Exploratory Evaluation of Alumina-Ceramic Housings for Deep Submergence Service

Third Generation Housings
Volume 2: Appendices

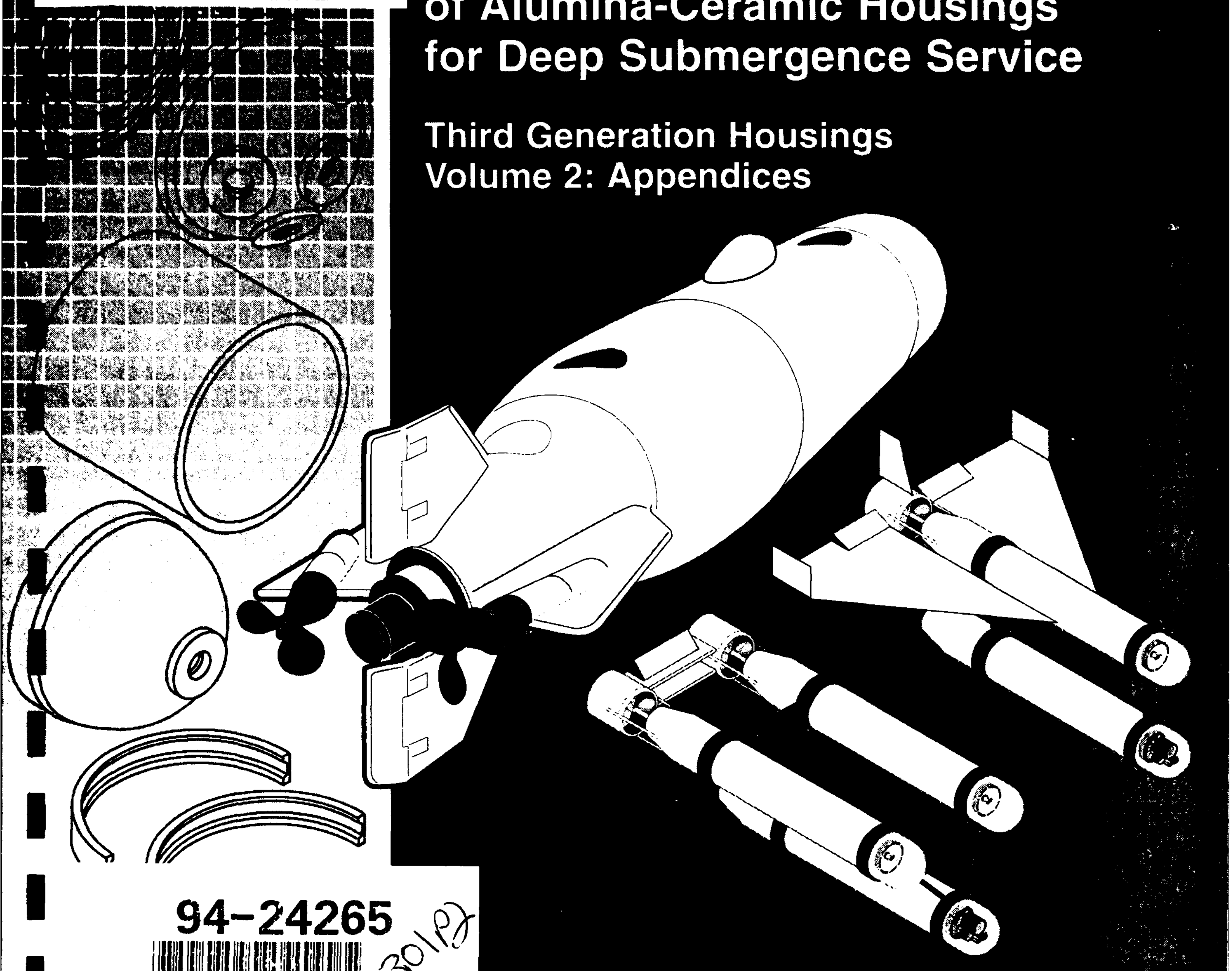

J. D. Stachiw

Technical Report 1314
September 1989
Revised June 1993

Technical Report 1314
September 1989
Revised June 1993

Exploratory Evaluation of Alumina-Ceramic Housings for Deep Submergence Service

Third Generation Housings
Volume 2: Appendices

J. D. Stachiw

NAVAL COMMAND, CONTROL AND OCEAN SURVEILLANCE CENTER
RDT&E DIVISION
San Diego, California 92152–5001

K. E. EVANS, CAPT, USN
Commanding Officer

R. T. SHEARER
Executive Director

ADMINISTRATIVE INFORMATION

This work was performed by the Marine Materials Technical Staff, RDT&E Division of the Naval Command, Control and Ocean Surveillance Center, for the Naval Sea Systems Command, Washington, DC 20362.

Because the program extended over several years and covered many technical areas, publication of this report was delayed until now.

Released by
J. D. Stachiw
Marine Materials
Technical Staff

Under authority of
N. B. Estabrook, Head
Ocean Engineering
Division

Accession For
NTIS GRA&I ☑
DTIC TAB ☐
Unannounced ☐
Justification
By
Distribution/
Availability Codes
Dist | Avail and/or Special
A-1

ES

VOLUME 2 CONTENTS

APPENDIX A: SCALE-MODEL 6-INCH-DIAMETER HOUSINGS

All appendix A figures and tables are placed at the end of appendix A text.

FIGURES

TABLES

APPENDIX A: SCALE-MODEL 6-INCH-DIAMETER HOUSINGS

TEST SPECIMENS

Scale-model 6-inch-diameter housings served as test specimens. The reason for choosing the scale-model housings for the first phase of the program was purely economical. Some of the more risky design options could be evaluated here with only minor loss of investment in case of catastrophic failure. Also, the scale-model housings could be tested inexpensively in small pressure vessels equipped for automatic pressure cycling, while the larger 12-inch-diameter housings could only be pressure cycled at the Naval Command, Control and Ocean Surveillance Center (NCCOSC) RDT&E Division (NRaD) in large vessels set up for manual operation.

To keep the number of variables to a minimum, all cylinders were fabricated from 94-percent alumina ceramic to the same dimensions (6.038-inch OD *by 9-inch* L *by* 0.207-*inch* t) as the Model 2 cylinders in second generation NRaD ceramic housings (figure A-1). The design hoop stress in these cylinders at 9,000 psi design depth was 137,000 psi.

Since there were two Model 1 cylinders from 99.5-percent alumina left over from the Second Generation Housing Program (figure A-2), they were also used in this test program. The design hoop stress in these cylinders at 9,000-psi design depth was −148,000 psi.

TEST FIXTURES

Three kinds of end closures served as bulkheads for testing the scale-model 6-inch-diameter cylinders. Plane steel discs 3-inches thick with a 0.25-inch-deep seat were used for destructive testing of individual cylinders and cylinder assemblies (figure A-3). The critical pressure generated by testing with plane bulkheads represent the maximum elastic stability attainable by a monocoque cylinder. Titanium hemispheres Model 2 were used in tests where the cylinder, or cylindrical assembly, was to be cycled to pressures exceeding the 9,000-psi design pressure (figure A-4). Titanium hemispheres Model 1 represent the lightest bulkheads that can be safely used in proof testing to 10,000 psi and subsequent pressure cycling of ceramic cylinders, or cylindrical assemblies, to 9,000-psi design pressure (figure A-5). Model 1 titanium hemispheres, because of their low weight, would also be the designer's choice for 6-inch-diameter operational pressure housings.

CERAMIC END CLOSURES

The *first goal* of Phase 1 was to demonstrate that the titanium hemispherical end closures (figures A-4 and A-5) on the ceramic cylinders can be replaced with ceramic hemispheres without any loss in structural performance of the ceramic cylinder. The ceramic hemispheres selected for this purpose were off-the-shelf, as-fired 6-inch-diameter hemispheres manufactured by Coors Ceramics for industrial applications (figure A-6). These hemispheres were twice as thick as it is required to meet the 137,000-psi design stress.

No attempt was made, however, to optimize their thickness by grinding since the goal of the experiment with the scale-model hemispheres was not to optimize their design, but to demonstrate that ceramic hemispheres could be mated to the ceramic cylinder by means of a metallic ring (figure A-7) similar in design to the metallic caps (figure A-8) developed for model cylinders in the second generation NRaD ceramic housing study. The primary function of both the metal caps on the cylinders and the nose mounting rings was to encapsulate the ceramic bearing surfaces from direct bearing contact with each other, that in time would lead to fretting and chipping of the ceramic surfaces due to relative movement between each other during external pressure loading (figure A-9). The encapsulation materials and procedures were identical to those employed previously on scale-model cylinders during the second generation Naval Ocean Systems Center (NOSC)* ceramic housing study (figure A-10).

---

*NOSC is now the Naval Command, Control and Ocean Surveillance Center (NCCOSC) RDT&E Division (NRaD).

The experimental evaluation of the scale-model ceramic hemispheres and the associated metallic mounting rings consisted of fitting them to a ceramic cylinder (figure A-11) and subjecting the assembled ceramic housing (figure A-12) to a series of pressure tests consisting of a proof test to 10,000 psi, followed by 100 pressure cycles to 9,000 psi and a single overpressure test to destruction (table A-1). The housing withstood the proof and cyclic tests without initiation of cracking or spalling, but imploded at 14,250 psi during short-term pressurization to failure. Inspection of the imploded housing components disclosed that the implosion was initiated by shearing at two locations of the thin flange on the metallic end cap bonded to the ceramic hemisphere. Based on this observation, one can conclude that the cylinder was deforming into an ellipse and, as a result of this deformation, the radial forces applied by the cylinder to the end cap on the hemisphere were maximized at the minor diameter of the ellipse. Increasing the thickness of the flange on the end cap would not significantly increase the critical pressure of the cylinder.

REMOVABLE JOINT STIFFENERS

The *second goal* of Phase 1 was to demonstrate that the radial end support provided by the titanium, or ceramic, hemispheres to the ends of a ceramic cylinder can be replaced with removable metallic joint ring stiffeners whose weight and elastic stability can be extensively modified by machining hoies in the web of the stiffener. The evaluation of stiffeners was performed with a 6-inch-diameter housing assembled first from two (Type Y) and later from four (Type W) ceramic cylinders joined by ring stiffeners and enclosed at the ends with titanium spherical bulkheads with penetrations for instrumentation heads (figures A-13 and A-14). Seven stiffeners were incorporated into nine cylindrical pressure housings assembled from two or more cylinders closed off at the ends by bulkheads (table A-1).

As the starting point in evaluation of joint ring stiffeners served the titanium ring stiffeners, Types B and C with T and I cross sections (figures A-15 and A-16) were developed during a previous program on the Second Generation NRaD ceramic housings (reference 8). In that program, joint stiffeners B and C were proof tested 10 times to 10,000 psi and pressure cycled 10 and 100 times to 9,000 psi, respectively, while mounted in a Type Y pressure housing assembly (figures A-17 and A-18). These tests were repeated in the current program to serve as a benchmark for succeeding tests in which stiffeners with lightening holes in the web were evaluated (table A-2).

To reduce the weight of the joint stiffener C configuration and to make it operationally more acceptable, a series of holes were drilled in the web of the stiffener at equal 20-degree intervals (figures A-19 and A-20), resulting in a new stiffener configuration, Type D. After proof testing it successful"y to 10,000 psi in a housing configuration Type Y (figure A-13), the stiffener was removed and the holes enlarged to form a new stiffener configuration, Type F (figures A-21 and A-22). This stiffener configuration was subsequently integrated into the housing assembly Type Y, where it was proof tested to 10,000 psi and pressure cycled 100 times to 9,000 psi. Following this, it was incorporated into housing assembly Type W and proof tested to 10,000 psi. After successful completion of these tests, no further enlargement of the holes in the web of the stiffener was contemplated as it was concluded that any further reduction of the stiffener cross section would not reduce its weight significantly, while, at the same time, it probably would reduce sufficiently the stiffener's elastic stability to trigger buckling of the housing assembly during proof testing to 10,000 psi. The effect of holes on the weight of the titanium stiffener is shown in table A-3.

After optimization of the titanium joint ring stiffener configuration, similar procedures were followed in the optimization of the aluminum joint-ring stiffener Type E (figure A-23). The high-strength aluminum 7,000 alloy series was investigated as the potential replacement for the expensive Ti–6Al–4Va alloy used in the fabrication of ring stiffener Types C, D, and F. It was postulated that the high-strength aluminum alloys could handle without yielding the radial and axial loads to which the joint ring stiffener is subjected, as the maximum axial bearing and hoop stresses in the stiffener were calculated

not to exceed –68,000 and –35,000 psi at 10,000-psi proof pressure. The only drawback associated with the use of aluminum joint rings is their susceptibility to corrosion on surfaces exposed to seawater. This drawback, however, can be eliminated by placing the seal at a location that the seawater does not wet any portion of the stiffener.

The aluminum joint ring stiffener configurations Type G (figure A-24) and Type H (figure A-25), which were created by machining holes in the web of stiffener Type E, were pressure proof tested after being integrated into ceramic housing assemblies Type Y and Type W, consisting of two and four ceramic cylinders, respectively (figures A-26 and A-27). The test results were satisfactory: No permanent deformation of the aluminum stiffeners or cracking of the ceramic cylinders was observed. The weights of the aluminum joint ring stiffeners are shown in table A-3. It should be noted that drilling holes in the webs of joint ring stiffeners reduced their weight by approximately 18 percent.

INTERIOR RING STIFFENERS

The *third goal* of Phase 1 was to demonstrate that it is feasible to increase the elastic stability of ceramic monocoque cylinders by providing radial support at midbay with a metallic ring stiffener bonded to the interior surface of the cylinder with epoxy adhesive. The feasibility of this arrangement was to be demonstrated by fabricating Model 3 (figure A-28) from the same material and with the same internal and external diameters as pressure hull Model 2 (figure A-1) used in preceding studies on the optimization of joint ring stiffeners. The only difference between Models 3 and 2 was the length; Model 3 was twice as long as Model 2, and without a midbay stiffener the longer Model 3 cylinder, supported only at the ends, buckled at 8,800 psi instead of 17,500 psi.

Thus, the function of the fixed midbay stiffener was to provide the same radial support to a single $L/_D = 3$ cylinder (figures A-29 and A-30) as the joint ring stiffener provided to two $L/_D = 1.5$ cylinders (figures A-13 and A-31). The internal ring stiffener has many advantages over a joint ring stiffener. It does not have to be fabricated from materials that (1) are corrosion resistant in seawater, and (2) have a compressive yield point in excess of 65,000 psi, since the internal stiffener is neither exposed to seawater, nor is it subjected to axial bearing loads between mating ends of cylinders. The many materials from which a midbay stiffener may be fabricated besides titanium are aluminum, magnesium, silicon-carbide reinforced cast aluminum, glass or graphite-fiber reinforced plastic, ceramic, or cermet.

The use of a midbay stiffener represents significant weight savings, as it eliminates one set of end caps and a single clamp band associated with a joint ring stiffener (figure A-32). The cylinder with a midbay stiffener also generates less hydrodynamic drag since one of the external clamp bands has been eliminated. The reduction in cost is also significant as the grinding of one pair of ceramic bearing surfaces and the machining of two metallic end caps and a single clamp band has been eliminated from the cylindrical housing section.

The midbay stiffeners were machined from 7076–T6 aluminum plate to fit the interior diameter of the ceramic cylinders with only 0.005-inch radial clearance. Prior to inserting the stiffener into the ceramic cylinder, the interior of the cylinder at midbay was liberally coated with epoxy adhesive (figures A-32 and A-33). After the epoxy had set, a bead of elastomeric adhesive (i.e., room-temperature vulcanizing silicone rubber) was placed on the ceramic surface near the edge of the exterior flange on the midbay stiffener. While the primary purpose of the epoxy adhesive was to *fill* the annular clearance and to *serve as a bearing gasket* between the interior surface of the cylinder and the exterior surface of the stiffener, the purpose of the elastomer adhesive bead was to keep the stiffener from sliding axially in case the brittle epoxy debonded from the aluminum stiffener.

The bonding arrangement performed well for the Model 3 ceramic cylinder with Mod 0 midbay stiffener (figure A-34) during subsequent proof testing to 10,000 psi, followed by 1,000 pressure cycles to 9,000 psi. After successful completion of pressure cycling with the Mod 0 stiffener, similar testing was initiated with Mod 1 and Mod 2 stiffeners (figures A-33 and A-37). During pressure testing, strains were recorded on all three types of

stiffeners (figures A-38 through A-55). The Mod 1 stiffener failed during the proof test by buckling at 9,900 psi (figure A-44), while the Mod 2 stiffener, like Mod 0, passed all the tests successfully.

Comparison of the data generated by tests of the Mods 0, 1, and 2 midbay stiffeners (tables A-4 through A-9) resulted in several interesting observations:

1. Tensile stresses are generated in the stiffeners only on the interior surface of the inside flange in axial direction; their magnitude at 9,000-psi design pressure is in the 8,500- to 10,500-psi range for all three stiffener configurations.

2. The presence of holes in the stiffener web introduces large bending moments in the interior flange oriented in the hoop direction. As a result of this bending, the hoop stresses measured on the concave surface of the interior flange varied with their locations; *maximum compressive* stresses are found midway between web sections directly under the holes in the web above, while *minimum compressive* stresses are located directly under the remaining web sections. For example, in the Mod 2 stiffener, the average value of hoop stress in the internal flange, midway between web sections, is –23,632 psi, while the average value of hoop stress in the same flange under the web sections is only –6,366 psi.

3. The presence of holes also introduces high radial compressive stresses in the web sections. In the Mod 0 stiffener without holes, the radial compressive stress on the web is only –10,249 psi, while in Mod 1 and Mod 2 stiffeners, the value of radial compressive stress on the web between holes has increased to –36,371 and –41,066 psi, respectively.

The evaluation of internal midbay stiffeners was concluded by testing to implosion two Mod 3 ceramic cylinders with Mod 0 and Mod 2 midbay stiffeners. For these tests, the titanium hemispherical end closures were replaced with thick, flat-steel bulkheads (figure A-57) designed not to fail at pressures below 20,000 psi. Model 3 ceramic cylinders with a Mod 0 midbay stiffener imploded at 18,000 psi, while the one with a Mod 2 midbay stiffener imploded at 15,000 psi. There was no need to perform an implosion test on a Model 3 cylinder supported by a Mod 1 midbay stiffener, as one of them had already failed at 9,900 psi during proof testing of the cylinder.

When one compares the critical pressures of the three different midbay stiffener configurations (table A-10), it becomes apparent that the drilling of lightening holes in the web of stiffeners cannot be justified solely on the basis of weight reduction, as a 5-percent decrease in weight (Mod 2 versus Mod 0 stiffener design) is accompanied by a 16.6-percent reduction in critical pressure of the ceramic cylinder. There is no doubt that an equivalent weight reduction can be achieved without a decrease in critical pressure by making the web and flanges of Mod 0 stiffeners approximately 5-percent thinner and the height of the web 5-percent higher.

Incorporating holes into the web of the midbay or joint ring stiffeners is readily justifiable, however, by the packaging requirements of electronic and hydraulic subsystems to be located inside the cylindrical housings some time in the future. The large holes in the webs of the stiffeners allow placement of cables and/or hydraulic lines next to the wall of the cylinder without having to make provisions for U-shaped bends where the cables and/or hydraulic lines have to clear the stiffeners.

Since the critical pressure of the cylindrical housing decreases exponentially with the size of holes in the stiffener web, it behooves the housing designer to keep the size of the holes to a minimum. If required for placing cables, the holes should be round, and smaller in diameter than the height of the midbay stiffener web. Elliptical holes are less desirable than round holes as they are more conducive to buckling of the flanges on the stiffener. Elliptical holes can be safely incorporated into the web of the stiffeners, provided they do not exceed the sizes of the holes in interior midbay stiffener Mod 2 or joint ring stiffeners F (for titanium) and H (for aluminum).

CONCLUSIONS—PHASE I

1. The short-term critical pressure of 6-inch-diameter Model 2 94-percent alumina-ceramic cylinders with $t/D_0 = 0.034$ and $L/D_0 = 1.5$ and Model 1 99.5-percent alumina-ceramic cylinders with $t/D_0 = 0.032$ and $L/D_0 = 1.5$ has been found to be in the range of 17,700 to 18,000 psi when radially supported at the ends by plane-steel bulkheads (*figures* A-56 and A-57), and 14,250 psi when supported by ceramic or titanium Model 2 hemispheres (table A-10). With Model 1 titanium hemispheres, the short-term critical pressure is only 11,250, as these hemispheres were designed to provide maximum buoyancy with the absolute minimum safety factor (SF) for a housing with 9,000 psi design pressure. Thus, the SF against buckling at 9,000-psi design depth varies from 1.25 to 2, depending on the type of radial support to the cylinder ends.

2. At 9,000-psi design pressure, the maximum compressive stress of 94-percent alumina Model 2 cylinders with $t/D_0 = 0.0344$ and $L/D_0 = 1.5$ is –135,785 psi in hoop direction. This provides the Model 2 cylinder at design pressure with a nominal SF of 2.2 based on the nominal uniaxial compressive strength of –300,000 psi for 94-percent alumina ceramic. For a 99-percent alumina Model 1 cylinder with a $t/D_0 = 0.0313$ and $L/D_0 = 1.5$, the maximum compressive hoop stress is –148,350 psi, providing it with an SF of 2 based on its compressive strength.

3. External pressure housings made up of a single monocoque ceramic cylinder supported at the ends by plane or hemispherical bulkheads can be extended in length by mechanically joining several cylindrical sections with removable joint stiffeners that provide radial support to the cylinder ends. By selecting the proper moment of inertia for the joint stiffener, the buckling pressure of the housing made up of several cylindrical sections can be made to equal, or surpass, the buckling pressure of a single monocoque cylinder supported radially at the ends with plane or spherical bulkheads.

4. The length of a single monolithic monocoque Model 2 cylinder with $t/D_0 = 0.0344$ can be increased beyond $L/D_0 = 1.5$ without decreasing its buckling pressure, provided that metallic ring stiffeners are bonded to its interior at $L/D_0 \leq 1.5$ intervals.

   Extending the length of a single monocoque cylinder from t/Do = 1.5 to 3 and inserting an internal stiffener adds less weight to the structure than joining two $L/D_0 = 1.5$ cylinders with a joint stiffener (approximately 4 percent less). It also is less expensive to fabricate, as it eliminates the grinding of two ceramic bearing areas and the machining of two titanium end caps.

5. The cyclic fatigue of 94-percent alumina-ceramic monolithic cylinders with $t/D_0 = 0.0344$ and 99.5-percent alumina cylinders with $t/D_0 = 0.313$ thickness is in excess of 1,000 pressure cycles to 9,000 psi when the ends are protected by metallic end caps bonded to them by epoxy adhesive. The *depth* of the annular seat in the end cap exceeds the thickness of the cylinder by 50 percent. Without end caps, the cyclic fatigue life is less than 50 cycles, as the differential movement between the bare ends of cylinders and metallic bearing surfaces initiates shear cracks in the ceramic bearing surface that propagate inward with each succeeding pressure cycle.

6. The cyclic fatigue life of Model 2 alumina-ceramic polylithic cylinder assembly consisting of 94-percent alumina rings joined by nickel brazing was found also to exceed 1,000 pressure cycles when the ends of the cylinder were protected by metallic end caps in the same manner as the monolithic Model 2 cylinder.

7. The ceramic hemispheres provide the required radial support to the ceramic cylinder ends by bonding to its equator a metallic end cap with a lip that matches the internal diameter of the end cap on the cylinder.

   The monocoque ceramic cylinders, Models 1 and 2, supported at their ends by ceramic, or titanium, hemispheres with equivalent radial

stiffness fail by buckling at pressures that are approximately 20-percent smaller than when they are supported by plane-metallic bulkheads.

8. The external pressure at which a single ceramic monocoque cylinder supported radially at the ends by plane bulkheads will buckle can be predicted with ± 10 percent accuracy by the graphic solution of the von Mises equation for elastic instability of cylinders (figures A-58 through A-61). The same graphic solution applies to a single ceramic monocoque cylinder supported radially at the ends by ceramic or metallic hemispherical bulkheads, provided that (1) the radial stiffness of the hemispheres equals that of the cylinder, and (2) one substitutes the expression ($L + 0.33\ D_0$) for L in the L/D_0 ratio while reading the graph's abscissa.

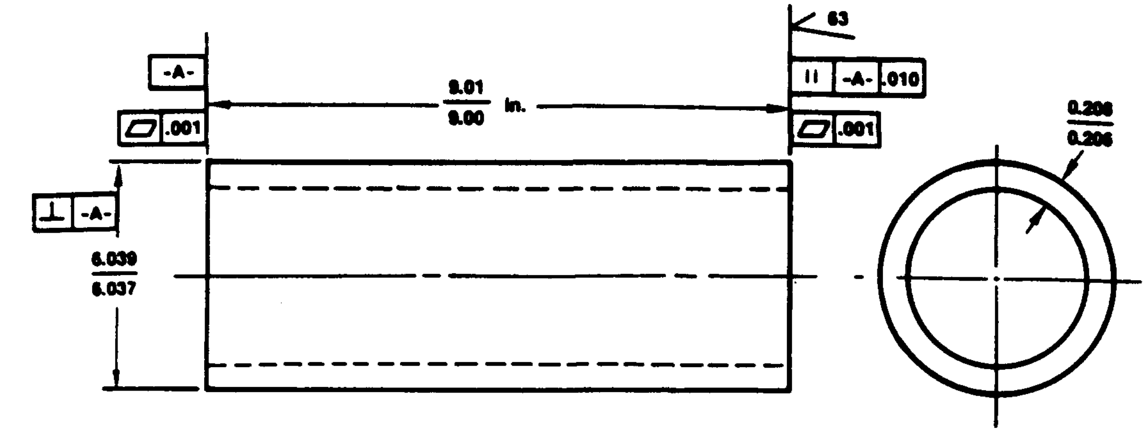

MATERIAL REQUIREMENTS:

CERAMIC COMPOSITION	94% Al_2O_3
MODULUS OF ELASTICITY	41×10^6 psi
COMPRESSIVE STRENGTH	> 300,000 psi
FLEXURAL STRENGTH	> 50,000 psi
POISSON'S RATIO	0.21
SHEAR MODULUS	17×10^6
BULK MODULUS	24×10^6
SPECIFIC GRAVITY	3.62
COEFF OF THERMAL EXPANSION AT ROOM TEMP	2×10^{-6}/°F

Figure A-1. Model 2 ceramic cylinder.

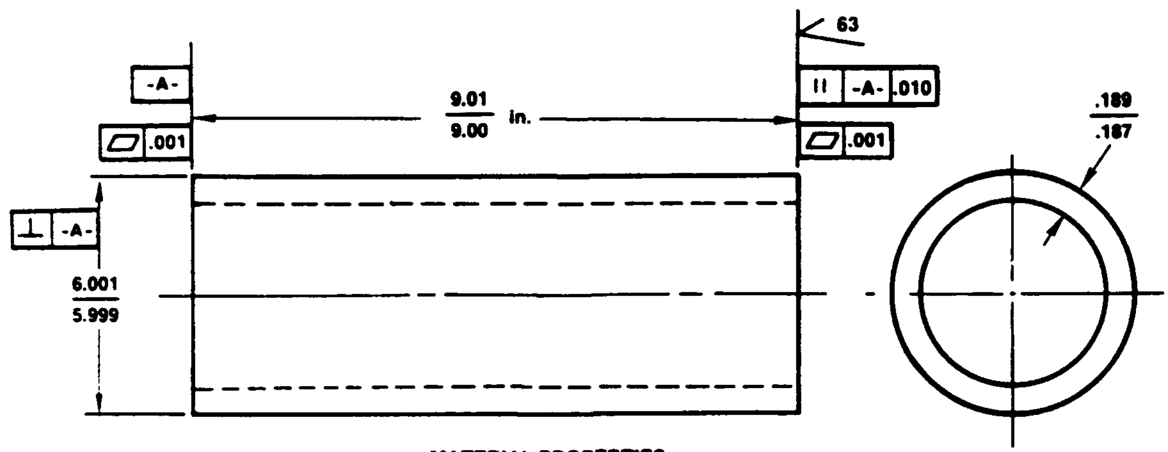

MATERIAL PROPERTIES

CERAMIC COMPOSITION	99.5% Al_2O_3
MODULUS OF ELASTICITY	54×10^6 psi
COMPRESSIVE STRENGTH	> 300,000 psi
FLEXURAL STRENGTH	> 50,000 psi
POISSON'S RATIO	0.22
SHEAR MODULUS	22×10^6
BULK MODULUS	33×10^6
SPECIFIC GRAVITY	3.89
COEFF OF THERMAL EXPANSION AT ROOM TEMP	2×10^{-6}/°F

Figure A-2. Model 1 ceramic cylinder.

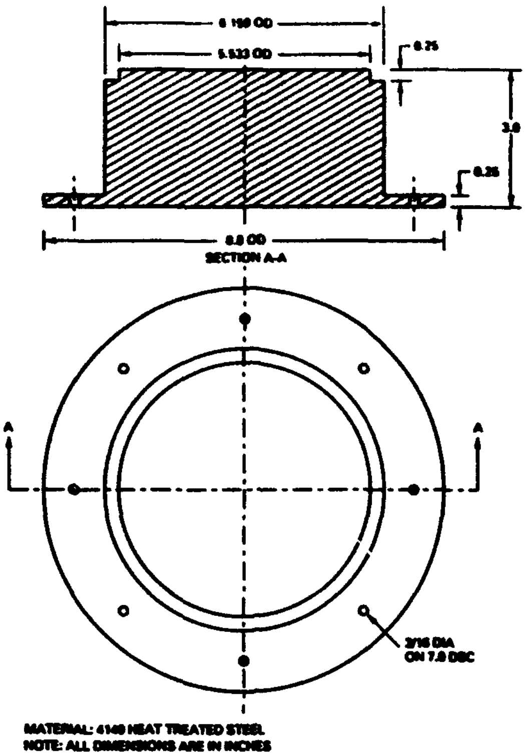

Figure A-3. Steel plug serving as end closure for 6-inch-OD ceramic cylinder.

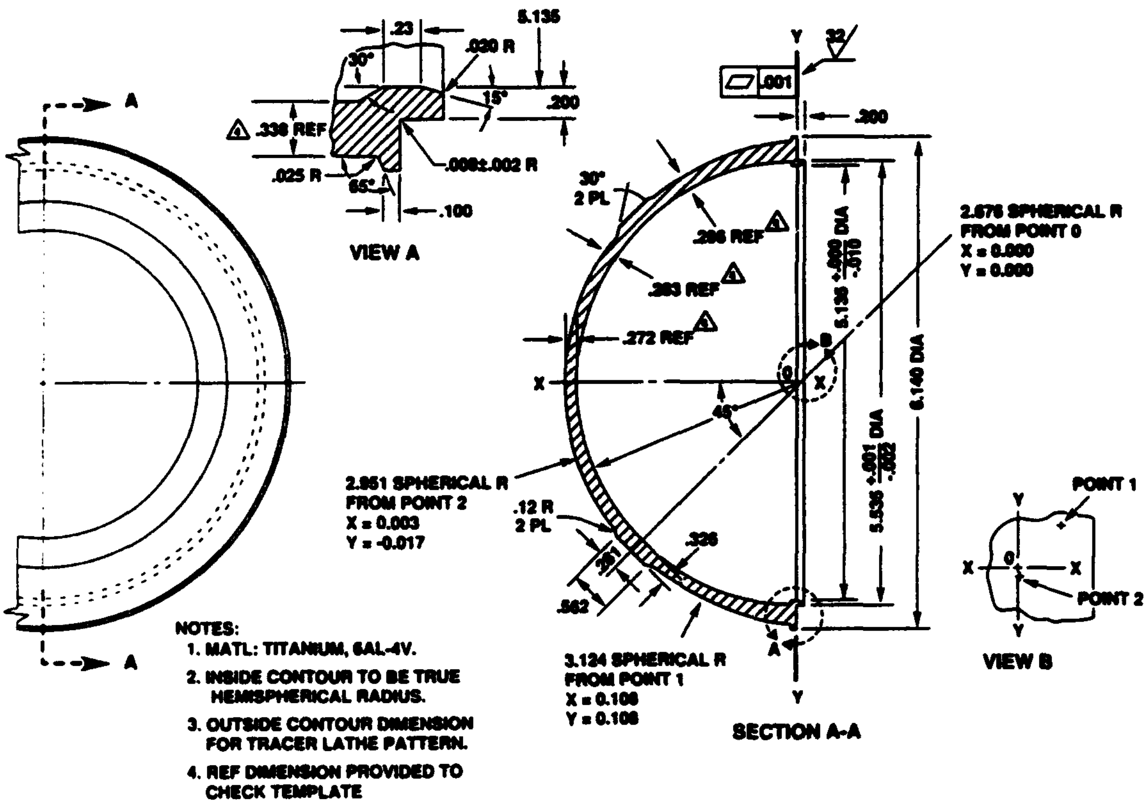

Figure A-4. Model 2 titanium hemisphere; 20,000-psi design pressure.

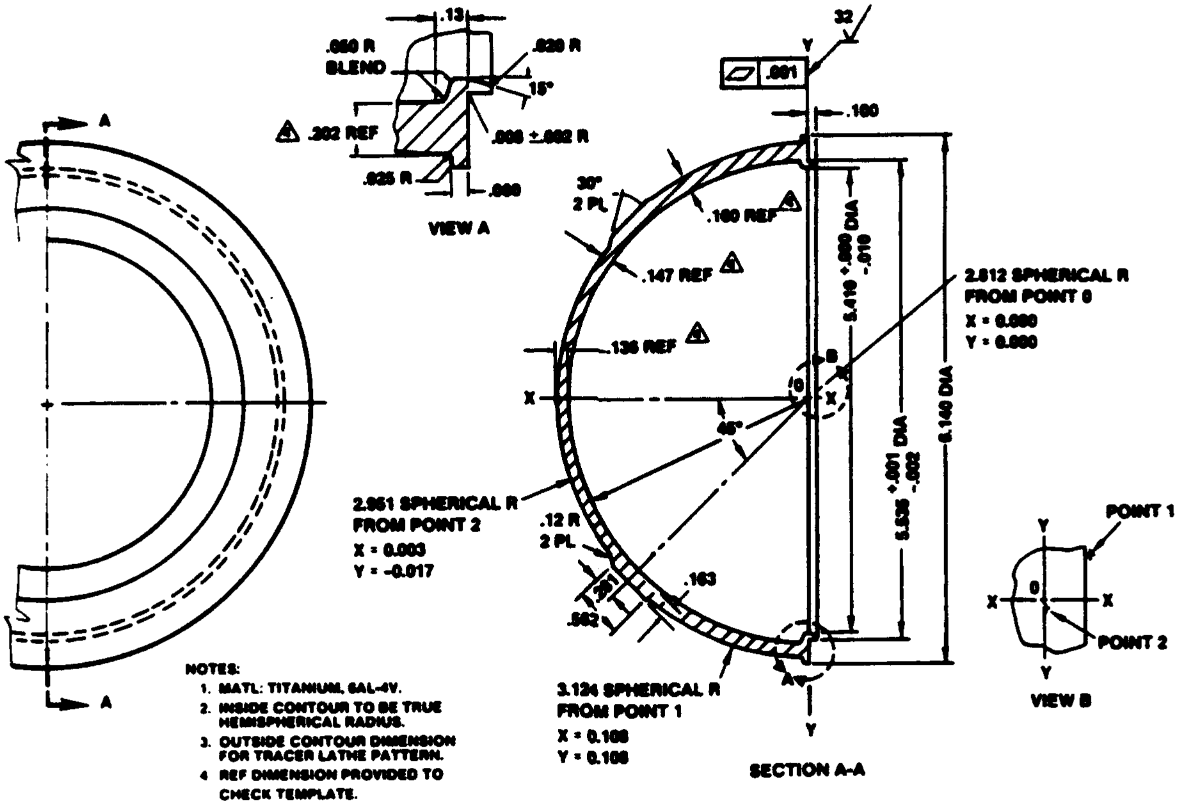

Figure A-5. Model 1 titanium hemisphere; 9,000-psi design pressure.

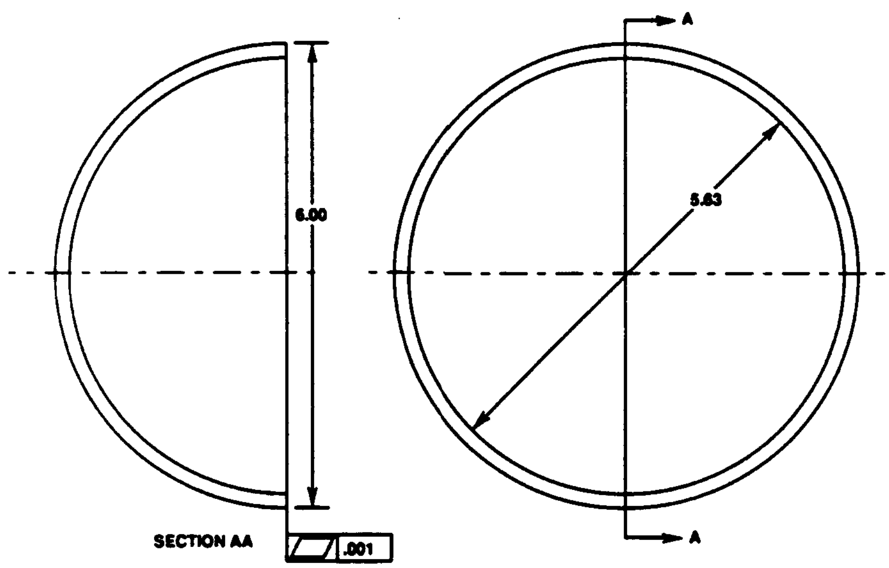

MATERIAL REQUIREMENTS

CERAMIC COMPOSITION	99.8 AL_2O_3
MODULUS OF ELASTICITY	>54 x 10^6 psi
COMPRESSIVE STRENGTH	>300,000 psi
FLEXURAL STRENGTH	> 50,000 psi
POISSON'S RATIO	0.22
SHEAR MODULUS	>20 x 10^6
BULK MODULUS	>30 x 10^6
SPECIFIC GRAVITY	3.86
COEFF OF THERMAL EXPANSION AT ROOM TEMP	4 x 10^{-6}/°F

Figure A-6. Ceramic hemisphere; 20,000-psi design.

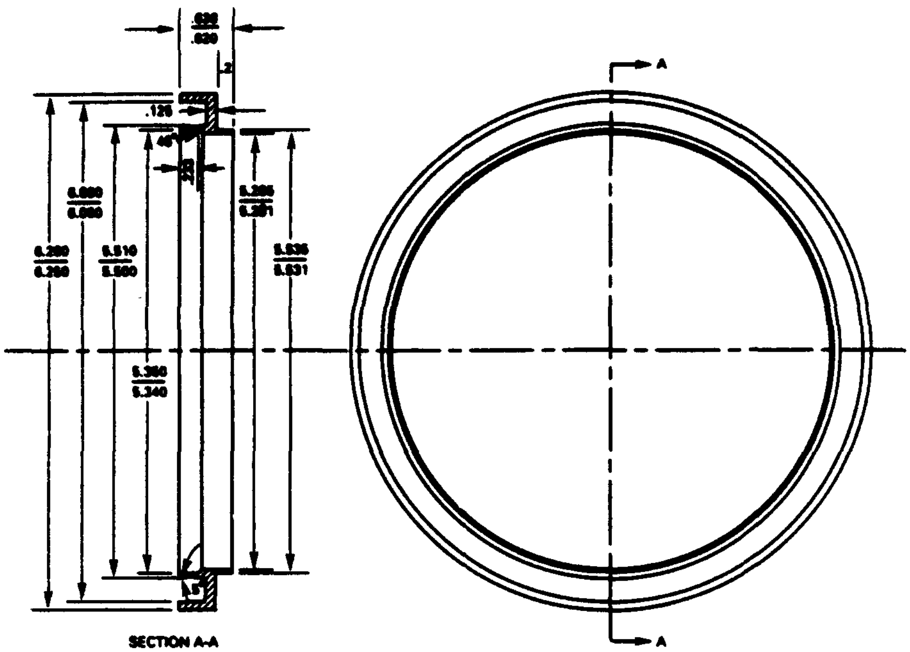

MATERIAL: TITANIUM ALLOY 6Al4Va

Figure A-7. End ring for ceramic hemisphere.

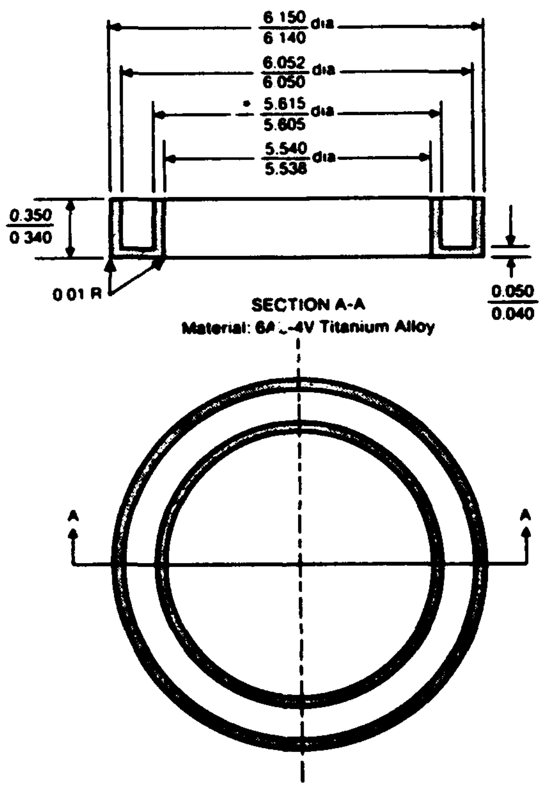

ALL MEASUREMENT IN inches

* 6.012/6.010 for MODEL 1 cylinders

Figure A-8. End cap for Models 2 and 3 ceramic cylinders.

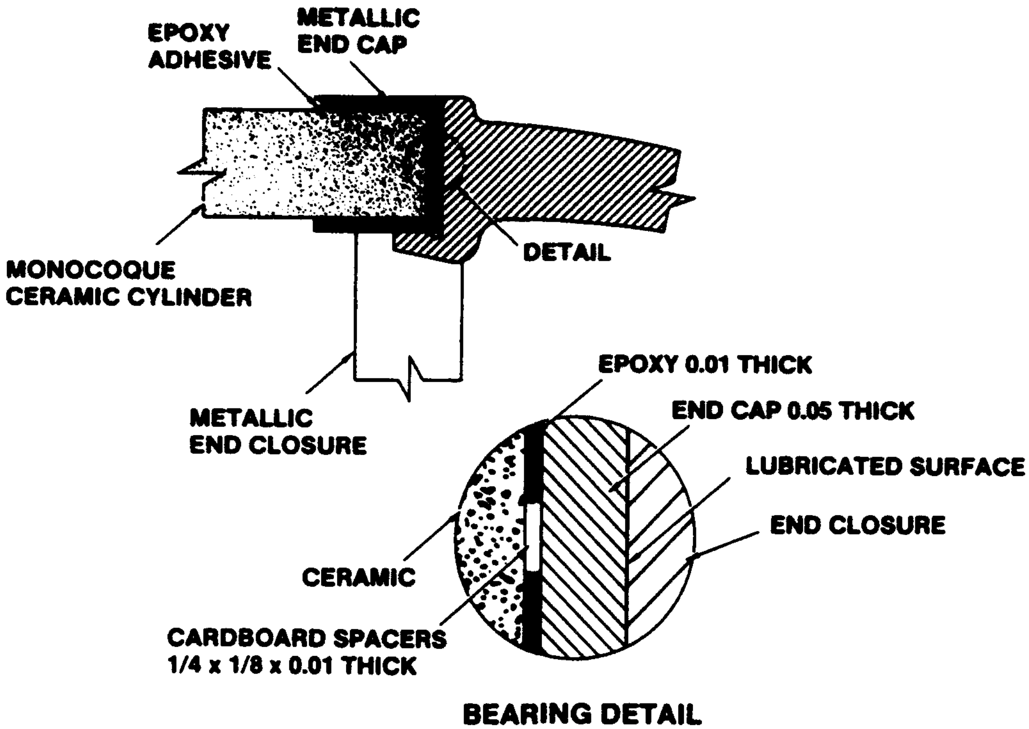

Figure A-9. Encapsulation of ceramic bearing surfaces in metallic end caps against fretting.

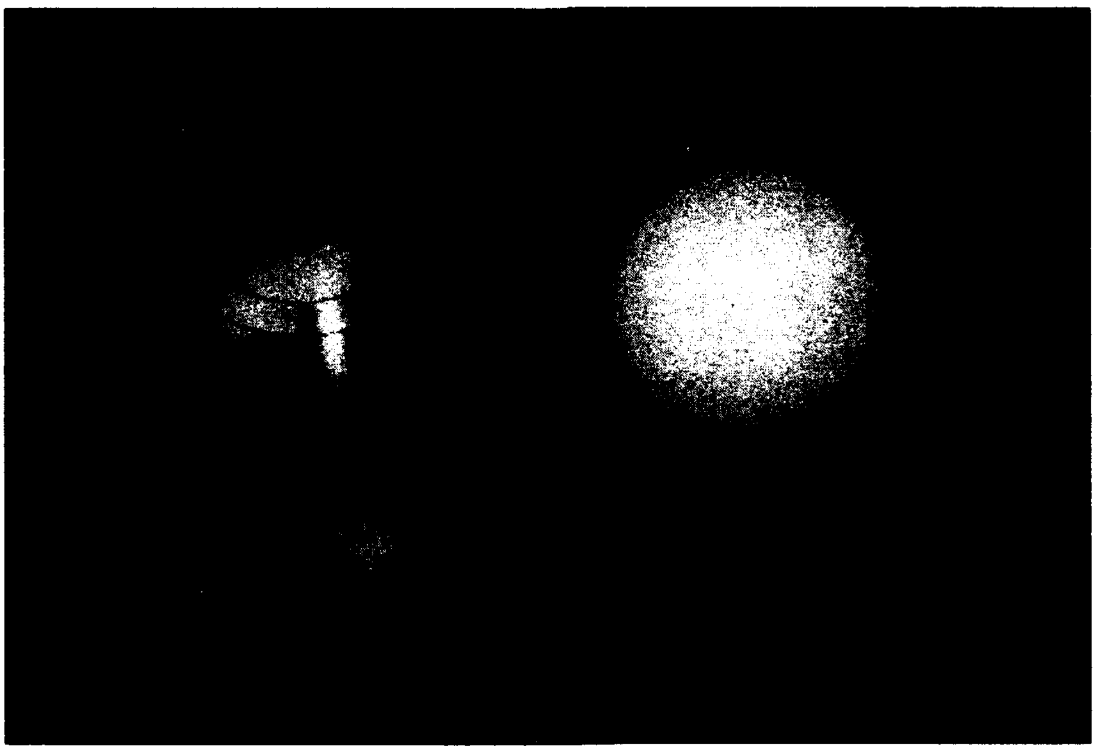

Figure A-10. Titanium and ceramic hemispheres serving as end closures for 6-inch-OD ceramic cylinders.

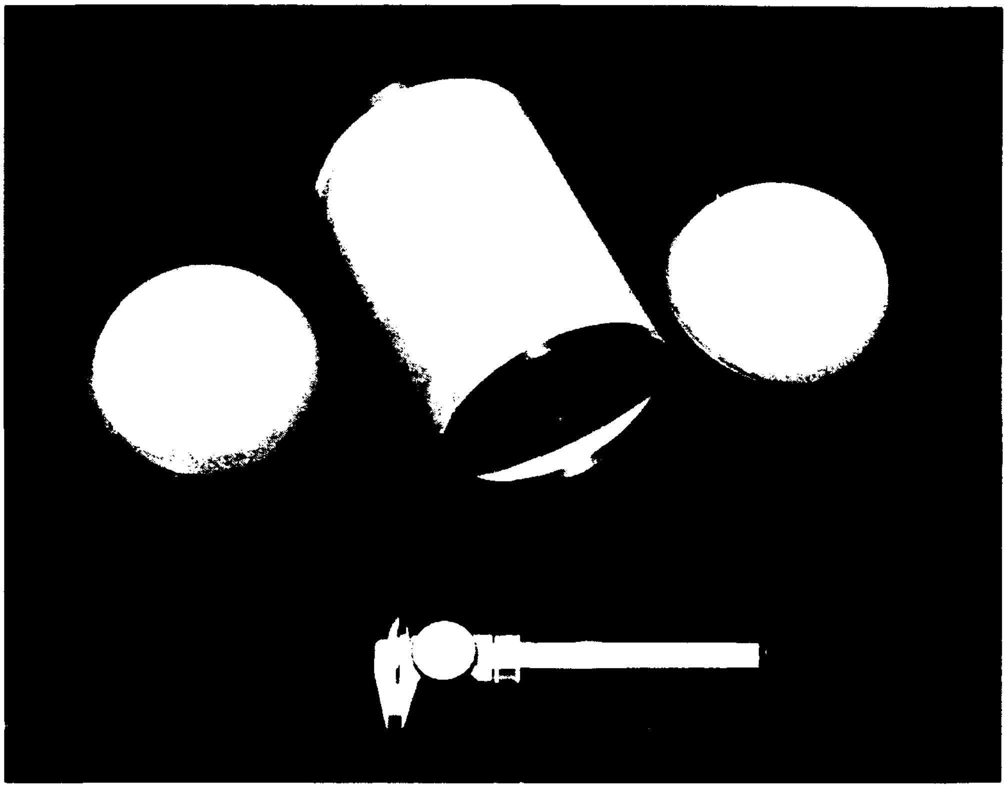

Figure A-11. Components of 6-inch-OD ceramic housing assembly.

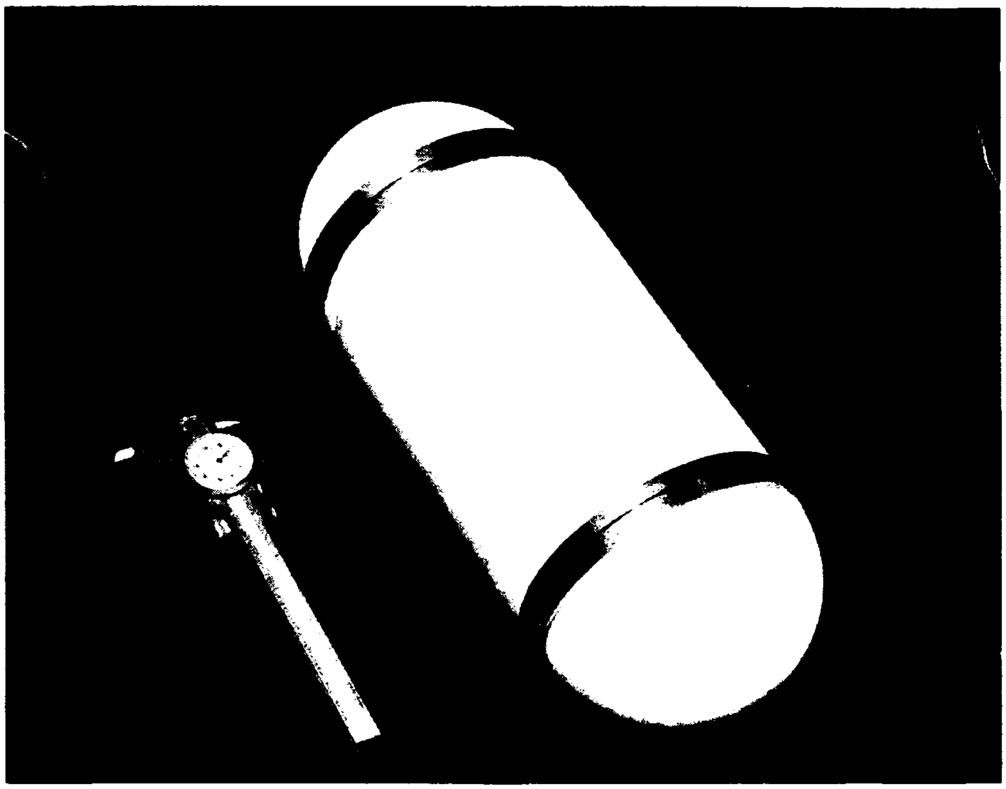

Figure A-12. The 6-inch-OD ceramic housing assembly using ceramic end closures.

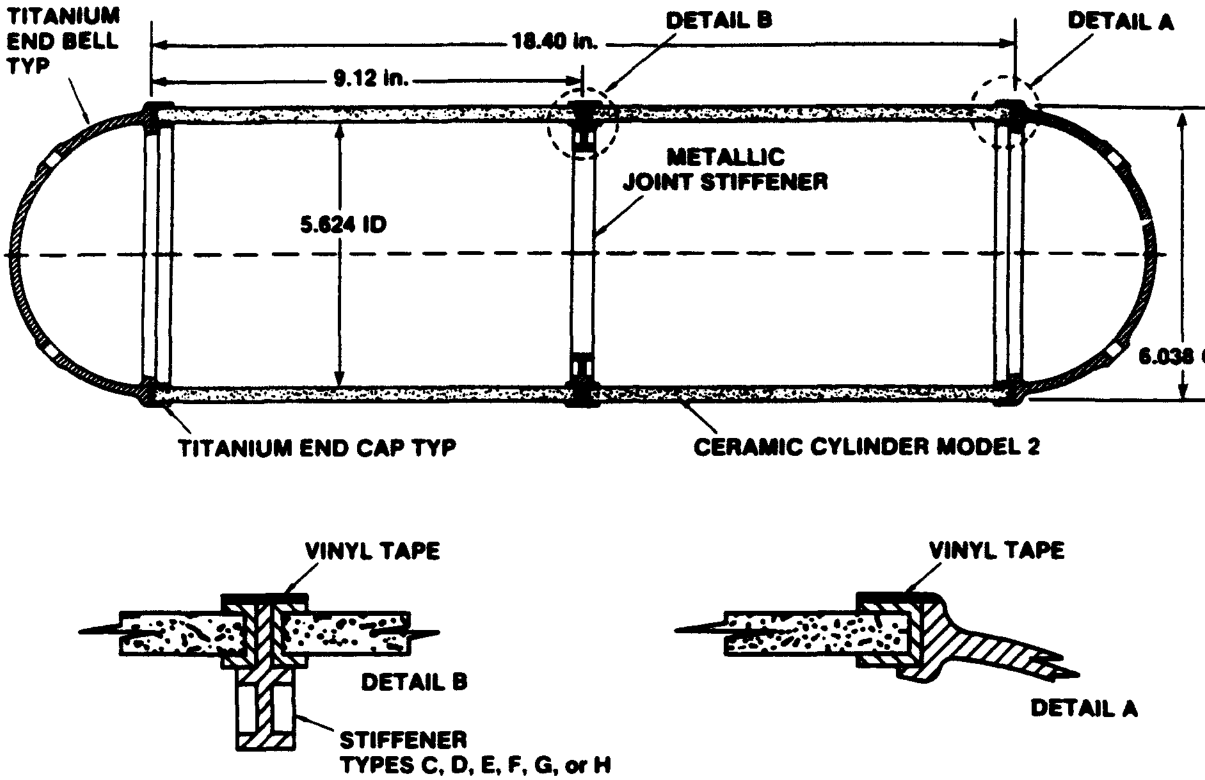

Figure A-13. Joint stiffened ceramic housing assembly; Type Y; 2 cylinder sections Mod 2.

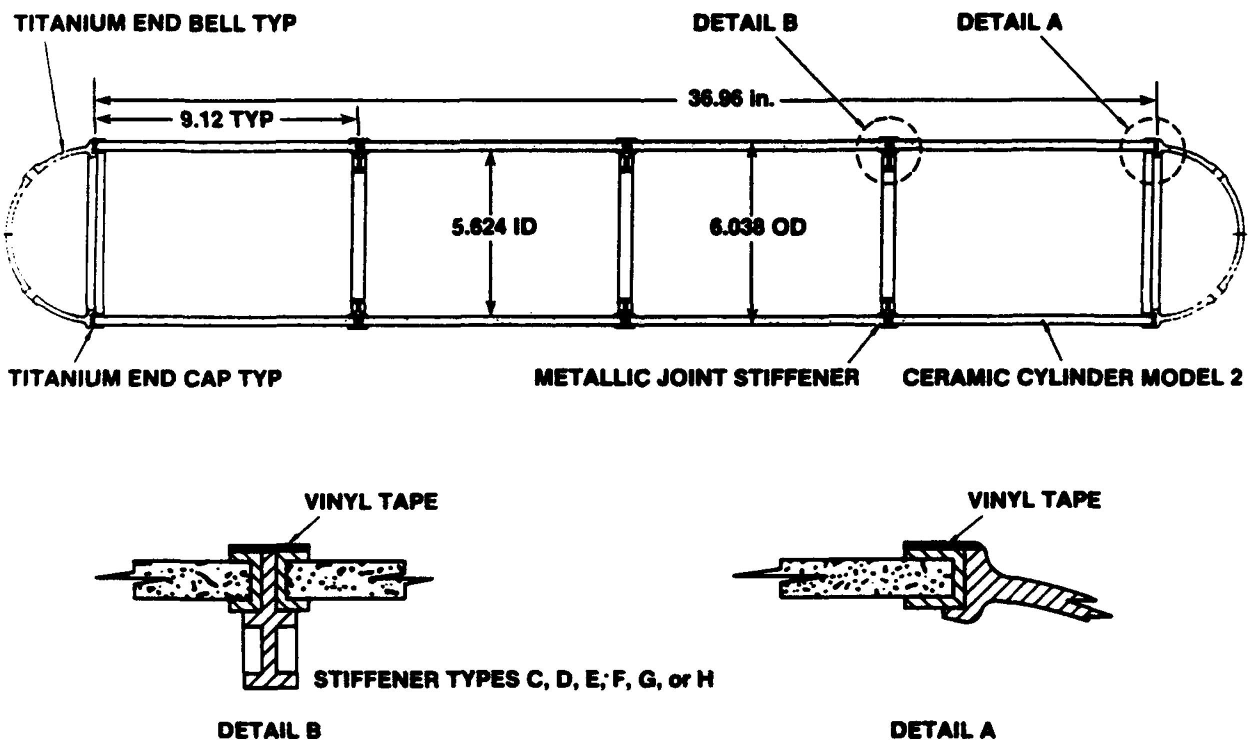

Figure A-14. Joint stiffened ceramic housing assembly; Type W; 4 cylinder sections Mod 2.

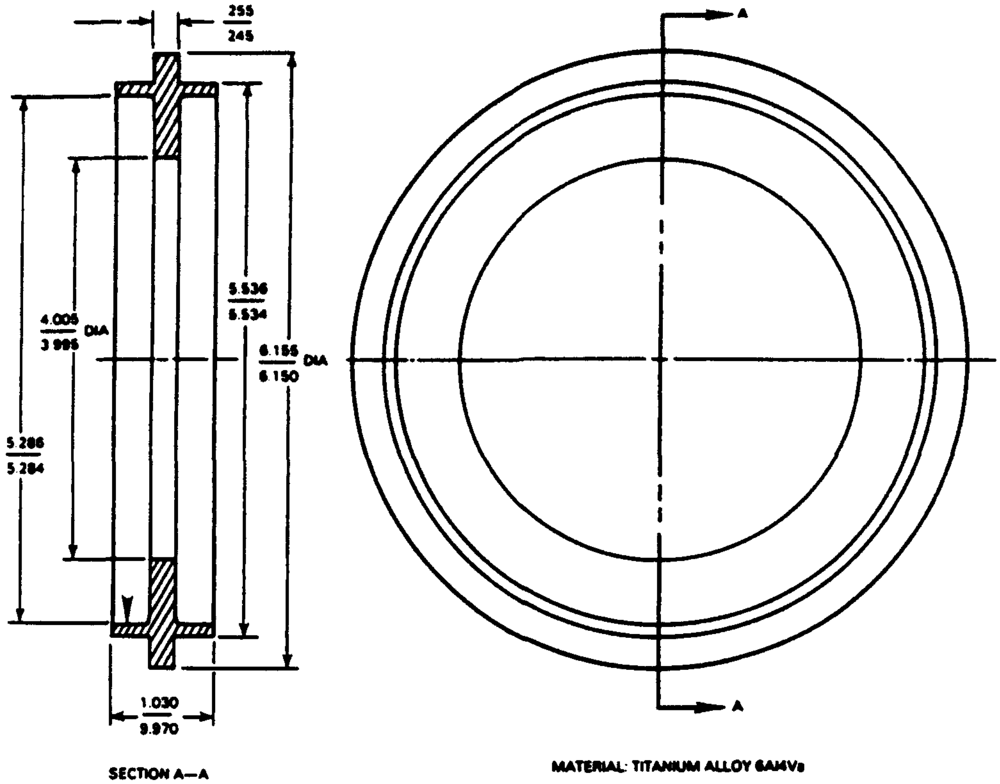

Figure A-15. Joint ring stiffener B; critical pressure ≥18,000 psi.

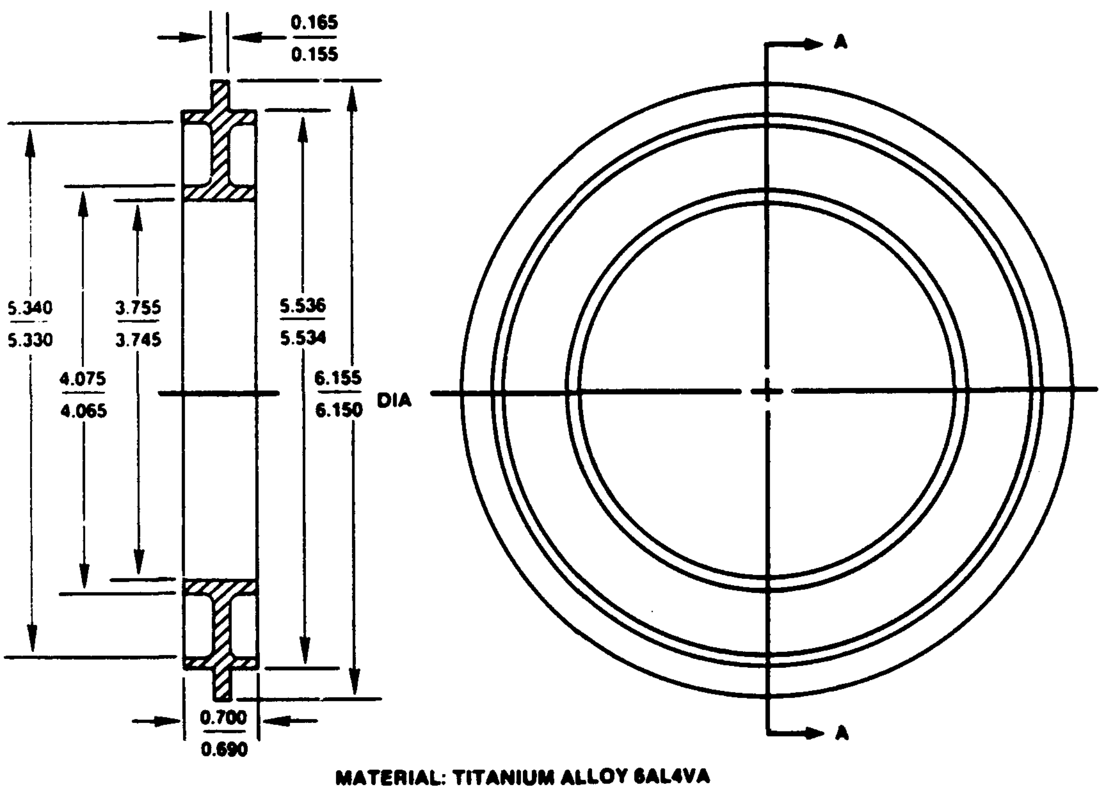

Figure A-16. Joint ring stiffener C; critical pressure ≥18,000 psi.

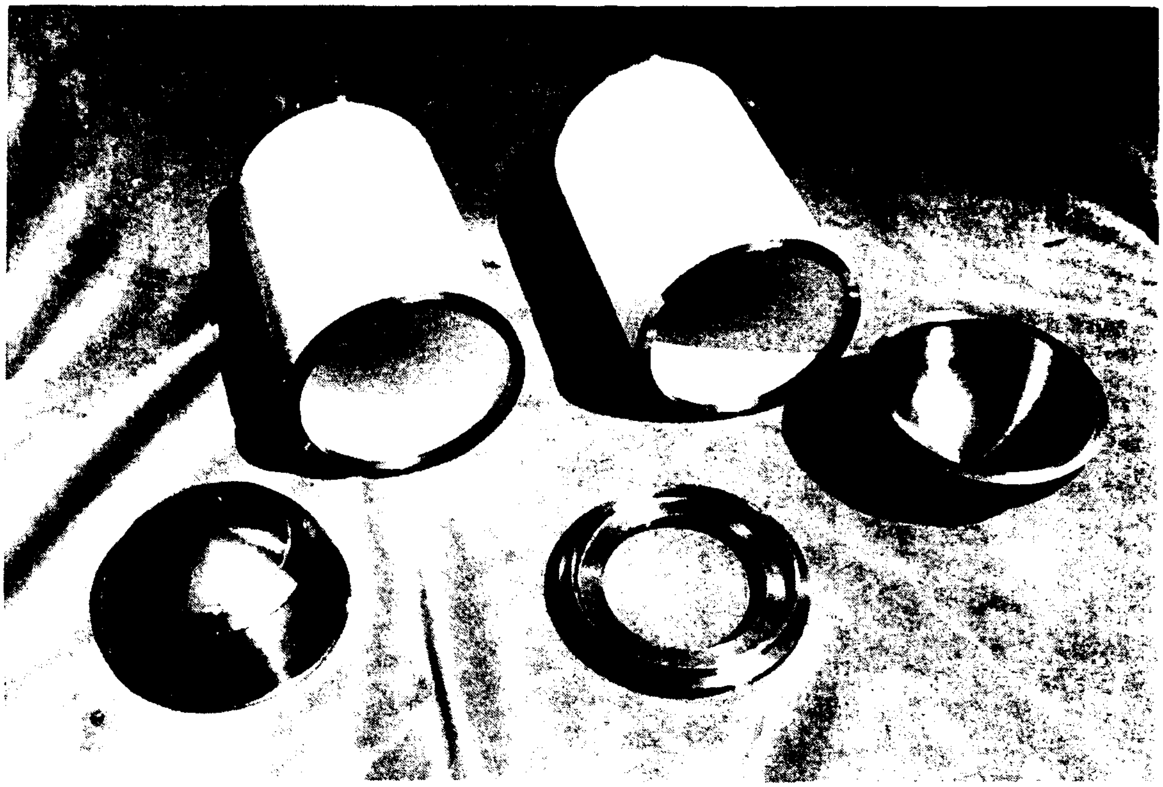

Figure A-17. Components of 6-inch-OD ceramic housing Type Y; joint ring stiffener B.

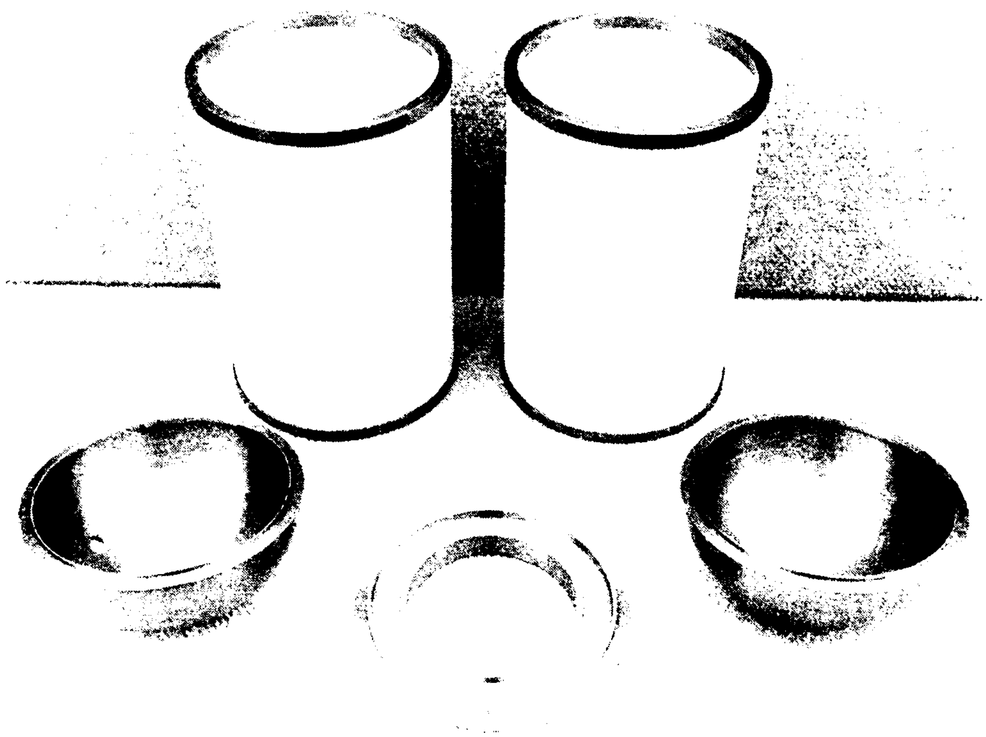

Figure A-18. Components of 6-inch-OD ceramic housing Type Y; joint ring stiffener C.

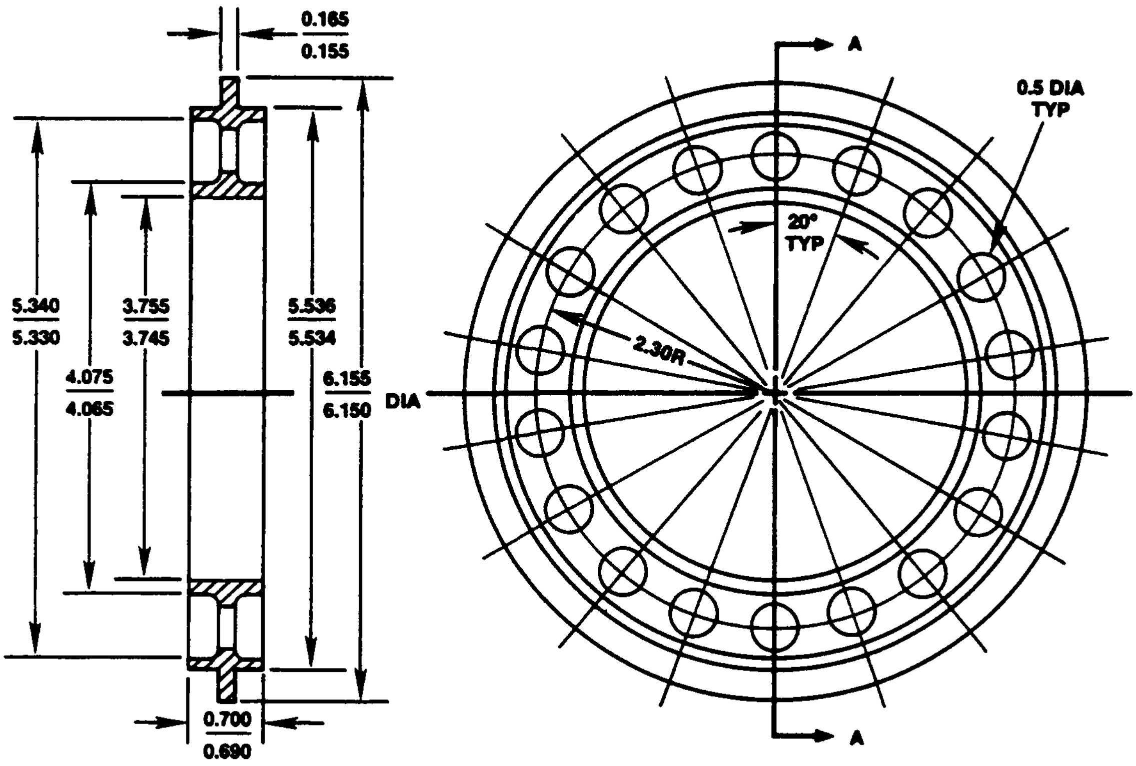

Figure A-19. Joint ring D; drawing.

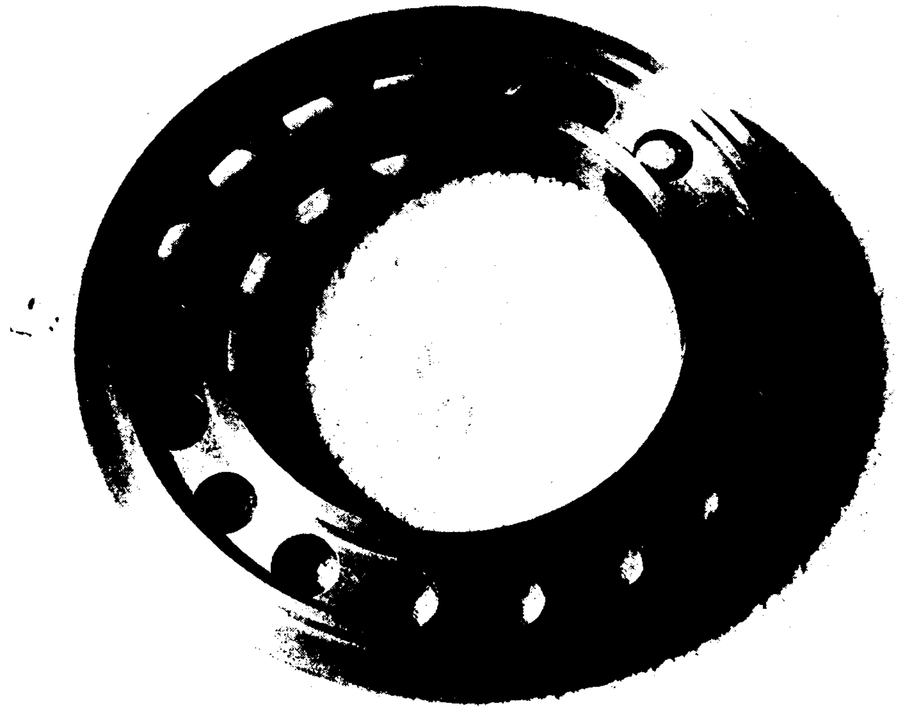

Figure A-20. Joint ring D; exterior view.

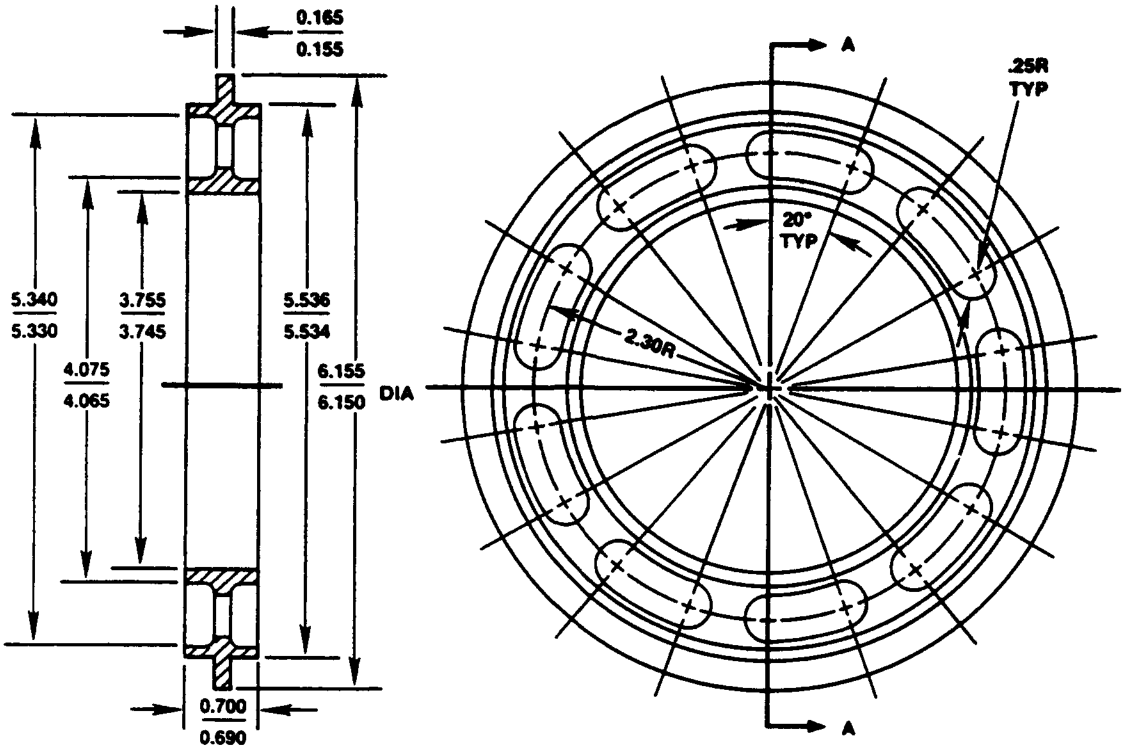

MATERIAL: TITANIUM ALLOY 6AL4VA

Figure A-21. Joint ring F; drawing.

Figure A-22. Joint ring F; exterior view.

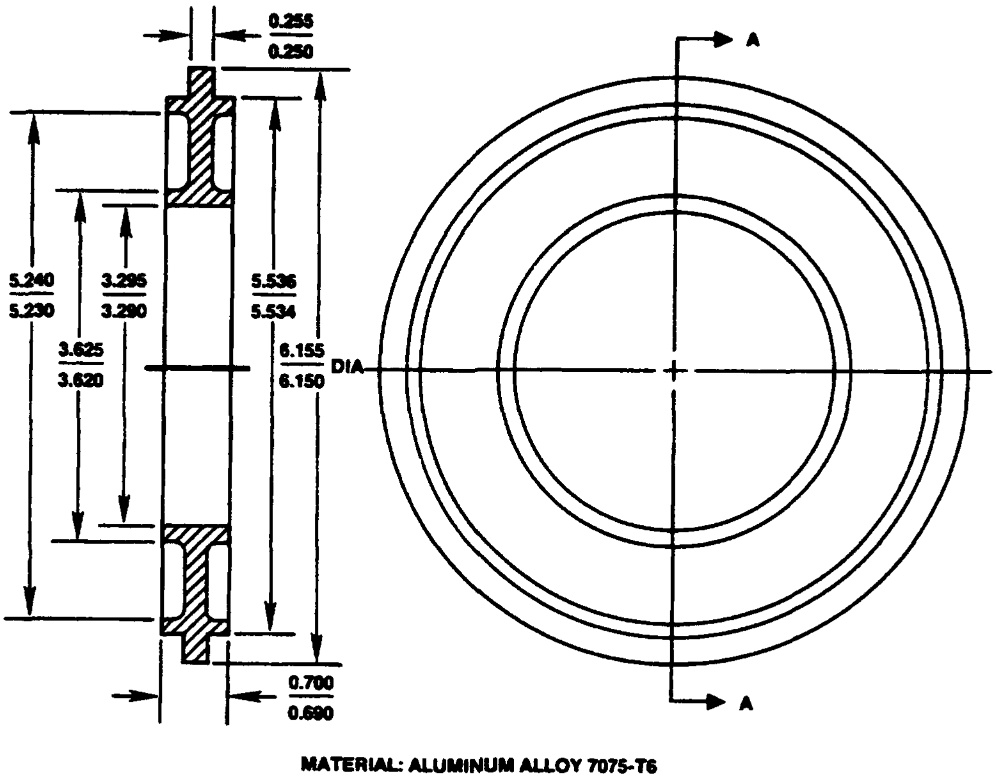

Figure A-23. Joint ring E; drawing.

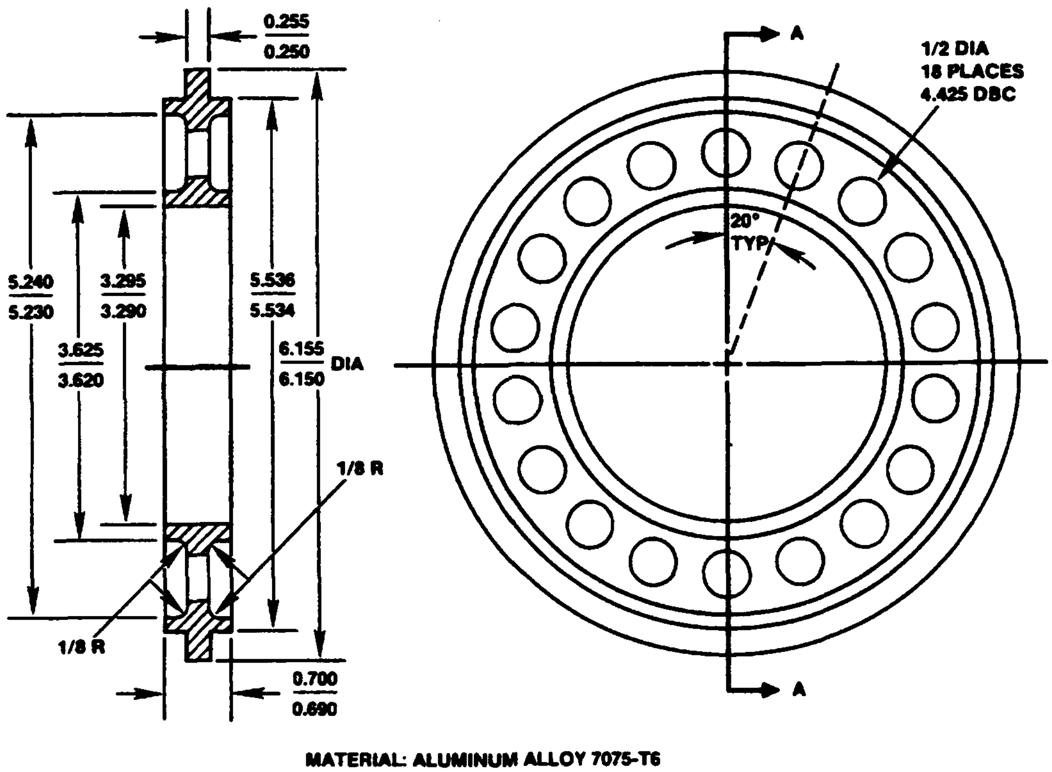

Figure A-24. Joint ring G; drawing.

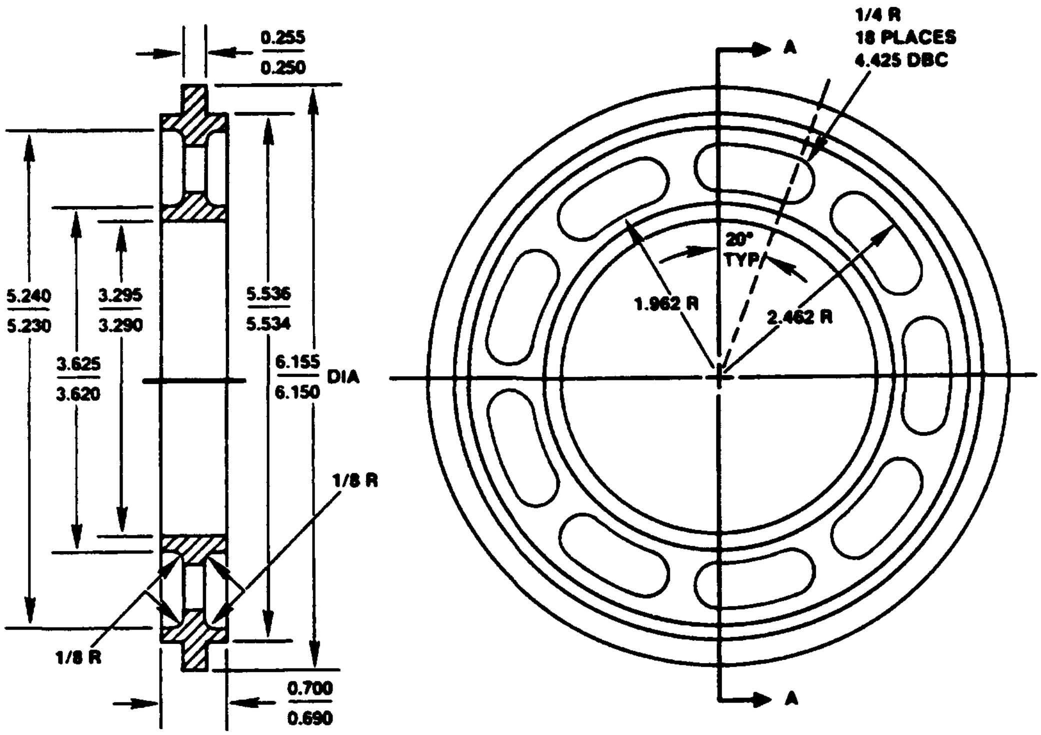

MATERIAL: ALUMINUM ALLOY 7075-T6

Figure A-25. Joint ring H; drawing.

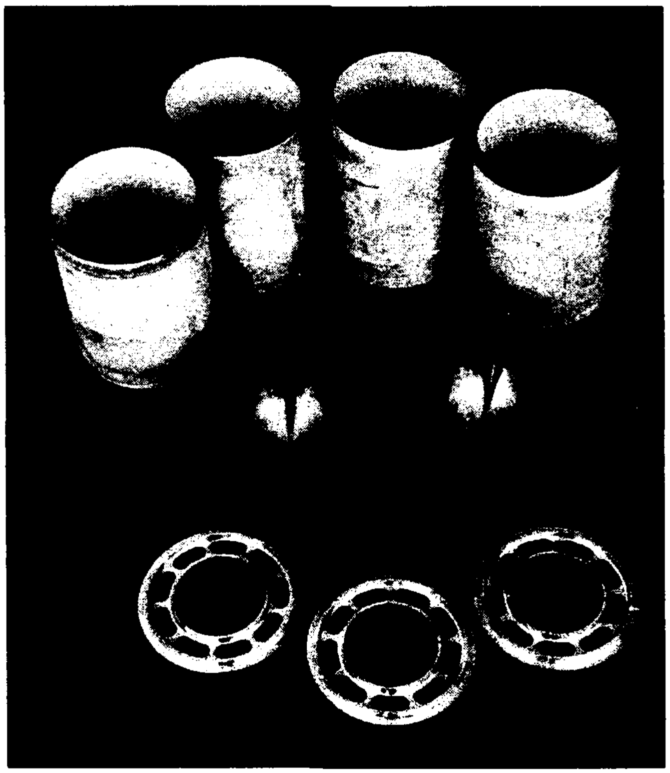

Figure A-26. Type W ceramic housing components prior to assembly.

Figure A-27. Type W ceramic housing components assembled.

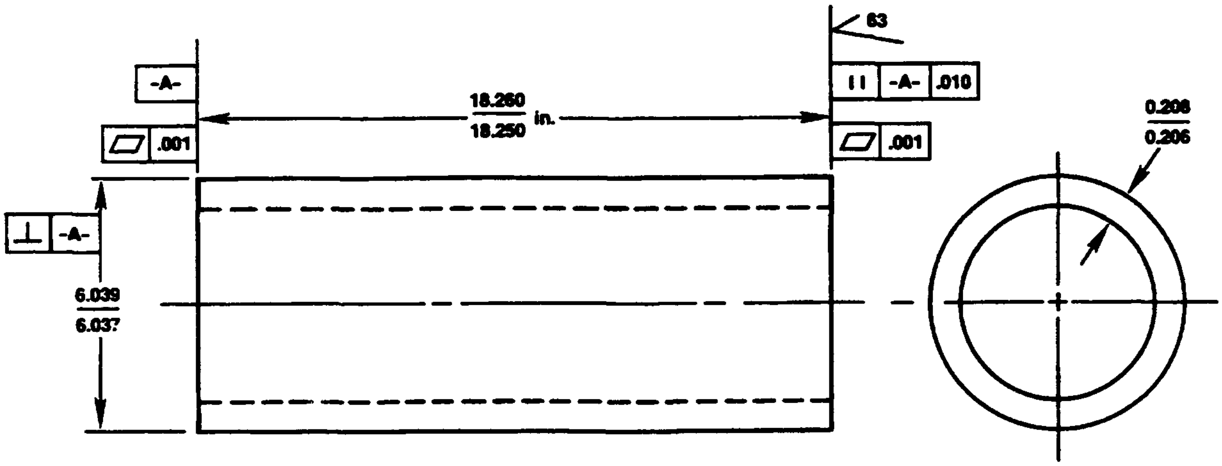

MATERIAL REQUIREMENTS:

CERAMIC COMPOSITION	94% Al_2O_3
MODULUS OF ELASTICITY	41×10^6 psi
COMPRESSIVE STRENGTH	> 300,000 psi
FLEXURAL STRENGTH	> 50,000 psi
POISSON'S RATIO	0.21
SHEAR MODULUS	17×10^6
BULK MODULUS	24×10^6
SPECIFIC GRAVITY	3.62
COEFF OF THERMAL EXPANSION AT ROOM TEMP	$2 \times 10^{-6}/°F$

Figure A-28. Model 3 ceramic cylinder.

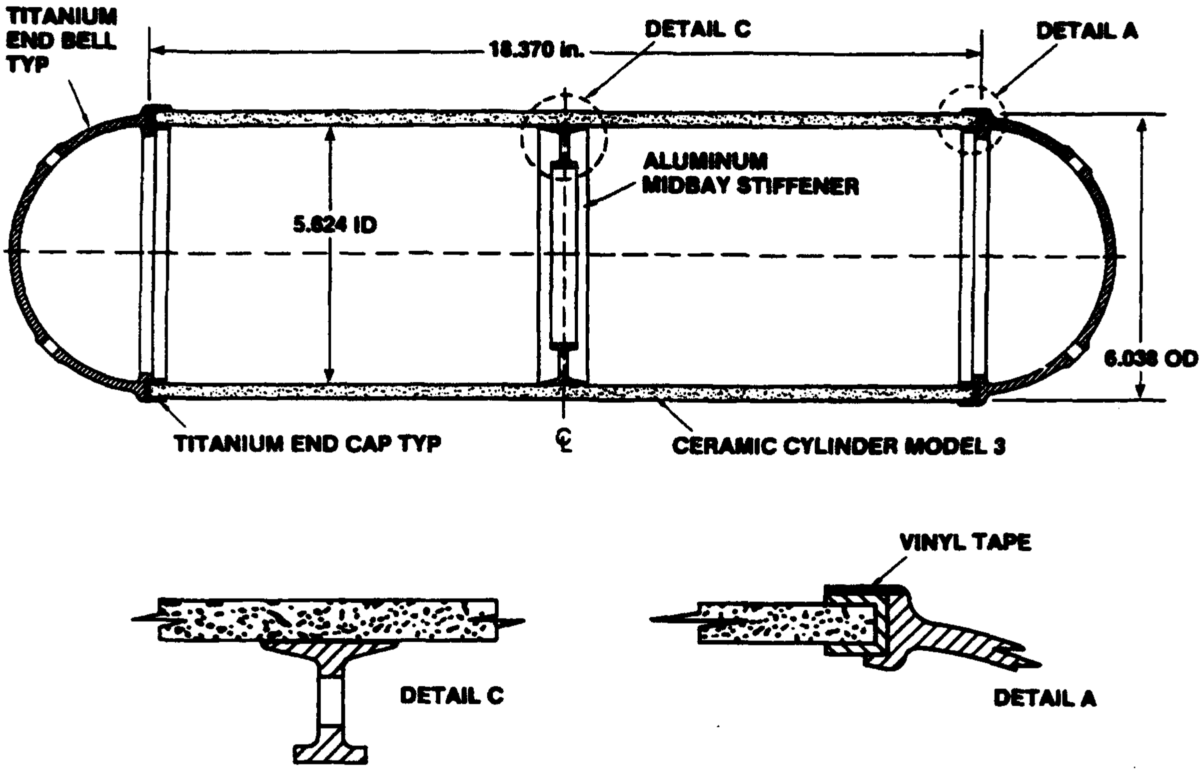

Figure A-29. Internally stiffened ceramic housing Type X.

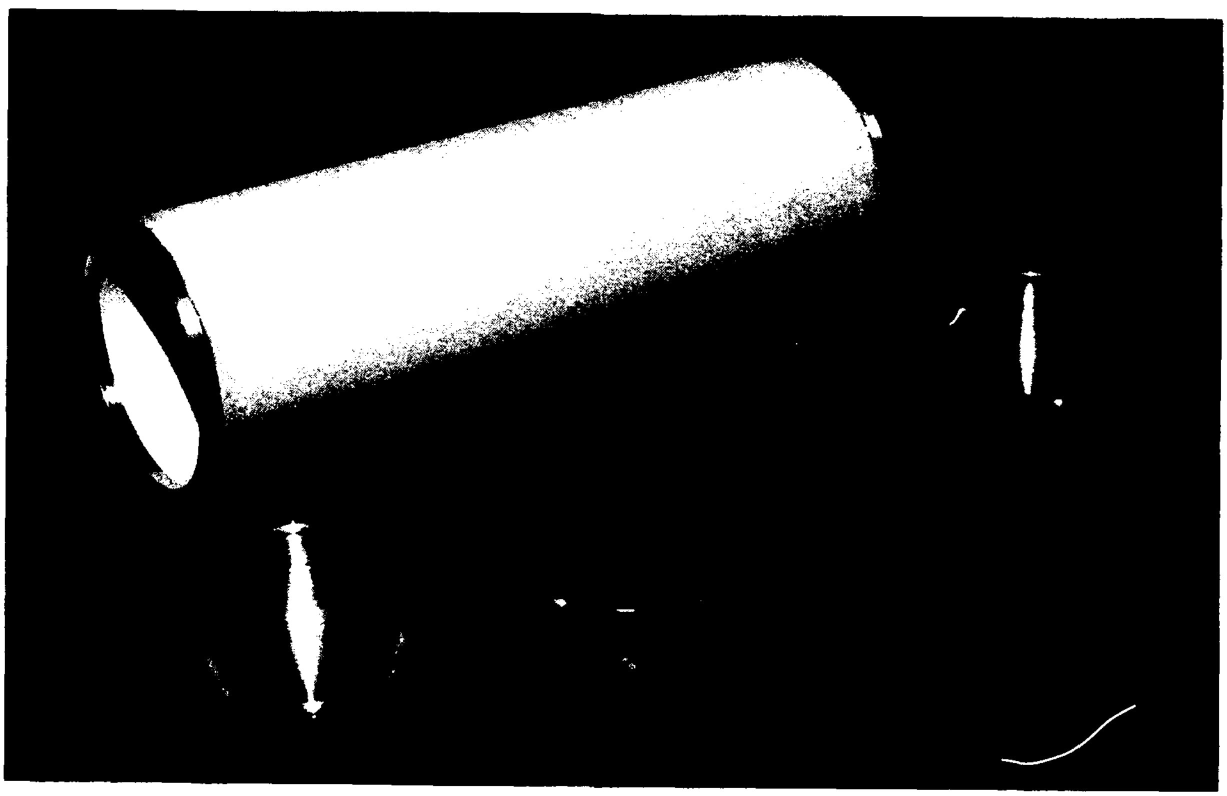

Figure A-30. Components of 6-inch-OD ceramic housing Type X.

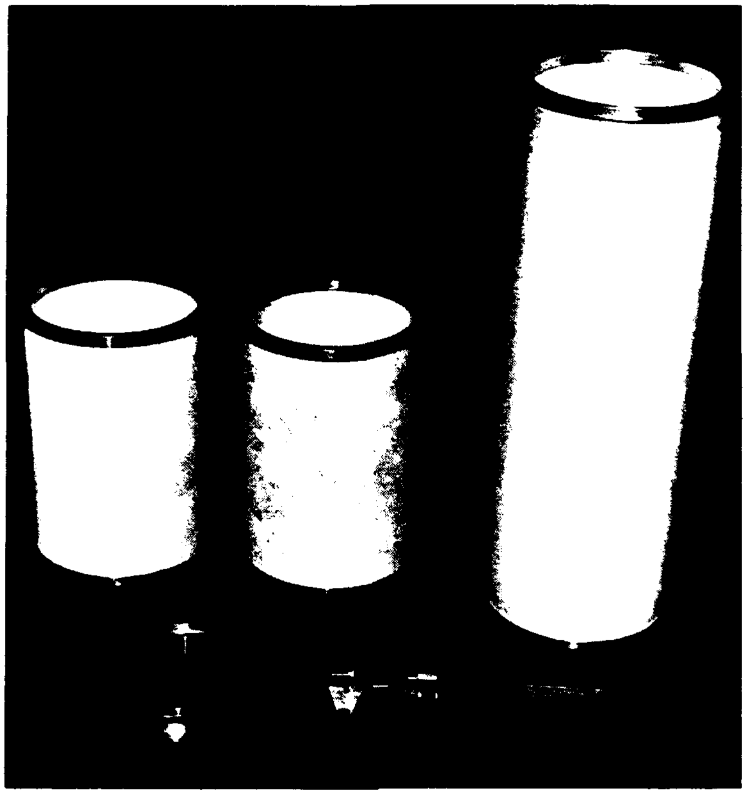

Figure A-31. A single Type 3 internally stiffened ceramic cylinder replaces two Type 2 ceramic cylinders and a joint stiffener.

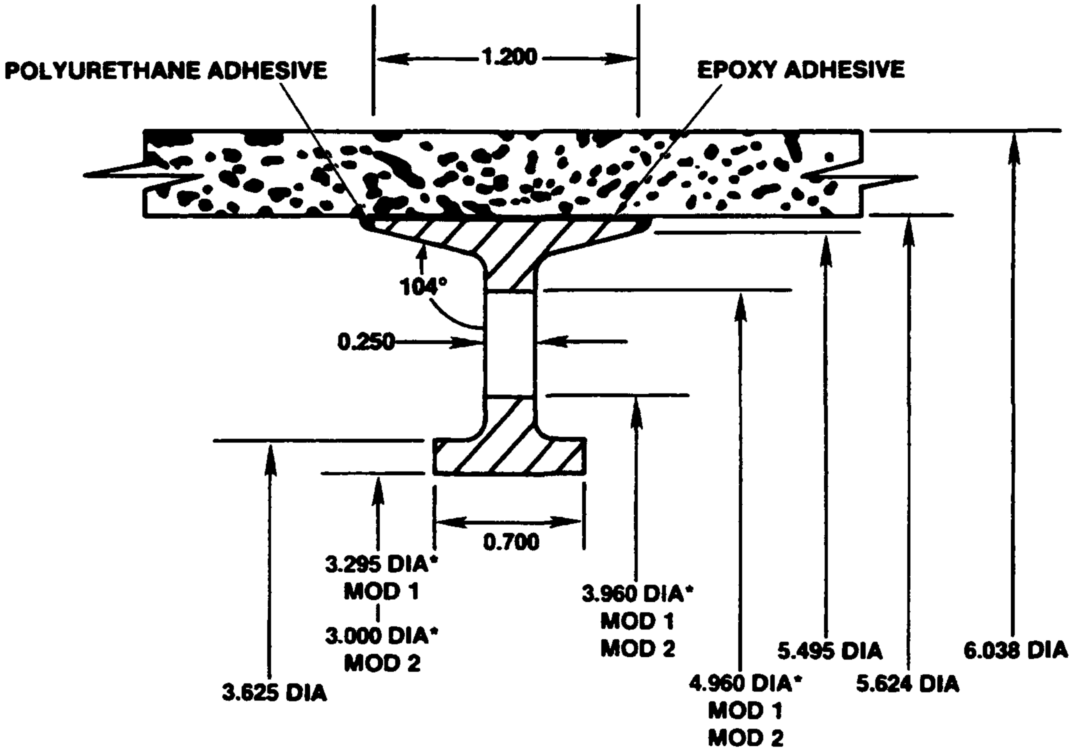

Figure A-32. Internal midbay stiffeners for Type 3 ceramic cylinders.

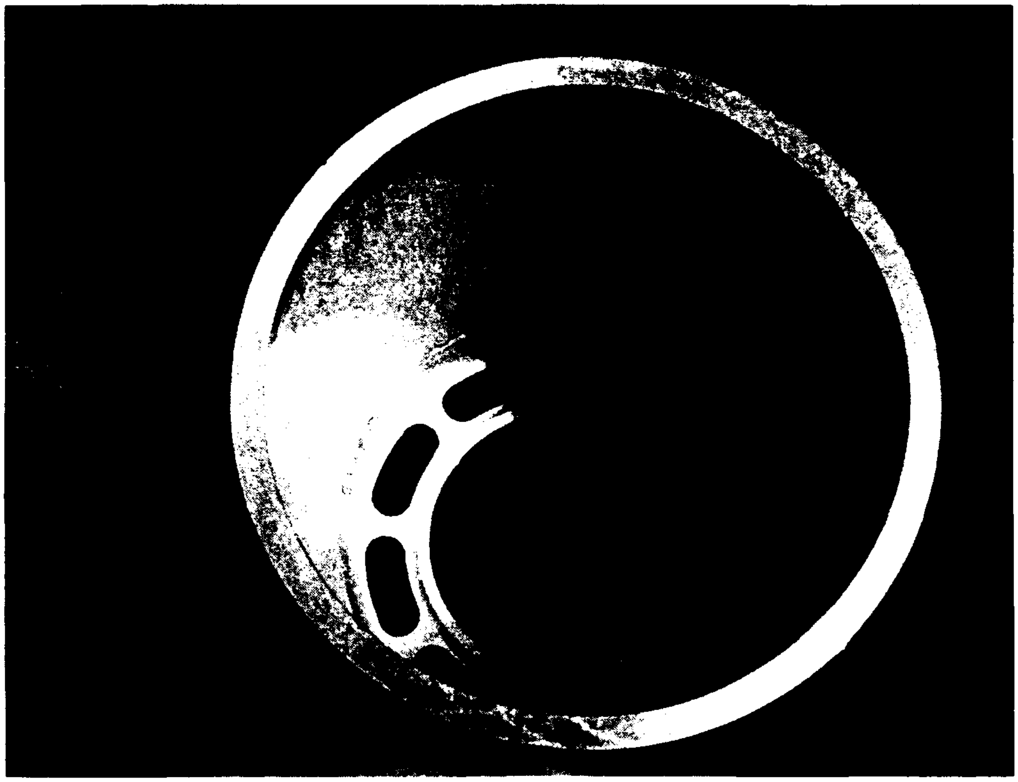

Figure A-33. Type 3 ceramic cylinder with internal midbay stiffener.

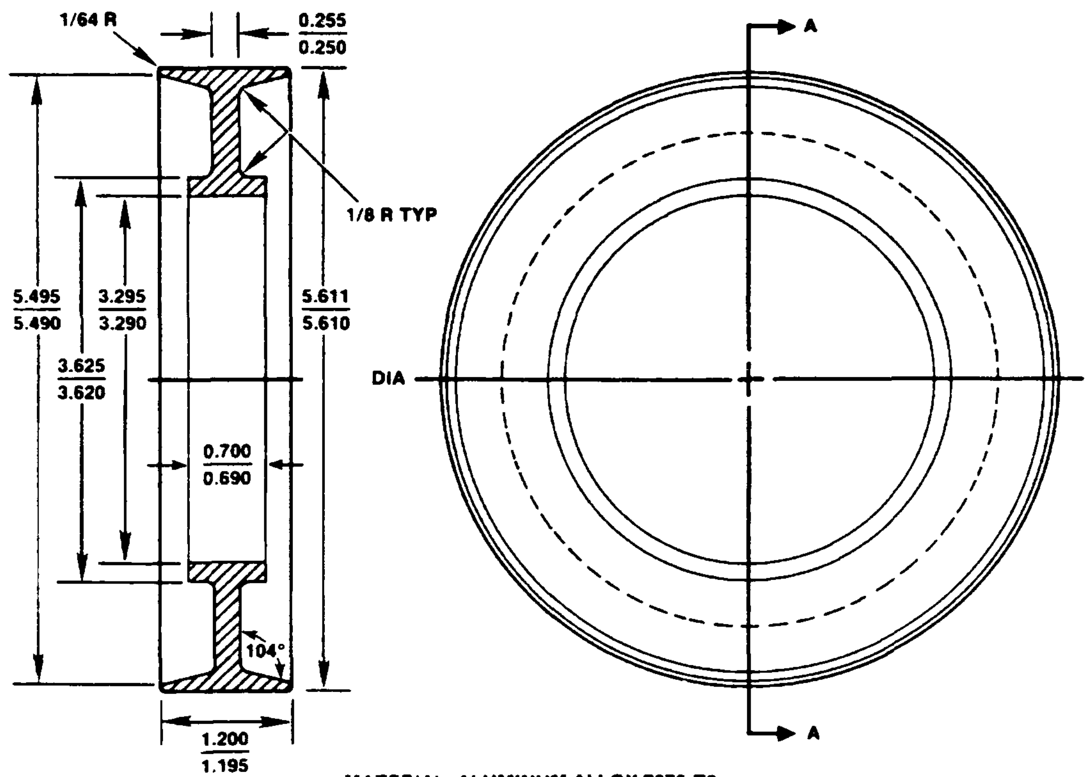

Figure A-34. Internal midbay stiffener; Mod 0.

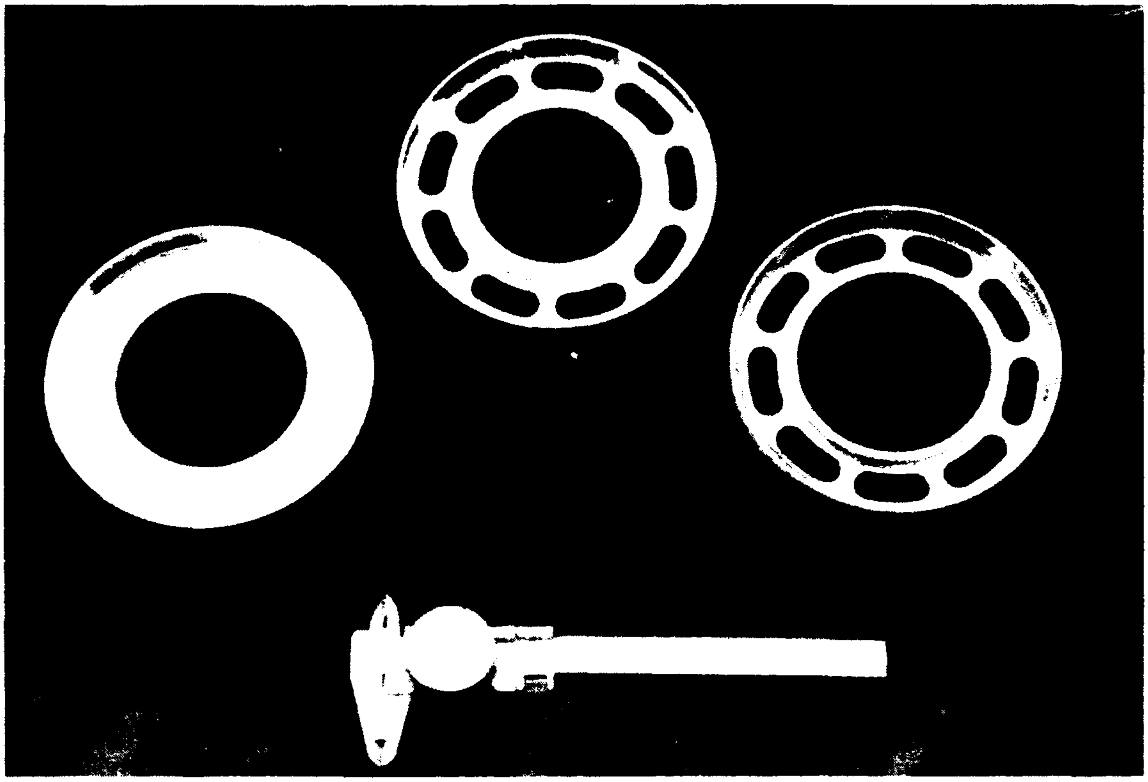

Figure A-35. Internal midbay stiffeners for Type 3 ceramic cylinders. Critical pressure of Type 3 cylinders is 18,000 psi with Mod 0, 9,800 psi with Mod 1, and 15,000 psi with Mod 2 internal stiffeners.

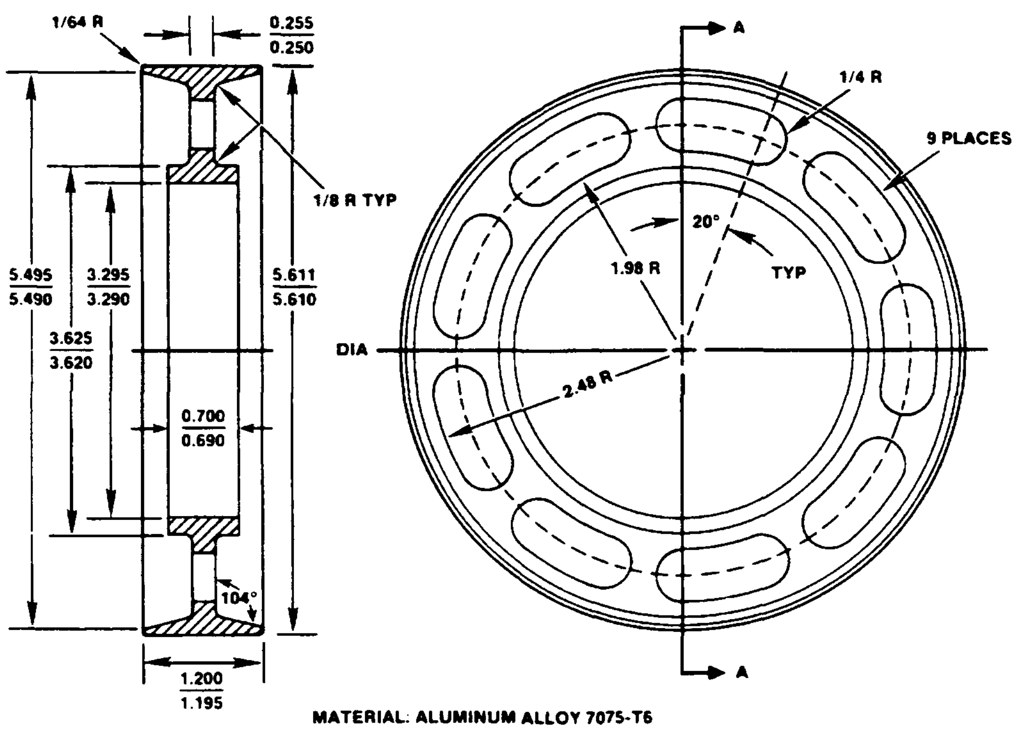

Figure A-36. Midbay stiffener Mod 1.

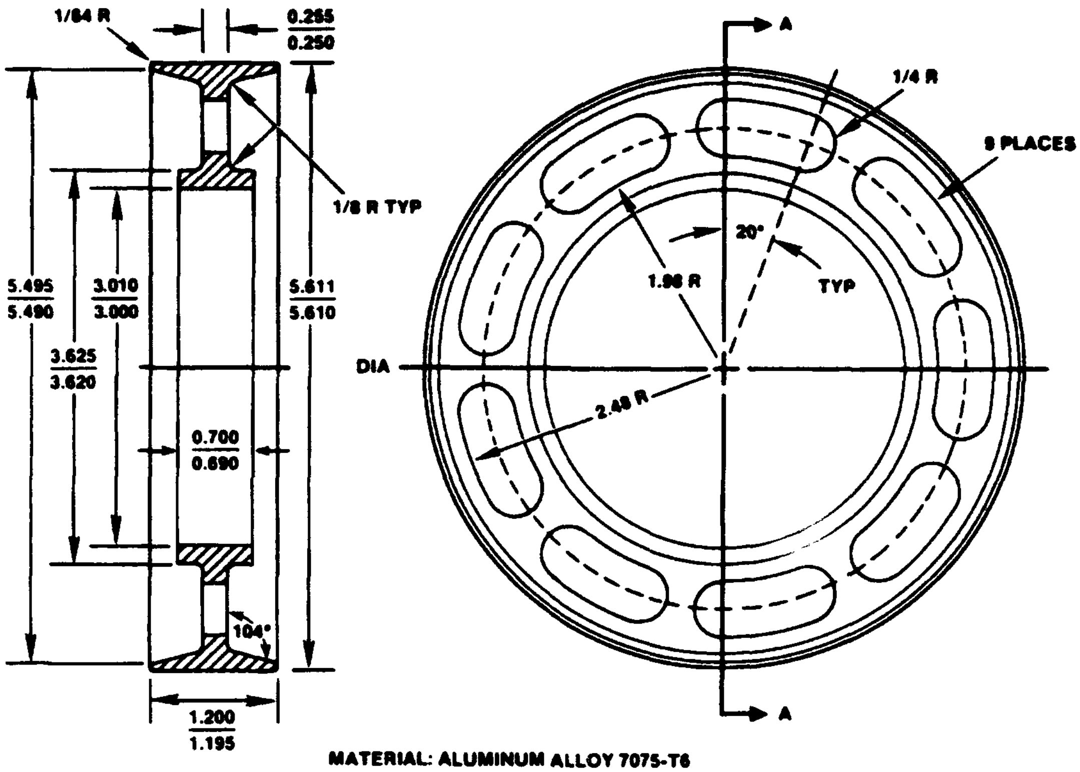

Figure A-37. Midbay stiffener Mod 2.

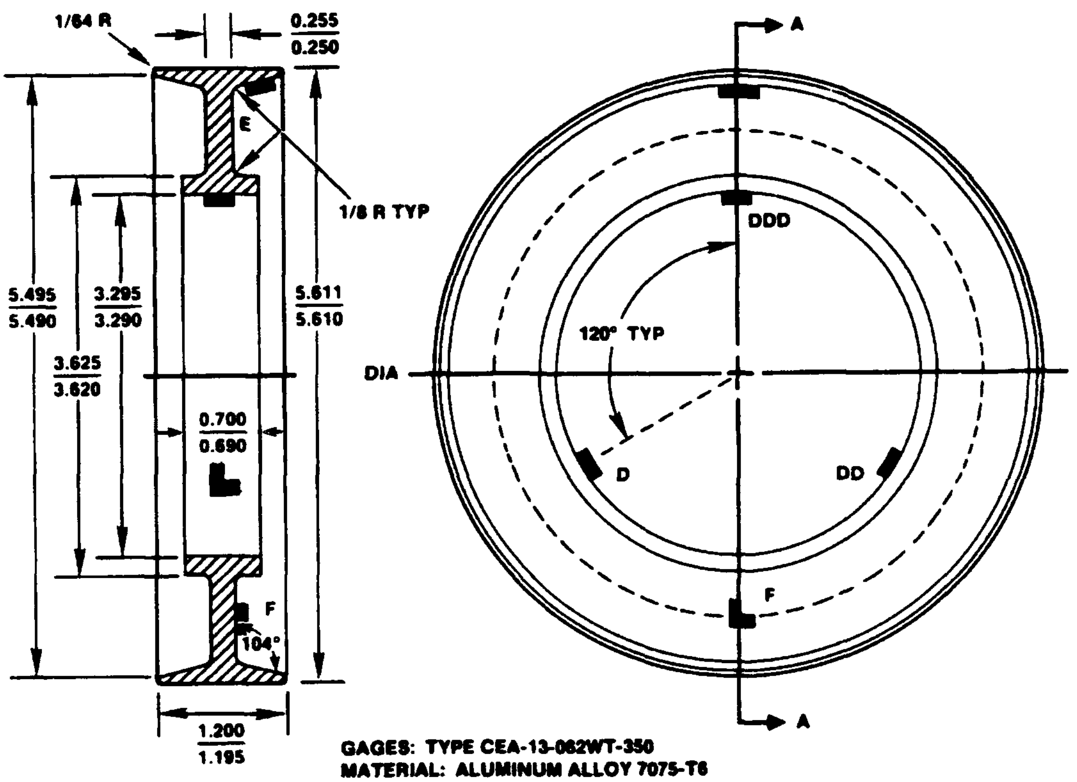

Figure A-38. Location of strain gages on midbay stiffener Mod 0.

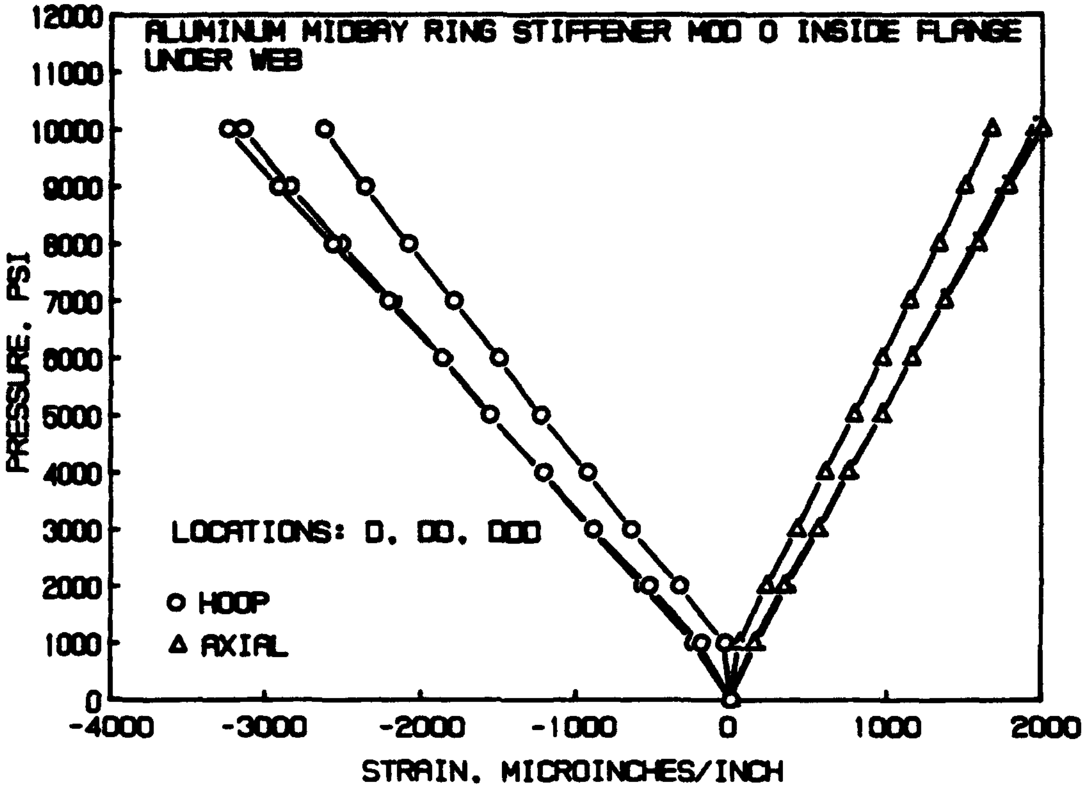

Figure A-39. Strains on midbay stiffener Mod 0; locations D, DD, DDD.

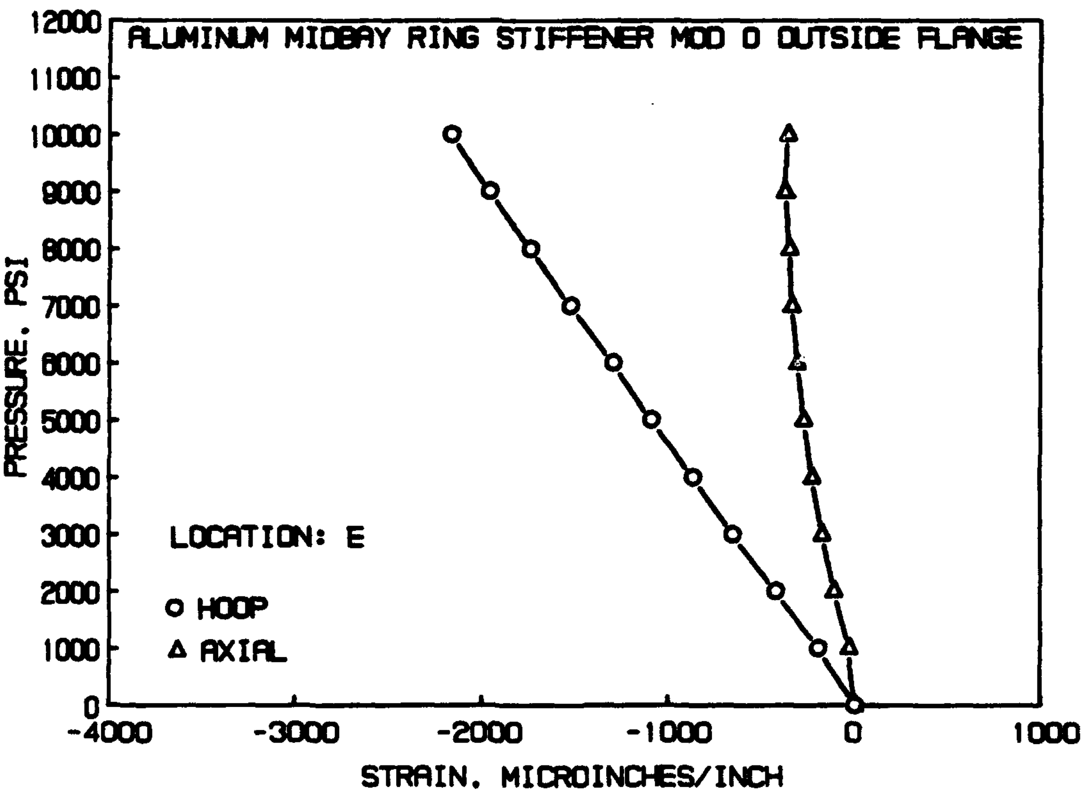

Figure A-40. Strains on midbay stiffener Mod 0; location E.

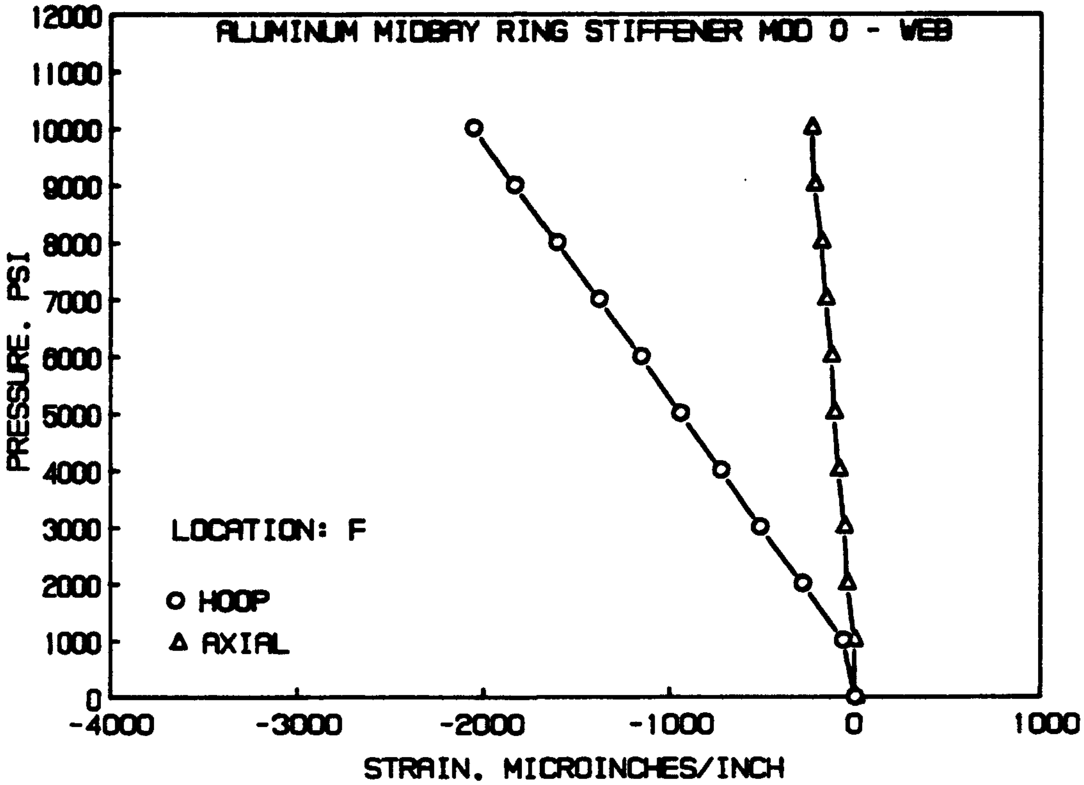

Figure A-41. Strains on midbay stiffener Mod 0; location F.

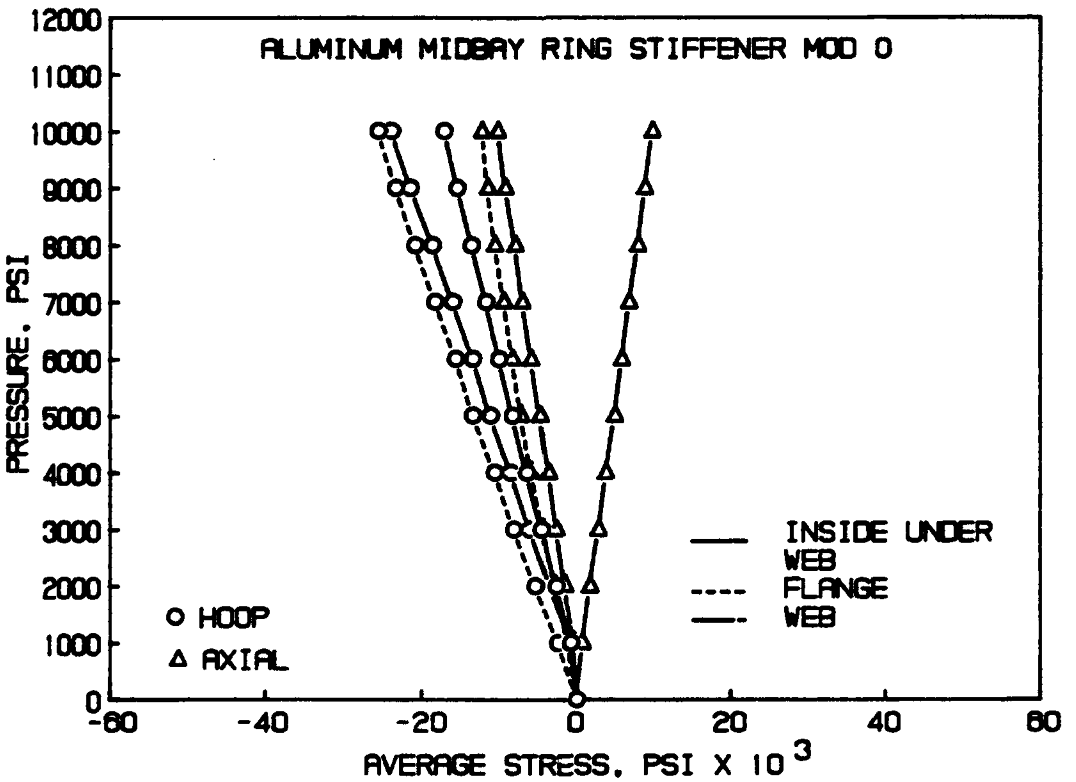

Figure A-42. Stresses on midbay stiffener Mod 0.

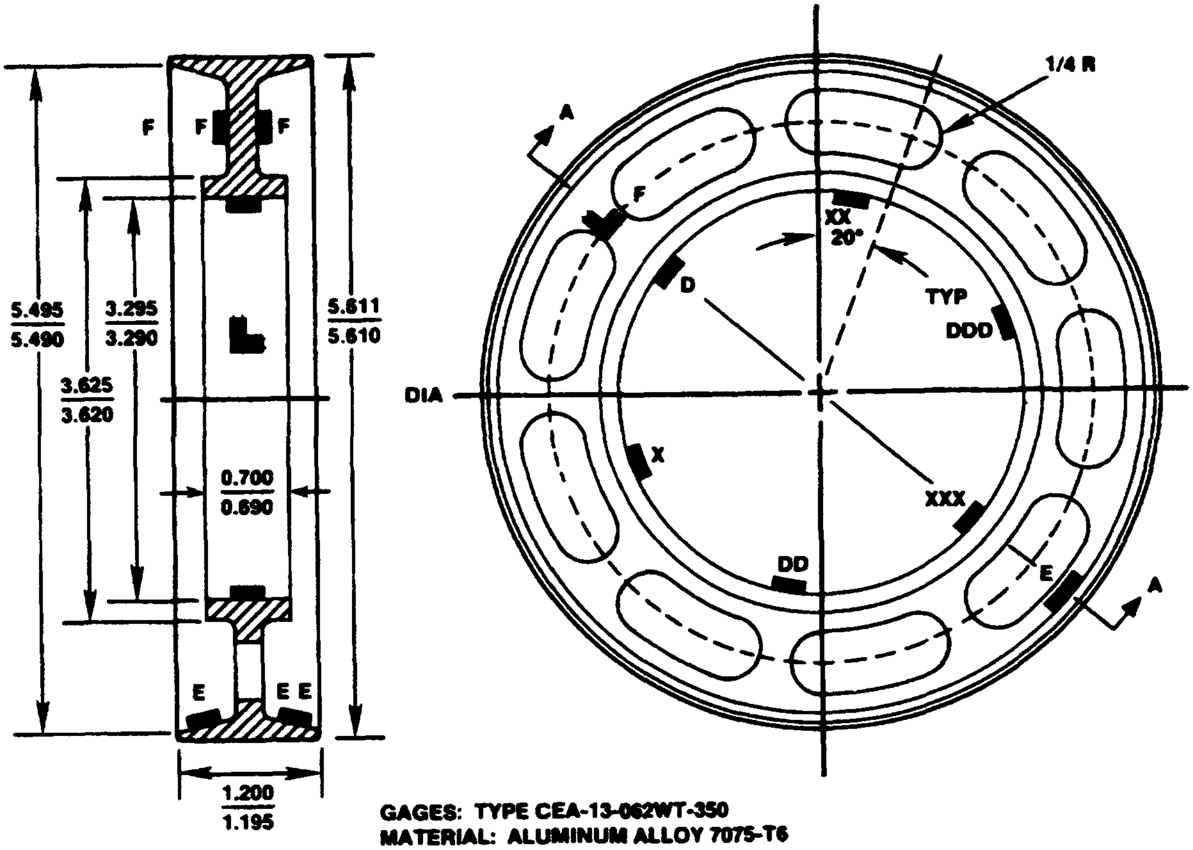

Figure A-43. Location of strain gages on midbay stiffener Mod 1.

Figure A-44. Midbay stiffeners Mod 1 before and after failure of Model 3 ceramic cylinder at 9,800 psi.

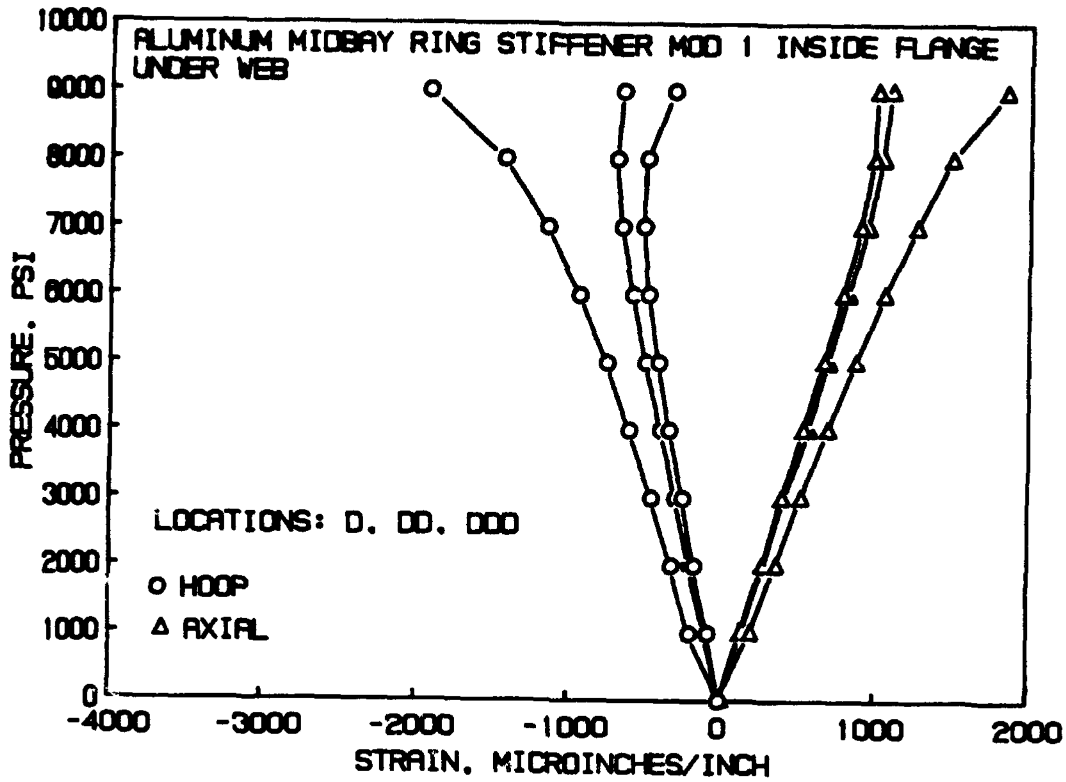

Figure A-45. Strains on midbay stiffener Mod 1; locations D, DD, DDD.

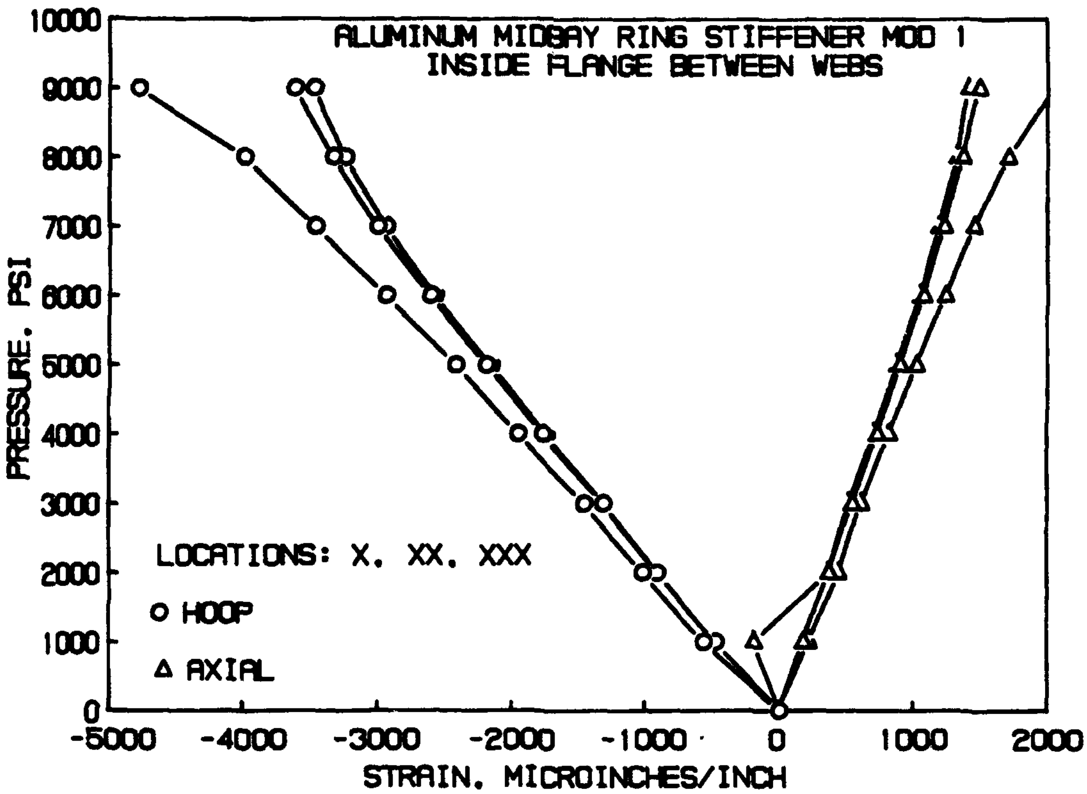

Figure A-46. Strains on midbay stiffener Mod 1; locations X, XX, XXX.

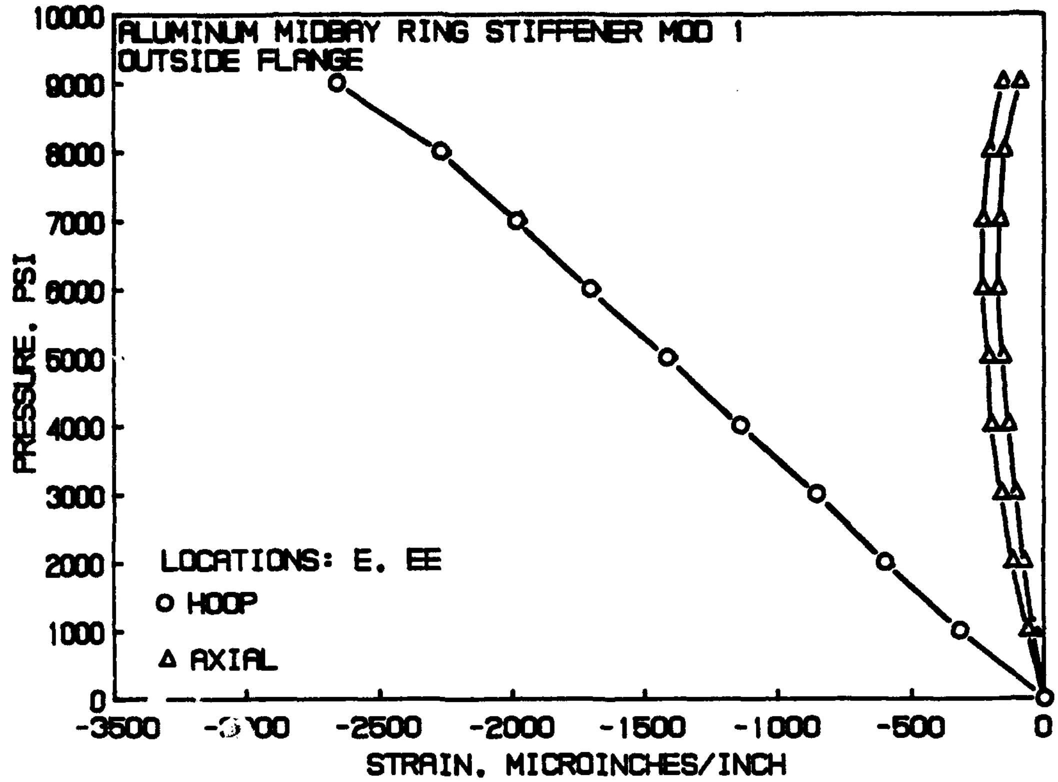

Figure A-47. Strains on midbay stiffener Mod 1; locations E, EE.

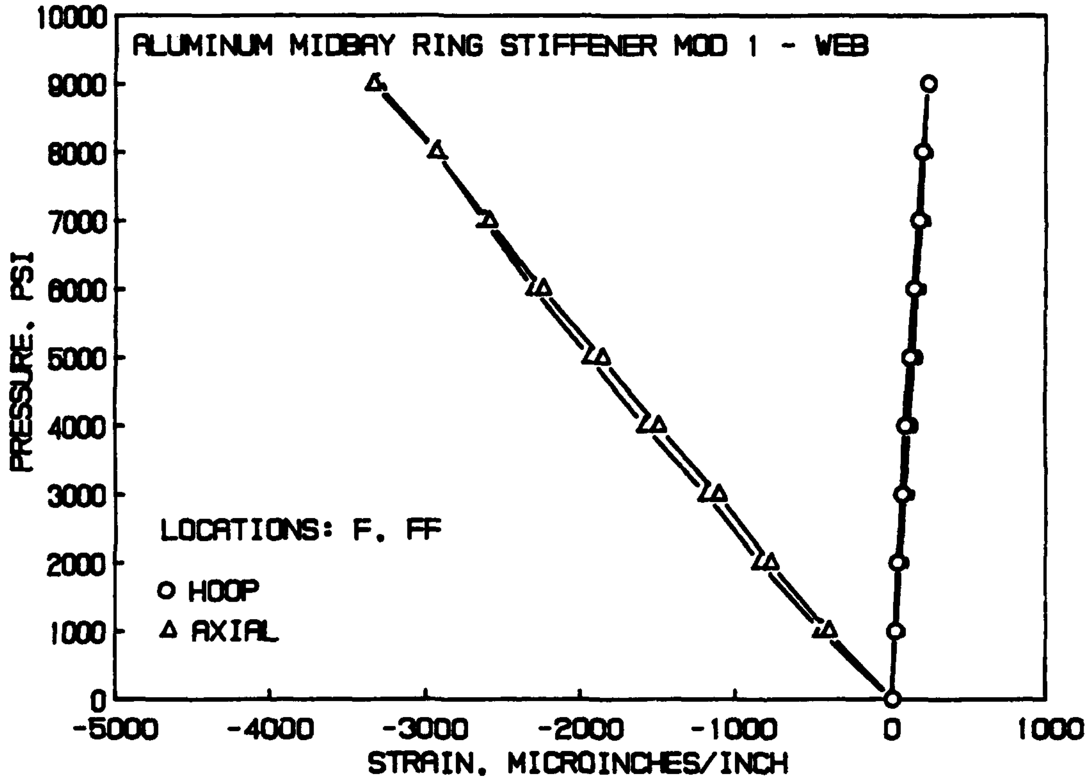

Figure A-48. Strains on midbay stiffener Mod 1; locations F, FF.

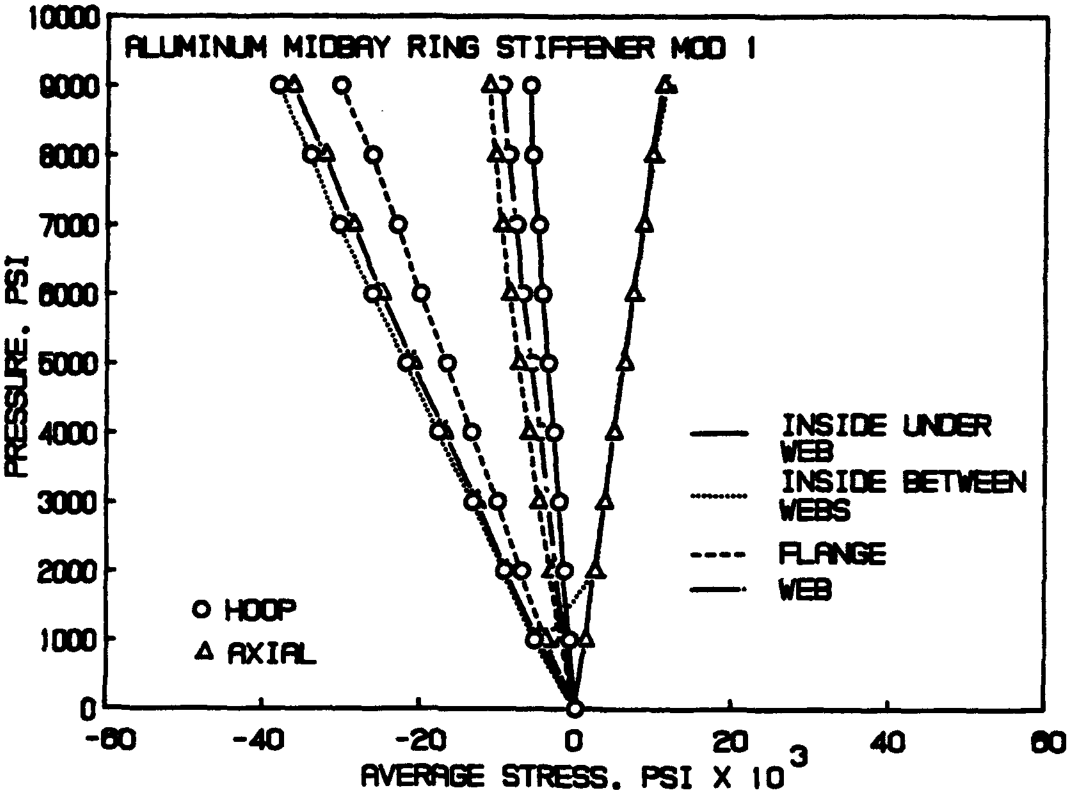

Figure A-49. Stresses on midbay stiffener Mod 1.

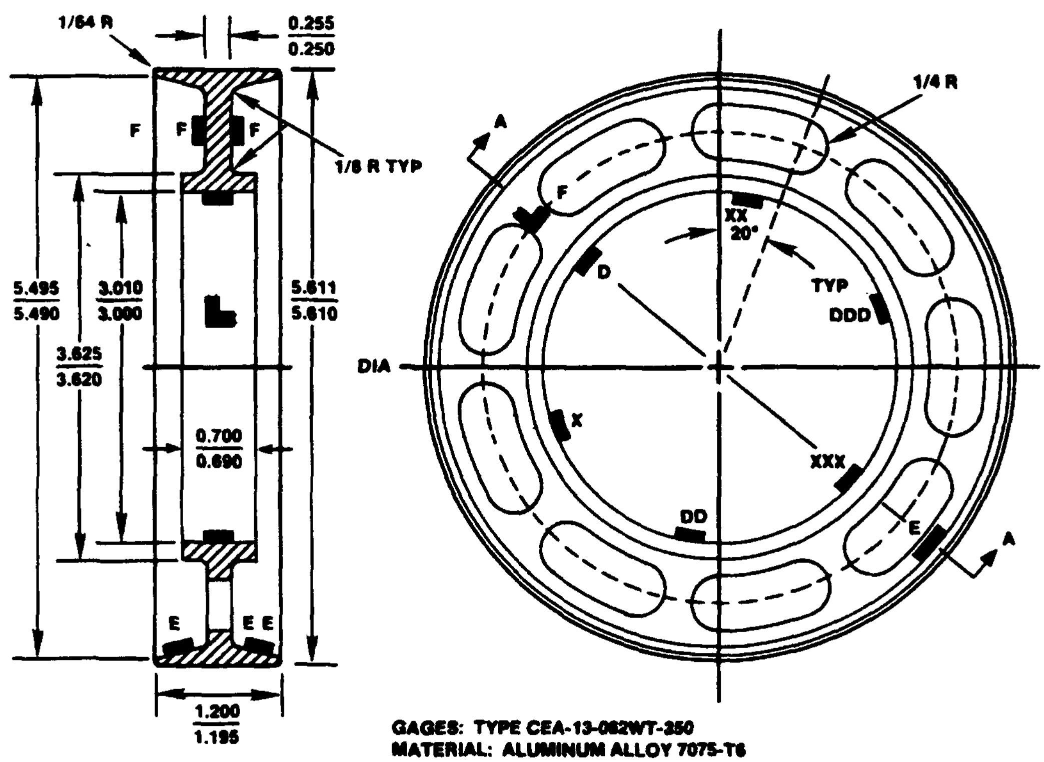

Figure A-50. Location of strain gages on midbay stiffener Mod 2.

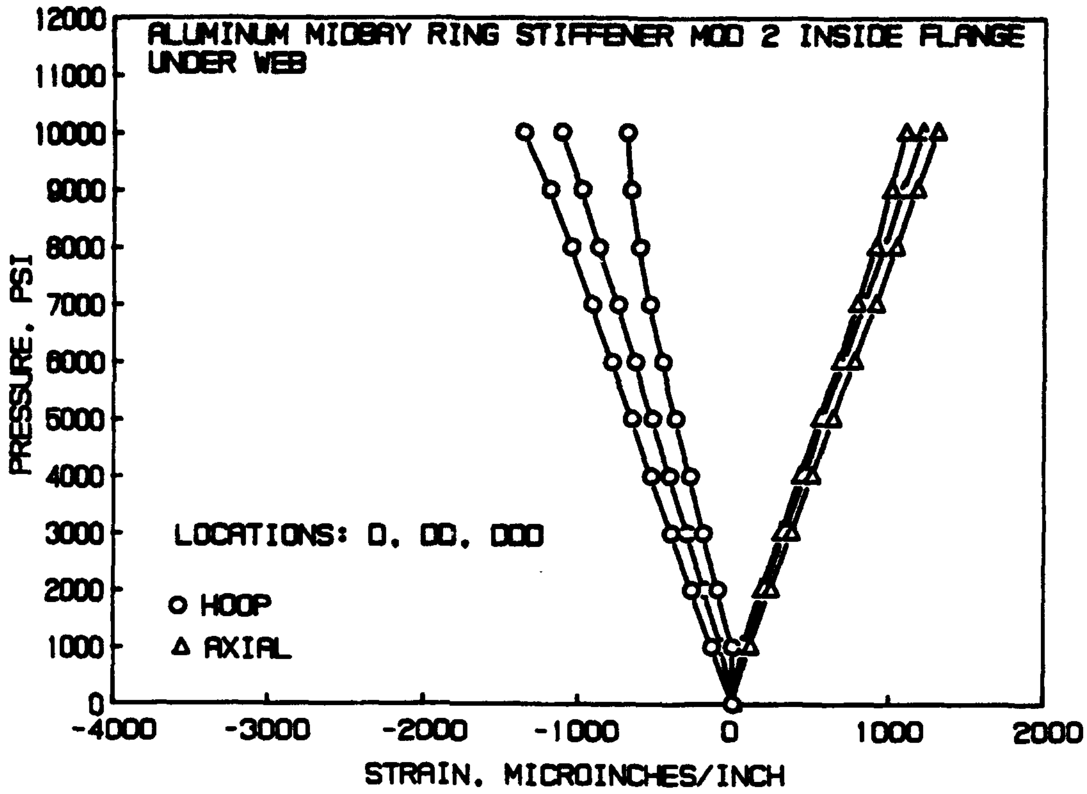

Figure A-51. Strains on midbay stiffener Mod 2; locations D, DD, DDD.

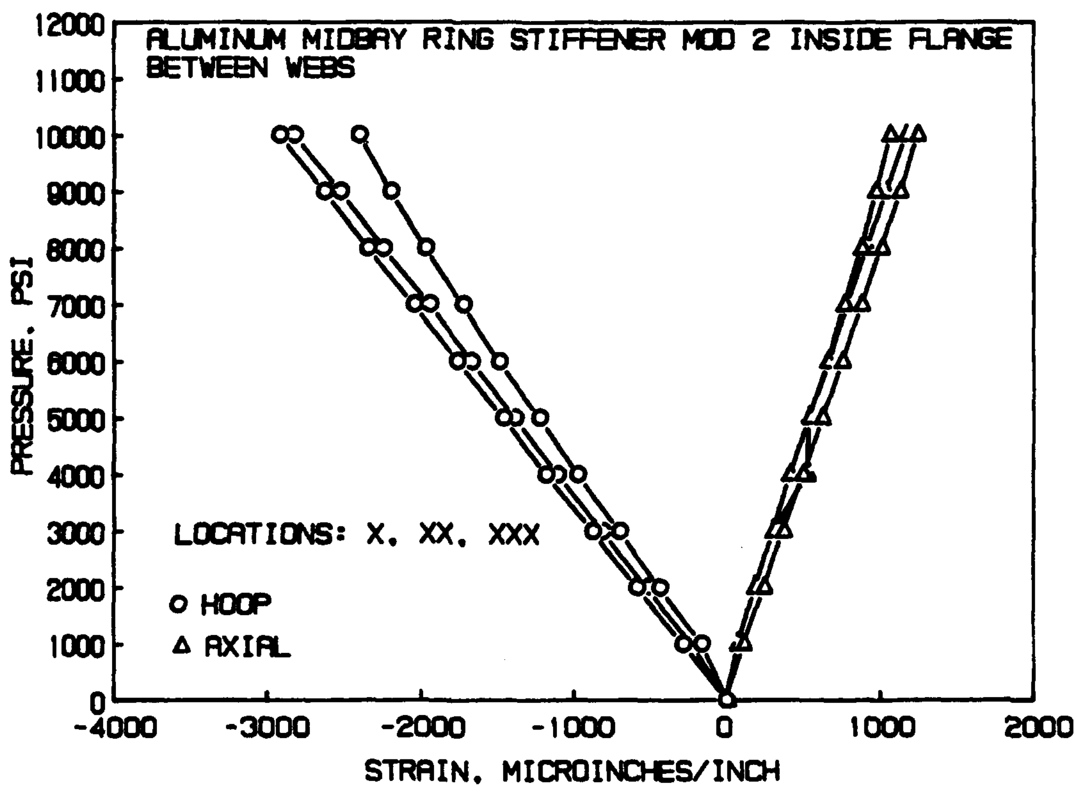

Figure A-52. Strains on midbay stiffener Mod 2; locations X, XX, XXX.

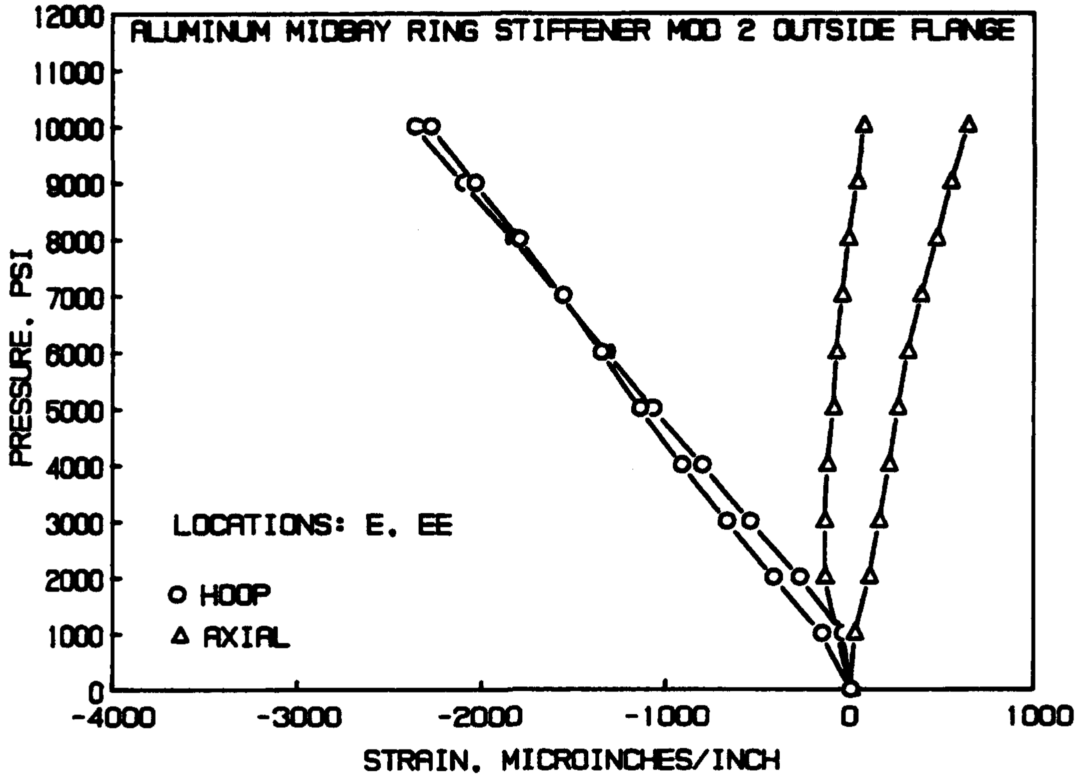

Figure A-53. Strains on midbay stiffener Mod 2; locations E, EE.

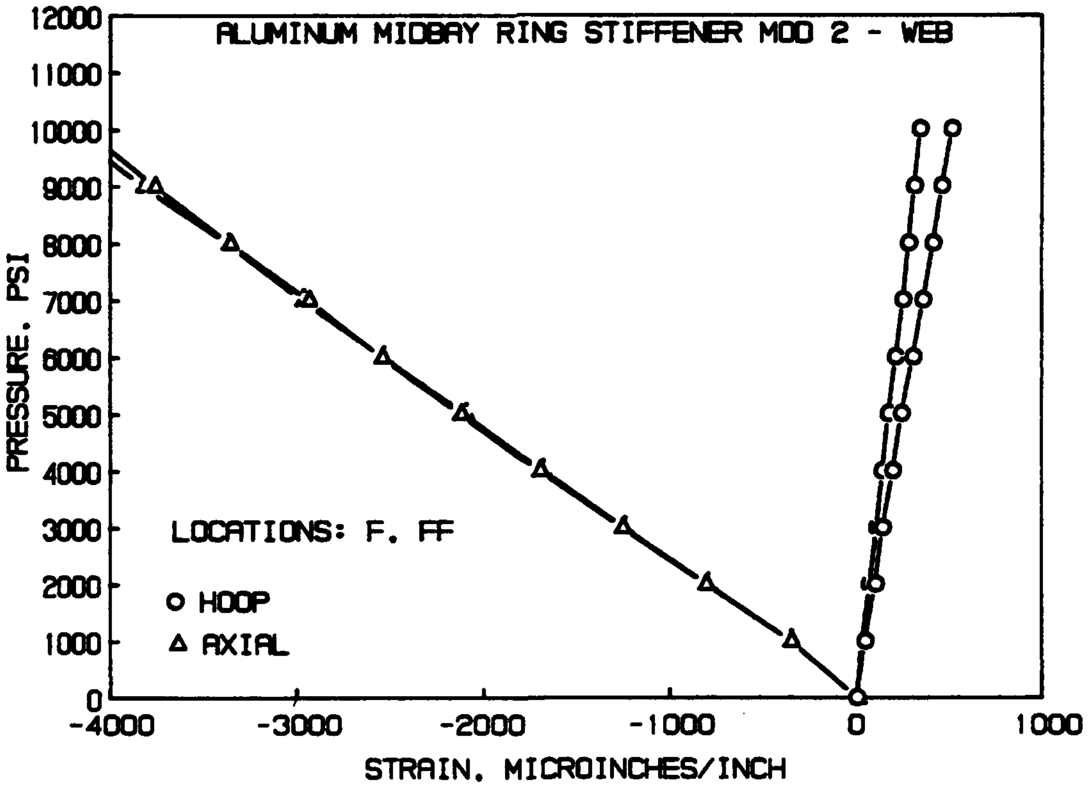

Figure A-54. Strains on midbay stiffener Mod 2; locations F, FF.

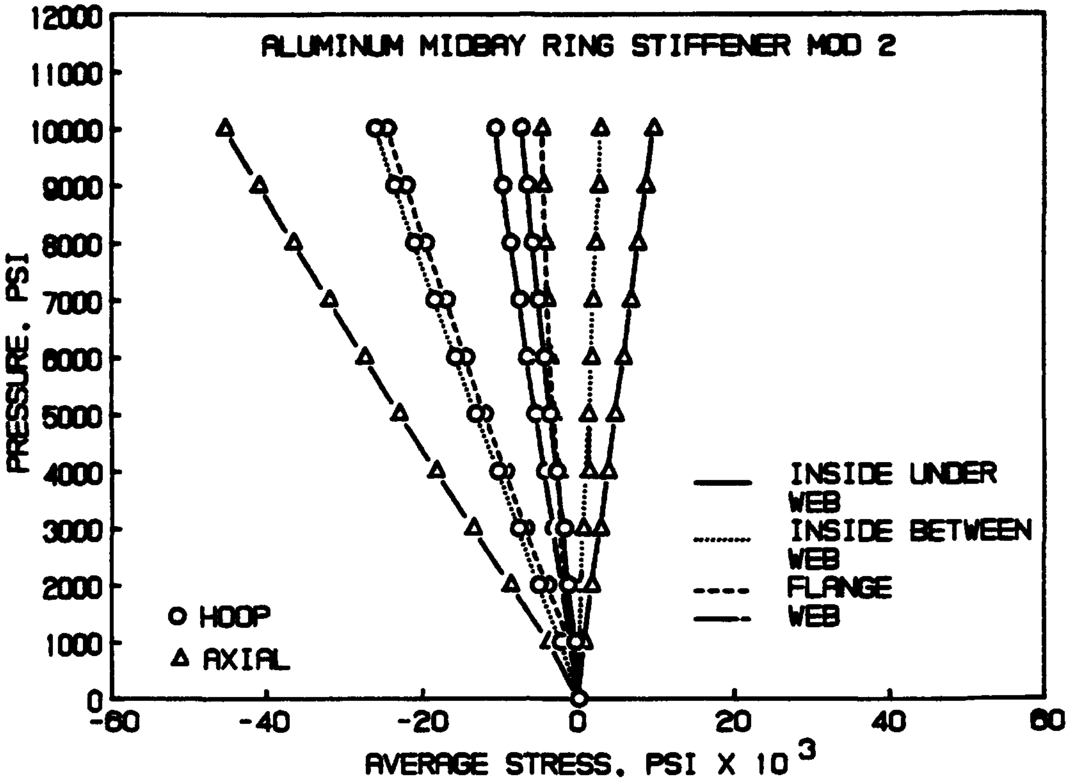

Figure A-55. Stress on midbay stiffener Mod 2.

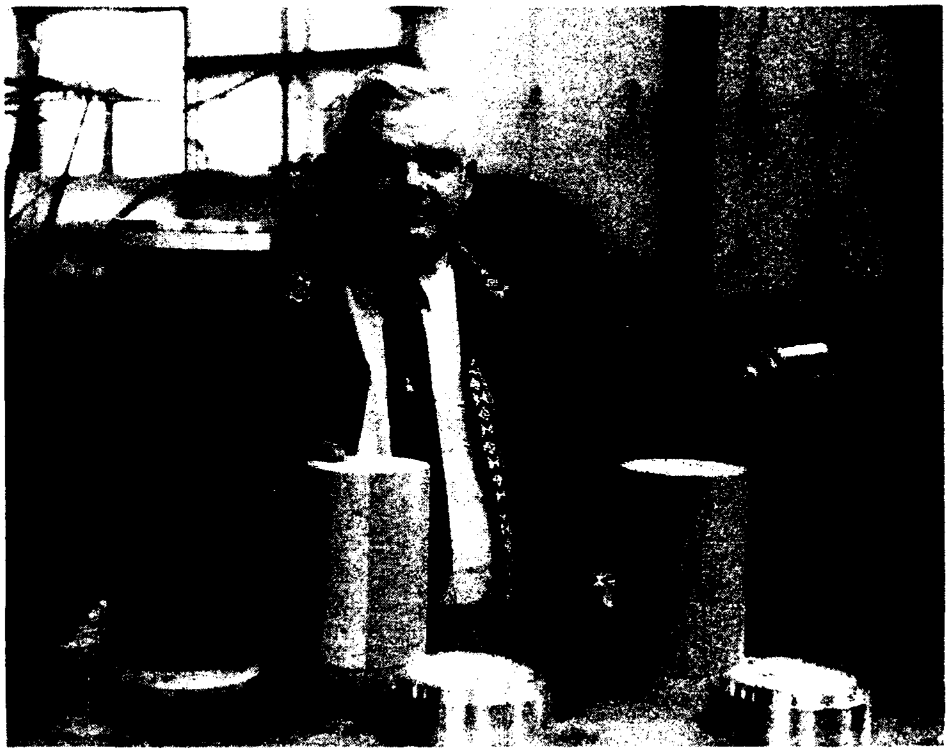

Figure A-56. Ceramic cylinder Model 3 prior to assembly with wooden plugs and metal bulkheads for implosion testing.

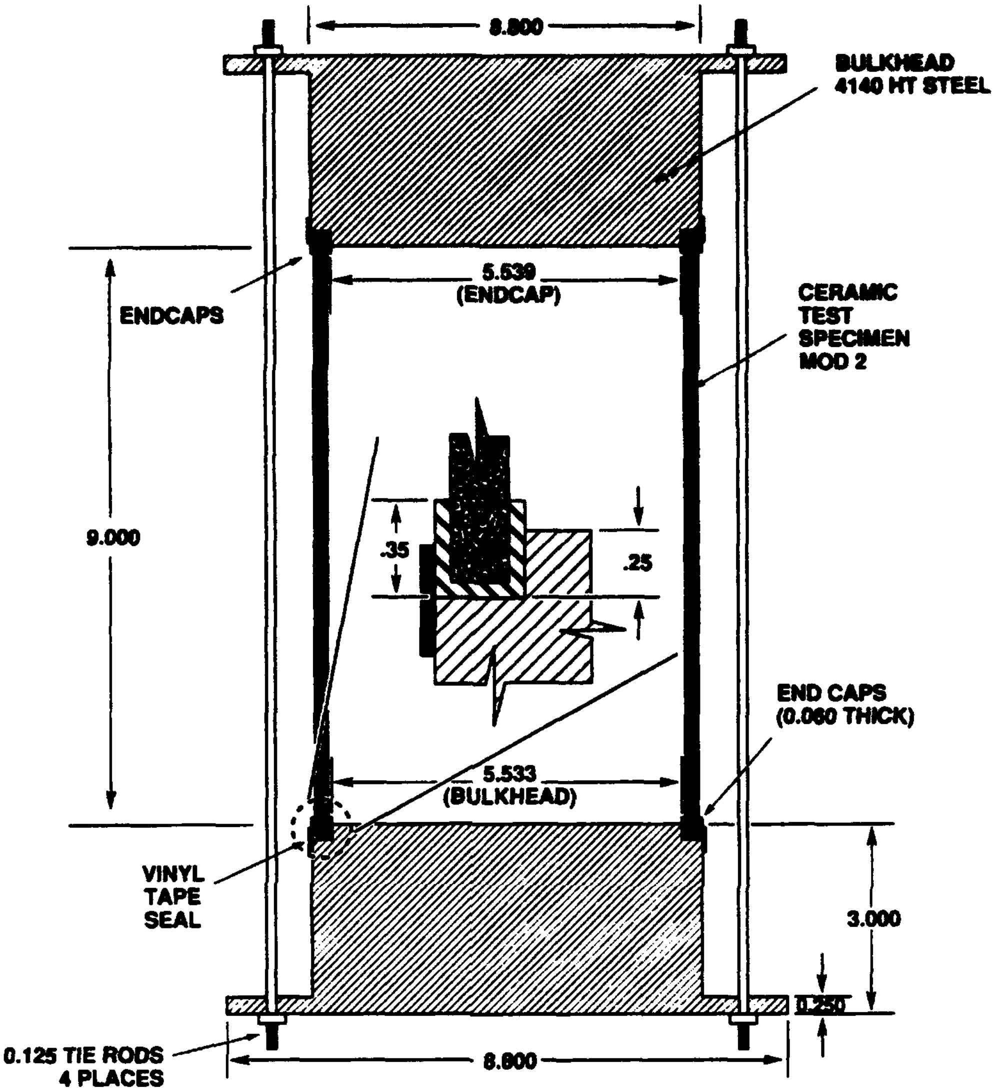

Figure A-57. Typical setup for implosion testing of Models 1 and 2 ceramic cylinders.

NUMBER OF LOBES INTO WHICH A TUBE WILL COLLAPSE WHEN SUBJECTED TO UNIFORM RADIAL AND AXIAL EXTERNAL PRESSURE

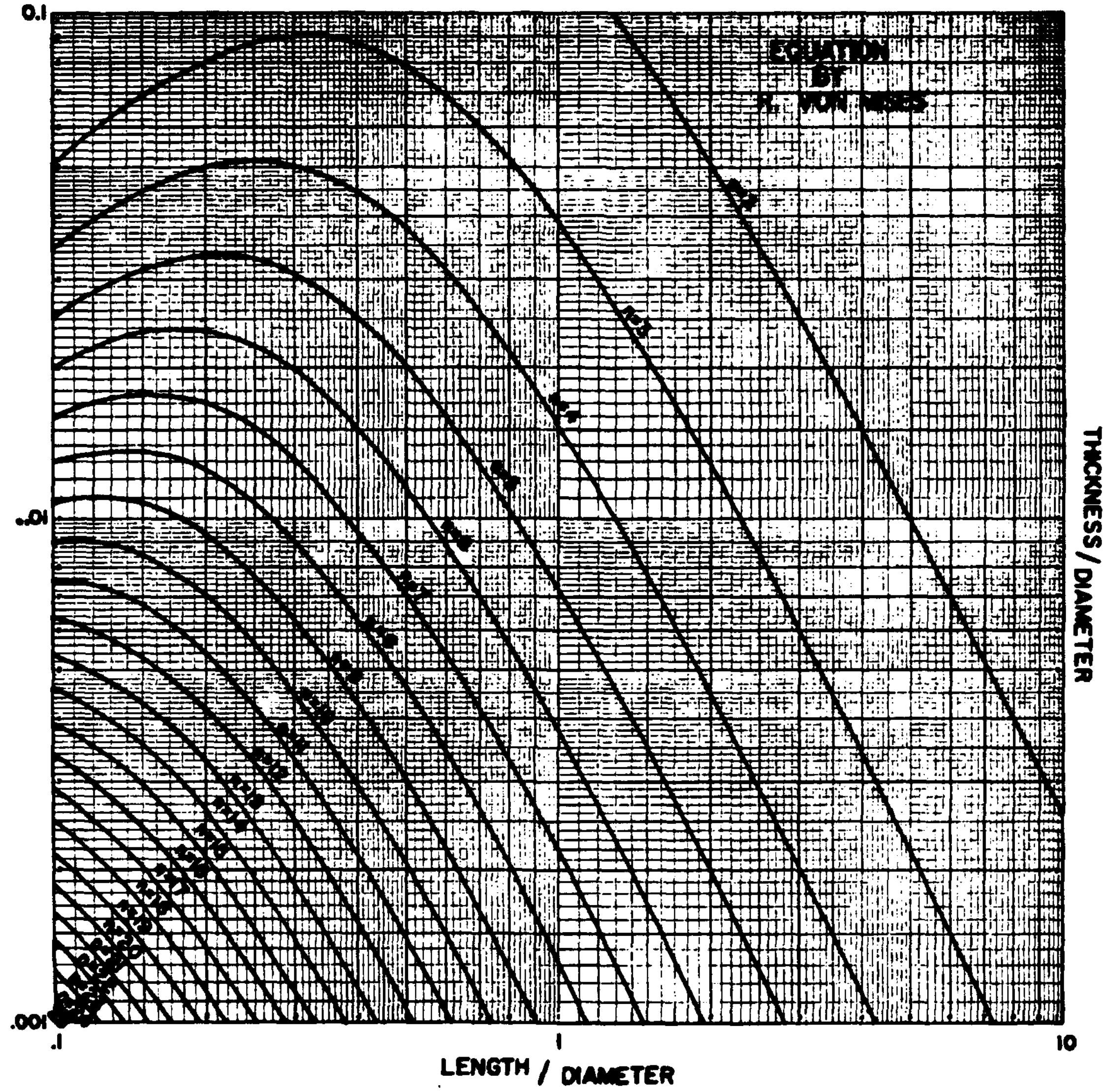

Figure A-58. Graphic solution to R. von Mises analytical equation for buckling of monocoque cylinders between plane bulkheads providing radial support. If hemispherical bulkheads are used, add 0.3D to the length of the cylinder.

COLLAPSING PRESSURE OF TUBES
SUBJECTED TO UNIFORM RADIAL AND AXIAL EXTERNAL PRESSURE

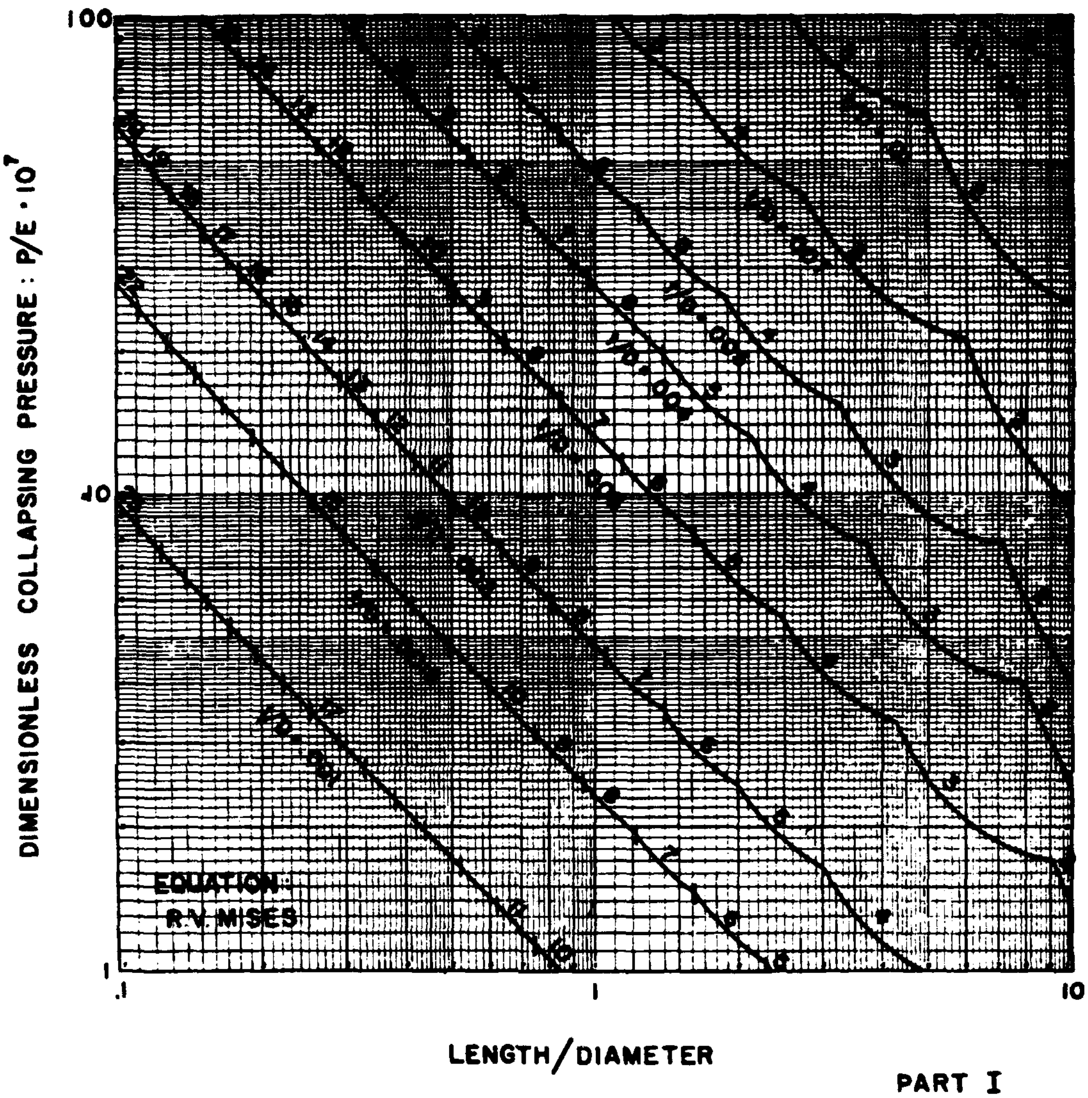

Figure A-59. Graphic solution to R. von Mises analytical equation for buckling.

COLLAPSING PRESSURE OF TUBES
SUBJECTED TO UNIFORM RADIAL AND AXIAL EXTERNAL PRESSURE

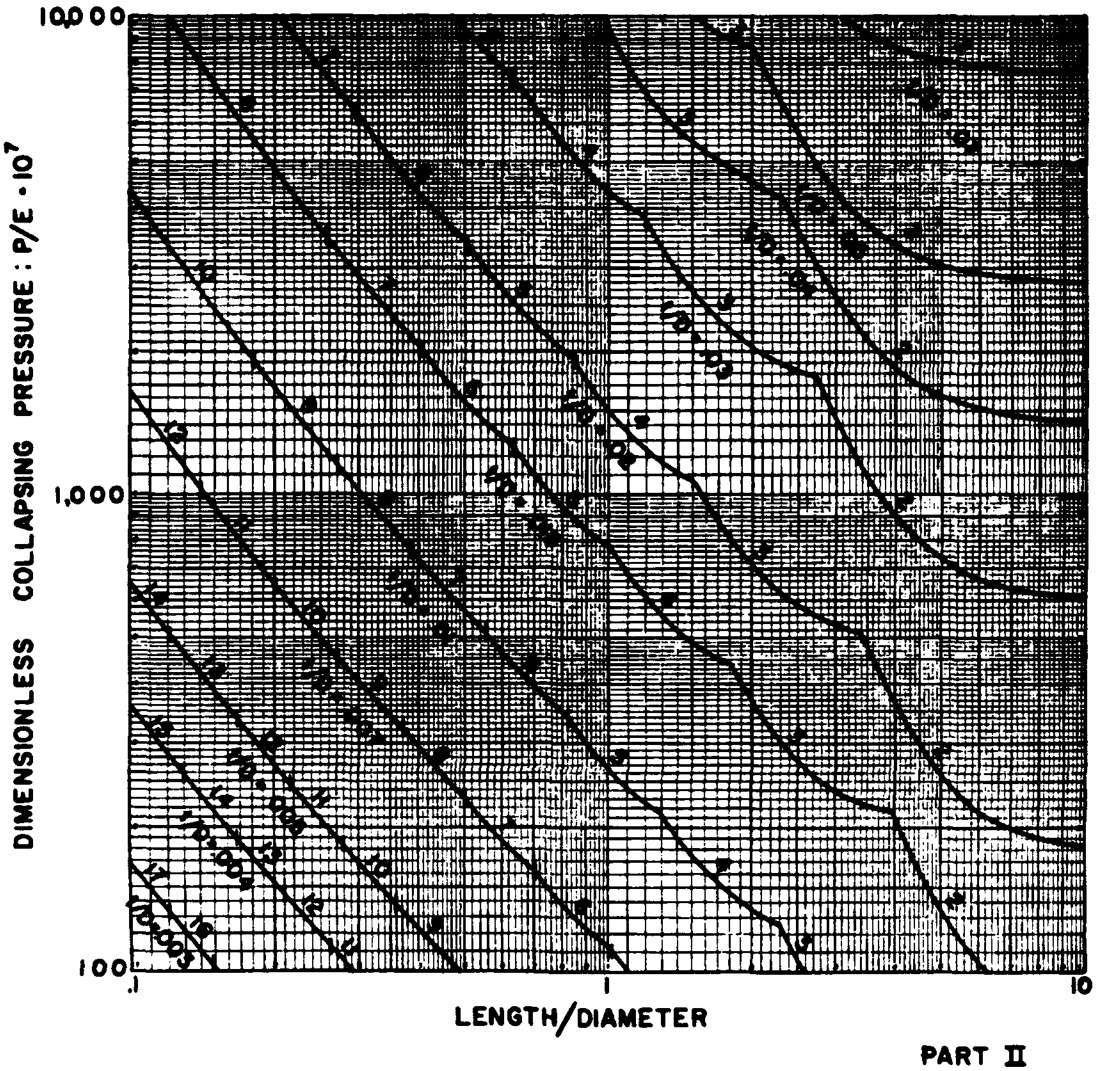

Figure A-60. Graphic solution to R. von Mises analytical equation for buckling.

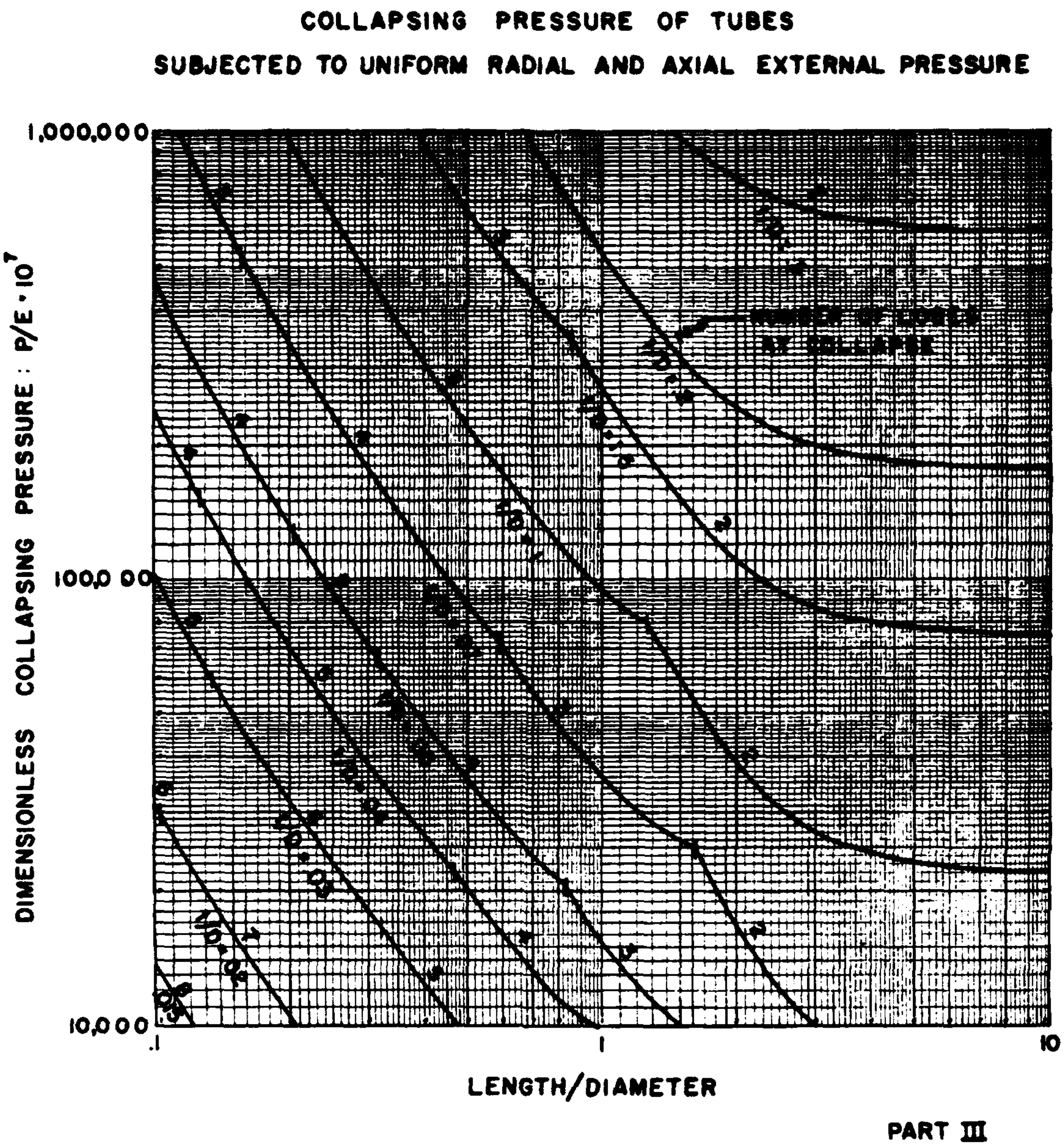

Figure A-61. Graphic solution to R. von Mises analytical equation for buckling.

Table A-1. Six-inch-diameter housing test assemblies used in pressure testing.

	Assy I	Assy II	Assy III	Assy IV	Assy V
End Bells	Titanium	Ceramic	Titanium	Titanium	Titanium
Cylinders	Mod 2	Mod 2	Mod 1, Mod 1	Mod 2, Mod 2	Mod 2, Mod 2
Stiffeners			Type B Titanium	Type C Titanium	Type D Titanium
End Caps	Titanium	Titanium	Titanium	Titanium	Titanium
Overall Length	L/D = 2.5	L/D = 2.5	L/D = 4	L/D = 4	L/D = 4

	Assy VI	Assy VII	Assy VIII	Assy IX	Assy X
End Bells	Titanium	Titanium	Titanium	Titanium	Titanium
Cylinders	Mod 2, Mod 2,	Mod 2	Mod 2	Mod 2, Mod 2	Mod 2, Mod 2, Mod 1, Mod 1
Stiffeners	Type E Aluminum	Type F Titanium	Type G Aluminum	Type H Aluminum	Type D, Type C, Type D Titanium
End Caps	Titanium	Titanium	Titanium	Titanium	Titanium
Overall Length	L/D = 4	L/D = 4	L/D = 4	L/D = 4	L/D = 7

	Assy XI	Assy XII	Assy XIII	Assy XIV
End Bells	Titanium	Titanium	Titanium	Titanium
Cylinders	Mod 2, Mod 2, Mod 1, Mod 1	Mod 3	Mod 3	Mod 3
Stiffeners	Type H, Type H, Type H Aluminum	Midbay Mod 0 Aluminum	Midbay Mod 1 Aluminum	Midbay Mod 2 Aluminum
End Caps	Titanium	Aluminum	Aluminum	Aluminum
Overall Length	L/D = 7	L/D = 4	L/D = 4	L/D = 4

Table A-2. Summary of pressurizations performed on 6-inch-diameter housing assemblies.

	Assy I	Assy II	Assy III	Assy IV	Assy V
Proof Tests to 10,000 psi	1	1	1	1	1
Cyclic Tests to 9000 psi	1000 Cycles	100 Cycles	10 Cycles	1000 Cycles	10 Cycles

	Assy VI	Assy VII	Assy VIII	Assy IX	Assy X
Proof Tests to 10,000 psi	1	1	1	1	1
Cyclic Tests to 9000 psi	10 Cycles	10 Cycles	10 Cycles	10 Cycles	10 Cycles

	Assy XI	Assy XII	Assy XIII	Assy XIV
Proof Tests to 10,000 psi	1	1	Imploded at 9900 psi	1
Cyclic Tests to 9000 psi	10 Cycles	1000 Cycles	0	1000 Cycles

Table A-3. Weight of structural components in 6-inch-diameter housing assemblies.

Cylinder, Ceramic Model 2, 94% alumina 6.04 in OD X 9 in L X 0.206 in thick	2056 grams
Cylinder, Ceramic Model 3, 94% alumina 6.04 in OD X 18 in L X 0.206 in thick	4110 grams
Hemisphere, Titanium, Model 1* (single)	673 grams
Hemisphere, Titanium, Model 2* (single)	1257 grams
Hemisphere, Ceramic with end ring (single)	765 grams
End Caps	
Titanium (pair)	120 grams
Aluminum (pair)	70 grams
Joint Ring Stiffener, Titanium	
Type B	441 grams
Type C	357 grams
Type D	317 grams
Type F	294 grams
Joint Ring Stiffener, Aluminum	
Type E	346 grams
Type G	302 grams
Type H	283 grams
Midbay Stiffener, Aluminum	
Mod 0	319 grams
Mod 1	261 grams
Mod 2	304 grams
Weight/Displacement	
Cylinder, Model 2 with Titanium end caps	0.503
Cylinder, Model 2 with Titanium end caps and two Titanium Hemispheres Model 1	0.567
Cylinder, Model 3 with Titanium end caps, Mod 2 interior midbay stiffener and two Titanium hemispheres Model 1	0.56
Cylindrical Assembly, two Model 2 cylinders joined with Type F ring stiffener, and closed by two Titanium Hemispheres Model 1	0.57
Cylinder, Model 3 with Titanium end caps, Mod 0 interior midbay stiffener, and two Titanium Hemispheres Model 2	0.64

* The critical buckling pressure of titanium hemispheres Model 1 is 11,250 psi and of Model 2 is 23,000 psi

Table A-4. Strains on aluminum midbay stiffener Mod 0 located inside the 6-inch-OD Model 3 ceramic cylinder.

Pressure (PSI)	D Hoop	D Axial	DD Hoop	DD Axial	DDD Hoop	DDD Axial	Flange E Hoop	Flange E Axial	Web F Hoop	Web F Axial
	Gage Locations									
	Inside Diameter Under Webs						Flange		Web	
0	0	0	0	0	0	0	0	0	0	0
1000	-190	143	-39	54	-237	165	-202	-36	-69	-6
2000	-531	335	-333	226	-564	353	-428	-112	-283	-39
3000	-883	550	-645	422	-907	565	-657	-175	-512	-60
4000	-1206	746	-926	598	-1220	758	-868	-229	-722	-86
5000	-1551	961	-1226	787	-1550	966	-1091	-276	-946	-111
6000	-1869	1156	-1497	961	-1852	1155	-1295	-312	-1153	-132
7000	-2212	1369	-1787	1145	-2183	1357	-1520	-337	-1380	-159
8000	-2567	1586	-2078	1331	-2513	1565	-1742	-356	-1607	-181
9000	-2916	1786	-2361	1498	-2839	1753	-1961	-376	-1837	-221
10000	-3252	1996	-2624	1670	-3148	1950	-2165	-367	-2053	-236

NOTES:

Gages: Gage Type: CEA-13-062-350; Gage Factor 2.15

Test Assembly:

1. One Ceramic Cylinder 6 in OD x 18 in L radially supported at Midbay by an aluminum ring stiffener bonded to the Ceramic Cylinder with epoxy
2. The Cylinder is capped with Titanium Hemispheres DWG 55910-0106069 on Both Ends

Materials: The Ceramic is Coors AD 94 (94% Alumina); The Aluminum is 7075-T6 alloy

Data: All Readings are in microinches/inch

Structural Performance: Did not implode at 10,000 psi

Table A-5. Stresses on aluminum midbay stiffener Mod 0 located inside the 6-inch-OD Model 3 ceramic cylinder.

	Gage Locations									
	Inside Diameter Under Webs						Flange		Web	
Pressure	D		DD		DDD		E		F	
(PSI)	Hoop	Axial	Hoop	Axial	Hoop	Axial	Hoop	Axial	Hoop	Axial
0	0	0	0	0	0	0	0	0	0	0
1000	-1602	901	-238	461	-2048	974	-2400	-1152	-796	-323
2000	-4717	1793	-2899	1303	-5021	1872	-5217	-2841	-3320	-1485
3000	-7871	2902	-5674	2347	-8085	2981	-8019	-4396	-5967	-2569
4000	-10769	3905	-8176	3281	-10882	3988	-10587	-5783	-8419	-3638
5000	-13844	5040	-10842	4291	-13814	5099	-13263	-7136	-11025	-4748
6000	-16690	6050	-13238	5240	-16503	6102	-15685	-8296	-13425	-5750
7000	-19750	7170	-15811	6230	-19469	7143	-18302	-9409	-16072	-6894
8000	-22929	8290	-18387	7240	-22401	8255	-20863	-10444	-18701	-7981
9000	-26105	9242	-20944	8066	-25363	9157	-23395	-11480	-21429	-9281
10000	-29097	10354	-23258	9022	-28100	10223	-25650	-12134	-23908	-10249

NOTES: All Stresses are in pounds per square inch, calculated on the basis of E = 10,000,000 and M = .33

Table A-6. Strains on aluminum midbay stiffener Mod 1 located inside the 6-inch-OD Model 3 ceramic cylinder.

	Gage Locations											
	Inside Diameter Under Webs						Inside Diameter Between Webs					
	D		DD		DDD		X		XX		XXX	
Pressure (PSI)	Hoop	Axial	Hoop	Axial	Hoop	Axial	Hoop	Axial	Hoop	Axial	Hoop	Axial
0	0	0	0	0	0	0	0	0	0	0	0	0
1000	-197	193	-79	129	-96	137	-467	183	-553	228	-464	-181
2000	-327	357	-170	265	-203	280	-913	365	-1014	439	-902	360
3000	-452	512	-249	390	-298	413	-1318	539	-1452	612	-1302	521
4000	-601	687	-338	526	-402	558	-1768	723	-1949	813	-1745	701
5000	-755	859	-417	653	-498	688	-2190	890	-2424	1010	-2156	870
6000	-935	1047	-483	775	-589	818	-2612	1067	-2932	1236	-2570	1040
7000	-1147	1253	-517	886	-663	940	-3006	1226	-3463	1454	-2935	1190
8000	-1430	1486	-506	971	-699	1030	-3330	1364	-3995	1700	-3242	1316
9000	-1921	1837	-327	995	-662	1088	-3614	1488	-4776	2057	-3472	1409

	Flange				Web			
	E		EE		F		FF	
Pressure (PSI)	Hoop	Axial	Hoop	Axial	Hoop	Axial	Hoop	Axial
0	0	0	0	0	0	0	0	0
1000	-320	-61	-315	-40	22	-397	34	-444
2000	-600	-114	-593	-74	44	-767	63	-830
3000	-855	-157	-850	-103	65	-1111	88	-1183
4000	-1141	-200	-1135	-132	89	-1492	116	-1575
5000	-1416	-209	-1410	-155	113	-1857	142	-1935
6000	-1707	-230	-1701	-169	140	-2242	167	-2301
7000	-1988	-230	-1981	-166	168	-2595	188	-2620
8000	-2272	-204	-2264	-146	197	-2933	210	-2925
9000	-2662	-152	-2658	-90	242	-3340	242	-3303

NOTES:
Gages:
Gage Type: CEA-13-062-350
Gage Factor: 2.15
Test Assembly:
1. One Ceramic Cylinder 6 in OD × 18 in L radially supported at Midbay by an aluminum ring stiffener bonded to ceramic with epoxy
2. The Cylinder is capped with Titanium Hemispheres DWG 55910-XXXX on Both Ends
Materials:
The Ceramic is Coors AD 94 (94% Alumina)
The Aluminum is 7075-T6 alloy
Data: All readings are in microinches/inch
Structural Performance: Imploded at 9800 psi

Table A-7. Stresses on aluminum midbay stiffener Mod 1 located inside the 6-inch-OD Model 3 ceramic cylinder.

	Gage Locations											
	Inside Diameter Under Webs						Inside Diameter Between Webs					
Pressure	D		DD		DDD		X		XX		XXX	
(PSI)	Hoop	Axial	Hoop	Axial	Hoop	Axial	Hoop	Axial	Hoop	Axial	Hoop	Axial
0	0	0	0	0	0	0	0	0	0	0	0	0
1000	-1496	1436	-409	1155	-570	1182	-4562	324	-5360	511	-5876	-3749
2000	-2347	2795	-926	2344	-1241	2390	-8892	715	-9752	1171	-8788	699
3000	-3176	4071	-1350	3454	-1814	3530	-12792	1168	-14025	1490	-12679	1025
4000	-4200	5483	-1845	4650	-2444	4772	-17160	1566	-18858	1905	-16983	1404
5000	-5291	6843	-2261	5783	-3040	5875	-21276	1877	-23458	2357	-20969	1779
6000	-6614	8285	-2550	6907	-3580	6997	-25356	2301	-28321	3012	-24985	2153
7000	-8230	9812	-2520	8027	-3958	8092	-29188	2626	-33471	3492	-28525	2485
8000	-10543	11378	-2082	9021	-4029	8968	-32312	2974	-38529	4282	-31503	2762
9000	-14752	13498	15	9953	-3399	9756	-35040	3314	-45970	5396	-33739	2954

	Flange				Web			
Pressure	E		EE		F		FF	
(PSI)	Hoop	Axial	Hoop	Axial	Hoop	Axial	Hoop	Axial
0	0	0	0	0	0	0	0	0
1000	-3816	-1869	-3682	-1615	-1223	-4373	-1262	-4856
2000	-7154	-3501	-6927	-3026	-2346	-8443	-2366	-9079
3000	-10174	-4927	-9918	-4303	-3384	-12225	-3393	-12947
4000	-13543	-6469	-13223	-5683	-4526	-16411	-4530	-17242
5000	-16661	-7588	-16394	-6960	-5608	-20417	-5571	-21185
6000	-20004	-8901	-19711	-8194	-6730	-24637	-6646	-25199
7000	-23157	-9941	-22841	-9197	-7723	-28494	-7591	-28700
8000	-26247	-10701	-25943	-10021	-8649	-32179	-8474	-32041
9000	-30430	-11562	-30156	-10851	-9651	-36579	-9514	-36164

NOTES: All Stresses are in pounds per square inch, caluclated on the basis of E = 10,000,000 and M = .33

Table A-8. Strains on aluminum midbay stiffener Mod 2 located inside the 6-inch-OD Model 3 ceramic cylinder.

	Gage Locations											
	Inside Diameter Under Webs						Inside Diameter Between Webs					
Pressure	D		DD		DDD		X		XX		XXX	
(PSI)	Hoop	Axial	Hoop	Axial	Hoop	Axial	Hoop	Axial	Hoop	Axial	Hoop	Axial
0	0	0	0	0	0	0	0	0	0	0	0	0
1000	-135	107	2	64	-73	78	-281	114	-159	70	-229	68
2000	-265	242	-93	188	-183	204	-583	245	-434	189	-524	188
3000	-399	369	-118	305	-296	324	-879	366	-702	301	-816	296
4000	-526	506	-279	431	-407	453	-1176	496	-970	521	-1106	415
5000	-652	634	-368	549	-516	574	-1464	618	-1229	531	-1390	529
6000	-785	772	-455	674	-630	706	-1760	750	-1487	651	-1666	664
7000	-915	905	-535	790	-745	830	-2040	870	-1728	760	-1939	781
8000	-1050	1040	-606	906	-865	965	-2341	1000	-1978	875	-2238	912
9000	-1190	1175	-662	1000	-983	1085	-2625	1123	-2199	970	-2526	1032
10000	-1360	1308	-692	1100	-1115	1208	-2917	1242	-2400	1057	-2820	1165

	Flange				Web			
Pressure	E		EE		F		FF	
(PSI)	Hoop	Axial	Hoop	Axial	Hoop	Axial	Hoop	Axial
0	0	0	0	0	0	0	0	0
1000	-160	18	-40	-70	44	-349	26	-350
2000	-416	99	-281	-148	98	-804	66	-791
3000	-668	152	-545	-141	139	-1248	104	-1240
4000	-910	209	-801	-127	191	-1697	140	-1680
5000	-1136	254	-1067	-96	239	-2117	172	-2093
6000	-1348	312	-1317	-80	306	-2541	209	-2536
7000	-1566	381	-1575	-49	355	-2938	244	-2962
8000	-1800	468	-1828	-15	411	-3359	276	-3366
9000	-2042	547	-2102	25	458	-3757	311	-3817
10000	-2276	640	-2365	68	515	-4130	343	-4225

NOTES:

Gages: Gage Type: CEA-13-062-350; Gage Factor 2.15

Test Assembly:

1. One Ceramic Cylinder 6 in OD x 18 in L radially supported at Midbay by an aluminum ring stiffener bonded to the Ceramic Cylinder with epoxy
2. The Cylinder is capped with Titanium Hemispheres DWG 55910-0106069 on Both Ends

Materials: The Ceramic is Coors AD 94 (94% Alumina); The Aluminum is 7075-T6 alloy

Data: All Readings are in microinches/inch

Structural Performance: Did not implode at 10,000 psi

Table A-9. Stresses on aluminum midbay stiffener Mod 2 located inside the 6-inch-OD Model 3 ceramic cylinder.

	Gage Locations											
	Inside Diameter Under Webs						Inside Diameter Between Webs					
Pressure	D		DD		DDD		X		XX		XXX	
(PSI)	Hoop	Axial	Hoop	Axial	Hoop	Axial	Hoop	Axial	Hoop	Axial	Hoop	Axial
0	0	0	0	0	0	0	0	0	0	0	0	0
1000	-1119	701	259	725	-530	605	-2731	239	-1525	197	-2318	-85
2000	-2077	1734	-347	1765	-1298	1611	-5634	590	-4170	514	-5183	169
3000	-3111	2663	-195	2985	-2121	2539	-8507	852	-6762	778	-8060	300
4000	-4028	3730	-1535	3803	-2889	3576	-11358	1211	-8954	2254	-10873	561
5000	-4968	4699	-2096	4797	-3664	4530	-14138	1513	-11823	1407	-13637	789
6000	-5949	5755	-2610	5878	-4455	5589	-16970	1898	-14274	1798	-16234	1282
7000	-6915	6766	-3078	6883	-5286	6554	-19668	2208	-16574	2129	-18864	1583
8000	-7930	7781	-3445	7922	-6132	7625	-22563	2552	-18953	2494	-21734	1946
9000	-9001	8777	-3725	8769	-7012	8534	-25294	2881	-21081	2741	-24521	2226
10000	-10416	9640	-3691	9780	-8038	9425	-28130	3135	-23014	2973	-27327	2630

	Flange				Web			
Pressure	E		EE		F		FF	
(PSI)	Hoop	Axial	Hoop	Axial	Hoop	Axial	Hoop	Axial
0	0	0	0	0	0	0	0	0
1000	-1729	-390	-708	-934	-799	-3753	-1004	-3831
2000	-4301	-430	-3701	-2701	-1877	-8658	-2188	-8631
3000	-6932	-768	-6637	-3600	-3061	-13488	-3424	-13528
4000	-9436	-1024	-9457	-4391	-4140	-18333	-4650	-18331
5000	-11805	-1356	-12327	-5028	-5157	-22868	-5820	-22847
6000	-13969	-1490	-15073	-5774	-5975	-27377	-7045	-27680
7000	-16160	-1523	-17853	-6381	-6895	-31650	-8229	-32330
8000	-18463	-1414	-20566	-6937	-7826	-36166	-9366	-36745
9000	-20886	-1423	-23492	-7502	-8772	-40458	-10643	-41675
10000	-23167	-1246	-26284	-7994	-9513	-44432	-11795	-46135

NOTES: All Stresses are in pounds per square inch, calculated on the basis of E = 10,000,000 and M = .33

Table A-10. Critical pressures of 6-inch-OD Model 1, 2, and 3 ceramic cylinders.

	Cylinder 1	Cylinder 2	Cylinder 3	Cylinder 4	Cylinder 5	Cylinder 6	Cylinder 7
Material	94% Al_2O_3	94% Al_2O_3	99.5% Al_2O_3	99.5% Al_2O_3	94% Al_2O_3	94% Al_2O_3	94%Al_2O_3
Dimensions	6.040 in. OD 5.624 in. ID 0.208 in. t 9.000 in. L	6.040 in. OD 5.624 in. ID 0.208 in. t 9.000 in. L	6.000 in. OD 5.624 in. ID 0.188 in. t 9.000 in. L	6.000 in. OD 5.624 in. ID 0.188 in. t 9.000 in. L	6.040 in. OD 5.624 in. ID 0.208 in. t 18.000 in. L	6.040 in. OD 5.624 in. ID 0.208 in. t 18.000 in. L	6.040 in. OD 5.624 in. ID 0.208 in. t 18.000 in. L
Radial Support	Ends Only	Ends Only	Ends & Joint Stiffener Type B		Ends & Midbay Stiffener Mod 0	Ends & Midbay Stiffener Mod 1	Ends & Midbay Stiffener Mod 2
Proof Pressure Tests to 10,000 psi	16	16	20	20	2	1	1
Design Pressure Tests to 9000 psi	1000	1000	2000	2000	1000	1	1000
Surface Spalling Initiation	None	None	None	None	None	None	None
Internal Delaminations	None	None	2 in. W x 1 in. L 1 in. W x 1 in. L	None	None	None	None
Internal Inclusions	Not Inspected	Not Inspected	None	None	Not Inspected	Not Inspected	Not Inspected
End Closures for Implosion Test	Plane Steel Bulkheads	Hemispherical Ceramic Bulkheads	Plane Steel Bulkheads	Plane Steel Bulkheads	Plane Steel Bulkheads	Plane Steel Bulkheads	Plane Steel Bulkheads
Implosion Pressure	17,700 psi	14,250 psi	Failed Together at 17,900 psi		18,000 psi	9900 psi	15,000 psi
Type of Failure	Buckling of Cylinder	Failure of Metallic Flange on Hemisphere	Buckling of Cylinder	Buckling of Cylinder	Buckling of Cylinder	Buckling of Midbay Stiffener	Buckling of Midbay Stiffener

APPENDIX B: MECHANICAL JOINTS WITH INTEGRAL JOINT RING STIFFENERS FOR CERAMIC CYLINDERS

All appendix B figures and tables are placed at the end of appendix B text.

FIGURES

TABLES

APPENDIX B: MECHANICAL JOINTS WITH INTEGRAL JOINT RING STIFFENERS FOR CERAMIC CYLINDERS

INTRODUCTION

The *basic* ceramic cylindrical housing consists of a ceramic monocoque cylinder sealed and radially supported at the ends by metallic or ceramic bulkheads. The resistance to buckling of the monocoque cylinder is a function not only of its E, t/D_0, and L/D_0 ratio, but also of the radial compliance of *supports provided by the bulkheads.*

For such a basic ceramic cylindrical housing, the only approach to increasing its payload rating is to *increase the diameter* without changing the t/D_0 and L/D_0 ratios, or to *increase the length and thickness* without changing the diameter. The first approach does not change the weight-to-displacement (W/D) ratio, while the second approach increases it significantly. Furthermore, serious manufacturing difficulties are encountered if the L/D_0 exceeds 1.5 for cylinders with $D_0 \geq 12$ inches.

Since there are many applications that call for additional payload capability while, at the same time, preclude increasing housing diameter, an alternate approach had to be developed that allows the extension in length of the cylindrical housing without a significant increase in manufacturing cost, or W/D ratio. The alternate approach developed by Dr. Stachiw of the Naval Ocean Systems Center (NOSC)* (Reference 1) consists of maintaining the same L/D_0 and t/D_0 for each cylindrical section even though the overall length of the housing is increased to generate the specified buoyancy for the housing. This is accomplished by NOSC mechanical joints that fasten together, provide radial support, and seal the ends of the cylindrical sections.

The NOSC mechanical joint consists of two end caps that enclose the ends of adjoining cylinders, a ring stiffener (with integral O-ring seals) that provides radial support to the end caps, and a split wedge band clamp that locks the end caps and the ring stiffener together. The radial compliance of the ring stiffener can be designed to simulate the radial support provided by either a hemispherical or plane bulkhead fabricated from metal or ceramic. In either case, the weight of stiffener is significantly less than that of the type of bulkhead it replaces.

Thus, the designer can extend a ceramic cylindrical housing to any length without increasing its W/D ratio. The ability to do this makes the cylindrical ceramic housing a more attractive choice, as it allows the designer to extend the length of the housing by adding identical shell sections, rather than having to increase the length and thickness of a single monocoque cylinder.

Since the removable joint ring stiffener is, beside the end caps, a key element of the joint, extensive efforts have been devoted in this program to their design and evaluation. The design of end caps is described in detail separately in appendix D.

DESIGN OF JOINT RING STIFFENERS

The primary objective of the joint ring stiffener design is to provide sufficient radial support to the ends of adjoining cylinders at the joint so that the failure of the housing takes place by buckling of individual cylinders at the midbay, rather than by general buckling of the whole cylindrical assembly. If this objective is attained, the structural performance of each cylindrical section becomes independent of other sections, and the length of the cylindrical housing assembly can be increased by any number of cylindrical section modules without reducing the critical pressure of the whole assembly.

Such an approach to joint ring stiffener design does not result, however, in the lightest structure, since housing assemblies of only two cylinders require, for example, joint ring stiffeners with less resistance to buckling than assemblies made up of three, four, or more cylindrical sections. Thus, for ceramic housing assemblies configured for an optimum W/D ratio, the joint ring stiffeners must be custom designed for a specific number of cylindrical sections. Adding another cylinder section to such a cylindrical housing assembly to

*NOSC is now the Naval Command, Control and Ocean Surveillance Center (NCCOSC) RDT&E Division (NRaD).

accommodate a bigger payload would, however, cause the housing to buckle at lesser pressure.

The approach used for the design of the joint ring stiffeners in this program consisted of sizing the H-shaped stiffener to provide adequate radial support for the ends of ceramic cylinders with $t/D_0=0.034$ and $L/D_0=1.5$ so that they would not buckle at pressures $\leq$13,500 psi when three or more of them are joined together to form a cylindrical housing supported at the ends by hemispherical bulkheads.

Since the critical pressures predicted by computer programs, like BOSOR4, for cylindrical housings consisting of several cylindrical sections fastened together by mechanical joints with integral ring stiffeners may depart by as much as 25 percent from the experimentally generated critical pressures, the basic stiffener was configured to prevent failure of the multi-section cylindrical housing at calculated pressures $\leq$16,000 psi. This provides adequate insurance for the potential margin of error between the calculated and actual critical pressures. Once this design was experimentally validated, holes were milled into the web of the stiffener to reduce its weight.

The perforated stiffener, after instrumentation with strain gages, was incorporated into a joint between two ceramic cylinders comprising a cylindrical housing assembly. If the strains on the ring stiffener did not indicate onset of buckling, the stiffener would be removed from the housing and the holes enlarged further. This process was reiterated several times until, during a proof test to 10,000 psi, the divergence of strains signaled the initiation of buckling. At that point, the design of the holes in the stiffeners would be frozen and the stiffeners would be considered to represent the minimum weight design for 9,000-psi design pressure of cylindrical housings incorporating two cylinder sections. Some of the holes in the stiffeners were milled out too large, and because of it, the stiffeners either failed during the pressurization to 10,000 psi, or the pressurization was terminated at lower pressure to preclude catastrophic failure during the pressure test.

TEST SPECIMENS

Two classes of joint ring stiffeners were designed, fabricated, and experimentally evaluated in this program. The design of stiffeners in Class T centered around the physical properties of Ti-6Al–4V alloy, while the design of stiffeners in Class A centered around the physical properties of 7178–T651 aluminum alloy. The goals of both stiffener classes were, however, the same: (1) design a *basic stiffener configuration* capable of providing radial support to alumina-ceramic cylinders with $t/D_0=0.034$ and $L/D_0=1.5$ dimensions at 150-percent overpressure, and (2) reduce the weight of the basic stiffener configuration by incorporating lightening holes into the webs of the stiffeners until the critical pressure of a cylindrical multi-section ceramic housing supported by these stiffeners exceeds the 9,000-psi design pressure by only 15 to 25 percent.

Class T Stiffeners

Stiffener Class T consisted of three designs. The *basic stiffener* configuration (figure B-1A DWG 0119738 and figures B-14 through B-32), was designed to provide a housing assembly of three or more cylindrical ceramic sections (L/Do=1.5 and t/Do=0.034) with critical pressure $\geq$13,500 psi. The design of the basic stiffener was arrived at by scaling up the scale-model stiffener C (appendix A, figure A-16) whose performance has shown to exceed the design requirements of this program.

The first modification to the basic stiffener configuration consisted of milling nine elliptical slots with 0.75-inch width and 20-degree arc length at 20-degree intervals (figure B-1B DWG 0123943 and figures B-33 through B-40). The second modification consisted of enlarging the elliptical slots to a 1-inch width (figure B-1C DWG 0121604 and figures B-41 through B-49).

Class A Stiffeners

Stiffener Class A also consisted of three designs. The basic stiffener configuration (figure B-1D DWG 0124007 and figures B-50 through B-56) was designed to provide a housing assembly of three or more cylindrical ceramic sections (L/Do=1.5 and t/Do=0.034) with critical pressure $\geq$13,500 psi. The design was arrived at by scaling up the aluminum scale-model stiffener (appendix A,

figure A-23) whose performance has shown to exceed the design requirements of this program.

The first modification to the basic stiffener configuration consisted of milling nine elliptical slots with 0.75-inch width and 20-degree arc length at 20-degree intervals (figure B-1F DWG 0124008 and figures B-57 through B-64). The second modification consisted of enlarging the elliptical slots to a 1-inch width (figure B-1E DWG 0121605 and figures B-65 through B-71).

The decision to mill these slots was driven by weight consideration. Table B-3 lists the housing component weights, including the weight of the six different stiffeners.

TEST SETUP

The joint ring stiffeners were experimentally evaluated by incorporating them into a ceramic cylindrical housing assembly (figures B-2 through B-5 DWG 0119733) consisting of two ceramic cylindrical sections (figure B-6 DWG 0119735) radially supported at the central joint by the ring stiffener and at the ends by titanium end bells (figure B-11 DWG 0119737). Each cylindrical section consisted of two end caps (figure B-8 DWG 0119736) epoxy-bonded to an alumina-ceramic cylinder (figure B-6) which in turn was protected by a polyurethane jacket (figure B-7). Split aluminum bands (figure B-10 DWG 0119740) clamped around each joint held all the components of the housing together. By using the same housing assembly for evaluation of all joint ring stiffeners, the radial loading to which the stiffeners were subjected during the tests was held constant.

After all of the joint ring stiffeners were experimentally evaluated by testing them as a part of the ceramic housing assembly made up of two cylinders, some of them were incorporated into larger housing assemblies made up of three and four ceramic cylinder sections. To preclude buckling because of the extra radial loading on the stiffeners, caution was exercised in selection of the stiffener types. For the housing with four ceramic cylinders, only the stiffeners without lightening holes were selected. The housing with three cylindrical sections was fitted with titanium and aluminum stiffeners with 0.75-inch wide slots. Table B-1, Sheets 1 and 2, summarizes the housing configuration tested.

INSTRUMENTATION

All components of the housing test assembly (figure B-4 DWG 0119733) were instrumented with electric strain gages to provide an overview of the structural performance of all housing components during the first proof test with the titanium joint ring stiffener. If implosion occurred during that test, the strain data would help identify the component whose nonlinear deformation initiated buckling of the housing assembly. If the first proof test was successful, the recording of strains from gages from all components, except for stiffener, would be discontinued as it was already shown that these components were capable of withstanding proof pressure of 10,000 psi.

All stiffeners were instrumented with electrical resistance strain gages at the same locations to facilitate comparison of strain data generated by gages on different stiffeners. The locations of interest were (1) the inner surface of the inner flange, (2) the inner surface of the outer flange, and (3) the web between flanges. A nonlinear strain increase at any of these locations would signal incipient buckling or material yielding, and the test would be terminated unless someone wished to observe the failure of the stiffener.

TEST PROCEDURE

The test procedure consisted of proof testing each test housing to 10,000 psi while the strains were recorded at 1,000 psi intervals. After sustained pressurization of 60 minute's duration, the pressure was decreased at 1,000-psi/minute rate to zero. The proof test was followed by cyclic pressure testing to 9,000 psi. Following the cyclic pressure tests, the housings were taken apart and inspected for permanent deformation of the joint ring stiffeners.

TEST OBSERVATIONS

Buckling

Titanium and aluminum joint ring stiffeners without lightening holes did not fail at 10,000-psi proof test pressure. All strains were linear to 10,000 psi.

The titanium joint ring stiffener with 1-inch-wide slots (figure B-1C DWG 0121604) buckled at

9,910 psi (figure B-44). The strains departed linearity at 7,500 psi external pressure loading. The cause of failure was local elastic buckling of the inner flange under excessively large lightening holes in the web of the stiffener. Because of the excessive long spans between web supports, the inner flange formed a series of lobes between these supports with maximum tensile hoop stresses *under* each web support, and maximum compressive hoop stresses midway between supports. At the moment of failure, the compressive stresses midway between web supports exceeded –85,000 psi.

The test on the aluminum joint ring stiffener with 1-inch-wide slots (figure B-1E DWG 0124008) was terminated at 7,000 psi without failure or departure of strains from linearity. Table B-1 lists the different test assemblages, and table B-2 is a summary of proof and cyclic pressure tests run on all test assemblies. Tables B-4 through B-20 show complete strain and stress breakdowns.

Stress Distribution

Maximum tensile stresses were recorded in all joint stiffeners on the inside surface of the inner flange in *axial* direction. Their magnitude on titanium stiffeners at 9,000-psi design pressure varied from 20,000 to 42,000 psi depending on the absence or presence of lightening holes and their size. On aluminum stiffeners, the maximum tensile stress varied from 12,000 to 16,000 psi at the same location.

Maximum compressive stresses were recorded in all joint stiffeners on the inside surface of the inner flange in *hoop* direction. Their magnitude on titanium stiffeners at 9,000-psi design pressure varied from –30,000 to –39,000 psi at the same locations.

On joint stiffeners without lightening holes, the compressive hoop stress was uniform around the whole circumference of the inner flange, indicating that the stiffener contracted uniformly under radial loading. This was not the case on stiffeners with elliptical lightening holes. On such stiffeners, the inner flange did not contract uniformly; instead, the inner flange formed ripples, each ripple corresponding to the location of an elliptical hole above. These local ripples at some strain level spawned buckling of the inner flange.

Compressive stresses also were recorded on the inside surface of the outer flange and on the web of the stiffener. Their magnitude, however, did not exceed the compressive stresses on the inside surface of the inner flange.

FINDINGS

1. Joint ring stiffeners can be scaled up or down linearly without reduction of their elastic stability.
2. Milling of holes in the webs of joint stiffeners is not an effective approach to reducing their weight; the *small* reduction in weight is accompanied by a large reduction in elastic stability.
3. Aluminum 7178–T6 alloy joint ring stiffeners provide more elastic stability to the cylindrical housing than Ti–6Al–4V alloy stiffeners of equal weight.
4. The joint ring stiffener provides higher elastic stability to the cylindrical housing than a hemispherical bulkhead of the same material and weight.

CONCLUSIONS

1. The NOSC mechanical joint, composed of two end caps bonded to the ends of ceramic cylinders, split band clamp, and a joint ring stiffener, successfully performed three functions. It aligns and couples mating cylinders together, seals the interface between them, and radially supports their ends against buckling.
2. It is feasible to assemble cylindrical housing of infinite length from many identical ceramic monocoque cylinders by incorporating the NOSC mechanical joints with integral joint ring stiffeners.
3. The elastic stability of a cylindrical housing assembled from many cylindrical ceramic monocoque cylinders and coupled together by NOSC mechanical joints can be predicted by the BOSOR4 computer program within 20 percent of critical pressure.

RECOMMENDATIONS

1. For optimum fatigue life of the adjoining ceramic cylinders, the ends of the cylinders must be encapsulated in NOSC Mod 1 type 2 end caps (see appendix D).
2. Joint ring stiffeners without lightening holes are preferred, as stiffeners incorporating lightening holes are more prone to local buckling of the stiffener web and flanges.
3. If there is a requirement for holes in the webs of stiffeners to act as feedthroughs for electric cables or hydraulic lines, it should be met preferentially by 18 circular holes of 0.75-inch diameter located uniformly at 20-degree intervals on the web's mean diameter. Only as the last resort should one replace the circular holes with elliptical slots of the same width.

REFERENCE

B-1. Stachiw, J. D., 1987, "Exploratory Evaluation of Alumina Ceramic Cylindrical Housings for Deep Submergence Service: The Second Generation NOSC Ceramic Housings," NOSC TR 1176 (Sep). Naval Ocean Systems Center, San Diego, CA.

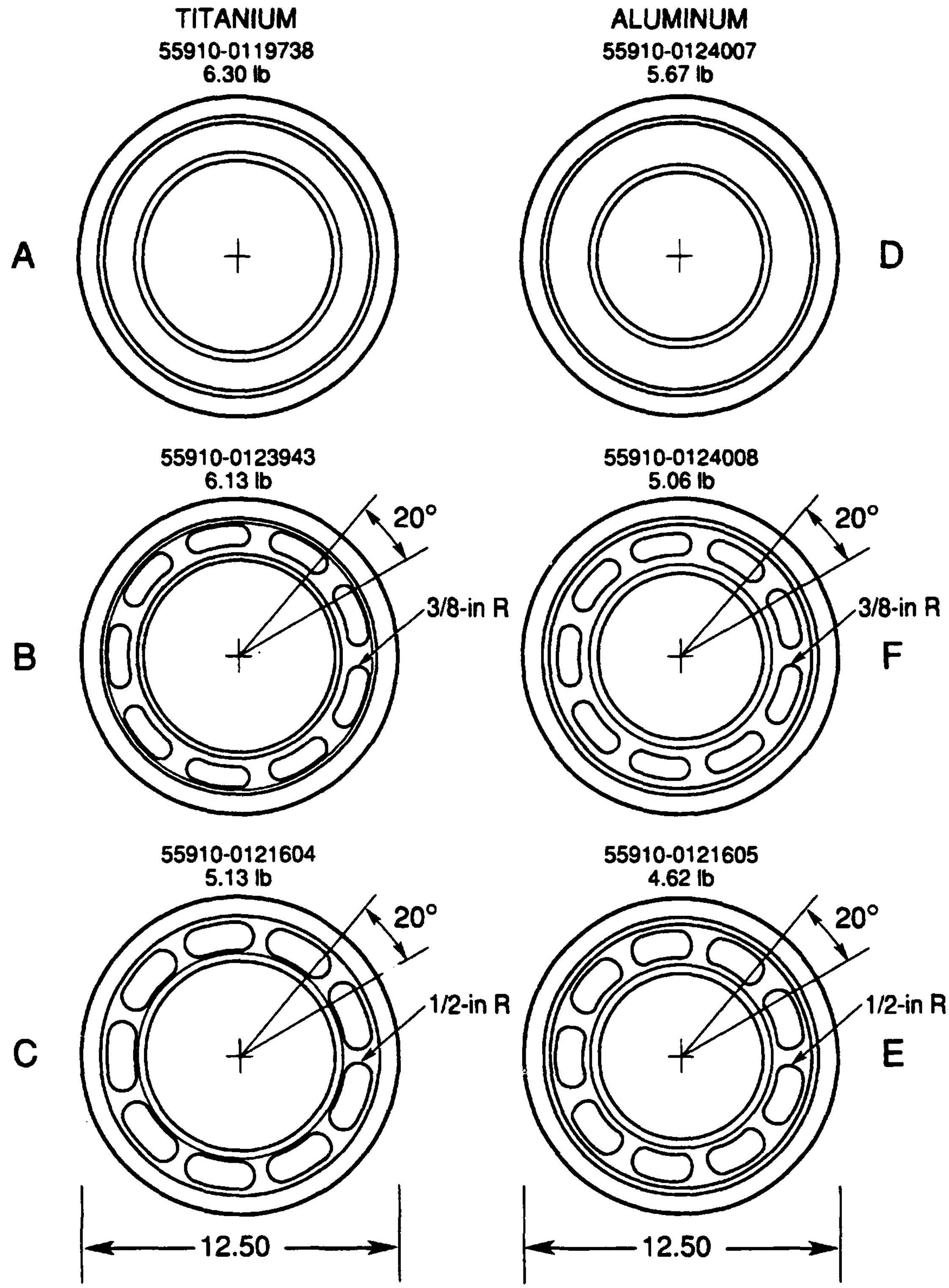

Figure B-1. Configuration of joint ring stiffeners described in appendix B.

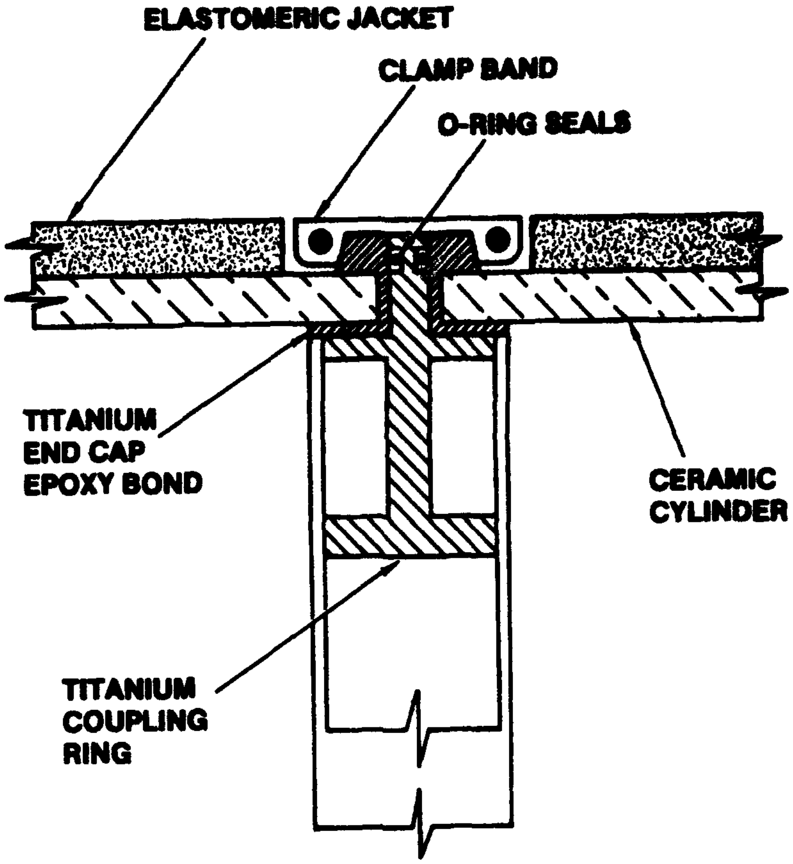

Figure B-2. Joint stiffener and coupling for ceramic cylinders for housing test assemblies 1A through 1F.

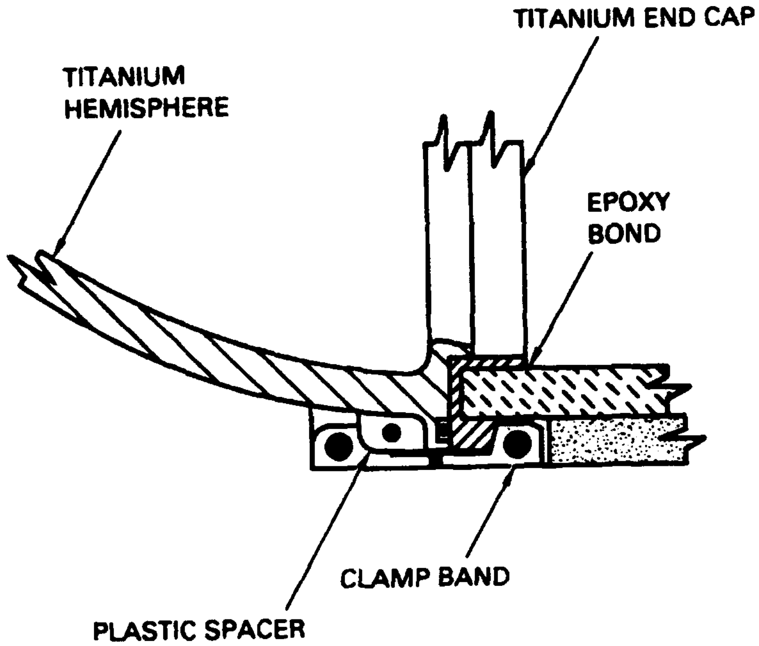

Firgure B-3. Coupling of ceramic cylinders to titanium bulkheads for housing test assemblies 1A through 1F.

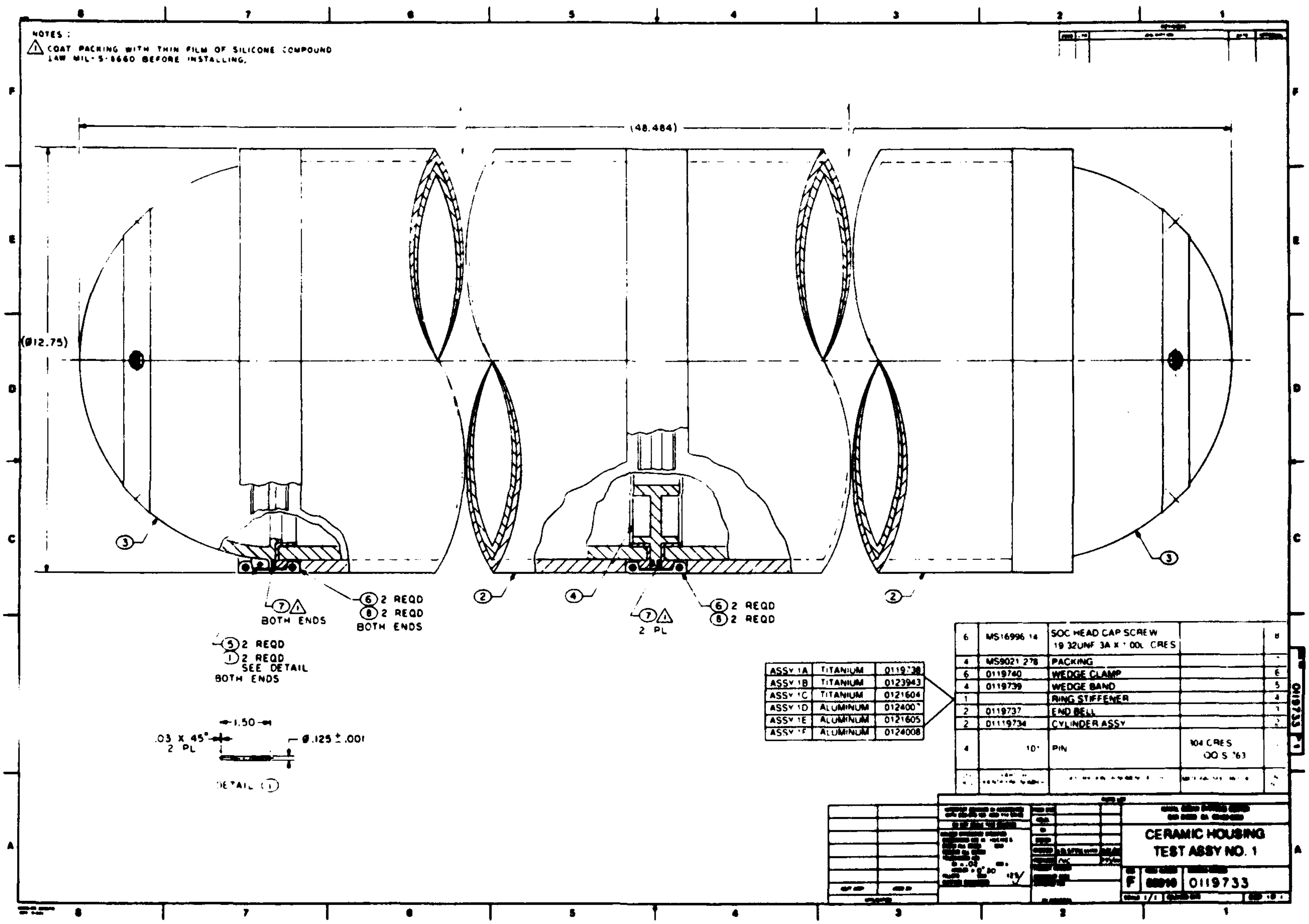

Figure B-4. List of components comprising housing test assemblies 1A through 1F.

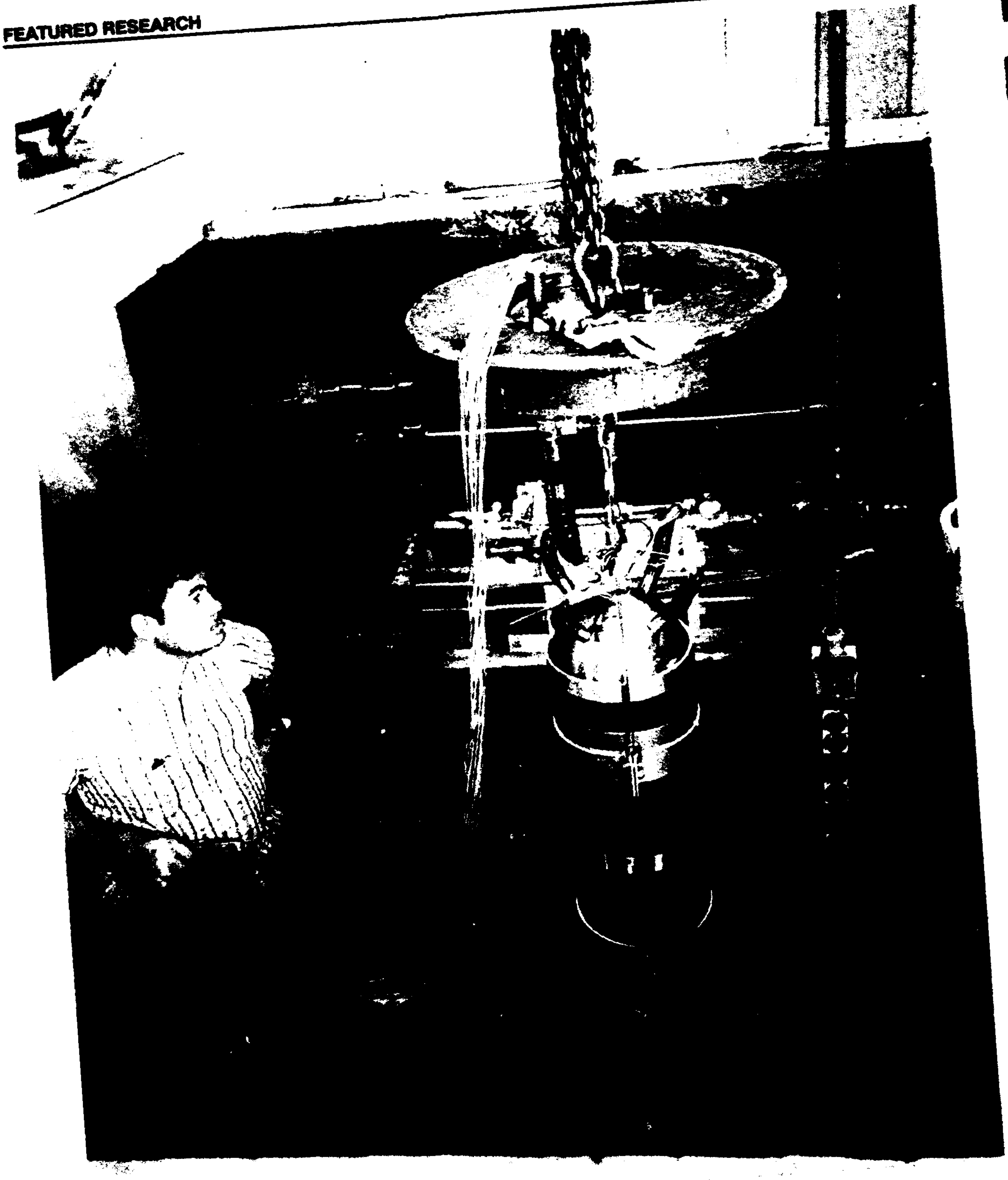

Figure B-5. Housing assembly 1A during placement in the pressure vessel for external pressure testing.

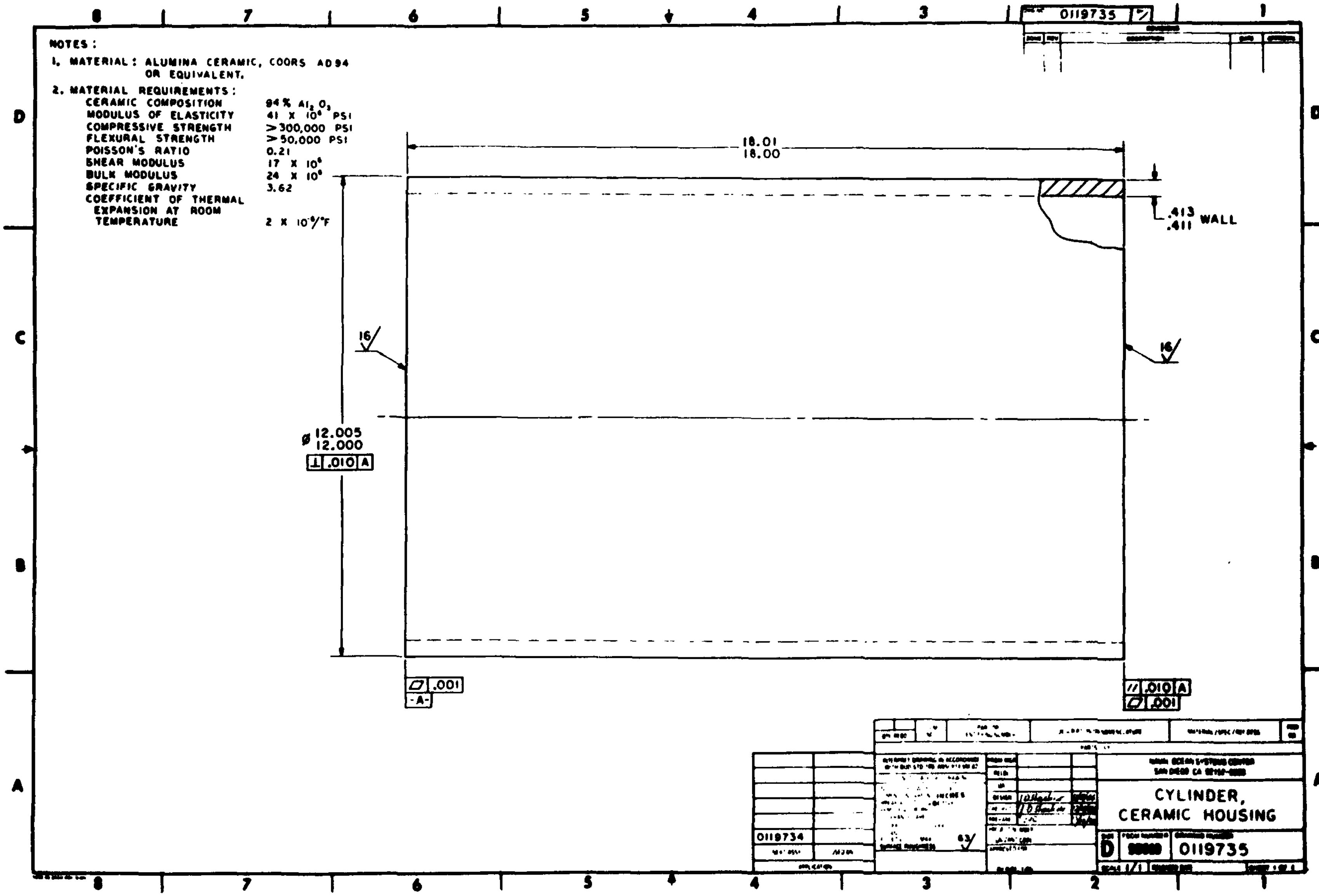

Figure B-6. Ceramic cylinders used in housing test assemblies.

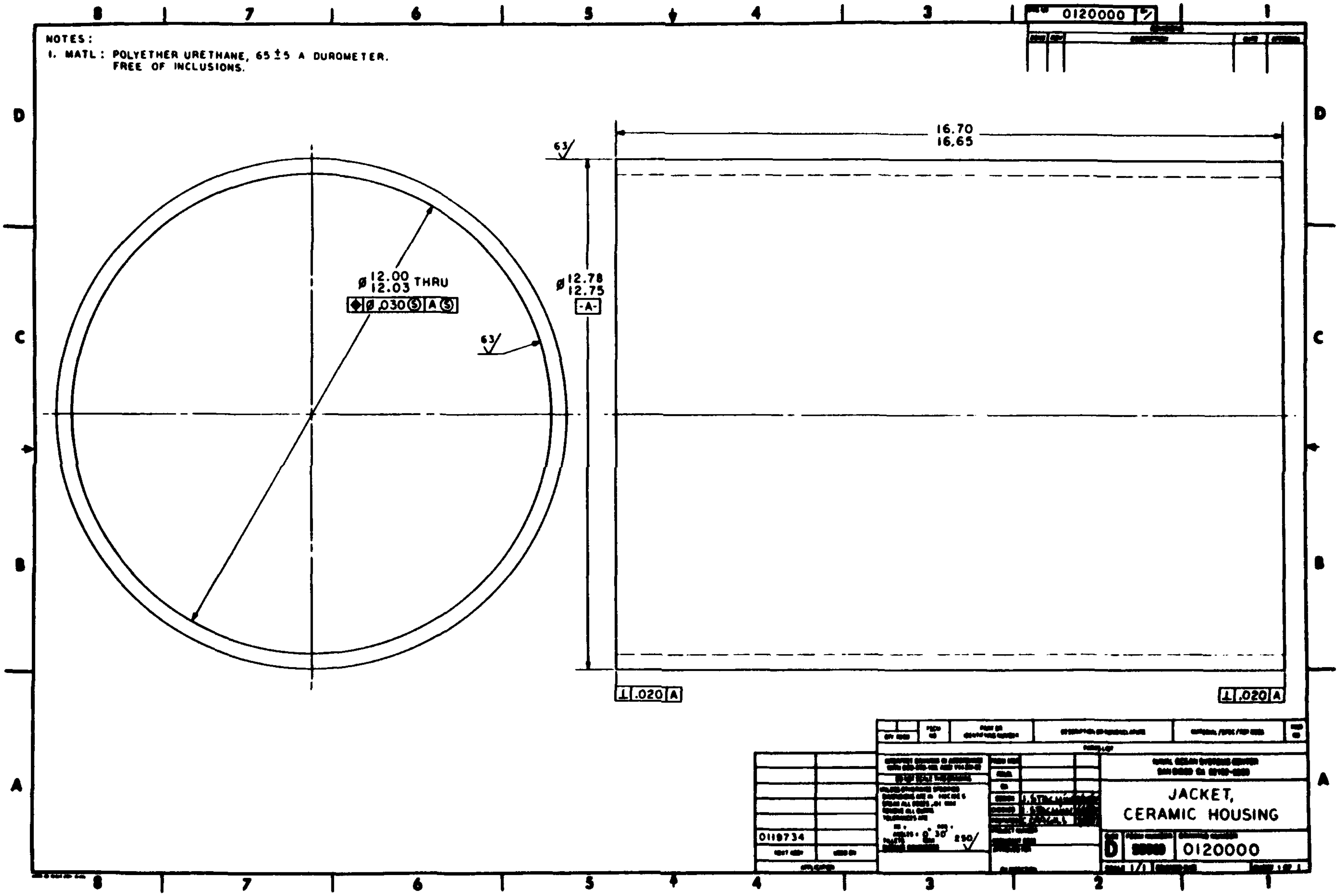

Figure B-7. Polyurethane jacket for ceramic cylinders.

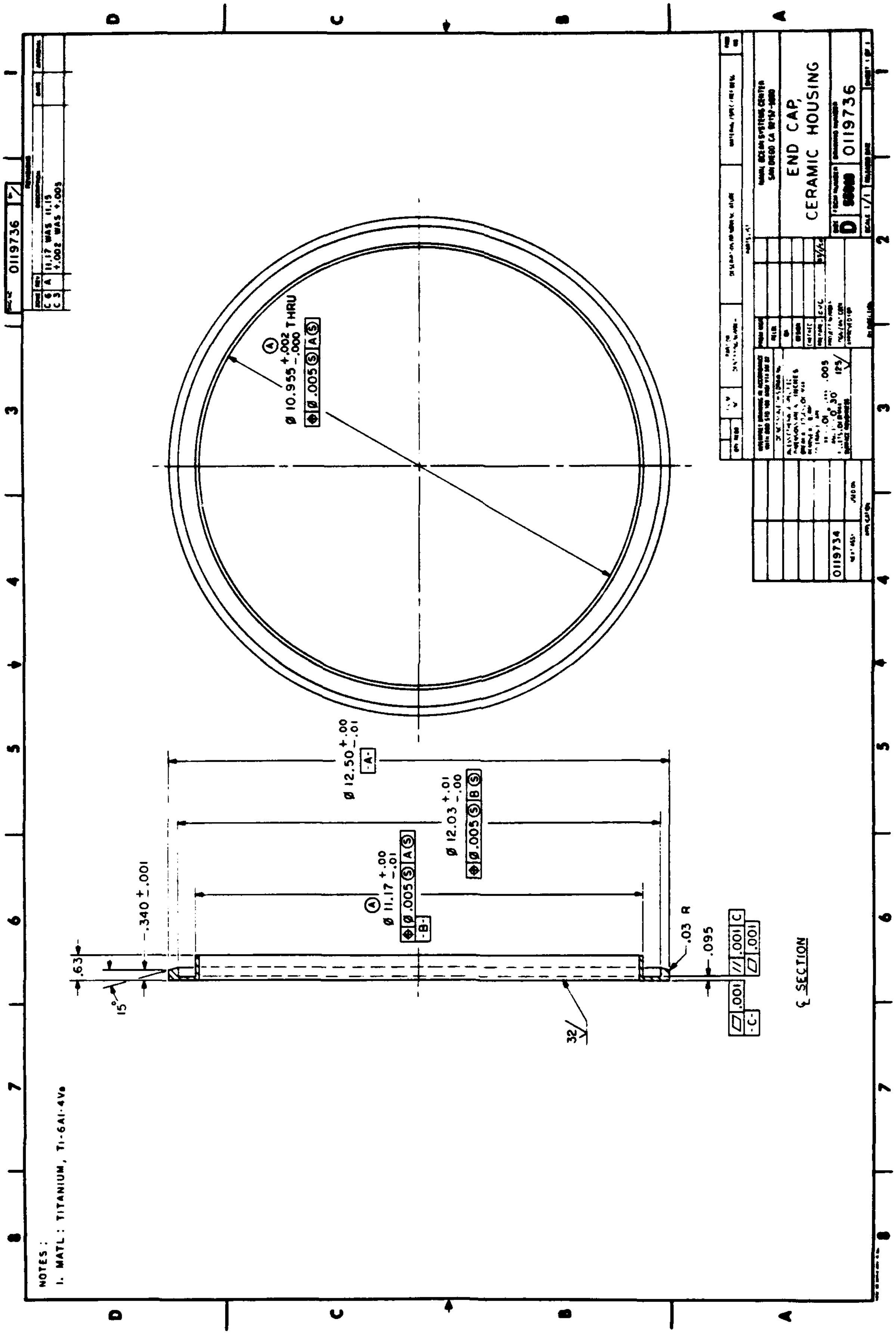

Figure B-8. Mod 0 end cap for ceramic cylinders.

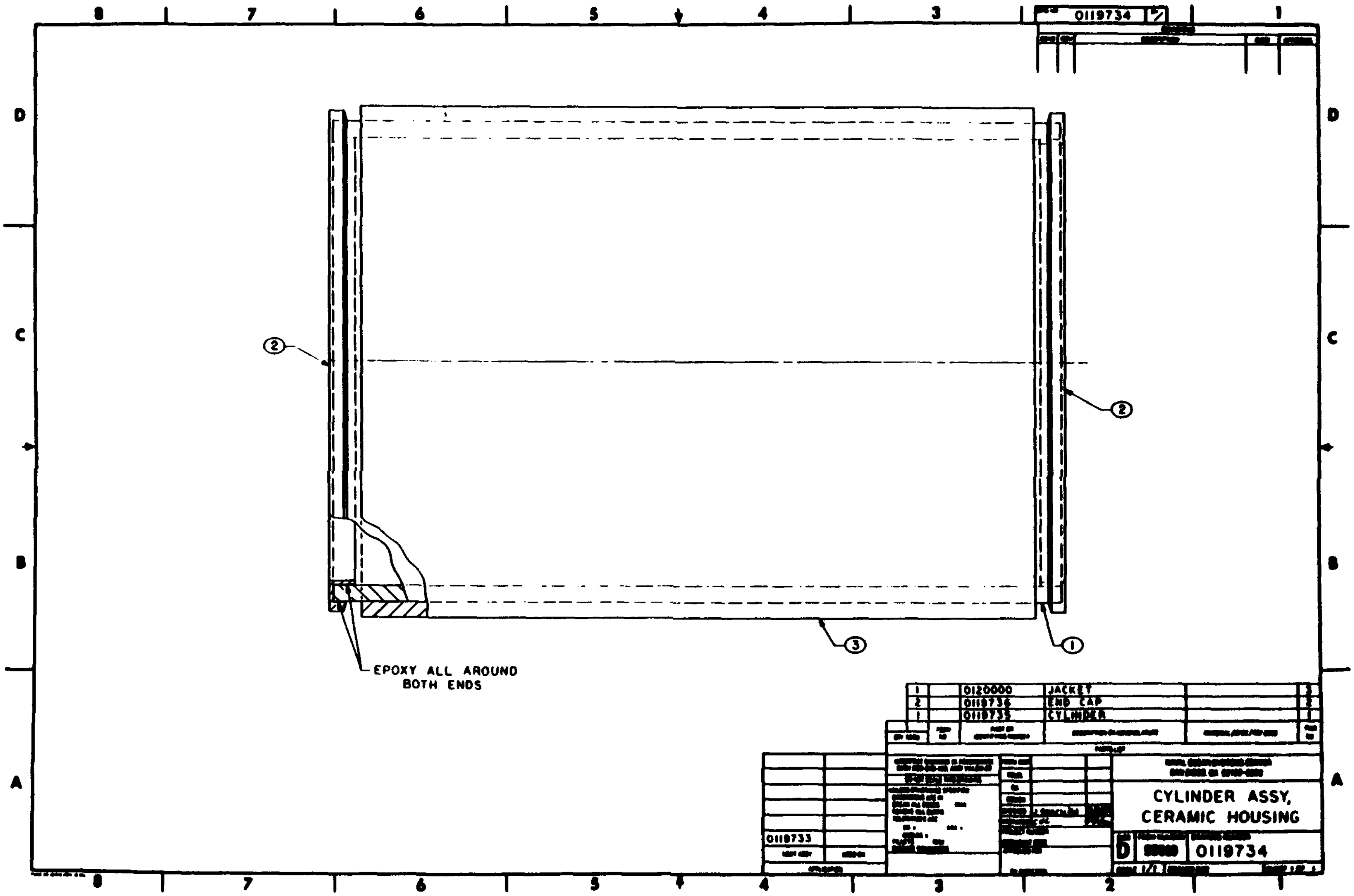

Figure B-9. Ceramic cylinder assembly.

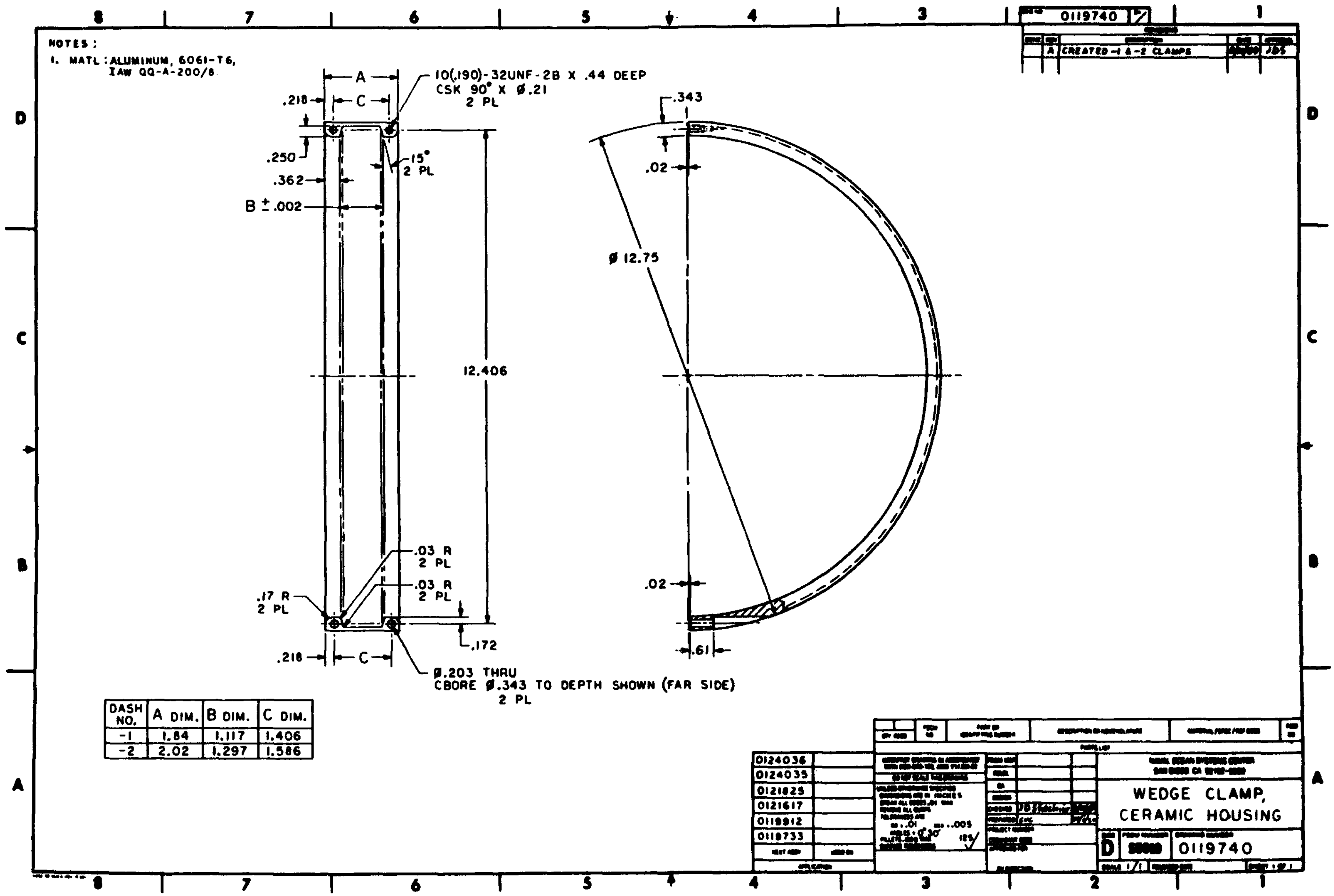

DASH NO.	A DIM.	B DIM.	C DIM.
-1	1.84	1.117	1.406
-2	2.02	1.297	1.586

Figure B-10. Wedge clamp for coupling cylinder assemblies and bulkheads in housing test assemblies.

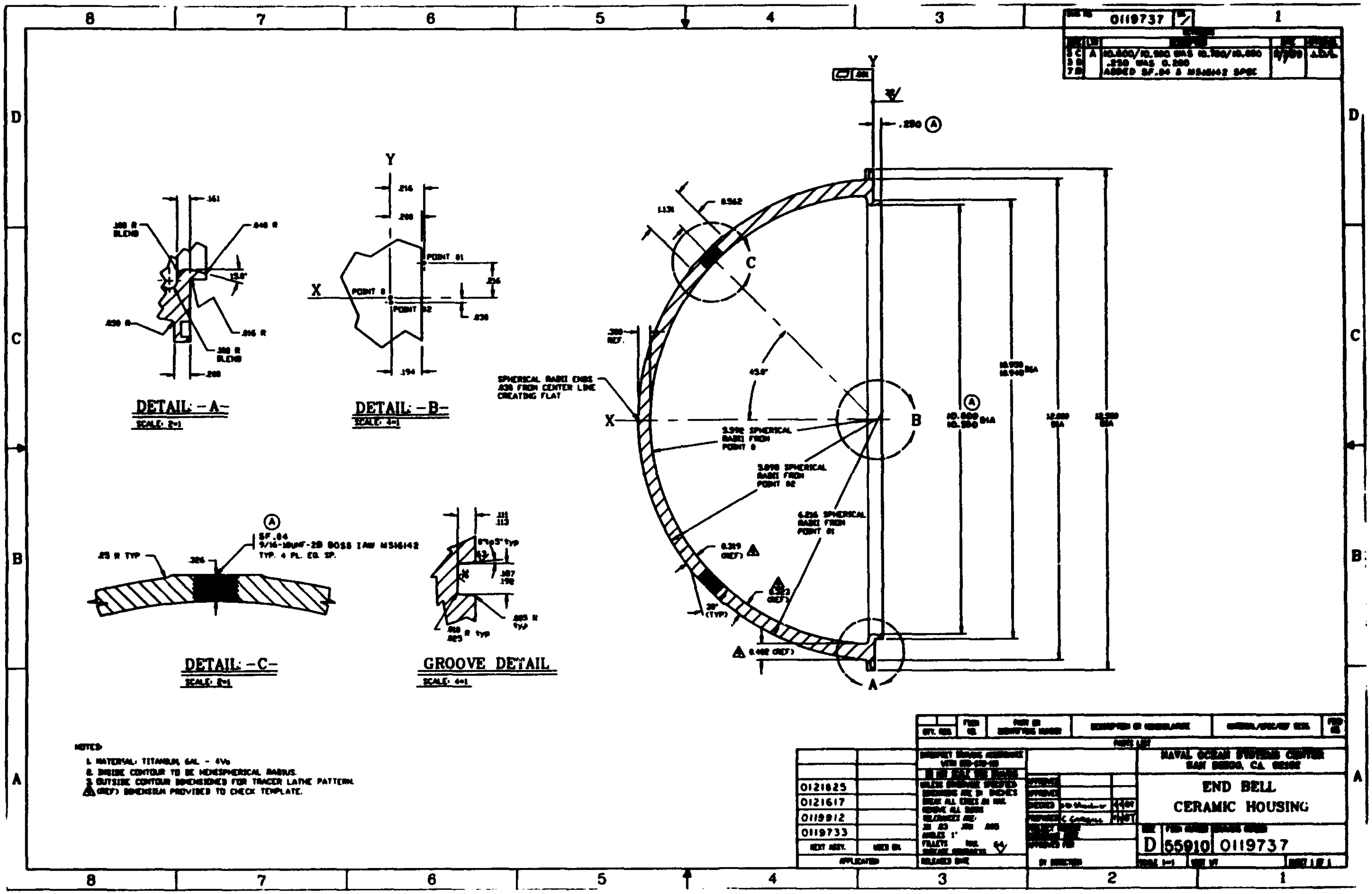

Figure B-11. Optimized titanium end bell for 9,000-psi service used as bulkhead in housing test assemblies.

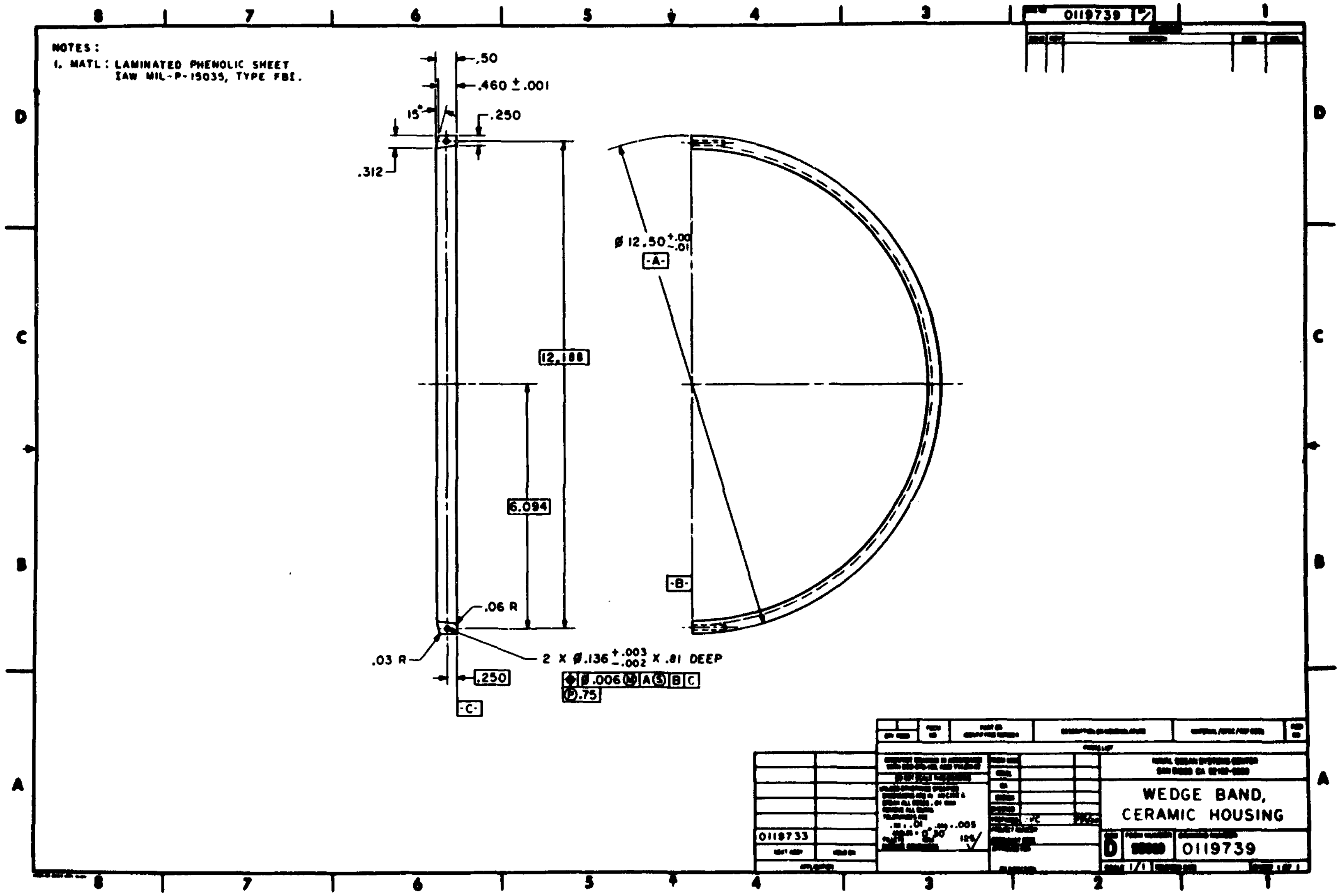

Figure B-12. Wedge band for coupling ceramic cylinders to titanium end bells.

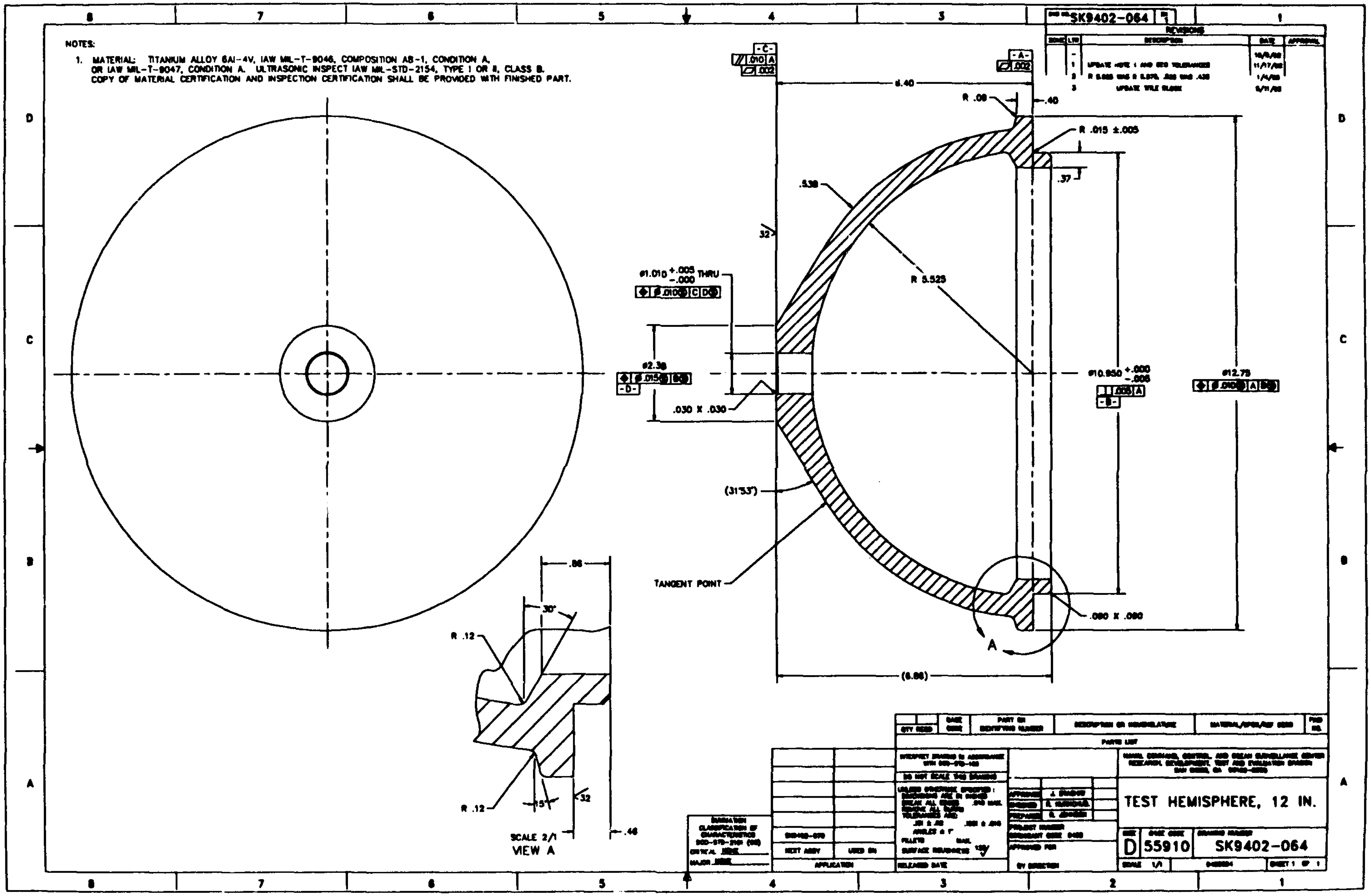

Figure B-13. Titanium end bell for 10,000-psi service (not used in this test program).

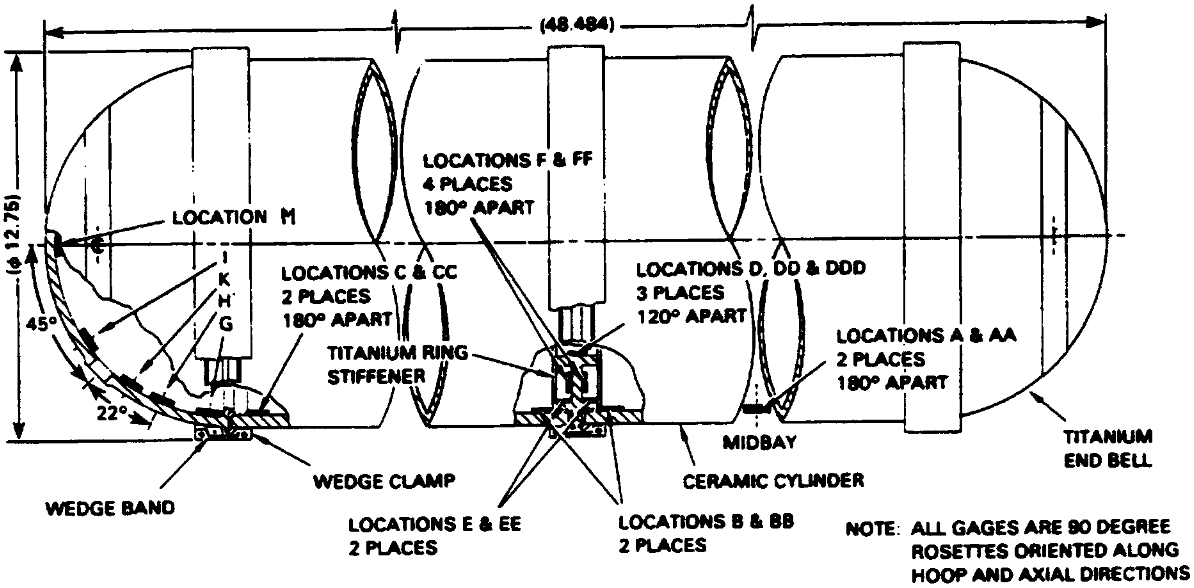

LOCATION OF STRAIN GAGES
ON
CERAMIC HOUSING ASSY NO. 1A

Figure B-14. Ceramic housing test assembly 1A.

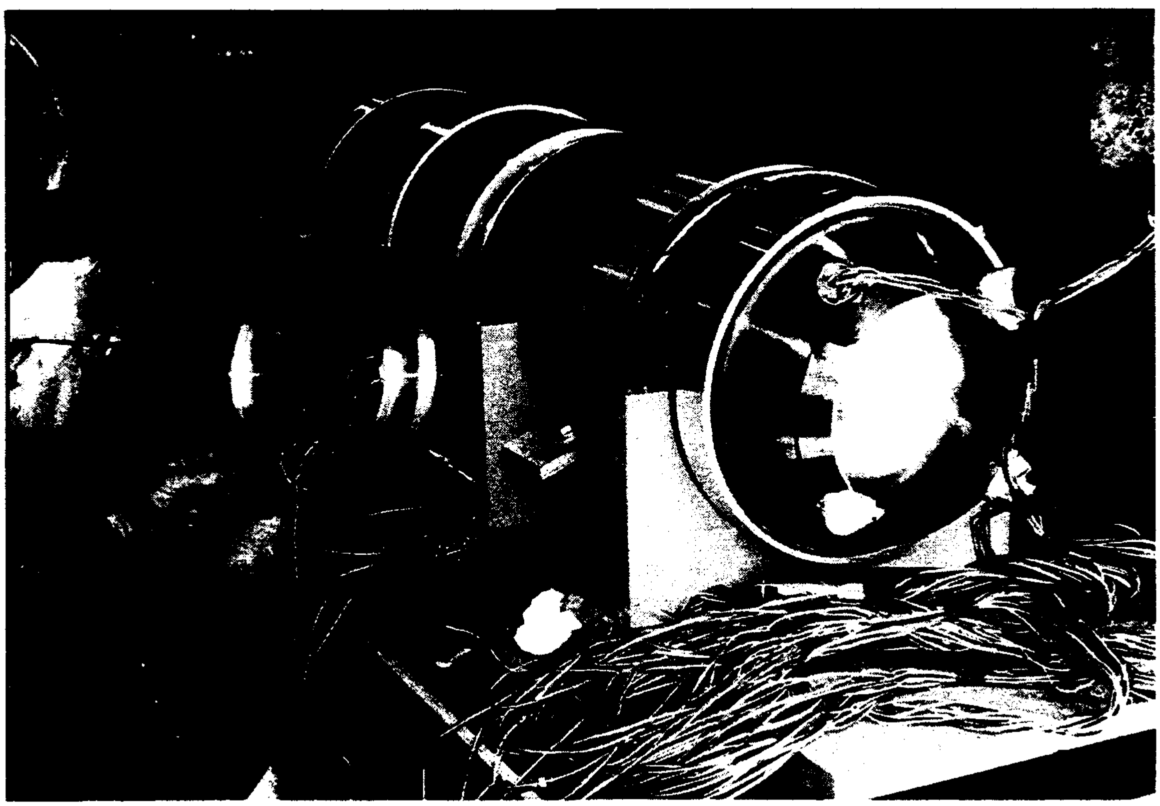

Figure B-15. Ceramic housing test assembly 1A during instrumentation with strain gages.

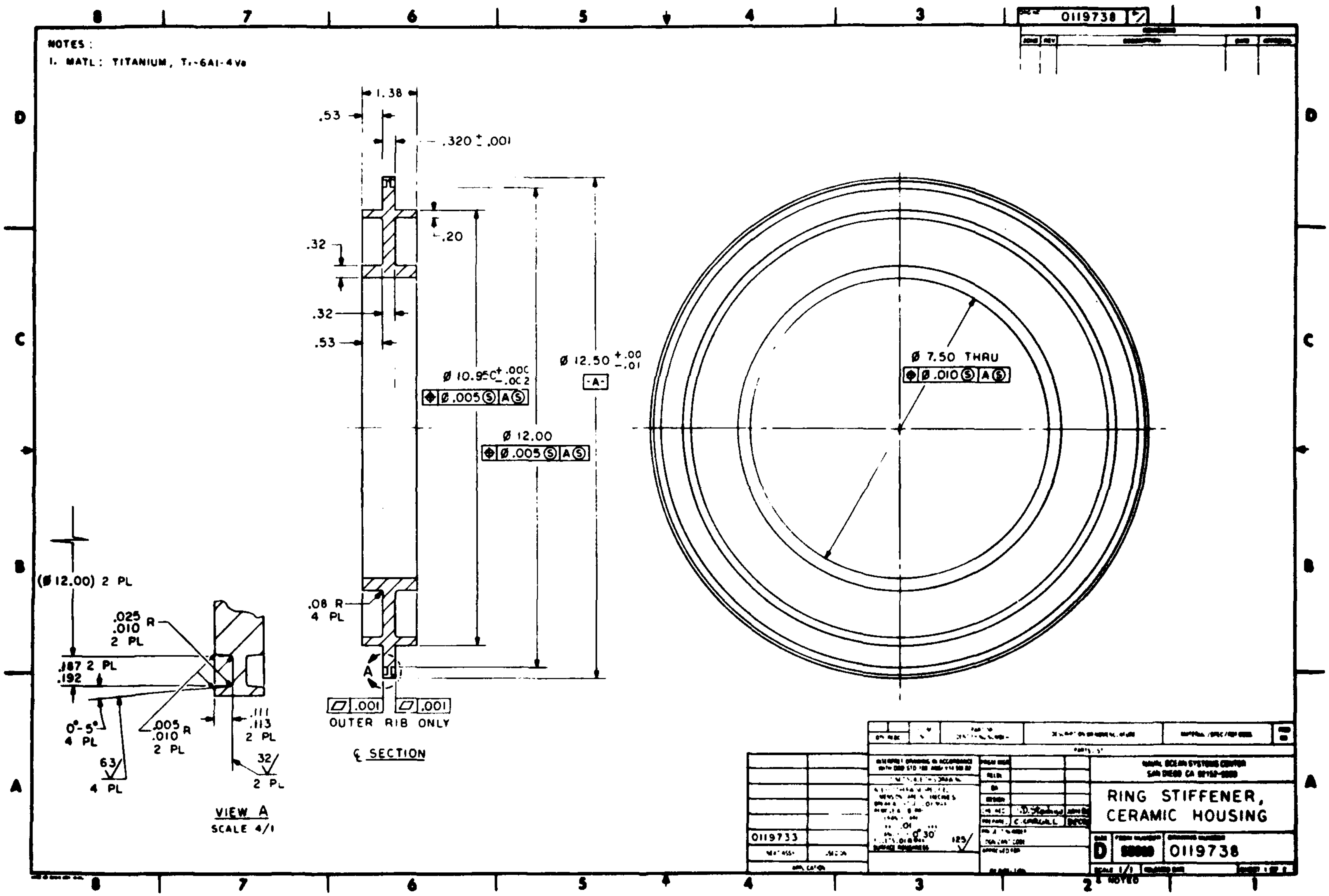

Figure B-16. Titanium ring stiffener DWG 0119738; fabrication drawing.

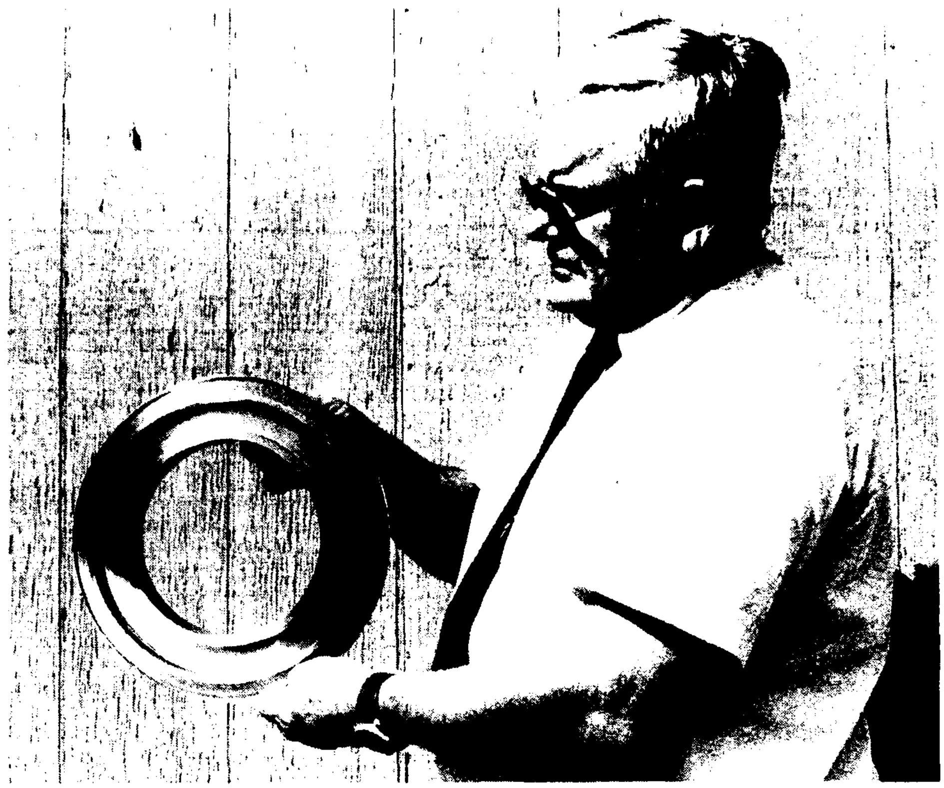

Figure B-17. Titanium ring stiffener DWG 0119738; exterior view.

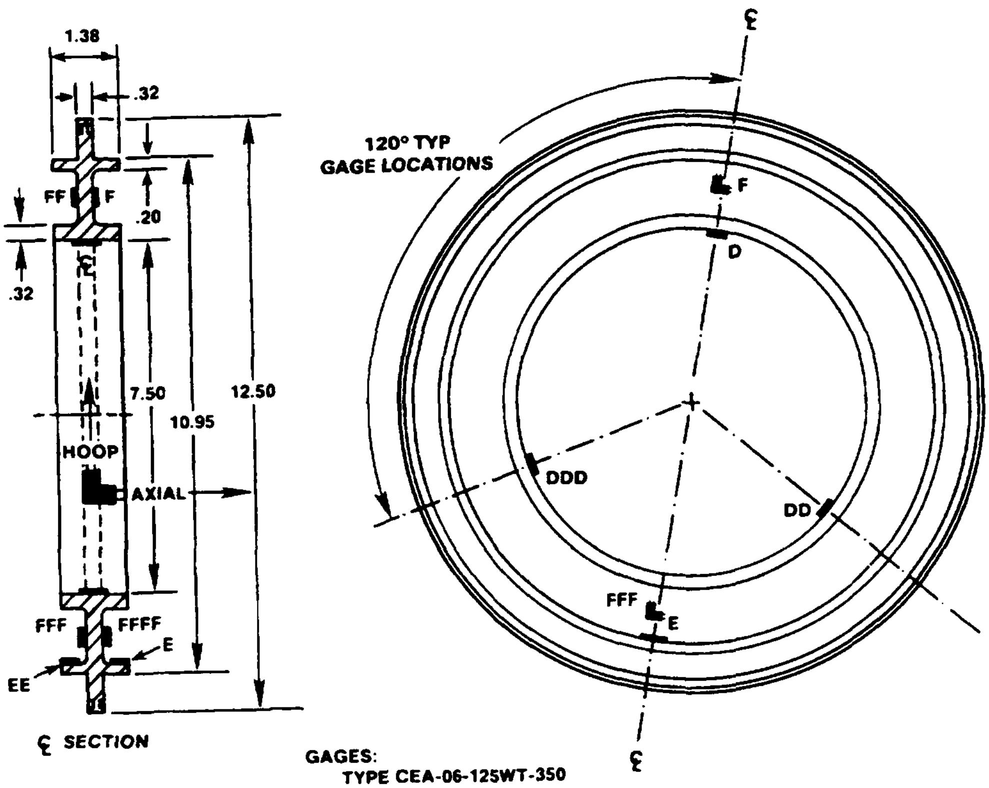

Figure B-18. Titanium ring stiffener DWG 0119738; locations of strain gages.

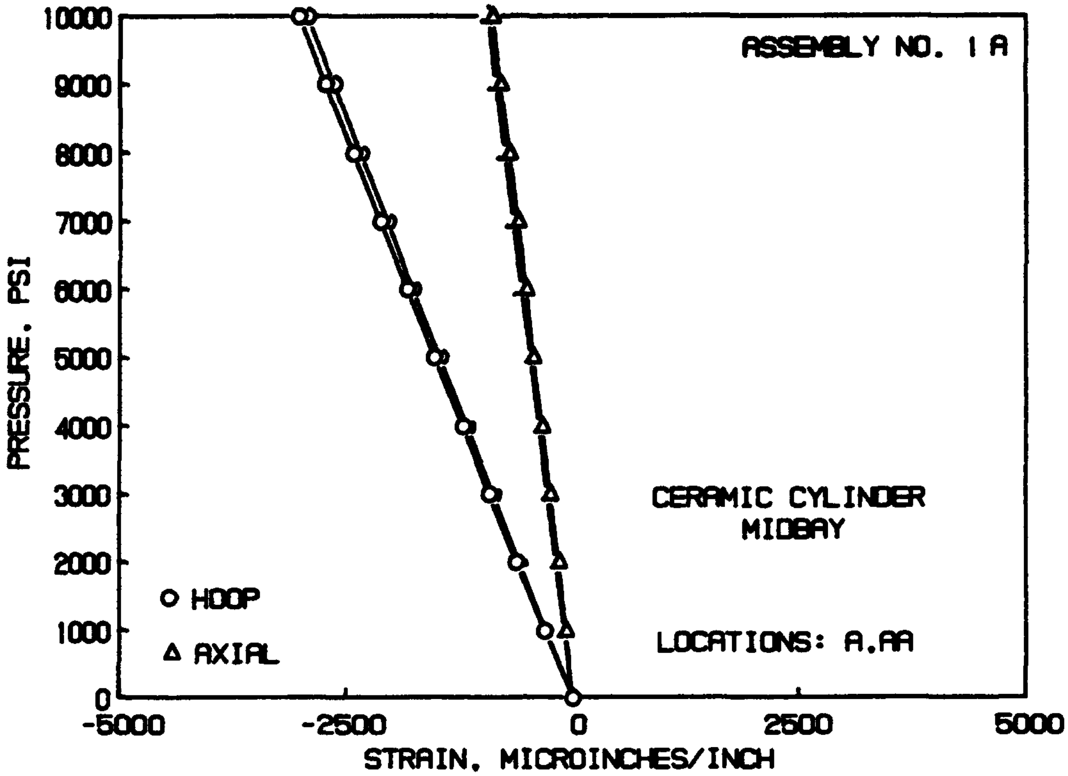

Figure B-19. Strains on housing test assembly 1A; locations A, AA.

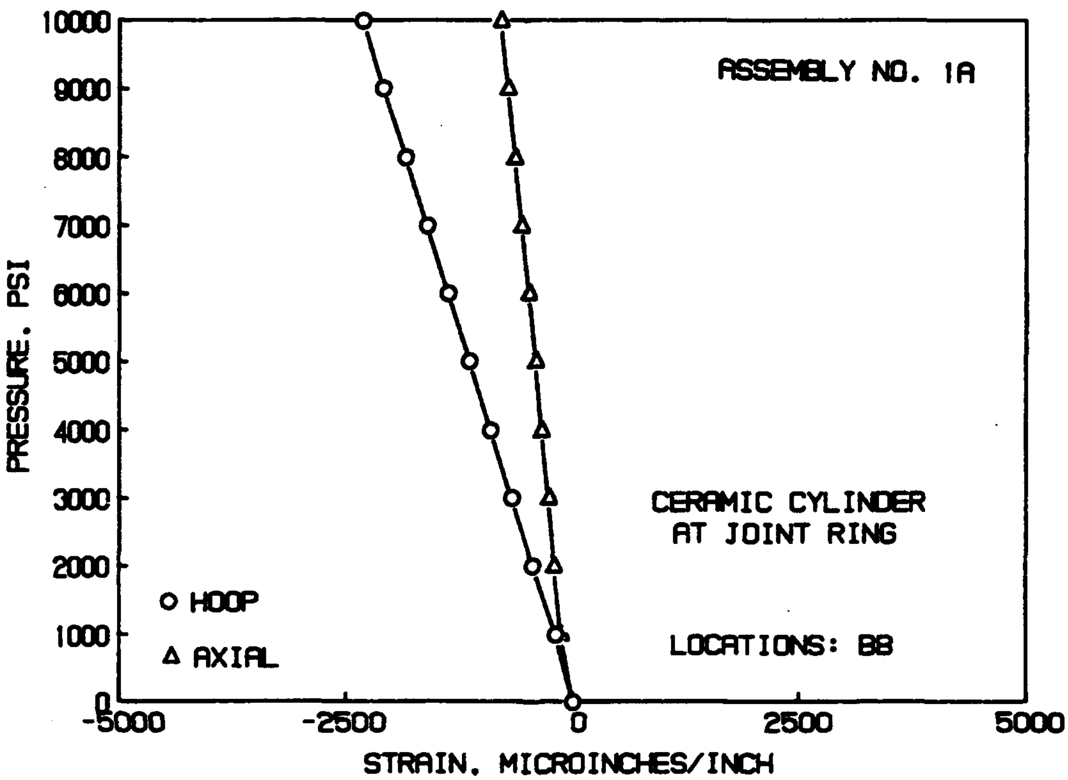

Figure B-20. Strains on housing test assembly 1A; location BB.

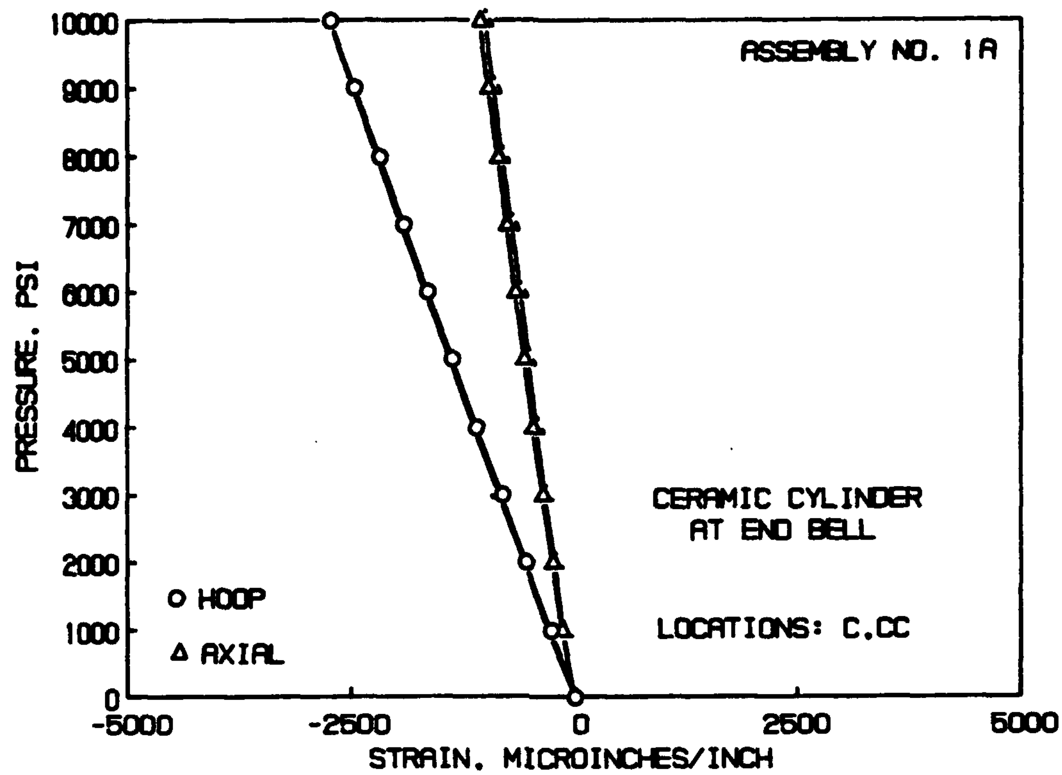

Figure B-21. Strains on housing test assembly 1A; locations C, CC.

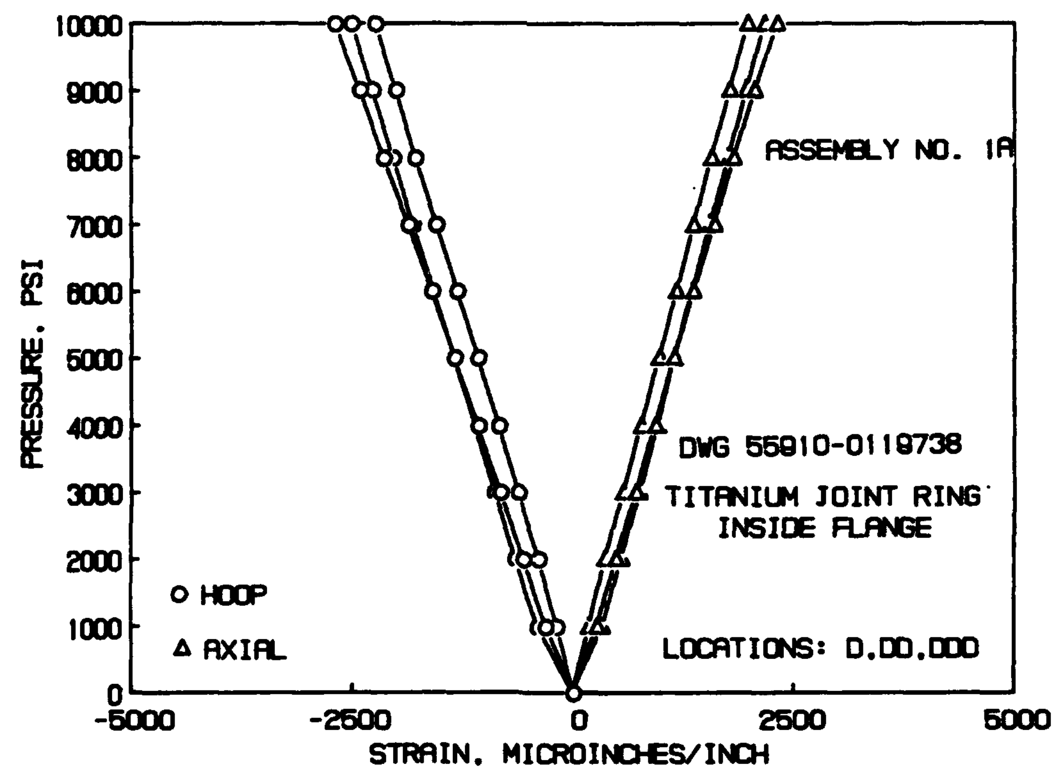

Figure B-22. Strains on housing test assembly 1A; locations D, DD, DDD.

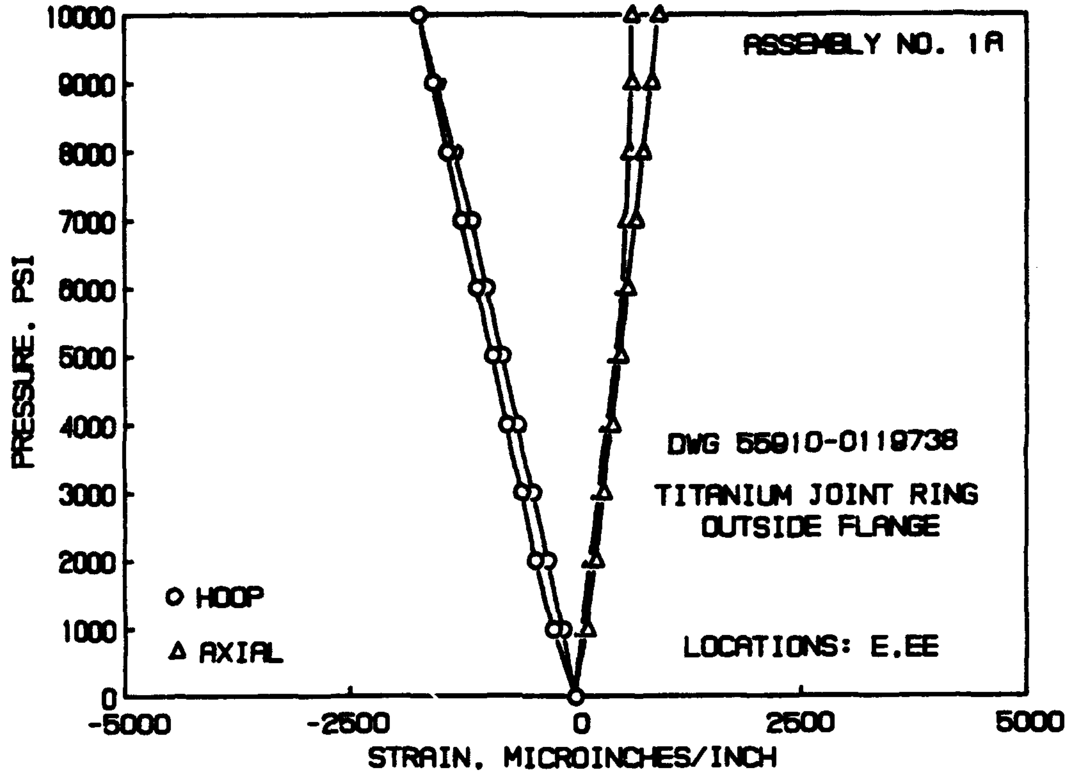

Figure B-23. Strains on housing test assembly 1A; locations E, EE.

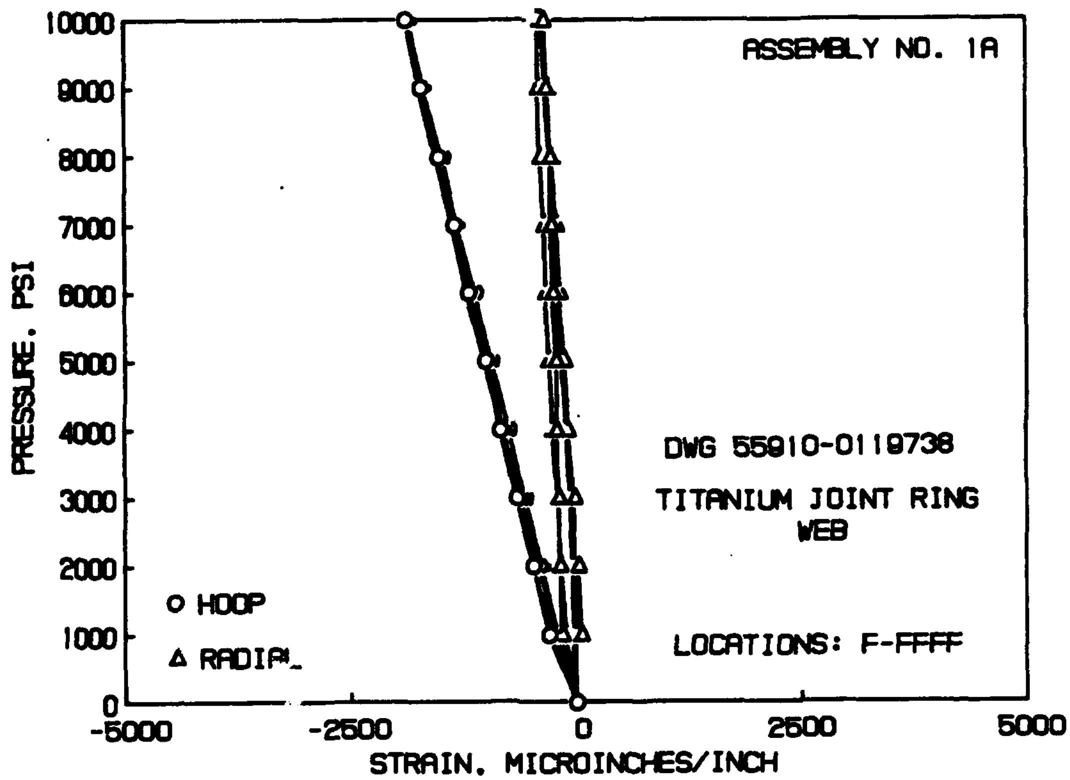

Figure B-24. Strains on housing test assembly 1A; locations F, FF.

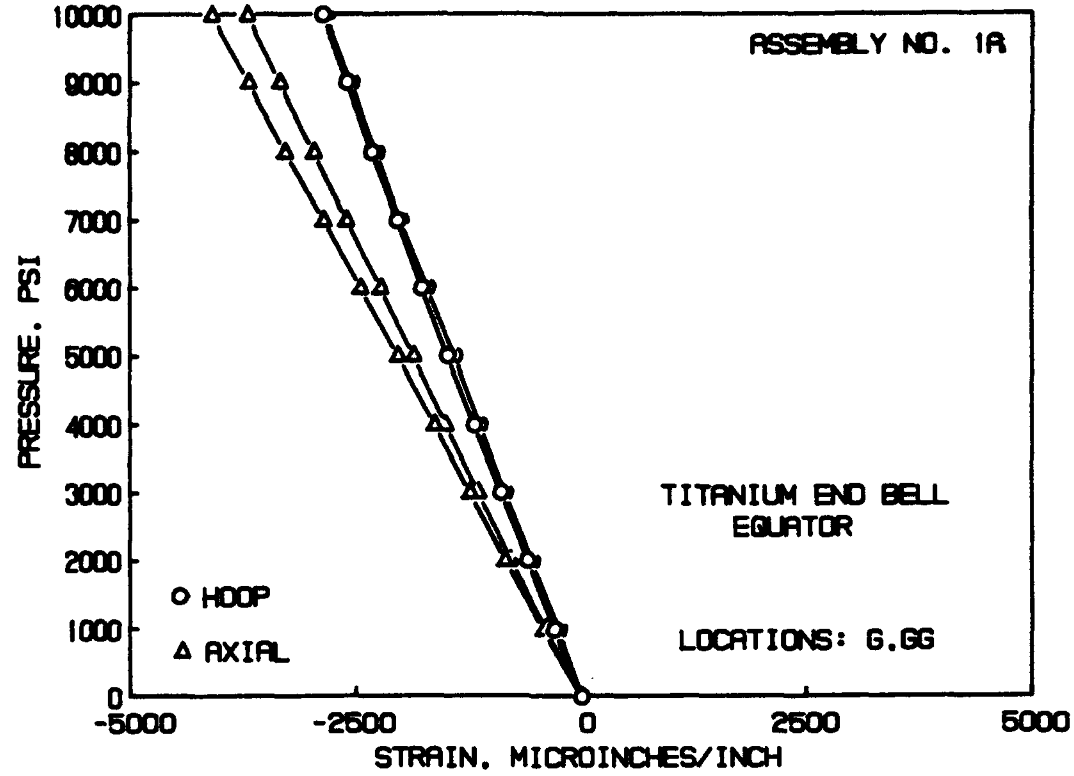

Figure B-25. Strains on housing test assembly 1A; locations G, GG.

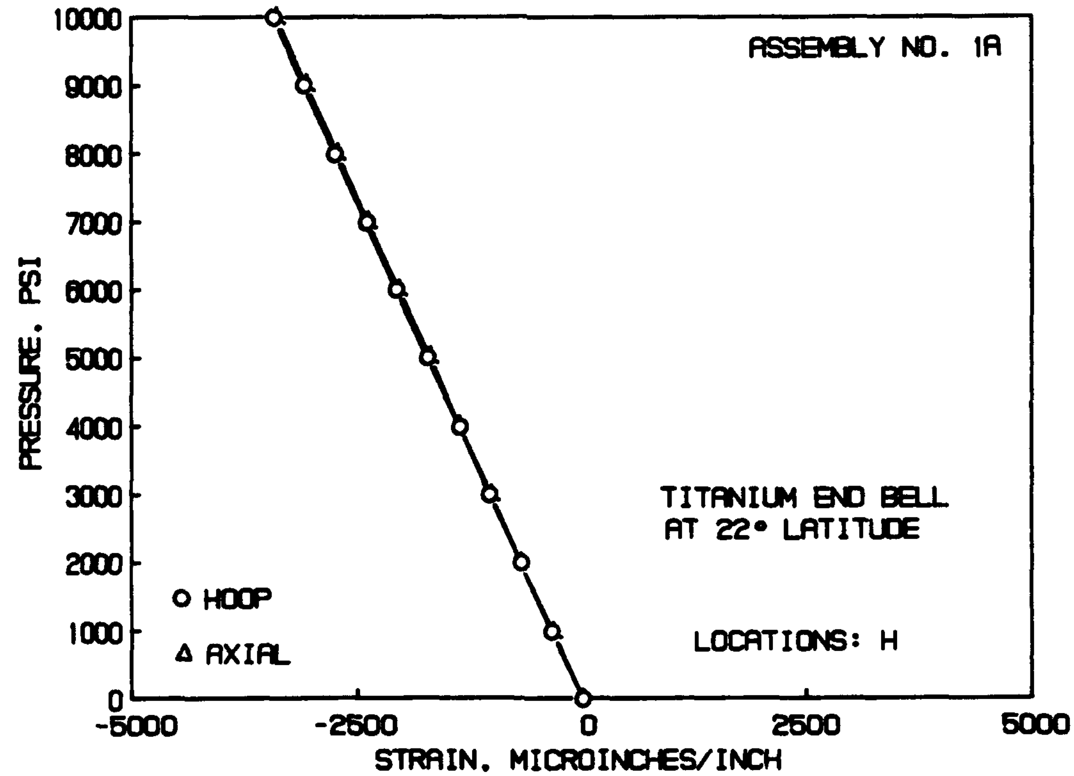

Figure B-26. Strains on housing test assembly 1A; location H.

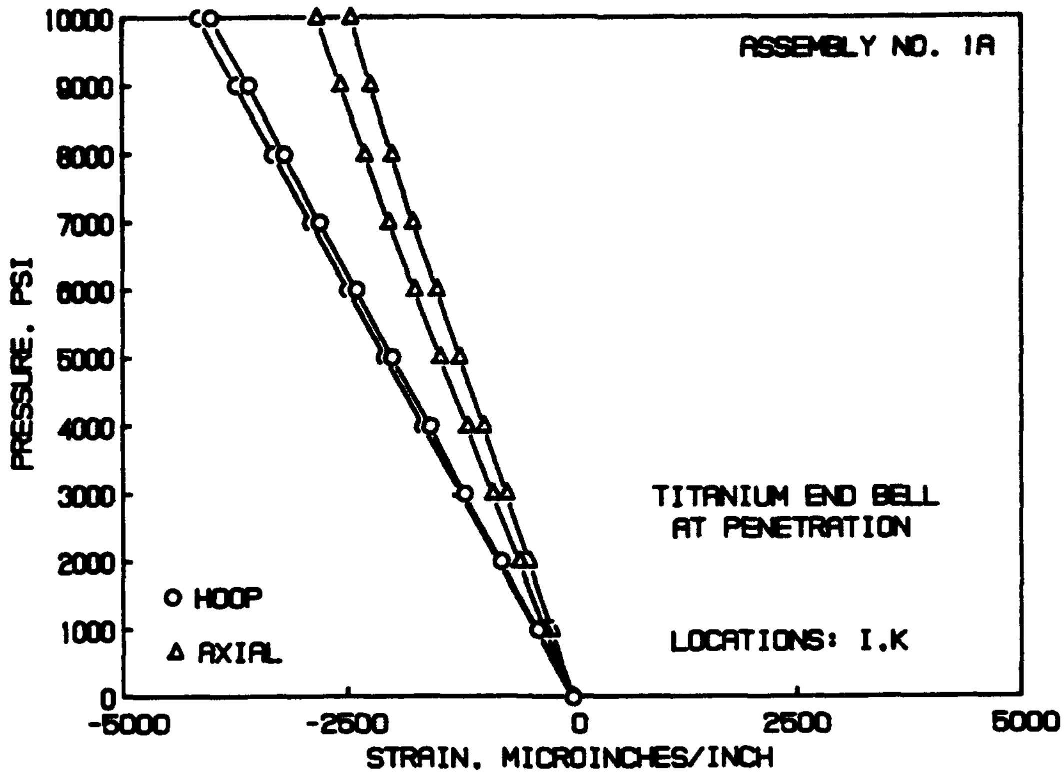

Figure B-27. Strains on housing test assembly 1A; locations I, K.

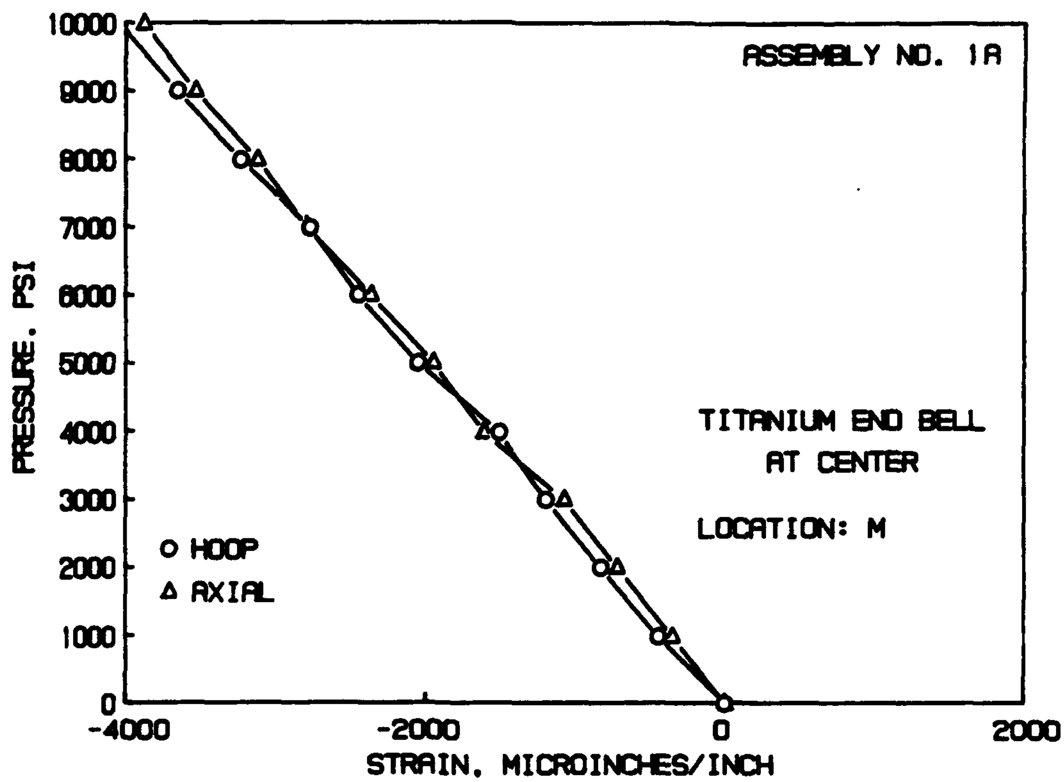

Figure B-28. Strains on housing test assembly 1A; location M.

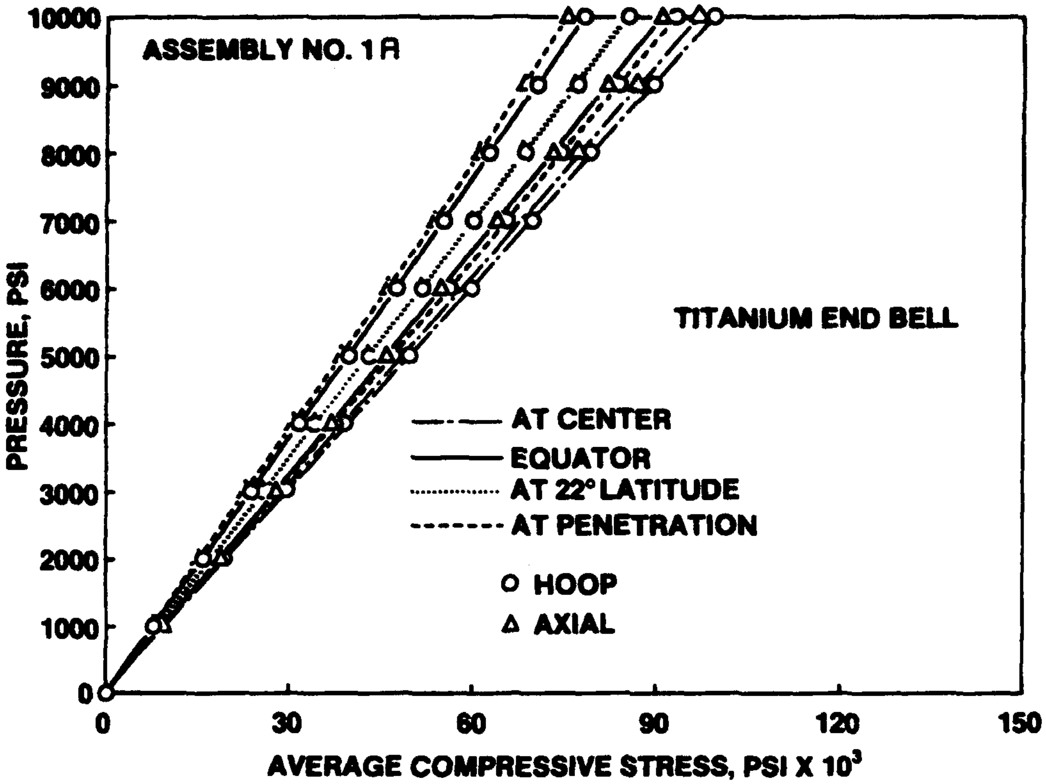

Figure B-29. Stresses on housing test assembly 1A; location–titanium end bell DWG 0119737.

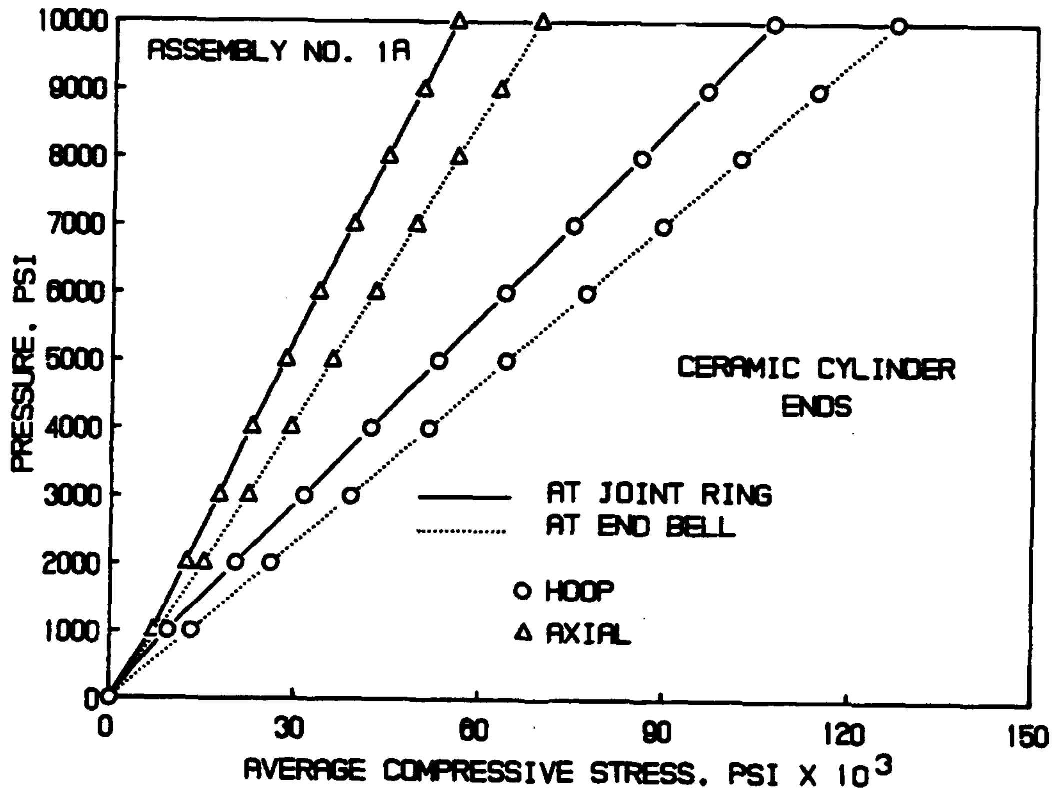

Figure B-30. Stresses on housing test assembly 1A; location–ceramic cylinder ends.

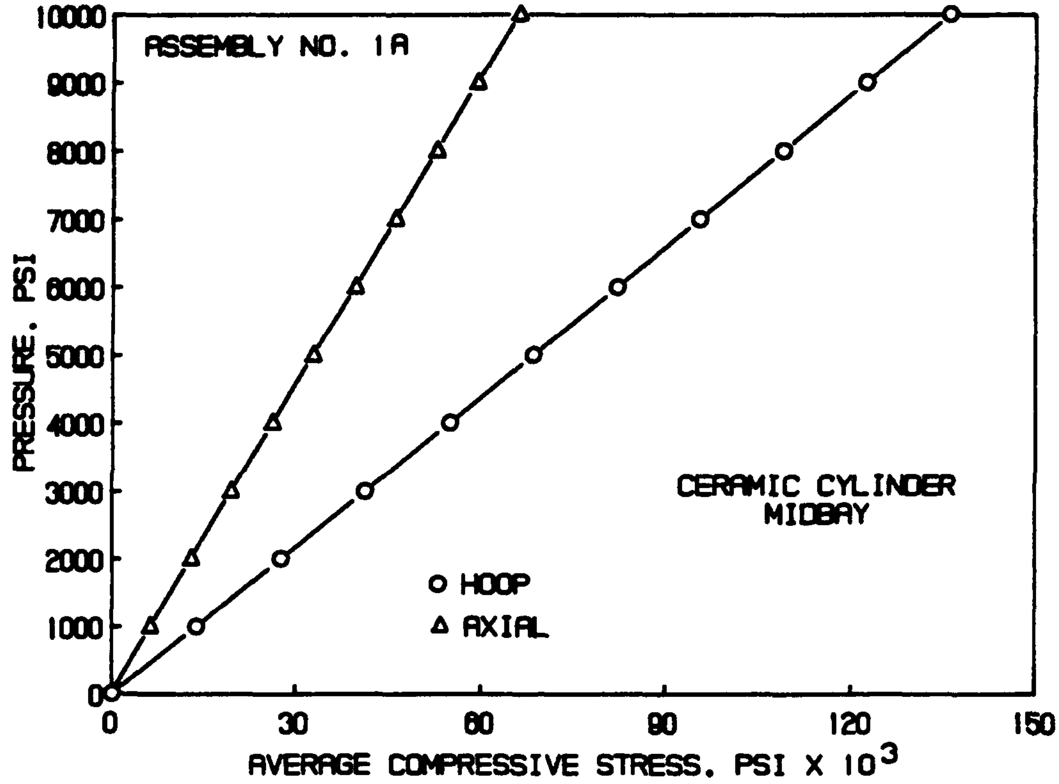

Figure B-31. Stresses on housing test assembly 1A; location–ceramic cylinder midbay.

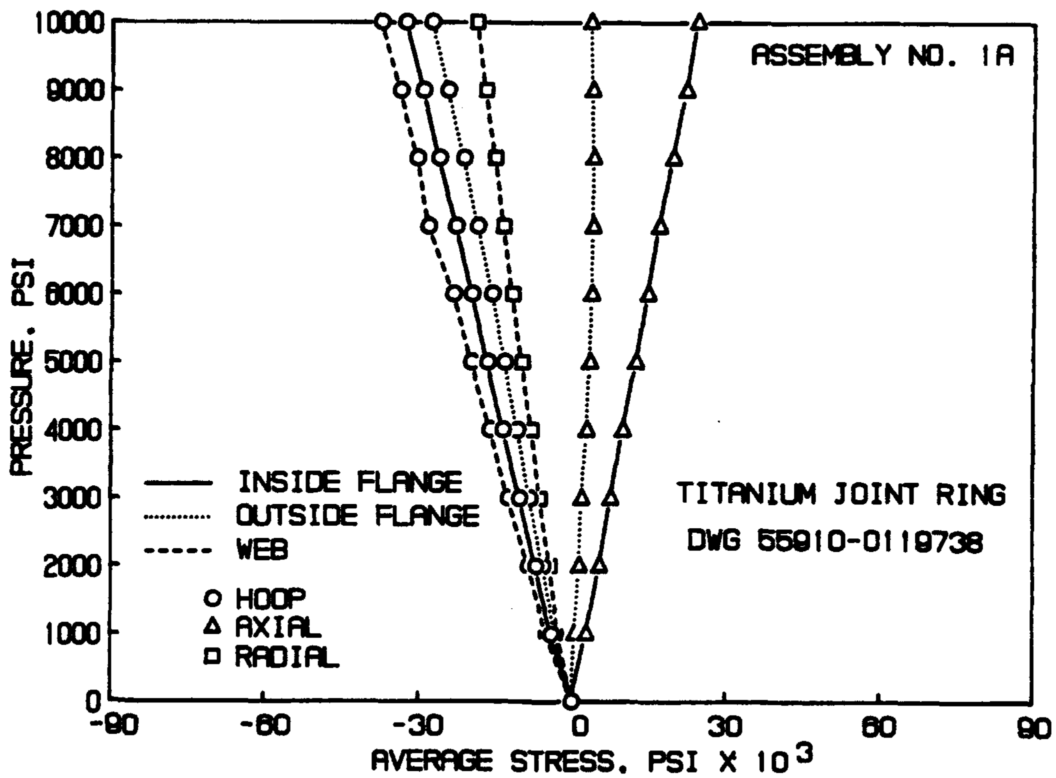

Figure B-32. Stresses on housing test assembly 1A; location–titanium joint ring DWG 0119738.

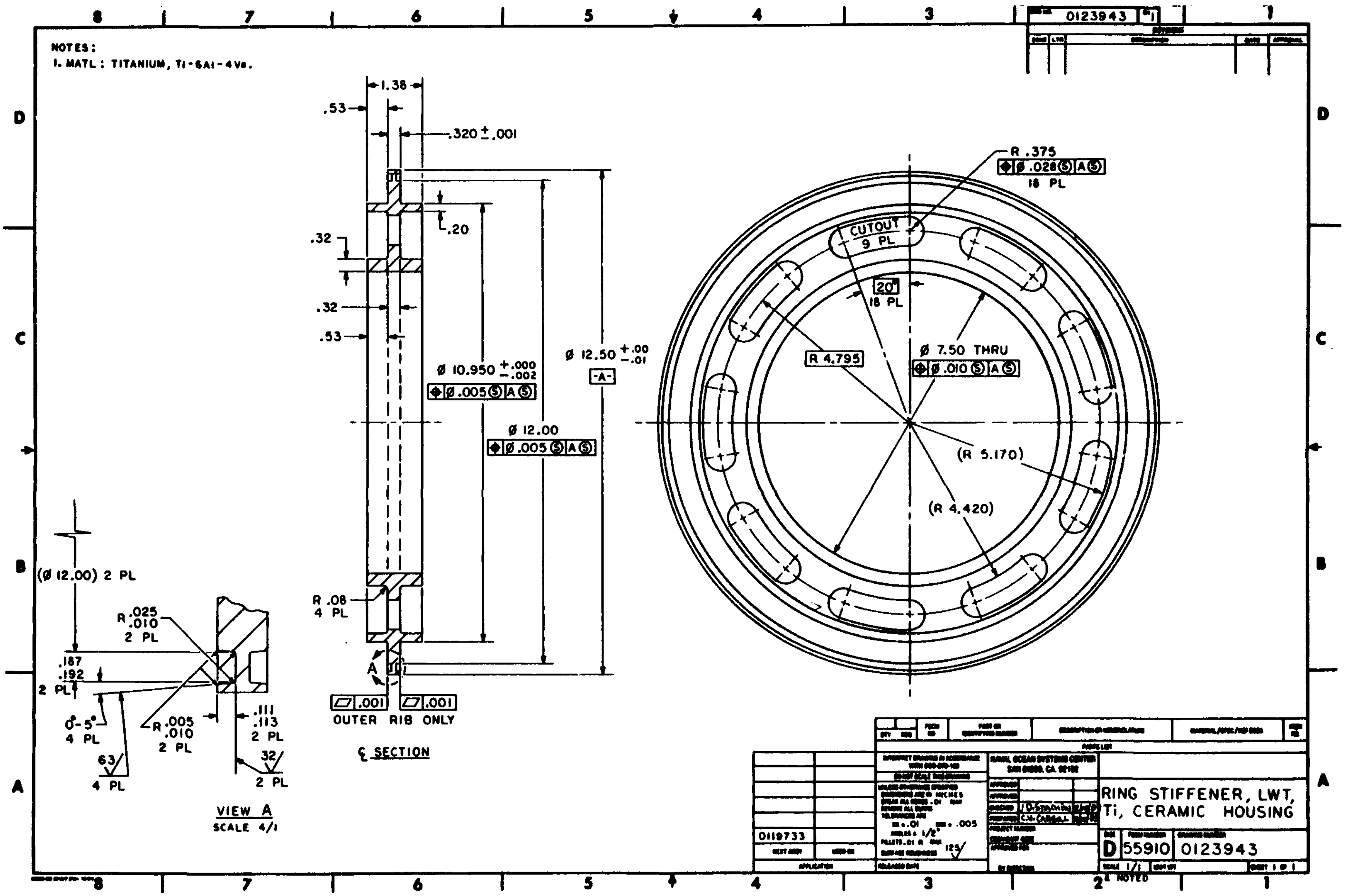

Figure B-33. Titanium ring stiffener DWG 0123943; fabrication drawing.

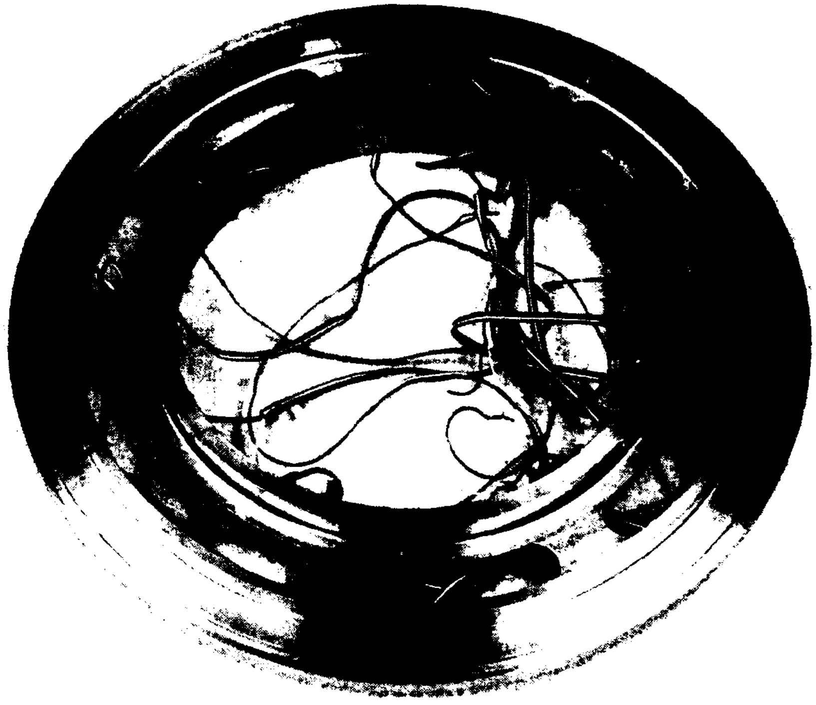

Figure B-34. Titanium ring stiffener DWG 0123943; exterior view.

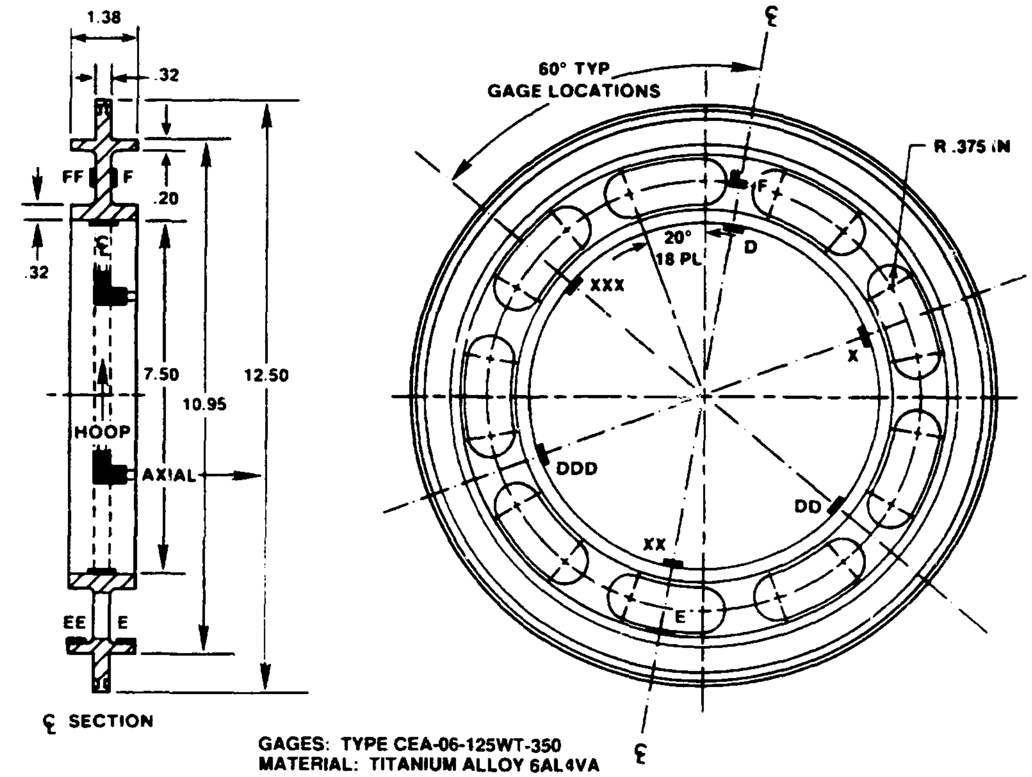

Figure B-35. Titanium ring stiffener DWG 0123943; location of gages.

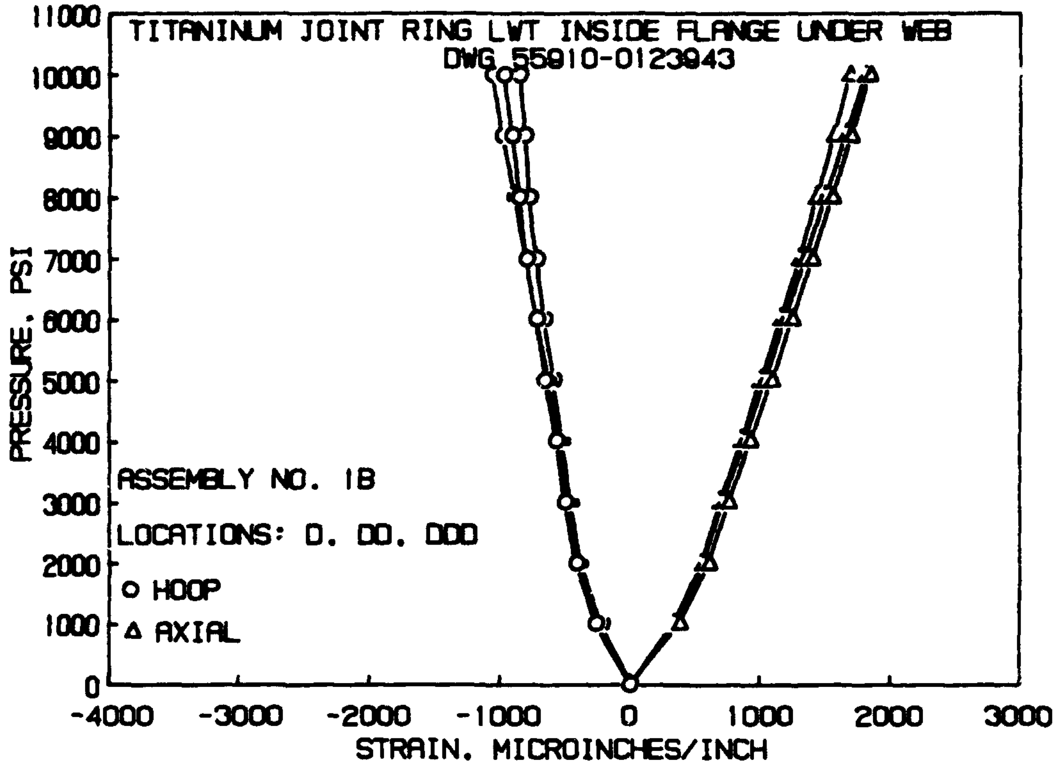

Figure B-36. Strains on housing test assembly 1B; locations D, DD, DDD.

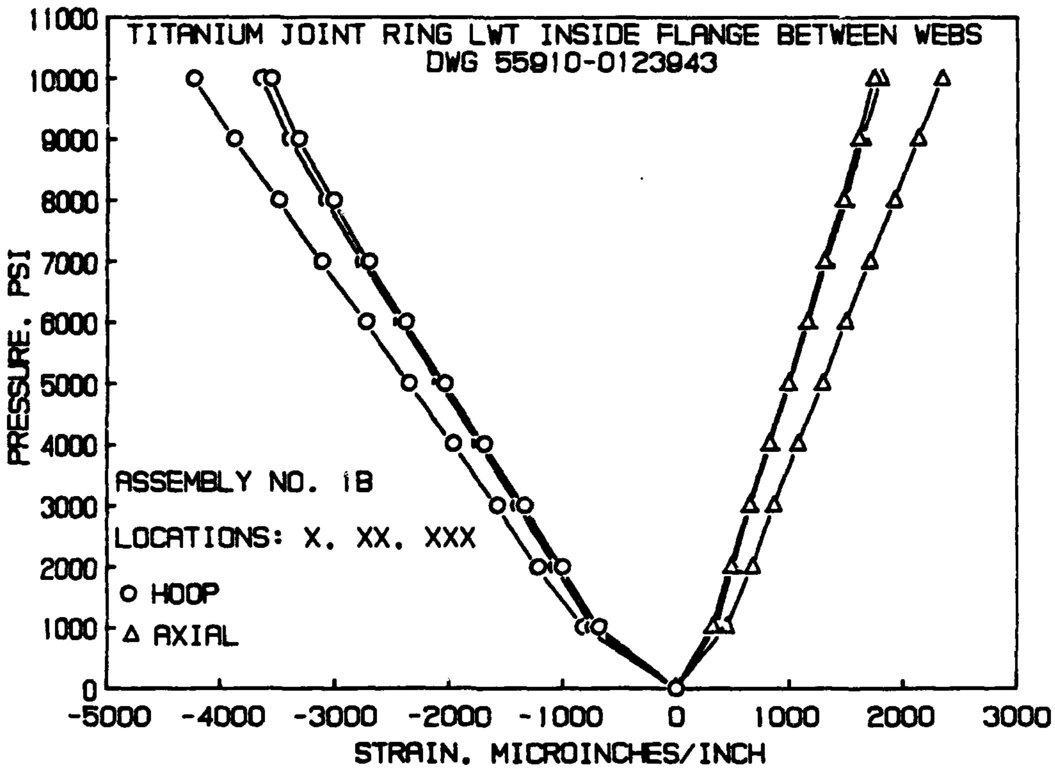

Figure B-37. Strains on housing test assembly 1B; locations X, XX, XXX.

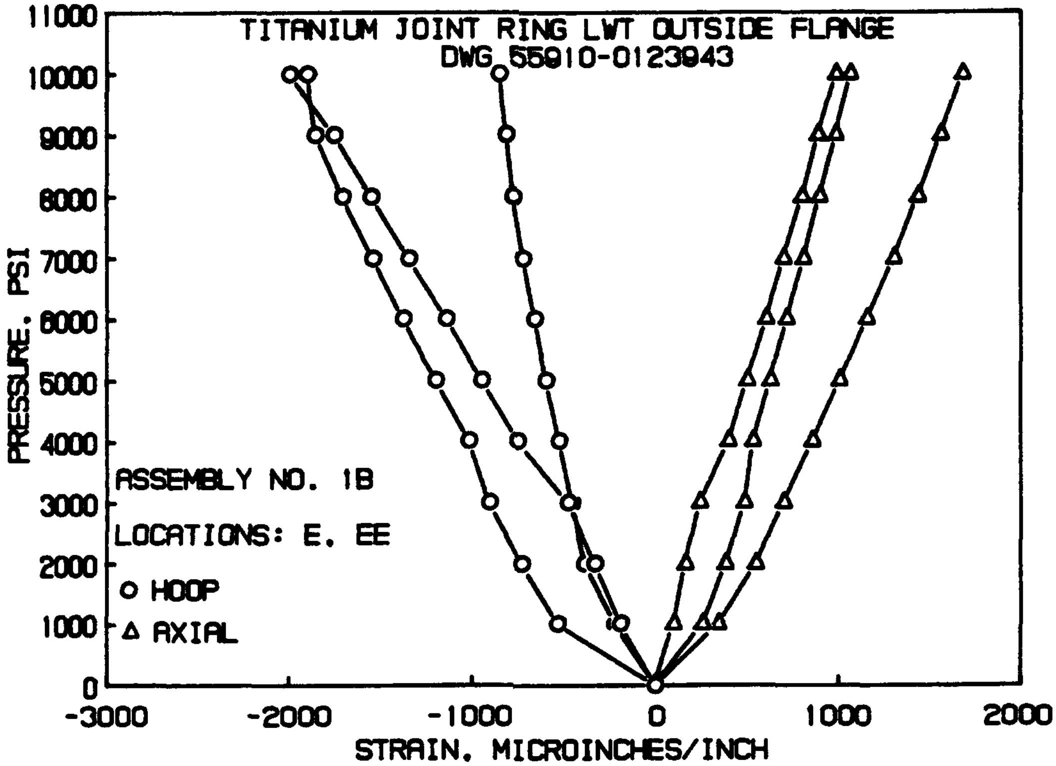

Figure B-38. Strains on housing test assembly 1B; locations E, EE.

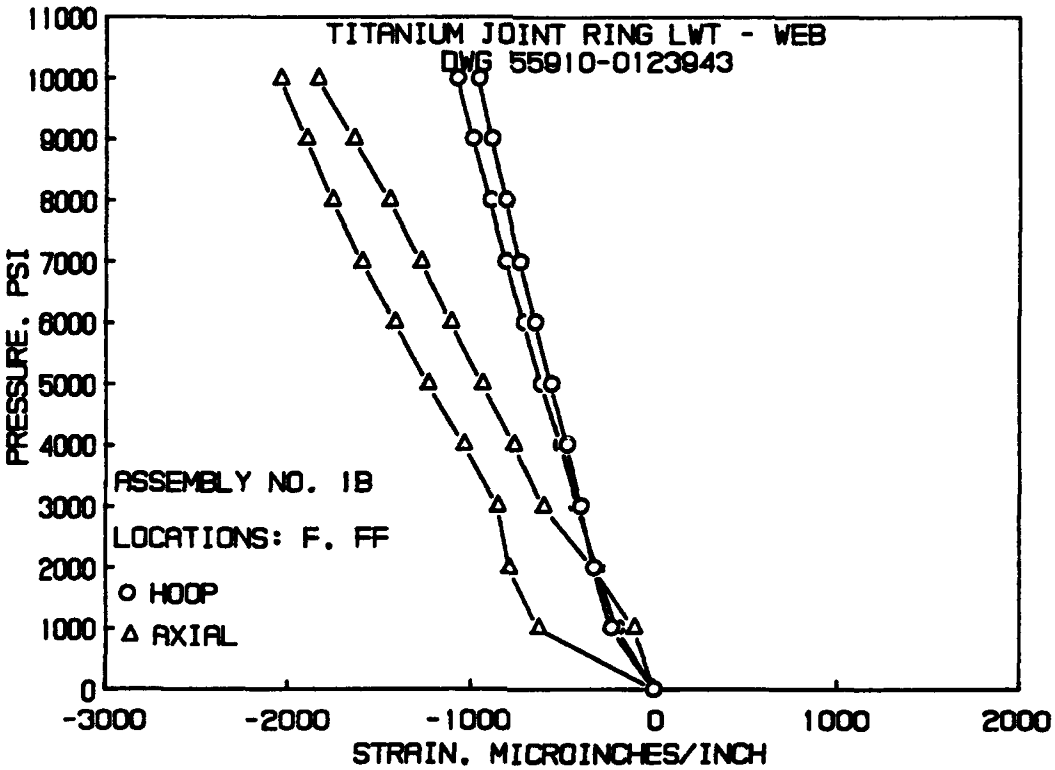

Figure B-39. Strains on housing test assembly 1B; locations F, FF.

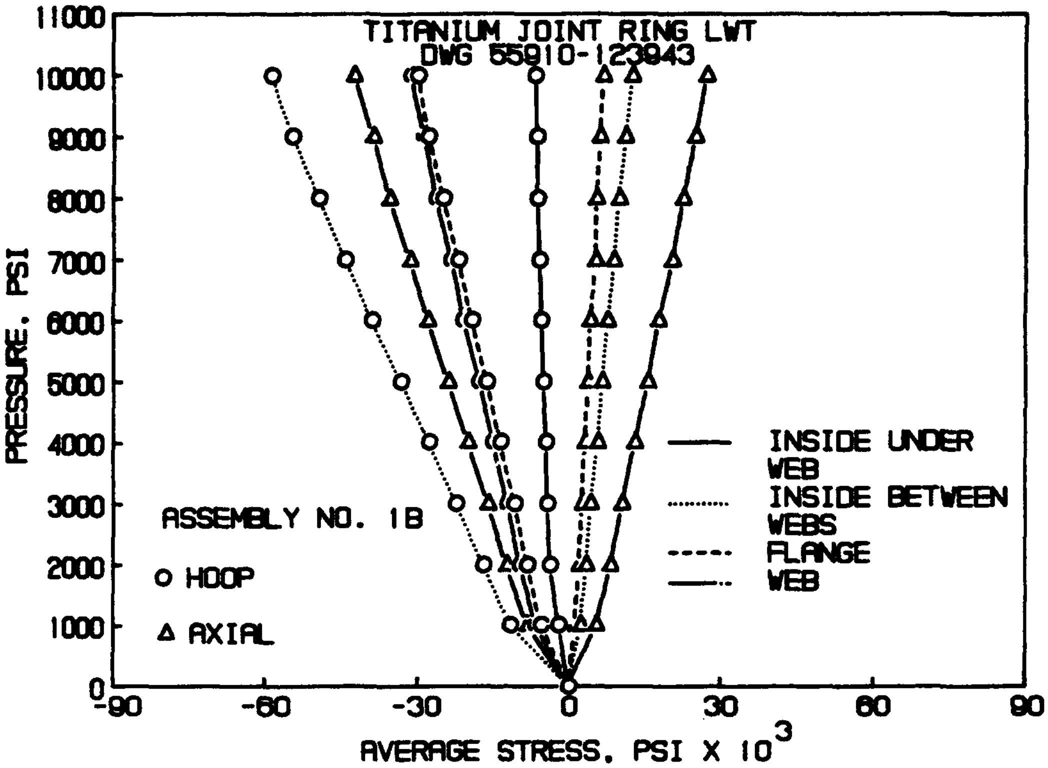

Figure B-40. Stresses on housing test assembly 1B; location–titanium joint ring DWG 0123943.

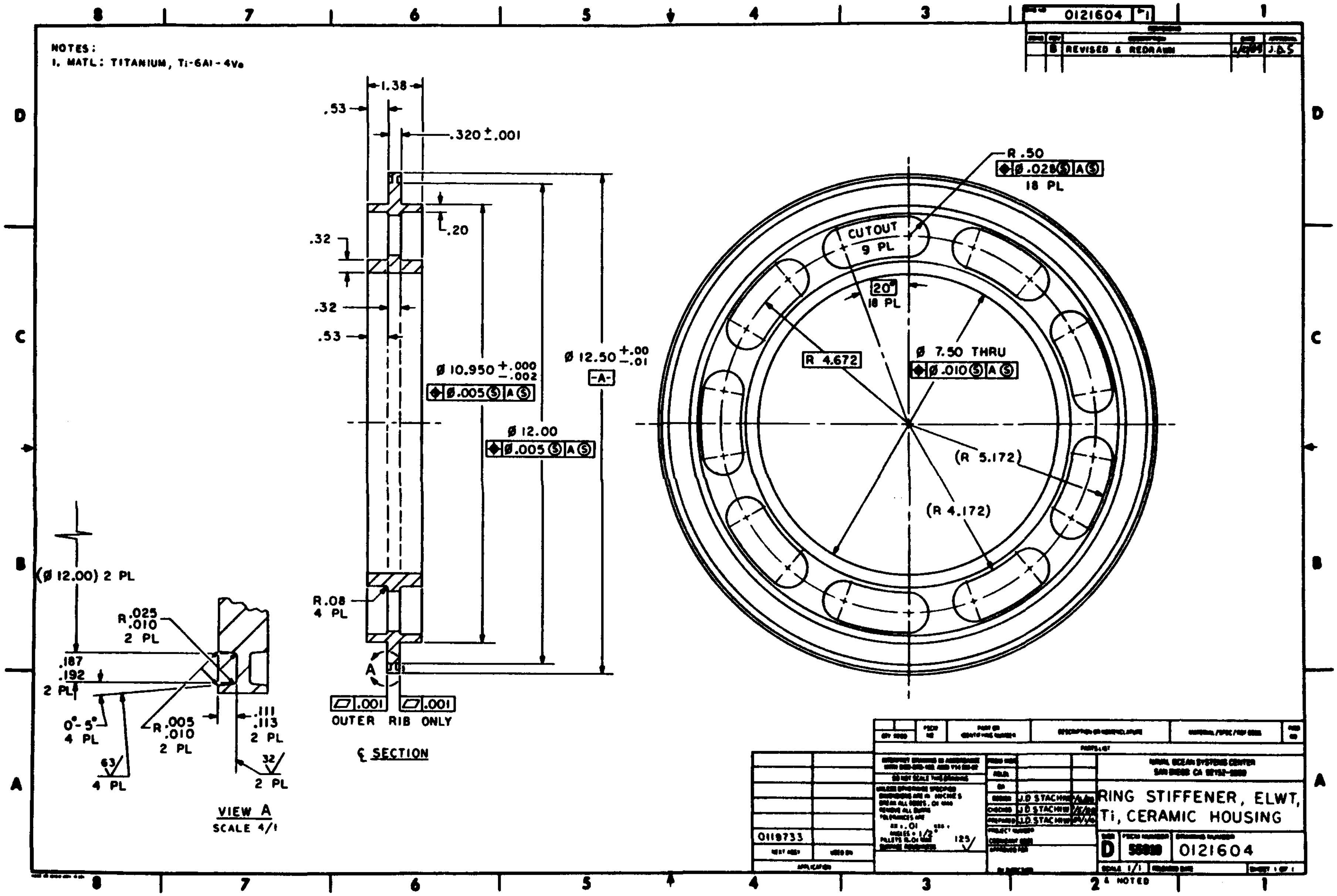

Figure B-41. Titanium ring stiffener DWG 0121604; fabrication drawing.

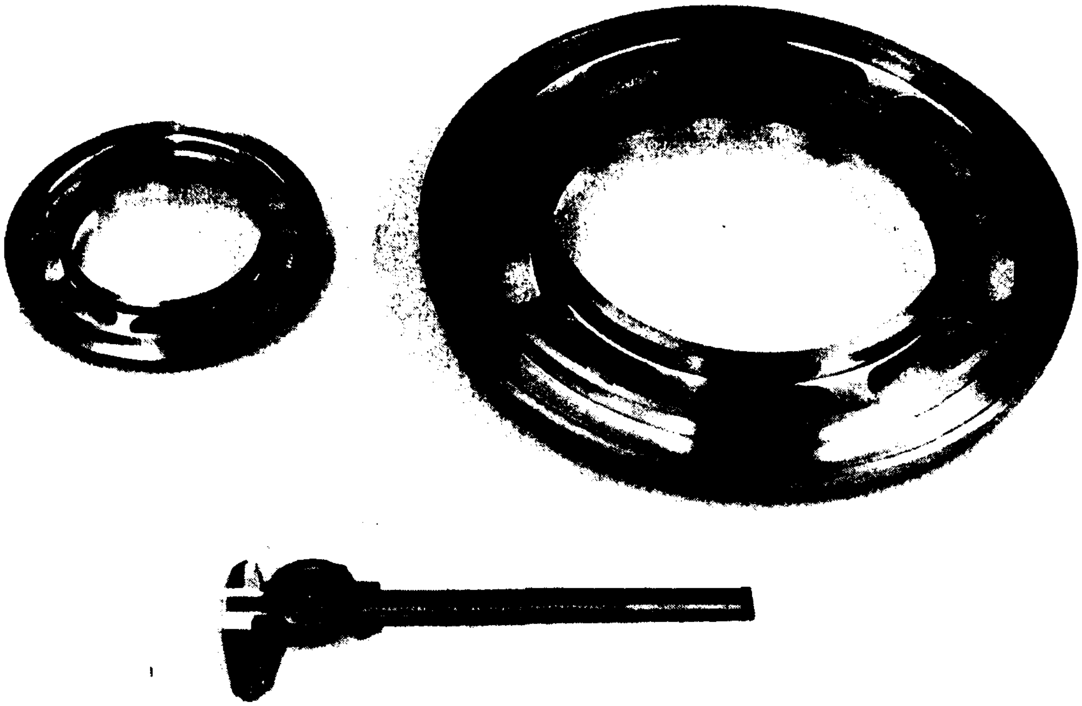

Figure B-42. Titanium ring stiffener DWG 0121604; exterior view.

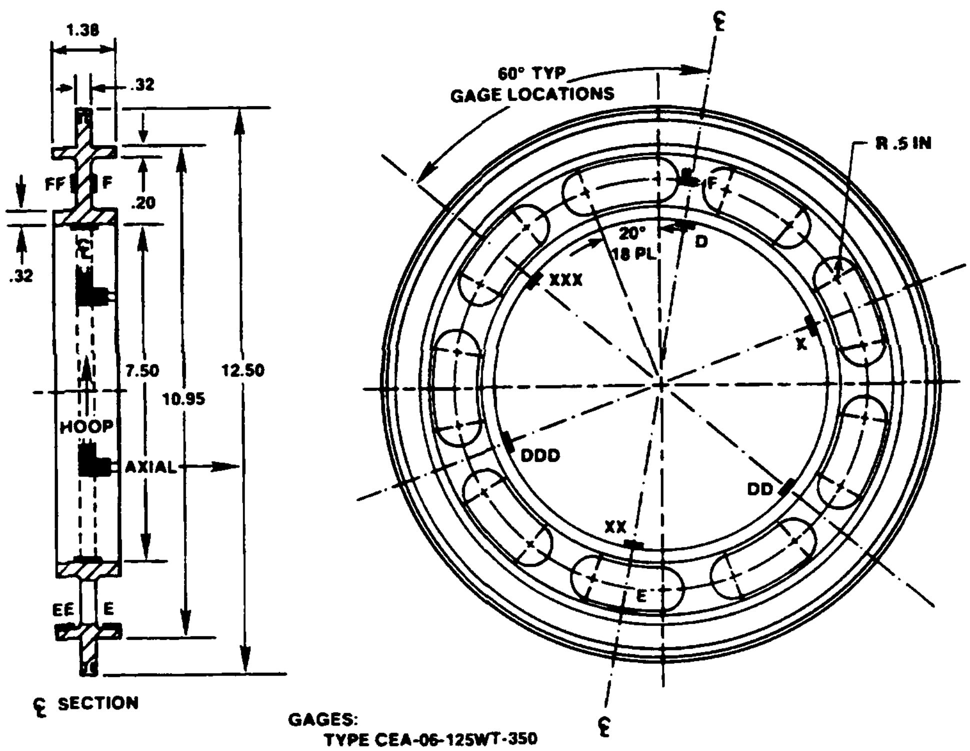

Figure B-43. Titanium ring stiffener DWG 0121604; location of gages.

Figure B-44. Failed ring stiffener DWG 0121604 after implosion of housing test assembly 1C at 9,910 psi.

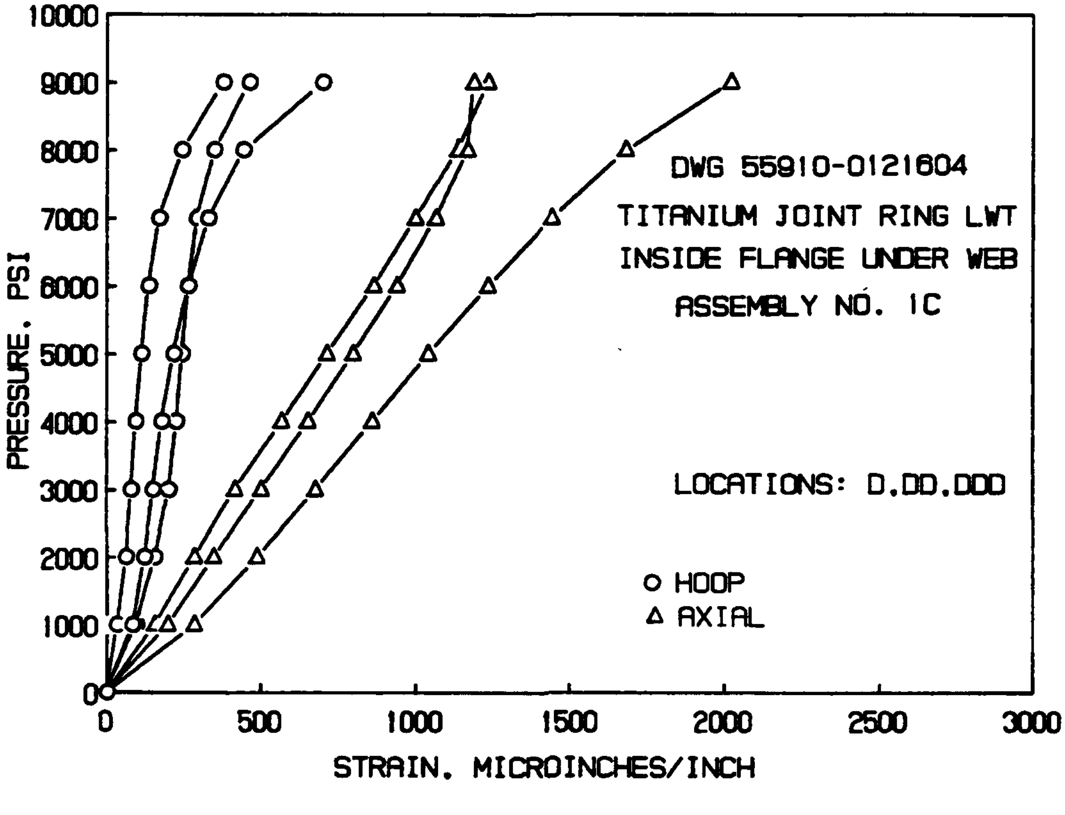

Figure B-45. Strains on housing test assembly 1C; locations D, DD, DDD.

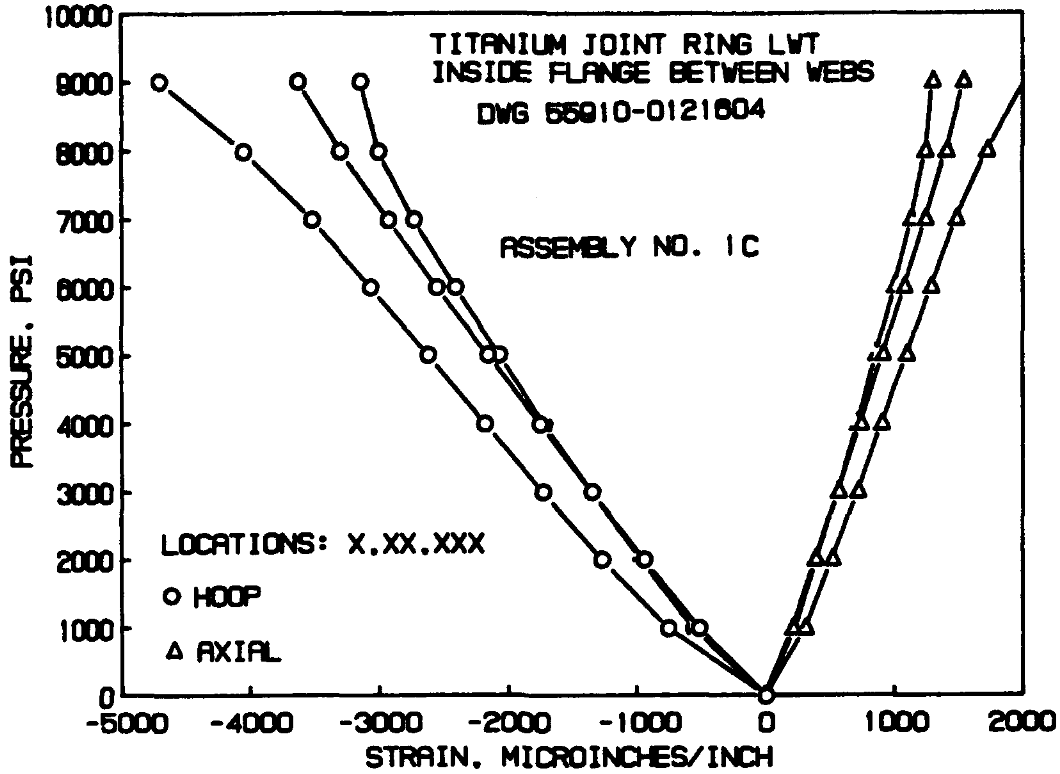

Figure B-46. Strains on housing test assembly 1C; locations X, XX, XXX.

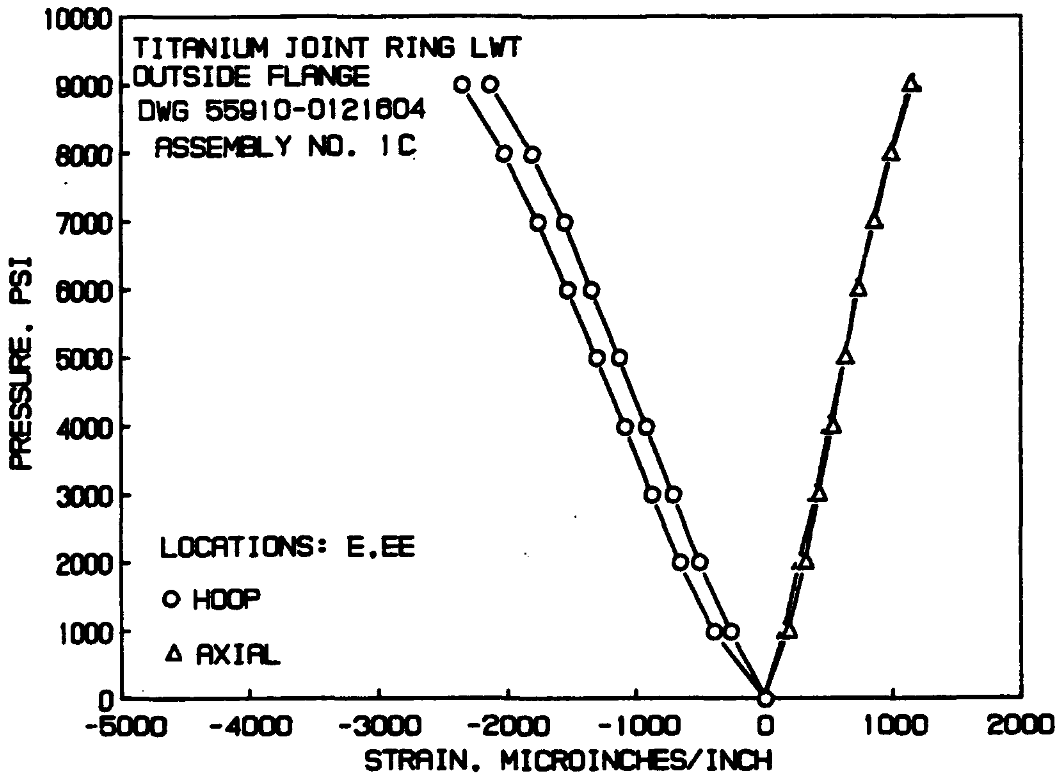

Figure B-47. Strains on housing test assembly 1C; locations E, EE.

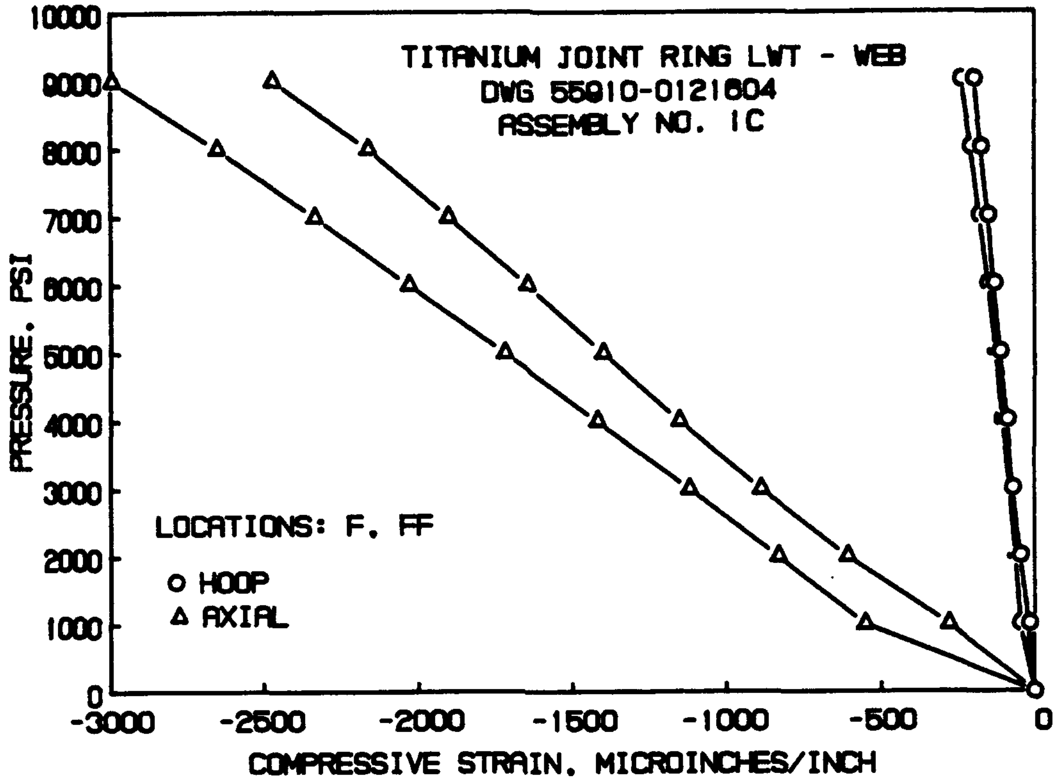

Figure B-48. Strains on housing test assembly 1C; locations F, FF.

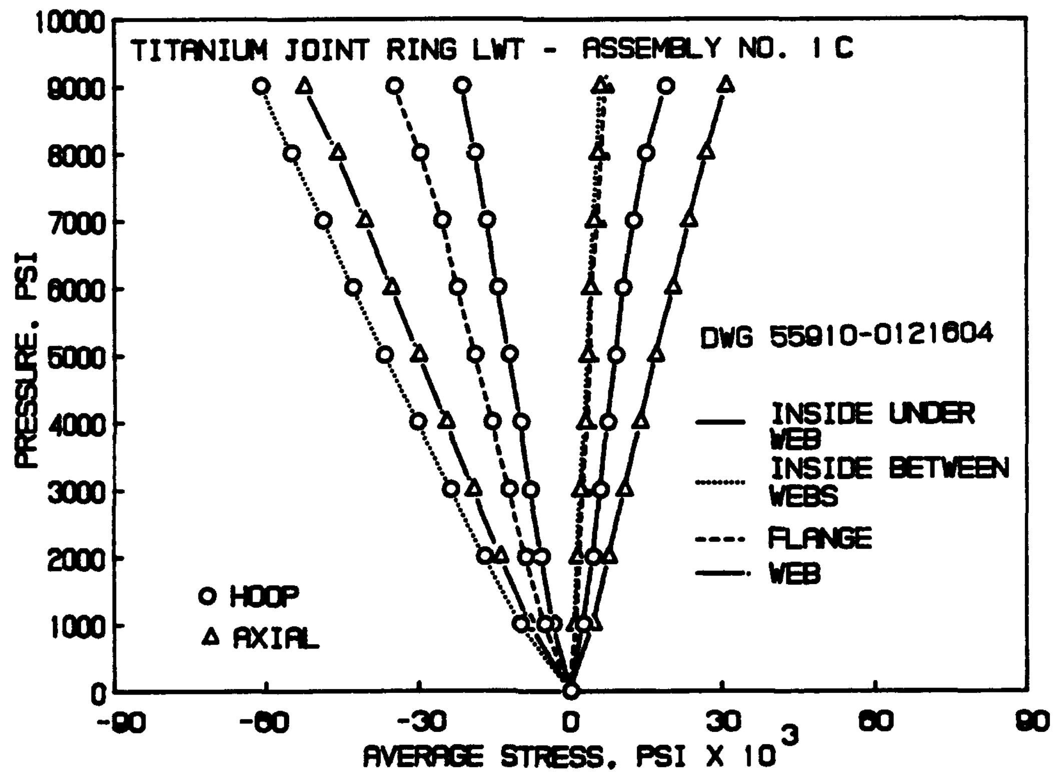

Figure B-49. Stresses on housing test assembly 1C; location–titanium joint ring DWG 0121604.

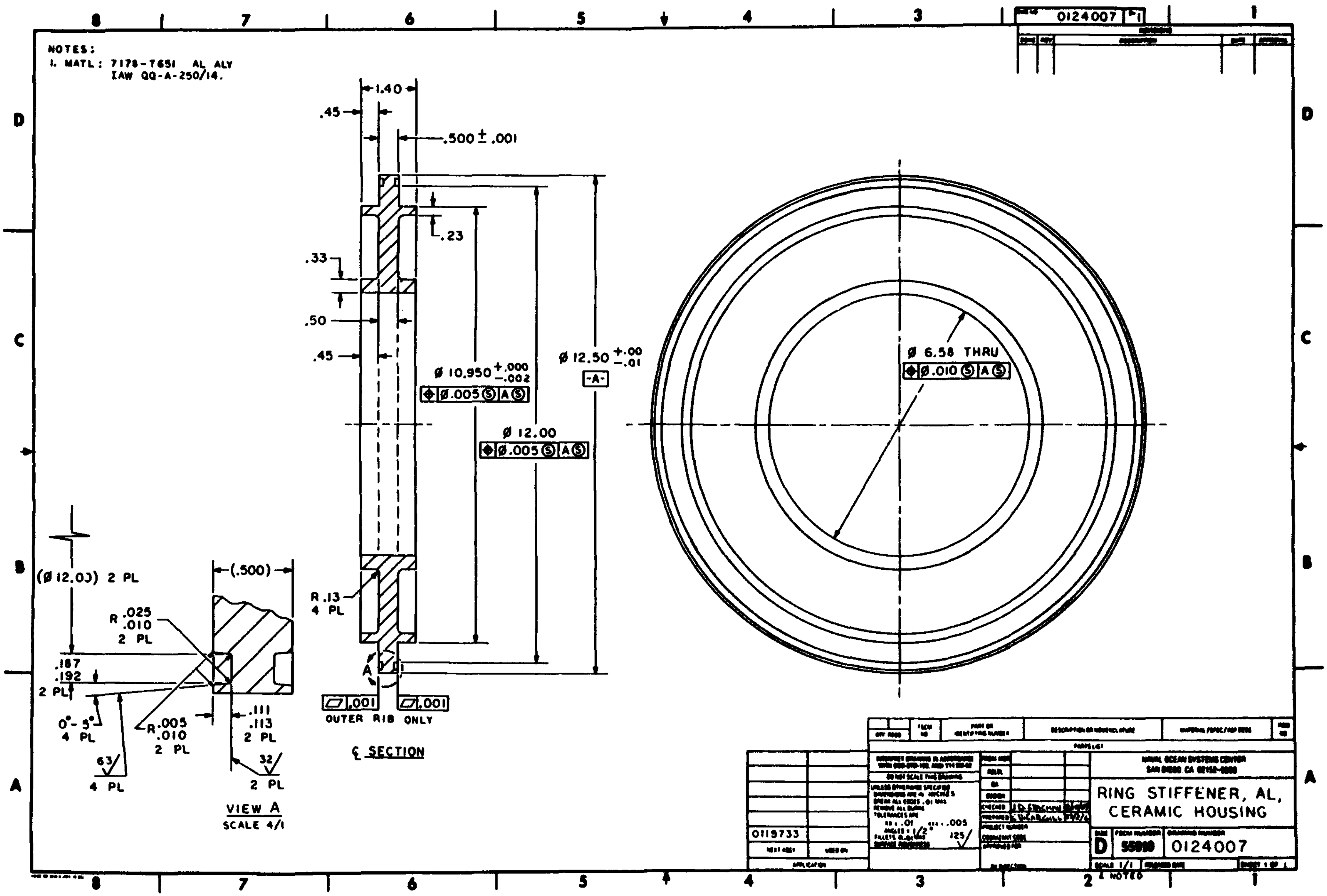

Figure B-50. Aluminum ring stiffener DWG 0124007; fabrication drawing.

Figure B-51. Aluminum ring stiffener DWG 0124007; exterior view.

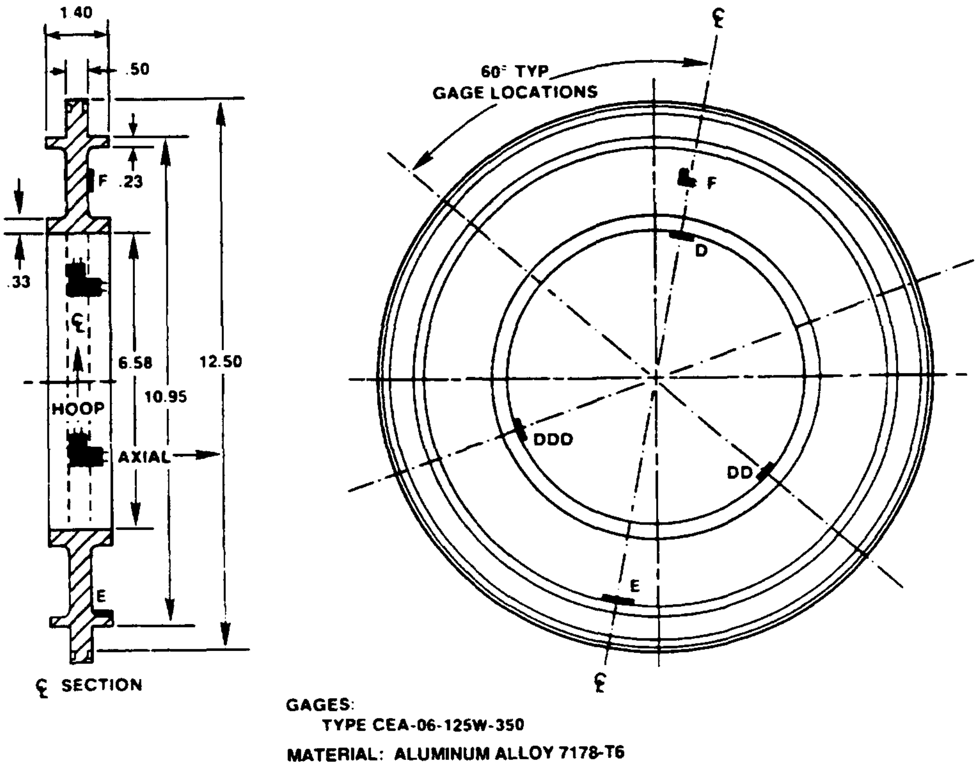

Figure B-52. Aluminum ring stiffener DWG 0124007; location of gages.

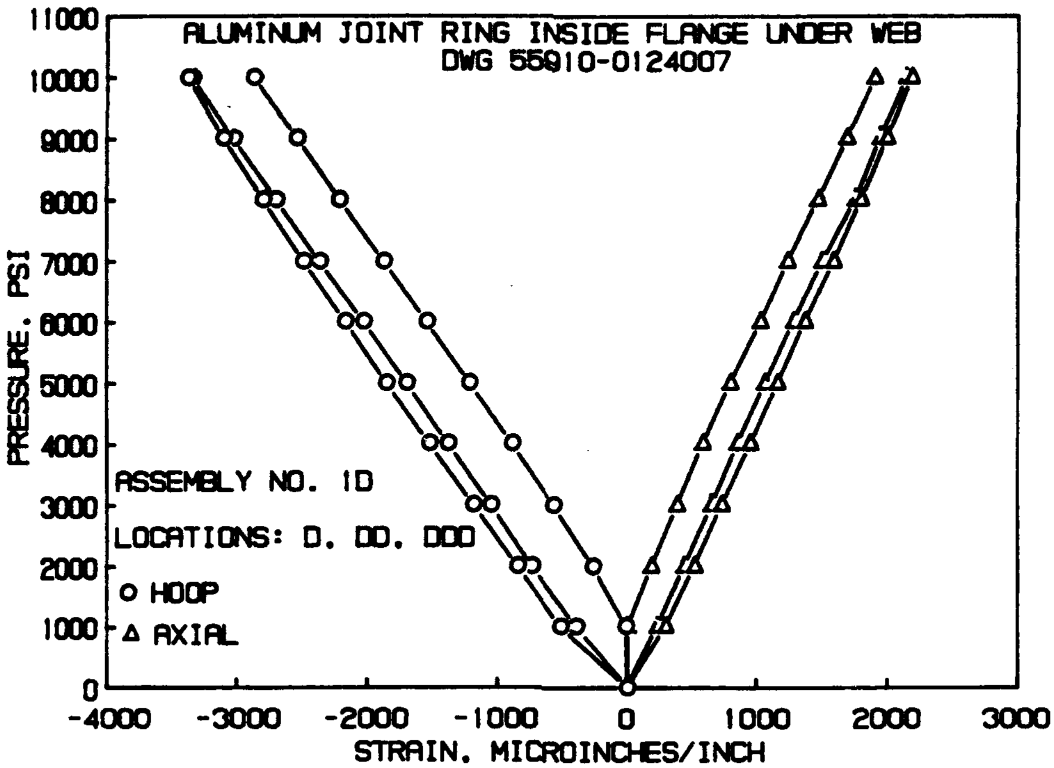

Figure B-53. Strains on housing test assembly 1D; locations D, DD, DDD.

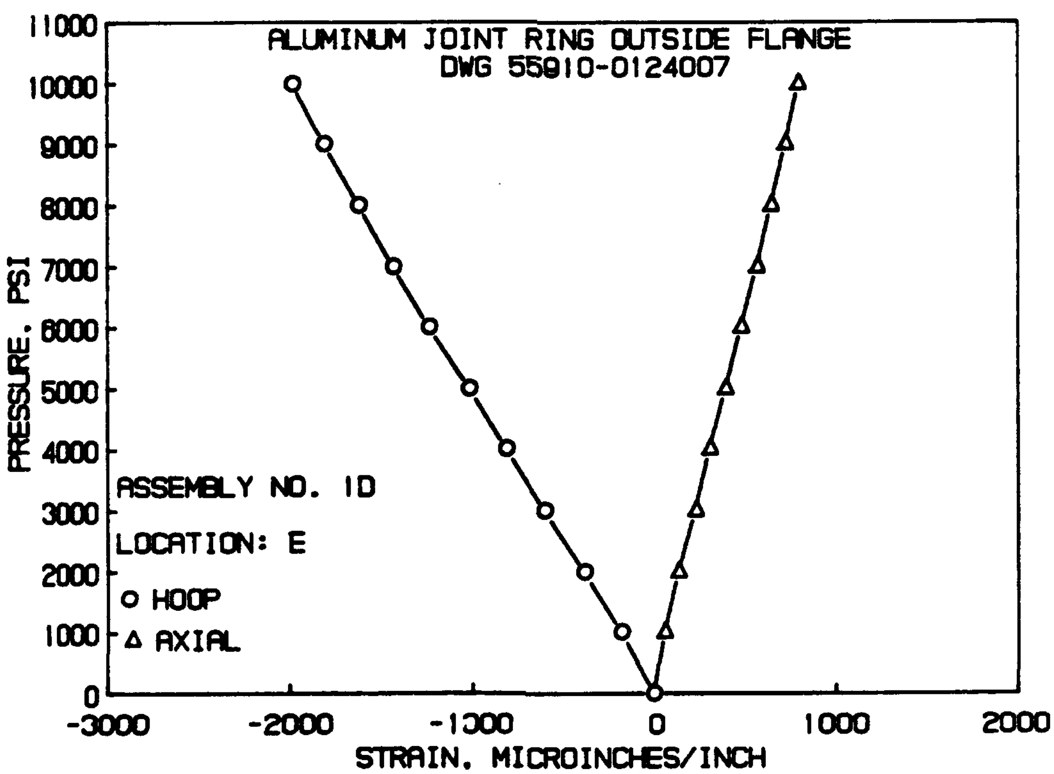

Figure B-54. Strains on housing test assembly 1D; location E.

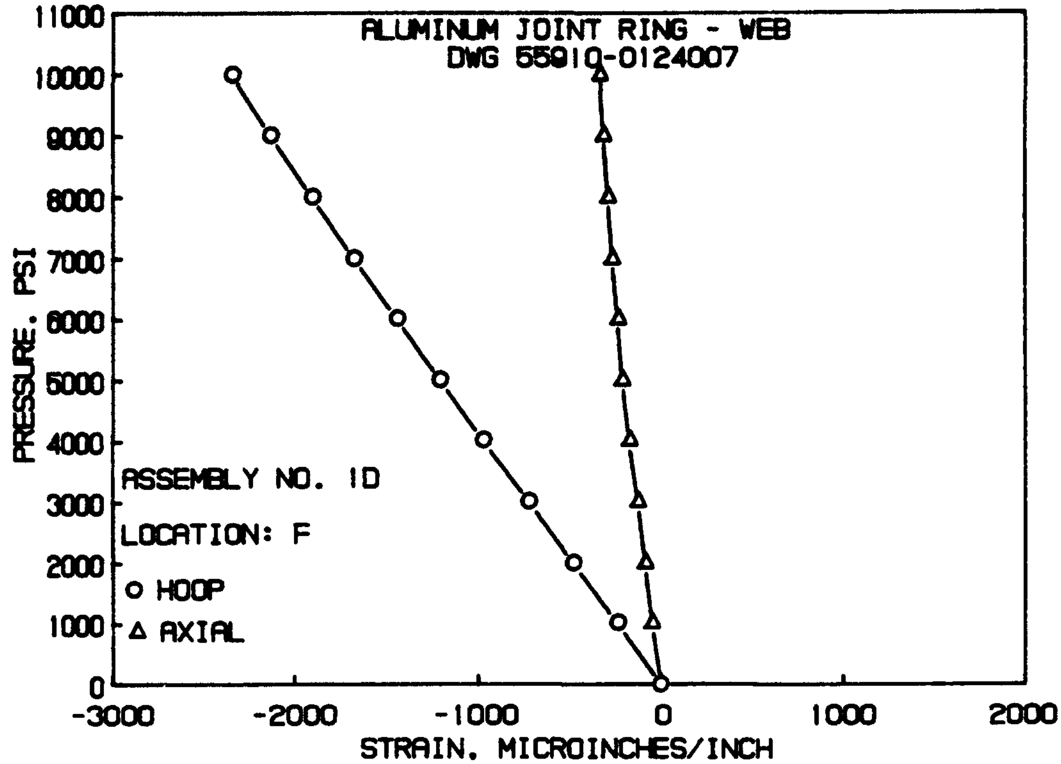

Figure B-55. Strains on housing test assembly 1D; location F.

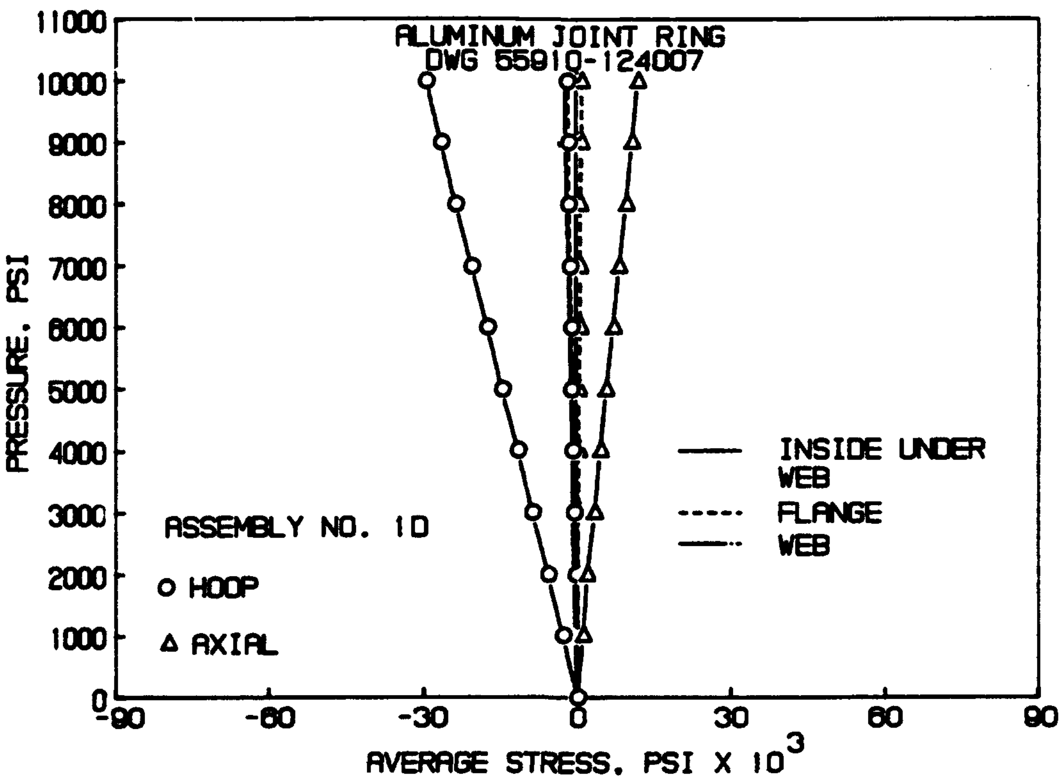

Figure B-56. Stresses housing test assembly 1D; location–aluminum joint ring DWG 0124007.

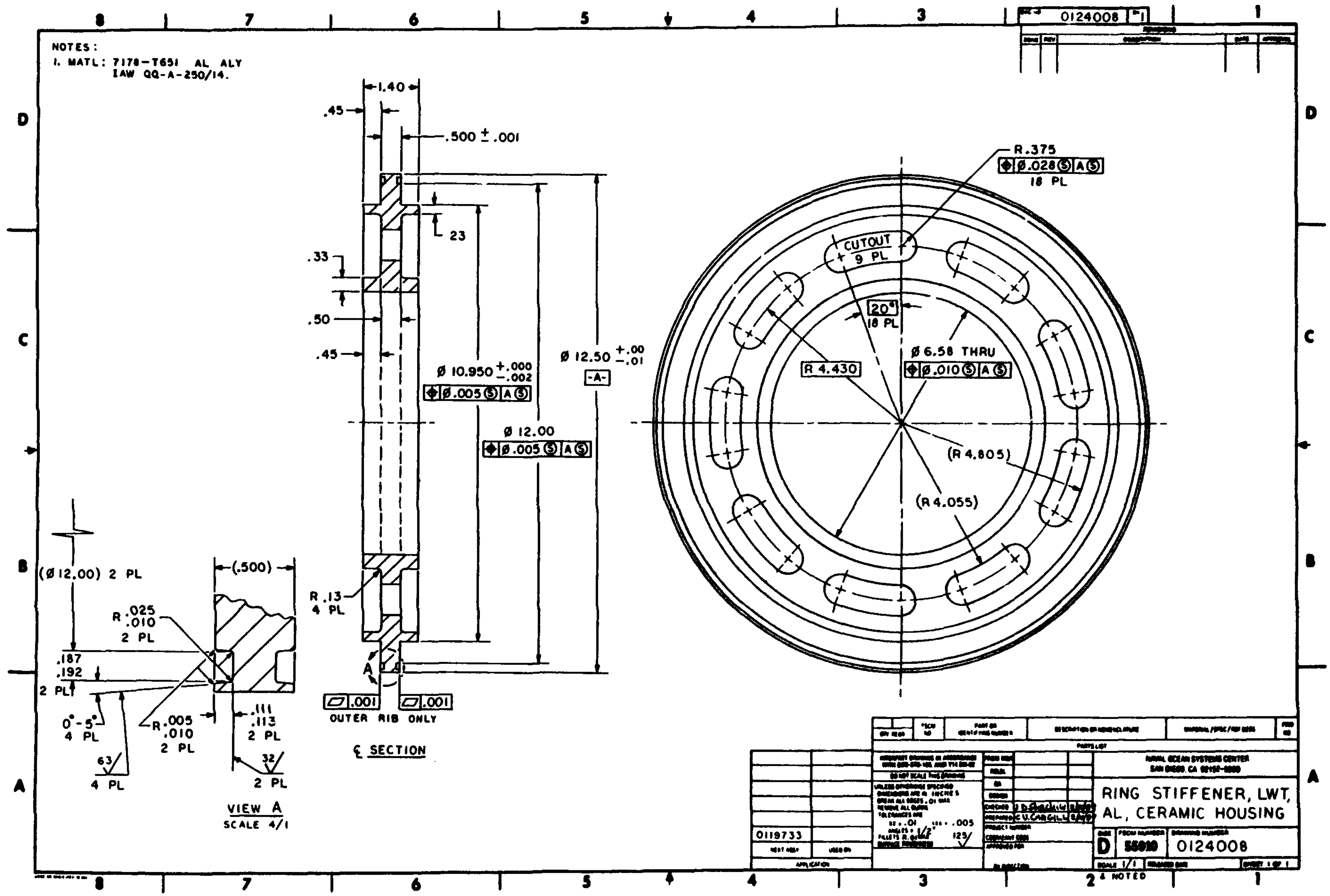

Figure B-57. Aluminum ring stiffener DWG 0124008; fabrication drawing.

Figure B-58. Aluminum ring stiffener DWG 0124008; exterior view.

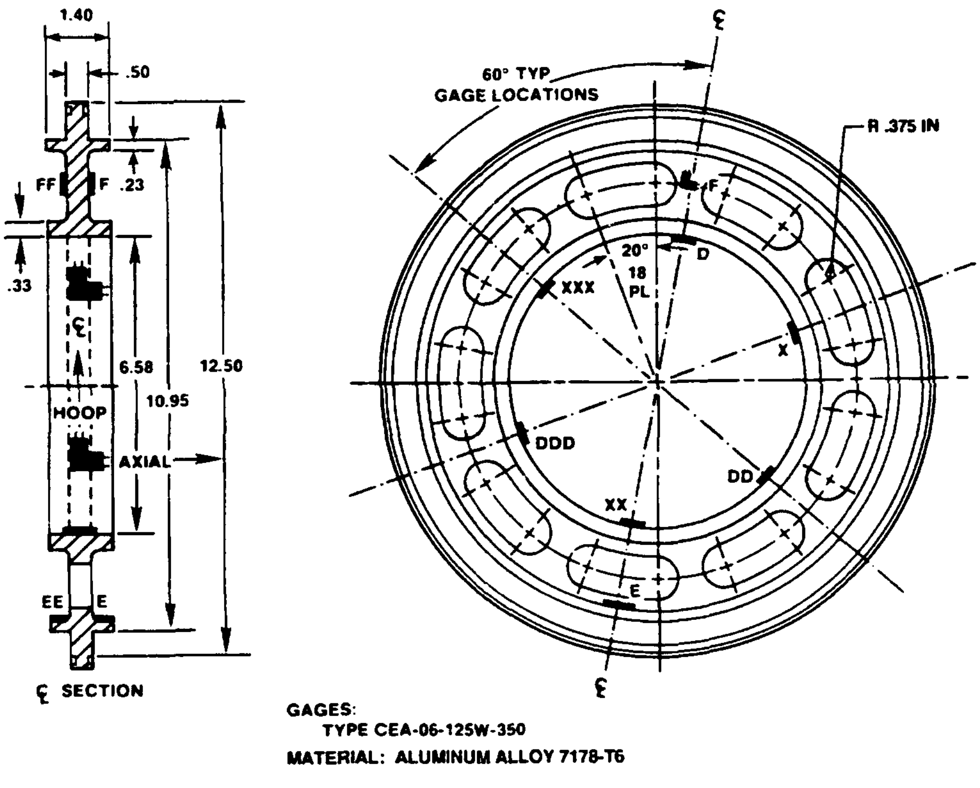

Figure B-59. Aluminum ring stiffener DWG 0124008; location of gages.

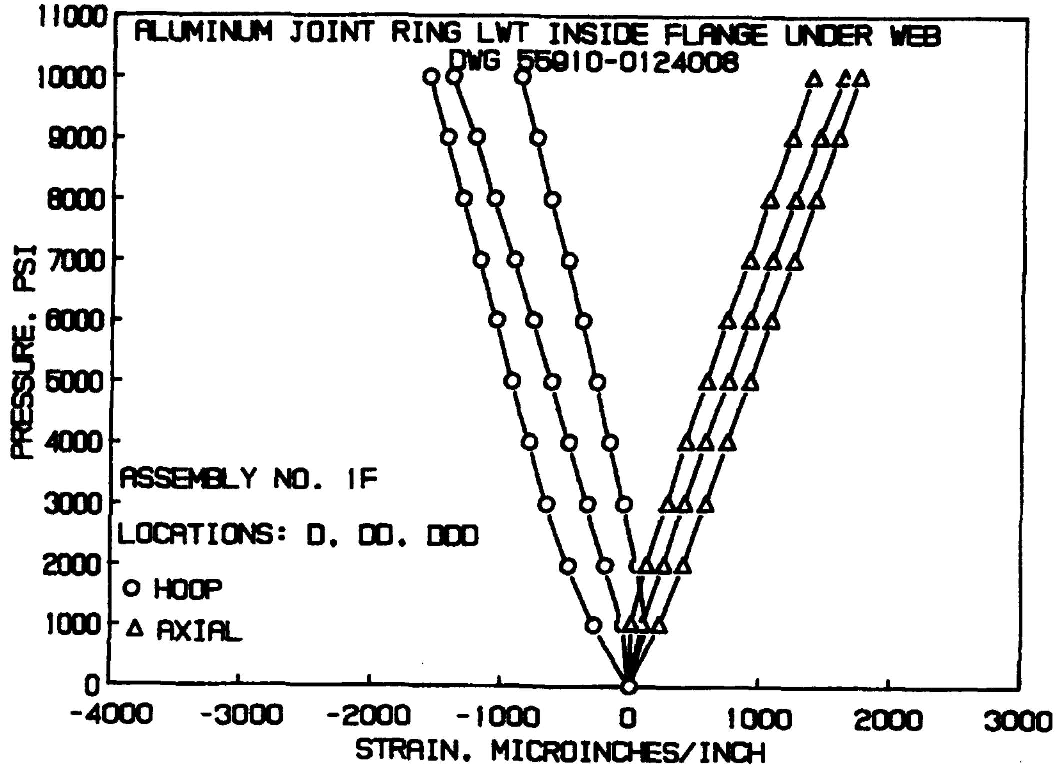

Figure B-60. Strains on housing test assembly 1F; locations D, DD, DDD.

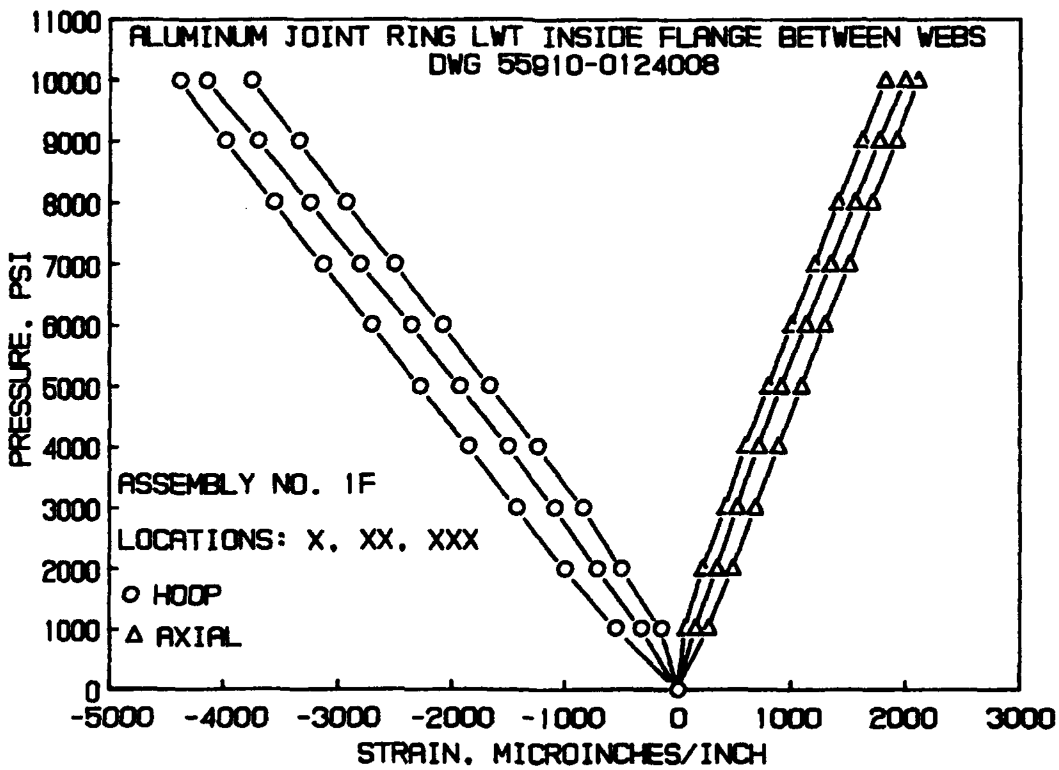

Figure B-61. Strains on housing test assembly 1F; locations X, XX, XXX.

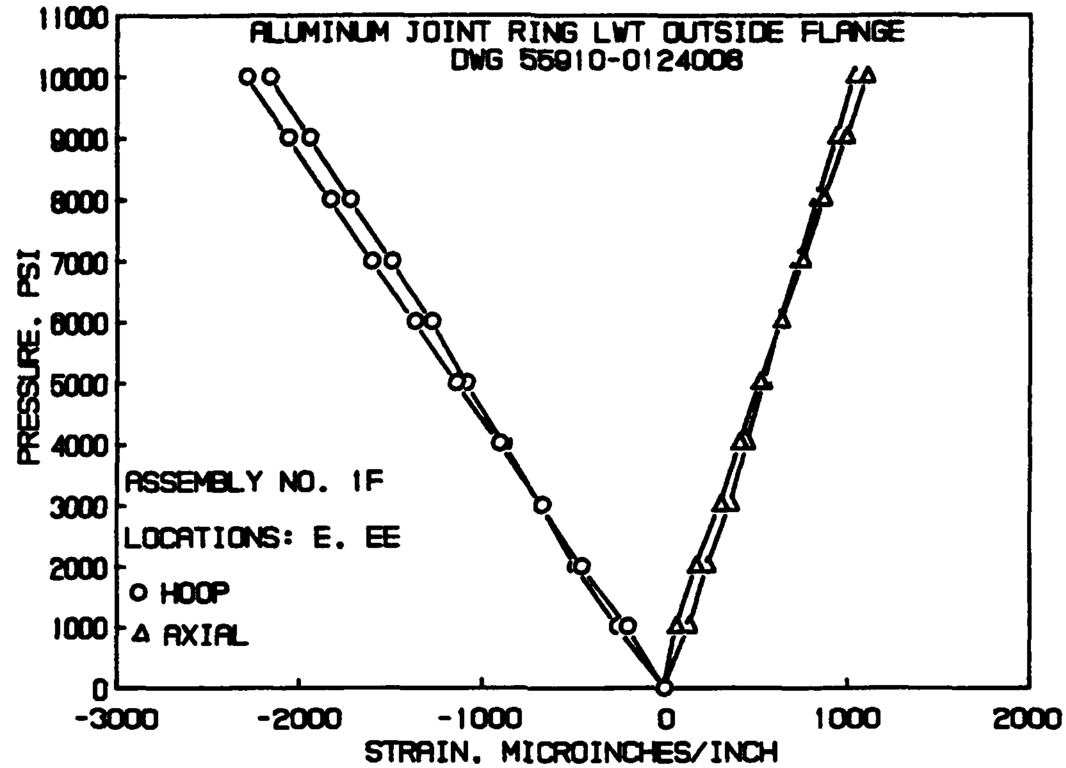

Figure B-62. Strains on housing test assembly 1F; locations E, EE.

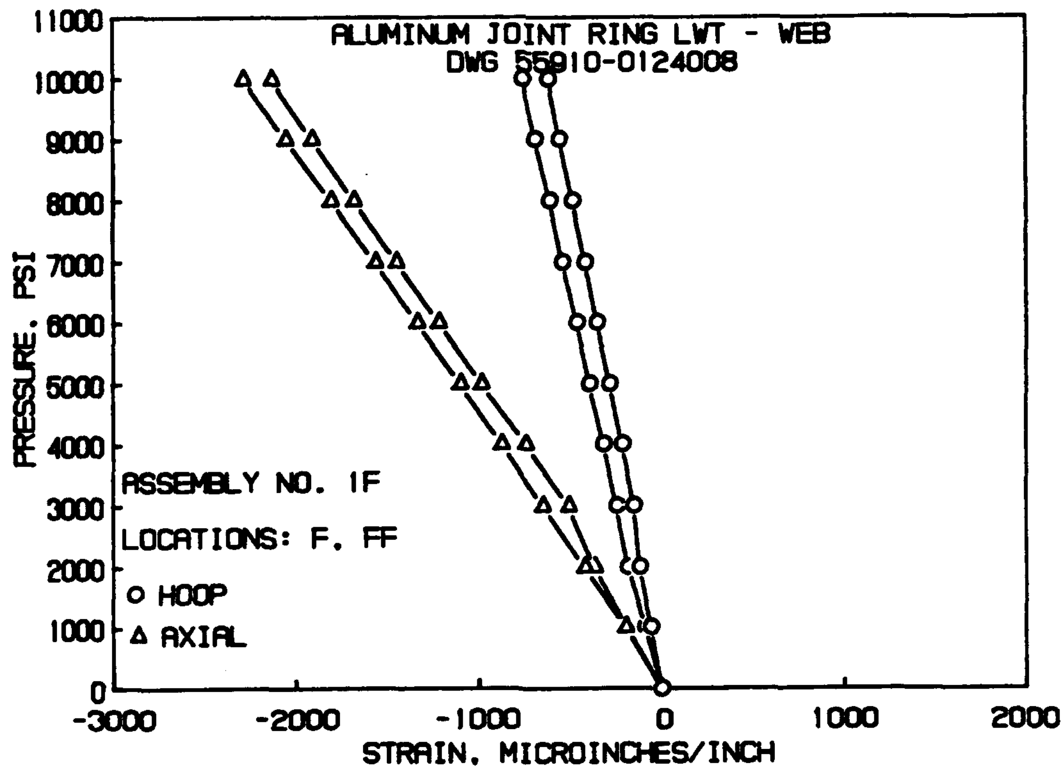

Figure B-63. Strains on housing test assembly 1F; locations F, FF.

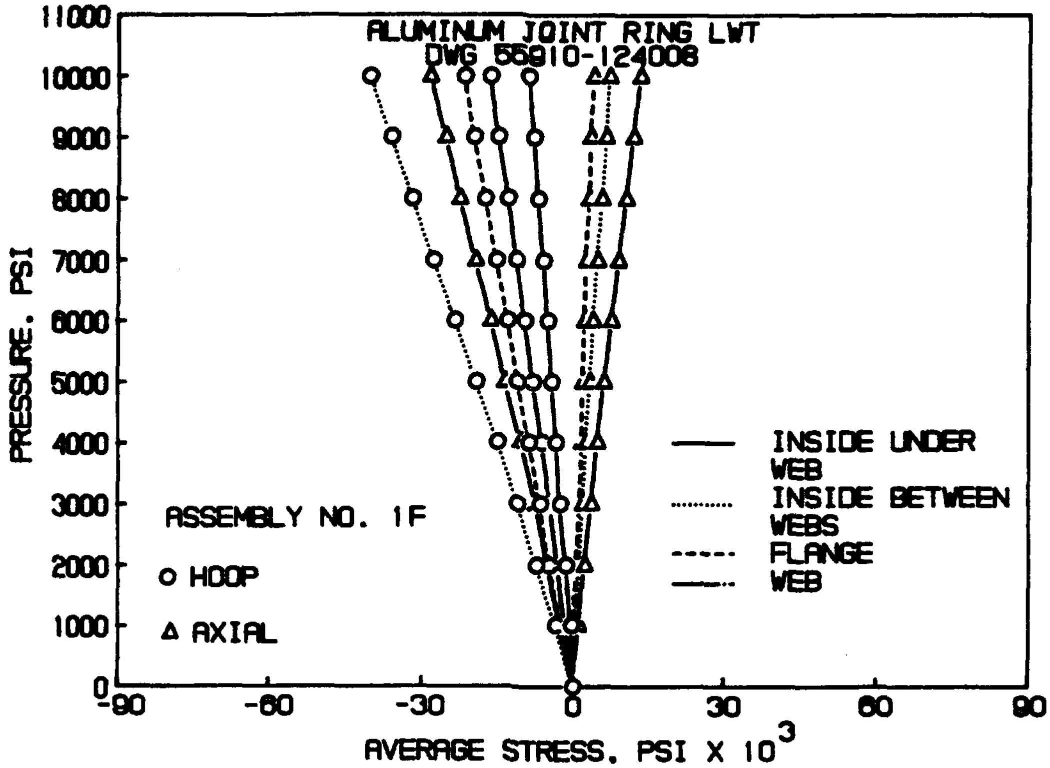

Figure B-64. Stresses on housing test assembly 1F; location--titanium joint ring DWG 0124008.

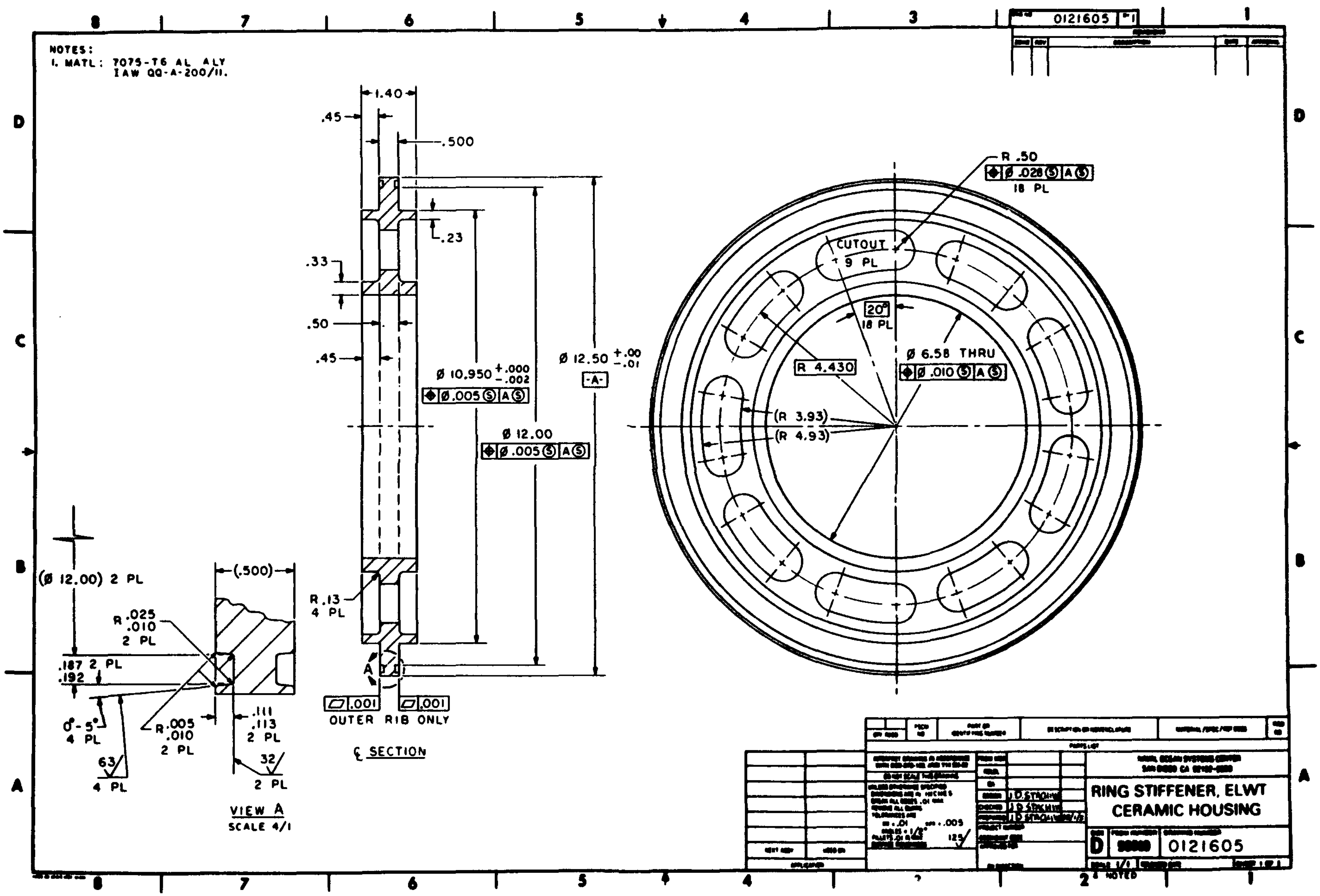

Figure B-65. Aluminum ring stiffener DWG 0121605; fabrication drawing.

Figure B-66. Aluminum ring stiffener DWG 0121605; exterior view.

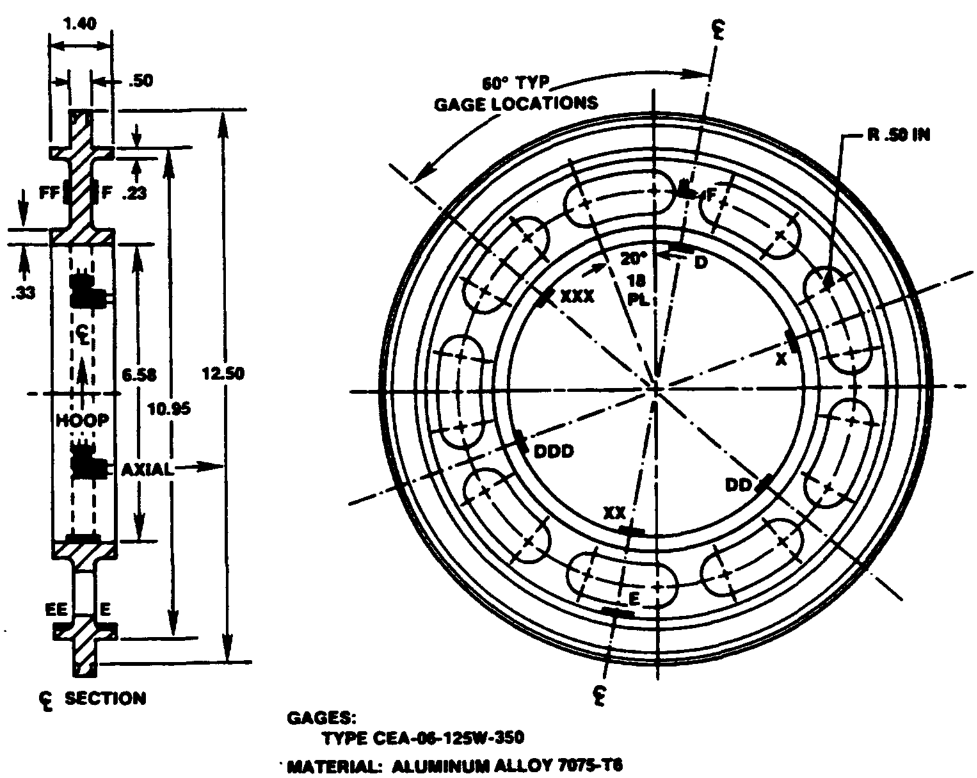

Figure B-67. Aluminum ring stiffener DWG 0121605; location of gages.

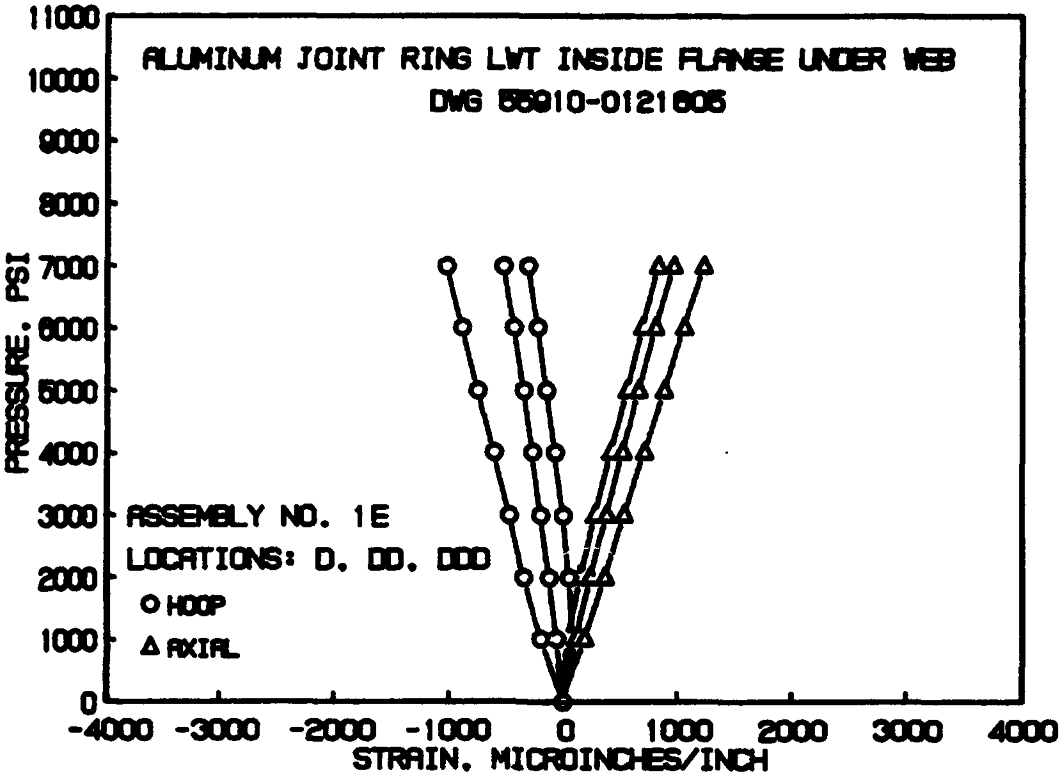

Figure B-68. Strains on housing test assembly 1E; locations D, DD, DDD.

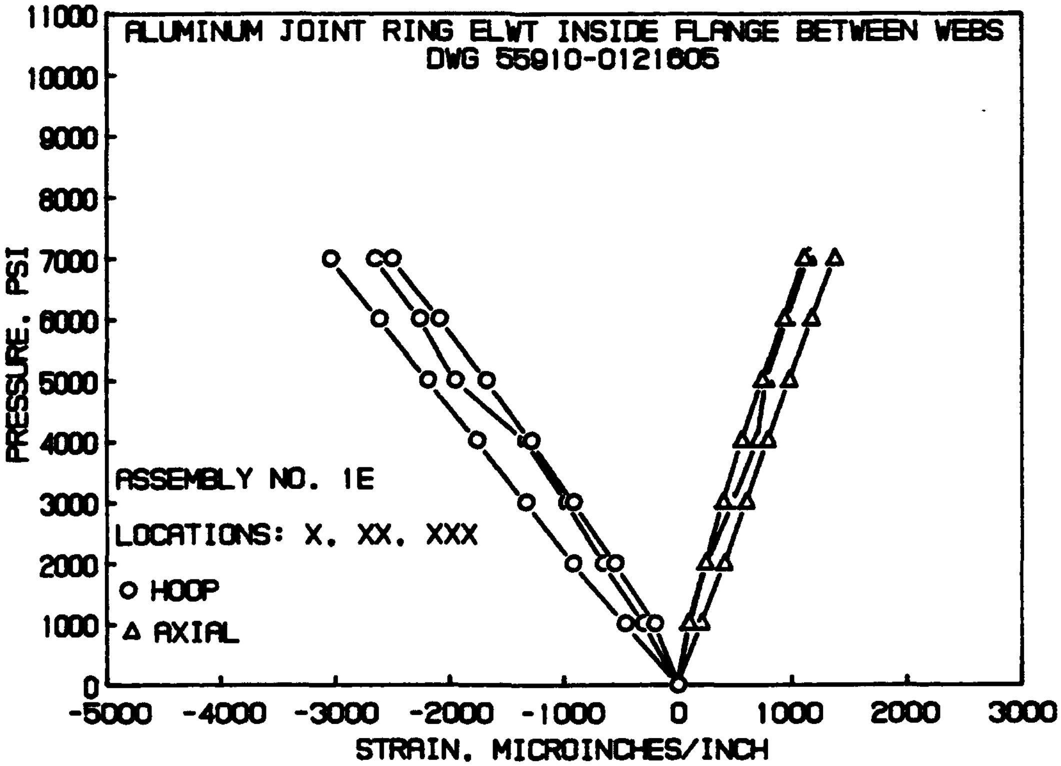

Figure B-69. Strains on housing test assembly 1E; locations X, XX, XXX.

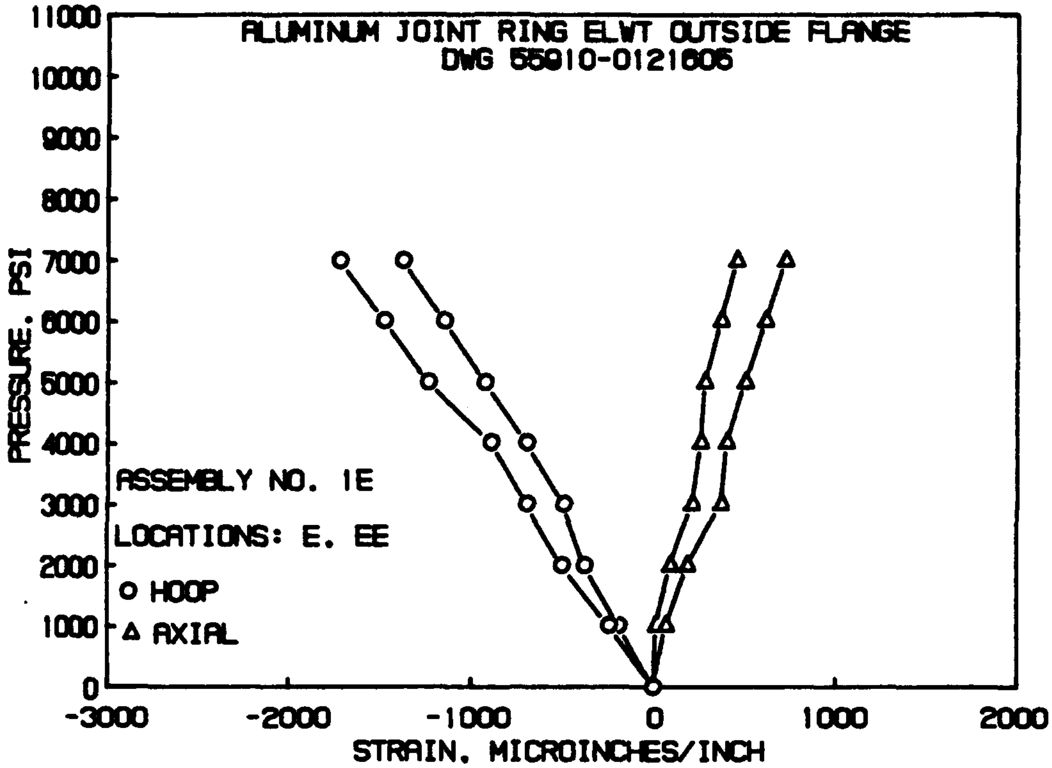

Figure B-70. Strains on housing test assembly 1E; locations E, EE.

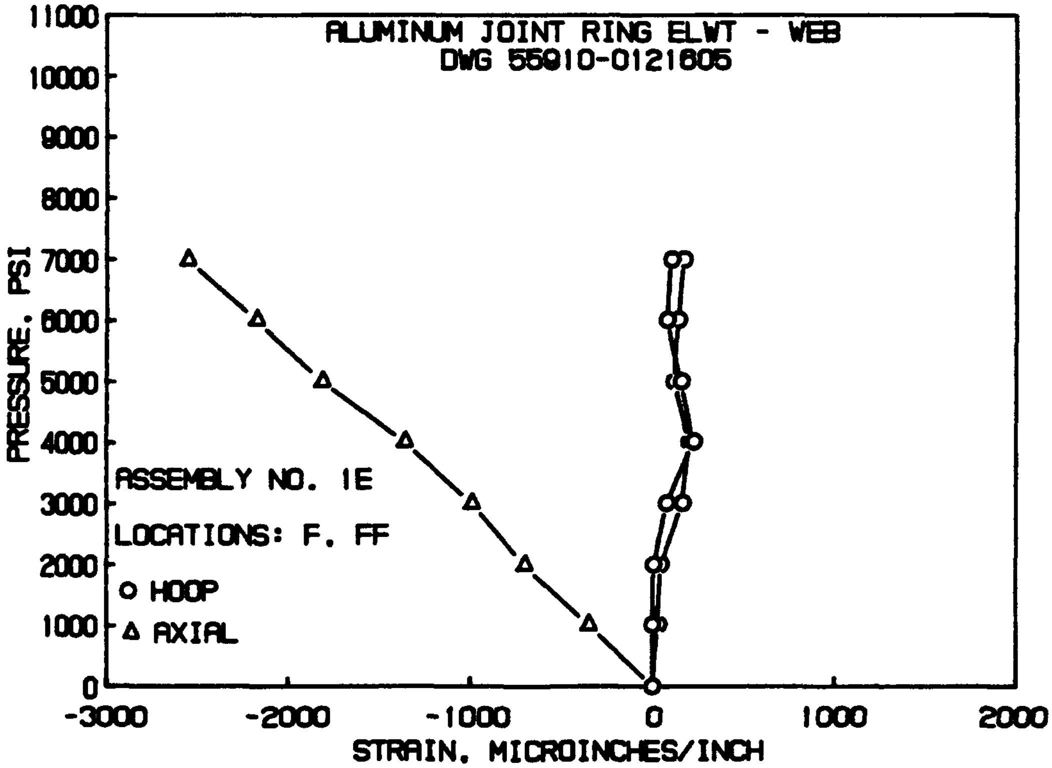

Figure B-71. Strains on housing test assembly 1E; locations F, FF.

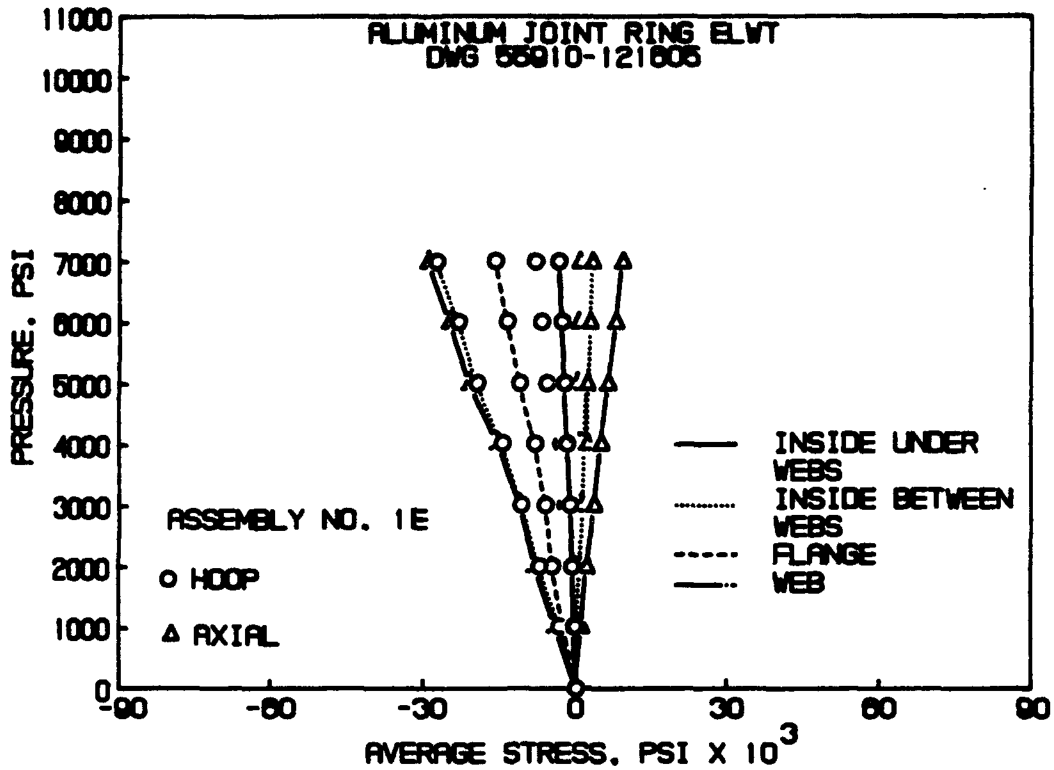

Figure B-72. Stresses housing test assembly 1E; location–aluminum joint ring DWG 0121605.

	Assy 1A	Assy 1B	Assy 1C
			
End Bells	Titanium, DWG 0119737 Titanium, DWG 0119737	Titanium, DWG 0119737 Titanium, DWG 0119737	Titanium, DWG 0119737 Titanium, DWG 0119737
Cylinder	Ceramic, DWG 0119735	Ceramic, DWG 0119735	Ceramic, DWG 0119735
Stiffener	Titanium, DWG 0119738	Titanium, DWG 0123943	Titanium, DWG 0121604
End Caps	Titanium, DWG 0119736	Titanium, DWG 0119736	Titanium, DWG 0119736
Hemi End Rings	—	—	—
Band Clamps	Aluminum, DWG 0119740	Aluminum, DWG 0119740	Aluminum, DWG 0119740
Overall Length	L/D = 4	L/D = 4	L/C = 4

	Assy 1D	Assy 1E	Assy 1F
	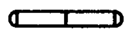		
End Bells	Titanium, DWG 0119737 Titanium, DWG 0119737	Titanium, DWG 0119737 Titanium, DWG 0119737	Titanium, DWG 0119737 Titanium, DWG 0119737
Cylinder	Ceramic, DWG 0119735	Ceramic, DWG 0119735	Ceramic, DWG 0119735
Stiffener	Aluminum, DWG 0124007	Aluminum, DWG 0121605	Aluminum, DWG 0124008
End Caps	Titanium, DWG 0119736	Titanium, DWG 0119736	Titanium, DWG 0119736
Hemi End Rings	—	—	—
Band Clamps	Aluminum, DWG 0119740	Aluminum, DWG 0119740	Aluminum, DWG 0119740
Overall Length	L/D = 4	L/D = 4	L/D = 4

Table B-1. Twelve-inch-diameter ceramic housing test configurations for evaluation of joint ring stiffeners, Sheet 1.

	Assy 3A	Assy 3B	Assy 4A
	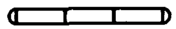	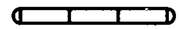	
End Bells	Ceramic, DWG 0119913 Ceramic, DWG 0121710	Titanium, DWG 0119737 Titanium, DWG 0119737	Titanium, DWG 0119737 Ceramic, DWG 0119913
Cylinder	Ceramic, DWG 0119735	Ceramic, DWG 0119735	Ceramic, DWG 0119735
Stiffeners	Titanium, DWG 0123943 Titanium, DWG 0123943	Aluminum, DWG 0124008 Aluminum, DWG 0124008	Aluminum, DWG 0124007 Titanium, DWG 0119738 Aluminum, DWG 0124007
End Caps	Titanium, DWG 0119736	Titanium, DWG 0119736	Titanium, DWG 0119736
Hemi End Rings	Titanium, DWG 0119915	Titanium, DWG 0119915	
Band Clamps	Aluminum, DWG 0119740	Aluminum, DWG 0119740	Aluminum, DWG 0119740
Overall Length	L/D = 7	L/D = 7	L/D = 7

Notes: All cylinders and hemisphered are equipped with Mod 0 end caps and end rings except for assembly 2F where the 12-inch diameter cylinder is equipped with Mod 1 end caps.

Table B-1. Twelve-inch-diameter ceramic housing test configurations for evaluation of joint ring stiffeners, Sheet 2.

	Assy 1A	Assy 1B	Assy 1C
Proof Tests	1	1	Failed at 9910
Cyclic Tests	10	10	0

	Assy 1D	Assy 1E	Assy 1F
Proof Tests	1	Test Terminated at 7000 psi without implosion	1
Cyclic Tests	10		10

	Assy 3A	Assy 3B	Assy 4A
Proof Tests	1	1	1
Cyclic Tests	50	50	50

1. Proof testing: Pressurize to 10,000 psi, hold pressure for 15 minutes.
2. Cycling Test: Pressurize to 9000 psi, hold pressure for 1 minute.

Table B-2. Summary of test performed on 12-inch-diameter ceramic test housings during evaluation of joint ring stiffeners.

Ceramic Cylinder, 12 in OD X 18 in L X 0.412 in, 94% alumina		35.0 lbs
End Caps for Cylinder (pair)		
Titanium Mod 0	DWG.55910-0119736	4.0 lbs
Titanium Mod 1	DWG.55910-0125186	5.1 lbs
Aluminum Mod 0	DWG.55910-0119736	1.44 lbs
Aluminum Mod 1	DWG.55910-0125186	3.28 lbs
Joint Ring Stiffener, Titanium		
DWG. 55910-0119738		6.30 lbs
DWG. 55910-0123943		6.00 lbs
DWG. 55910-0121604		5.13 lbs
Joint Ring Stiffener, Aluminum		
DWG. 55910-0124007		5.67 lbs
DWG. 55910-0124008		5.06 lbs
DWG. 55910-0121605		4.62 lbs
Jacket, Polyurethane, DWG.55910-0120000		9.8 lbs
Hemisphere*, Titanium Type 1	DWG.55910-0119737	12.5 lbs
Titanium Type 2	DWG.55910-SK9402-064	24.0 lbs
Hemisphere, Ceramic		
Mod 1, DWG. 55910-0119913		6.57 lbs
Mod 2, DWG. 55910-0120247		8.21 lbs
Mod 3, DWG. 55910-0121707		5.40 lbs
Mod 4, DWG. 55910-0121710		8.80 lbs
Mod 5, DWG. 55910-0121837		7.88 lbs
End Ring for ceramic hemisphere Mod 0		
Titanium DWG.55910-0119915		2.22 lbs
End Ring for ceramic hemisphere Mod 1		
Titanium DWG.55910-0125666		4.10 lbs
Wedge Clamp Band, Aluminum	DWG.55910-0119740	1.5 lbs
Connector Inserts, Titanium (each)	DWG.55910-0120248	0.6 lbs
Weight/Displacement		
Cylinder with end caps, Mod 0 Titanium		0.512
Cylinder with end caps, Mod 1 Titanium		0.525
Cylinder with end caps, Mod 0 Aluminum		0.48
Cylinder with end caps, Mod 1 Aluminum		0.49
Cylinder with end caps, Mod 1 Titanium and two Titanium hemispheres Type 1		0.62
Cylinder with end caps, Mod 1 Titanium; two ceramic hemispheres, Mod 1; with end rings, Mod 1 Titanium; Aluminum clamp bands and connector inserts		0.60

*The critical buckling pressure of Titanium hemispheres Type 1 is 12,500 psi, and of Type 2 is 23,000 psi

Table B-3. Weights of structural components in 12-inch-diameter ceramic test housings.

Pressure (PSI)	Gage Locations D Hoop	D Axial	DD Hoop	DD Axial	DDD Hoop	DDD Axial	E Hoop	E Axial	EE Hoop	EE Axial
0	0	0	0	0	0	0	0	0	0	0
1000	-309	266	-182	175	-409	329	-253	133	-142	74
2000	-566	486	-395	364	-651	542	-432	230	-304	174
3000	-825	705	-623	562	-888	747	-602	320	-474	270
4000	-1080	925	-853	762	-1119	950	-768	410	-650	364
5000	-1342	1149	-1088	966	-1351	1152	-932	500	-814	460
6000	-1603	1369	-1323	1170	-1580	1351	-1098	584	-984	530
7000	-1867	1596	-1552	1370	-1813	1554	-1266	672	-1144	566
8000	-2145	1826	-1781	1575	-2043	1760	-1428	760	-1344	594
9000	-2409	2060	-2012	1778	-2274	1960	-1588	841	-1530	620
10000	-2690	2300	-2240	1977	-2502	2160	-1747	924	-1740	634

Note: All strain readings are in microinches per inch

Table B-4. Strains on titanium ring stiffener DWG 0119738 in housing test assembly 1A, Sheet 1.

Pressure	Gage Locations							
	F		FF		FFF		FFFF	
(PSI)	Hoop	Radial	Hoop	Radial	Hoop	Radial	Hoop	Radial
0	0	0	0	0	0	0	0	0
1000	-290	-150	-222	64	-270	-102	-198	-10
2000	-470	-170	-408	36	-464	-150	-384	-30
3000	-660	-190	-606	-20	-660	-210	-564	-64
4000	-830	-206	-798	-74	-836	-256	-740	-98
5000	-1000	-226	-986	-120	-1012	-290	-940	-150
6000	-1190	-254	-1180	-180	-1200	-334	-1106	-190
7000	-1350	-260	-1350	-210	-1360	-350	-1318	-240
8000	-1528	-288	-1544	-264	-1548	-386	-1480	-280
9000	-1702	-318	-1718	-300	-1720	-410	-1670	-326
10000	-1876	-340	-1888	-388	-1888	-424	-1844	-374

Note: All strain readings are in mircoinches per inch

Table B-4. Strains on titanium ring stiffener DWG 0119738 in housing test assembly 1A, Sheet 2.

Pressure (PSI)	D Hoop	D Axial	DD Hoop	DD Axial	DDD Hoop	DDD Axial	E Hoop	E Axial	EE Hoop	EE Axial
	Gage Locations									
0	0	0	0	0	0	0	0	0	0	0
1000	-4078	3003	-2285	2110	-5544	3544	-3877	877	-2180	480
2000	-7477	5477	-5061	4286	-8708	5983	-6601	1551	-4568	1318
3000	-10920	7920	-8058	6533	-11829	8304	-9202	2152	-7131	2031
4000	-14282	10407	-11081	8806	-14851	10626	-11728	2778	-9818	2668
5000	-17749	12924	-14171	11121	-17898	12923	-14217	3416	-12269	3419
6000	-21223	15373	-17261	13436	-20908	15183	-16781	3931	-14996	3646
7000	-24709	17933	-20265	15715	-23968	17492	-19357	4507	-17753	3303
8000	-28436	20461	-23237	18087	-26952	19877	-21821	5121	-21307	2557
9000	-31877	23152	-26259	20409	-29993	22143	-24293	5617	-24612	1862
10000	-35598	25847	-29251	22676	-32978	24428	-26732	6157	-28441	791

Note: All stresses are in pounds per square inch, calculated on the basis of E=16,5000,000 and M=.34

Table B-5. Principal stresses on titanium ring stiffener DWG 0119738 on housing test assembly 1A, Sheet1.

Pressure (PSI)	Gage Locations: F Hoop	F Radial	FF Hoop	FF Radial	FFF Hoop	FFF Radial	FFFF Hoop	FFFF Radial
0	0	0	0	0	0	0	0	0
1000	-6362	-4638	-3736	-214	-5684	-3616	-3758	-1443
2000	-9847	-6153	-7384	-1916	-9608	-5742	-7355	-2996
3000	-13519	-7731	-11433	-4217	-13646	-8105	-10929	-4772
4000	-16792	-9108	-15358	-6443	-17221	-10079	-14428	-6522
5000	-20091	-10560	-19157	-8493	-20720	-11830	-18489	-8761
6000	-23813	-12288	-23157	-10843	-24507	-13843	-21840	-10561
7000	-26836	-13414	-26519	-12482	-27594	-15157	-26112	-12838
8000	-30335	-15066	-30481	-14720	-31330	-17021	-29389	-14612
9000	-33771	-16729	-33956	-16495	-34691	-18560	-33225	-16676
10000	-37157	-18244	-37686	-19215	-37914	-19887	-36776	-18675

Note: All stresses are in pounds per square inch, calculated on the basis of E=16,5000,000 and M=.34

Table B-5. Principal stresses on titanium ring stiffener DWG 0119738 in housing test assembly 1A, Sheet 2.

Pressure (PSI)	A Hoop	A Axial	AA Hoop	AA Axial	B Hoop	B Axial	BB Hoop	BB Axial	C Hoop	C Axial	CC Hoop	CC Axial
	Gage Locations											
0	0	0	0	0	0	0	0	0	0	0	0	0
1000	-320	-72	-293	-92	58	-3285	-194	-123	-263	-137	-292	-122
2000	-625	-162	-590	-185	120	-5239	-435	-200	-542	-252	-570	-224
3000	-926	-252	-884	-277	180	-6686	-672	-272	-819	-365	-850	-325
4000	-1230	-343	-1178	-372	209	-7726	-910	-340	-1093	-470	-1125	-420
5000	-1530	-434	-1471	-464	187	-8528	-1146	-415	-1364	-572	-1395	-515
6000	-1830	-525	-1764	-560	147	-9160	-1384	-488	-1640	-673	-1670	-613
7000	-2128	-617	-2056	-652	83	-9566	-1622	-567	-1913	-770	-1941	-712
8000	-2425	-708	-2346	-745	45	-10250	-1857	-646	-2185	-867	-2211	-810
9000	-2725	-802	-2636	-839	0	-10962	-2094	-728	-2459	-966	-2480	-910
10000	-3026	-896	-2927	-935	-376	-13330	-2327	-804	-2732	-1066	-2750	-1009

Note: All strain readings are in microinches per inch

Table B-6. Strains on ceramic cylinder DWG 0119735 in housing test assembly 1A.

Pressure (PSI)	A Hoop	A Axial	AA Hoop	AA Axial	B Hoop	B Axial	BB Hoop	BB Axial	C Hoop	C Axial	CC Hoop	CC Axial
0	0	0	0	0	0	0	0	0	0	0	0	0
1000	-14374	-5971	-13396	-6585	-27101	-140378	-9429	-7023	-12515	-8245	-13623	-7863
2000	-28267	-12578	-26973	-13249	-42042	-223630	-20459	-12497	-25517	-15691	-26466	-14742
3000	-41988	-19150	-40412	-19844	-52502	-285155	-31273	-17720	-38416	-23033	-39386	-21596
4000	-55847	-25791	-53877	-26566	-60626	-329501	-42094	-22780	-51114	-30004	-52037	-28148
5000	-69534	-32396	-67274	-33152	-68794	-364099	-52892	-28123	-63657	-36820	-64473	-34655
6000	-83221	-39002	-80706	-39908	-76202	-391567	-63758	-33397	-76405	-43638	-77151	-41335
7000	-96832	-45632	-94059	-46485	-82604	-409557	-74678	-38930	-88988	-50258	-89667	-48022
8000	-110390	-52210	-107335	-53086	-90395	-439238	-85469	-44435	-101528	-56868	-102130	-54658
9000	-124105	-58944	-120620	-59730	-98738	-470182	-96373	-50087	-114172	-63583	-114569	-61370
10000	-137862	-65687	-133967	-66468	-136195	-575137	-107052	-55445	-126783	-70331	-127041	-68048

Note: All stresses are in pounds per square inch calculated on the basis of E=41,000,000 and M=.21

Table B-7. Principal stresses on ceramic cylinder DWG 0119735 in housing test assembly 1A.

Pressure (PSI)	Gage Locations G Hoop	G Axial	GG Hoop	GG Axial	H Hoop	H Axial	I Hoop	I Axial	K Hoop	K Axial
0	0	0	0	0	0	0	0	0	0	0
1000	-302	-430	-254	-390	-348	-330	-396	-308	-410	-242
2000	-600	-840	-552	-790	-694	-690	-800	-600	-830	-490
3000	-888	-1240	-844	-1150	-1040	-1026	-1200	-890	-1242	-732
4000	-1194	-1630	-1130	-1500	-1368	-1358	-1590	-1174	-1660	-990
5000	-1488	-2030	-1416	-1860	-1720	-1700	-2000	-1470	-2080	-1250
6000	-1770	-2444	-1710	-2230	-2066	-2044	-2400	-1750	-2490	-1510
7000	-2040	-2860	-2000	-2598	-2400	-2382	-2800	-2036	-2900	-1770
8000	-2320	-3278	-2272	-2964	-2740	-2714	-3190	-2310	-3318	-2008
9000	-2596	-3688	-2554	-3338	-3084	-3050	-3594	-2574	-3732	-2242
10000	-2870	-4094	-2840	-3702	-3420	-3390	-4010	-2830	-4160	-2458

Note: All strain readings are in microinches per inch

Table B-8. Strains on titanium end bell DWG 0119737 in housing test assembly 1A.

Pressure (PSI)	Gage Locations G Hoop	G Axial	GG Hoop	GG Axial	H Hoop	H Axial	I Hoop	I Axial	K Hoop	K Axial
0	0	0	0	0	0	0	0	0	0	0
1000	-8362	-9938	-7213	-8887	-8586	-8364	-9342	-8258	-9184	-7116
2000	-16523	-19478	-15310	-18241	-17325	-17276	-18732	-16269	-18594	-14407
3000	-24433	-28768	-23041	-26809	-25912	-25739	-28034	-24217	-27815	-21535
4000	-32616	-37985	-30597	-35154	-34137	-34014	-37112	-31989	-37251	-29000
5000	-40639	-47313	-38217	-43684	-42874	-42628	-46639	-40113	-46736	-36515
6000	-48526	-56825	-46049	-52452	-51511	-51240	-55878	-47874	-56034	-43967
7000	-56202	-66300	-53794	-61158	-59887	-59665	-65155	-55747	-65333	-51419
8000	-64078	-75874	-61190	-69712	-68336	-68016	-74169	-63333	-74641	-58511
9000	-71828	-85274	-68824	-78478	-76885	-76467	-83381	-70821	-83850	-65502
10000	-79515	-94587	-76469	-87083	-85311	-84942	-92766	-78236	-93205	-72247

Note: All stresses are in pounds per square inch, calculated on the basis of E=16,5000,000 and M=.34

Table B-9. Principal stresses on titanium end bell DWG 0119737 in housing test assembly 1A.

Strains on Titanium End Bell
Gage Location

Pressure (PSI)	M Hoop	M Axial
0	0	0
1000	-442	-354
2000	-830	-714
3000	-1200	-1074
4000	-1508	-1614
5000	-2050	-1950
6000	-2450	-2360
7000	-2772	-2790
8000	-3230	-3114
9000	-3656	-3534
10000	-4050	-3880

Principal Stresses on Titanium End Bell
Gage Location

Pressure (PSI)	M Hoop	M Axial
0	0	0
1000	-10492	-9408
2000	-20014	-18586
3000	-29201	-27650
4000	-38373	-39678
5000	-50616	-49385
6000	-60680	-59572
7000	-69415	-69637
8000	-80015	-78587
9000	-90627	-89125
10000	-100173	-98080

Note: All strain readings are in microinches per inch

All stresses are in pounds per square inch, calculated on the basis of E = 16,500,000 and M=.34

Table B-10. Principal strains and stresses at apex of titanium end bell DWG 0119737.

Pressure (PSI)	Inside Diameter Under Webs: D Hoop	D Axial	DD Hoop	DD Axial	DDD Hoop	DDD Axial	Inside Diameter Between Webs: X Hoop	X Axial	XX Hoop	XX Axial	XXX Hoop	XXX Axial
0	0	0	0	0	0	0	0	0	0	0	0	0
1000	-254	394	-245	364	-217	348	-684	322	-737	352	-822	442
2000	-408	606	-390	564	-380	552	-1014	480	-1060	504	-1228	662
3000	-496	761	-478	722	-456	701	-1340	640	-1383	661	-1572	852
4000	-566	929	-549	877	-520	856	-1687	813	-1725	832	-1960	1067
5000	-649	1088	-635	1032	-593	1007	-2036	978	-2075	998	-2349	1278
6000	-723	1245	-718	1185	-660	1154	-2376	1140	-2419	1162	-2736	1485
7000	-791	1402	-801	1341	-721	1300	-2708	1300	-2755	1326	-3120	1696
8000	-854	1550	-888	1495	-774	1436	-3025	1453	-3080	1485	-3500	1907
9000	-905	1692	-983	1652	-810	1559	-3321	1595	-3394	1638	-3887	2120
10000	-970	1834	-1060	1809	-850	1682	-3560	1737	-3640	1791	-4230	2333

Pressure (PSI)	Flange: E Hoop	E Axial	EE Hoop	EE Axial	Web: F Hoop	F Axial	FF Hoop	FF Axial
0	0	0	0	0	0	0	0	0
1000	-183	105	-530	261	-237	-106	-206	-635
2000	-326	168	-730	388	-325	-326	-314	-789
3000	-478	245	-910	490	-395	-601	-411	-849
4000	-747	404	-1014	538	-478	-763	-511	-1044
5000	-949	506	-1194	628	-566	-937	-614	-1235
6000	-1145	603	-1374	718	-652	-1108	-714	-1420
7000	-1346	702	-1542	810	-735	-1274	-810	-1601
8000	-1549	798	-1703	897	-815	-1451	-902	-1763
9000	-1756	890	-1859	979	-890	-1644	-990	-1902
10000	-2000	982	-1900	1060	-965	-1837	-1080	-2045

NOTES:
Gages:
Gage Type: CEA-06-125WT-350
Gage Factor: 2.09
Test Assembly:
1. Two ceramic cylinders joined and supported by a metallic ring stiffener.
2. The Cylinder is capped with Titanium Hemispheres DWG 55910-0119737 on both ends
Materials:
The Ceramic is Coors AD 94 (94% Alumina)
The Titanium is Ti6Al4Va Alloy
Data: All readings are in microinches/inch
Structural Performance: Sustained external loading to 10,000 psi without implosion

Table B-11. Strains on the titanium ring stiffener DWG 0123943 in housing test assembly 1B.

Pressure (PSI)	Inside Diameter Under Webs: D Hoop	D Axial	DD Hoop	DD Axial	DDD Hoop	DDD Axial	Inside Diameter Between Webs: X Hoop	X Axial	XX Hoop	XX Axial	XXX Hoop	XXX Axial
0	0	0	0	0	0	0	0	0	0	0	0	0
1000	-2240	5740	-2262	5237	-1841	5116	-10719	1669	-11517	1892	-12532	3032
2000	-3768	8718	-3699	8049	-3588	7888	-15873	2523	-16579	2679	-18711	4561
3000	-4427	11052	-4338	10438	-4061	10186	-20941	3440	-21610	3559	-23924	5924
4000	-4667	13742	-4680	12880	-4272	12672	-26317	4467	-26906	4580	-29799	7474
5000	-5207	16182	-5301	15226	-4676	15026	-31782	5331	-32383	5457	-35718	8943
6000	-5592	18642	-5879	17554	-4993	17344	-37098	6197	-37760	6335	-41626	10350
7000	-5864	21140	-6438	19938	-5205	19681	-42277	7076	-42989	7263	-47451	11851
8000	-6101	23501	-7084	22259	-5331	21882	-47220	7920	-48044	8168	-53203	13377
9000	-6152	25827	-7861	24586	-5223	23948	-51842	8692	-52931	9031	-59072	14896
10000	-6464	28064	-8301	27027	-5189	25989	-55400	9825	-56550	10325	-64120	16694

Pressure (PSI)	Flange: E Hoop	E Axial	EE Hoop	EE Axial	Web: F Hoop	F Axial	FF Hoop	FF Axial
0	0	0	0	0	0	0	0	0
1000	-2748	798	-8233	1507	-5094	-3481	-7871	-13154
2000	-5016	1066	-11158	2608	-8131	-8144	-10863	-16712
3000	-7364	1539	-13870	3369	-11182	-13718	-13054	-18447
4000	-11374	2799	-15505	3605	-13758	-17267	-16156	-22719
5000	-14496	3421	-18293	4143	-16504	-21072	-19289	-26936
6000	-17537	3987	-21080	4680	-19193	-24808	-22329	-31022
7000	-20659	4559	-23631	5331	-21794	-28431	-25268	-35008
8000	-23838	5062	-26083	5933	-24410	-32241	-28012	-38614
9000	-27116	5466	-28473	6473	-27033	-36318	-30536	-41766
10000	-31085	5634	-28724	7724	-29657	-40394	-33122	-45004

NOTES: All Stresses are in pounds per square inch, calculated on the basis of E = 16,500,000

Table B-12. Principal stresses on the titanium ring stiffener DWG 0123943 in test housing assembly 1B.

Gage Locations

Pressure (PSI)	Inside Diameter Under Webs D Hoop	D Axial	DD Hoop	DD Axial	DDD Hoop	DDD Axial	X Hoop	X Axial	Inside Diameter Between Webs XX Hoop	XX Axial	XXX Hoop	XXX Axial
0	0	0	0	0	0	0	0	0	0	0	0	0
1000	86	284	32	196	96	153	-517	212	-756	306	-560	234
2000	123	482	61	345	157	281	-936	388	-1265	519	-962	400
3000	149	671	78	499	204	416	-1345	562	-1731	715	-1346	558
4000	179	854	95	650	225	562	-1751	740	-2178	905	-1714	711
5000	214	1040	112	797	243	711	-2158	910	-2620	1095	-2072	858
6000	263	1234	137	937	262	859	-2550	1082	-3066	1287	-2414	1000
7000	328	1439	170	1064	292	997	-2931	1245	-3521	1487	-2724	1129
8000	442	1680	243	1166	346	1131	-3301	1405	-4040	1721	-3000	1247
9000	695	2019	376	1187	459	1231	-3628	1538	-4700	2027	-3141	1301

Pressure (PSI)	Flange E Hoop	E Axial	EE Hoop	EE Axial	Web F Hoop	F Axial	FF Hoop	FF Axial
0	0	0	0	0	0	0	0	0
1000	-391	189	-269	153	-20	-554	-48	-281
2000	-650	316	-500	274	-48	-832	-63	-609
3000	-870	423	-715	395	-70	-1120	-82	-890
4000	-1088	528	-922	509	-91	-1419	-103	-1152
5000	-1307	630	-1132	624	-111	-1722	-127	-1402
6000	-1536	730	-1344	714	-132	-2032	-152	-1647
7000	-1765	852	-1551	856	-152	-2336	-178	-1903
8000	-2032	982	-1812	993	-173	-2651	-206	-2164
9000	-2358	1137	-2134	1159	-198	-2995	-242	-2475

Notes:
- Gages:
  - CEA-06-125WT-350
  - Gage Factor 2.165
- Test Assembly:
  1. Two Ceramic Cylinders Joined and Supported by Titanium Ring Stiffener
  2. The Cylinders are capped with Titanium Hemispheres DWG 55910-XXXX on Both Ends
- Materials:
  - The Ceramic is Coors AD 94 (94% Alumina)
  - The Titanium is Ti 6Al 4Va Alloy
- Data:
  - All readings are in microinches/inch

Table B-13. Strains on titanium ring stiffener DWG 0121604 in housing test assembly 1C.

Gage Locations

Pressure (PSI)	Inside Diameter Under Webs Gage Locations D Hoop	D Axial	DD Hoop	DD Axial	DDD Hoop	DDD Axial	Inside Diameter Between Webs X Hoop	X Axial	XX Hoop	XX Axial	XXX Hoop	XXX Axial
0	0	0	0	0	0	0	0	0	0	0	0	0
1000	3406	5844	1840	3860	2762	3463	-8301	676	-12164	913	-8964	813
2000	5352	9773	3327	6824	4712	6239	-15002	1302	-20309	1659	-15411	1360
3000	7036	13464	4621	9805	6445	9055	-21529	1953	-27760	2359	-21573	1872
4000	8757	17069	5896	12730	7763	11912	-27974	2699	-34894	3069	-27468	2393
5000	10590	20761	7145	15580	9044	14807	-34489	3289	-41935	3810	-33215	2864
6000	12735	24691	8500	18351	10337	17688	-40712	4011	-49038	4563	-38695	3344
7000	15248	28928	9921	20929	11772	20453	-46786	4636	-56259	5408	-43660	3784
8000	18903	34148	11930	23296	13630	23296	-52674	5274	-64457	6481	-48061	4235
9000	25774	42077	14545	24531	16372	25878	-57931	5681	-74830	8004	-50349	4348

Pressure (PSI)	Flange E Hoop	E Axial	EE Hoop	EE Axial	Web F Hoop	F Axial	FF Hoop	FF Axial
0	0	0	0	0	0	0	0	0
1000	-6096	1046	-4048	1148	-3887	-10463	-2678	-5547
2000	-10123	1772	-7590	1940	-6173	-15827	-5039	-11762
3000	-13548	2373	-10834	2834	-8411	-21340	-7175	-17125
4000	-16950	2949	-13973	3648	-10699	-27052	-9229	-22146
5000	-20388	3463	-17161	4461	-12994	-32831	-11263	-26963
6000	-24026	3876	-20546	4796	-15352	-38748	-13283	-31692
7000	-27525	4700	-23507	6132	-17654	-44547	-15392	-36633
8000	-31682	5431	-27508	7032	-20044	-50557	-17570	-41680
9000	-36781	6255	-32462	8087	-22693	-57134	-20215	-47711

Note: All stresses are in pounds per square inch, calculated on the basis of E = 16,5000,000 and M = .34

Table B-14. Principal stresses on titanium ring stiffener DWG 0121604 in housing test assembly 1C.

	Gage Locations									
	Inside Diameter Under Webs						Flange		Web	
Pressure	D		DD		DDD		E		F	
(PSI)	Hoop	Axial	Hoop	Axial	Hoop	Axial	Hoop	Axial	Hoop	Axial
0	0	0	0	0	0	0	0	0	0	0
1000	-510	303	20	7	-395	236	-182	57	-237	-48
2000	-842	515	-261	188	-726	444	-382	138	-474	-88
3000	-1179	728	-566	385	-1050	651	-603	226	-722	-127
4000	-1520	944	-887	590	-1373	855	-817	310	-974	-168
5000	-1850	1157	-1210	800	-1692	1061	-1018	391	-1205	-209
6000	-2165	1370	-1540	1020	-2027	1279	-1234	480	-1440	-236
7000	-2484	1580	-1875	1238	-2366	1500	-1433	564	-1676	-264
8000	-2797	1790	-2210	1460	-2699	1750	-1622	644	-1906	-291
9000	-3105	1996	-2546	1680	-3027	1932	-1806	724	-2129	-314
10000	-3380	2180	-2875	1891	-3337	2132	-1983	797	-2338	-339

NOTES:
Gages:
Gage Type: CEA-06-125WT-350
Gage Factor: 2.12
Test Assembly:
1. Two ceramic cylinders joined and supported by a metallic ring stiffener.
2. The Cylinder is capped with Titanium Hemispheres DWG 55910-0119737 on both ends
Materials:
The Ceramic is Coors AD 94 (94% Alumina)
The Aluminum is 7178-T651 alloy
Data: All readings are in microinches/inch
Structural Performance: Sustained external loading to 10,000 psi without implosion

Table B-15. Strains on aluminum ring stiffener DWG 0124007 in housing test assembly 1D.

Pressure (PSI)	Inside Diameter Under Web D Hoop	D Axial	DD Hoop	DD Axial	DDD Hoop	DDD Axial	Flange E Hoop	E Axial	Web F Hoop	F Axial
0	0	0	0	0	0	0	0	0	0	0
1000	-4785	1572	260	159	-3701	1233	-1905	-36	-2951	-1473
2000	-7843	2768	-2322	1189	-6763	2386	-3927	139	-5871	-2853
3000	-10956	3956	-5123	2313	-9747	3554	-6167	315	-8916	-4263
4000	-14104	5163	-8080	3470	-12731	4691	-8341	471	-12015	-5712
5000	-17135	6378	-11041	4677	-15661	5866	-10375	643	-14869	-7080
6000	-19991	7651	-14045	5973	-18731	7120	-12553	849	-17715	-8300
7000	-22906	8873	-17115	7227	-21836	8394	-14552	1063	-20577	-9536
8000	-25750	10119	-20170	8528	-24760	10029	-16450	1269	-23366	-10737
9000	-28551	11337	-23244	9802	-27887	10890	-18289	1494	-26057	-11864
10000	-31052	12425	-26271	10997	-30735	12030	-20074	1664	-28592	-12961

NOTES: All Stresses are in pounds per square inch, calculated on the basis of E = 10,400,000 and M = .33

Table B-16. Principal stresses on aluminum ring stiffener DWG 0124007 in housing test assembly 1D.

Pressure (PSI)	D Hoop	D Axial	DD Hoop	DD Axial	DDD Hoop	DDD Axial	X Hoop	X Axial	XX Hoop	XX Axial	XXX Hoop	XXX Axial
	Inside Diameter Under Webs								Inside Diameter Between Webs			
0	0	0	0	0	0	0	0	0	0	0	0	0
1000	-205	193	-61	108	90	41	-202	88	-464	207	-296	107
2000	-348	363	-130	237	52	[illegible]	-547	236	-911	401	-653	258
3000	-480	532	-204	373	-4	[illegible]	-906	392	-1337	588	-979	482
4000	-620	700	-280	511	-74	[illegible]	-1286	560	-1760	775	-1336	690
5000	-753	874	-352	656	-150	548	-1682	734	-2186	966	-1953	766
6000	-888	1049	-441	807	-230	689	-2092	913	-2618	1162	-2265	946
7000	-1030	1225	-527	960	-310	830	-2500	1095	-3045	1358	-2655	1128

Pressure (PSI)	Flange E Hoop	E Axial	EE Hoop	EE Axial	Web F Hoop	F Axial	FF Hoop	FF Axial
0	0	0	0	0	0	0	0	0
1000	-242	73	-186	21	-3	--	30	-350
2000	-500	186	-371	94	9	--	46	-704
3000	-698	367	-492	211	82	--	167	-992
4000	-895	400	-693	263	225	--	209	-1364
5000	-1240	500	-923	285	157	--	116	-1818
6000	-1480	612	-1152	371	80	--	142	-2181
7000	-1724	723	-1380	460	103	--	172	-2550

NOTES:
Gages:
Gage Type: CEA-06-125WT-350
Gage Factor: 2.165
Test Assembly:
1. Two ceramic cylinders joined and supported by a metallic ring stiffener.
2. The Cylinder is capped with Titanium Hemispheres DWG 55910-0119913 on both ends
Materials:
The Ceramic is Coors AD 94 (94% Alumina)
The Aluminum is 7075-T6 alloy
Data: All readings are in microinches/inch
Structural Performance: Sustained external loading to 7,000 psi without implosion

Table B-17. Strains on aluminum ring stiffener DWG 0121605 in housing test assembly 1E.

Gage Locations

Pressure (PSI)	Inside Diameter Under Webs: D Hoop	D Axial	DD Hoop	DD Axial	DDD Hoop	DDD Axial	Inside Diameter Between Webs: X Hoop	X Axial	XX Hoop	XX Axial	XXX Hoop	XXX Axial
0	0	0	0	0	0	0	0	0	0	0	0	0
1000	-1649	1463	-296	1026	1208	825	-2019	249	-4618	629	-3043	109
2000	-2663	2896	-604	2265	1200	1998	-5475	648	-9088	1171	-6627	496
3000	-3553	4360	-944	3568	1020	3217	-9064	1086	-13339	1713	-9570	1855
4000	-4540	5782	-1300	4885	708	4477	-12852	1583	-17556	2267	-12935	2907
5000	-5422	7300	-1582	6300	360	5818	-16804	2088	-21792	2855	-19843	1418
6000	-6324	8823	-2039	7720	-31	7155	-20899	2598	-26079	3479	-22791	2317
7000	-7303	10330	-2453	9174	-421	8493	-24960	3151	-30308	4122	-26642	2939

Pressure (PSI)	Flange: E Hoop	E Axial	EE Hoop	EE Axial	Web: F Hoop	F Axial	FF Hoop	FF Axial
0	0	0	0	0	0	0	0	0
1000	-2543	-80	-2090	-471	--	--	-998	-3969
2000	-5119	245	-3968	-332	--	--	-2175	-8039
3000	-6733	1595	-4929	568	--	--	-1872	-10934
4000	-8905	1221	-7075	400	--	--	-2814	-15114
5000	-12546	1060	-9675	-229	--	--	-5648	-20771
6000	-14916	1443	-12016	-107	--	--	-6743	-24908
7000	-17336	1798	-14334	54	--	--	-7814	-29099

NOTES: All Stresses are in pounds per square inch, calculated on the basis of E = 10,400,000 and M = .33

Table B-18. Principal stresses on aluminum ring stiffener DWG 0121605 in housing test assembly 1E.

Pressure (PSI)	Inside Diameter Under Webs D Hoop	D Axial	DD Hoop	DD Axial	DDD Hoop	DDD Axial	Inside Diameter Between Webs X Hoop	X Axial	XX Hoop	XX Axial	XXX Hoop	XXX Axial
0	0	0	0	0	0	0	0	0	0	0	0	0
1000	-280	226	139	3	-48	95	-325	155	-553	266	-150	64
2000	-477	412	63	130	-193	253	-709	340	-995	477	-493	221
3000	-652	580	-53	275	-340	410	-1093	517	-1427	679	-839	412
4000	-789	741	-164	423	-480	570	-1500	709	-1850	881	-1243	596
5000	-924	904	-271	574	-621	736	-1927	912	-2276	1085	-1665	791
6000	-1050	1064	-383	726	-767	902	-2359	1116	-2702	1286	-2083	989
7000	-1180	1230	-505	888	-914	1074	-2800	1328	-3131	1494	-2500	1194
8000	-1315	1394	-631	1050	-1066	1245	-3243	1540	-3557	1697	-2927	1395
9000	-1445	1562	-752	1212	-1225	1425	-3695	1760	-3980	1903	-3340	1608
10000	-1570	1722	-874	1370	-1399	1608	-4152	1980	-4389	2100	-3753	1813

Pressure (PSI)	Flange E Hoop	E Axial	EE Hoop	EE Axial	Web F Hoop	F Axial	FF Hoop	FF Axial
0	0	0	0	0	0	0	0	0
1000	-205	61	-257	135	-52	-192	-87	-186
2000	-452	171	-482	239	-113	-418	-177	-368
3000	-673	307	-675	359	-146	-647	-240	-504
4000	-911	413	-886	449	-208	-875	-314	-743
5000	-1143	522	-1085	539	-278	-1102	-393	-986
6000	-1371	633	-1279	632	-348	-1335	-464	-1218
7000	-1603	751	-1493	730	-415	-1567	-540	-1452
8000	-1835	865	-1720	830	-485	-1808	-612	-1680
9000	-2059	986	-1940	933	-553	-2048	-688	-1910
10000	-2288	1101	-2160	1031	-615	-2286	-757	-2130

NOTES:
Gages:
Gage Type: CEA-06-125WT-350
Gage Factor: 2.12
Test Assembly:
1. Two ceramic cylinders joined and supported by a metallic ring stiffener.
2. The Cylinder is capped with Titanium Hemispheres DWG 55910-0119737 on both ends
Materials:
The Ceramic is Coors AD 94 (94% Alumina)
The Aluminum is 7178-T651 alloy
Data: All readings are in microinches/inch
Structural Performance: Sustained external loading to 10,000 psi without implosion

Table B-19. Strains on aluminum ring stiffener DWG 0124008 in housing test assembly 1F.

Gage Locations

Pressure (PSI)	Inside Diameter Under Webs D Hoop	D Axial	DD Hoop	DD Axial	DDD Hoop	DDD Axial	Inside Diameter Between Webs X Hoop	X Axial	XX Hoop	XX Axial	XXX Hoop	XXX Axial
0	0	0	0	0	0	0	0	0	0	0	0	0
1000	-2397	1559	1634	570	-194	924	-3196	557	-5430	975	-1504	169
2000	-3980	2971	1236	1760	-1278	2209	-6965	1237	-9776	1735	-4903	681
3000	-5376	4258	441	3005	-2389	3476	-10765	1824	-14039	2429	-8205	1577
4000	-6355	5609	-285	4305	-3407	4804	-14776	2498	-18198	3157	-12212	2169
5000	-7302	6992	-952	5655	-4413	6198	-18978	3222	-22384	3897	-16386	2819
6000	-8157	8374	-1674	6998	-5478	7573	-23234	3939	-26582	4602	-20502	3520
7000	-9035	9811	-2474	8419	-6531	9014	-27564	4715	-30788	5378	-24579	4307
8000	-9978	11205	-3320	9824	-7646	10425	-31918	5483	-34978	6106	-28788	5008
9000	-10849	12665	-4109	11249	-8809	11913	-36346	6310	-39121	6881	-32788	5903
10000	-11691	14051	-4924	12623	-10135	13379	-40832	7117	-43136	7605	-36819	6705

Pressure (PSI)	Flange E Hoop	E Axial	EE Hoop	EE Axial	Web F Hoop	F Axial	FF Hoop	FF Axial
0	0	0	0	0	0	0	0	0
1000	-2158	-78	-2480	586	-1346	-2441	-1732	-2506
2000	-4617	255	-4705	933	-2929	-5314	-3483	-4977
3000	-6672	991	-6495	1590	-4196	-8113	-4742	-6807
4000	-9042	1311	-8611	1828	-5798	-11013	-6526	-9881
5000	-11330	1690	-10587	2112	-7489	-13932	-8384	-13021
6000	-13563	2107	-12493	2450	-9203	-16921	-10106	-16002
7000	-15816	2591	-14613	2770	-10879	-19887	-11895	-19026
8000	-18085	3028	-16877	3062	-12624	-22969	-13613	-21964
9000	-20233	3578	-19048	3417	-14342	-26032	-15386	-24941
10000	-22463	4038	-21239	3714	-15982	-29049	-17038	-27775

NOTES: All Stresses are in pounds per square inch, calculated on the basis of E = 10,400,000 and M = .33

Table B-20. Principal stresses on aluminum ring stiffener DWG 0124008 in housing test assembly 1F.

APPENDIX C: HEMISPHERICAL CERAMIC BULKHEADS FOR 12-INCH-DIAMETER CERAMIC CYLINDRICAL HOUSINGS

All appendix C figures and tables are placed at the end of appendix C text.

FIGURES

TABLES

APPENDIX C: HEMISPHERICAL CERAMIC BULKHEADS FOR 12-INCH-DIAMETER CERAMIC CYLINDRICAL HOUSINGS

INTRODUCTION

In prior studies of ceramic housings for underwater vehicles, no effort was devoted to the design and evaluation of ceramic hemispherical bulkheads. Instead, all effort focused on the ceramic cylinders that provide the bulk of the buoyancy in an underwater housing. It was felt that if it could be demonstrated that ceramic cylinders could be designed reliably, fabricated economically, and tested successfully, more interest would be generated in the Navy to fund further investigations into application of ceramic housings to underwater vehicles.

The preliminary investigations into the structural performance of ceramic cylindrical housings conducted with 6-inch-OD scale-model monocoque cylinders radially supported at the ends with titanium hemispherical bulkheads were very promising. A weight-to-displacement (W/D) of 0.64 was attained by housings with a design depth of 20,000 feet which provided them with the capability to carry twice as heavy a payload as housings made of titanium. If the titanium hemispherical bulkheads could be successfully replaced with ceramic bulkheads, not only the overall buoyancy, but also the elastic stability of the housing would improve significantly.

Because of the importance that ceramic hemispherical bulkheads have in the ceramic housing assembly, a major portion of this investigation was devoted to their design, fabrication, and experimental evaluation.

OBJECTIVES

The exploratory investigation into the feasibility of replacing 12-inch-OD hemispherical titanium bulkheads with ceramic bulkheads focused on the following objectives:

1. *Design and evaluation of ceramic hemispheres with single or multiple penetrations* that will not act as crack initiators when the hemisphere is, after proof testing to 10,000 psi, pressure cycled repeatedly to 9,000-psi design pressure. The penetrations are to be adequately sized to handle 1.5-inch-diameter electrical bulkhead penetrators.
2. *Design and evaluation of metallic inserts for penetrations* in ceramic hemispheres to accommodate threaded, commercially available electrical or hydraulic bulkhead penetrators. These inserts are not to initiate cracks on the ceramic shell in contact with the inserts when the hemisphere is, after proof testing to 10,000 psi, pressure cycled repeatedly to 9,000-psi design pressure.
3. *Design and evaluation of a metallic end ring* for the equatorial bearing surface of the hemisphere. The end ring is to serve three functions: (1) as an end cap enclosing the equatorial bearing surface of the hemisphere, (2) as a radial support for the cylinder end, and (3) as an attachment point for the split wedge band fastening the hemisphere to the cylinder.

APPROACH

Five 12-inch-OD bulkheads with penetrations were designed and fabricated from 94-percent alumina-ceramic (figure C-1). After fitting out with titanium penetration inserts and joint end rings, they were instrumented on their interior surfaces with electric resistance strain gages (figure C-2), mated with a single monocoque ceramic cylinder to form a 12-inch cylindrical housing (table C-1) and subsequently subjected to external pressure testing (tables C-2 and C-3).

All pressure housings satisfactorily withstood a proof test to 10,000 psi, followed by many pressurizations to 9,000-psi design pressure. The compressive stresses in all hemispheres, except for the Mod 3 hemisphere, did not exceed the design stress of −150,000 psi at 9,000-psi design pressure (figure C-3). In Mod 3, while the nominal membrane stresses were below −150,000 psi, the peak hoop stress around the unreinforced polar opening approached −300,000 psi. Some spalling took place on the bearing surfaces of hemispheres

and cylinders after repeated pressure cycling. The causes of early spalling were identified and recommendations were formulated to eliminate them in future designs.

DESIGN DETAILS

Hemispheres

The *nominal thickness* of the hemisphere was selected to equal one-half of the cylinder thickness. This equalized the hoop membrane stresses in both ceramic shells, and, as a result, it equalized also their radial deflections. Because of this, the bending stresses at the joint between the hemisphere and the cylinder were minimized.

The *nominal membrane stresses* in the spherical shell with 0.200-inch thickness were calculated to be 152,475 psi at 10,000-psi proof pressure, just slightly above the design stress of –150,000 psi selected for 94-percent alumina-ceramic pressure housings. At this design stress level, the *nominal safety factor* (SF) is 2, based on minimum material strength of 94-percent alumina ceramic obtained by uniaxial testing of cylindrical test specimens. The *real* SF is in excess of 2.4 as hydrostatic testing of 94-percent alumina-ceramic spheres to catastrophic failure by other investigators has demonstrated compressive strengths in excess of 360,000 psi.

Peak stresses in the spheres were calculated to increase by approximately 100 percent above the nominal membrane stresses at penetrations in a shell of constant thickness. To reduce the magnitude of peak stresses, steps were taken to increase the shell thickness around penetrations by 100 percent. There are several approaches to achieve this, and hemispheres Mod 1, 2, 3, and 4 demonstrate these approaches.

Diameters of penetrations in hemispheres varied from 2 to 3 inches (i.e., $0.15<d/D_o<0.25$). The 2-inch-diameter penetration was the smallest hole capable of accommodating standard, commercially available 1.5-inch-diameter electrical bulkhead penetrators threaded into metallic penetration inserts. The other-sized holes were created by enlarging the 2-inch-diameter holes after the edges of the smaller holes were damaged either during assembly of the penetrators, or during pressure testing.

Single Penetrations

Single penetrations were incorporated into the spherical shell using the following design procedures:

Procedure 1. The shell is reinforced *locally* around the penetration to reduce the peak membrane stress at this location to –150,000 psi at design pressure. For a single polar penetration, the reinforcement took the shape of a boss centered at the pole of the hemisphere (figure C-4). The nominal thickness of the shell at the edge of the penetration increased from 0.2 to 0.5 inch in order to reduce the hoop stress around the penetration from –300,000 psi to <–150,000 psi design stress value.

Several iterations of boss configuration had to be performed to minimize bending stresses in the transition zone between the massive reinforcement around the polar penetration and the thin spherical shell. The resulting reinforcement around the polar penetration was well proportioned; the hoop stress on the interior surface was only –35,000 psi while the radial stress was positive, but less than 5,000 psi. At all other locations on the interior surface, the compressive stresses were fairly uniform and in the –100,000 to –130,000 psi range. Some bending between the thick polar reinforcement around the penetration and the thin shell took place, as shown by the reduced compressive stress on the interior surface at this location.

Procedure 2. The shell thickness is increased gradually by approximately 100 percent from areas without penetrations to where penetrations are located. For hemispheres with a single polar penetration (figure C-27), the shell is increased in thickness from the calculated nominal value at the equator to its maximum thickness at the pole.

For the 12-inch-diameter hemisphere Mod 2 with a single polar penetration, the thickness of the shell was increased from 0.205 inch at the equator to 0.44 inch at the edge of the penetration. Because of the gradual increase in thickness, bending moments are not introduced into the shell near the

penetration, as is the case with Mod 1 hemispheres. Also, because of the increase in shell thickness, the magnitude of hoop membrane stresses over the whole shell area is less than −100,000 psi at 9,000-psi design pressure. Only at the equator does the meridional (axial) stress increase to −121,000 psi; still far below the specified −150,000-psi design stress level at 9,000-psi design pressure.

Procedure 3. The nominal shell thickness based on −150,000-psi design stress is kept constant everywhere on the hemisphere regardless of where the penetrations are located (figure C-42). Since there is no reinforcement around a single penetration, or multiple penetrations, the compressive stresses around the edge of the penetration increase by 100 percent from the nominal stress value of −150,000 psi. This is a very high stress level for 94-percent alumina ceramic as it reduces the actual SF to less than 1.2.

This is not a structurally desirable approach for incorporating penetrations in the ceramic hemispheres as the resulting peak stresses around penetrations are too close to the ultimate strength of the ceramic and, thus, are incompatible with prudent design criteria. Still, hemisphere Mod 3 with constant shell thickness incorporating a penetration was designed, fabricated, and pressure cycled in this program to provide a structural performance baseline for other hemispheres with reinforcements around penetrations.

The Mod 3 hemisphere designed by this approach on the basis of −150,000-psi design stress has only a nominal shell thickness of 0.2 inch. The Mod 3 hemisphere represents the lightest design for a 12-inch-diameter hemisphere with a single polar penetration. Although it has been shown subsequently that the Mod 3 hemisphere is capable of successfully withstanding a proof test to 10,000 psi and at least 34 pressure cycles to 9,000-psi design pressure, this design is not recommended for service where a fatigue life in excess of 100 cycles is expected. Maximum hoop stress of −190,000 psi was recorded near the penetration at design pressure.

The picture changes dramatically, however, when penetrations are not incorporated into the hemisphere. In that case, the maximum hoop stress at design pressure does not exceed the −150,000-psi design stress at 9,000-psi design pressure. The resulting ceramic hemispherical bulkhead assembly with Mod 1 end rings has a 0.43 W/D ratio, a significant improvement over the 0.7 W/D ratio of a titanium hemispherical bulkhead with a critical pressure of 13,500 psi. Because of the acceptable stress levels and outstanding W/D ratio, ceramic hemispherical bulkheads with $t/D_0=0.017$ uniform shell thickness are considered to represent a cost-effective replacement for titanium hemispherical bulkheads without penetrations.

Multiple Penetrations

Multiple penetrations were incorporated into the spherical shell using the same design procedures as those for single penetrations:

Procedure 1. The shell of the hemisphere with multiple penetrations is thickened only locally around the penetrations on the circumference of the hemisphere at a 45-degree latitude (figure C-54). Since it is time-consuming, difficult, and, therefore, expensive to carve out circular pads around several individual penetrations that would reinforce their edges, a continuous band of thicker shell material was substituted. The replacement of many reinforcement pads around penetrations with a single reinforcement band girding the hemisphere between 30° and 60° latitudes had also a beneficial effect on the structural performance of the hemisphere by decreasing local deformations of the shell known to initiate buckling at a lower pressure. The replacement of many pads with a single band added weight to the hemisphere. However, the associated reduction in fabrication cost and improvement in structural performance made this a very cost-effective design change.

The Mod 4 hemispherical shell incorporating this design approach was 100-percent thicker around the penetrations than at the equator. As a result of this variation in shell thickness, there are bending movements generated in the transition zones between the thick- and thin-shell areas. Still, the maximum compressive stress at 9,000-psi design

pressure did not exceed 141,000 psi on the interior surface, and there was a total absence of tensile stresses.

Procedure 2. The shell of the hemisphere with multiple penetrations is increased in thickness from a nominal value at the pole to its maximum value at the equator. The reason for increasing the shell thickness at the equator instead of at the pole, as it was done with design Procedure 2 for the Mod 2 hemisphere with a single polar penetration, is that one cannot locate many large penetrations in the polar region as, otherwise, the separation between their edges would not be adequate.

To minimize the increase in shell thickness and weight, while at the same time providing adequate reinforcement, penetrations must be located as close as it is structurally feasible to the equator, where the shell is the thickest. An acceptable location is at 30° latitude, since at that location the distance between the edge of the penetration and the equator still exceeds the minimum structurally acceptable spacing between the edges of adjacent penetrations. A conservative value for this spacing is the diameter of the penetration. To keep the peak compressive stresses around the penetrations below –150,000 psi, the minimum shell thickness at any location around the penetration's circumference will have to exceed by 100 percent the nominal shell thickness, calculated on the basis of –150,000-psi design stress under proof-test pressure of 10,000 psi.

One additional feature of thickening the shell at the equator and not at the pole is the decrease by at least 50 percent of the axial bearing stress on the plane-equatorial bearing surface. Since the cyclic fatigue life of the ceramic component is inversely related to the axial stress on the ceramic bearing surface, reducing its magnitude by 50 percent increases the cyclic fatigue life by a factor of 10, or more.

The design of Mod 4 did not follow this procedure because the design requirement called for not only four penetrations around the circumference of the hemisphere at 45° latitude, but also for a single polar penetration. The only approach to providing all of these penetrations with material thickness that exceeds the nominal shell values by 100 percent is to increase the nominal shell thickness either (1) by 100 percent over the whole hemisphere, or (2) by about 200 percent at the pole, and then decreasing it toward the nominal shell thickness at the edge.

Neither approach was chosen, as there was insufficient funding to have another hemisphere fabricated for testing at this time. The approach chosen instead was to modify the already tested hemisphere Mod 2 in which the shell thickness was increased from the nominal 0.200-inch value at the equator to the maximum 0.445-inch value at the pole. Four penetrations were cored into the Mod 2 hemisphere at the 45° latitude (figure C-66). The thickness of the shell around these four penetrations varied from 0.27 to 0.35 inch, while around the central penetrations it was 0.42 inch. Because of this arrangement, the stresses around the penetrations varied from approximately –150,000 psi at the polar penetration to –220,000 psi at the penetrations on the 45° latitude. Thus, the maximum stress around the four penetrations was higher than the design stress of –150,000 psi, but probably acceptable as it still provided a nominal SF of 1.36 for 94-percent alumina ceramic. When one takes into account the increase in compressive strength under biaxial loading that exists in ceramic hemispheres, the real SF probably increases to 1.5, making this hemisphere design acceptable.

Connector Inserts for Penetrations

Standard commercial, high pressure, electrical bulkhead penetrators with steel bodies are not well suited for direct installation in the ceramic shell without custom made inserts. Such inserts are required to eliminate point contact between the threaded steel body of the bulkhead penetrator and the ceramic surfaces and to provide a threaded hole for seating the penetrator.

The original concept of the connector insert was a flanged tube threaded on the inside to receive a threaded electrical bulkhead penetrator, and threaded on the outside to engage with a nut. The exterior threads did not extend the whole length of the tube; the exterior of the tube contacting the ceramic shell was radially smooth and its diameter

was only 0.002 to 0.004 inch smaller than the diameter of the penetrations.

Sealing was originally accomplished with an axially compressed O-ring seal held captive by an O-ring groove in the flanged head of the tube. Both Mod 1 and Mod 2 hemispheres were equipped with such connector inserts (figures C-6 and C-29). After a single proof test to 10,000 psi, however, followed by 34 pressure cycles to 9,000 psi, a crack was detected on the exterior surface of the Mod 2 hemisphere directly beneath the O-ring groove in the flange of the connector insert. No cracks were detected under the connector insert in Mod 1 hemispheres.

Following the inspection, the polar penetration in the Mod 2 hemisphere was enlarged to eliminate the circular crack paralleling the circumference of the penetration. When completed, the diameter of the polar penetration was 3 inches. In addition to enlarging the polar penetration, four equally spaced 2-inch-diameter holes were cored out from the hemispheres at 45° latitude. The reworked sphere was returned for further pressure cycling as a Mod 5 sphere configuration after being equipped with modified connector inserts.

The modification to connector inserts consisted of modifying the flange on the connector insert to eliminate any axial bearing contact between the metallic flange on the connector insert and the ceramic shell. This was achieved by interposing a laminated phenolic bearing washer between the metallic flange and the ceramic surface on the sphere (figures C-7 and C-30).

The phenolic washers served two functions; they acted (1) as a vertically compliant, but radially restrained, gasket between the flange of the metallic connector insert and the exterior surface of the sphere, and (2) as a spacer between the flange and the sphere controlling the extent to which the O-ring seal beneath the flange was axially compressed. The laminated, cloth-reinforced phenolic material was chosen because of its high compressive strength and low creep under load. In all cases, the curvature of the lower surface on the washer was machined to match the spherical curvature of the ceramic sphere while the upper surface on the washer was plane, matching that of the flange on the connector insert. The axial compressive loading on the laminated phenolic bearing gasket varied from one connector insert design to another. The highest loading at 10,000-psi proof pressure applied to the bearing gasket was 12,400 psi on Mod 1 spheres, and the lowest value was 7,400 psi on Mod 3 and 4 spheres.

The modified connector insert with the phenolic washer performed satisfactorily; no cracking was observed on any of the ceramic hemispheres on the exterior surface of the spheres after repeated pressure cycling. However, a crack-free cyclic fatigue life has not been established experimentally for a connector insert resting upon a laminated phenolic washer since pressure cycling of ceramic housings did not continue beyond 121 pressurizations to design depth. It appears that a connector insert resting upon a laminated phenolic washer will not initiate cracks on the surface of the sphere in less than 1,000 pressurizations to design pressure.

Although the above connector insert performed satisfactorily, it has one drawback that should be eliminated in future designs. The present connector insert design requires a very small radial clearance between the insert body and the edge of the penetration in the ceramic shell for the proper performance of the O-ring seal as, otherwise, the O-ring will squeeze through under pressure. Because of the snug fit, the ceramic shell contacts the metallic insert when pressurized and, as a result, generates some compressive bearing stress in the ceramic shell edge that, after many repeated pressurizations, may initiate cracks in it.

This shortcoming of the penetrator insert design may be eliminated by decreasing the interior and exterior diameters of the phenolic pad until the internal diameter contacts the connector body. The O-ring is placed now in the space between the exterior diameter of the pad and the lip on the connector insert flange Since the O-ring is trapped between the exterior diameter of the pad, insert flange, and the surface of the shell, the radial clearance between the body of the insert and the

penetration insert can be increased to 0.005–0.010 inch eliminating any radial bearing stress on the ceramic shell at that location.

End Ring

The end ring is designed to perform three functions. It serves as (1) an end cap for the equatorial bearing surface on the hemispheres, (2) a flange providing radial support to the end of the adjoining cylinder, and (3) a component of a mechanical joint for fastening the hemisphere to the cylinder. The Mod 0 end ring designed for the 12-inch-diameter hemisphere performed all three functions satisfactorily. None of the five hemispheres equipped with these end rings failed catastrophically during the test program.

During pressure cycling, however, it became apparent that the Mod 0 end cap is not providing adequate bearing support to the hemisphere, as evidenced by appearance of spalling on the exterior surface of the hemisphere after approximately 50 pressure cycles to design pressure. This finding was corroborated in another program by the testing of 20-inch-diameter hemispheres also equipped with Mod 0 end rings (Reference 1). In that case, spalls were visible after 100 pressure cycles, and catastrophic implosion occurred on the 109th cycle.

The inability to provide adequate support for the equatorial bearing surface on the hemisphere by a Mod 0 end joint was corrected by extending the length of the flanges on the end ring. The design of improved Mod 1 end rings is discussed in detail in appendix D. Due to financial and scheduling constraints, Mod 1 end rings for 12-inch-OD hemispheres were neither fabricated, nor evaluated in this program.

TEST RESULTS

The *12-inch-diameter hemispheres* did not fail during proof testing to 10,000 psi, or cyclic testing to 9,000-psi design pressure.

Penetrations in the hemispheres did not initiate cracking even though the peak compressive stresses at the edges of the penetrations in the Mod 3 hemisphere approach 300,000 psi during proof testing.

The *connector inserts* did not initiate any cracks in the ceramic shell when high-pressure-laminated phenolic washers served as axial bearing gaskets between the metallic flange of the insert and the ceramic shell.

The *Mod 0 end ring* did not provide adequate support to the equatorial bearing surface on the hemisphere, resulting in spalling of this surface after only about 50 pressure cycles to design pressure. Catastrophic failure is expected after 100 cycles. The redesigned Mod 1 end ring described in appendix D has eliminated early spalling and, for this reason, will be used in all future hemisphere assemblies.

CONCLUSIONS

1. Ceramic hemispheres have been successfully designed and fabricated in 94-percent alumina incorporating single, or multiple penetrations equipped with metallic inserts capable of mating with threaded electrical, or hydraulic, bulkhead penetrators.

2. When properly reinforced with additional ceramic material around penetrations, the peak compressive stresses in ceramic hemispheres with nominal $t=0.017D_0$ shell thickness can be reduced below −150,000-psi design stress level and the tensile stresses completely eliminated when pressurized externally to 9,000-psi design pressure.

3. The cyclic fatigue life of ceramic hemispheres equipped with Mod 0 end rings, although adequate for the purposes of this program, does not meet the operational needs of typical deep submergence underwater vehicles that require as a minimum a cyclic fatigue life of 500 dives to design depth. This shortcoming in performance can be resolved by redesigning (1) the shape of the equatorial bearing surfaces on the hemisphere and (2) the size of the annular seat in the titanium end ring, or both.

4. The W/D ratio of ceramic hemispherical bulkheads with 9,000-psi design depth varies from 0.5 for complete hemisphere assemblies without penetration, to 0.73 for hemispheres with four penetrations (table C-4). This represents a payload increase of approximately 58 percent over titanium hemispheres with the same design depth and number of penetrations.
5. Besides an increase in payload capability, the ceramic hemispheres also provide stiffer radial support to the ends of monocoque ceramic cylinders resulting in higher critical pressure of the whole housing assembly.

RECOMMENDATIONS

1. Ceramic hemispherical bulkheads are to be preferred over titanium hemispherical bulkheads, as they increase both the payload capability and the critical pressure of the cylindrical housing assembly.
2. All ceramic hemispherical bulkheads should terminate at the equator with a cylindrical skirt whose thickness matches that of the adjoining cylinder. This reduces the axial stress on the ceramic bearing surface and, as a result of the bearing stress reduction, the cyclic fatigue life of the ceramic bearing surface will increase significantly.
3. The length of cylindrical skirts should match or exceed the depth of the annular seat on the Naval Ocean Systems Center (NOSC)* Mod 1 joint ring which is bonded to the cylindrical skirt. The depth of the seat should be $\leq$3.4t of the skirt thickness. With such support to the equatorial surfaces on ceramic hemispheres their cyclic fatigue life exceeds 500 cycles to design depth.
4. The membrane design stress should not exceed −150,000 psi at design pressure for ceramic hemispheres fabricated from 94-percent alumina. For 96-percent alumina, the membrane design stress can increase to −160,000 psi at design depth.
5. *For bulkheads without penetrations*, one should select a hemisphere with uniform wall thickness, except at the equator where it transitions into a cylindrical skirt whose thickness matches that of the adjoining cylinder.
6. *For bulkheads with a single polar penetration*, the recommended design is a ceramic hemisphere of constant thickness, except for the boss at the pole and the cylindrical skirt at the equator where the shell doubles in thickness to match that of the adjoining cylinder.
7. *For bulkheads with multiple penetrations* equally spaced around their circumferences at 45° latitude, the recommended shape is a ceramic hemisphere of constant thickness except around the penetrations and the cylindrical skirt at the equator where the shell doubles in thickness.
8. *For bulkheads with multiple penetrations* located both at the pole and around the circumference at 45° elevation, the recommended design is a ceramic hemisphere whose thickness uniformly decreases from the pole toward the equator that terminates in a cylindrical skirt whose thickness matches that of the cylinder. In this design, the thickness of the shell at the pole is based on a membrane stress of −75,000 psi at design depth. Because of the uniformly decreasing wall thickness from the pole to the equator, the peak stresses around the penetrations at 45° latitude will increase above −150,000 psi, but not sufficiently to be a source of concern.

---

*NOSC is now the Naval Command, Control and Ocean Surveillance Center (NCCOSC) RDT&E Division (NRaD).

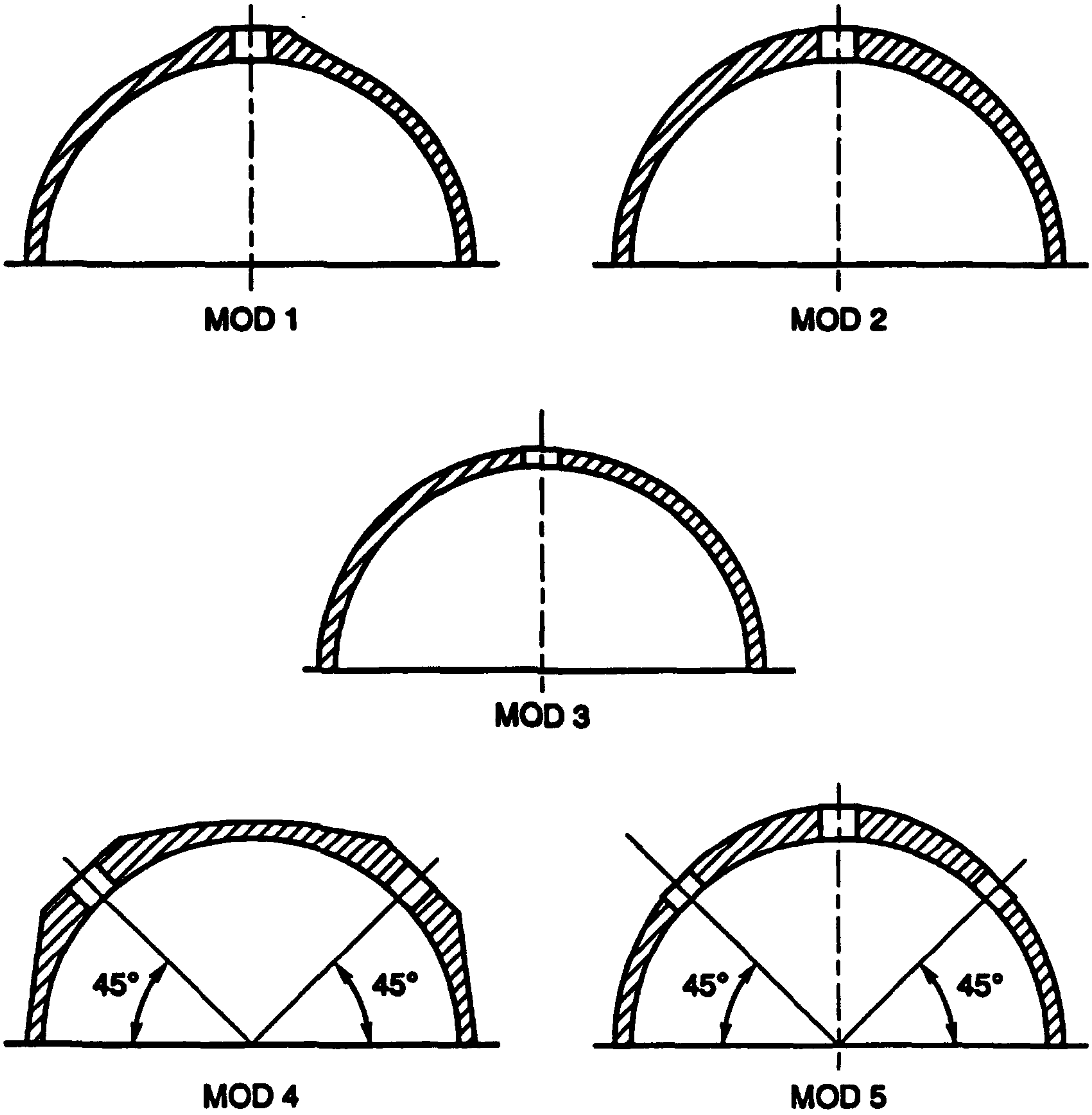

Figure C-1. Configurations of hemispherical ceramic bulkheads described in appendix C.

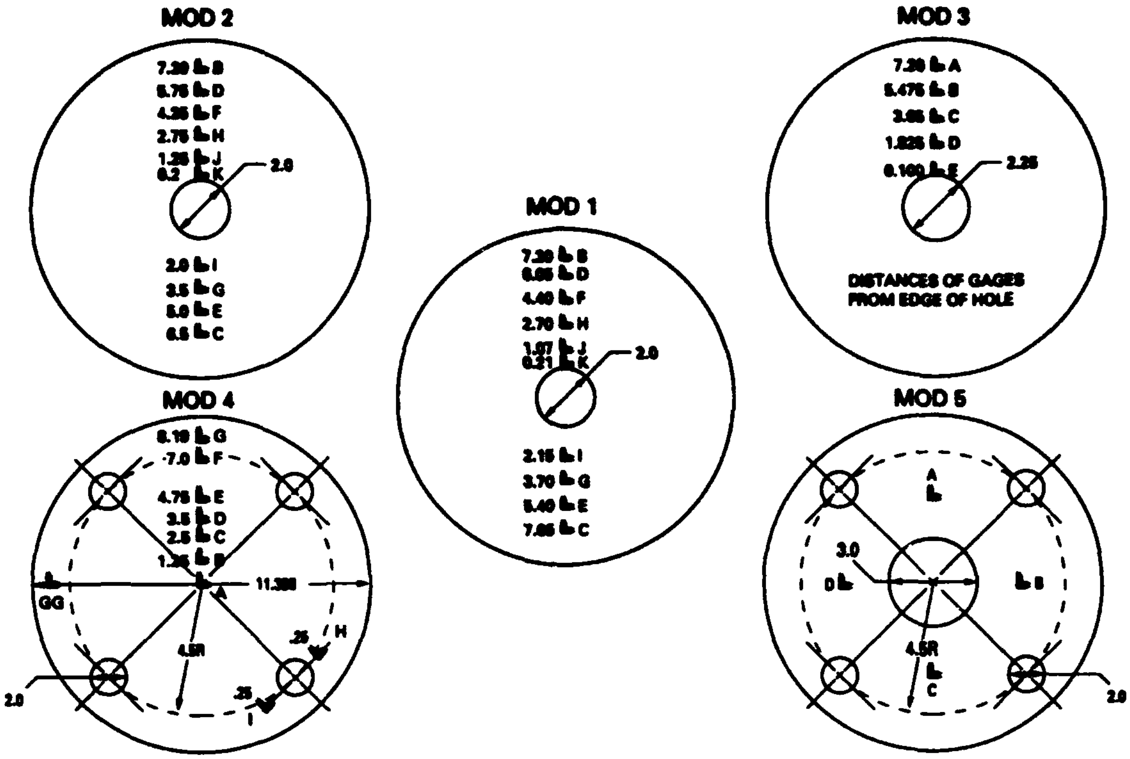

Figure C-2. Location of strain gages on ceramic hemispheres.

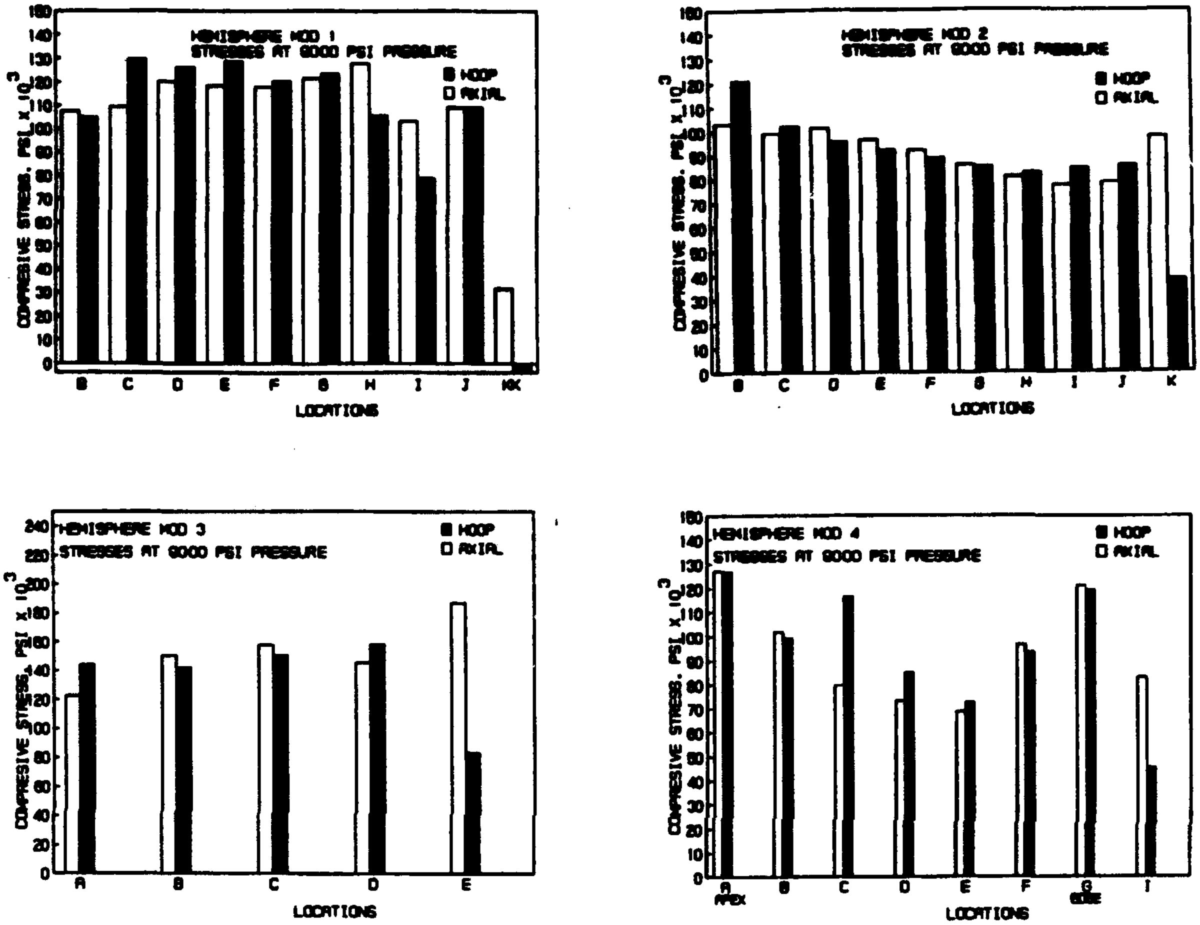

Figure C-3. Distribution of stresses in hemispherical ceramic bulkheads.

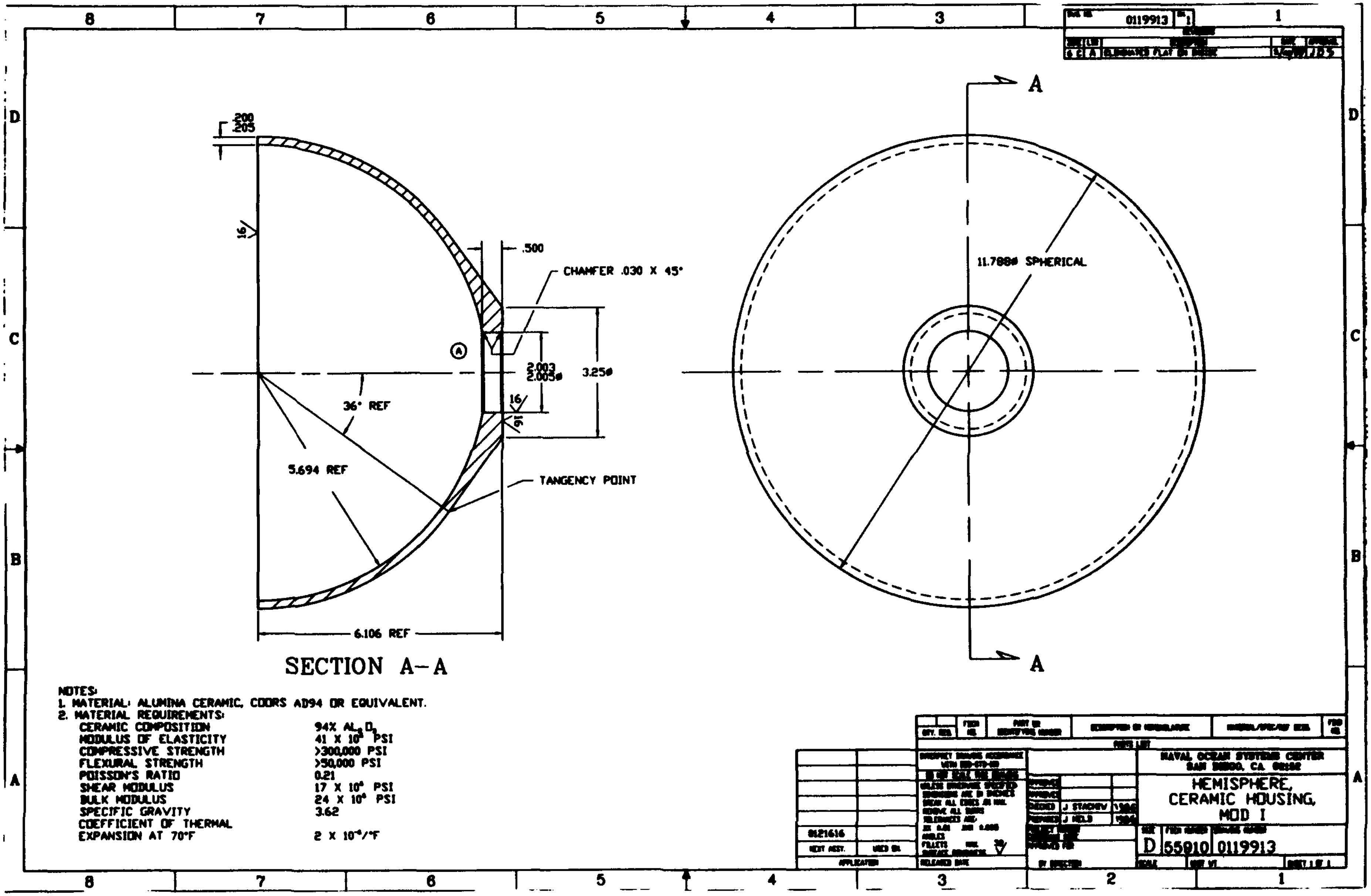

Figure C-4. Mod 1 ceramic hemisphere dimensions.

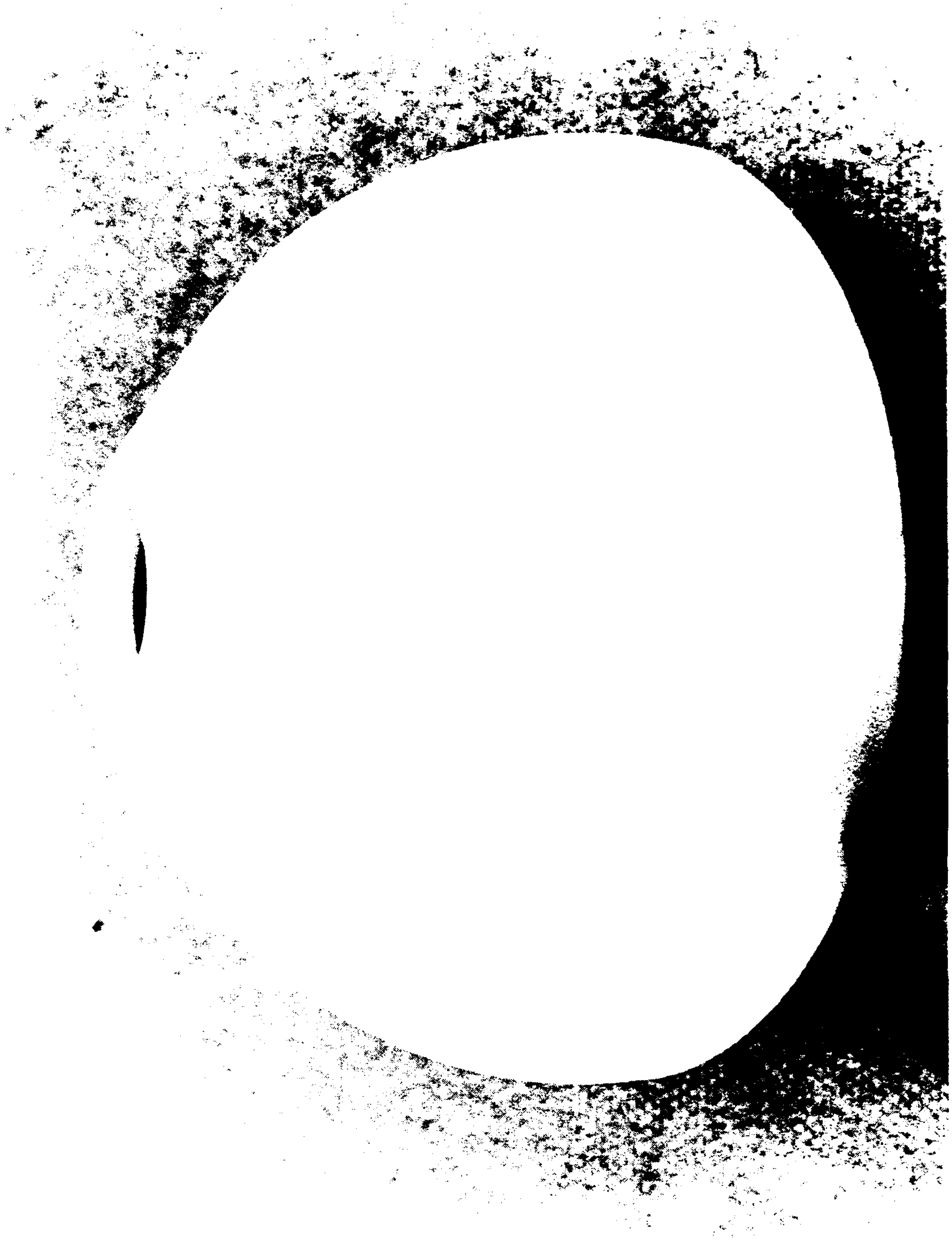

Figure C-5. Exterior view of Mod 1 hemisphere.

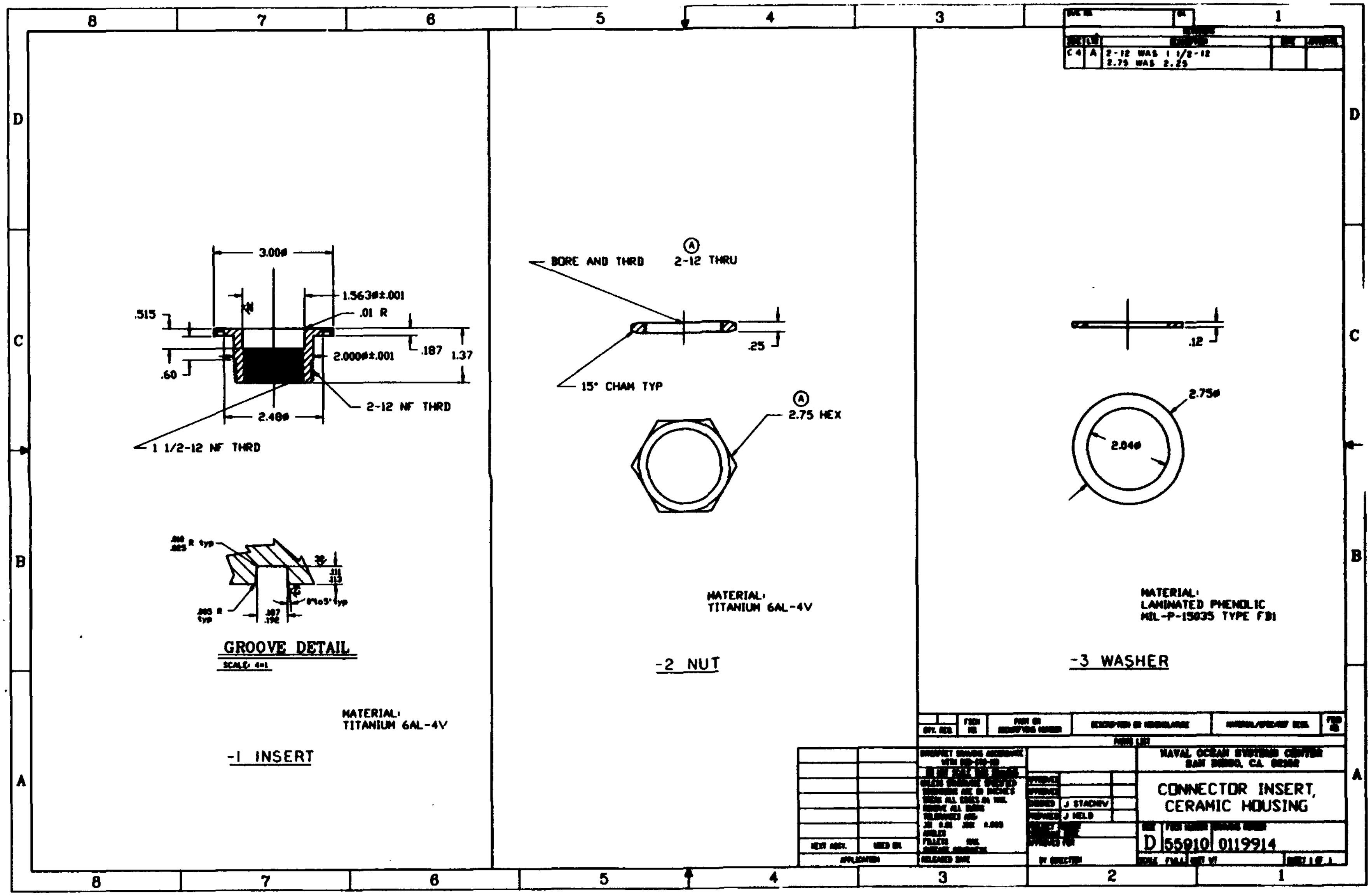

Figure C-6. Connector insert (Revision 0) without phenolic bearing pad for Mod 1 ceramic hemisphere.

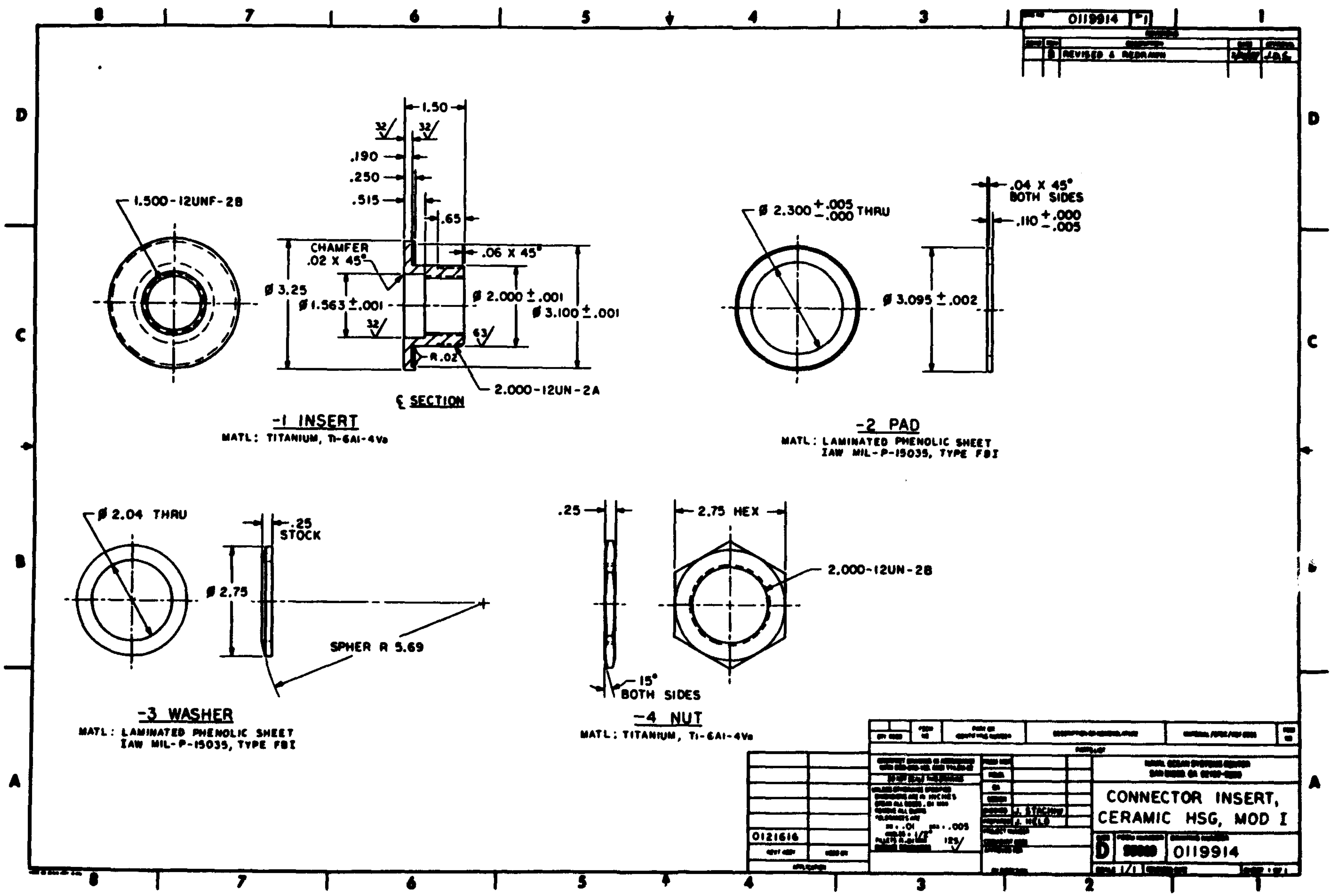

Figure C-7. Improved connector insert (Revision A) for Mod 1 ceramic hemisphere after incorporation of phenolic bearing pad.

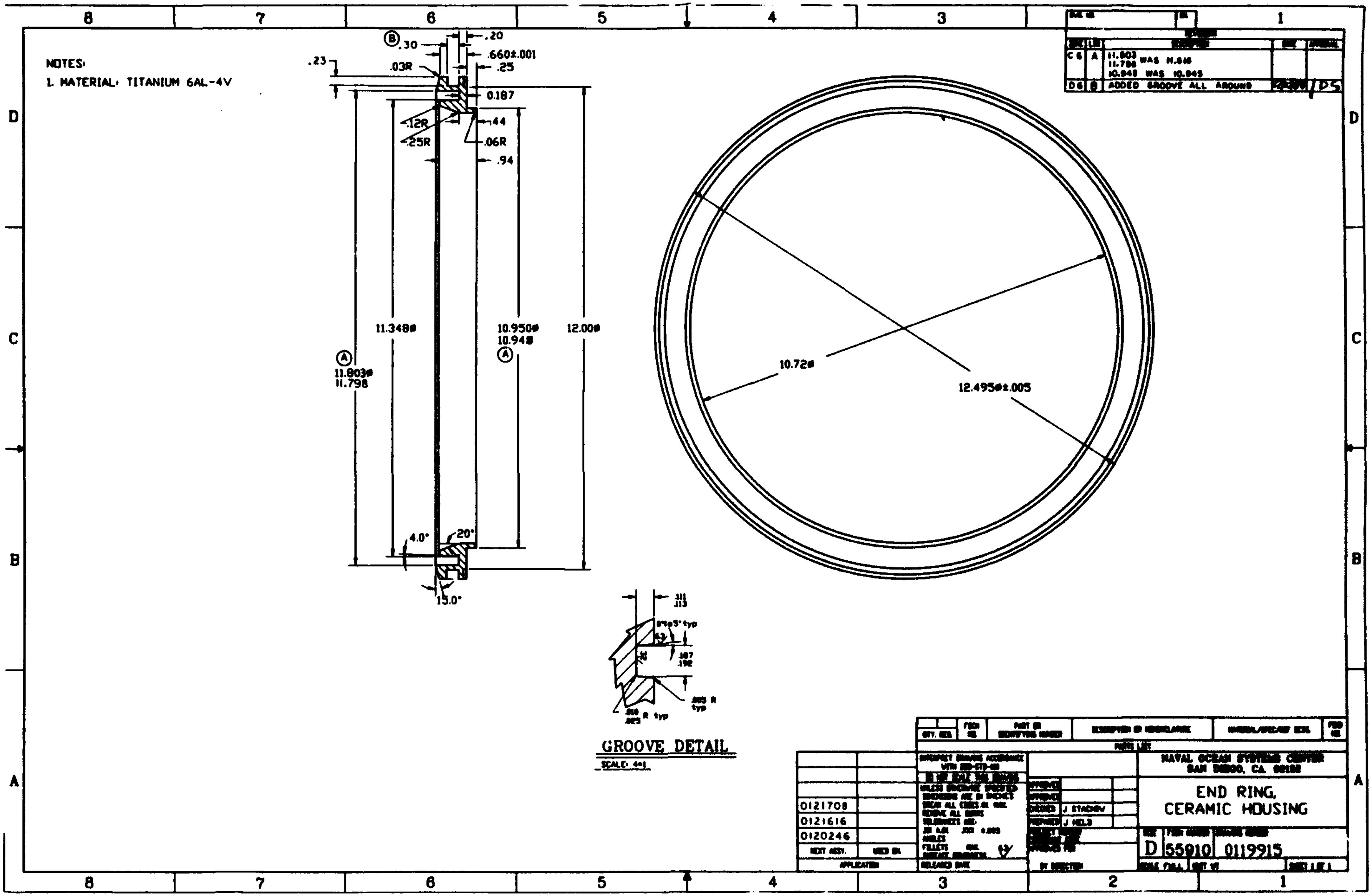

Figure C-8. Mod 0 end ring for ceramic hemispheres.

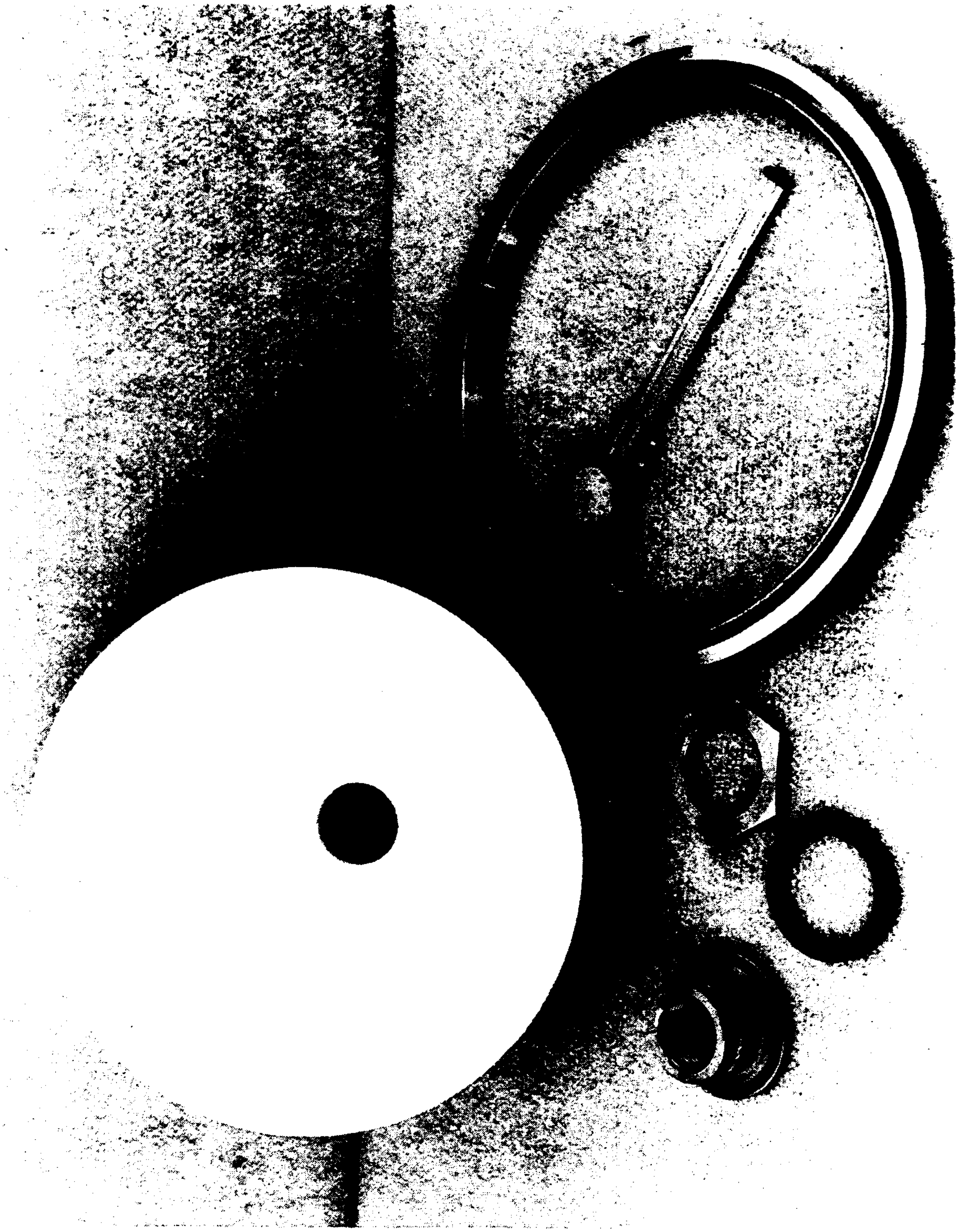

Figure C-9. Components of Mod 1 ceramic bulkhead assembly.

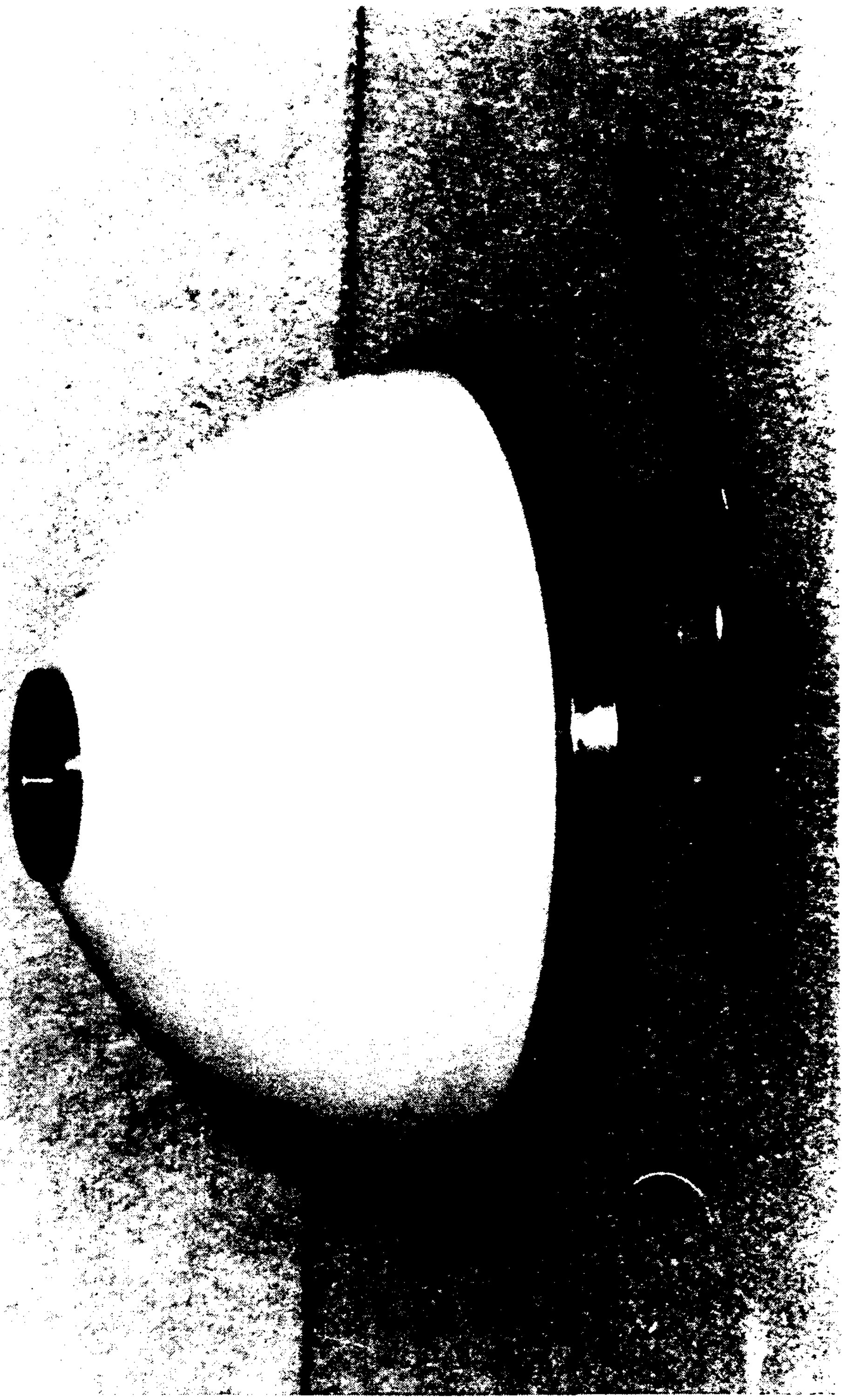

Figure C-10. Ceramic bulkhead assembly Mod 1; exterior view.

Figure C-11. Ceramic bulkhead assembly Mod 1; interior view.

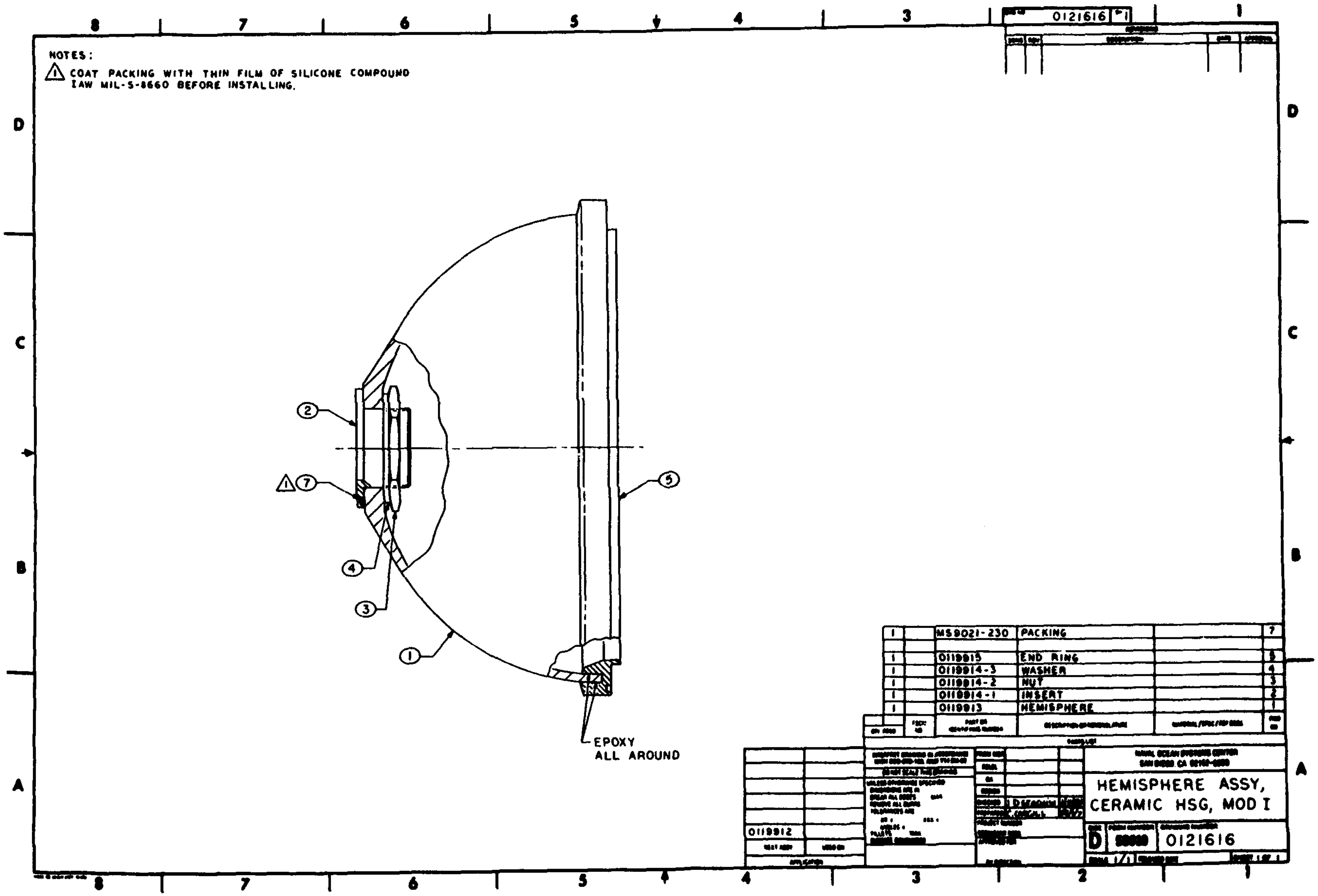

Figure C-12. Ceramic housing test assembly 2A incorporating the Mod 1 ceramic bulkhead

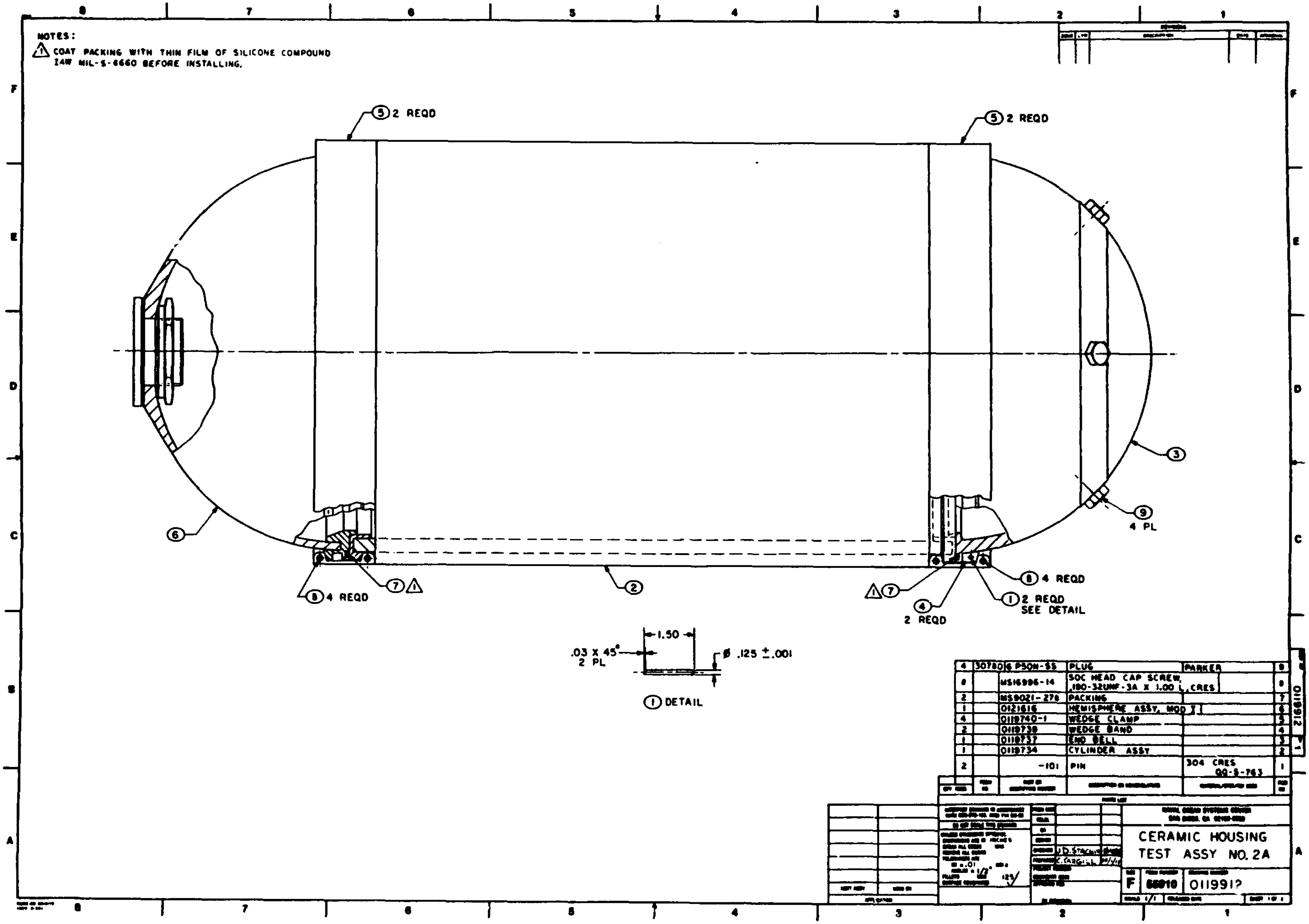

Figure C-13. Mod 1 ceramic housing test assembly 2A.

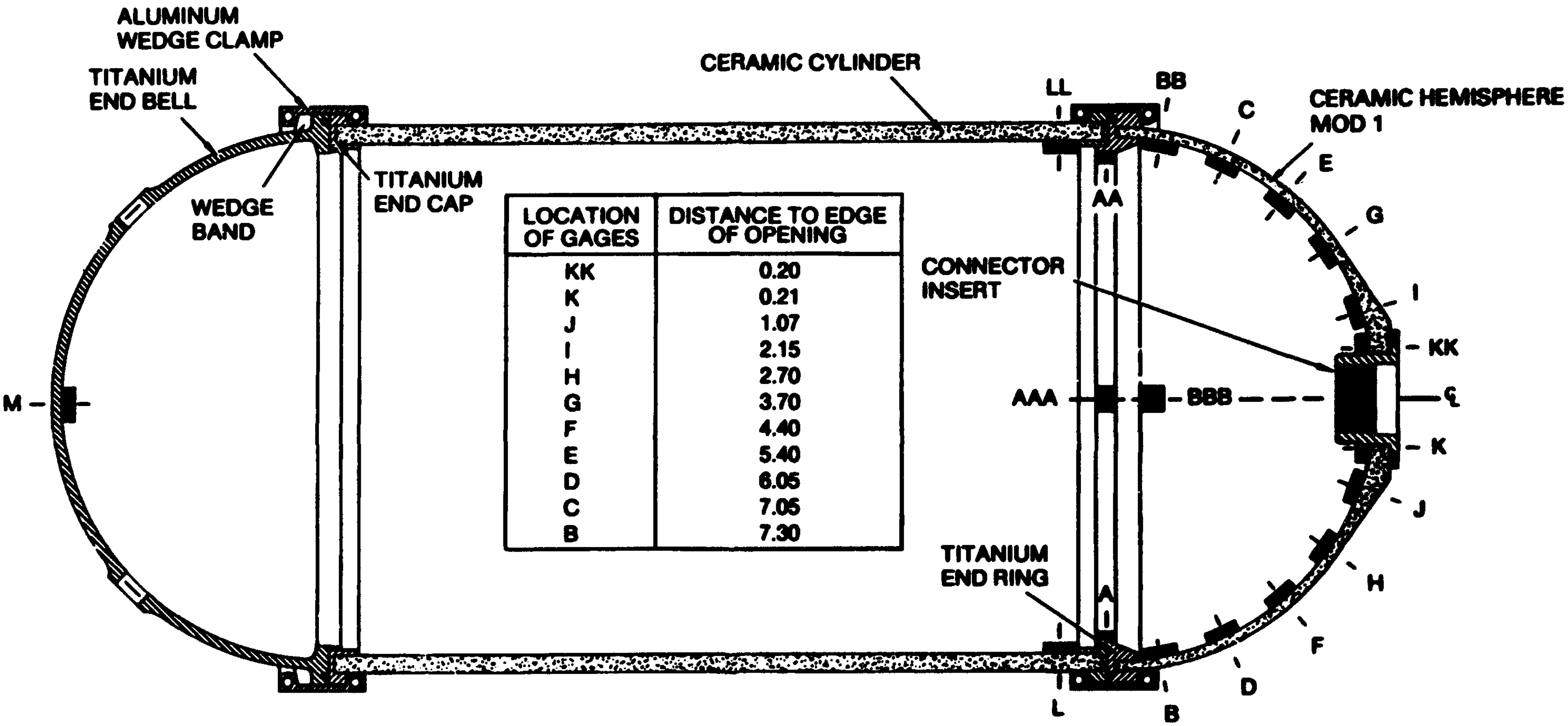

LOCATION OF GAGES	DISTANCE TO EDGE OF OPENING
KK	0.20
K	0.21
J	1.07
I	2.15
H	2.70
G	3.70
F	4.40
E	5.40
D	6.05
C	7.05
B	7.30

NOTE: ALL GAGES ARE 90 DEGREE ROSETTES ORIENTED ALONG HOOP AND AXIAL DIRECTIONS

GAGE TYPE: CEA-06-125WT-120
GAGE FACTOR: 2.085

Figure C-14. Location of strain gages on ceramic housing test assembly 2A.

Figure. C-15. Instrumented ceramic housing test assembly 2A prior to pressure testing.

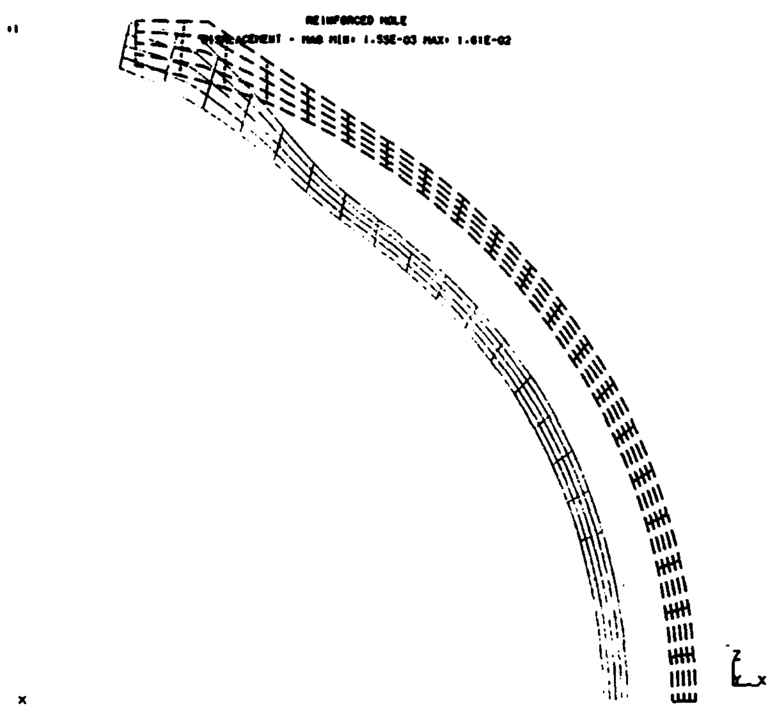

Figure. C-16. Displacement of the ceramic shell on Mod 1 ceramic hemisphere under 9,000-psi external design pressure calculated with a finite-element computer program.

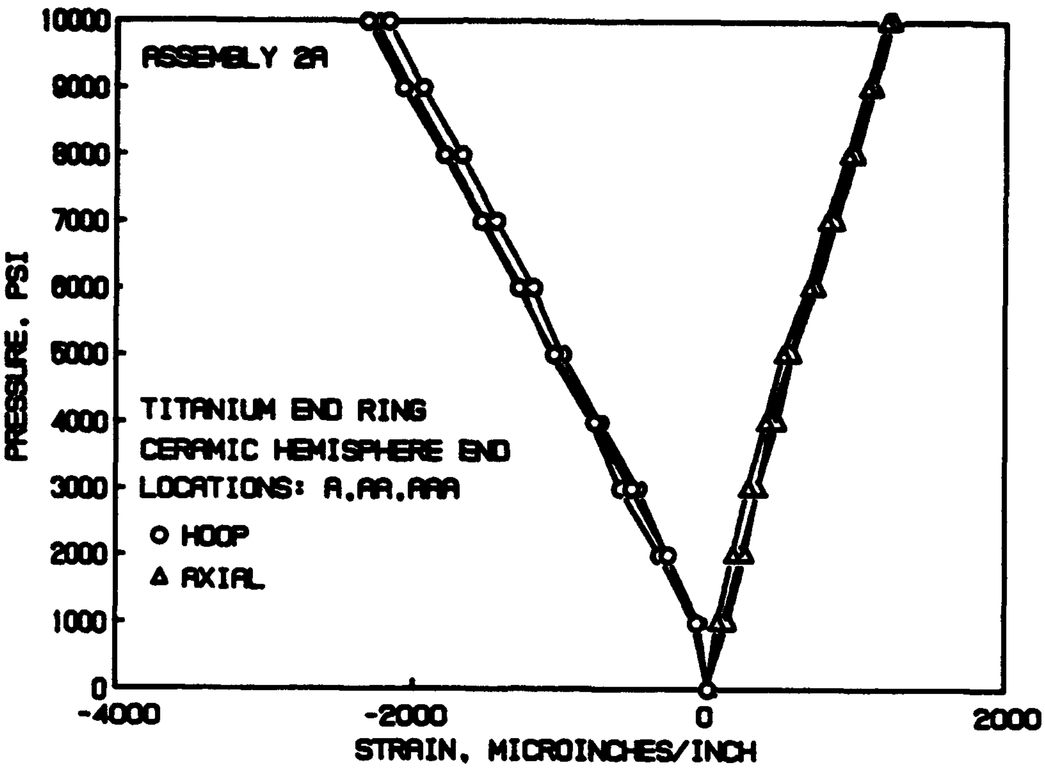

Figure. C-17. Stains on test assembly 2A; locations A, AA, AAA.

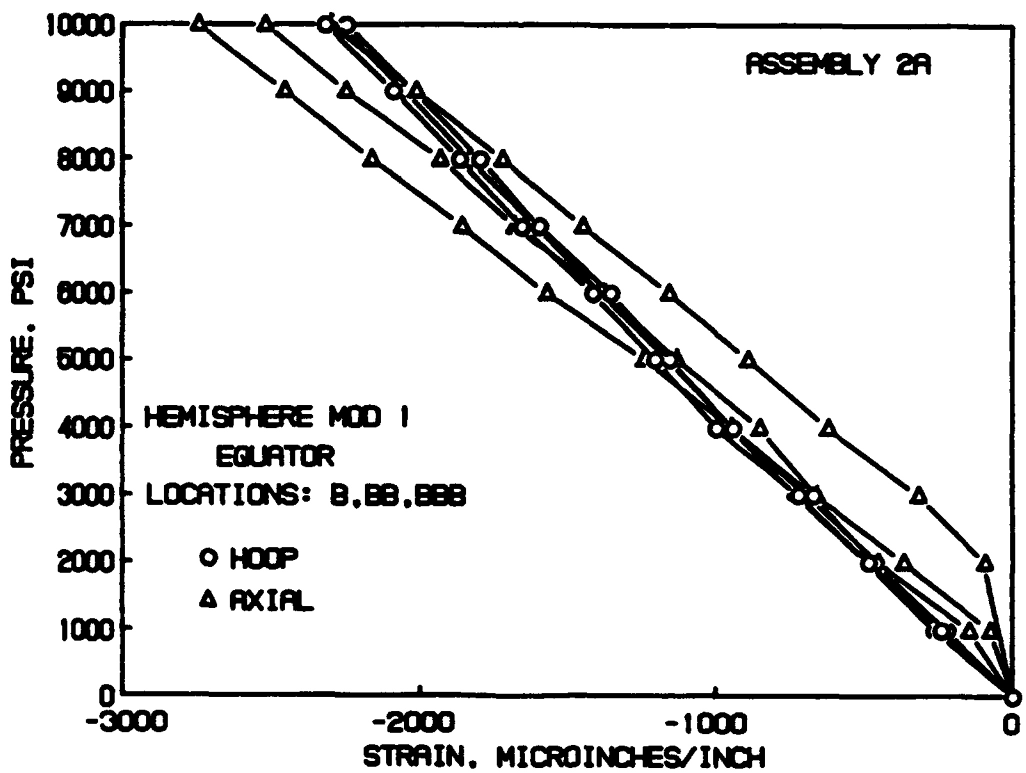

Figure. C-18. Strains on test assembly 2A; locations B, BB, BBB.

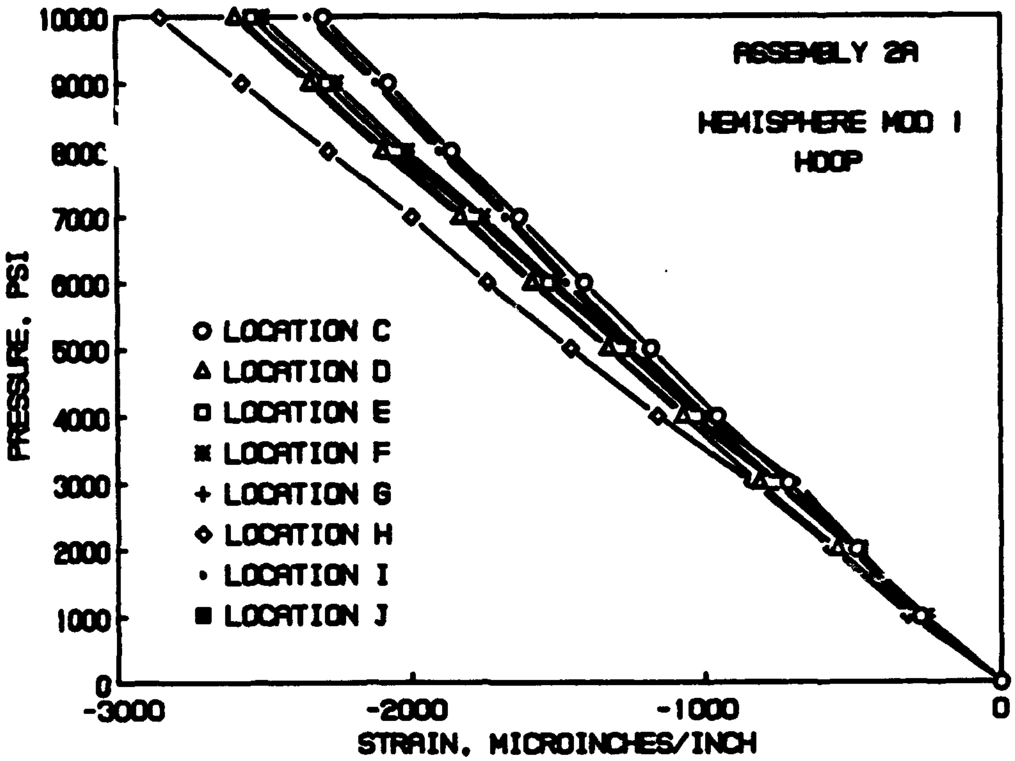

Figure. C-19. Strains on test assembly 2A; locations C, D, E, F, G, H, I, J in hoop orientation.

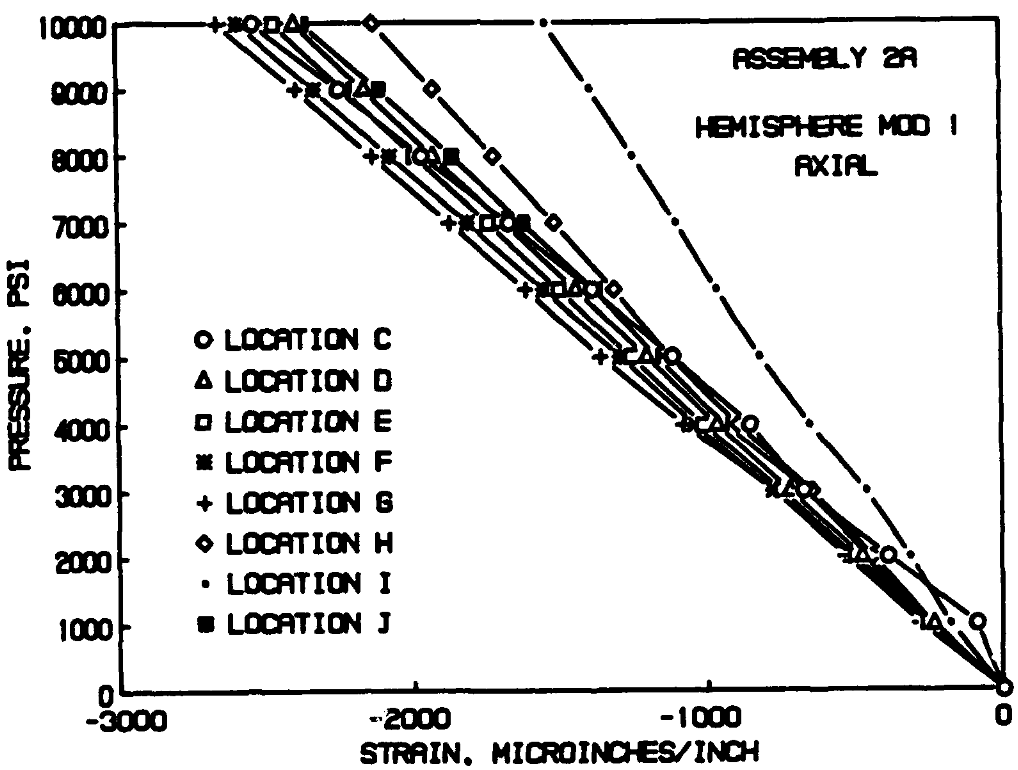

Figure. C-20. Strains on test assembly 2A; locations C, D, E, F, G, H, I, J in axial orientation.

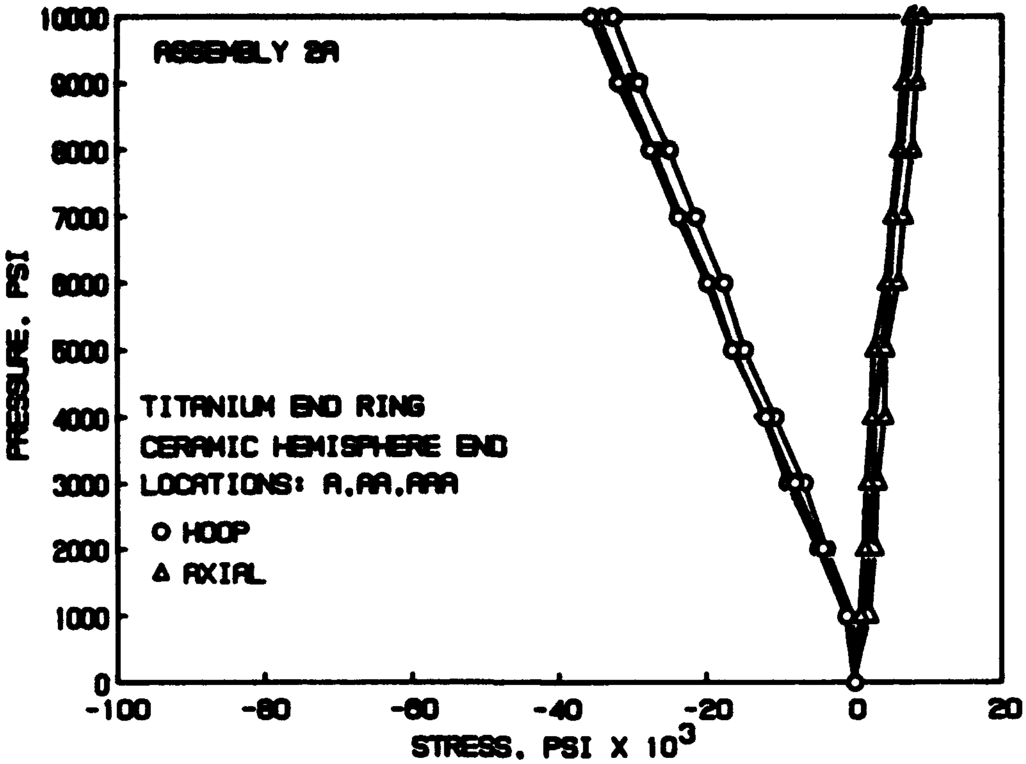

Figure. C-21. Stress on test assembly 2A; locations A, AA, AAA.

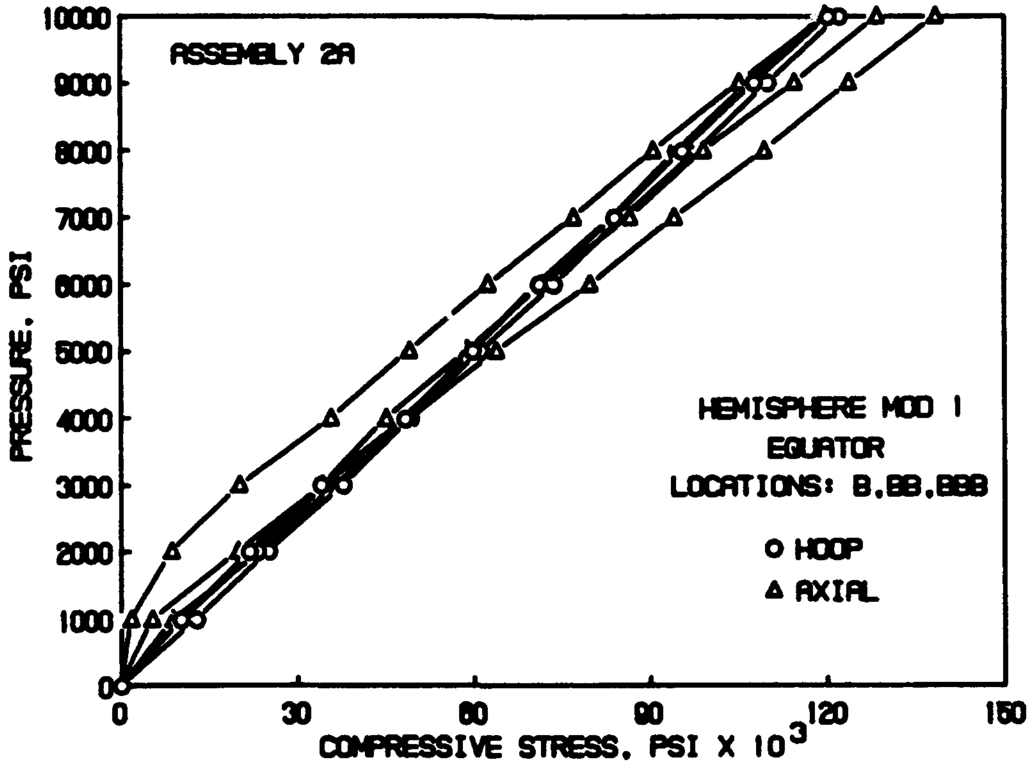

Figure. C-22. Stress on test assembly 2A; locatio[illegible] BBB.

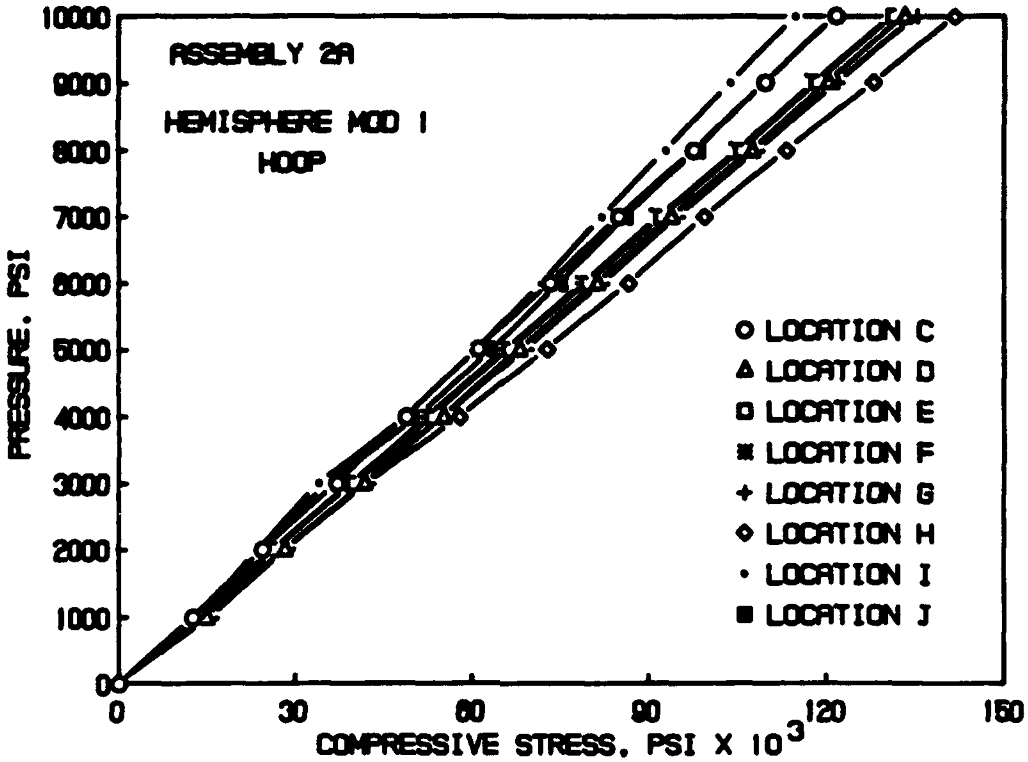

Figure. C-23. Stress on test assembly 2A; locations C, D, E, F, G, H, I, J in hoop orientating.

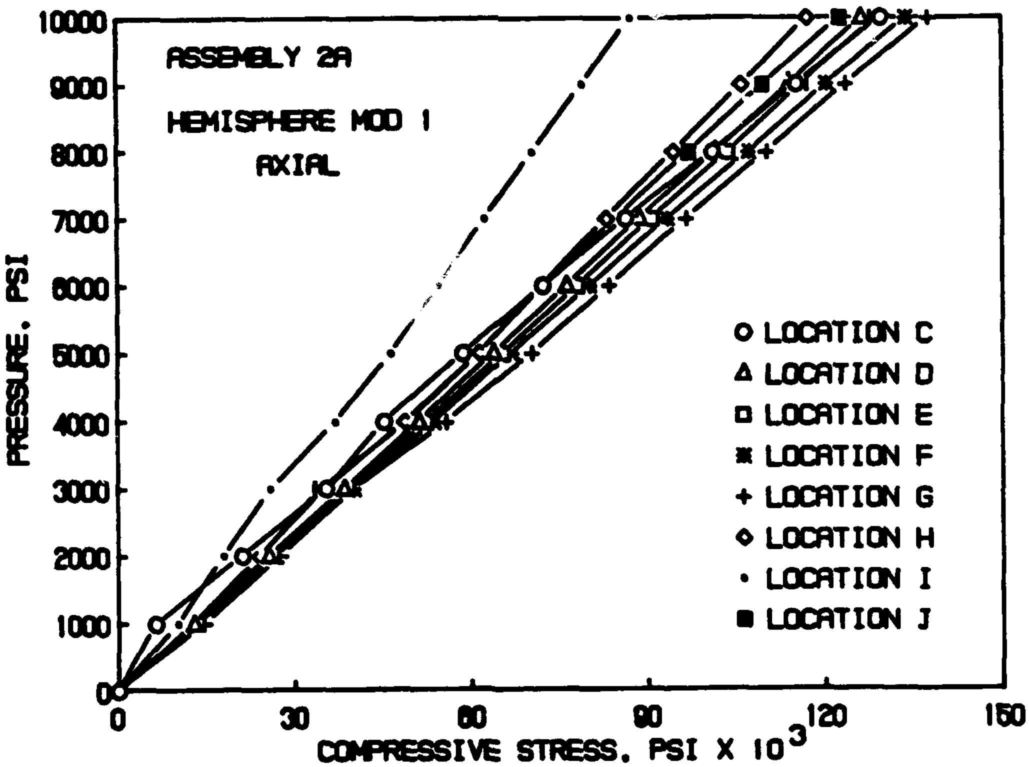

Figure. C-24. Stress on test assembly 2A; locations C, D, E, F, G, H, I, J in axial orientation.

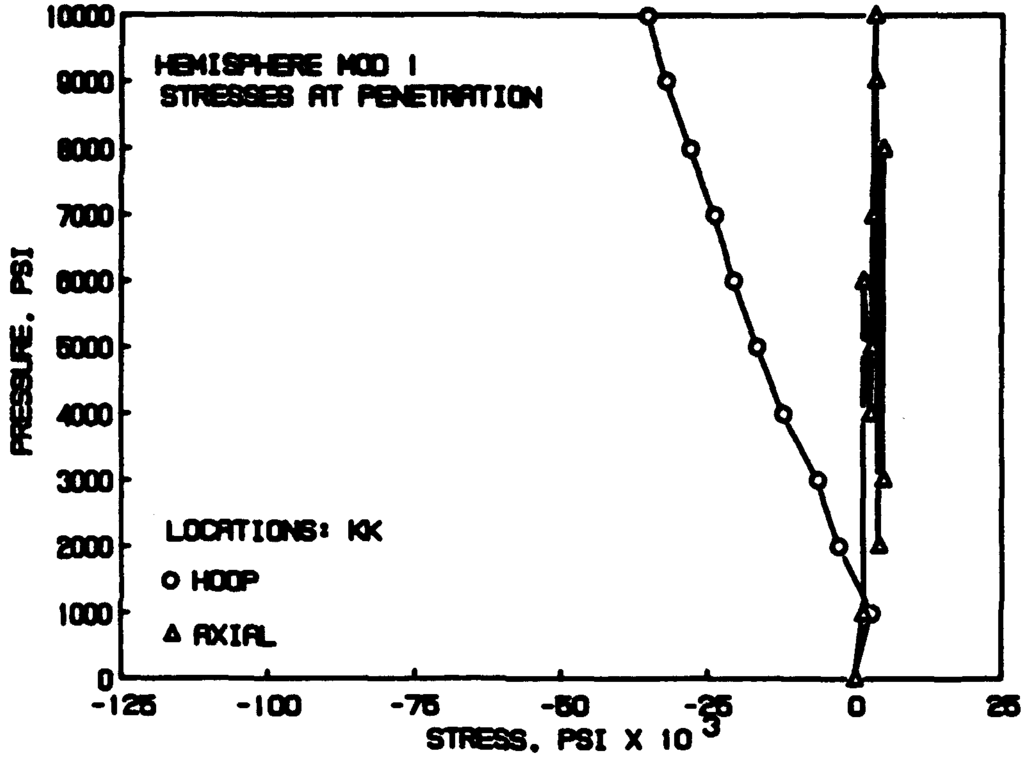

Figure. C-25. Stress on test assembly 2A; location KK at polar penetration in Mod 1 hemisphere.

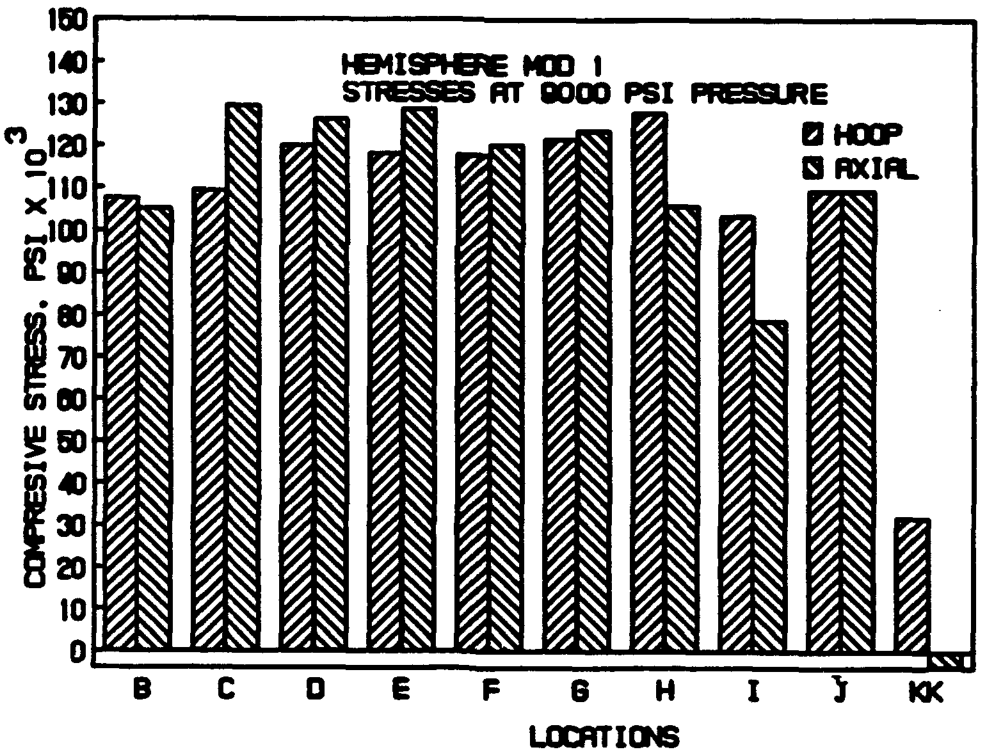

Figure. C-26. Distribution of stress in Mod 1 hemisphere.

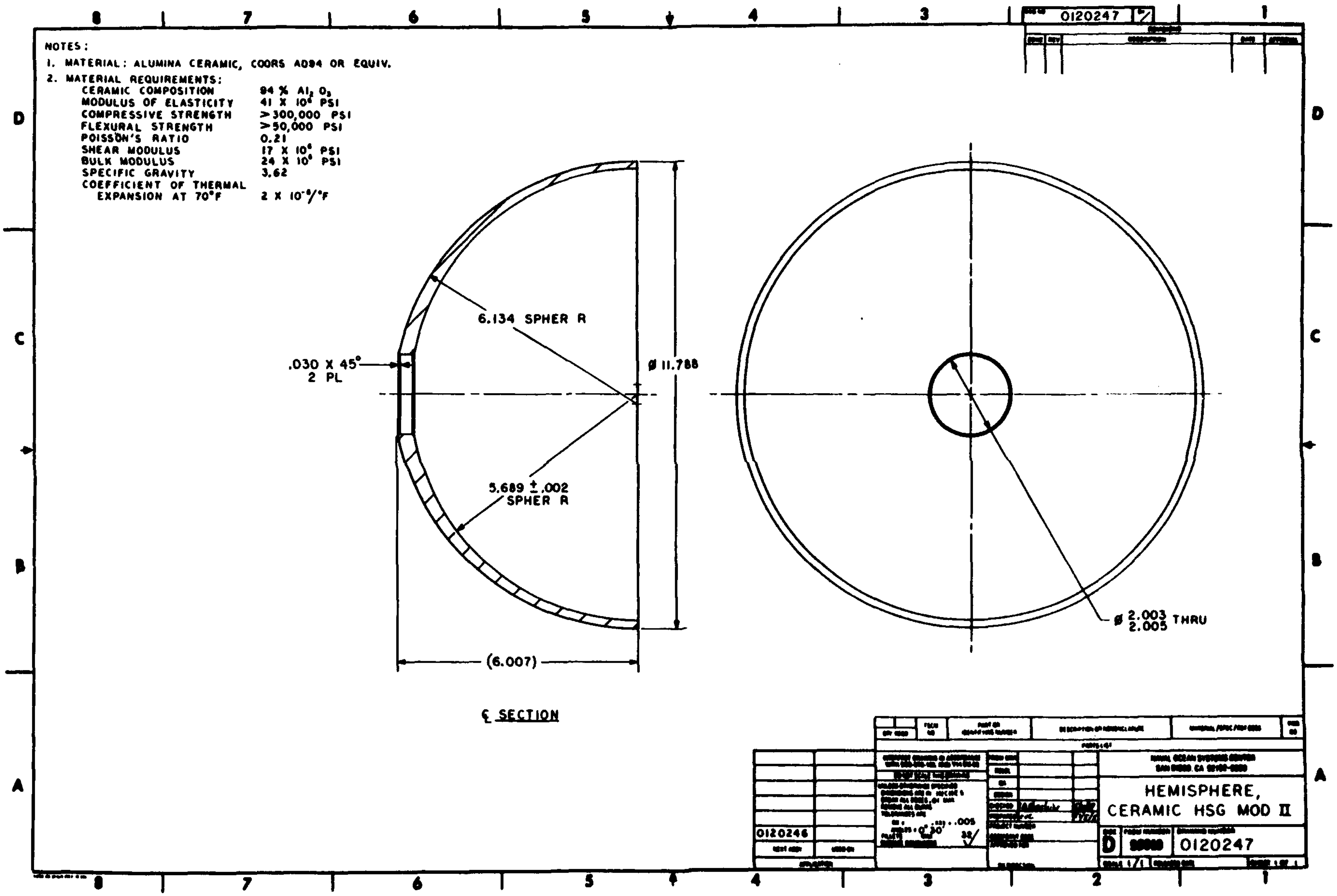

Figure C-27. Mod 2 ceramic hemisphere dimensions.

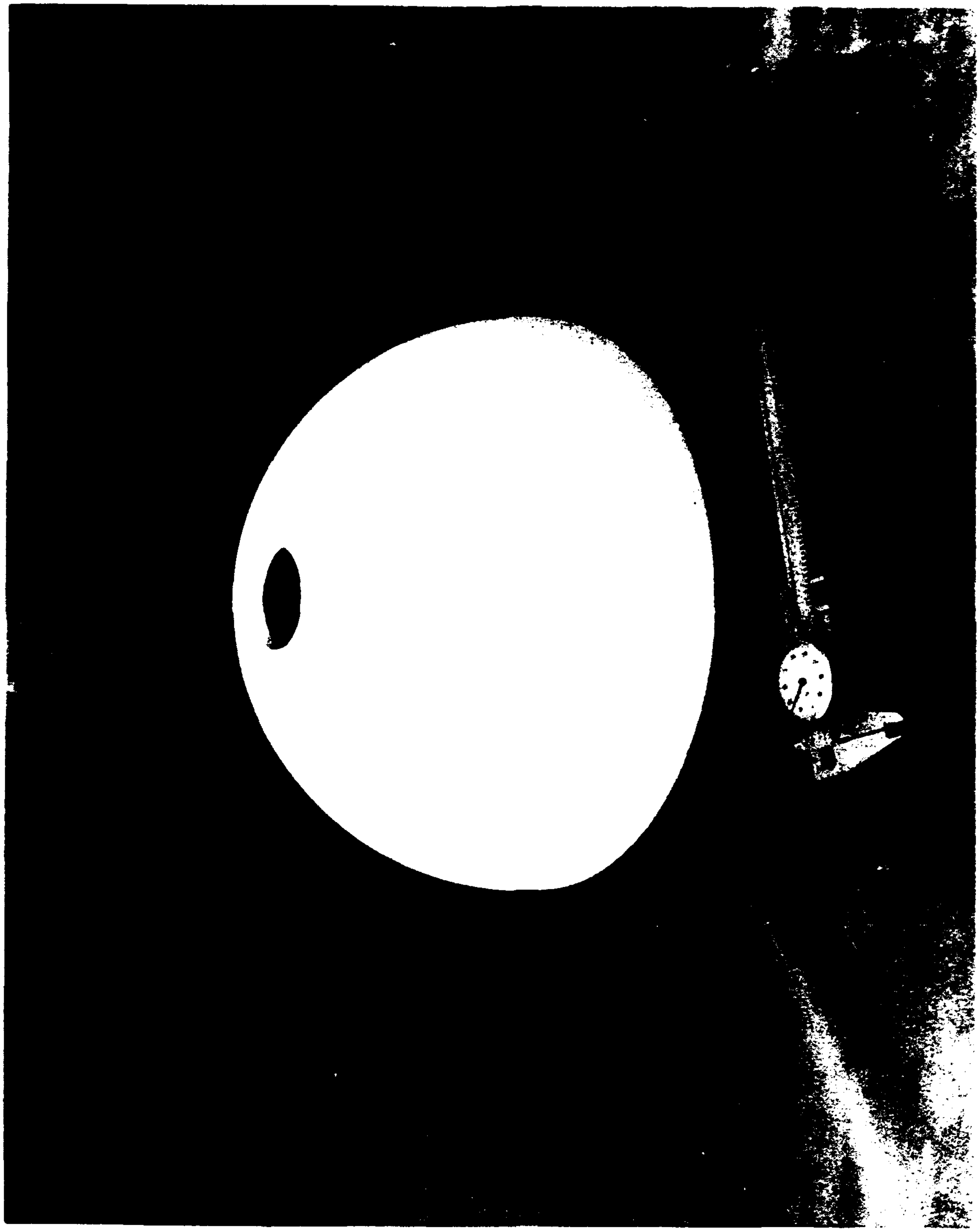

Figure C-28. Exterior view of Mod 2 hemisphere.

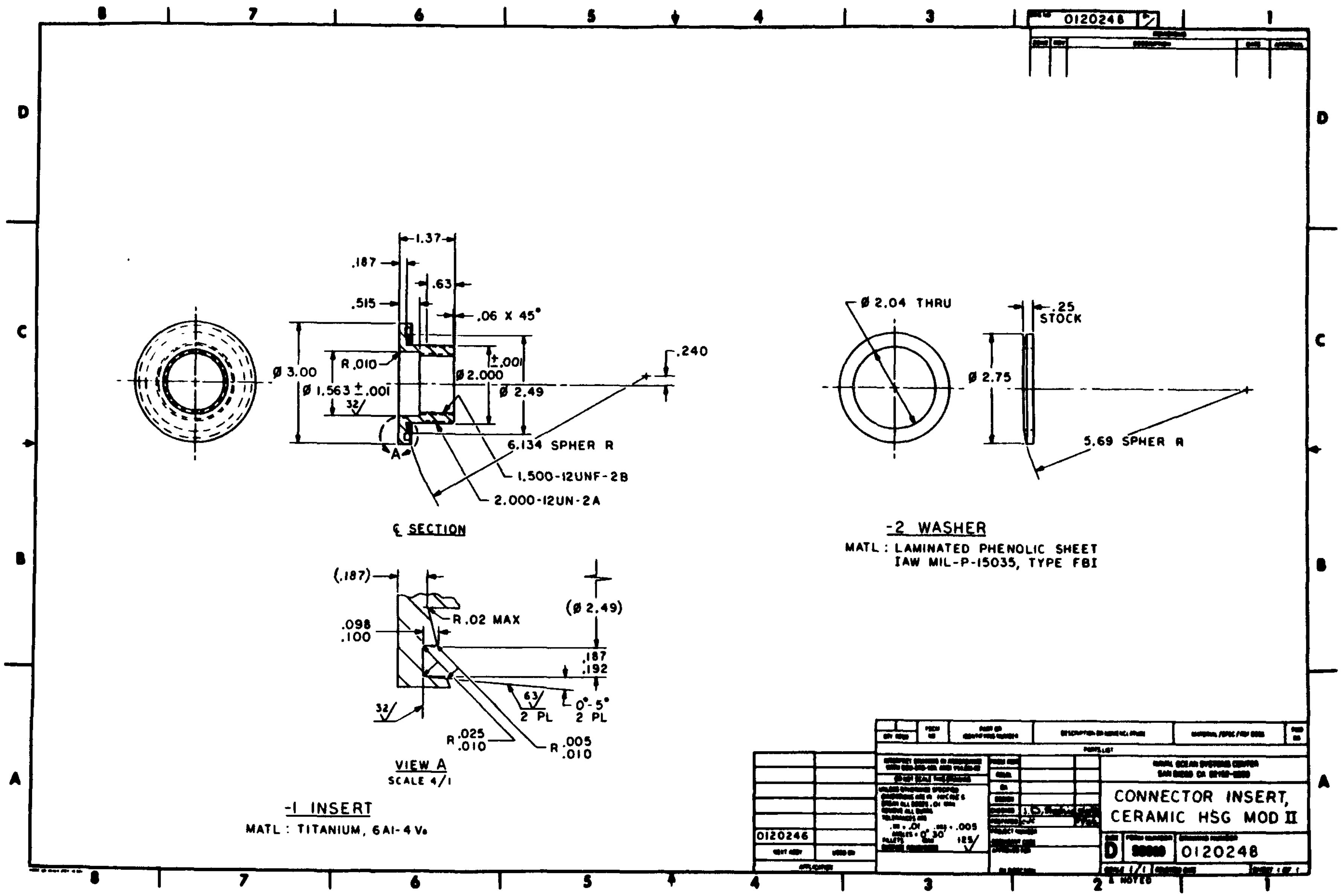

Figure C-29. Connector Insert (Revision 0) without phenolic bearing pad for Mod 2 hemisphere that initiated cracks at the edge of penetration.

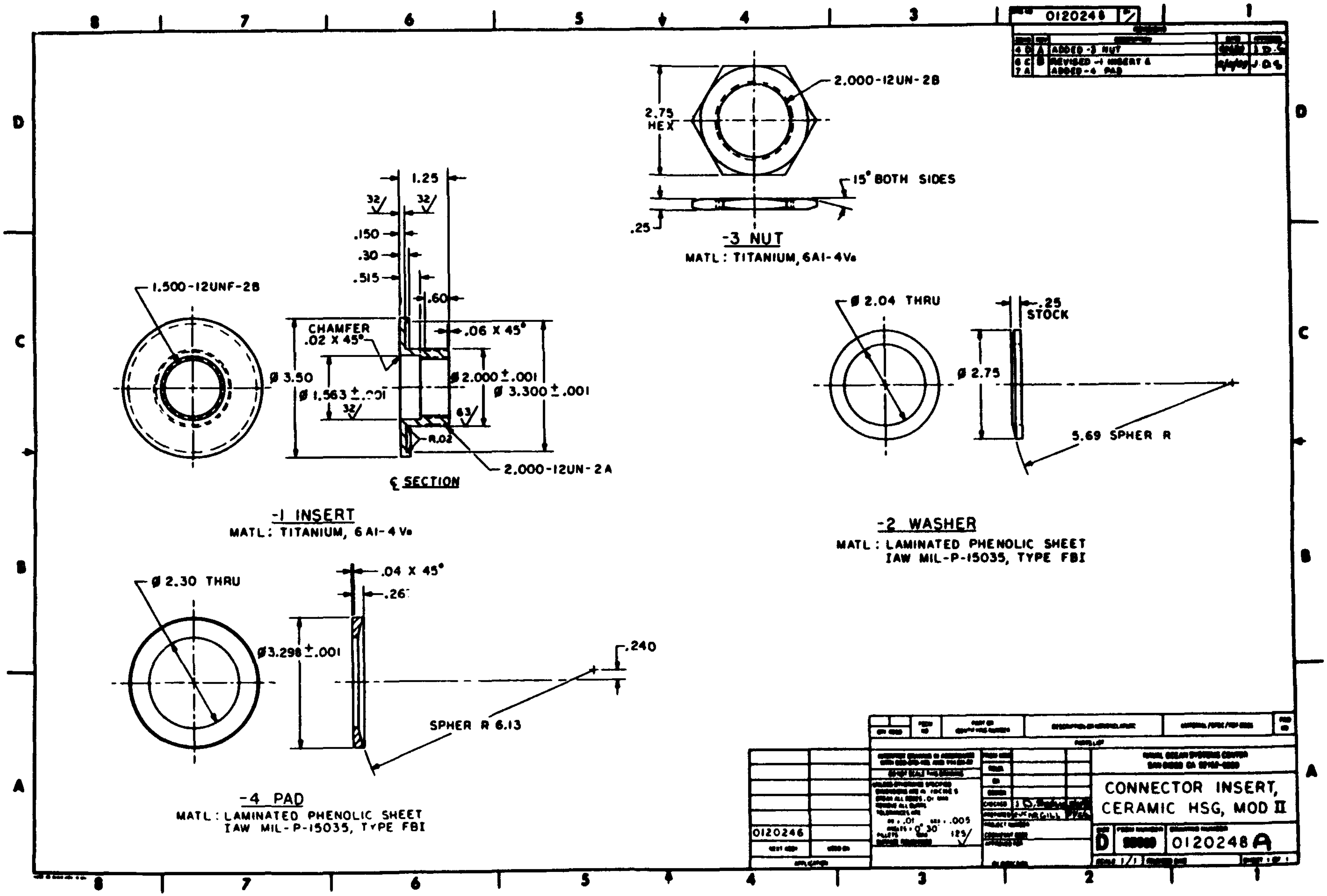

Figure C-30. Improved connector insert (Revision A for Mod 2 hemisphere) after incorporation of phenolic bearing pad.

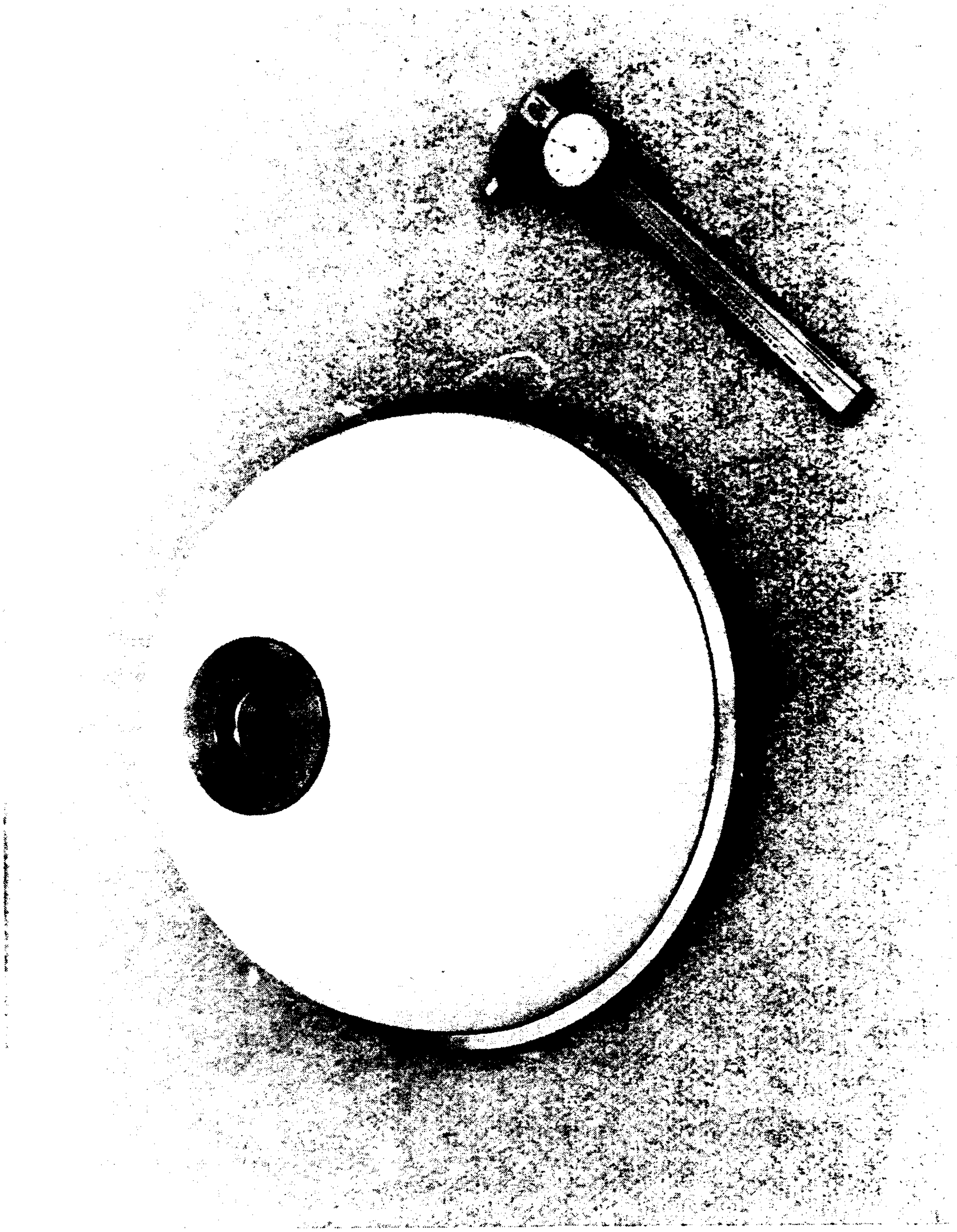

Figure C-31. Ceramic bulkhead assembly Mod 2; exterior view.

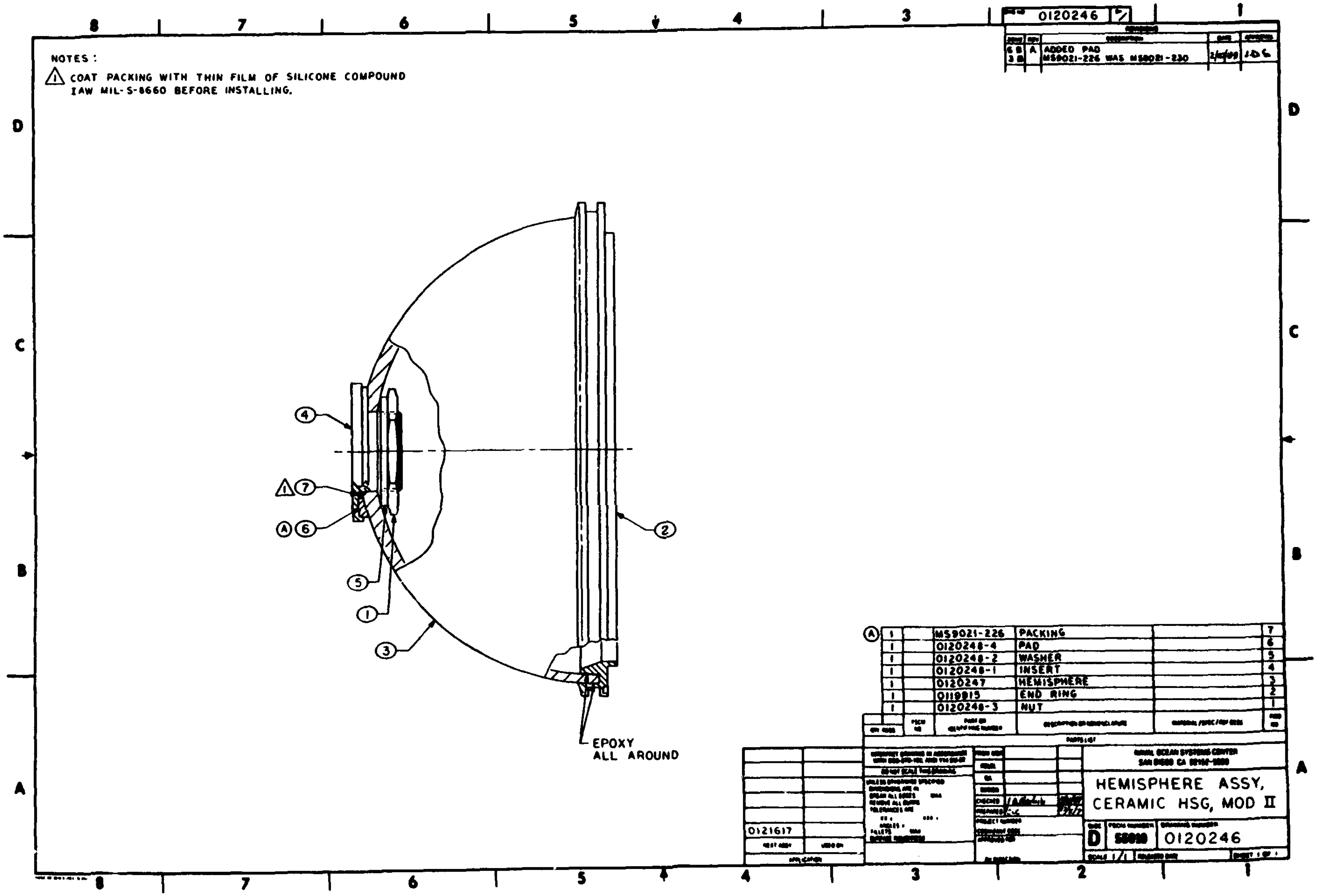

Figure C-32. Ceramic bulkhead assembly Mod 2; list of components.

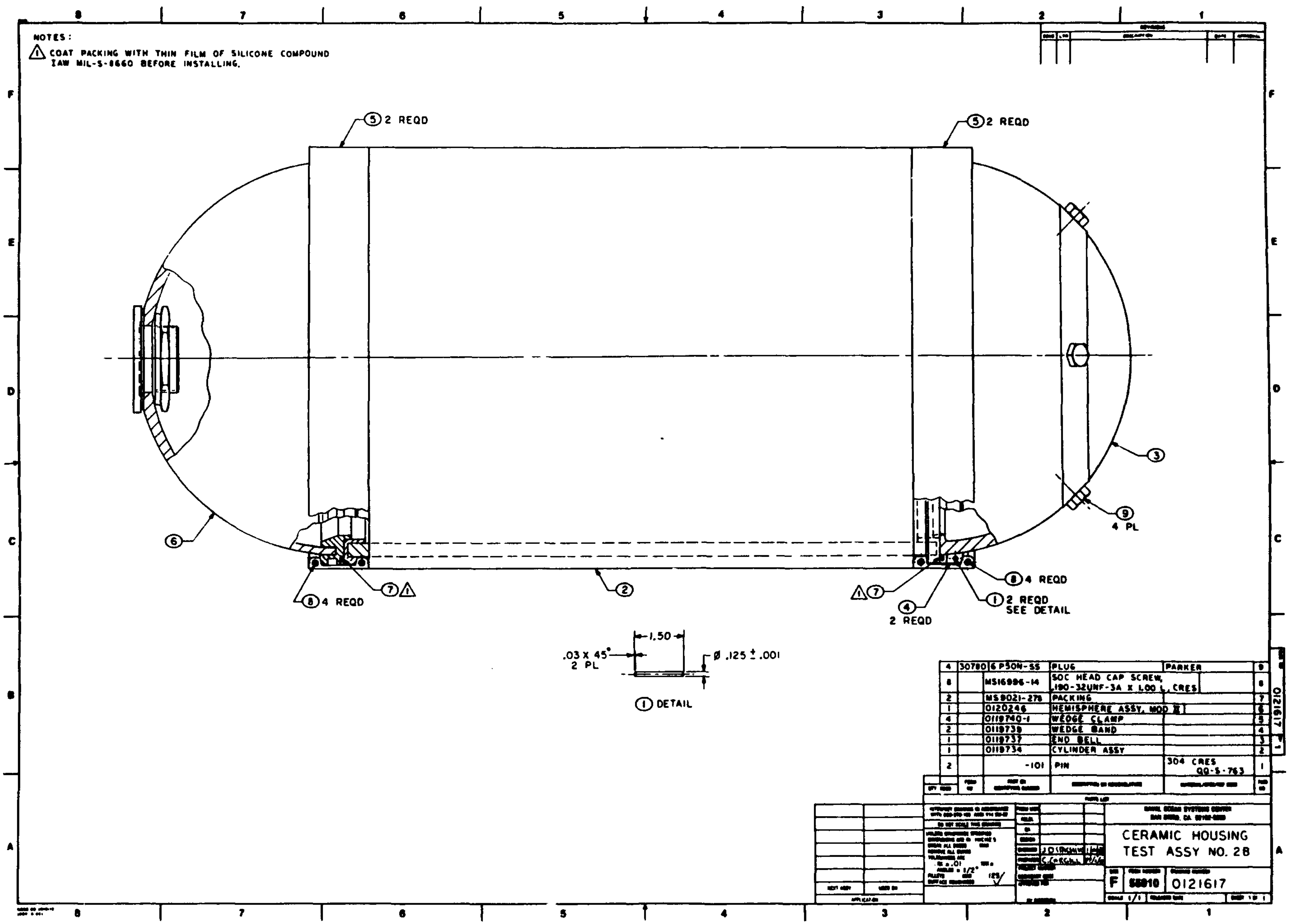

Figure C-33. Ceramic housing test assembly 2B incorporating the Mod 2 ceramic bulkhead.

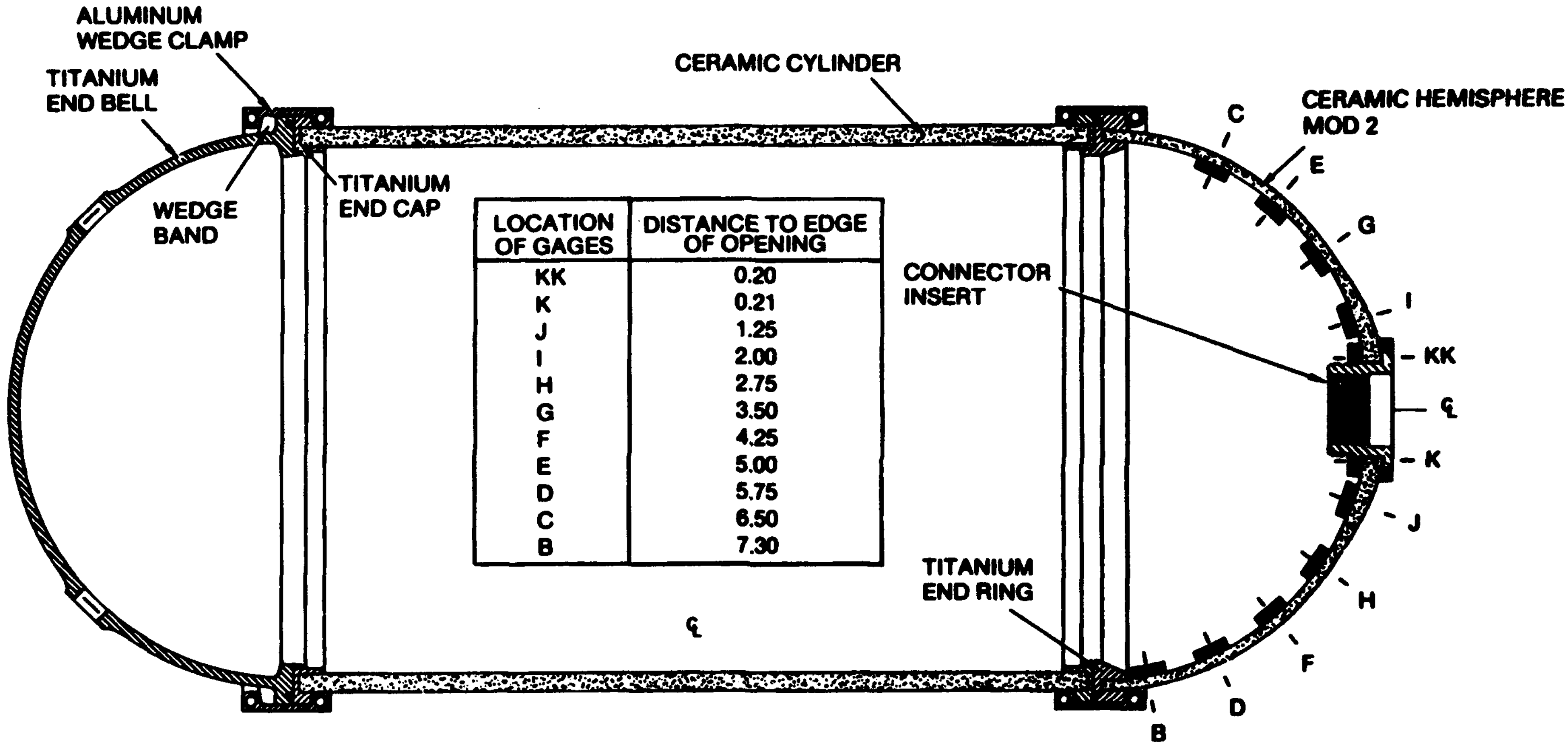

LOCATION OF GAGES	DISTANCE TO EDGE OF OPENING
KK	0.20
K	0.21
J	1.25
I	2.00
H	2.75
G	3.50
F	4.25
E	5.00
D	5.75
C	6.50
B	7.30

NOTE: ALL GAGES ARE 90 DEGREE ROSETTES ORIENTED ALONG HOOP AND AXIAL DIRECTIONS

GAGE TYPE: CEA-06-125WT-120
GAGE FACTOR: 2.11

Figure C-34. Location of strain gages on ceramic test assembly 2B.

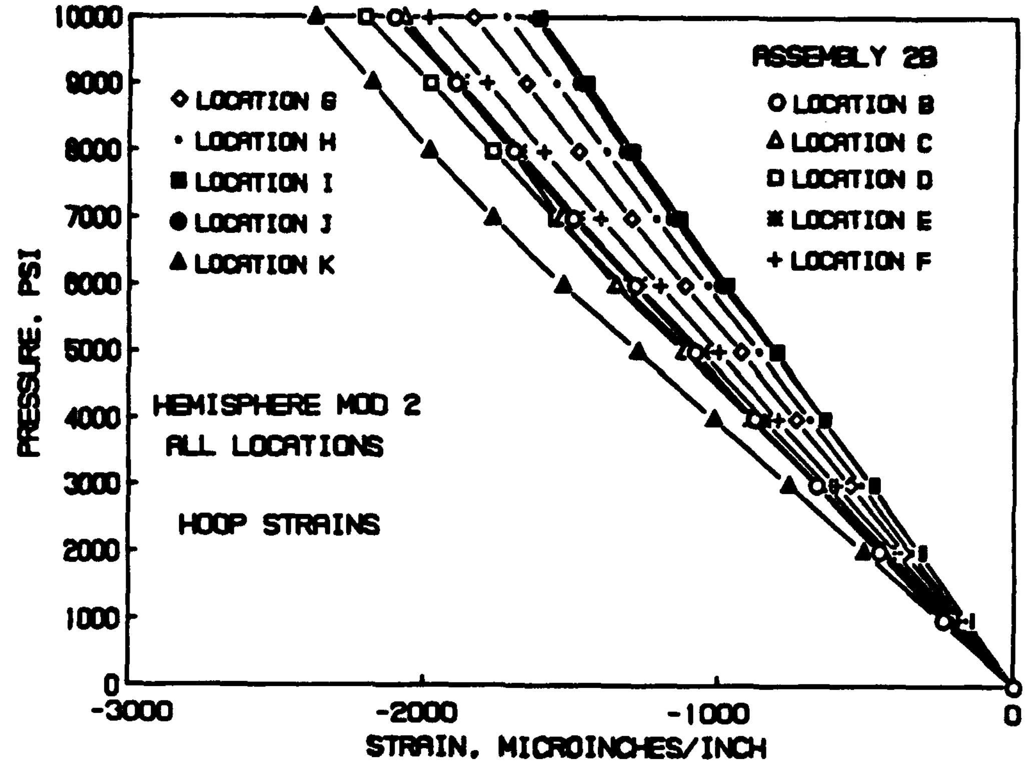

Figure. C-35. Strains on test assembly 2B; locations B, C, D, E, F, G, H, I, J, K in hoop orientation.

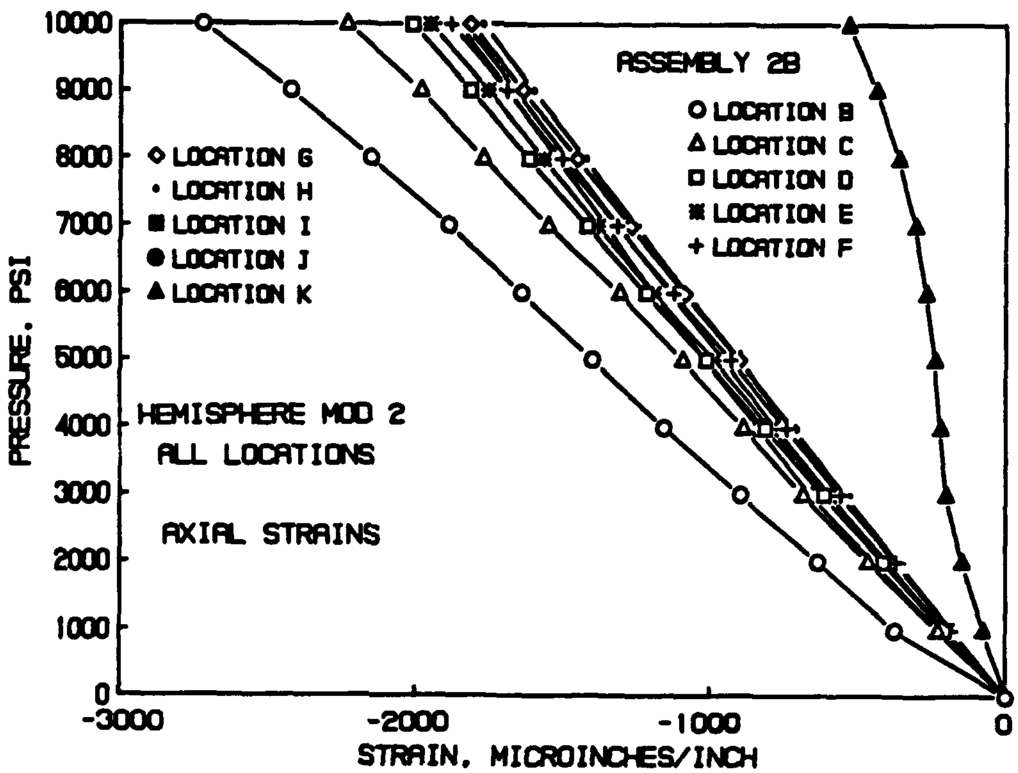

Figure. C-36. Strains on test assembly 2B; locations B, C, D, E, F, G, H, I, J, K in axial orientation.

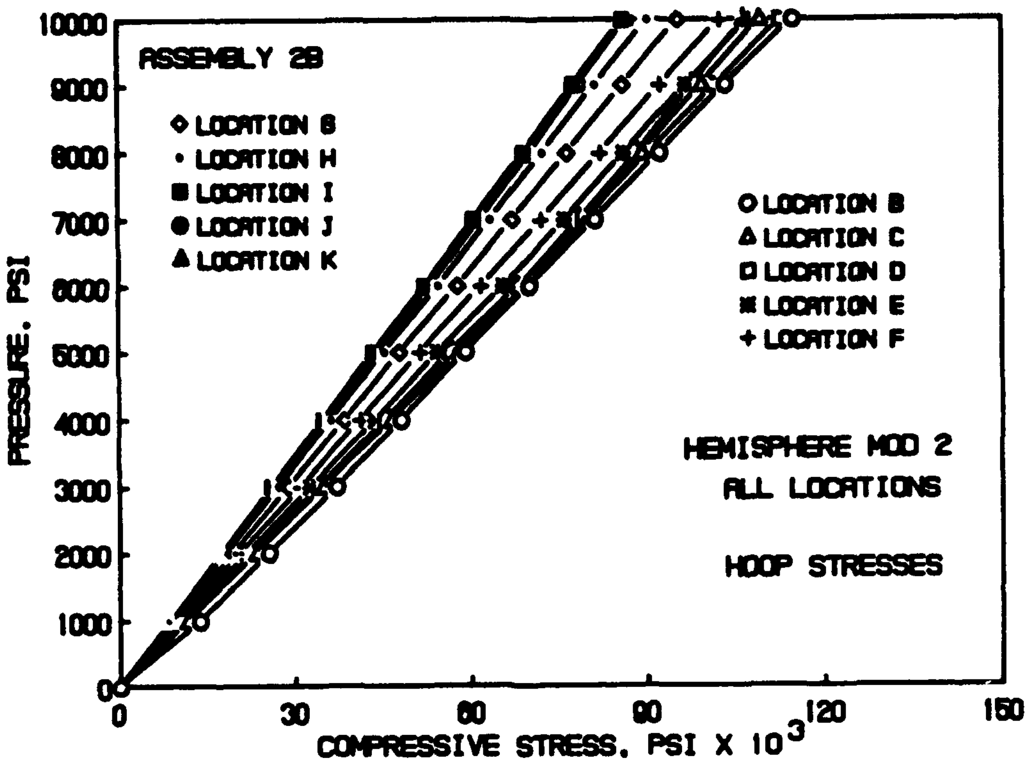

Figure. C-37. Stresses on test assembly 2B; locations B, C, D, E, F, G, H, I, J, K in hoop orientation.

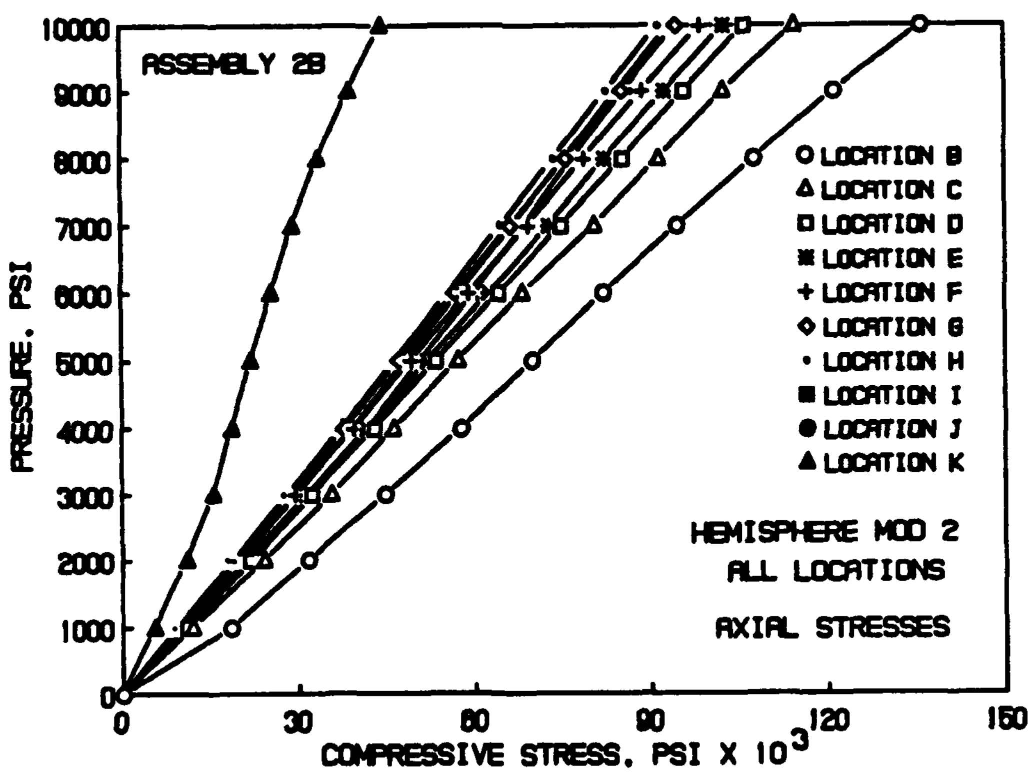

Figure. C-38. Stresses on test assembly 2B; locations B, C, D, E, F, G, H, I, J, K in axial orientation.

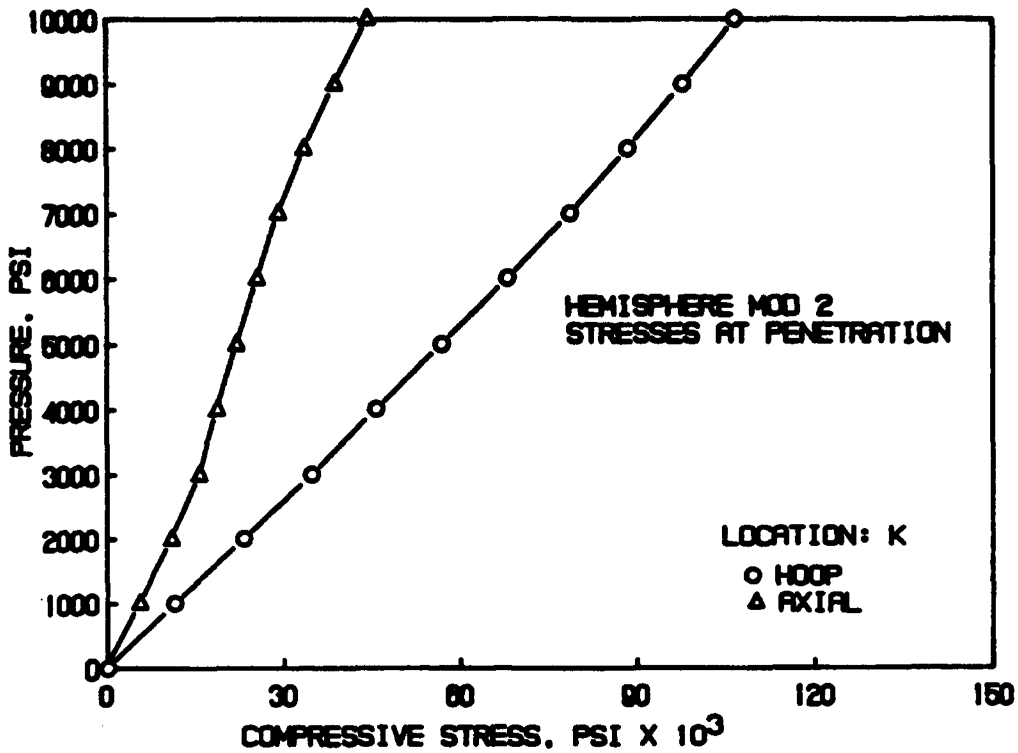

Figure. C-39. Stresses on test assembly 2B; location K at polar penetration in Mod 2 hemisphere.

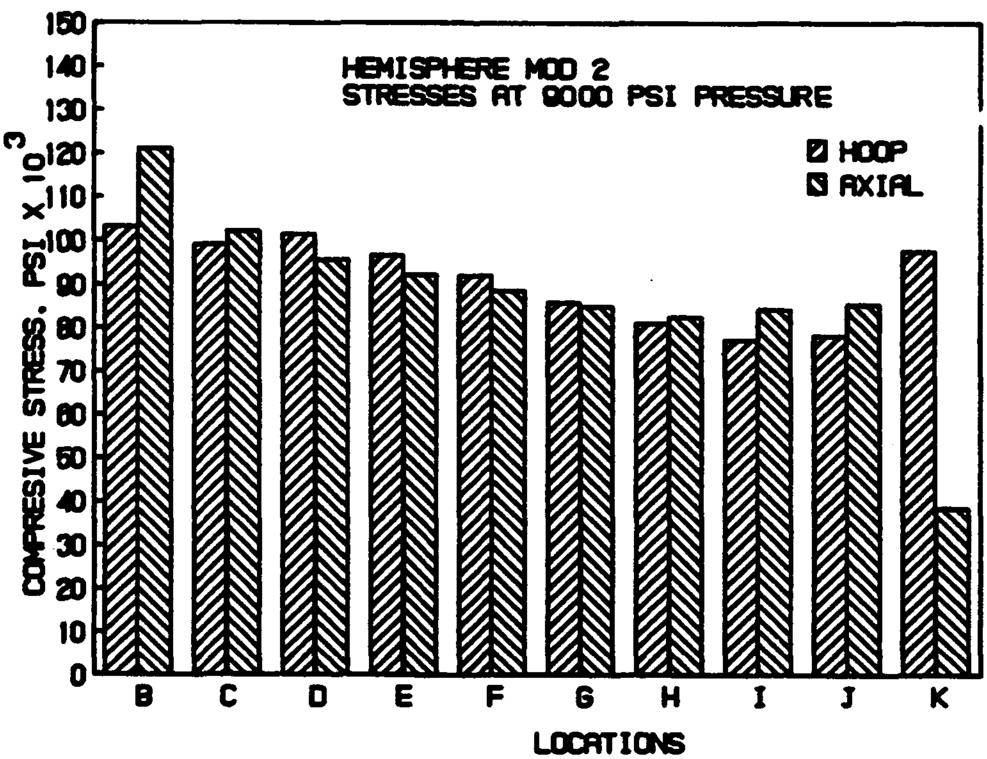

Figure. C-40. Distribution of stresses on Mod 2 hemisphere.

Figure C-41. Circular crack around the polar penetration in hemisphere Mod 2 generated by connector insert Revision 0 shown on figure C-29.

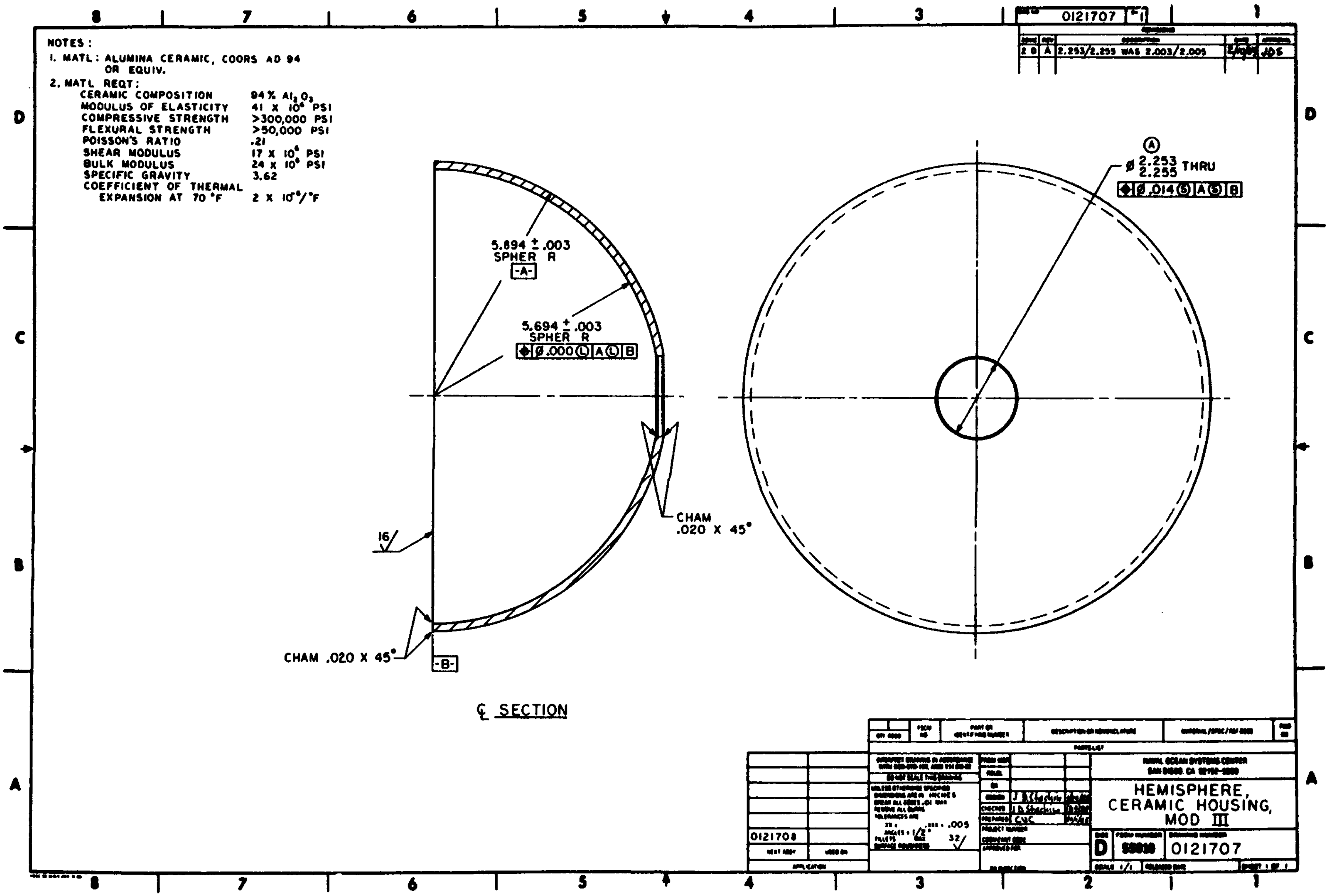

Figure C-42. Mod 3 ceramic hemisphere dimensions.

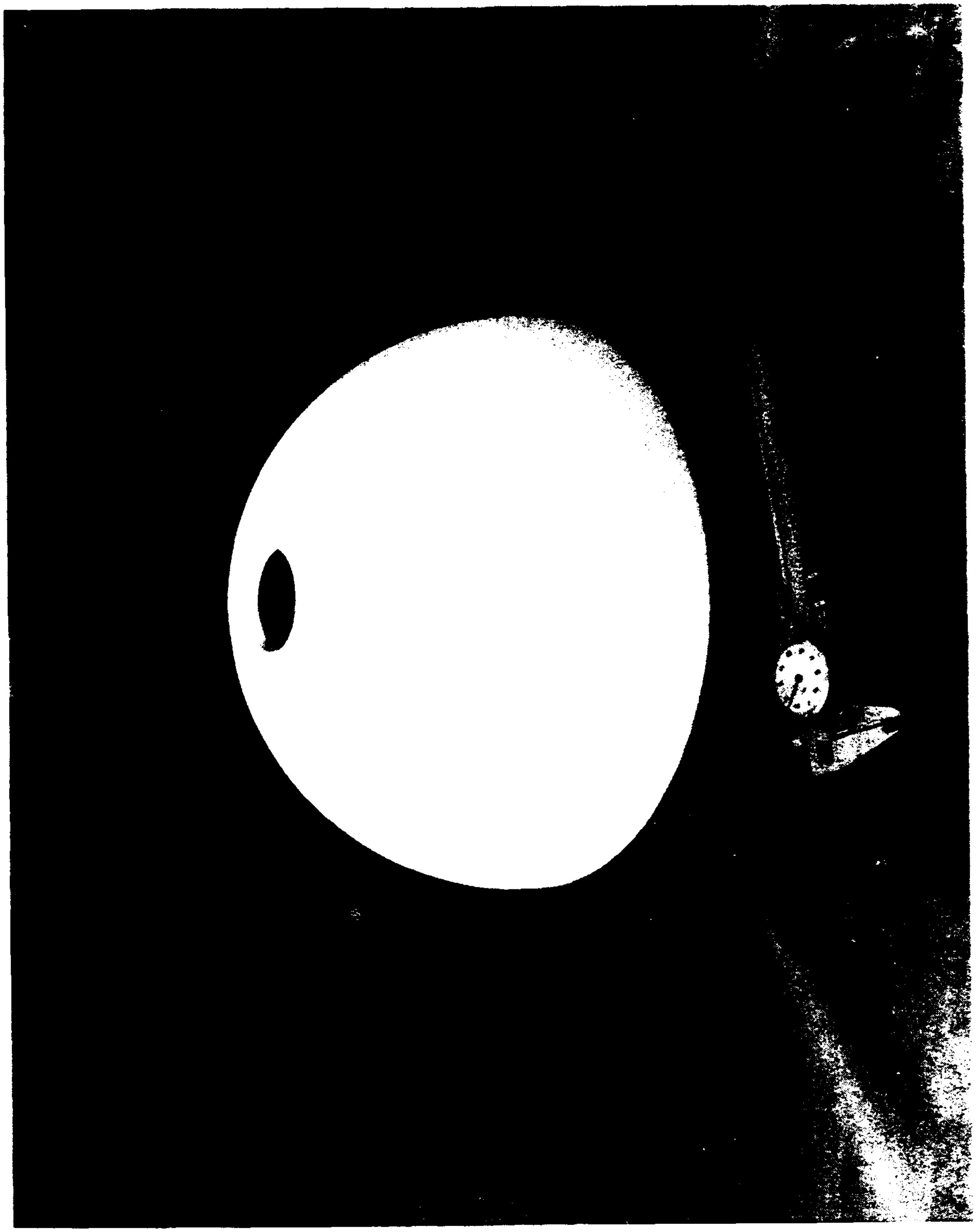

Figure C-43. Exterior view of Mod 3 hemisphere.

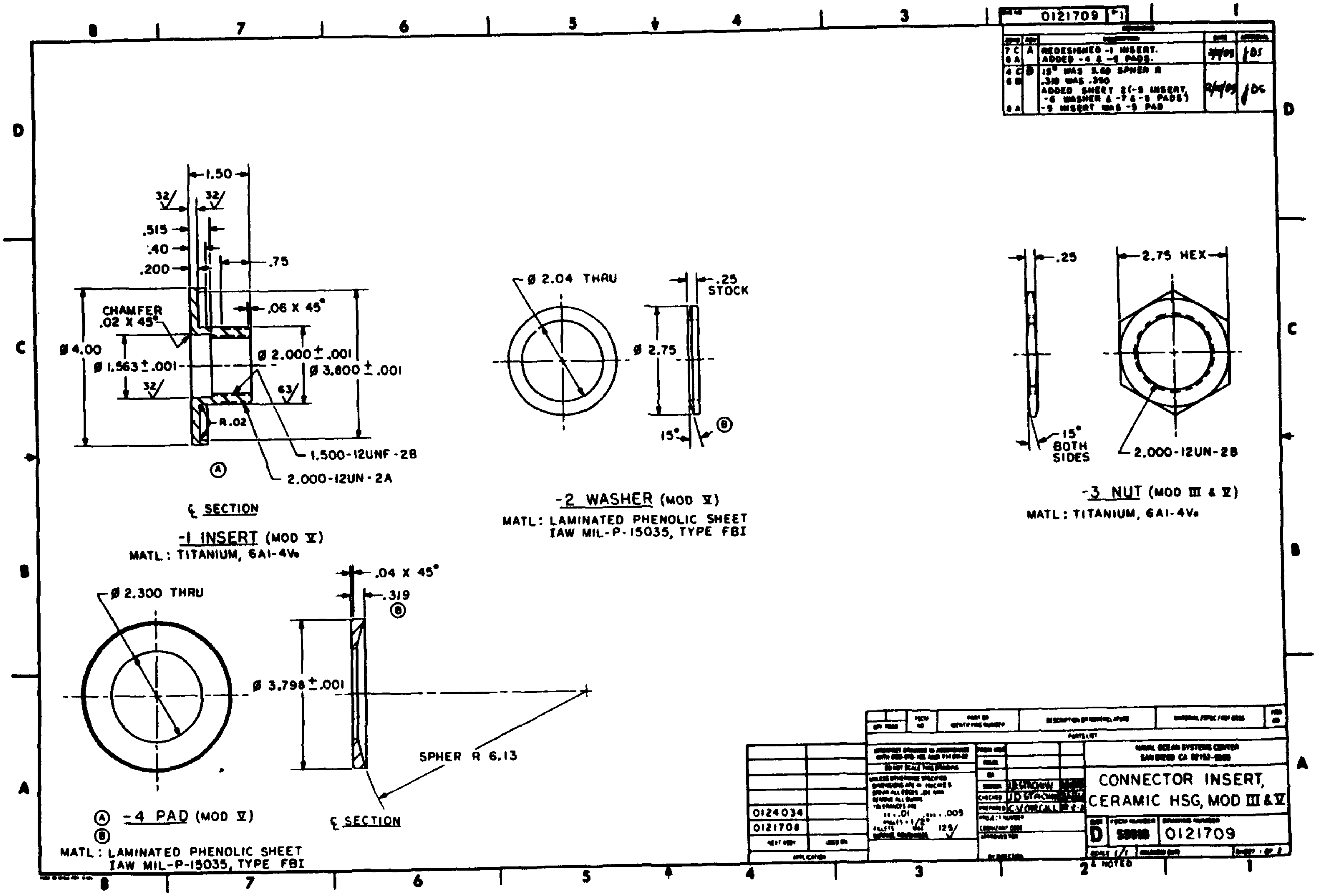

Figure C-44. Connector insert for Mod 3 hemisphere incorporating phenolic bearing pads, Sheet 1.

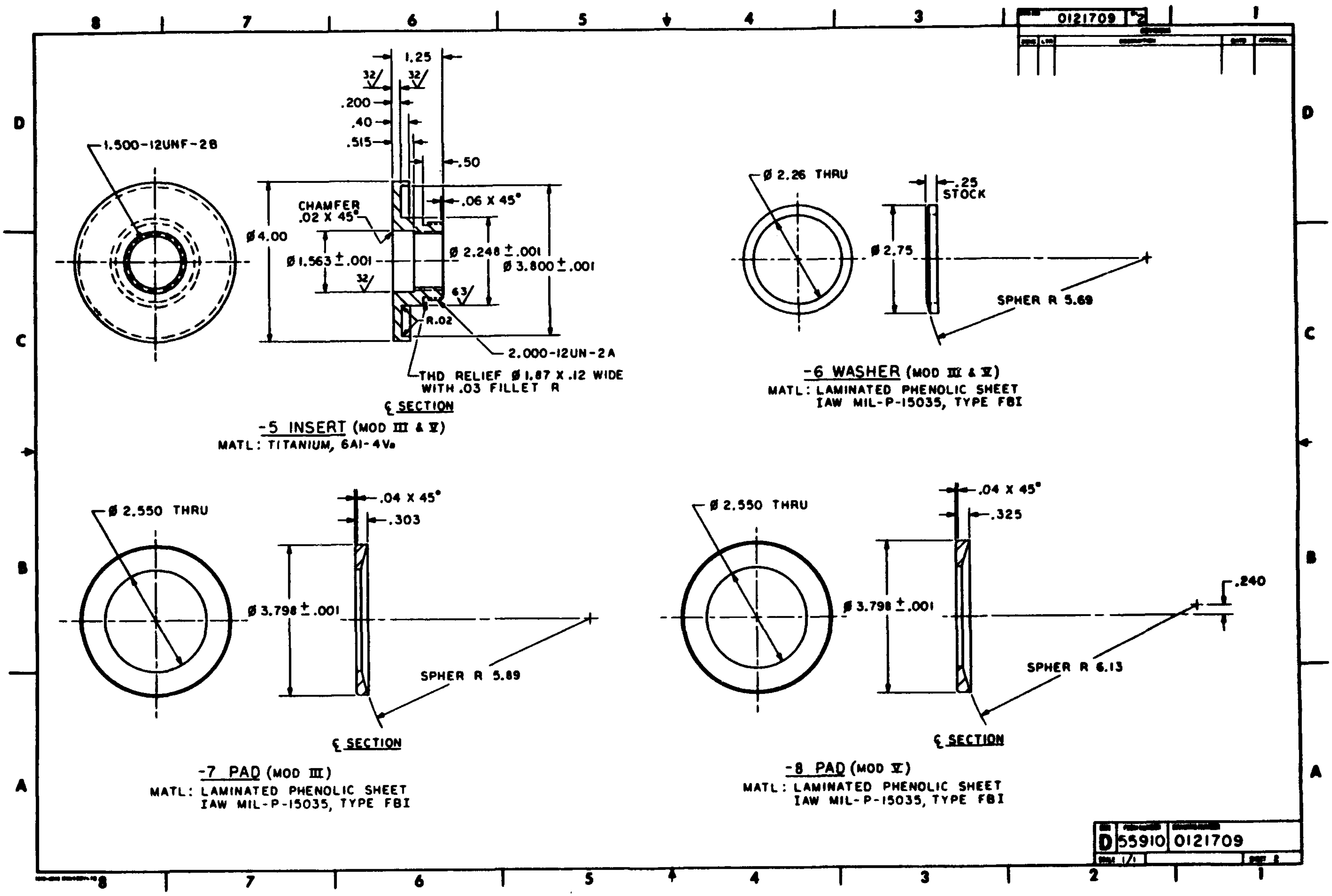

Figure C-44. Connector insert for Mod 3 hemisphere incorporating phenolic bearing pads, Sheet 2.

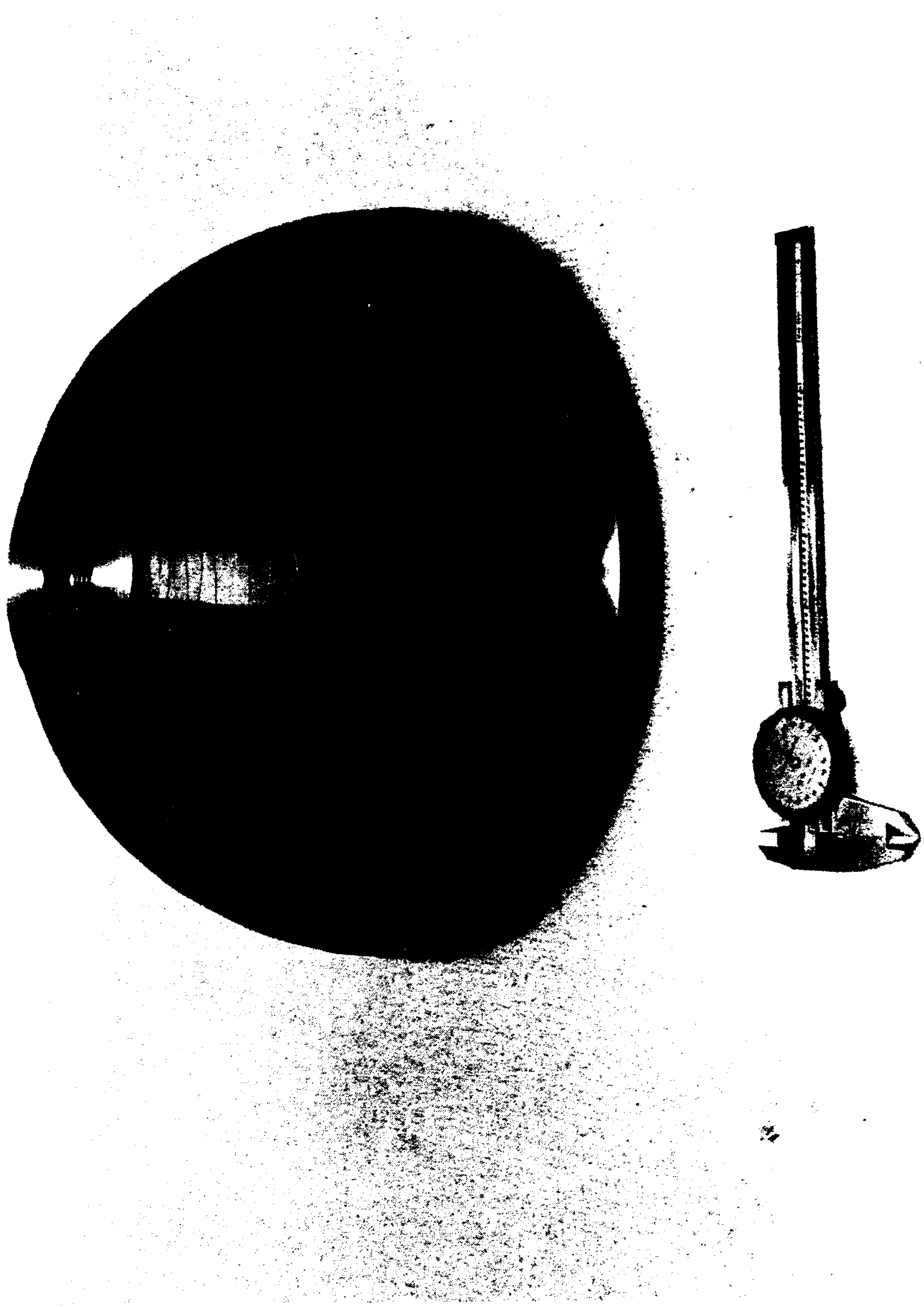

Figure C-45. Exterior view of the hemispherical Mod 3 assembly protected by a neoprene coating.

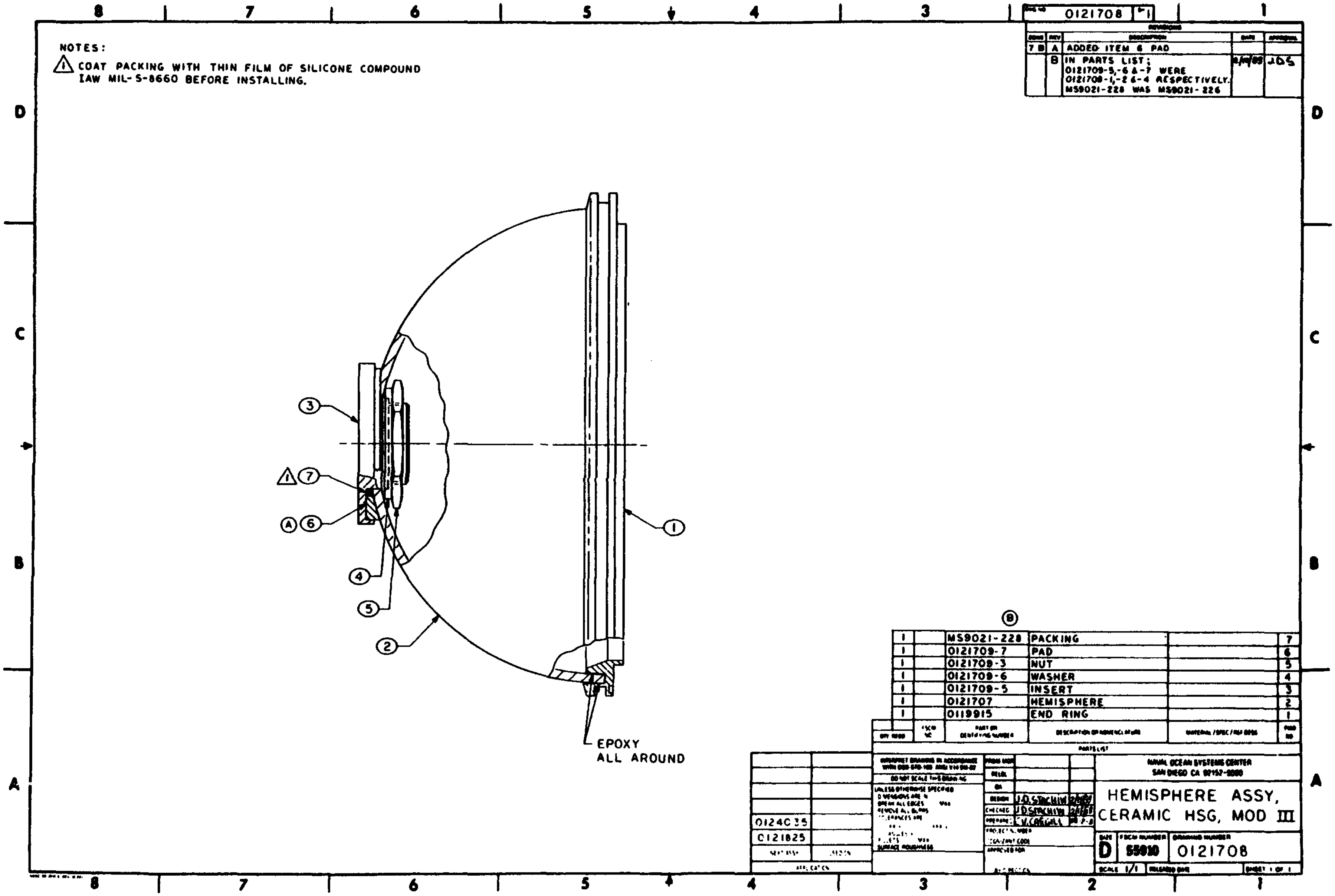

Figure C-46. Ceramic bulkhead assembly Mod 3; list of components.

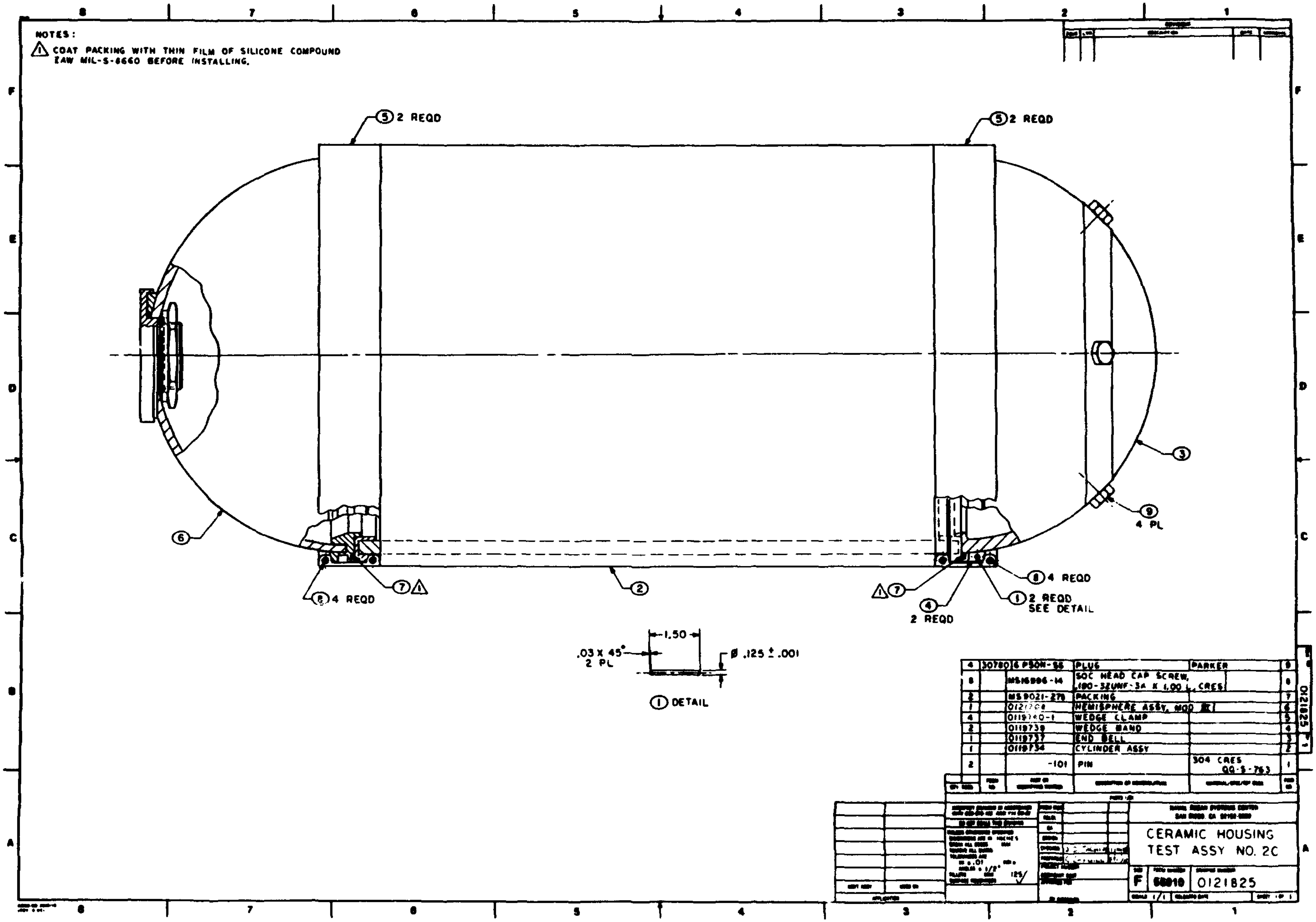

Figure C-47. Ceramic housing test assembly 2C incorporating the Mod 3 ceramic bulkhead.

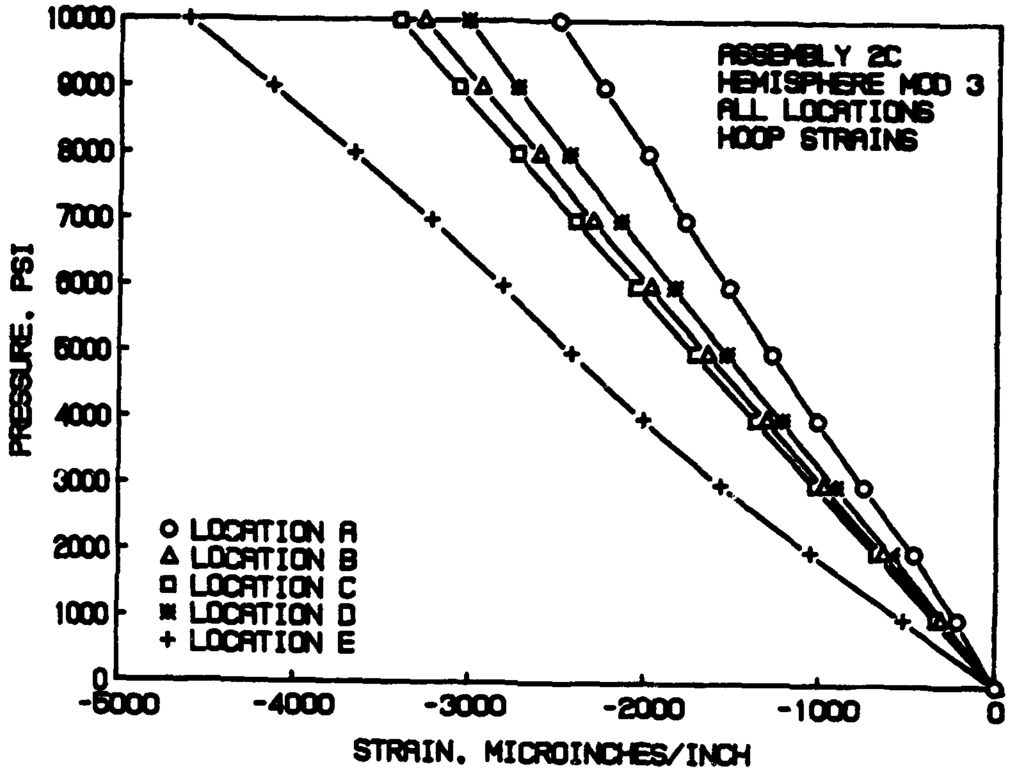

Figure. C-48. Strains on test assembly 2C; locations A, B, C, D, E in hoop orientation.

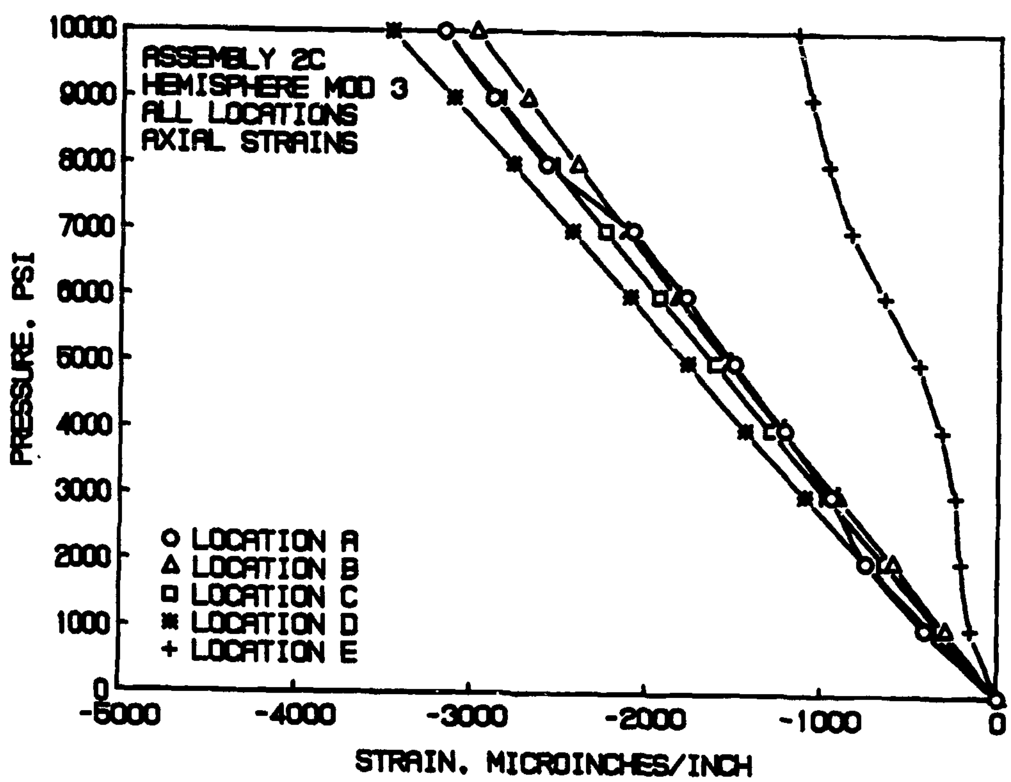

Figure. C-49. Strains on test assembly 2C; locations A, B, C, D, E in axial orientation.

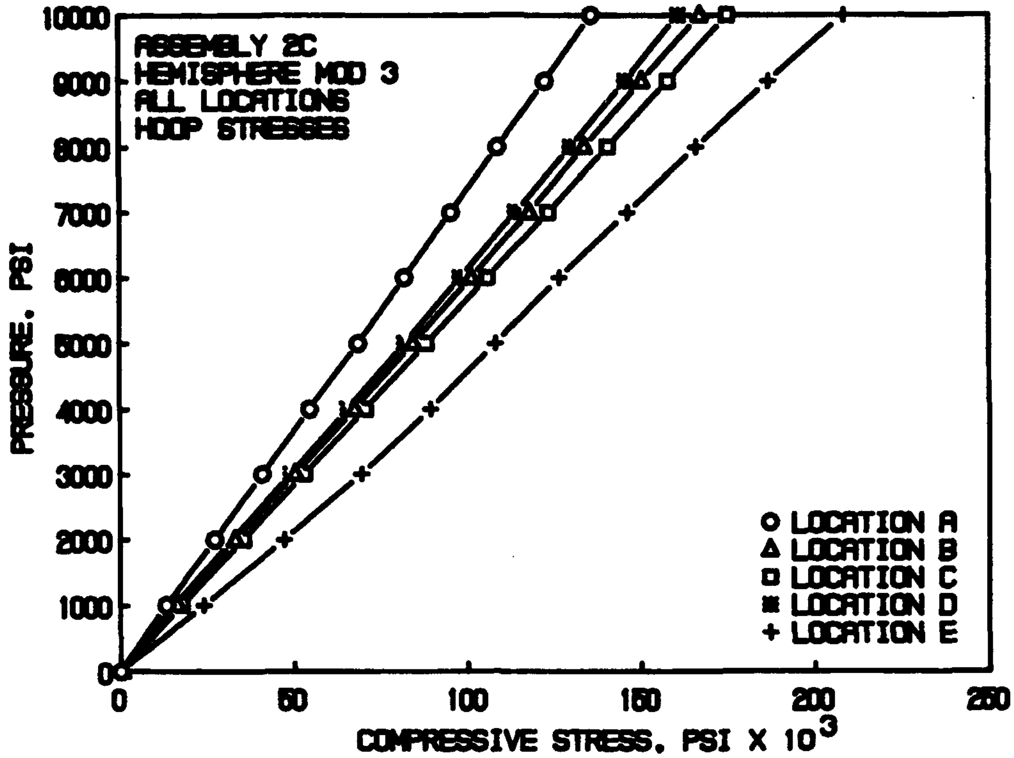

Figure. C-50. Stresses on test assembly 2C; locations A, B, C, D, E in hoop orientation.

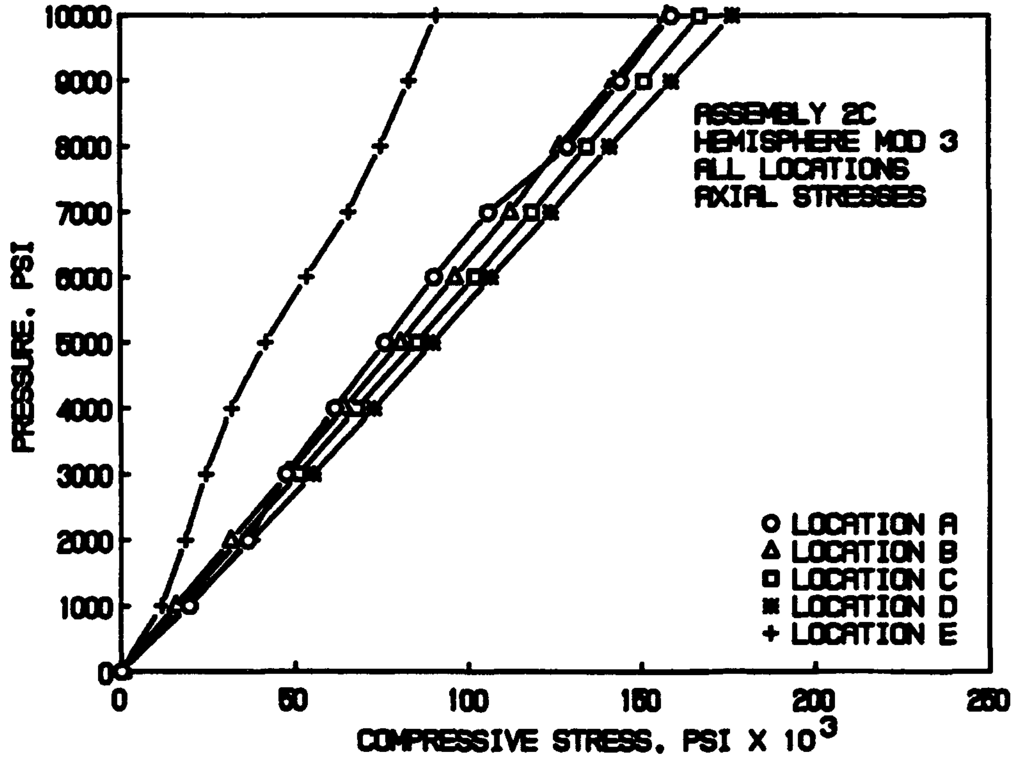

Figure. C-51. Stresses on test assembly 2C; locations A, B, C, D, E in axial orientation.

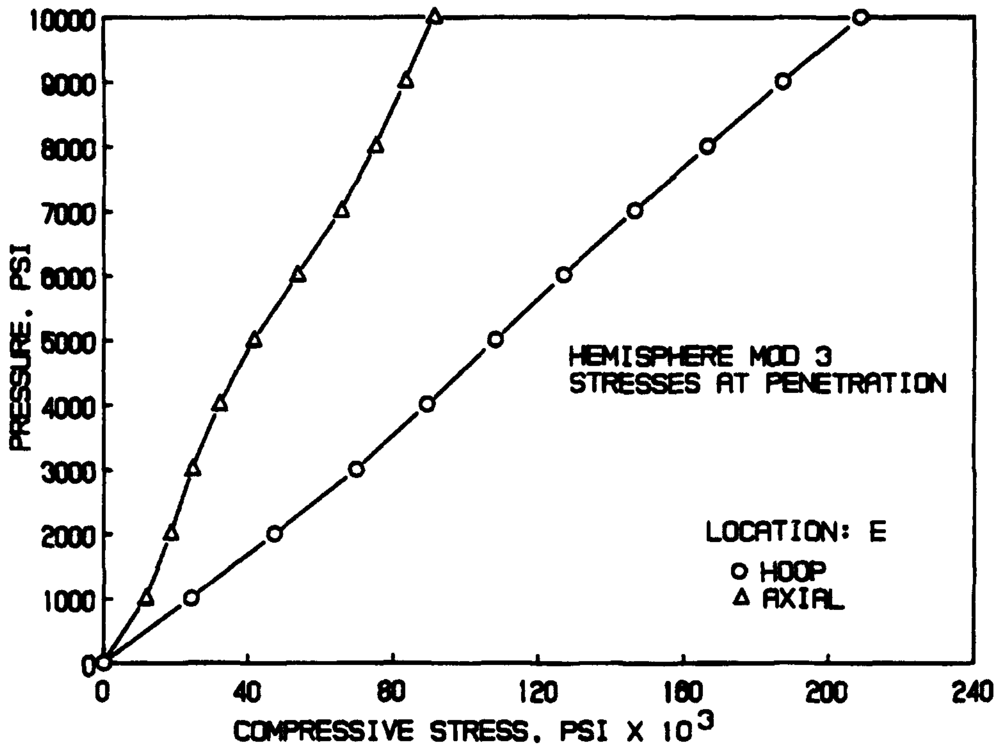

Figure. C-52. Stress on test assembly 2C; location E at polar penetration in Mod 3 hemisphere.

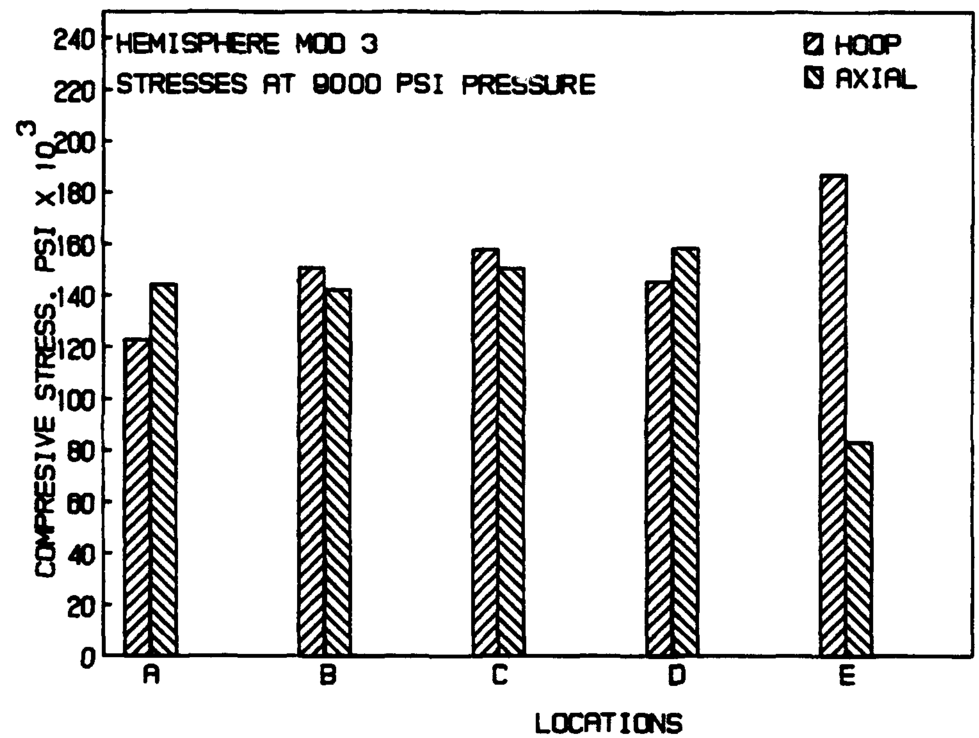

Figure. C-53. Distribution of stresses on Mod 3 hemisphere at 9000psi pressure.

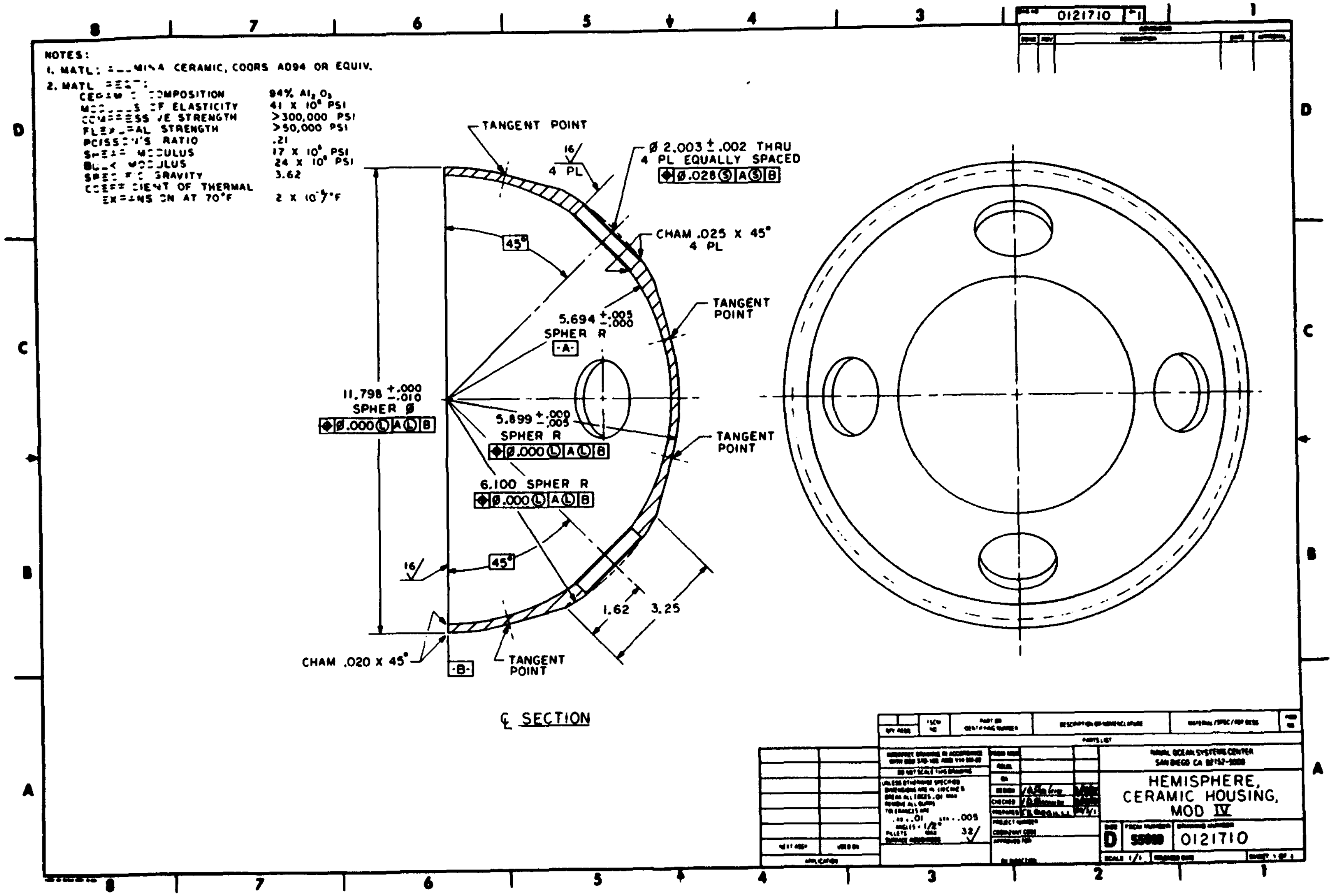

Figure C-54. Mod 4 ceramic hemisphere dimensions.

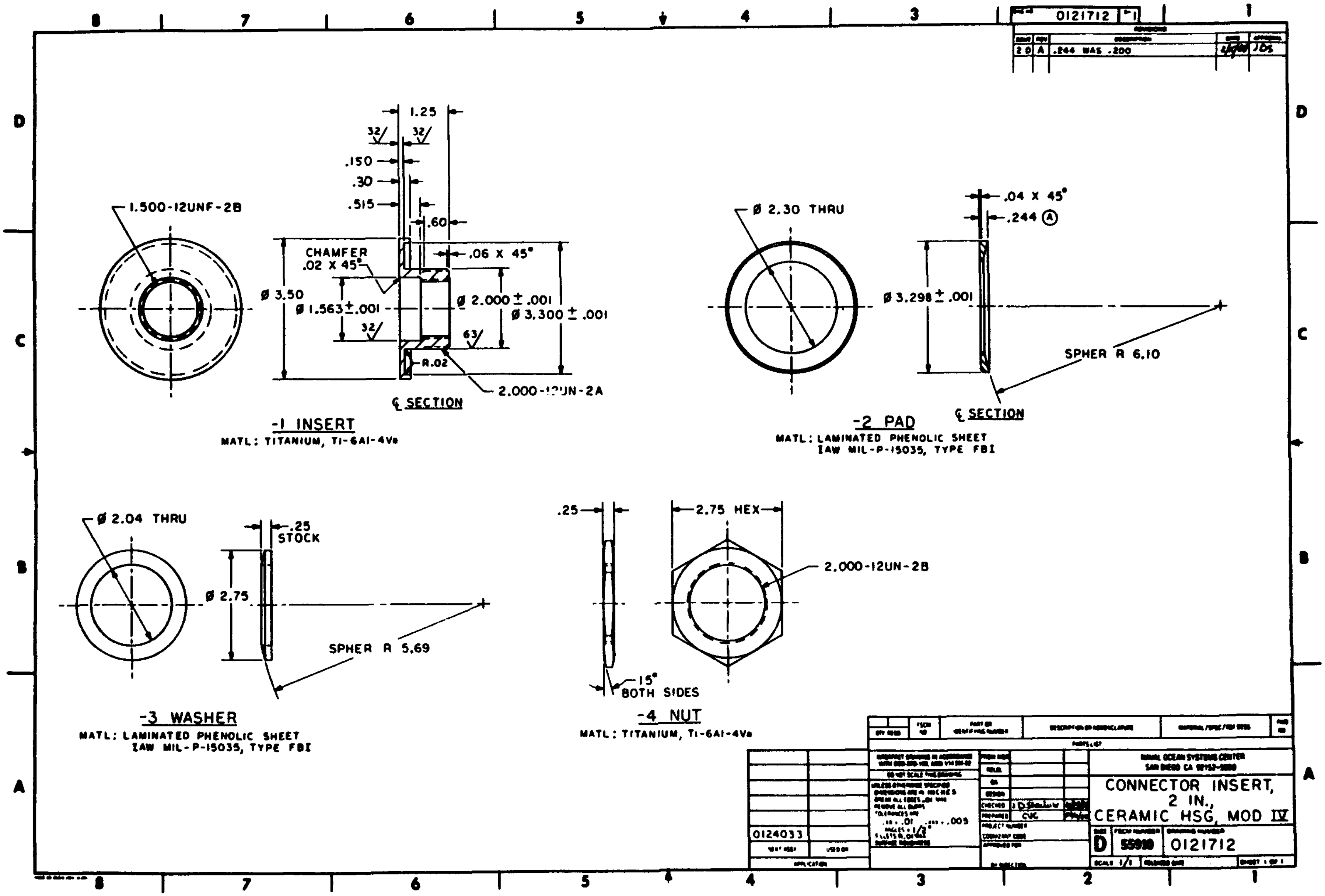

Figure C-55. Connector insert for Mod 4 hemisphere incorporating phenolic bearing pads.

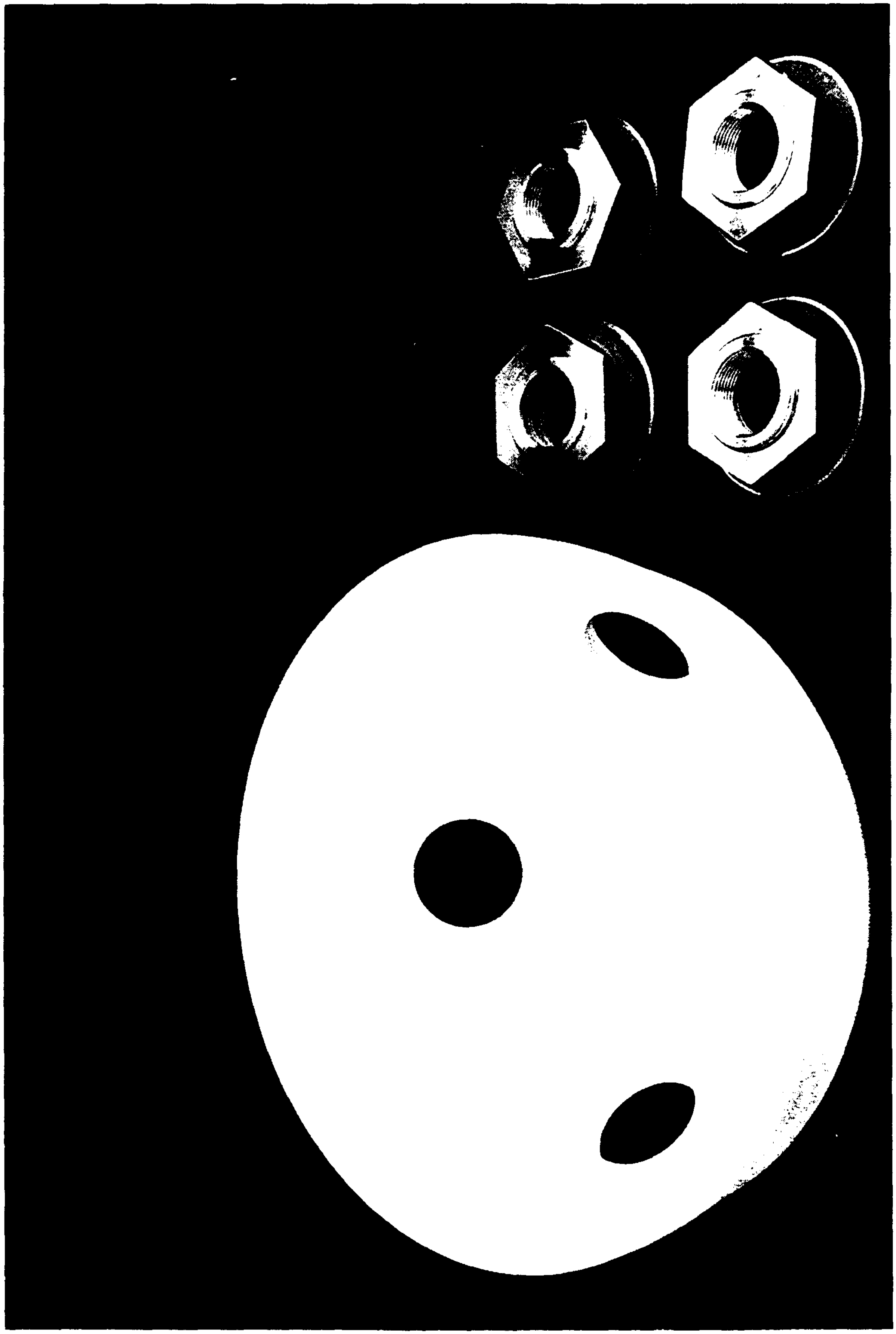

Figure C-56. Mod 4 hemisphere with connector inserts ready for installation.

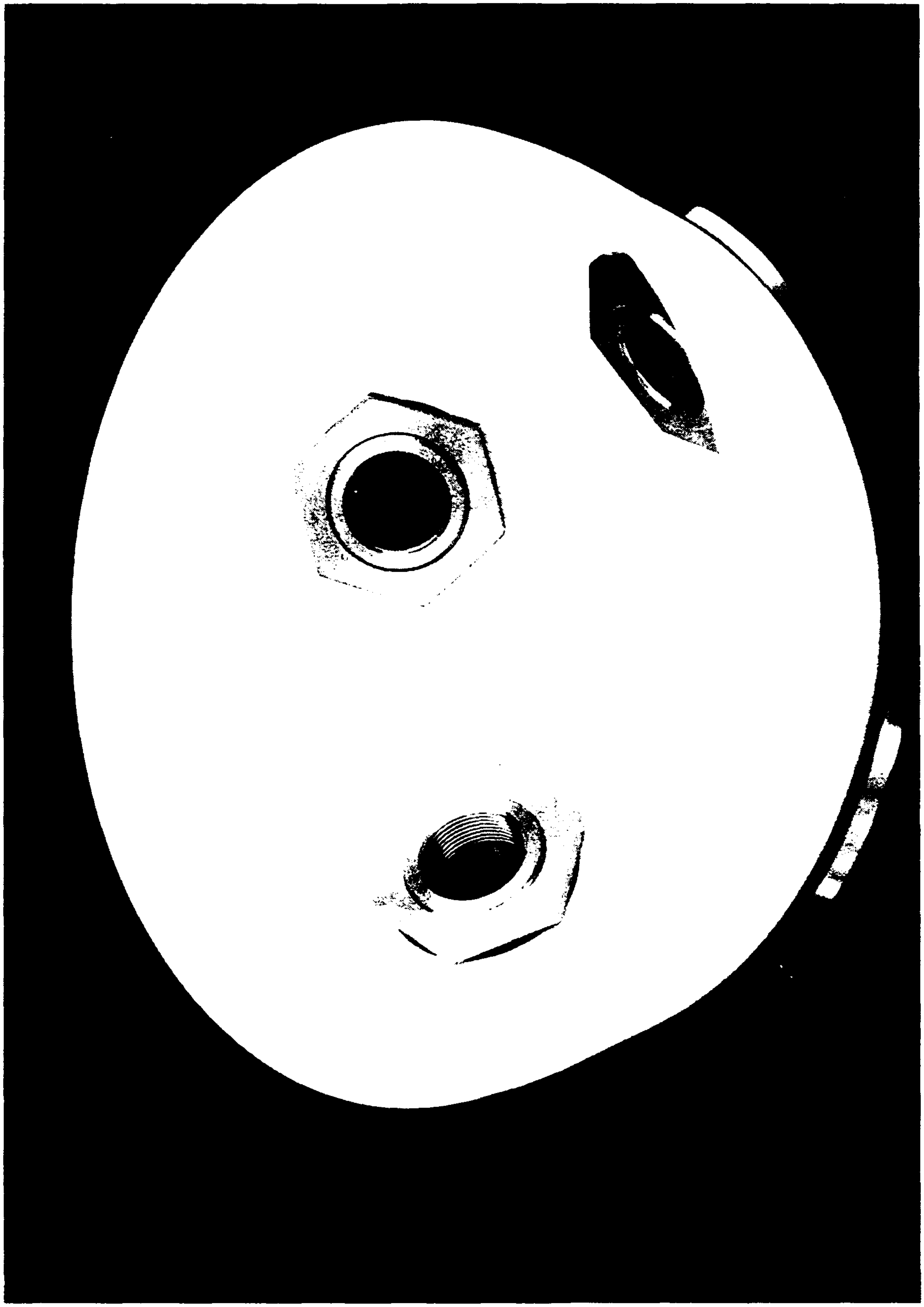

Figure C-57. Mod 4 hemisphere after installation of connector inserts—interior view.

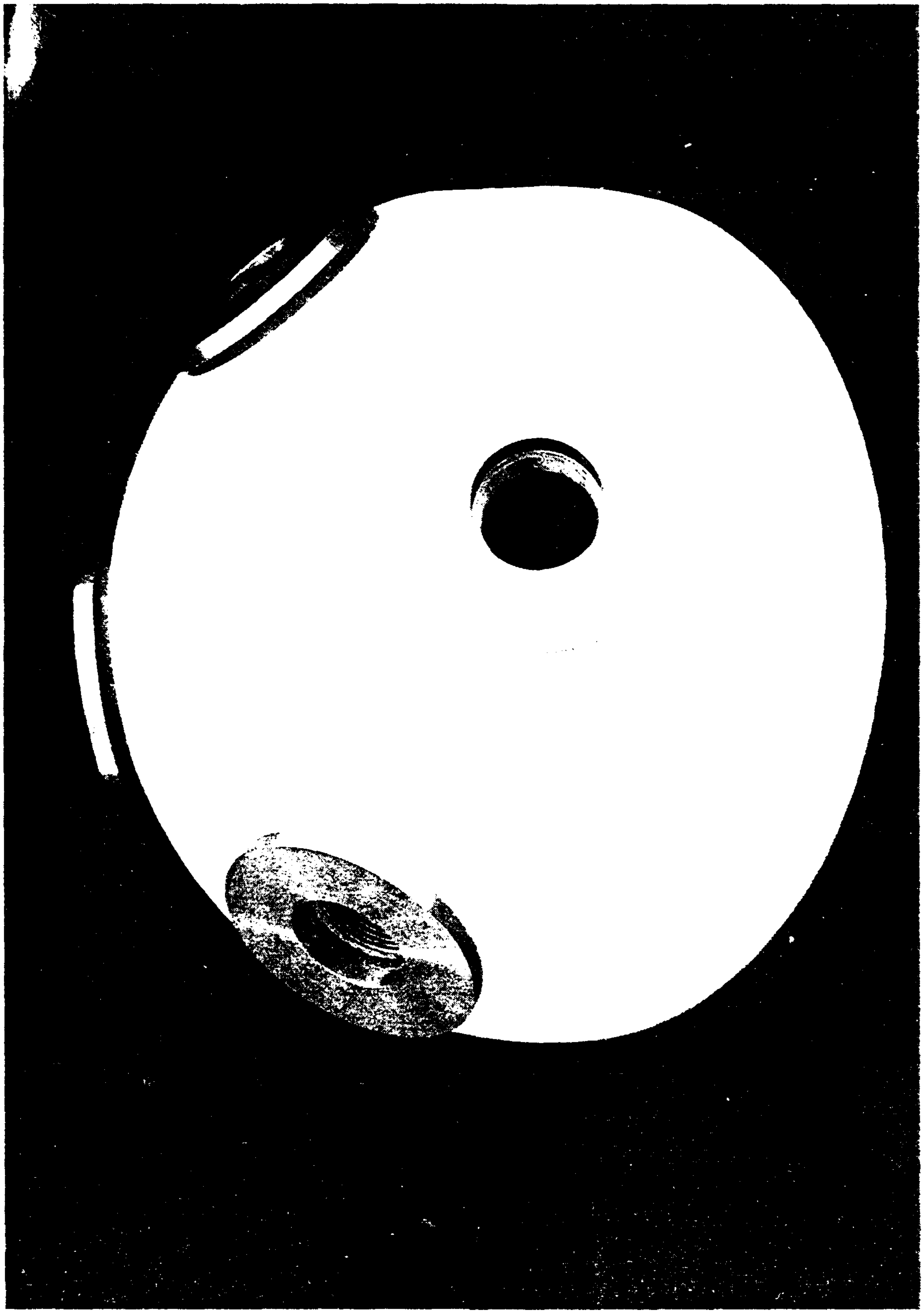

Figure C-58. Mated hemisphere after test [illegible]

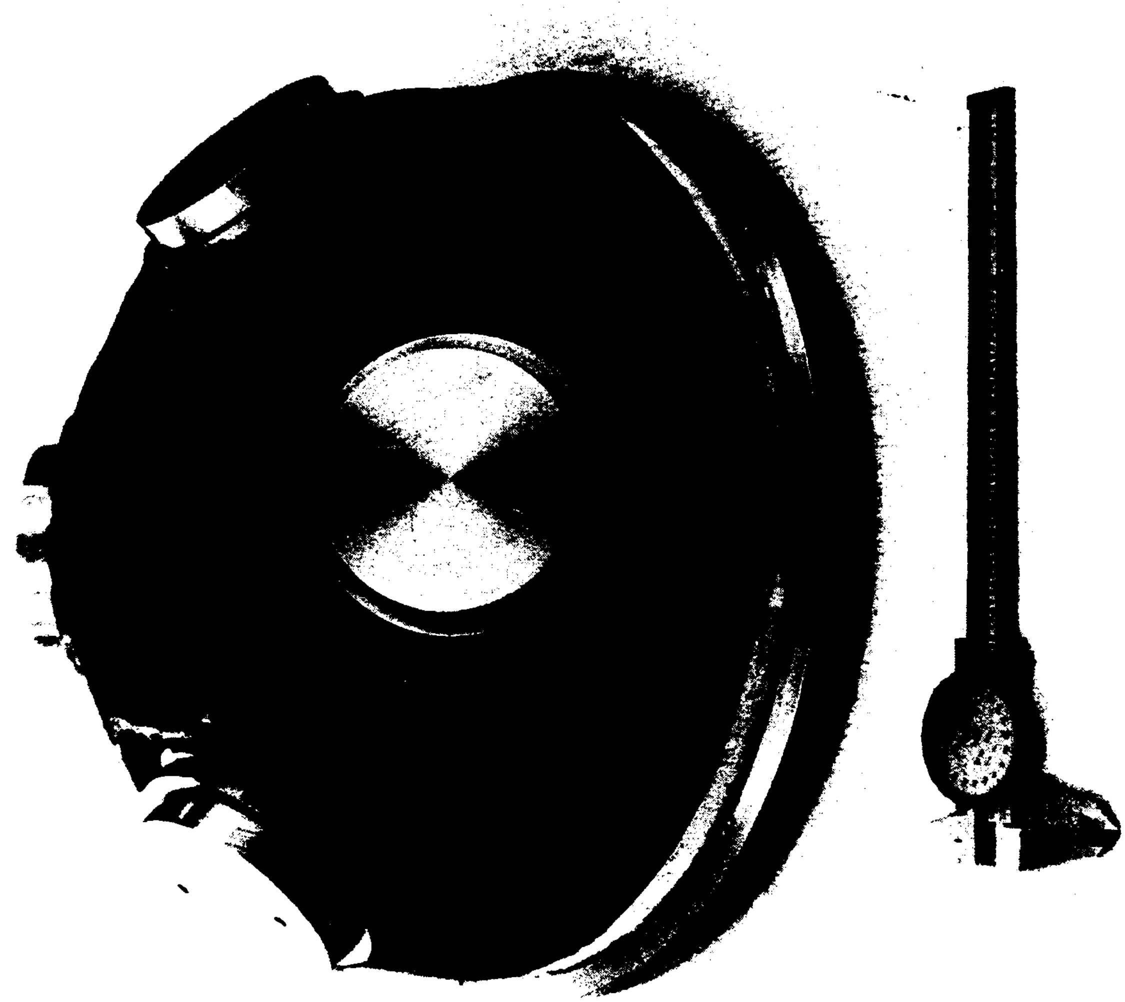

Figure C-59. Mod 4 hemisphere assembly after application of neoprene coating.

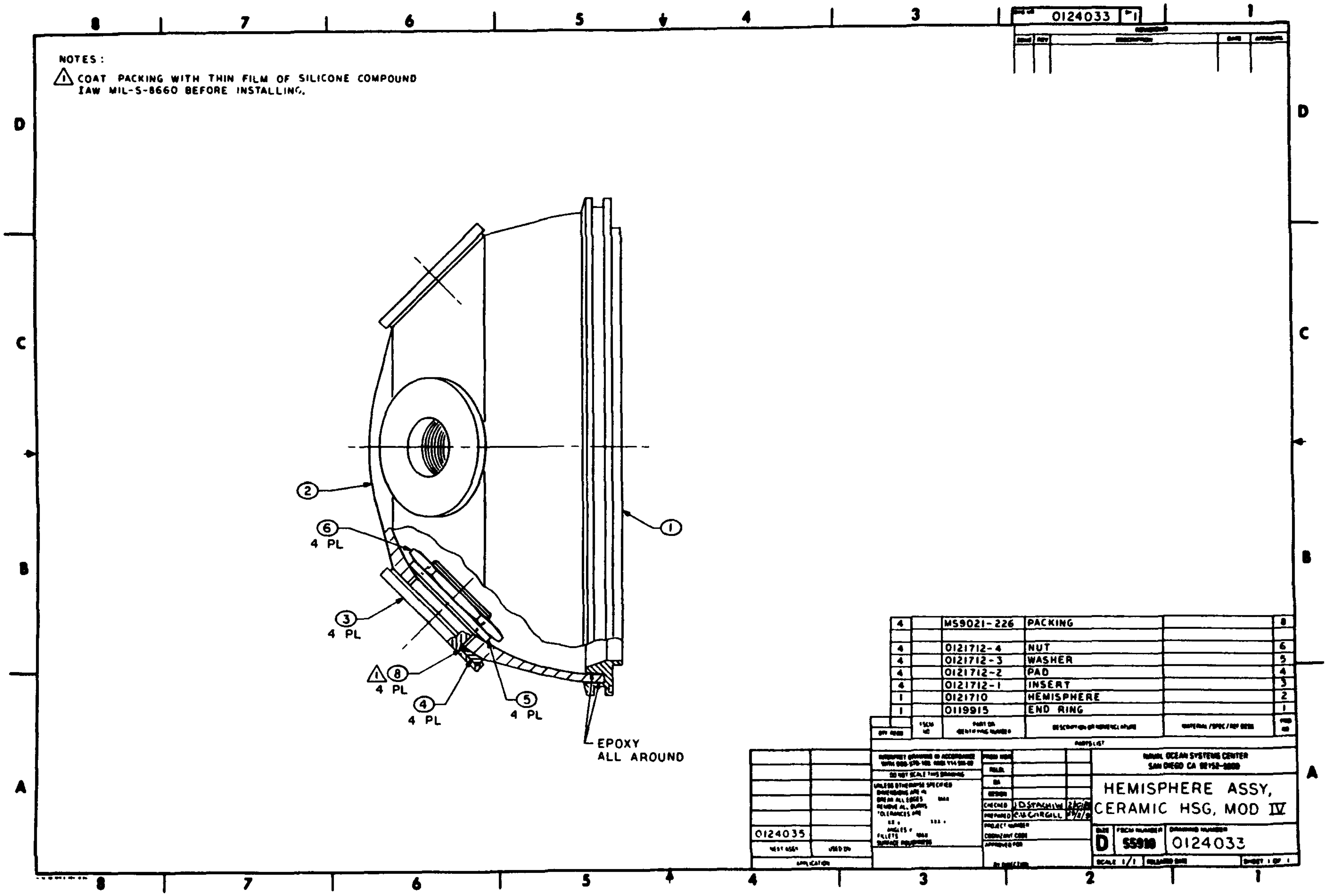

Figure C-60. Ceramic bulkhead assembly Mod 4; list of components.

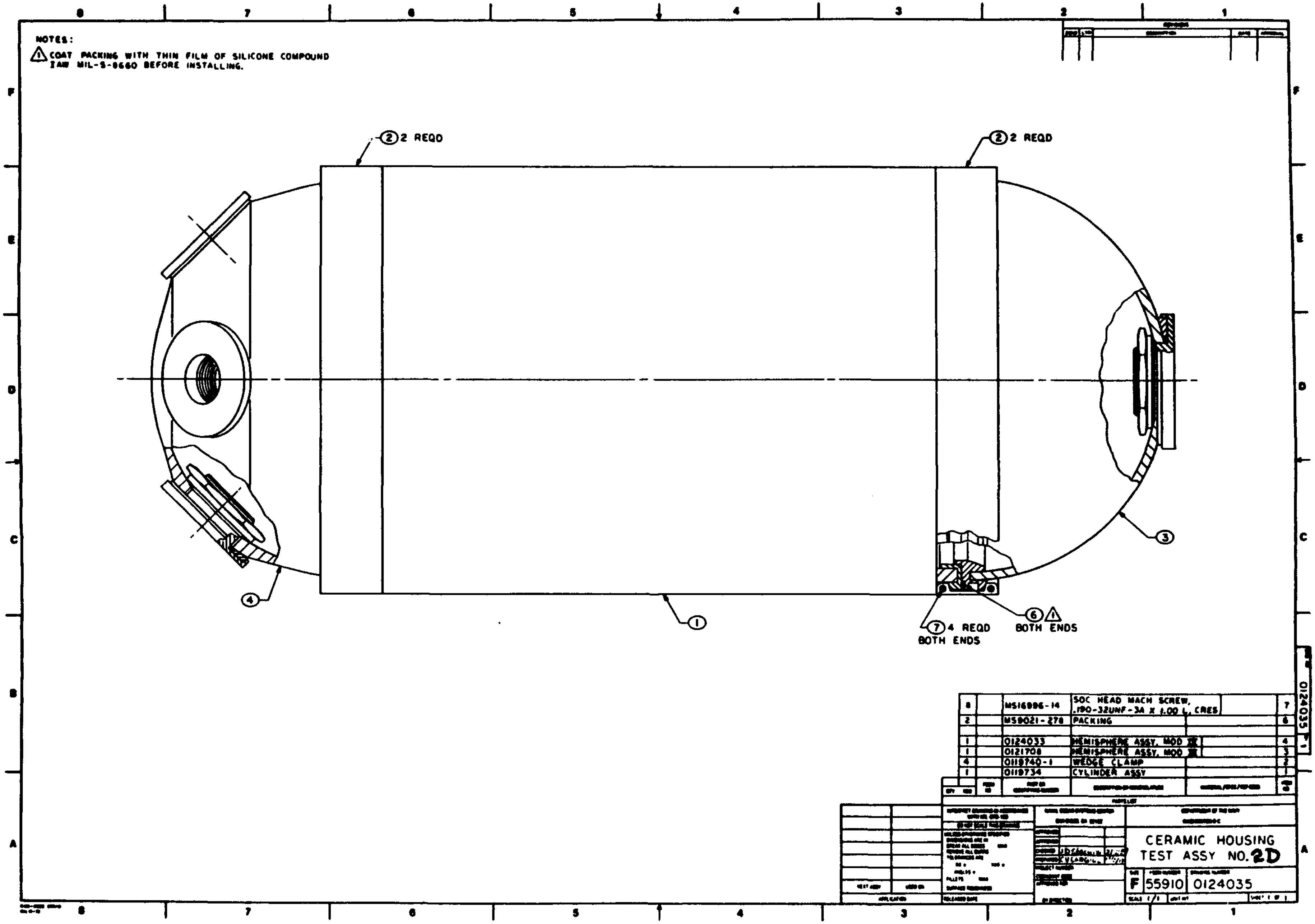

Figure C-61. Ceramic housing test assembly 2D incorporating the Mod 4 ceramic bulkhead.

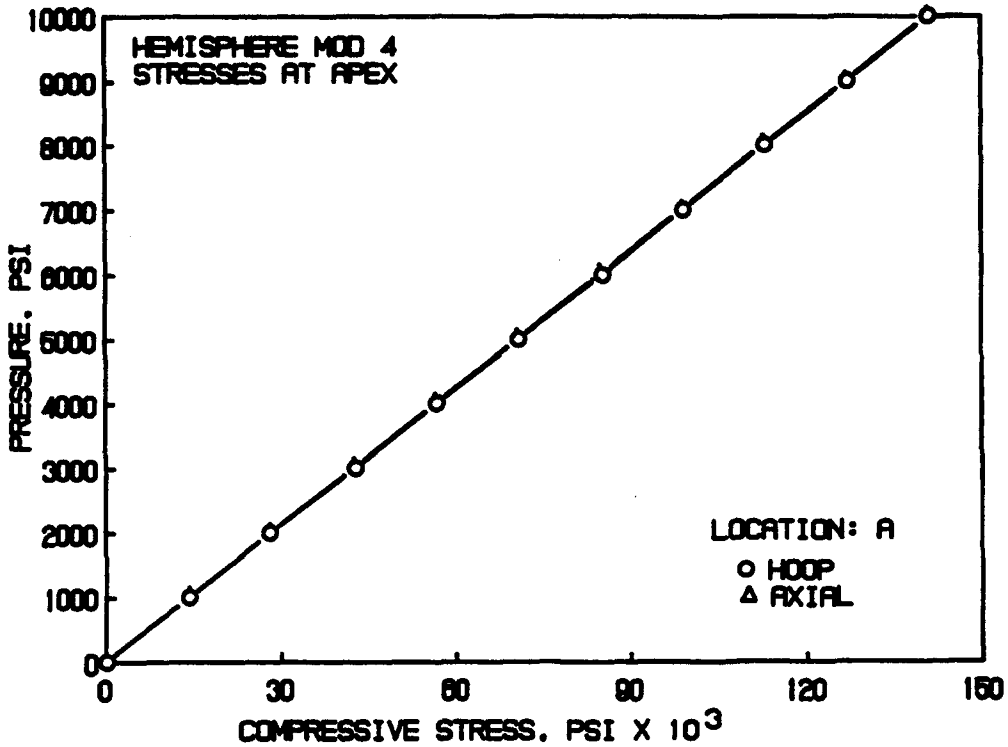

Figure. C-62. Stresses at apex of ceramic hemisphere Mod 4.

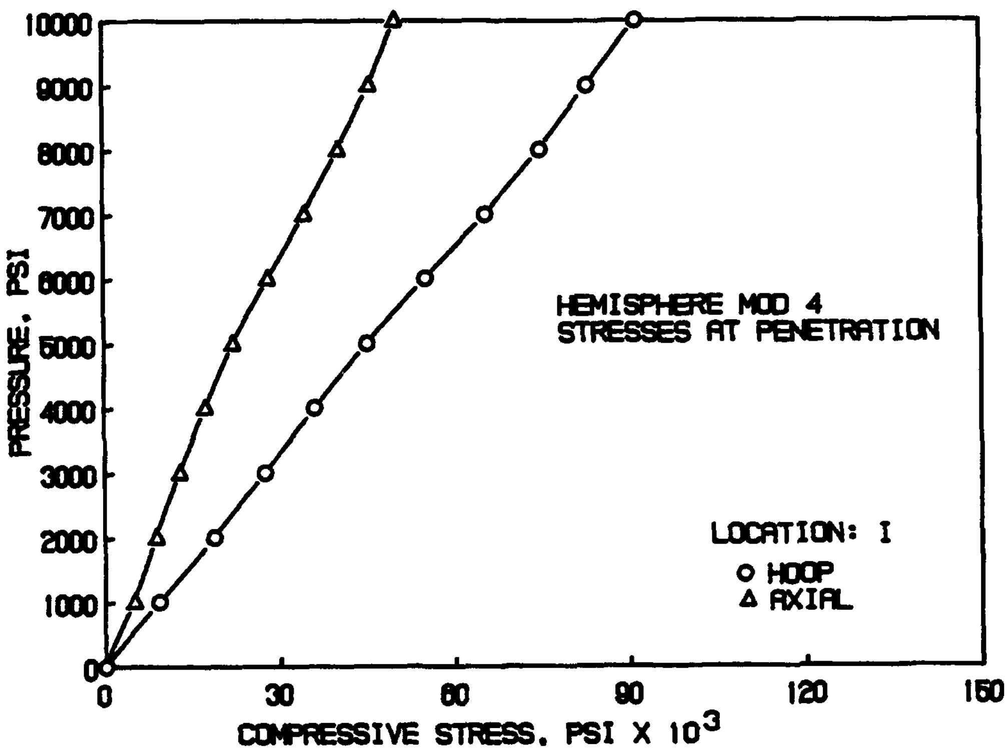

Figure. C-63. Stresses at penetration in hemisphere Mod 4.

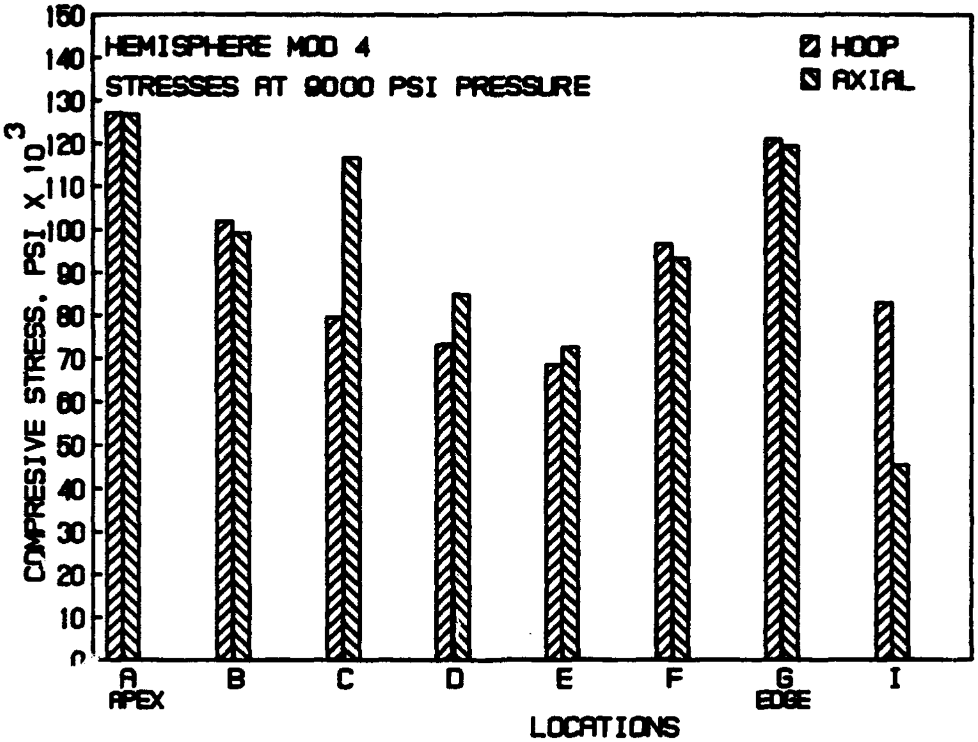

Figure. C-64. Distribution of stresses on ceramic hemisphere Mod 4.

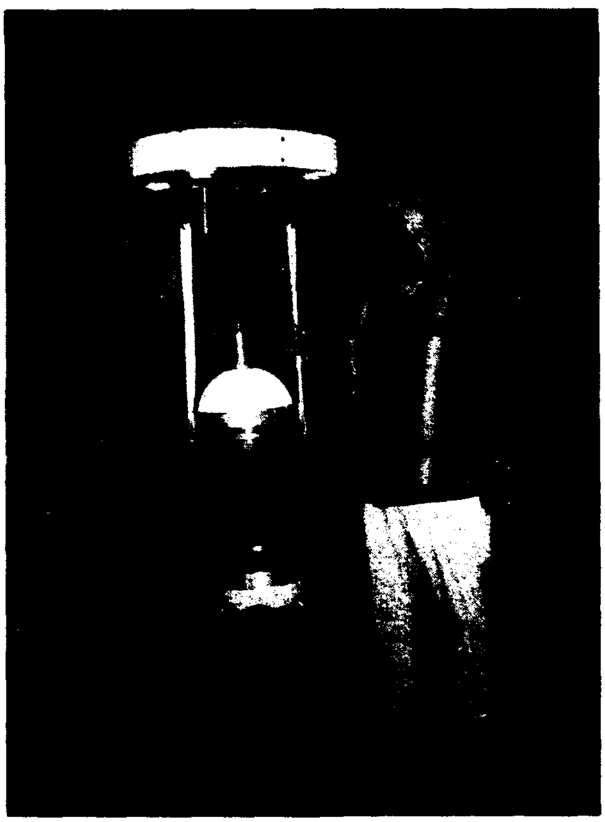

Figure. C-65. Ceramic housing test assembly 2D incorporating both Mod 4 and Mod 3 ceramic bulkheads.

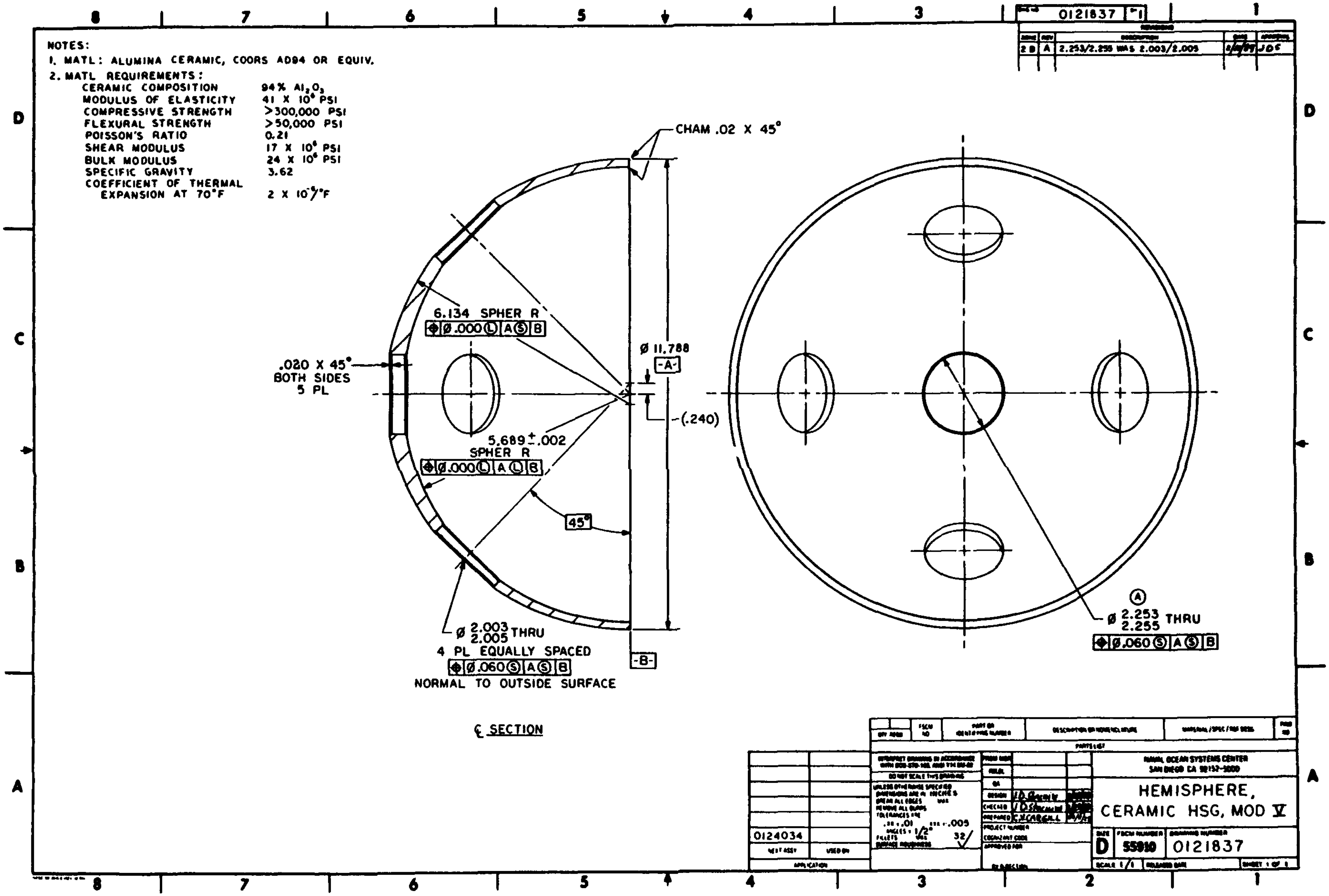

Figure C-66. Mod 5 ceramic hemisphere dimensions; the polar opening was subsequently enlarged to 3 inches.

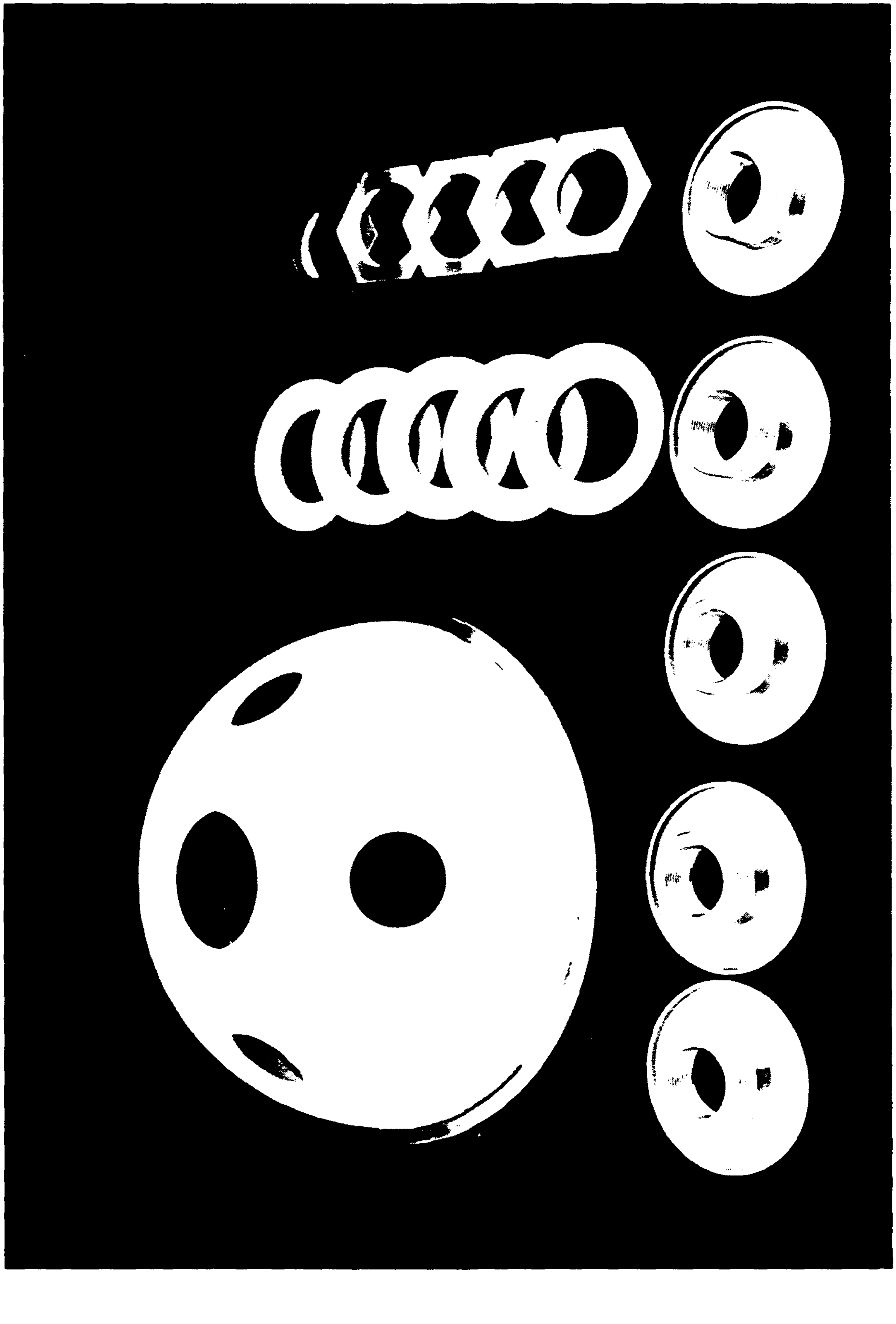

Figure C-67. Mod 5 hemisphere prior to mounting of connector inserts.

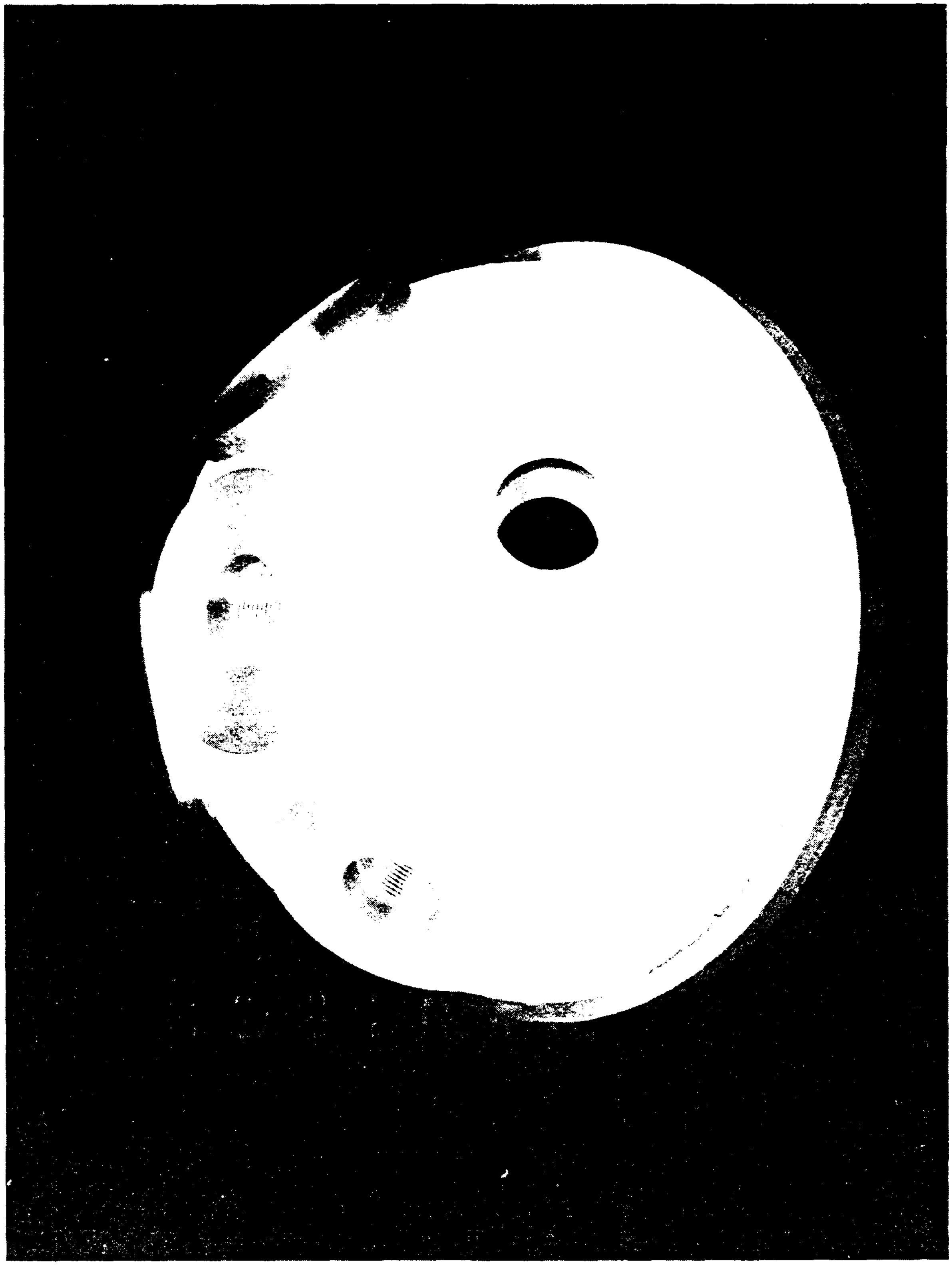

Figure C-68. Mod 5 hemispherical bulkhead assembly; exterior view.

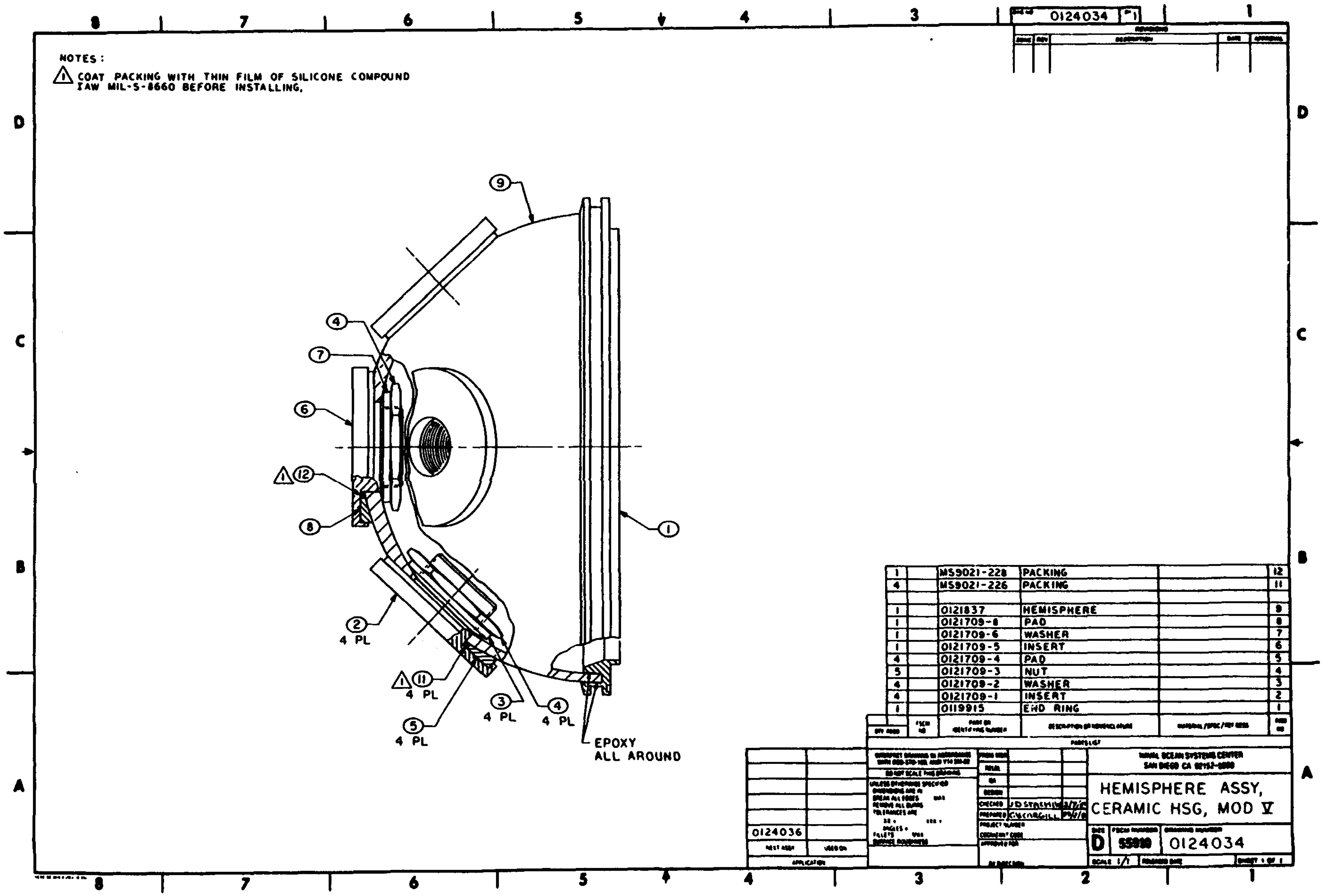

Figure C-69. Mod 5 ceramic bulkhead assembly; list of components.

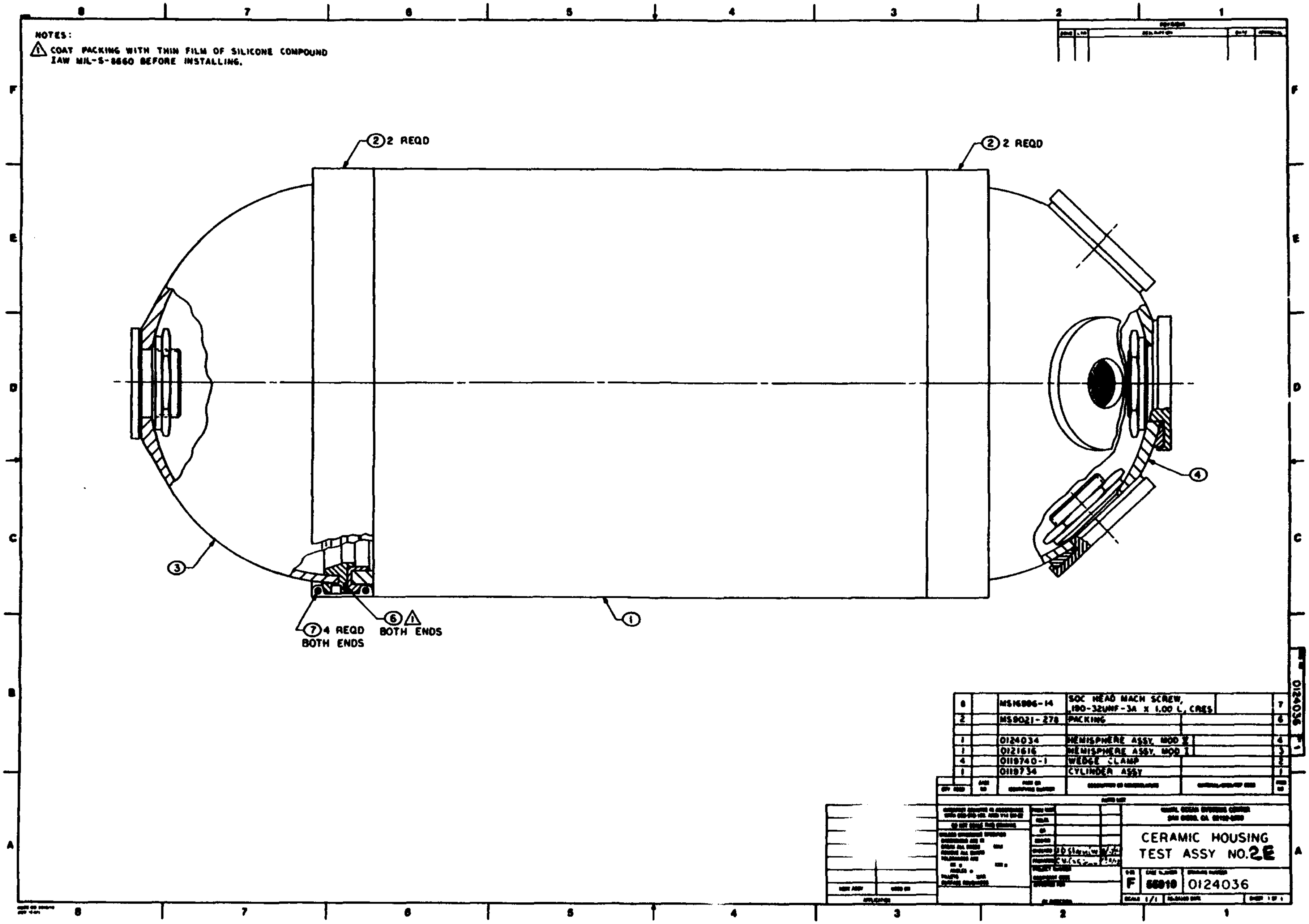

Figure C-70. Ceramic housing test assembly 2E incorporating Mod 5 and Mod 1 ceramic bulkheads.

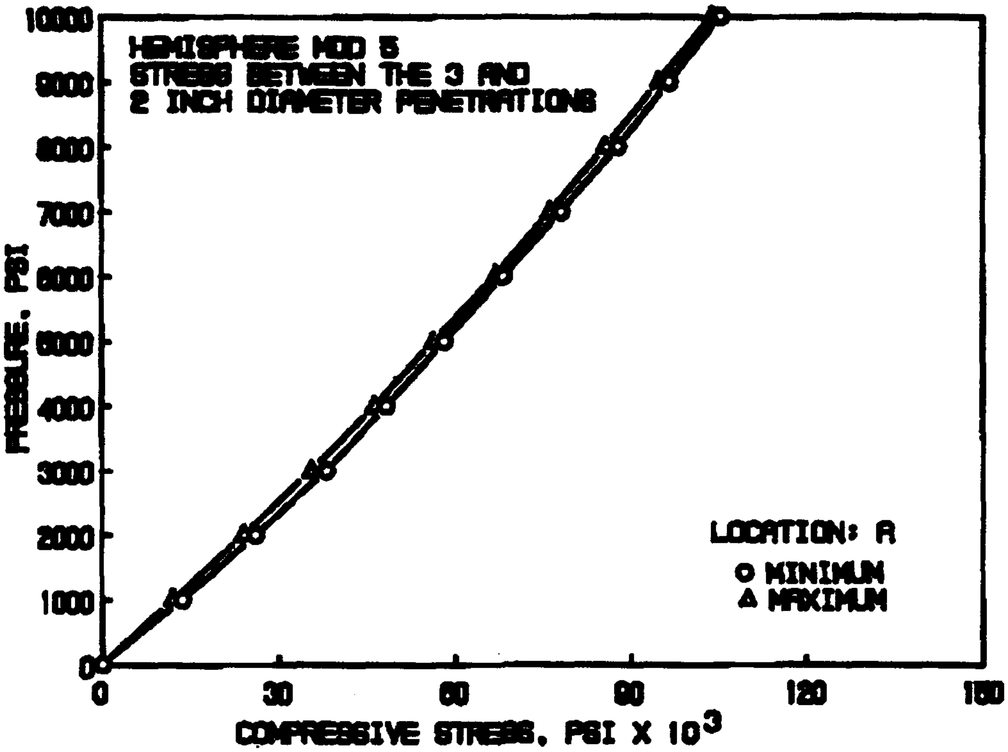

Figure. C-71. Stress on Mod 5 ceramic hemisphere between penetrations.

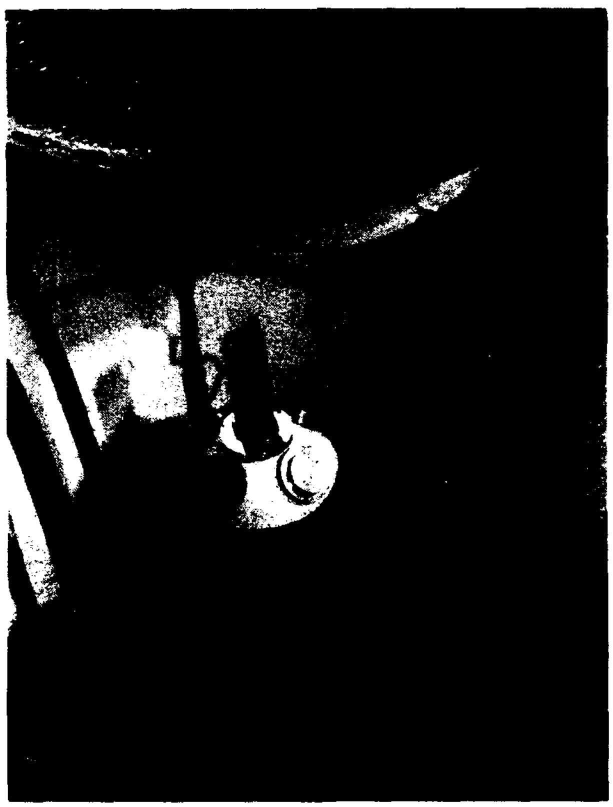

Figure C-72. Ceramic housing test assembly 2E during placement into the pressure vessel for external pressure testing.

Table C-1. Housing test assemblies with 12-inch diameters used in the evaluation of ceramic hemispherical bulkheads.

	Assy 2A	Assy 2B	Assy 2C
End Bells	Titanium, DWG 0119737 Ceramic, DWG 0119913	Titanium, DWG 0119737 Ceramic, DWG 0120247	Titanium, DWG 0119737 Ceramic, DWG 0121707
Cylinder	Ceramic, DWG 0119735	Ceramic, DWG 0119735	Ceramic, DWG 0119735
Stiffener	—	—	—
End Caps	Titanium, DWG 0119736	Titanium, DWG 0119736	Titanium, DWG 0119736
Hemi End Rings	Titanium, DWG 0119915	Titanium, DWG 0119915	Titanium, DWG 0119915
Band Clamps	Aluminum, DWG 0119740	Aluminum, DWG 0119740	Aluminum, DWG 0119740
Overall Length	L/D = 2.5	L/D = 2.5	L/D = 2.5

	Assy 2D	Assy 2E	Assy 2F
End Bells	Ceramic, DWG 0121707 Ceramic, DWG 0121710	Ceramic, DWG 0119913 Ceramic, DWG 0121837	Titanium, DWG 0119737 Titanium, DWG 0119737
Cylinder	Ceramic, DWG 0119735	Ceramic, DWG 0119735	Ceramic, DWG 0119735
Stiffener	—	—	—
End Caps	Titanium, DWG 0119736	Titanium, DWG 0119736	Aluminum, DWG 0125186
Hemi End Rings	Titanium, DWN 0119915	Titanium, DWN 0119915	—
Band Clamps	Aluminum, DWG 0119740	Aluminum, DWG 0119740	Aluminum, DWG 0119740
Overall Length	L/D = 2.5	L/D = 2.5	L/D = 2.5

Table C-2. Summary of proof and pressure test applied to 12-inch-diameter ceramic cylinders in housing test assemblies.

	Assy 2A	Assy 2B	Assy 2C
Proof Tests	1	1	1
Cyclic Tests	34	34	5

	Assy 2D	Assy 2E	Assy 2F
Proof Tests	2	1	1
Cyclic Tests	5	37*	500

1. Proof testing: Pressurize to 10,000 psi, hold pressure for 15 minutes.
2. Cycling Test: Pressurize to 9000 psi, hold pressure for 1 minute.

*Ceramic hemisphere Mod II was converted to Mod V by enlarging polar opening to 3 inches and adding four 2-in holes at 90° intervals at 45° elevation.

Table C-3. Summary of proof and pressure test applied to 12-inch-diameter ceramic hemispheres in housing test assemblies.

Ceramic Hemisphere	Hemisphere End Rings	Proof Testing to 10,000 psi	Pressure Cycling to 9000 psi	Condition of Hemisphere
Mod I	Mod 0	3	121 Cycles	a. No visible cracks around penetration. b. No spalling visible above the metal end ring.
Mod II	Mod 0	1	34 Cycles*	a. Visible cracks around penetration. b. Visible spalling above end ring.
Mod III	Mod 0	1	4 Cycles	a. No visible cracks around penetration. b. No visible cracks above end ring.
Mod IV	Mod 0	2	54 Cycles	a. No visible cracks around penetrations. b. Visible spalling above end ring.
Mod V	Mod 0	1	71 Cycles	a. No visible cracks around penetrations. b. Visible spalling above end ring.

* At completion of cycling the central penetration was enlarged from 2 to 3 inches to remove cracked material. In addition, 4 equally spaced penetrations with 2-in diameter were ground into the hemisphere at 45° elevation. The modified hemisphere saw further service as Mod V.

Table C-4. Weights of structural components in 12-inch-diameter ceramic housing test assemblies.

Ceramic Cylinder 12 in OD X 18 in L X 0.412 in, 94% alumina	35.0 lbs
End Caps for Cylinder (pair)	
Titanium MOD 0 DWG 55910-0119736	4.0 lbs
Titanium MOD 1 DWG 55910-0125186	5.2 lbs
Aluminum MOD 0 DWG 55910-0119736	1.44 lbs
Aluminum MOD 1 DWG 55910-0125186	3.28 lbs
Hemisphere, Titanium Type 1 DWG 55910-0119737	12.5 lbs
Hemisphere, Ceramic	
MOD 1 DWG 55910-0119913	6.57 lbs
MOD 2 DWG 55910-0120247	8.21 lbs
MOD 3 DWG 55910-0121710	5.40 lbs
MOD 4 DWG 55910-0121710	8.80 lbs
MOD 5 DWG 55910-0121837	7.88 lbs
End Ring for ceramic hemisphere MOD 0 Titanium DWG 55910-0119915	2.22 lbs
End Ring for ceramic hemisphere MOD 1 Titanium DWG 55910-0125666	4.10 lbs
Wedge Clamp Band, Aluminum DWG 55910-0119740	1.50 lbs
Connector Inserts, Titanium (each) DWG 55910-0120248	0.60 lbs
Weight/Displacement	
Cylinder with end caps, MOD 0 Titanium	0.512
Cylinder with end caps, MOD 1 Titanium	0.526
Cylinder with end caps, MOD 0 Aluminum	0.48
Cylinder with end caps, MOD 1 Aluminum	0.50
Cylinder with end caps, MOD 1 titanium and two Titanium hemispheres Type 1	0.62
Cylinder with end caps, MOD 1 Titanium; two ceramic hemispheres, MOD 1; with ends rings, MOD 1 Titanium; Aluminum clamp bands and connector inserts	0.60

*The critical buckling pressure of Titanium hemisphere Type 1 is 12,500 psi, and of Ceramic MOD 1 is 23,000 psi

Table C-5. Strains on the titanium end ring bonded to the 12-inch-diameter ceramic hemisphere Mod 1 DWG 55910-0119913.

Pressure (PSI)	Gage Locations A Hoop	A Axial	AA Hoop	AA Axial	AAA Hoop	AAA Axial
0	0	0	0	0	0	0
1000	-75	66	-58	137	-96	112
2000	-280	165	-280	250	-330	222
3000	-525	270	-476	332	-592	342
4000	-776	385	-732	470	-795	420
5000	-1050	500	-990	575	-1063	565
6000	-1290	670	-1187	727	-1277	700
7000	-1550	800	-1438	860	-1530	820
8000	-1800	942	-1677	993	-1773	957
9000	-2070	1065	-1936	1116	-2023	1080
10000	-2320	1192	-2172	1240	-2270	1207

Note: All strain readings are in microinches per inch

Table C-6. Strains on 12-inch-diameter ceramic hemisphere Mod 1 DWG 55910-0119913, Sheet 1.

Pressure (PSI)	Gage Locations B Hoop	B Axial	BB Hoop	BB Axial	BBB Hoop	BBB Axial	C Hoop	C Axial	D Hoop	D Axial	E Hoop	E Axial
0	0	0	0	0	0	0	0	0	0	0	0	0
1000	-238	11	-223	-75	-265	-148	-272	-89	-294	-233	-265	-256
2000	-484	-96	-459	-366	-487	-452	-491	-384	-557	-475	-510	-499
3000	-721	-313	-670	-656	-730	-693	-720	-673	-820	-721	-767	-750
4000	-995	-620	-940	-850	-945	-946	-959	-849	-1078	-964	-1028	-1009
5000	-1206	-888	-1153	-1130	-1163	-1241	-1186	-1116	-1333	-1204	-1281	-1255
6000	-1414	-1155	-1352	-1380	-1385	-1570	-1412	-1388	-1588	-1445	-1535	-1500
7000	-1653	-1447	-1593	-1680	-1602	-1857	-1630	-1669	-1836	-1682	-1782	-1739
8000	-1865	-1720	-1796	-1932	-1832	-2162	-1863	-1966	-2098	-1930	-2044	-1990
9000	-2087	-2012	-2018	-2248	-2050	-2453	-2080	-2248	-2348	-2165	-2291	-2227
10000	-2318	-2301	-2248	-2522	-2270	-2746	-2300	-2540	-2600	-2400	-2542	-2470

Note: All strain readings are in microinches per inch

Table C-6. Strains on 12-inch-diameter ceramic hemisphere Mod 1 DWG 55910-0119913, Sheet 2.

	Gage Locations											
	F		G		H		I		J		K	
Pressure (PSI)	Hoop	Axial	Hoop	Axial	Hoop	Axial	Hoop	Axial	Hoop	Axial	Hoop	Axial
0	0	0	0	0	0	0	0	0	0	0	0	0
1000	-255	-259	-284	-280	-312	-238	-272	-180	-270	-238	-350	-244
2000	-498	-514	-512	-532	-574	-436	-490	-312	-482	-458	-274	-274
3000	-753	-775	-760	-770	-844	-642	-690	-460	-686	-658	-262	-320
4000	-1007	-1037	-1060	-1078	-1160	-892	-1000	-650	-990	-936	-218	-372
5000	-1258	-1295	-1328	-1358	-1460	-1124	-1250	-818	-1232	-1170	-202	-416
6000	-1509	-1554	-1574	-1614	-1740	-1314	-1470	-964	-1452	-1380	-172	-404
7000	-1756	-1810	-1820	-1870	-2000	-1516	-1680	-1098	-1664	-1622	-142	-414
8000	-2014	-2078	-2080	-2134	-2282	-1722	-1904	-1244	-1892	-1864	-120	-444
9000	-2259	-2333	-2334	-2394	-2576	-1930	-2122	-1394	-2110	-2110	-88	-472
10000	-2507	-2593	-2592	-2660	-2854	-2130	-2350	-1540	-2330	-2370	-54	-524

Note: All strain readings are in microinches per inch

Table C-6. Strains on 12-inch-diameter ceramic hemisphere Mod 1 DWG 55910-0119913, Sheet 3.

Pressure (PSI)	KK Hoop	KK Axial
0	0	0
1000	64	20
2000	-90	116
3000	-180	150
4000	-312	126
5000	-420	154
6000	-510	142
7000	-600	198
8000	-712	260
9000	-800	250
10000	-882	264

Note: All strain readings are in microinches per inch

Table C-7. Strains on ceramic cylinder assembly 2A gage locations.

Pressure (PSI)	L		LL	
	Hoop	Axial	Hoop	Axial
0	0	0	0	0
1000	-242	182	-344	38
2000	-580	-44	-580	0
3000	-794	-134	-884	-44
4000	-1066	-318	-1196	-116
5000	-1350	-390	-1240	-242
6000	-1630	-666	-1684	-310
7000	-1910	-920	-1924	-386
8000	-2190	-1190	-2280	-474
9000	-2472	-1960	-2510	-500
10000	-2744	-2548	-2800	-626

Note: All strain readings are in microinches per inch

Table C-8. Strains on titanium end bell gage location.

Pressure (PSI)	Gage Location M Hoop	Gage Location M Axial
0	0	0
1000	-442	-354
2000	-830	-714
3000	-1200	-1074
4000	-1508	-1614
5000	-2050	-1950
6000	-2450	-2360
7000	-2772	-2790
8000	-3230	-3114
9000	-3656	-3534
10000	-4050	-3880

Note: All strain readings are in microinches per inch

Table C-9. Principal stresses on titanium end ring bonded to the 12-inch-diameter ceramic hemisphere Mod 1 DWG 55910-0119913,.

Pressure (PSI)	Gage Locations A		AA		AAA	
	Hoop	Axial	Hoop	Axial	Hoop	Axial
0	0	0	0	0	0	0
1000	-981	756	-213	2188	-1081	1481
2000	-4177	1302	-3638	2888	-4749	2049
3000	-8082	1707	-6775	3175	-8876	2625
4000	-12036	2260	-10676	4125	-12168	2793
5000	-16418	2668	-14823	4448	-16248	3798
6000	-19817	4317	-17534	6034	-19385	4959
7000	-23844	5093	-21373	6923	-23344	5593
8000	-27607	6157	-24989	7889	-27008	6608
9000	-31864	6739	-29041	8540	-30892	7317
10000	-35723	7523	-32657	9357	-34695	8120

Note: All stresses are in pounds per square inch, calculated on the basis of E = 16,500,000 and M=.34

Table C-10. Stresses on 12-inch-diameter ceramic hemisphere Mod 1 DWG 55910-0119913, Sheet 1.

Pressure (PSI)	Gage Locations B Hoop	B Axial	BB Hoop	BB Axial	BBB Hoop	BBB Axial	C Hoop	C Axial	D Hoop	D Axial	E Hoop	E Axial
0	0	0	0	0	0	0	0	0	0	0	0	0
1000	-10109	-1672	-10240	-5226	-12699	-8735	-12468	-6267	-14709	-12642	-13672	-13367
2000	-21624	-8477	-22984	-19833	-24960	-23774	-24519	-20893	-28169	-25391	-26370	-25997
3000	-33744	-19919	-34646	-34172	-37553	-36299	-36944	-35352	-41666	-38311	-39654	-39078
4000	-48262	-35555	-47975	-44925	-49054	-49088	-48781	-45053	-54921	-51058	-53181	-52538
5000	-59726	-48951	-59633	-58853	-61061	-63704	-60922	-58550	-68020	-63649	-66249	-65368
6000	-71053	-62277	-70420	-71369	-73547	-79816	-73066	-72252	-81128	-76283	-79350	-78164
7000	-83934	-76954	-83459	-86407	-85440	-94080	-84947	-86269	-93900	-88682	-92097	-90640
8000	-95486	-90573	-94436	-99044	-98052	-109234	-97616	-101106	-107372	-101679	-105596	-103766
9000	-107638	-105097	-106805	-114598	-110024	-123679	-109464	-115156	-120211	-114010	-118325	-116156
10000	-120149	-119573	-119138	-128422	-122099	-138228	-121530	-129663	-133137	-126360	-131280	-128840

Note: All stresses are in pounds per square inch calculated on the basis of E=41,000,000 and M=.21

Table C-10. Stresses on 12-inch-diameter ceramic hemisphere Mod 1 DWG 55910-0119913, Sheet 2.

Pressure (PSI)	F Hoop	F Axial	G Hoop	G Axial	H Hoop	H Axial	I Hoop	I Axial	J Hoop	J Axial	K Hoop	K Axial
	Gage Locations											
0	0	0	0	0	0	0	0	0	0	0	0	0
1000	-13270	-13406	-14703	-14568	-15526	-13019	-13288	-10171	-13725	-12640	-17210	-13618
2000	-25990	-26532	-26753	-27430	-28547	-23871	-23827	-17796	-24799	-23986	-14220	-14220
3000	-39278	-40024	-39534	-39872	-41984	-35139	-33739	-25945	-35351	-34402	-14120	-16085
4000	-52533	-53549	-55175	-55785	-57789	-48708	-48747	-36887	-50894	-49064	-12701	-17919
5000	-65623	-66876	-69193	-70209	-72747	-61361	-60983	-46345	-63382	-61281	-12411	-19663
6000	-78721	-80246	-82050	-83405	-86468	-72033	-71734	-54589	-74709	-72270	-11016	-18878
7000	-91622	-93451	-94907	-96601	-99439	-83039	-81949	-62228	-85982	-84559	-9820	-19036
8000	-105102	-107270	-108437	-110267	-113390	-94415	-92871	-70508	-97941	-96993	-9146	-20125
9000	-117907	-120415	-121673	-123707	-127874	-105984	-103573	-78905	-109508	-109508	-8026	-21038
10000	-130886	-133800	-135136	-137440	-141599	-117067	-114667	-87221	-121286	-122641	-7036	-22962

Note: All stresses are in pounds per square inch calculated on the basis of E=41,000,000 and M=.21

Table C-10. Stresses on 12-inch-diameter ceramic hemisphere Mod 1 DWG 55910-0119913, Sheet 3.

Pressure (PSI)	KK Hoop	KK Axial
0	0	0
1000	2925	1434
2000	-2815	4165
3000	-6369	4812
4000	-12247	2594
5000	-16628	2822
6000	-20596	1497
7000	-23952	3088
8000	-28197	4739
9000	-32062	3517
10000	-35453	3379

Note: All stresses are in pounds per square inch calculated on the basis of E=41,000,000 and M=.21

Table C-11. Principal stresses on ceramic cylinder gage location.

Pressure (PSI)	L Hoop	L Axial	LL Hoop	LL Axial
0	0	0	0	0
1000	-8741	5627	-14413	-1469
2000	-25274	-7111	-24877	-5224
3000	-35263	-12899	-38313	-9850
4000	-48587	-23241	-52344	-15748
5000	-61417	-28888	-55366	-21549
6000	-75913	-43248	-75022	-28465
7000	-90210	-56665	-86001	-33886
8000	-104652	-70768	-102063	-40867
9000	-123683	-106334	-112163	-44054
10000	-140646	-134005	-125736	-52071

Note: All stresses are in pounds per square inch calculated on the

Table C-12. Principal stresses on titanium end bell gage location.

Pressure (PSI)	M Hoop	Axial
0	0	0
1000	-10492	-9408
2000	-20014	-18586
3000	-29201	-27650
4000	-38373	-39678
5000	-50616	-49385
6000	-60680	-59572
7000	-69415	-69637
8000	-80015	-78587
9000	-90627	-89125
10000	-100173	-98080

Note: All stresses are in pounds per square inch, calculated on the basis of E = 16,500,000 and M=.34

Table C-13. Strains on 12-inch-diameter ceramic hemisphere Mod 2; DWG 55910-0120247, Sheet 1.

Pressure (PSI)	Gage Locations											
	B		C		D		E		F		G	
	Hoop	Axial	Hoop	Axial	Hoop	Axial	Hoop	Axial	Hoop	Axial	Hoop	Axial
0	0	0	0	0	0	0	0	0	0	0	0	0
1000	-240	-378	-222	-230	-212	-207	-208	-202	-199	-182	-184	-184
2000	-458	-636	-442	-467	-438	-413	-422	-398	-401	-372	-372	-365
3000	-670	-900	-662	-687	-660	-615	-634	-595	-601	-560	-557	-544
4000	-878	-1156	-891	-889	-881	-814	-845	-793	-800	-745	-740	-723
5000	-1082	-1400	-1118	-1097	-1102	-1014	-1058	-989	-1000	-933	-925	-903
6000	-1286	-1641	-1350	-1307	-1328	-1216	-1274	-1188	-1200	-1125	-1113	-1085
7000	-1494	-1892	-1537	-1550	-1551	-1418	-1481	-1381	-1400	-1316	-1296	-1268
8000	-1696	-2155	-1703	-1773	-1768	-1616	-1680	-1565	-1596	-1503	-1475	-1453
9000	-1898	-2424	-1896	-1984	-1986	-1814	-1885	-1756	-1793	-1691	-1660	-1635
10000	-2105	-2724	-2072	-2232	-2204	-2012	-2087	-1953	-1990	-1880	-1837	-1817

Note: All strain readings are in microinches per inch

Table C-13. Strains on 12-inch-diameter ceramic hemisphere Mod 2; DWG 55910-0120247, Sheet 2.

Pressure (PSI)	H Hoop	H Axial	I Hoop	I Axial	J Hoop	J Axial	K Hoop	K Axial	KK Hoop	KK Axial
0	0	0	0	0	0	0	0	0	0	0
1000	-173	-180	-159	-200	-160	-225	-248	-75	-292	-72
2000	-347	-364	-321	-398	-322	-448	-506	-146	-534	-150
3000	-518	-543	-480	-592	-482	-657	-764	-200	-790	-220
4000	-690	-719	-642	-774	-646	-837	-1017	-219	-1040	-260
5000	-863	-897	-806	-956	-814	-1015	-1273	-241	-1270	-300
6000	-1040	-1075	-973	-1135	-986	-1188	-1530	-269	-1530	-340
7000	-1212	-1250	-1135	-1311	-1152	-1353	-1767	-305	-1760	-386
8000	-1383	-1424	-1293	-1488	-1313	-1518	-1985	-362	-1960	-436
9000	-1555	-1598	-1454	-1661	-1472	-1686	-2184	-439	-2150	-520
10000	-1727	-1771	-1613	-1836	-1629	-1858	-2374	-532	-2322	-620

Note: All strain readings are in microinches per inch

Table C-14. Principal stresses on 12-inch-diameter ceramic hemisphere Mod 2; DWG 55910-0120247, Sheet 1.

Pressure (PSI)	Gage Locations B Hoop	B Axial	C Hoop	C Axial	D Hoop	D Axial	E Hoop	E Axial	F Hoop	F Axial	G Hoop	G Axial
0	0	0	0	0	0	0	0	0	0	0	0	0
1000	-13699	-18375	-11594	-11865	-10958	-10788	-10741	-10538	-10175	-9599	-9549	-9549
2000	-25373	-31405	-23165	-24012	-22507	-21660	-21685	-20872	-20550	-19568	-19243	-19006
3000	-36844	-44638	-34583	-35430	-33848	-32323	-32553	-31231	-30822	-29433	-28791	-28350
4000	-48072	-57492	-46224	-46157	-45120	-42850	-43387	-41625	-41024	-39160	-38252	-37676
5000	-59019	-69795	-57834	-57123	-56400	-53419	-54288	-51950	-51296	-49026	-47809	-47063
6000	-69940	-81969	-69677	-68220	-67913	-64118	-65345	-62431	-61604	-59062	-57512	-56563
7000	-81122	-94609	-79886	-80327	-79298	-74791	-75962	-72574	-71902	-69056	-67009	-66061
8000	-92156	-107709	-89015	-91387	-90389	-85238	-86155	-82258	-81994	-78842	-76353	-75608
9000	-103243	-121066	-99194	-102176	-101523	-95695	-96668	-92297	-92137	-88680	-85928	-85081
10000	-114824	-135798	-108977	-114398	-112657	-106151	-107107	-102566	-102289	-98562	-95159	-94481

Note: All stresses are in pounds per square inch calculated on the basis of E=41,000,000 and M=.21

Table C-14. Principal stresses on 12-inch-diameter ceramic hemisphere Mod 2; DWG 55910-0120247, Sheet 2.

Pressure (PSI)	Gage Locations									
	H		I		J		K		KK	
	Hoop	Axial	Hoop	Axial	Hoop	Axial	Hoop	Axial	Hoop	Axial
0	0	0	0	0	0	0	0	0	0	0
1000	-9042	-9279	-8621	-10011	-8889	-11092	-11313	-5451	-13173	-5718
2000	-18162	-18738	-17353	-19962	-17847	-22116	-23018	-10820	-24255	-11244
3000	-27109	-27956	-25920	-29716	-26592	-32522	-34571	-15460	-35866	-16552
4000	-36072	-37054	-34508	-38981	-35247	-41719	-45594	-18554	-46950	-20520
5000	-45095	-46247	-43182	-48265	-44057	-50867	-56772	-21803	-57175	-24307
6000	-54291	-55477	-51957	-57447	-52992	-59837	-68048	-25319	-68687	-28364
7000	-63244	-64532	-60491	-66455	-61598	-68409	-78537	-28998	-78967	-32409
8000	-72146	-73535	-68862	-75470	-69990	-76937	-88401	-33406	-87996	-36355
9000	-81091	-82548	-77326	-84340	-78323	-85575	-97630	-38502	-96902	-41670
10000	-90026	-91517	-85722	-93279	-86607	-94366	-106618	-44202	-105180	-47508

Note: All stresses are in pounds per square inch calculated on the basis of E=41,000,000 and M=.21

Table C-15. Strains on 12-inch-diameter ceramic hemisphere Mod 3; DWG 55910-0121707.

Pressure	A		B		C		D		E	
	Hoop	Axial	Hoop	Axial	Hoop	Axial	Hoop	Axial	Hoop	Axial
0	0	0	0	0	0	0	0	0	0	0
1000	-223	-414	-317	-296	-340	-320	-290	-380	-528	-159
2000	-470	-749	-643	-595	-684	-646	-597	-743	-1055	-212
3000	-752	-952	-981	-913	-1028	-971	-908	-1100	-1570	-240
4000	-1017	-1218	-1312	-1220	-1372	-1295	-1221	-1440	-2011	-322
5000	-1280	-1504	-1646	-1526	-1718	-1618	-1535	-1770	-2424	-458
6000	-1532	-1780	-1977	-1827	-2062	-1938	-1843	-2102	-2818	-654
7000	-1782	-2095	-2307	-2124	-2403	-2252	-2148	-2437	-3232	-845
8000	-2000	-2586	-2617	-2404	-2746	-2553	-2447	-2778	-3672	-975
9000	-2253	-2891	-2944	-2694	-3083	-2869	-2741	-3123	-4135	-1071
10000	-2507	-3173	-3272	-2983	-3418	-3171	-3027	-3474	-4614	-1155

NOTES
Strain Gages:
CEA-13-125WT-350
Gage Factor 2.165
Test Assembly:
One Ceramic Cylinder Capped on One End With Ceramic Hemisphere Mod 4
DWG 55910-0121631 and on the Other End With Ceramic Hemisphere Mod 3
DWG 55910-0121632
Materials:
The Ceramic is: Coors AD 94 (94 percent Alumina)
The Titanium is: Ti 6Al 4Va
Data: All Strains are in microinches/inch

Table C-16. Stresses on 12-inch-diameter ceramic hemisphere Mod 3; DWG 55910-0121707.

Pressure	A Hoop	A Axial	B Hoop	B Axial	C Hoop	C Axial	D Hoop	D Axial	E Hoop	E Axial
0	0	0	0	0	0	0	0	0	0	0
1000	-13294	-19766	-16263	-15551	-17466	-16788	-15861	-18911	-24079	-11576
2000	-26906	-36360	-32939	-31312	-35157	-33869	-32299	-37246	-47161	-18596
3000	-40830	-47607	-50301	-47997	-52839	-50908	-48854	-55360	-69502	-24436
4000	-54592	-61403	-67263	-64146	-70512	-67903	-65342	-72762	-89156	-31925
5000	-68449	-76039	-84345	-80279	-88262	-84874	-81782	-89745	-108096	-41478
6000	-81744	-90147	-101254	-96171	-105899	-101698	-97983	-106759	-126760	-53434
7000	-95304	-105910	-118083	-111882	-123354	-118237	-114083	-123876	-146238	-65355
8000	-109077	-128933	-133902	-126685	-140777	-134237	-129979	-141195	-166282	-74895
9000	-122676	-144294	-150540	-142069	-158078	-150827	-145697	-158641	-187005	-83183
10000	-136110	-158678	-167211	-157419	-175167	-166798	-161126	-176272	-208307	-91100

Note: All stresses are in pounds per square inch calculated on the basis of E=41,000,000 and Poison's Ratio = 0.21

Table C-17. Strains on 12-inch-diameter ceramic hemisphere Mod 4; DWG 55910-0121710.

Pressure	A		B		C		D		E	
	Hoop	Axial	Hoop	Axial	Hoop	Axial	Hoop	Axial	Hoop	Axial
0	0	0	0	0	0	0	0	0	0	0
1000	-273	-270	-223	-226	-185	-257	-181	-186	-183	-146
2000	-542	-538	-442	-442	-350	-519	-351	-369	-342	-303
3000	-820	-812	-666	-654	-503	-789	-515	-556	-492	-470
4000	-1094	-1086	-889	-866	-653	-1062	-670	-744	-637	-630
5000	-1366	-1356	-1110	-1073	-796	-1332	-810	-933	-774	-790
6000	-1640	-1631	-1333	-1285	-940	-1608	-951	-1127	-914	-952
7000	-1910	-1900	-1551	-1493	-1078	-1881	-1087	-1314	-1045	-1103
8000	-2178	-2170	-1767	-1700	-1215	-2161	-1221	-1505	-1177	-1260
9000	-2450	-2440	-1980	-1900	-1344	-2437	-1349	-1697	-1301	-1419
10000	-2715	-2709	-2196	-2106	-1472	-2720	-1473	-1887	-1425	-1571

Pressure	F		G		GG		H		I	
	Hoop	Axial	Hoop	Axial	Hoop	Axial	Hoop	Axial	Hoop	Axial
0	0	0	0	0	0	0	0	0	0	0
1000	-225	-184	-298	-247	-239	-420	-172	-95	-198	-72
2000	-433	-380	-564	-420	-483	-737	-338	-198	-409	-119
3000	-640	-580	-828	-612	768	-977	-495	-291	-601	-172
4000	-846	-781	-1088	-812	-1025	-1210	-651	-382	-791	-234
5000	-1060	-984	-1336	-982	-1286	-1433	-811	-487	-984	-304
6000	-1263	-1181	-1587	-1182	-1546	-1652	-987	-615	-1199	-402
7000	-1475	-1386	-1848	-1393	-1809	-1873	-1164	-756	-1420	-501
8000	-1676	-1585	-2107	-1610	-2078	-2082	-1386	-890	-1617	-598
9000	-1880	-1783	-2362	-1840	-2340	-2290	-1480	-1000	-1791	-685
10000	-2095	-1978	-2626	-2107	-2602	-2485	-1622	-1094	-1967	-754

NOTES
Strain Gages:
CEA-13-125WT-350
Gage Factor 2.13
Test Assembly:
One Ceramic Cylinder Capped on One End With Ceramic Hemisphere Mod 4 DWG 55910-0121631 and on the Other End With Ceramic Hemisphere Mod 1 DWG 55910-0119913
Materials:
The Ceramic is: Coors AD 94 (94 percent Alumina)
The Titanium is: Ti 6Al 4Va
Data: All Strains are in microinches/inch

Table C-18. Stresses on 12-inch-diameter ceramic hemisphere Mod 4; DWG 55910-0121710.

Pressure	A Hoop	A Axial	B Hoop	B Axial	C Hoop	C Axial	D Hoop	D Axial	E Hoop	E Axial
0	0	0	0	0	0	0	0	0	0	0
1000	-14141	-14040	-11601	-11702	-10250	-12690	-9439	-9608	-9164	-7911
2000	-28093	-27958	-22939	-22939	-19687	-25414	-18379	-18989	-17398	-16077
3000	-42485	-42214	-34457	-34050	-28681	-38372	-27097	-28487	-25336	-24591
4000	-56706	-56435	-45931	-45152	-37574	-51433	-35439	-37947	-32997	-32760
5000	-70804	-70466	-57275	-56021	-46140	-64302	-43146	-47314	-40314	-40856
6000	-85034	-84729	-68749	-67123	-54802	-77437	-50942	-56905	-47778	-49066
7000	-99038	-98699	-79973	-78008	-63180	-90390	-58459	-66151	-54757	-56723
8000	-112965	-112694	-91103	-88832	-71579	-103634	-65927	-75550	-61833	-64646
9000	-127063	-126724	-102040	-99329	-79598	-116634	-73147	-84939	-68584	-72582
10000	-140853	-140649	-113160	-110111	-87637	-129925	-80177	-94205	-75272	-80219

Pressure	F Hoop	F Axial	G Hoop	G Axial	GG Hoop	GG Axial	H Hoop	H Axial	I Hoop	I Axial
0	0	0	0	0	0	0	0	0	0	0
1000	-11308	-9919	-15007	-13279	-14034	-20167	-8233	-5624	-9141	-4872
2000	-21995	-20199	-27974	-23095	-27355	-35962	-16281	-11537	-18615	-8788
3000	-32675	-30642	-41027	-33708	24141	-34988	-23853	-16940	-27327	-12791
4000	-43321	-41119	-53980	-44628	-54863	-61132	-31363	-22249	-36035	-17162
5000	-54329	-51753	-66149	-54154	-68067	-73048	-39172	-28193	-44944	-21902
6000	-64810	-62032	-78716	-64993	-81191	-84783	-47874	-35269	-55048	-28042
7000	-75750	-72734	-91812	-76394	-94462	-96631	-56736	-42911	-65419	-34279
8000	-86164	-83080	-104875	-88035	-107883	-108018	-67465	-50658	-74743	-40214
9000	-96697	-93410	-117884	-100197	-120994	-119300	-72487	-56223	-82990	-45513
10000	-107675	-103711	-131613	-114027	-133988	-130024	-79425	-61534	-91160	-50058

NOTES
Modulus of Elasticity 41 x 10E+06 psi
Poisson's Ratio 0.21

Table C-19. Strains on 12-inch-diameter ceramic hemisphere Mod 5; DWG 55910-0121837.

Pressure	A 1	A 2	A 3	B 1	B 2	B 3	C 1	C 2	C 3	D 1	D 2	D 3
0	0	0	0	0	0	0	0	0	0	0	0	0
1000	-258	-259	-226	-243	-260	-338	-250	-266	-238	-106	-243	-256
2000	-494	-502	-460	-484	-495	-452	-475	-503	-488	-444	-487	-498
3000	-720	-734	-687	-711	-729	-655	-699	-730	-730	-1032	-716	-728
4000	-930	-930	-890	-905	-905	-835	-895	-912	-935	-2273	-905	-925
5000	-1125	-1115	-1078	-1088	-1107	-1009	-1070	-1067	-1132	-2900	-1074	-1118
6000	-1320	-1301	-1280	-1270	-1300	-1184	-1250	-1231	-1325	-3135	-1246	-1300
7000	-1510	-1480	-1460	-1450	-1472	-1355	-1432	-1400	-1520	-3412	-1428	-1486
8000	-1690	-1650	-1645	-1628	-1633	-1525	-1614	-1573	-1710	-3660	-1620	-1673
9000	-1860	-1824	-1828	-1801	-1802	-1690	-1795	-1747	-1895	-3750	-1811	-1848
10000	-2025	-2000	-2005	-1966	-1990	-1845	-1967	-1925	-2068	-4270	-2009	-2019

NOTES
Strain Gages:
A,B,C
FABR-25-12-120
Gage Factor 2.17
D
WA-06-250WR-120
Gage Factor 2.05
Test Assembly:
One Ceramic Cylinder capped on one end with Ceramic Hemisphere Mod 5 DWG 55910-0121837 and on the other end with Ceramic Hemisphere Mod 1 DWG 55910-0119913
Materials:
The Ceramic is: Coors AD 94 (94 percent Alumina)
The Titanium is: Ti 6Al 4Va
Data: All Strains are in microinches/inch

Table C-20. Stresses on 12-inch-diameter ceramic hemisphere Mod 5; DWG 55910-0121837.

Pressure	A		B		C		D	
	Hoop	Axial	Hoop	Axial	Hoop	Axial	Hoop	Axial
0	0	0	0	0	0	0	0	0
1000	-13430	-11689	-17181	-12973	-13513	-11813	-13021	-5767
2000	-25883	-23629	-25458	-23119	-25826	-24152	-25614	-23275
3000	-37803	-35218	-37454	-33440	-37899	-36265	-54005	-37336
4000	-48282	-46174	-46997	-43307	-48241	-46734	-119045	-46927
5000	-58177	-56156	-57047	-51785	-58855	-55426	-152404	-56125
6000	-68215	-66722	-66838	-60522	-69347	-64292	-164892	-65279
7000	-78020	-76119	-75926	-69650	-79876	-73329	-179412	-74788
8000	-87604	-85479	-84668	-78969	-90025	-82487	-192172	-84604
9000	-96656	-94747	-93541	-87637	-99854	-91652	-206838	-94071
10000	-105248	-103904	-102767	-95019	-108634	-100778	-222787	-103605

NOTES
Modulus of Elasticity 41 x 10E+06 psi
Poisson's Ration 0.21

APPENDIX D: END CAPS FOR PROTECTION OF BEARING SURFACES ON CERAMIC CYLINDERS AND HEMISPHERES

All appendix D figures and tables are placed at the end of appendix D text.

FIGURES

TABLES

APPENDIX D: END CAPS FOR PROTECTION OF BEARING SURFACES ON CERAMIC CYLINDERS AND HEMISPHERES

INTRODUCTION

Experience has shown that contact between bare ceramic bearing surfaces on cylinders or hemispheres and metallic joint rings or bulkheads results in fretting and cracking of ceramic surfaces. This is caused by differential displacements of these components due to the difference in moduli of elasticity and Poisson's ratios between ceramics and metals.

A successful solution to this problem is a U-shaped circular end cap bonded with epoxy adhesive to ceramic. The thin layer of adhesive acts as a cushion between the mating metallic and ceramic bearing surfaces, eliminating point contacts that generate high stress concentrations. To ensure an even thickness of epoxy layer, some form of a spacer must be inserted between the mating surfaces.

Ideally, a spacer for controlling the thickness of the adhesive layer is made of material with the same physical properties as the polymerized (hardened) epoxy layer. Such a spacer could be produced by casting thin layers of epoxy upon Teflon sheets. The thin layer of hardened epoxy subsequently would be removed from the Teflon sheet and cut into pieces small enough to fit into the annular space between the flanges on the end cap.

The pre-cut pieces of epoxy would be placed at regular intervals on the bottom of the end cap prior to filling it with epoxy resin. Upon insertion of the ceramic cylinder end into the end cap, the epoxy would overflow the flanges of the end cap until the cylinder end came to rest upon the precast epoxy spacers. Since it was difficult to reliably cast epoxy layers of 0.01-inch thicknesses for the fabrication of spacers, manila stock paper of 0.01-inch thickness was selected for this purpose instead.

The spacers were cut into 1-inch-long circular segments whose outside and inside radii matched those of the ceramic component. After pre-filling the end caps with epoxy resin mixture (100 parts CIBA Geigy 610 resin with 70 parts CIBA Geigy 283 hardener), the spacers were placed on the bottom of the annular seat 0.25 inch apart. During insertion of the paper gasket segments, care was taken so that the segments did not overlap, as this would not only increase the thickness of the epoxy layer at this point, but also would result in point loading to the ceramic bearing surface during pressurization of the housing.

During the design of the end caps (appendix A) for the 6-inch-diameter cylinders, no thought was given to the effect that flange height might have on the magnitude of tensile radial stresses on the ceramic bearing surface resulting from a mismatch of elasticity moduli and Poisson's ratios at the bearing interface.

The height of the flanges was selected, instead, on the basis of surface area needed on the ceramic component to prevent extrusion of the epoxy layer from the annular space between the mating axial bearing surfaces compressed beyond its yield point. The height h=1.44t (0.300 inch) selected for 6-inch cylinders was found to be adequate for 68,000-psi axial bearing loading to which the end cap was subjected at 9,000-psi design pressure (figure D-1). During extensive pressure cycling (1,000 cycles) of 6-inch cylinders to design pressure, neither extrusion of adhesive, nor spalling of ceramic was observed on cylinder ends. Based on this observation, it was concluded that the height of the flanges on the end cap and the radial clearance between the flanges and the ceramic shell were properly sized to prevent extrusion of adhesive through the annular spaces between the ceramic shell and the end cap.

During the design of end caps for 12-inch-diameter ceramic cylinders and hemispheres, the same design philosophy was followed. Thus, the height of the external flange on the Mod 0 end cap for a 12-inch cylinder is 0.300 inch, the same height as of flanges on end caps for 6-inch-diameter cylinders (figure D-2). The ratio between the flange height and ceramic shell thickness h/t_c, however, is radically different for the two cylinder diameters since the flanges on the Mod 0 end cap are 50-percent shorter than what the ratio calls for

($h=1.44t_c$ versus $h=0.73t_c$). Similar flange height was selected for end caps on 12-inch-diameter hemispheres (figure D-3).

The relatively shorter flanges on Mod 0 end caps had no effect on the extrusion of adhesive, as the axial bearing loading of the epoxy layer did not change because of an increase in cylinder size. The effect on the magnitude of tensile radial stress on the ceramic bearing surface of the cylinder, however, was significant, as later studies have shown. The magnitude of tensile stress on the ceramic bearing surface increased as a result of flange height reduction by a factor of approximately 5, as shown by subsequent investigations (Reference 1).

FINDINGS

As a result of the inappropriately sized exterior flange on the Mod 0 end cap for 12-inch-diameter ceramic housing components, their cyclic fatigue life was reduced dramatically. Testing of cylinders and hemispheres equipped with Mod 0 end caps showed that external spalls began to appear on 12-inch-diameter cylinders (figure D-4) after 30 to 40 pressure cycles and on 12-inch-diameter hemispheres (figure D-5) after 50 to 100 cycles to 9,000-psi design pressure (tables D-1 and D-2).

In addition to the many spalls visible on the exterior surfaces, ultrasonic nondestructive testing (NDT) detected many internal fracture planes oriented parallel to the exterior surface of the ceramic component (appendix E). The internal fracture planes and external spalls reduced the critical pressure of the ceramic components significantly. If cycling had continued, the extent of internal delaminations and external spalling would have increased until the ceramic component weakened to such an extent that implosion would have occurred at, or below, design pressure.

None of the housings imploded prior to the termination of the cycling program. Some of the ceramic cylinders and hemispheres accumulated up to 130 pressure cycles without imploding (appendices B and E). It is not known how many more pressure cycles the ceramic components with titanium Mod 0 end caps would have withstood without catastrophic failure, but it is doubtful that the number of cycles would have exceeded 200.

The short fatigue life of 12-inch-diameter ceramic components with Mod 0 end caps was disappointing, but did not have a disastrous effect on the test program. The ability of cylinders and hemispheres to perform reliably in excess of 50 pressure cycles was sufficient to meet the goals of the Third Generation Ceramic Housing Program (i.e., evaluation of joint stiffener and ceramic hemisphere designs). In addition, the disparity in fatigue lives between 6-inch- and 12-inch-diameter ceramic housing components pinpointed the dependency of cyclic fatigue life of ceramic components on the height of the end cap flanges.

DISCUSSION

Once the effect of flange height on cyclic fatigue life of ceramic components became apparent, steps were taken to redesign the end caps and to evaluate the new Mod 1 end cap design experimentally. The modification to Mod 0 end caps consisted of (1) increasing the height of the flanges, and (2) incorporating an external seal between the edge of the external flange and the exterior of the ceramic component (figures D-6 and D-7).

The flanges on Mod 1 end caps for cylinders have been increased from 0.300 inch to 1.30 inches and for hemispheres from 0.50 inch to 1.30 inches. The height of the flange-to-shell thickness ratio of the Mod 1 end cap for cylinders is now $h=3.2t_c$ and for hemispheres, $h=6.3t_s$. These ratios exceed those of end caps on 6-inch-diameter cylinders by a factor of 2 (i.e., $h=3.2t_c$ for 12-inch-diameter cylinders versus $h=1.44t_c$ for 6-inch-diameter cylinders).

The reason for exceeding the $h/t_c=1.44$ ratio already experimentally validated on end caps for 6-inch cylinders is that the added height of the flanges will not only reduce further the tensile radial stresses on the ceramic bearing surface, but also prevent leakage until the tip of the spall extends beyond the elastomeric seal at the edge of the flange. Thus, even when a crack on the plane bearing surface grows into a spall, it will require many pressure cycles before the slow-growing spall extends beyond the edge of the flange.

It appears that extending the height of the flanges on the end cap lengthens the cyclic fatigue life of the ceramic housing by two ways: (1) the increase in radial restraint exerted by metallic end caps on the ceramic shell reduces the tensile radial stress on the ceramic bearing surface, delaying the initiation and propagation rate of delamination cracks, and (2) the increase in distance between the bearing surface and the elastomeric seal at the edge of the flange delays leakage through cracks surrounding spalls, as now the tip of the spall must extend *further* than in Mod 0 end caps to result in local leakage. To achieve this, the ceramic component must be subjected to a greater number of pressure cycles.

To experimentally validate the beneficial effect of extending the height of the flanges on Mod 1 end caps, a single 12-inch-diameter cylinder (cylinder #1) was equipped with Mod 1 end caps (figure D-8), mated with titanium hemispherical bulkheads, and cycled to 9,000-psi design pressure. The cycling was terminated after 500 cycles without any visual evidence of external spalling. Ultrasonic NDT performed by through-transmission techniques did not detect any internal delaminations extending above the flanges (appendix E).

When cylinder #1 was tested to implosion with plane steel bulkheads it failed catastrophically at 16,500 psi. This pressure was found to be in the range of critical pressures calculated for 94-percent aluminum cylinders with the dimensions of cylinder #1. Thus, it can be concluded that any delaminations hidden from ultrasonic NDT by Mod 1 end cap flanges were not significant enough to initiate premature implosion of the cylinder.

Based on the positive results of the cyclic and destructive tests to which cylinder #1 was subjected, a decision was made to abandon Mod 0 end caps and replace them with the Mod 1 end cap design (figure D-9). When the 12-inch-OD x 18-inch-L x 0.412-inch-t cylinders of 94-percent aluminum are equipped with Mod 1 titanium or aluminum end caps (figures D-10 and D-11), their fatigue lives can be expected to exceed 500 cycles to design depth when radially supported at the ends by ring stiffeners, or metallic hyperhemispherical bulkheads.

A different picture presents itself with Mod 1 end caps for ceramic hemispheres (figure D-12). Although the flanges on the Mod 1 end caps for hemispheres exceed the h/t ratio of end caps for cylinders (h/t_s=5.16 versus h/t_c=3.2), the projected cyclic fatigue life of hemispheres is probably shorter or, at best, the same as that of cylinders with Mod 1 end caps. The reason for it lies in the 100-percent greater axial compressive loading on the plane-equatorial bearing surface of the hemisphere.

The disparity in magnitudes of axial compressive stresses on the adjoining plane bearing surfaces of a cylinder and hemisphere is due to the fact that the spherical shell has been designed to be 50-percent thinner than the cylinder, so that the radial deflections of both shells match. Thus, the 0.59-percent increase in h/t ratio for the sphere does not compensate for the 100-percent increase in the axial stress on the equatorial bearing surface of the sphere, particularly when it has been demonstrated by other investigators that the fatigue life of ceramic bearing surfaces decreases in a nonlinear fashion with an increase in bearing stress (reference 1).

Two approaches have been considered to raise the fatigue life of ceramic hemispheres to equal that of the cylinders. One of the approaches considered is to make the shell thickness of the hemisphere equal to that of the cylinder (i.e., 0.412 inch). The other approach is to double the hemisphere's shell thickness only at the equator. This is to be accomplished by transitioning the shape of the spherical shell near the equator into a cylindrical shape (skirt) with twice the thickness of the spherical shell (figure D-13).

Of the two approaches considered, the second one appears to be a better solution to the problem. The good points of the hemisphere with a cylindrical skirt are:

a. The *increase in weight* over the original hemisphere design is insignificant, as the spherical shell retains its original wall thickness, except for a narrow equatorial band where its thickness is doubled to match the thickness of the cylinder.

b. The *fabrication cost* of the titanium end cap for a hemisphere with a cylindrical skirt is significantly less than for a true hemisphere, since it does not require machining of the spherical surface on the interior surface of the inside flange.

c. The *radial restraint* exerted by the outside flange of the end cap on the spherical ceramic shell around its equator has been significantly increased by the tight radial clearance between the flange on the end cap and the full height of the cylindrical skirt.

None of these approaches could be evaluated experimentally by pressure cycling in the program on Third Generation Ceramic Housings due to lack of funding. Plans were made, however, to pursue the evaluation of the skirted hemisphere concept in the future when funding for this purpose becomes available.

CONCLUSIONS

1. *Mod 0 end caps for cylinders* with flange height $h=0.73t_c$ (where t_c = thickness of cylinder shell) do not provide adequate radial support to the ends of the ceramic cylinder under external pressure loading, generating 68,000-psi axial bearing stress. As a result, spalling of the external surface initiates after about 50 cycles to design pressure.

2. *Mod 1 end caps for cylinders* with flange height $h \geq 1.44t_c$ appear to provide adequate radial support to the ends of the ceramic cylinder under external pressure loading, generating 68,000-psi axial bearing stress. As a result, spalling of the external surface *does not* initiate at $\prec$500 cycles to design pressure of 9,000 psi in 94-percent alumina-ceramic cylinders with $t/D_o = 0.034$.

3. *Mod 0 end caps for hemispheres* with flange height $h=2.37t_s$ (where t_s = thickness of spherical shell) do not provide adequate radial support to the ends of the ceramic hemisphere under external pressure loading, generating 134,000-psi axial bearing stress. As a result, spalling of the external spherical surface initiates after about 30 cycles to design pressure.

4. *Mod 1 end caps for hemispheres* with flange height $h=5.16t_s$ appear to be satisfactory. However, since they were not evaluated experimentally, it is not known whether the fatigue life of ceramic hemispheres equipped with Mod 1 end caps is shorter, or longer, than that of cylinders with Mod 1 end caps. Until this end cap design is validated experimentally, it can be assumed that the cyclic fatigue life of ceramic hemispheres with Mod 1 end caps is that of cylinders, i.e., $\succ$500 cycles to design depth.

RECOMMENDATIONS

1. *Mod 1 end cap* with flange heights $h \geq = 3.2\ t_c$ are to be used on 12-inch-diameter cylindrical shell sections of an external ceramic pressure housing. The additional height of the flange extends the cyclic fatigue life of the 94-percent alumina cylinder with $t/D_o = 0.034$ to >1,000 cycles.

2. *Epoxy compound* made up of 100 parts CIBA Geigy 610 resin and 70 parts CIBA Geigy 293 hardener is the recommended adhesive for bonding end caps to ceramic compounds.

3. *Manila stock cardboard gaskets* (or a single gasket) of 0.01-inch thickness are to be used as spacers between the mating-plane ceramic and metallic bearing surfaces. The OD and ID of gasket segments or of a continuous circular gasket shall match those of the ceramic component. If the gasket takes the form of a continuous ring, 0.25-inch diameter holes should be punched at 1-inch intervals on its center line prior to placement inside the end cap. Gaskets in the form of 1-inch-long ring segments should be uniformly spaced inside the end cap at $\prec$0.25-inch intervals.

4. Ceramic hemispheres should be 50-percent thinner than cylinders, except around penetrations, and at the equator where their thickness should equal that of cylinders. The transition of shell thickness from $0.5t_c$ to $1.0t_c$ at the equator should take the form of a cylindrical skirt whose width is equal to the height of flanges on Mod 1 end caps for cylinders. The height of flanges on Mod 1 end caps for hemispheres with cylindrical skirts should be identical to the height of flanges on Mod 1 end caps for cylinders.

REFERENCE

D-1. Kvitka, A. L., and I. Diachkov. 1983."Stress Distribution and Strength of Envelopes From Brittle Non-Metallic Materials," Ukrainian SSR Academy of Sciences, Kiev.

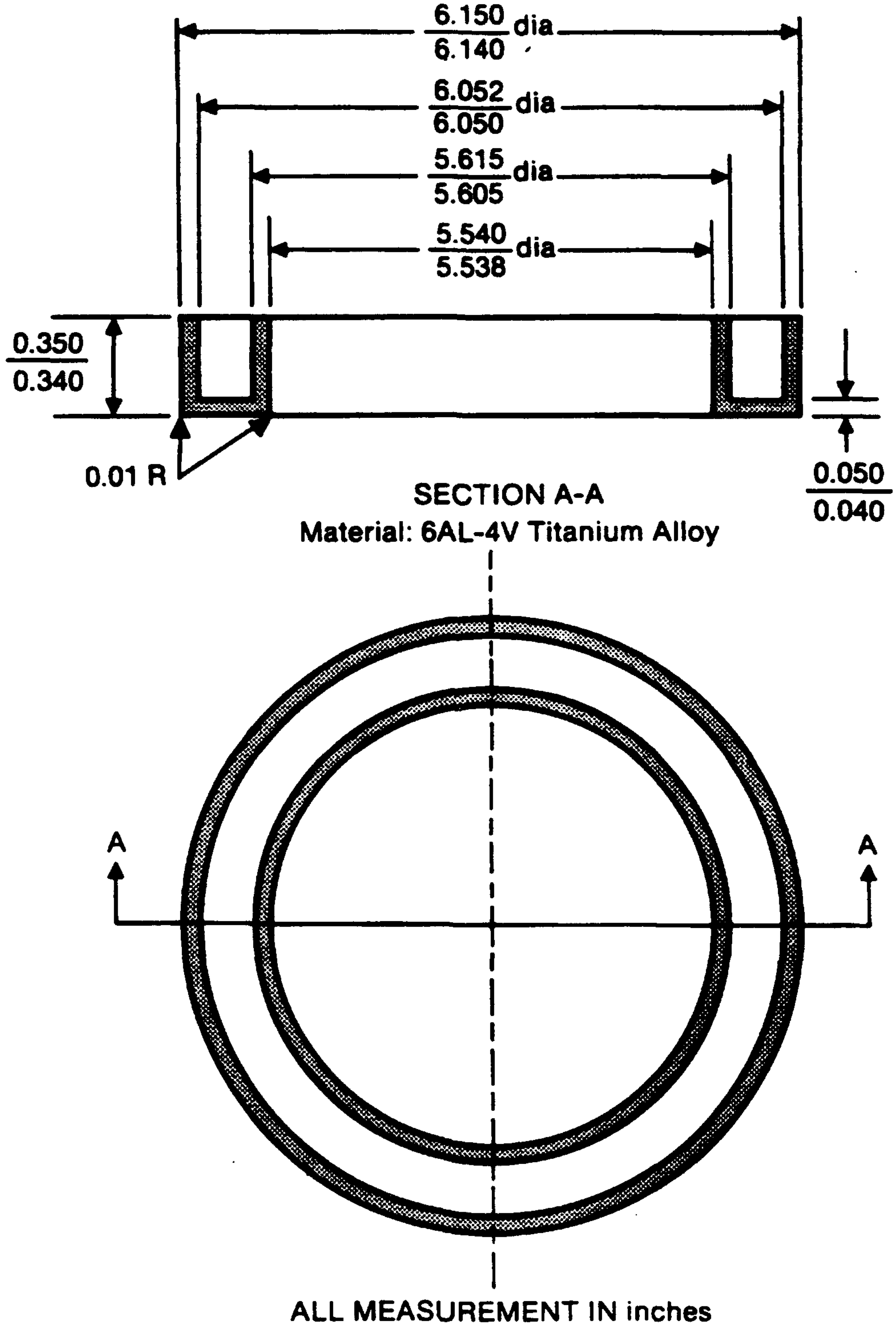

Figure D-1. End cap for 6.038-inch-OD x 5.626-inch-ID ceramic cylinder.

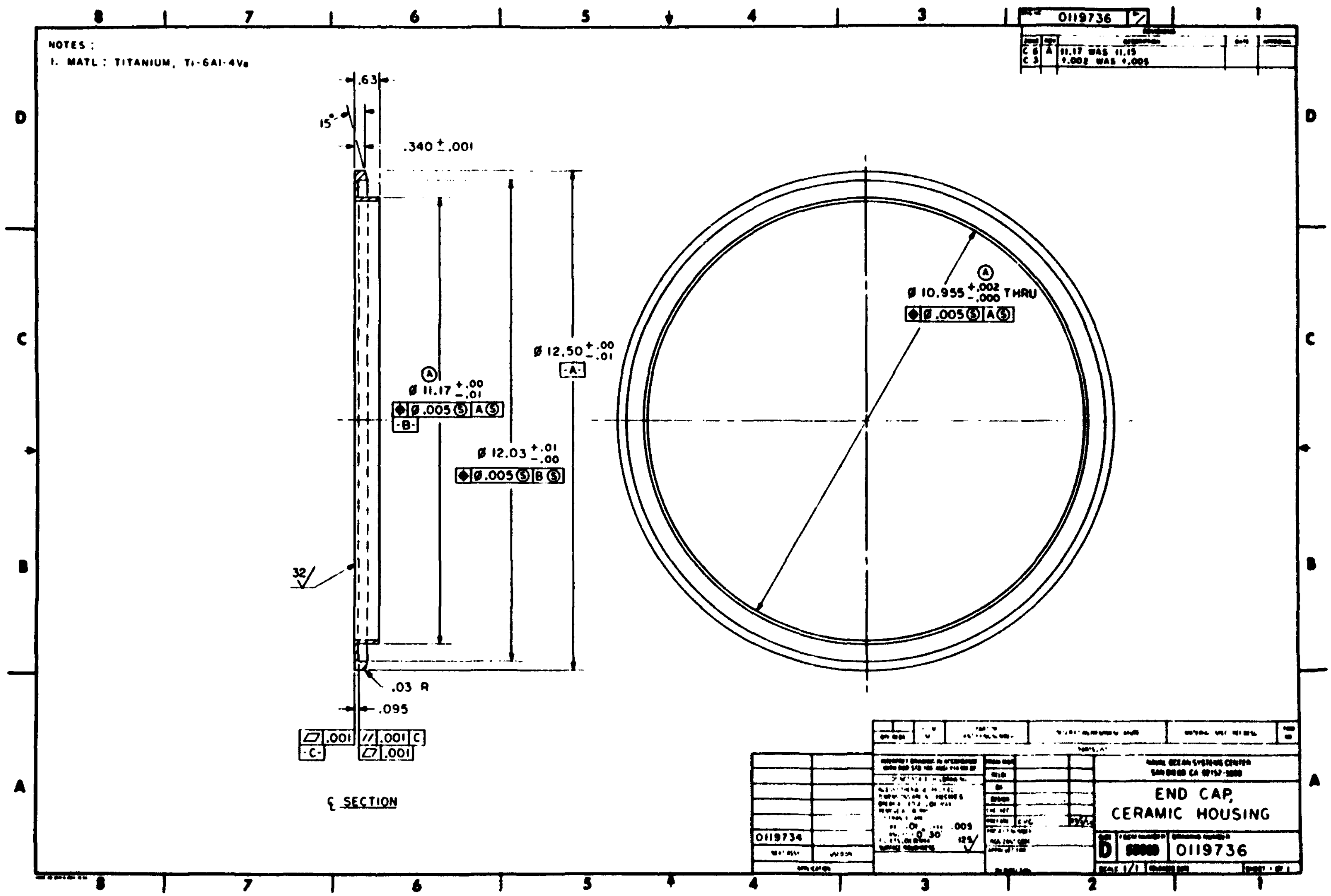

Figure D-2. End cap Mod 0 for 12-inch-OD x 11.174-inch-ID ceramic cylinder.

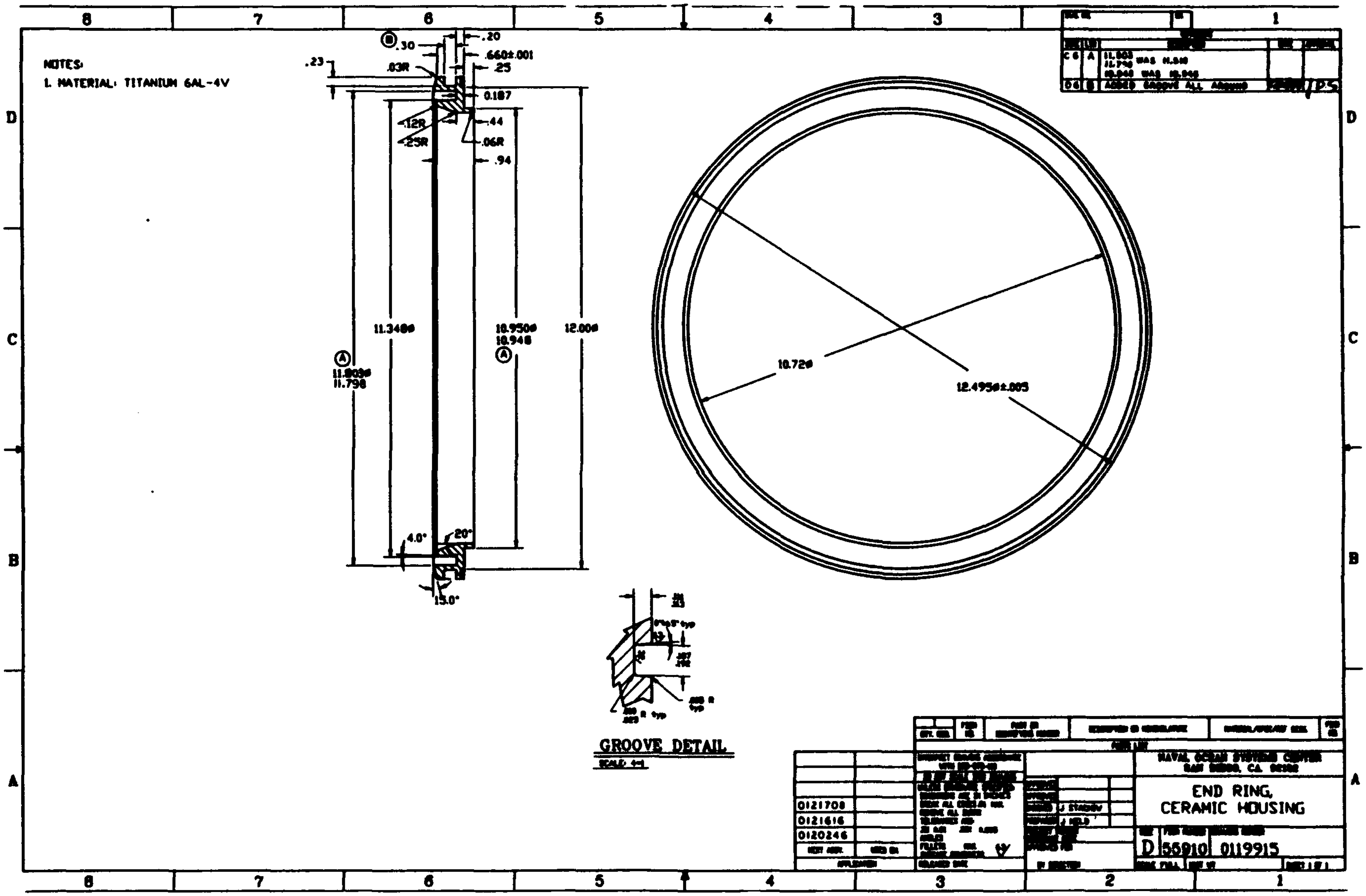

Figure D-3. End ring Mod 0 for 11.79-inch-OD x 11.37-inch-ID ceramic hemisphere.

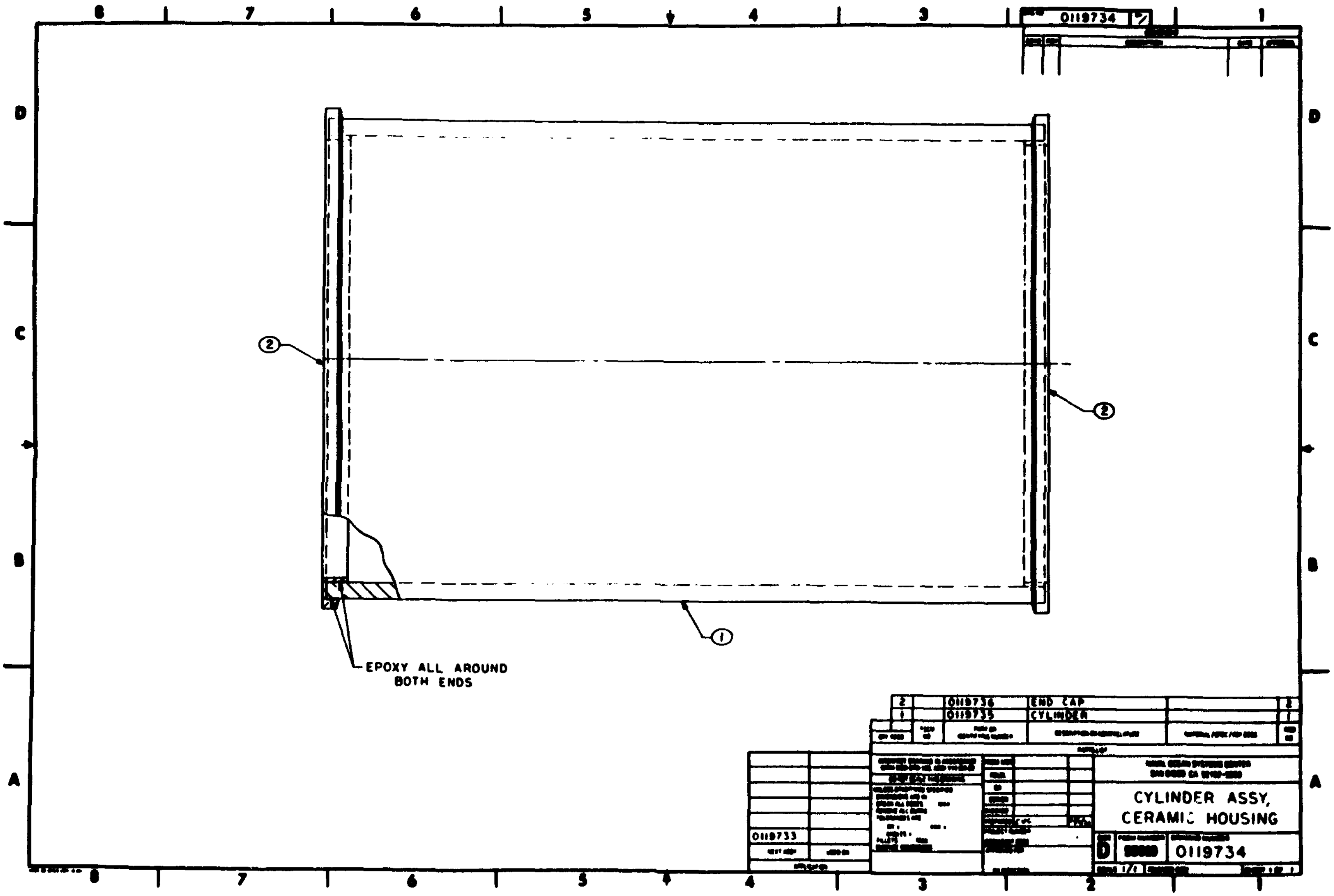

Figure D-4. 12-inch-diameter cylindrical ceramic housing section equipped with Mod 0 end caps.

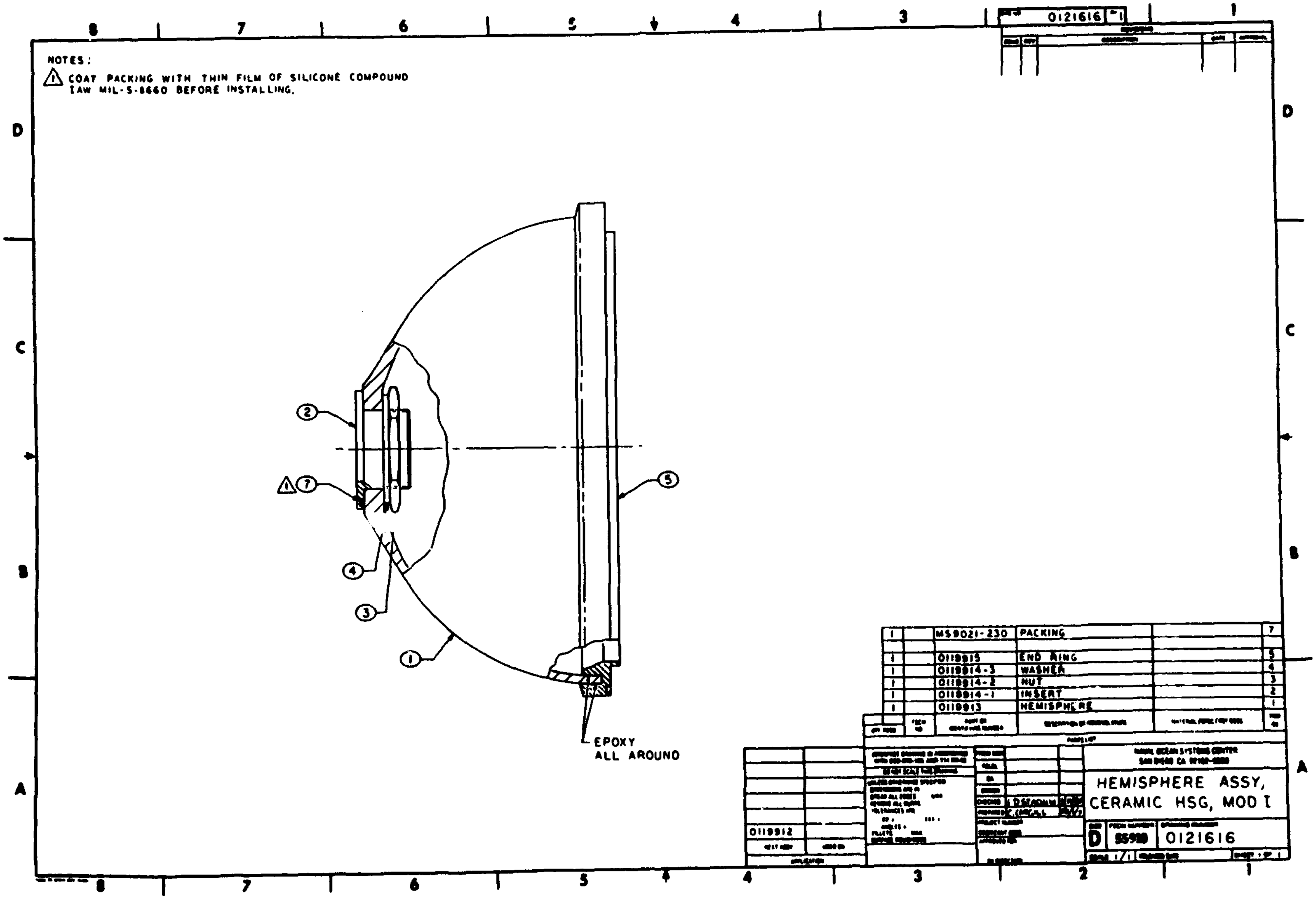

Figure D-5. 12-inch-diameter hemispherical ceramic housing section equipped with Mod 1 end ring.

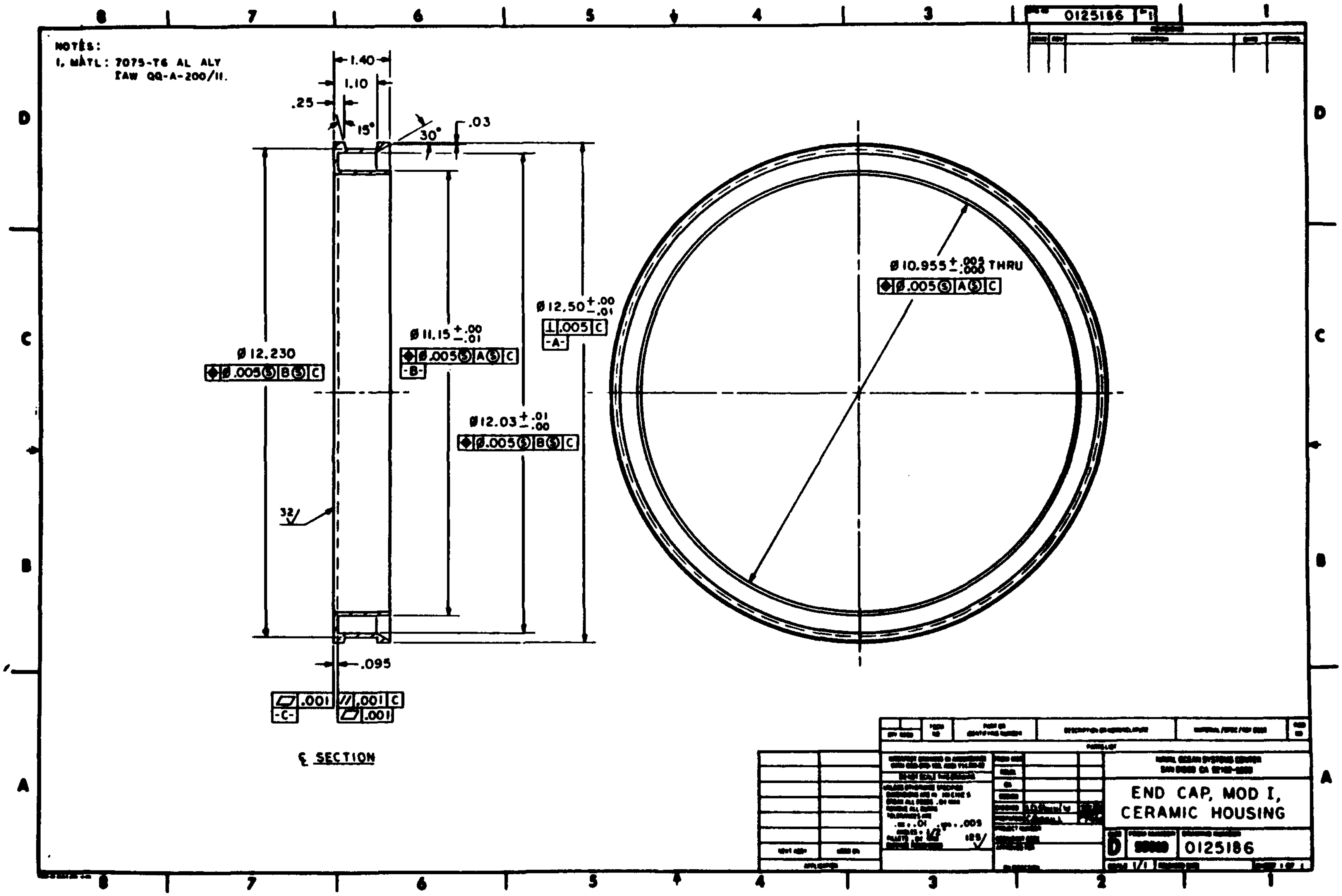

Figure D-6. Mod 1 end cap for 12-inch-OD x 11.174-inch-ID ceramic cylinder.

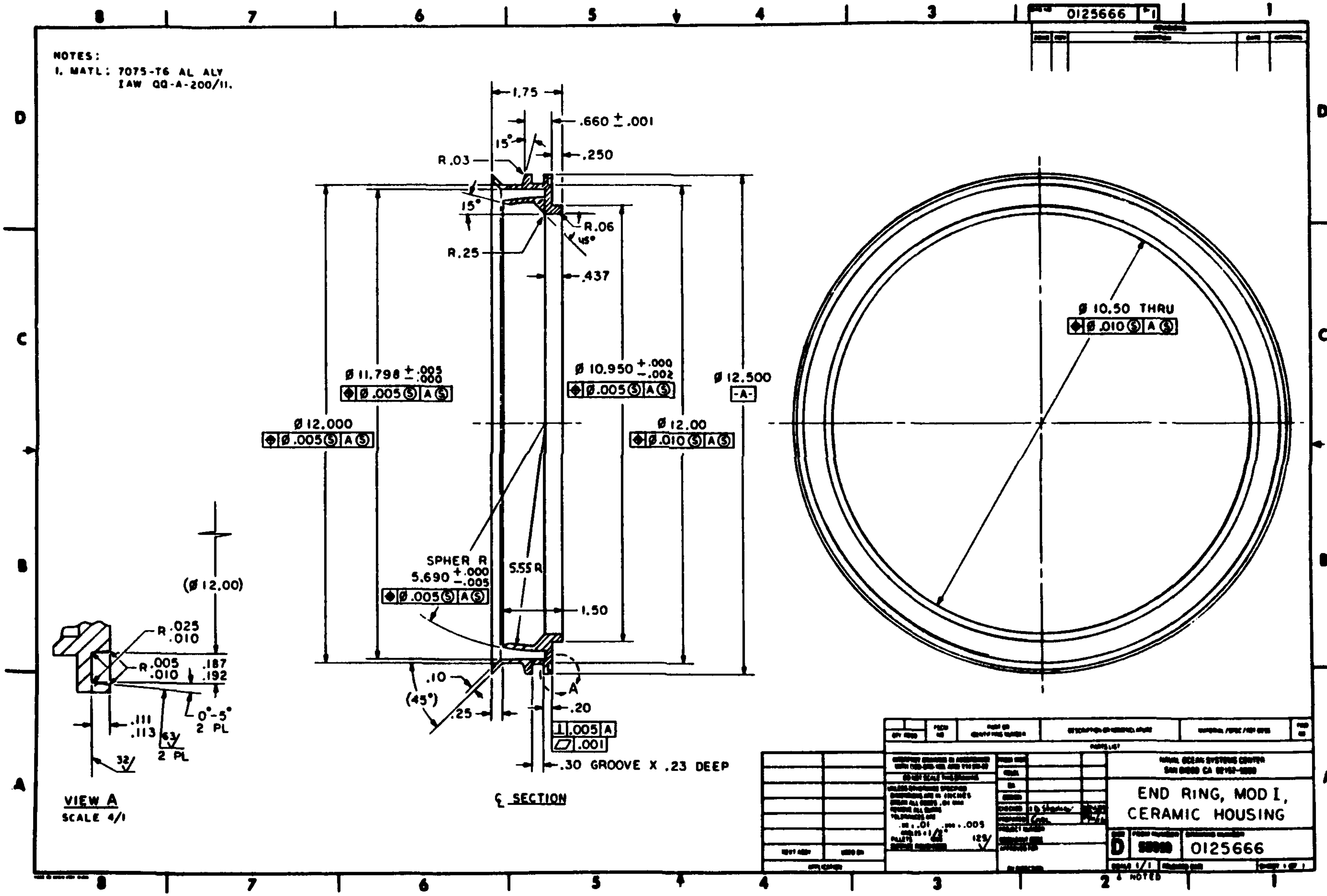

Figure D-7. Mod 1 end cap for 11.79-inch-OD x 11.37-inch-ID ceramic hemisphere.

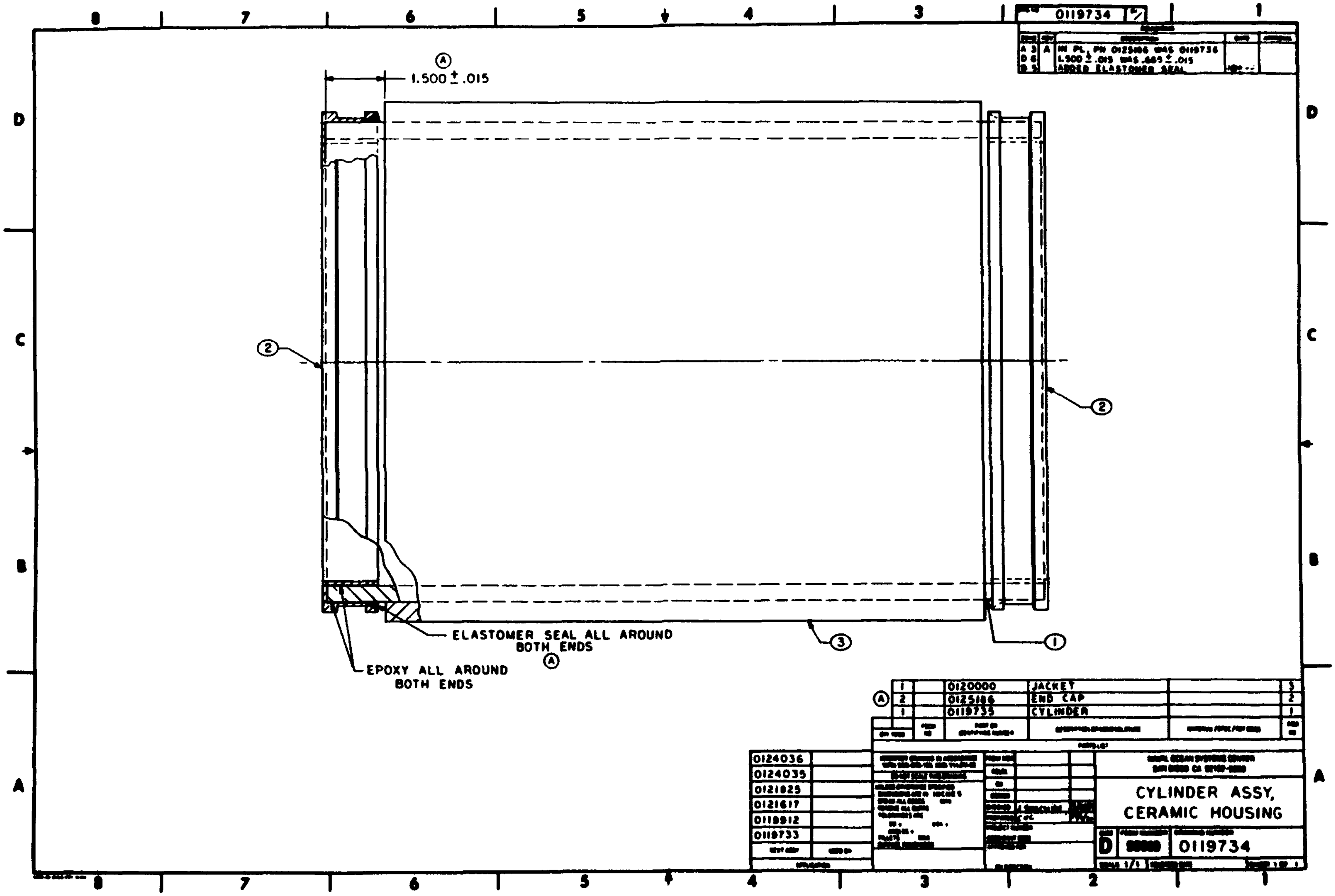

Figure D-8. 12-inch-diameter cylindrical ceramic housing section equipped with improved Mod 1 end caps.

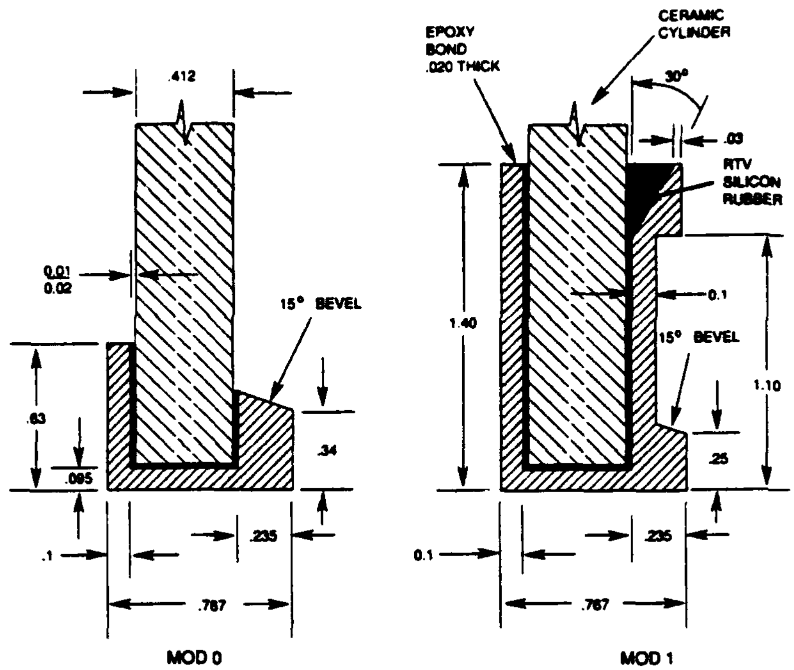

Figure D-9. Comparison of dimensions on Mod 0 and Mod 1 end caps for 12-inch-diameter ceramic cylinders.

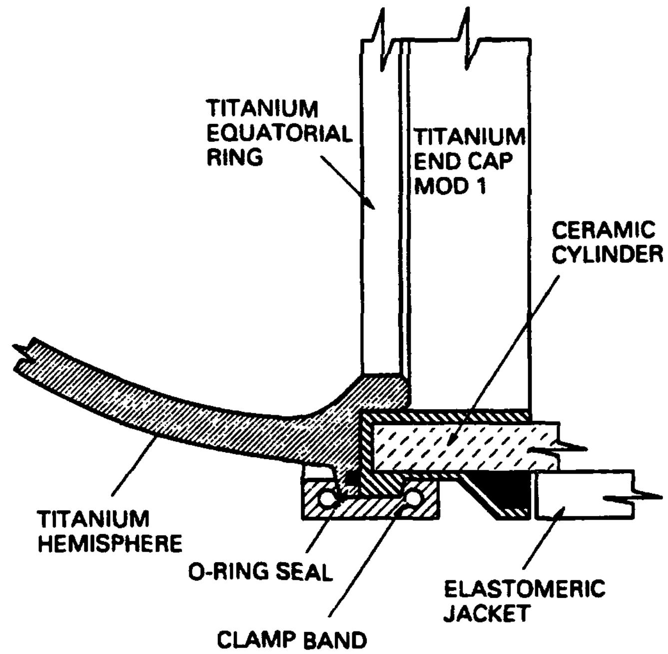

Figure D-10. Configuration of joint between titanium hemisphere and 12-inch-diameter ceramic cylinder equipped with Mod 1 end cap.

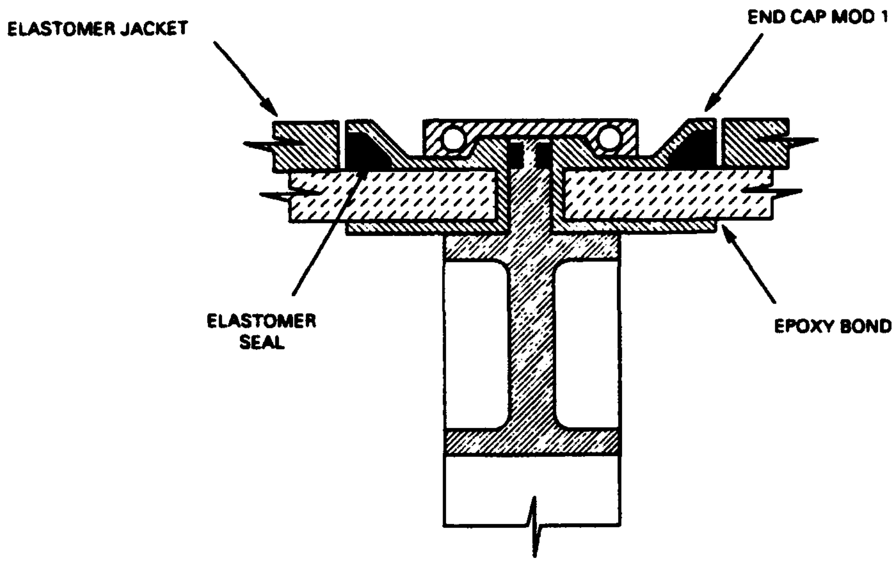

Figure D-11. Configuration of joint between 12-inch-diameter ceramic cylinders equipped with Mod 1 end caps, and radially supported by a joint ring stiffener.

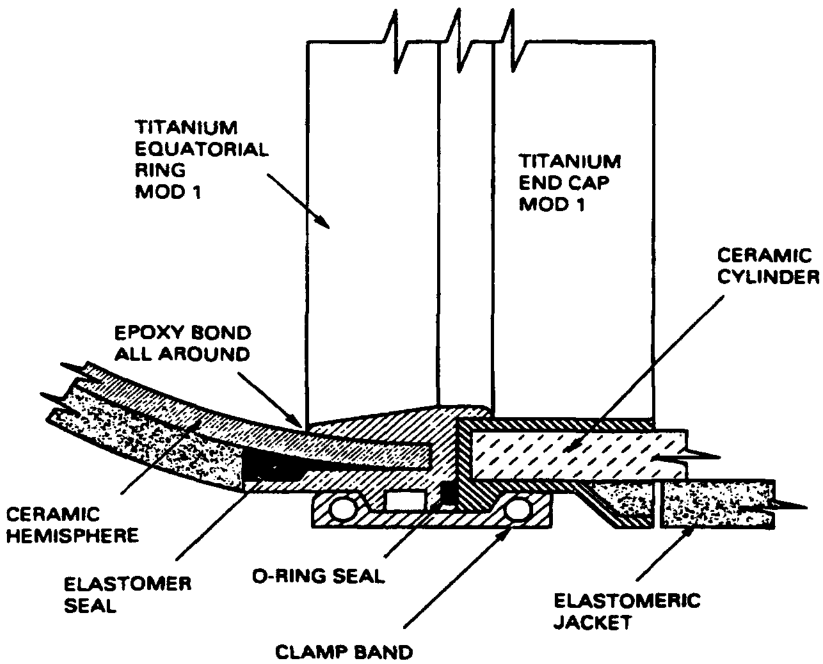

Figure D-12. Configuration of joint between 12-inch-diameter ceramic cylinder and hemisphere equipped with Mod 1 end caps.

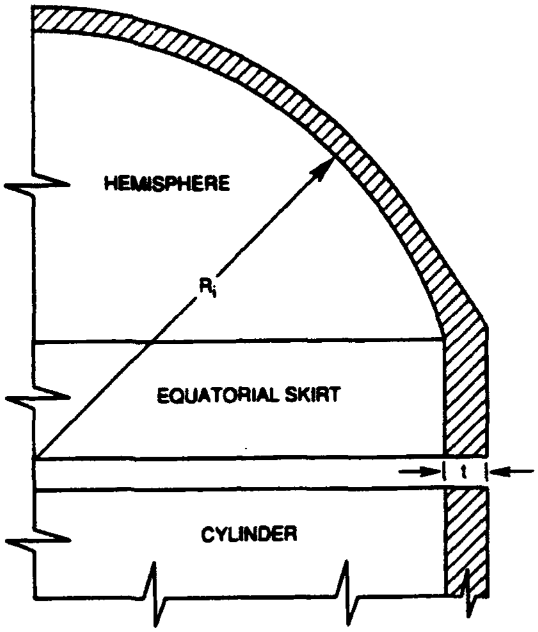

Figure D-13. Proposed configuration for axial and bearing surfaces in the equatorial region of the hemisphere.

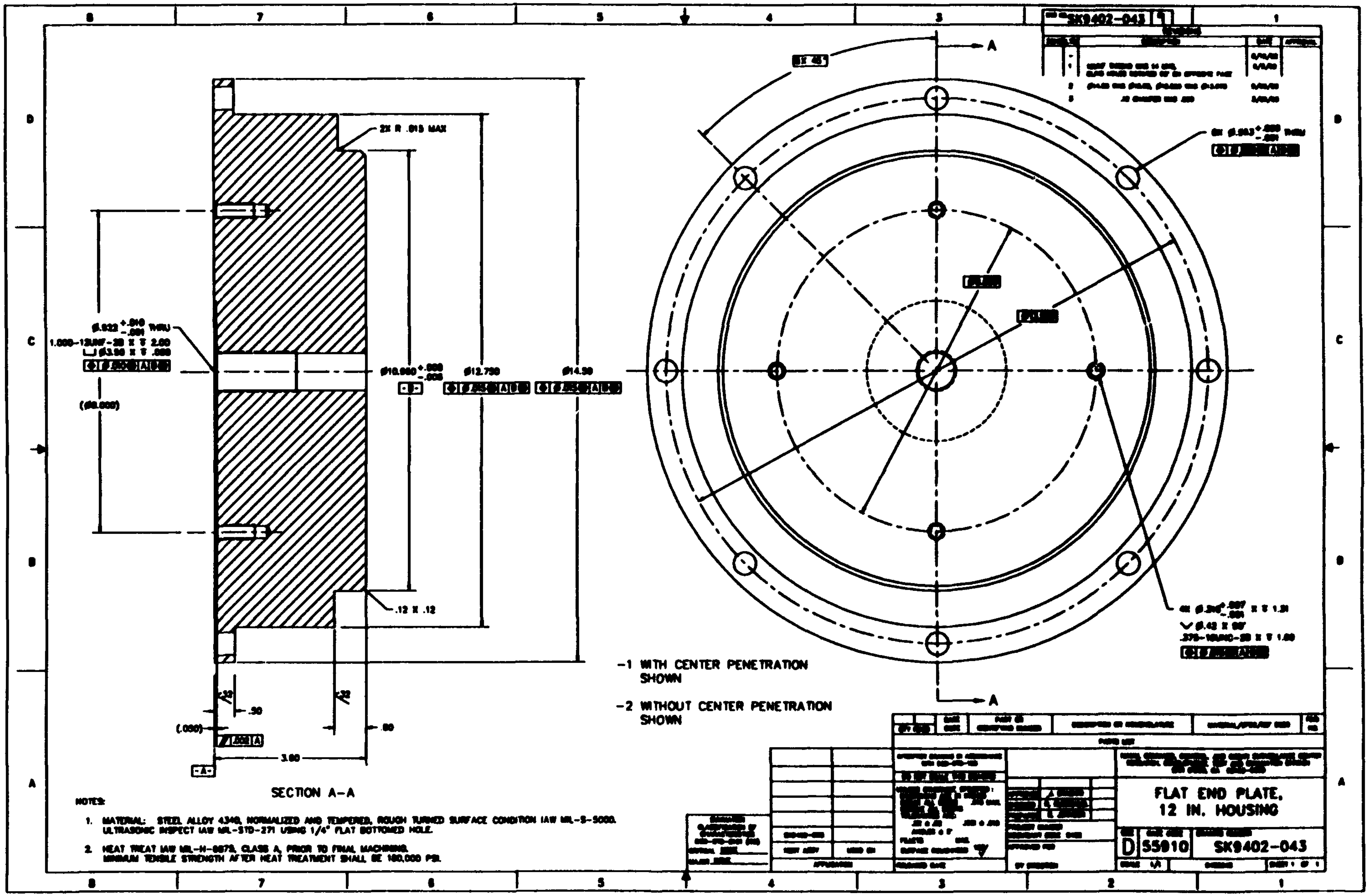

Figure D-14. Plane steel bulkhead used during pressure testing of individual cylinders to implosion.

Table D-1. Critical pressures of 12-inch-diameter 94-percent alumina-ceramic cylinders after testing to proof and design pressures.

	Cylinder 1	Cylinder 2	Cylinder 3	Cylinder 4	Cylinder 5
Proof Pressure Tests to 10,000 psi	1	2	3	2	1
Design Pressure Tests to 9000 psi	500 Cycles	90 Cycles	120 Cycles	130 Cycles	80 Cycles
End Cap Design	Mod 1	Mod 0	Mod 0	Mod 0	Mod 0
Surface Spalling –Initiation	None	30 Cycles	40 Cycles	34 Cycles	40 Cycles
–Outside Surface Top	No spalling	6W x 3.5L x 0.125 in T 6W x 1.5L x 0.060 in T	5W x 1.5L x 0.060 in T	6W x 2.5L x 0.125 in T	Minor spalling 0.03 in thick
Bottom	No spalling	5W x 2L x 0.06 in T 5W x 2.5L x 0.03 in T	No spalling	No spalling	Minor Spalling 0.03 thick
–Inside Surface	No spalling	No spalling	No spalling	No spalling	No spalling
Interior Delaminations	None	2W x 4.0 in L 1W x 2.0 in L 2.5W x 2.5 in L	2W x 1 in L Many 1W x 1.0 in L on both bearing surfaces	2W x 4 in L Many 1W x 0.5 in L on both bearing surfaces	Not inspected
Internal Inclusions	None over 0.017 in	Maximum size 0.06 in 0.015 in	None over 0.045 located 0.15 in from exterior surface at midbay	0.015 in	Not inspected
Implosion Pressure	16,5000 psi	13,250 psi	20,000 psi*+	12,100 psi	14,700 psi

Notes: Cylinders are 12.0 in OD x 11.176 in ID x 18.0 in L of 94% alumina ceramic.
Bulkheads are flat steel discs providing radial support.
*Test terminated without implosions,m only circumferential cracks at ends.
+Cylinder was shortened to 13 inches before testing to 20,000 psi

Table D-2. Results of proof and pressure tests on 12-inch-diameter ceramic hemispheres.

Ceramic Hemisphere	Hemisphere End Rings	Proof Testing to 10,000 psi	Pressure Cycling to 9000 psi	Condition of Hemisphere
Mod I	Mod 0	3	121 Cycles	a. No visible cracks around penetration. b. No spalling visible above the metal end ring.
Mod II	Mod 0	1	34 Cycles*	a. Visible cracks around penetration. b. Visible spalling above end ring.
Mod III	Mod 0	1	4 Cycles	a. No visible cracks around penetration. b. No visible cracks above end ring.
Mod IV	Mod 0	2	54 Cycles	a. No visible cracks around penetrations. b. Visible spalling above end ring.
Mod V	Mod 0	1	71 Cycles	a. No visible cracks around penetrations. b. Visible spalling above end ring.

* At completion of cycling the central penetration was enlarged from 2 to 3 inches to remove cracked material. In addition, 4 equally spaced penetrations with 2-in diameter were ground into the hemisphere at 45° elevation. The modified hemisphere saw further service as Mod V.

APPENDIX E: NONDESTRUCTIVE AND DESTRUCTIVE EVALUATIONS OF PRESSURE TREATED CYLINDERS

All appendix E figures and tables are placed at the end of appendix E text.

FIGURES

TABLES

APPENDIX E: NONDESTRUCTIVE AND DESTRUCTIVE EVALUATIONS OF PRESSURE TREATED CYLINDERS

INTRODUCTION

Overview

At the conclusion of pressure cycling tests performed on 12-inch-diameter by 18-inch-long 94-percent alumina cylinders (appendices B and C), a nondestructive evaluation (NDE) program was initiated to determine the physical condition of these cylinders. Since all of the cylinders were identical in size and in ceramic composition, any difference in extent of structural damage would be traceable either to the construction of the coupling rings (i.e., aluminum, titanium, Mod 0, or Mod 1 configuration), or to the number of pressure cycles to which they were individually subjected (table E-1).

The NDE program was prompted because as the pressure cycling progressed, signs of structural deterioration were observed at the ends of the cylinders and hemispheres which could lead to catastrophic failure if cycling was continued (figures E-1 and E-2). Thus, pressure cycling was terminated to preclude unexpected catastrophic failures, and to assess accurately the extent of damage that already took place.

All of the cylinders and hemispheres were surveyed visually, and ceramic cylinders #1, #2, #3, and #4 were subjected also to ultrasonic and radiographic NDE. The visual, X-ray film radiography, and ultrasonic inspections of the cylinders were performed by Martin Marietta Laboratories, while the digital radiography and radiographic computed tomography inspections were performed by Scientific Measurement Systems, Inc.

Following these inspections, cylinders #1, #2, and #4 were fitted out with Mod 0 end caps and pressurized to destruction. The objective of these tests was to determine what effect the internal fractures and external spalls had on the critical pressure of the 12-inch outside diameter (OD) x 18-inch length (L) x 0.412-inch-thick 94-percent alumina-ceramic monocoque cylinders radially supported by plane steel bulkheads. The test results showed conclusively that extensive spalling on the exterior surface, and delaminations inside the wall originating at the ends of cylinders, reduced the critical pressure of the cylinders significantly (approximately 25 to 35 percent).

Cylinder #3 was subjected to an additional set of evaluation procedures. Two 2.5-inch-wide rings were cut from both ends of the cylinder to remove all the shell material weakened by external spalls and internal delaminations. Following this procedure, the shortened cylinder was equipped with Mod 0 end caps, mounted between plane bulkheads, and subjected to short-term 20,000-psi external pressure.

The objective of this test was to determine whether any of the many voids detected by nondestructive (ND) inspections inside the cylinder would initiate cracking when subjected to principle stress of −290,000-psi magnitude in hoop and −145,000 psi in axial direction. The cylinder did not implode during pressurization to 20,000 psi in spite of severe spalling on the exterior surface at one end of the cylinder and the appearance of circumferential fractures originating on the exterior surface near both ends at the location of maximum tensile flexure stress. During removal of the end closures, both ends of the cylinder separated at the circumferential fractures. Since it was difficult to rotate the cylinder with fractured ends on a table during ND inspections, rings were cut from both ends further shortening the cylinder to 9.5 inches.

After cutting off the fractured ends, cylinder #3 was reinspected for internal cracks and voids. Inspection was conducted by five ND techniques.

1. Ultrasonic pulse-echo C-scan (US)
2. Scanning acoustic microscopy (SAM)
3. Film radiography (FR)
4. Digital radiography (DR)
5. Radiographic computed tomography (RCT)

The inspection of cylinder #3 with these ND techniques was concluded by a destructive inspection procedure. This procedure began with removing the material from the external surface of the cylinder by grinding. Grinding was continued until the

shell thickness was reduced from 0.412 to 0.162 inch. The locations of all voids exposed by removal of material were recorded, their dimensions measured, and their shapes photographed. There were two reasons for performing the destructive inspection: (1) to *evaluate and compare* the sensitivity and accuracy of the five ND techniques to which the cylinder was previously subjected, and (2) to *obtain* accurate three-dimensional definitions of the void shapes.

CONCLUSIONS

Comparison of ND Inspection Techniques

Voids in 0.412-inch-thick ceramic shells can be detected by several ND techniques. *Ultrasonic technique* detects voids ≥0.01 inch, *radiographic computed tomography* detects voids ≥0.02 inch, and *digital radiography* or *film radiography* detects voids only ≥0.03 inch.

The **size** of the voids can be measured accurately only by radiographic computed tomography. The *digital radiography* and *film radiography* techniques produce close approximations of the actual size, with the images of the voids slightly (approximately 1 to 3 percent) oversize. *Ultrasonic microscopy* presents images that are approximately 5- to 10-percent larger than voids. *Standard ultrasonic C-scans* generate images that are 100 to 200-percent larger than voids and, for this reason, are not suited for measurement of void sizes.

The **location** of the void in x–y coordinates can be precisely established by all ND techniques.

The **distance** of the void from the shell surface can be measured precisely only by *radiographic computed tomography*. Standard *ultrasonic pulse-echo A-scans* give a close approximation of the distance, provided that the void is not located within 0.05 inch of the surface facing the transducer.

Effect of Voids on Structural Performance

Voids do not act as crack initiators in 94-percent alumina-ceramic cylinders provided that the following conditions are satisfied.

1. Size of the void is ≤0.05 inch.
2. Distance of the void's center from the external surface of the cylinder is ≥ the void's diameter.
3. The *compressive membrane hoop stress* in the cylinder does not exceed –140,000 psi at design pressure and –280,000 psi at proof pressure.
4. Location of the void is outside regions where tensile stresses are present (i.e., within 0.2 inch of plane bearing surfaces).

RECOMMENDATIONS

All ceramic components must be ND inspected for external cracks and internal defects in the form of voids or cracks. Components with external cracks of any length are not acceptable. Voids with diameters >0.05 inch make the component unacceptable.

The following cost-effective ND quality-control inspection procedure is recommended for ceramic components.

1. Apply dye penetrant to all surfaces and visually inspect for cracks.
2. Perform ultrasonic C-scan at 0.01-inch intervals of the shell surface by means of pulse-echo or transmission techniques using ≥10 MHz transducers calibrated on a ceramic witness specimen with 0.03-inch flat bottom hole. Record location of voids with ≥0.015-inch diameter.
3. Place photographic film against the interior surface of the ceramic shell at locations where ultrasonic C-scan has located voids that *appear* to exceed 0.05 inch in size, and irradiate the cylinder with an X-ray source.
4. Develop the film and measure the images of voids. Use these measurements as the basis

for acceptance, or rejection, of ceramic component.

ULTRASONIC, VISUAL, AND DYE PENETRANT INSPECTION OF CYLINDER #1, #2, #3, AND #4

Introduction

Four 12-inch-diameter by 18-inch-long by 0.4-incn-thick alumina-ceramic cylinders (#1, #2, #3, and #4) which had been successfully proof tested to 10,000-psi external pressure and cyclically tested (to 9,000 psi) by the Naval Ocean Systems Center (NOSC)* were received by Martin Marietta Laboratories (MML) for NDE. This section summarizes the results of the visual and ND ultrasonic evaluation performed on these cylinders by Dr. L. Friant at the MML.

Each cylinder was assigned a number (1 to 4) and marked with a coordinate grid (0° to 360°, 0 inch to 18 inches). The origin of the grid markings on the cylinders was completely random, as was the choice for the top (0-inch mark) and bottom (18-inch mark). The configuration of the end caps serving as coupling rings on cylinder #2, #3, and #4 was the same, but, the materials varied. Cylinder #2 had an aluminum end cap on the top and titanium end cap on the bottom. Cylinder #3 had aluminum top and bottom end caps. Cylinder #4 had an aluminum end cap on the top and titanium end cap on the bottom. The end caps on cylinder #1 were both aluminum, but were of a different design (Mod 1) than the other three cylinders (Mod 0).

Test Procedures

After visually examining and marking each cylinder (figure E-2), they were inspected by ultrasonic NDE methods at MML. These methods included ultrasonic pulse-echo C-scans for rapid evaluation and defect mapping of the entire cylinder and scanning acoustic microscopy (SAM) to determine size and shape of some individual flaws detected by the C-scans. The Advanced Ultrasonic Test Bed (AUTB™) at MML, employing an automated scanning procedure, was used to produce the C-scans. It can accommodate both planar and cylindrical samples. For cylindrical shapes, such as the NOSC cylinders, the test article is centered on a 30-inch diameter turntable. The test parameters were optimized to provide high enough resolution to detect 0.01-inch voids with a scan time that was not excessively long.

The procedure selected to provide this high-resolution screening is based on through-transmission, i.e., where a tranducer on one side of the cylinder transmits a burst of acoustic energy and on the other side receives it. A waterjet probe was used to house the unfocused 10 MHz transmit and receive transducers and provide a quiet and uniform 0.187-inch-diameter water column to couple the ultrasound to the ceramic cylinders.

The through-transmission approach, when implemented with unfocused transducers, provides sensitivity to defects *through the entire wall thickness.* Single-sided pulse-echo methods suffer from a near "dead zone" where defects cannot be readily detected. If focused transducers are used, this can be improved somewhat by focusing them at the shell's mid thickness, but sensitivity to deeper defects suffers considerably.

The main advantage of using a waterjet rather than conventional full immersion are that more-rapid scanning speeds can be achieved, and that the waterjet provides a small aperture which can only receive transmitted sound from a small region on the surface, thereby reducing the effective probe diameter and increasing the lateral resolution. A test frequency of 10 MHz was the highest frequency that could provide penetration and adequate signal levels for rapid generation of C-scans. A scan is created from individual pixels that represent the amplitude of the signal transmitted through the cylinder at a particular location. Each pixel represented an area measuring 0.020 inch by 0.020 inch or 0.010 inch by 0.010 inch, and an amplitude value anywhere within 256 discrete levels.

This scanning procedure was previously developed and proven on 1-inch- and 2-inch-thick ceramic blocks of similar composition (reference 1). In that

*NOSC is now the Naval Command, Control and Ocean Surveillance Center (NCCOSC) RDT&E Division (NRaD).

study, simulated cylindrical (1-dimensional) voids on the order of 100 microns (0.004 inch) in diameter were detected in a 1-inch-thick block of ceramic. In addition, both horizontally and vertically oriented cracks were imaged in a 2-inch-thick block of ceramic. With this technique, defects measuring smaller than the 0.187-inch probe size can be detected, but *will not be sized accurately.*

SAM is a high-resolution, defect-imaging technique based on higher frequencies than used for conventional ultrasonics. This method has been shown to be able to locate and characterize defects in ceramic material. An example of a defect imaged by this method is shown in figure E-3. This defect was originally found in a large (50-inch-diameter, 3.25-inch-thick) ceramic cylinder by contact pulse-echo inspection. By sectioning the material, guided by Acoustic Microscopy, the defect was cross-sectioned through its center and optical micrographs of it were taken. The correlation between the size and shape predicted by SAM to the actual size and shape is excellent.

For the current application, a 30 MHz frequency was selected to provide the desired resolution. It was able to penetrate most of the 0.4-inch wall thickness of the cylinder. The probe used had a spherical focus, with a focal length of 1.25 inches from the probe end when measured in water. Since the speed of sound in alumina is almost six times greater than that in water, the actual focus distance in the cylinder is greatly foreshortened. As a general procedure, a first scan covering a 0.4-inch by 0.4-inch square was performed at 0.0015-inch pixel resolution in a suspect area and was followed up by a 0.0005-inch "zoom" scan (0.2-inch by 0.2-inch square) if a void was detected.

After the SAM analysis was performed, the end caps serving as coupling rings on cylinders #2, #3, and #4 were removed by dissolving the epoxy in the joints by immersing them in Dynasolve 160 stripper for 10 days. The areas on the cylinders under the rings were then visually examined and documented. Several pieces of the ceramic that had broken off were mounted, polished, and examined by metallographic methods at magnifications of up to 800X. These broken pieces came from the ends of the cylinders and contained cracks which produced the spalling found on the cylinders (discussed below). Dye penetrant was then applied to the ends of cylinders #3 and #4 to detect any cracks extending from the ends of the cylinders.

Findings

Visual Inspection

Visual examination showed no obvious damage to cylinder #1. Cylinders #2, #3, and #4 showed some damage, all of which was found at either, or both ends, but only on the outside diameter (table E-1). This damage was termed spalling. Pieces of the exterior surface near the ends of the cylinders appeared to have flaked off during testing (figure E-4). The flaking seemed to progress from the outside, inward, as some areas had multiple layers of material that flaked off easily by hand.

Cylinder #2 exhibited the most extensive damage to its exterior with five areas of spalling (figure E-1). On the top end of the cylinder, the spalling was located between 330° and 50° of circumference extending down to about 3 inches from the end of the cylinder, between 65° and 90° extending down about 1 inch, and between 145° and 210° extending down about 1.5 inches. The spalling on the bottom end of cylinder #2 was between 10° and 60° extending about 2 inches, between 125° and 163° extending about 2.5 inches from the end, and between 340° to 30° extending about 2 inches.

Cylinder #3 had spalling damage only on the top and only in one location (between 330° and 30° extending about 1.5 inches from the top end). Most of the ceramic material under the ring on the outer circumference in the spalled area came off with the ring, indicating that the cracks producing the spalling originated on the plane bearing surface of the cylinder end.

Cylinder #4 also had only one spalled area on the top between 310° and 50° of circumference extending down about 2.5 inches. Again, most of the ceramic material under the ring on the outer circumference came off with the ring, and what was left could easily be removed by hand.

Ultrasonic Inspections

After the visual examination, the cylinders were subjected to ultrasonic evaluation. Based on the previous success with test blocks, Dr. Friant of MML felt confident that similar methods could be directly applied for full area coverage (except under, and adjacent to, rings) of the NOSC cylinders. As it turned out, the method proved to be sensitive to internal defects, as well as external surface features such as spalled areas. In addition, drops of excess adhesive and pencil grid lines used to define a reference coordinate system showed up on some of the scans.

Ultrasonic C-scan performed on Cylinder #1 did not detect any internal cracks or external spalling. The ultrasonic images for cylinders #2, #3, and #4 are presented in figures E-5 and E-6. From these scans, it can be seen that cylinders #2 and #4 exhibited not only extensive spalling in several locations, but also delamination cracks. Table E-2 summarizes the information provided by the ultrasonic scans for the internal cracks detected in cylinder #2, #3, and #4. In cylinder #2, a suspect region between 15° and 55° coincides with a heavily spalled area. It is uncertain whether there is definitely an internal delamination in this area in addition to the surface spalling. In all other situations, cracks were detected in regions of little or no spalling, so there is no ambiguity about their presence.

The C-scans of the cylinders also revealed some randomly occurring low transmission regions measuring on the order of a few pixels (1 pixel = 0.020 inch by 0.020 inch). These regions appear as red dots on the scan images. It was postulated that these areas could be internal processing defects, such as voids. From a fracture mechanics standpoint, it would be extremely useful to know the size and distribution of defects in cylinders which have survived pressure cycling. These low transmission areas from the ultrasonic scans were selected for subsequent evaluation using SAM. For cylinders #2, #3, and #4, however, the majority of the suspect indications were visually correlated to external features, usually spots of epoxy adhesive adhering to the inside, or outside, diameter of the cylinder. Still, the C-scan of cylinder #1, which had very clean surfaces, exhibited a single axial band of voids clearly discernible several inches to the right of the tape marker (figure E-7). Discrete areas on the ultrasonic scans which did not correlate to some external feature on the cylinders were selected as candidates for SAM.

Acoustic microscopy was executed on all four cylinders starting at the 90° reference point, however, due to the fact that the objective was to characterize only a representative number of defects, most of the low-transmission regions were not scanned. Table E-2 provides a summary of the results; note that of the 44 total scans performed, 22 defects were confirmed. In some cases, multiple defects were observed in a single scan, whereas in other cases, no defects were detected. The two low-transmission regions in *cylinder #1*, shown as red dots in figure E-7, appear in the corresponding magnified SAM image, figure E-8, as two white patches. Individual "zoom" scans shown in figures E-9 and E-10 at a resolution of 0.0005 inch/pixel were subsequently performed to provide the best detail for sizing of the flaws. These two flaws were representative of those detected via SAM for cylinders #1, #3, and #4.

Cylinder #2 contained many suspect regions, but none of them could be verified using SAM. This was due in part to misleading indications from the large number of adhesive drops on the surface.

Cylinder #3 appeared to contain the highest concentration of actual defects since 12 were detected in the region between 90° and 120° in only 11 scans. Cylinder #3 also contained the largest defect out of the total of 22 detected. Regular and zoom images of this defect are shown as white patches in figures E-11 and E-12, respectively. This defect measured approximately 0.057 inch in diameter at a depth of 0.13 inch from the outside diameter. The smallest defect reported was 0.007 inch (cylinder #4), but smaller indications often surrounded the larger indications. In this particular configuration, it is estimated that a void as small as 0.004 inch (8 pixels across) could be reliably discriminated. It is unknown at this time how the detectability varies as a function of the void's distance from the shell surface. It is estimated that

defects lying within 0.05 inch of the outer surfaces will be very difficult, if not impossible, to detect.

Dye Penetrant Inspection

After ultrasonic scanning and SAM, the end caps on cylinders #3 and #4 were removed and their ends were examined by applying dye penetrant. The dye, which remains in cracks and voids that extend to the surface, revealed numerous internal cracks throughout the wall of the cylinders, but mostly on the plane surfaces of each cylinder that had visible spalled areas. These cracks were primarily circumferential, extending from 1/2 inch to 3 inches in length. They were not confined to the spalled areas, but were located at all areas around the circumference. On the ends that did not exhibit spalling, only a few small internal cracks were detected. The internal crack detected by the C-scans on the bottom of cylinder #4 was detected by dye penetrant and was located about at the center of the wall thickness. The dye penetrant also revealed what appeared to be damage on the inner diameter (ID) similar to the spalling found on the OD. No ceramic material was spalled off even though cracks existed close enough to the ID wall that the penetrant could be seen through the thin layer of ceramic remaining. Several such areas were found on the top of cylinders #3 and #4.

Pieces of ceramic that had spalled off cylinder #4 were mounted and polished. They were cross sectioned in the circumferential and longitudinal directions. The photomicrographs in figure E-13 show the numerous cracks in these small pieces. The crack propagation mode is primarily trans-granular, running straight through the grains whether alumina or glass. For the most part, the cracks were circumferential, but secondary cracks running perpendicular (radial) were also found. This appeared to be the method of the observed spalling.

RADIOGRAPHIC INSPECTIONS OF CYLINDERS #1, #2, #3, AND #4

Introduction

At the conclusion of ultrasonic NDE by MML, cylinders #1, #2, #3, and #4 were taken to Scientific Measurements Systems in Austin, Texas for NDE by digital radiography (DR) and radiographic computed tomography (RCT). Not much was expected of radiography, as its limitations have been well established over the years during the NDE of metal castings (it can not detect an internal delamination in a body of material if the fracture plane is at a right angle to the X-ray beam and the space between fracture surfaces is $\prec 3$ percent of shell thickness). In this respect, ultrasonic C-scan using a through-transmission technique is superior, as it not only detects surface spalls (due to an increase in the strength of the transmitted signal), but also internal delaminations (due to total, or partial, reflection of the signal at the fracture plane).

Its a different story with RCT, in which a computer reconstructs a tomographic slice of an object. In RCT, an object is placed between a collimated X-ray fan beam and detectors sensitive to X-ray radiation. The detectors measure the intensity of the X-ray signal as the object is fully rotated within the X-ray fan beam. A computer then reconstructs from the data a highly detailed internal view of that slice through the object. The quality of the resulting reconstruction depends on at least three major factors: how finely the object is sampled; how accurate the individual measurements are made; and how precisely each measurement can be related to an absolute frame of reference.

Mechanical RCT scanners have a spatial resolution on the order of 1,000 micrometers. State-of-the-art industrial scanners have resolutions in the 200- to 400-micrometer range. Such resolution is more than adequate for detection of delaminations (separations) wider than 0.005 inch, voids larger than 0.002 inch, and density variation in excess of 0.1 percent. There is, however, a drawback associated with the fine resolution. In order to attain this resolution, the tomographic slices through the object must be very narrow, thus increasing the number of RCT scans required to cover the full length of the object. Since the cost of such a thorough inspection was beyond the scope of the program, the objective of the RCT inspection became the measurement of wall thickness at locations where the greatest delaminations were observed. The locations where *greatest spalling* occurred was at the ends of cylinders, beginning at the exterior edge of coupling rings and continuing

for several inches along the length of the cylinder. Three tomographic scans were taken at these locations on the end of each cylinder.

Findings

The results of DR confirmed only some of the findings of ultrasonic NDE performed by MML. Radiographs of the ends of cylinder #2 presented digitized images (figure E-14) of external spalls identical to those generated by ultrasonic C-scans (figure E-4). The resolution of these images was not superior to that of the ultrasonic C-scans. Like C-scans, there was no positive way of determining whether the images of external spalls were on the exterior or interior shell surfaces, without visual examination of the internal and external surfaces of the cylinder. The digital radiographs did not detect internal delaminations previously found by ultrasonic C-scan since there was no separation of fractured surfaces inside the delamination.

The images generated by RCT presented data not shown by ultrasonic C-scans or DR. The images generated by RCT depicted accurately the cross sections of the cylinder wall at a selected location. These images allowed the observer to determine whether the defect shown on a high-resolution RGB monitor was a spall on the internal or external shell surface. The images of the cylinder cross section made it also feasible to measure the decrease in wall thickness at spall locations. Thus, figure E-15 shows that the wall thickness in cylinder #2 at a *0.375-inch* elevation above the cylinder end has been reduced by 30 percent due to extensive spalling on the external surface. In contrast, the images generated by RCT on cylinder #1 present evidence that leads one to conclude that there is a *total absence of spalling* in the ends hidden from visual observation or ultrasonic C-scan by Mod 1 coupling rings.

The greatest advantage of RCT is the ability of the system to generate images that represent thin slices of the component being evaluated. By taking a series of narrow beam RCT scans and presenting the results as thin slices of the component cross section, it is possible to determine where the delamination, crack, spall, or void originates, how it progresses along the length of the cylinder, and where it terminates. For cracks, spalls, and voids with large dimensions, the RCT scans may be taken at large intervals, thus keeping down the cost of NDE.

If one, however, intends to detect the presence of *small voids*, the distance between successive RCT scans must be no larger than the size of the void. This increases the cost of NDE by RCT to the point where it may exceed the cost of the item being inspected, losing its cost-effectiveness. Thus, the economics of the process may dictate that NDE by RCT technique will be used only for detection of shrinkage cracks, and not small voids in ceramics. If the location of voids has been previously discovered by DR, RCT may be applied to these locations in order to (1) establish the distance of the void from the exterior surface of the shell, and (2) define its shape.

To evaluate the ability of the DR and RCT to detect *voids* in ceramic, the 12-inch-OD cylinder #3 was first radiographed. Following DR, radiographic tomographs were taken at eight locations where DR had previously detected voids. All data was obtained on Scientific Measurements System's 101b+ tomographic analyzer. Two DRs and eight RCTs were taken in all. For all scans, the source was 420 kv X-rays at 3 ma with 0.025-inch brass filtration. The aperture setting for the detectors was .25 mm by .25 mm. For the two DRs, the approximate ray spacing and pixel size was .232 mm and the integration time was .15 second. The two DRs were taken 90 degrees to each other and cover the full height and about 237 mm of the center of the width at each 90-degree position.

The tomographs were taken with a ray spacing of .12 mm and reconstructed with a pixel size of .161 mm. The cylinder was marked with an arrow that points up and was centered in the first DR (345R1). The second DR was rotated 90 degrees in a counterclockwise direction looking at the tomograms, and, in the DRs, the front of the cylinder moves to the right. All of the RCTs were taken in the same orientation as the first DR. Some of the voids detected by DR and located by RCT were within 0.05 inch of the shell's exterior surface.

The DR did not encounter any difficulties in detecting voids with diameters ≥0.015 inch in the 0.412-inch-thick shell of 12-inch-OD cylinder #3. The tomographs taken through the centers of the voids clearly defined the cross sections of the voids and their location with respect to the shell's surfaces (figures E-16 through E-19). By taking a series of tomographs through any void, one could also define the void's three-dimensional shape (i.e., spherical, ellipsoidal, cubic, etc.).

DESTRUCTIVE EVALUATION OF CYLINDERS #1, #2, #3, AND #4

At the conclusion of the NDE program, all 12-inch-diameter cylinders were tested to implosion. Prior to testing, however, cylinder #3 was shortened from 18 to 13.5 inches to remove spalled and cracked ceramic material located at the ends of the cylinder. The removal of the spalled ends was intended to raise the critical pressure of the cylinder above 20,000 psi. The compressive stress at that pressure was below –300,000 psi, the nominal compressive strength of alumina. For this reason, catastrophic failure was not expected unless the presence of voids was to reduce the compressive strength of alumina to some lower value.

Since the size of voids in cylinder #3 ranged from 0.010 to 0.057 inch, a small decrease in critical pressure of the shortened cylinder would indicate that voids of up to 0.057-inch diameter can be tolerated in alumina-ceramic housings, as the decrease in material strength does not exceed the safety margin provided by the design safety factor of 2. A large reduction of critical pressure below 20,000 psi, on the other hand, would signify that the presence of a void with 0.057-inch diameter can not be tolerated, and ceramic cylinders or hemispheres in which NDE detected such voids should be rejected.

Findings

The 16,500-psi implosion pressure of cylinder #1 was the highest of all 12-inch OD by 18-inch L cylinders tested (table E-1), even though this cylinder was previously pressure cycled 500 times to 9,000 psi and a single time to 10,000 psi. This was to be expected as visual inspection, ultrasonic C-scan and RCT scan did not detect any external spalls or internal delaminations in cylinder #1 after completion of the cycling program. The absence of spalls and delaminations was thought to be due to the use of Mod 1 metallic end caps serving as coupling rings that provided better support to the ends of the cylinder than the Mod 0 end caps with which all the other cylinders were equipped.

The implosion pressures of the other 12-inch OD by 18-inch L cylinders (#2, #3, and #4) fell into the range between 12,100 to 14,700 psi. The magnitudes of implosion pressures appeared to reflect the extent of structural damage which these cylinders exhibited (i.e., the less spalling, the higher the implosion pressure). Cylinder #4, which failed at the lowest pressure, exhibited multilayer delamination at the top end that significantly decreased its structural performance.

Cylinder #3 did not implode, but the damage was substantial. A large area at the bottom of the cylinder spalled off (figure E-20) and circumferential fractures appeared on the exterior surface above each end cap. These fractures were the result of high flexure stresses caused by the rigid radial support provided by plane bulkheads.

To make the damaged cylinder #3 amenable to further ND inspections, it was shortened further to 9.5 inches by cutting away spalled and fractured material from both ends (figure E-21). The resulting cylinder was 3 inches shorter at the top and 5.5 inches shorter at the bottom than the original 18-inch length. But even at this shorter length, the external surface was still scarred at the bottom by the large spall that occurred during pressure testing to 20,000 psi. This scar served as a reference landmark in subsequent ND inspections.

FILM RADIOGRAPHY OF CYLINDER #3 AFTER HYDROTESTING TO 20,000 psi

The objective of the following X-ray film radiography and SAM nondestructive inspections was to compare the ability of X-ray film photography against pulse-echo SAM to detect and locate internal voids and any cracks originating from them that might have been generated by the

overpressurization to 20,000 psi. Both inspections were performed at MML.

Test Procedure

The *film radiography* inspection was performed by placing photographic film in contact with the interior surface of the cylinder and exposing it with X-rays of 90 kv intensity for 1.2 minutes from a distance of 60 inches. After exposure, the film negatives were developed and inspected visually on a light screen for images of voids. The size and location of each indication was noted (figure E-23 and table E-3) for subsequent comparison with indications generated by SAM.

The SAM was performed by using a pulse-echo immersion setup. A 30-MHz focused transducer was used, focusing between the outer and inner diameters of the cylinder. The acoustic microscopy scans were performed at a resolution of 0.0012 inch/pixel, covering a total area of 0.5 inch by 0.5 inch. The location and magnitude of each indication was noted (figure E-23 and table E-4).

Findings

There is a one-to-one correlation between some indications that appear in both the film radiography and corresponding SAM images (table E-5). However, there are some indications apparent in the X-ray images, which do not appear in the ultrasonic images, and vice-versa. This may be due to the character of the flaw (e.g., void, high-density void, low-density void, etc.), the orientation of the flaw, or its distance from the shell surface. Internal cracks were not detected by either inspection technique.

Neither inspection procedure provided information on the distance of the indication from the outside surface of the cylinder. There is no doubt, however, that SAM is more sensitive than X-ray film radiography. It routinely detected voids with diameters >-0.007 inch, while X-ray film radiography detected only voids with diameter >-0.02 inch. The indications generated by SAM are *always larger by about 20 percent* than indications generated by X-ray film radiography for the same voids.

DESTRUCTIVE INSPECTION OF CYLINDER #3 AFTER HYDROTESTING TO 20,000 psi

Following the X-ray film radiography and SAM, the 9.5-inch long cylinder #3 was subjected to a combination of standard, industrial ultrasonic pulse-echo C- and A-scans. After completion of these inspections, the external surface of the cylinder was ground away in 0.002-inch-thickness increments while the size and location of voids revealed by grinding was recorded.

The objective of these inspections was to evaluate the ability of a standard, industrial ultrasonic technique using pulse-echo C- and A-scans to detect, locate, and measure voids inside ceramic shells. The data generated by the destructive inspection would form an objective standard against which all the indications generated by all previous nondestructive inspection techniques could be evaluated.

The standard industrial ultrasonic pulse-echo scans were performed by J. B. Engineering of Weymouth, MA. Its results are similar to other industrial-grade ultrasonic inspections. The C-scan (figure E-24) produces indications whose size exceeds the actual size of voids, while A-scan displays for each indicate the distance from the shell surface to the void.

The destructive inspection was performed by WESGO, Inc. It consisted of applying DYKEM to the exterior cylinder surface, grinding away 0.002 inch of materal, visually inspecting the freshly ground surface, and recording the location of the remaining splotches of colored DYKEM. Splotches larger than 0.015 inch were photographed (figure E-25). This inspection was followed by application of fluorescent dye penetrant to all newly uncovered voids, followed by visual inspection under black light. Any microcracks radiating from voids would become visible under the black light illumination.

A total thickness of 0.250 inch was removed in 0.002-inch increments and inspected in the above manner at each 0.002-inch increment. Some of the larger voids were observed during removal of several layers (figures E-26 and E-27). When the images of the cross section of the same void exposed during several grinding intervals are

positioned above each other, a three-dimensional image of the void can be formed (figure E-28).

Findings

During grinding away of ceramic from the exterior surface, 32 voids with diameters ≤0.015 inch and 17 voids with diameters ≥0.015 inch were discovered. Their size, location, and distance from the shell surface were recorded.

The total number of voids exposed by removing 0.250 inch of wall thickness is significantly larger than the number of indications discovered by any of the ND inspection techniques in the 0.412-inch-thick shell prior to grinding. The *largest* number of indications was previously detected by acoustic microscopy, and the *least* number was detected by film radiography.

Still, the correlation between location of indications ≥0.01 inch detected by the industrial-grade ultrasonic pulse-echo C-scan and the voids uncovered by grinding is good.

The distances from shell surface to indications at mid thickness of the shell were found to be within 10 percent of the actual depth at which the voids were located. The distances to indications located within 0.05 inch of the shell surface were, however, off by 100 or more percent. The sizes of indications were 100- to 200-percent larger than voids.

The voids uncovered by grinding were mostly irregular in shape (figures E-25, E-26, and E-27). The long axis of all voids was found to be parallel, never perpendicular, to the surface of the cylinder.

Inspection with black light of the cylinder surface coated by fluorescent dye penetrant did not discover any microcracks originating at the voids. This indicated that voids up to 0.05 inch in size did not serve as crack initiators when located in a triaxial stress field subjected to hoop, axial, and radial principle stress of −290,000, −145,000, and −20,000 psi magnitude. This would seem to indicate that regular and irregular voids with ≤0.05-inch diameter can be tolerated in ceramic shells provided that the compressive stresses generated during prooftesting in ceramic components do not exceed above stress limits.

Some of the large voids uncovered during grinding were found to be located close to the external surface of the cylinder. The distance between the void envelope and the external cylinder surface in some cases (voids B, C, and D) did not exceed the radius of the void. Since the envelopes of the voids did not exhibit any microcracking even after pressurization to 20,000 psi, it can be postulated that voids can be located close to the pressurized shell surface provided that the distance between the void's envelope and the shell's surface is larger than the void's radius.

Although most of the voids were widely separated from each other, a few were encountered during grinding that were separated by less than 0.005 inch. Even there, cracking was not observed.

SUMMARY OF ND INSPECTIONS

Findings

The ***presence of voids*** with diameters ≥0.010 inch can be detected in ceramic shells with thicknesses of 0.412 inch by using ultrasonic pulse-echo or through-transmission data acquisition methods. To achieve such fine resolution, the C-scan of the ceramic cylinder or hemisphere must be performed at 0.01-inch increments using ≥10 MHz frequency.

The ***location of a void*** can be accurately pinpointed in the x–y plane by ultrasonic through-transmission or pulse-echo methods operating in C-scan mode, and its distance from the exterior surface of the shell estimated by pulse-echo method operating in A-scan mode.

The ***size of the void*** cannot be accurately determined by sonic inspection methods as the magnitude of the signal generated by echo from the void depends not only on its size, but also on its shape. As a rule, the image of an indication detected by an ultrasonic C-scan is 100- to 200-percent larger than the void itself.

The ***size of a void*** can be precisely determined by by radiographic inspection techniques. The most sensitive method is radiographic computed tomography, followed by digital radiography, and film radiography. The width of the void, or separation of fracture surfaces at right angles to the ray path, must be ≥3 percent of ceramic shell thickness in

order to be detectable by film radiography inspection techniques.

The ***distance of the void*** with respect to the front shell surface can be established accurately *only* by radiographic computed tomography. Ultrasonic pulse-echo A-scan provides a good approximation of the distance if the void is located in the central region of the wall thickness.

The ***three-dimensional shape of the void***, as well as its location inside the ceramic shell, can be accurately determined *only* by radiographic computed tomography. Because of the high cost, this technique must be applied only to locations where ultrasonic inspection has previously pinpointed the presence of a large void.

The ***magnitude of voids*** detected in the 6- and 12-inch diameter housings and hemispheres varied in size from 0.01 to 0.05 inch. The number of voids varied from one cylinder to another. The largest number of voids was found in cylinder #3 at an apparent density of 3 voids per cubic inch. Over 90 percent of voids detected were $\leq$0.015 inch in size. The sizes of voids in the remaining 10 percent of void population varied from 0.015 to 0.050 inch.

Some voids in the 0.04- to 0.05-inch range were found within 0.05 inch of the external surface. They did not implode or serve as crack initiators when the external surface of the cylinder was subjected to 20,000 psi test pressure.

Voids with diameter $\prec$0.05 inch do not initiate cracks in ceramic cylinders compressed hydrostatically to $\leq$300,000 psi compressive stress level.

Conclusions

ND inspection techniques are available for detection, location, and sizing of cracks, fracture surfaces, and voids inside ceramic components with ground exterior and interior surfaces. ND inspection techiques are a cost-effective approach for rejecting ceramic components that might have failed during proof testing or subsequent service life.

Recommendations

All structural ceramic components of external pressure housings should be inspected by ND techniques for cracks and internal inclusions in the form of voids.

The inspection should use three ND procedures. Application of:

a. Dye penetrant to external surfaces for detection of surface cracks.

b. Ultrasonic pulse-echo C-scan to the exterior surface for detection and location of internal cracks and voids.

c. Film or digital radiography for sizing of inclusions. FR or DR is to be used selectively only at locations where indications with apparent size larger than 0.05 inch have been previously detected by ultrasonic techniques. The images of flaws generated by FR or DR procedure shall be considered to represent the true sizes of flaws.

REFERENCE

E-1. SAMPE Journal, March–April 1990,
pp. 31–34.

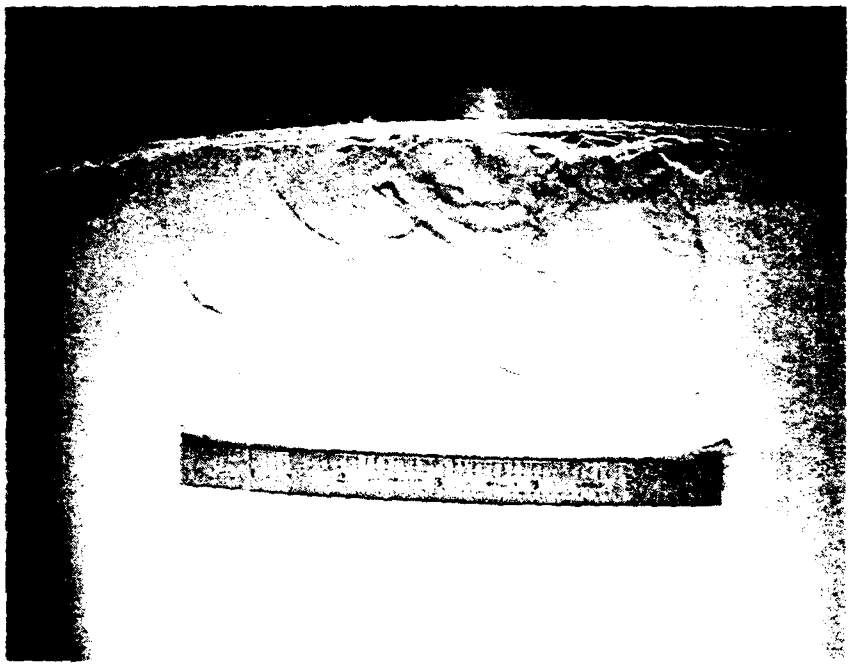

(a) Top end of cylinder, 330° to 50° location.

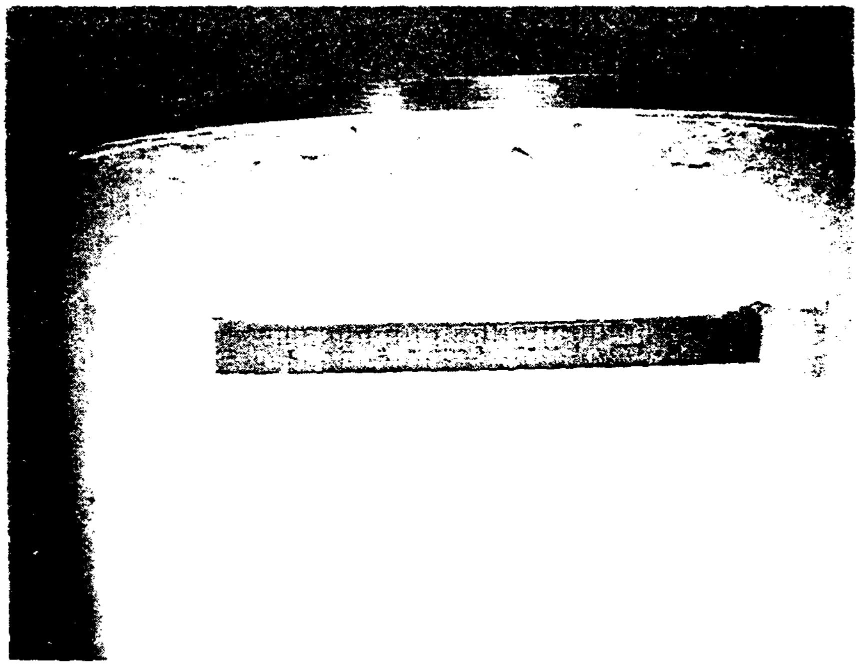

(b) Top end of cylinder, 145° to 210° location, sheet 1.

Figure E-1. Photomacrographs of spalling found on cylinder #2, sheet 1.

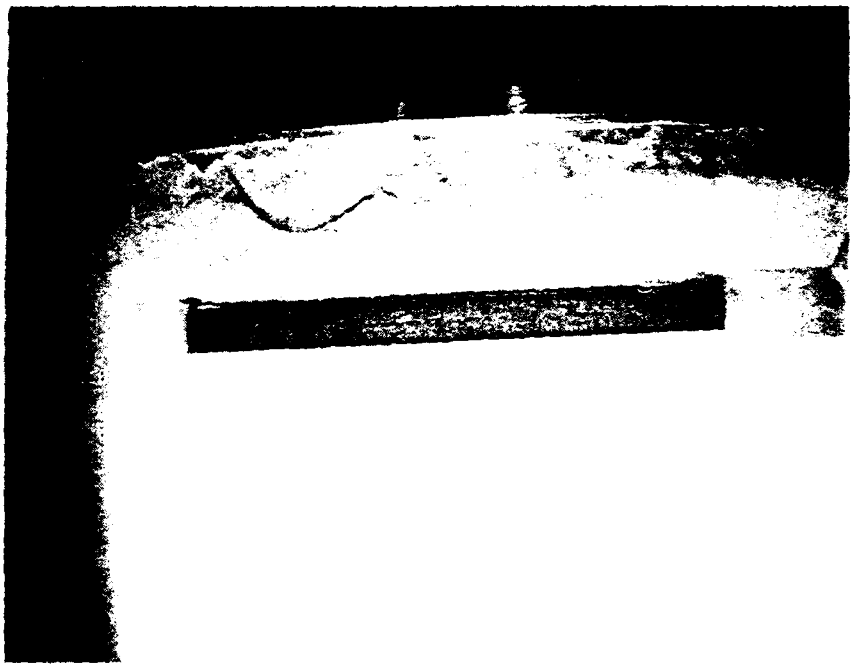

(c) Bottom end of cylinder, 10° to 60° location.

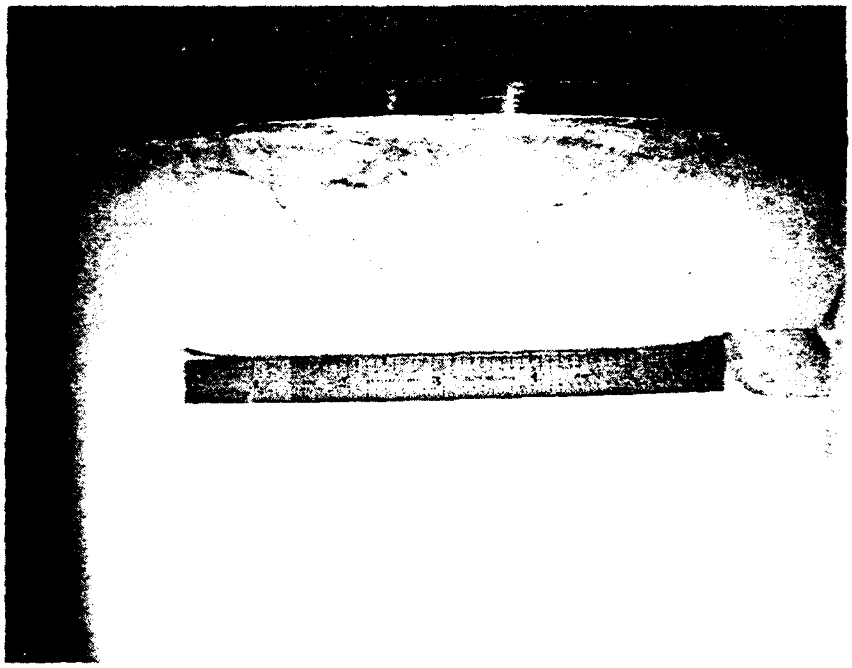

(d) Bottom end of cylinder, 145° to 210° location, sheet 2.

Figure E-1. Photomacrographs of spalling found on cylinder #2, sheet 2.

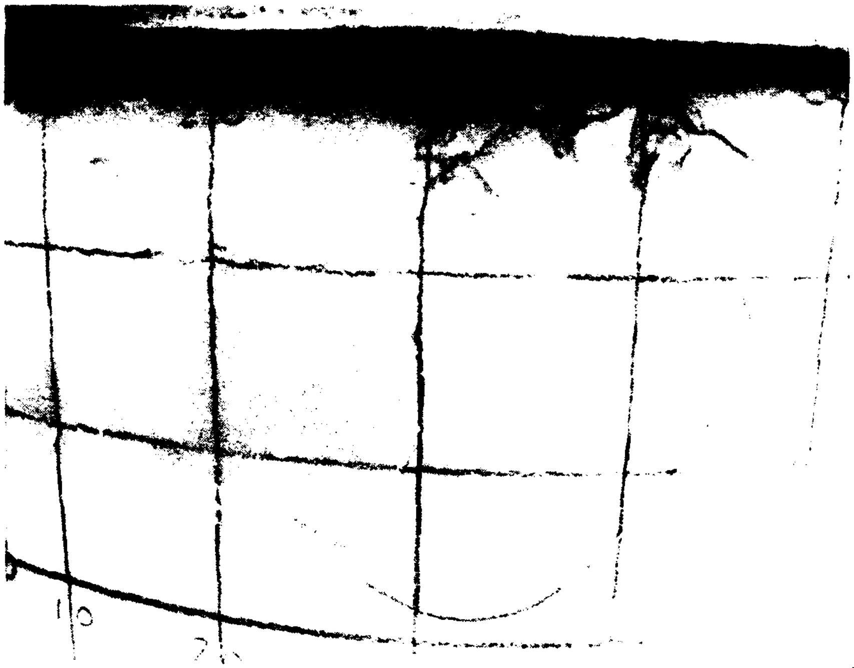

Figure E-2. Detail of spalling on top of cylinder #2, 10° to 50° location.

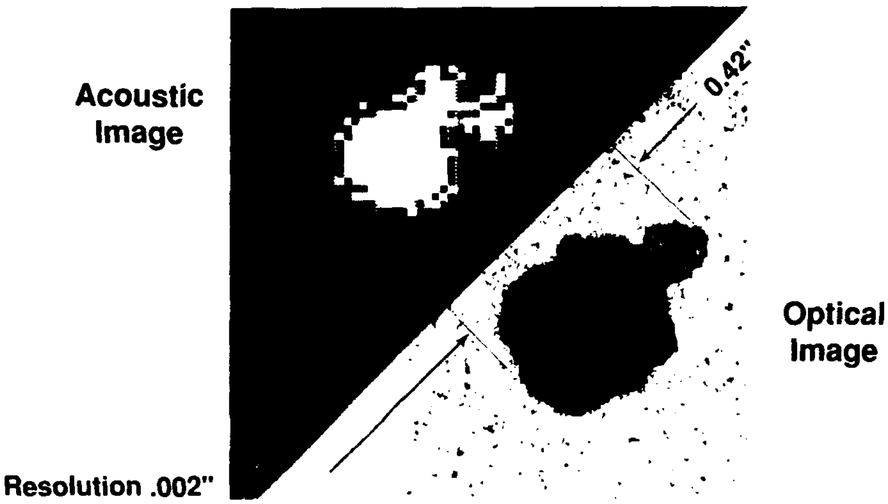

- Numerous flaws verified
- 95% of flaws less than 0.040 inch
- Fracture mechanics indicates small flaw propagation is self limiting
- Process adaptable to ful-size testing in factory and field
- Initial scan can be automated

Figure E-3. Definition of flaw shape and size by SAM performed on a 3.25-inch-thick ceramic specimen.

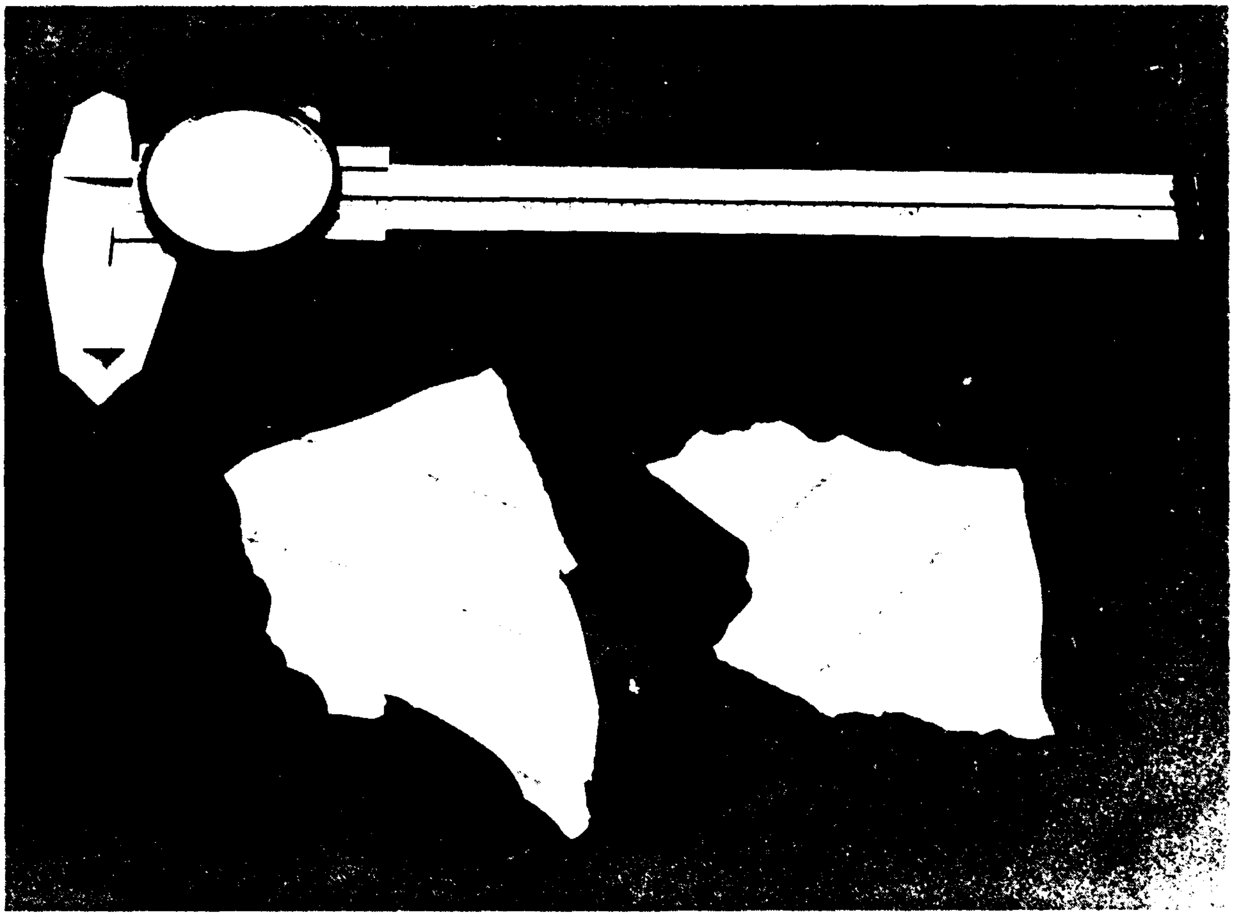

Figure E-4. Typical spall fragments from 12-inch-diameter ceramic cylinders. The fragments are approximately 0.06 inch thick.

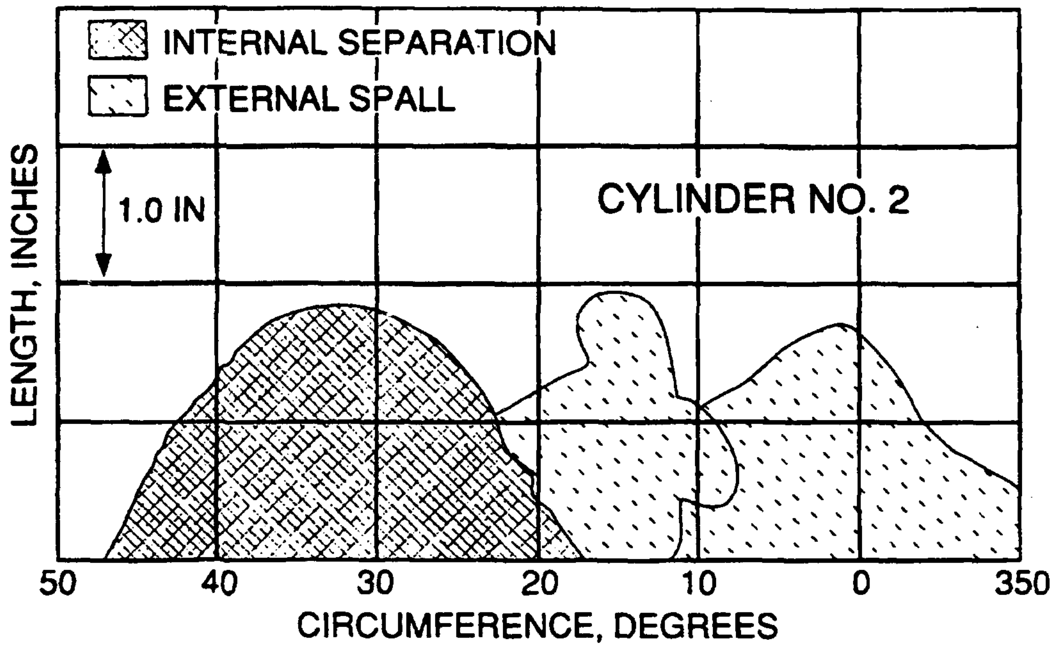

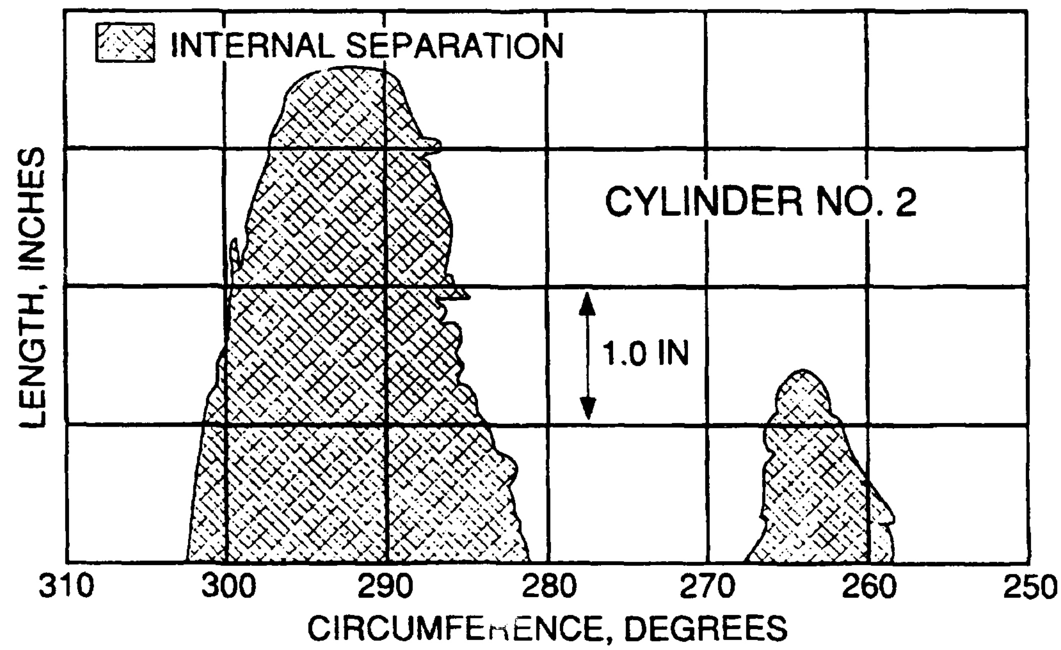

Figure E-5. Ultrasonic C-scan of spalled and delaminated areas above the end cap on cylinder #2.

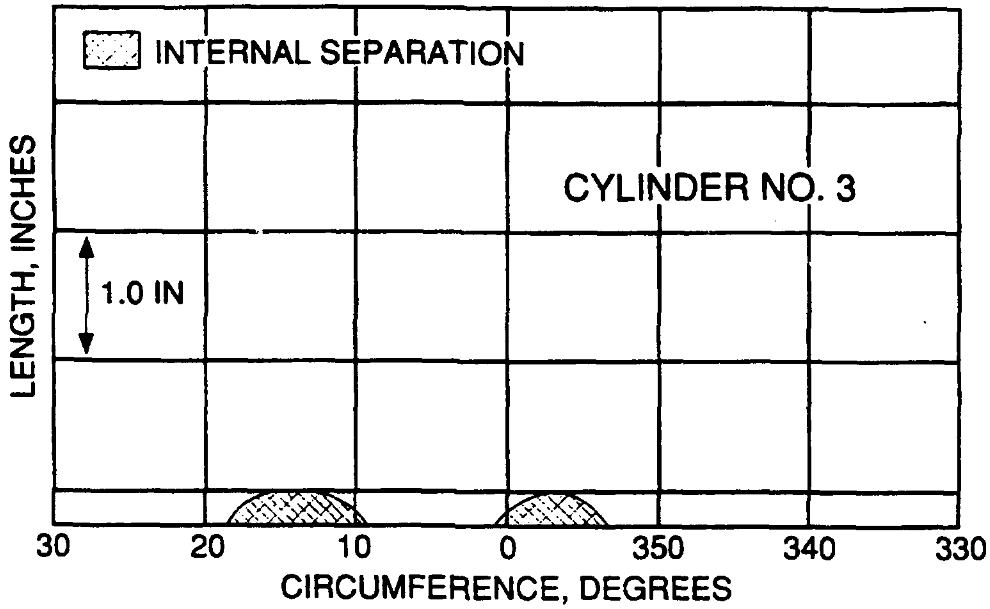

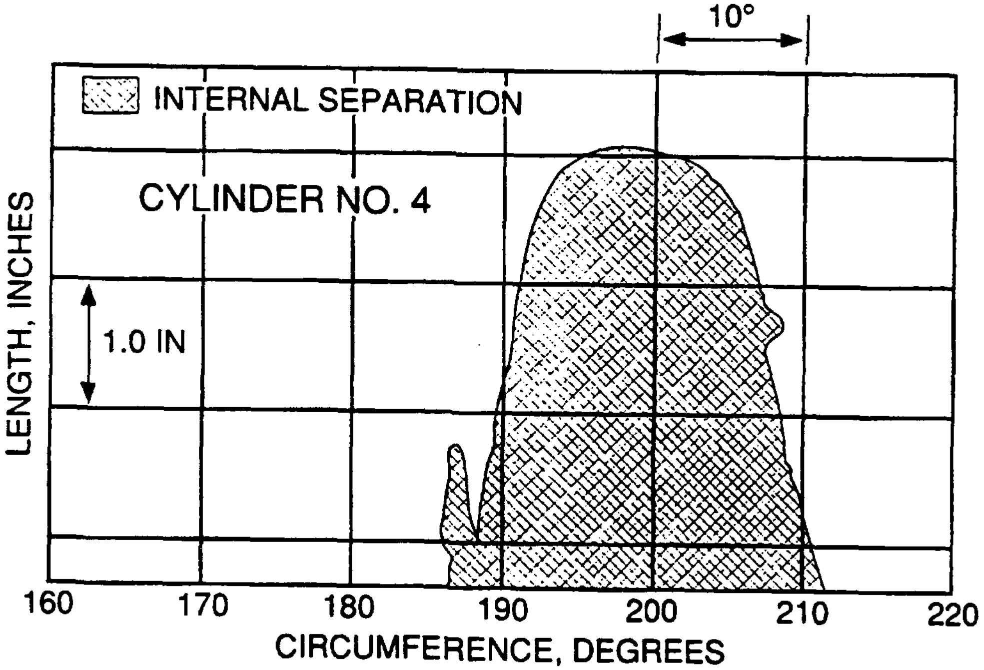

Figure E-6. Ultrasonic C-scan of spalled and delaminated areas above the end cap on cylinders #2, #3, and #4.

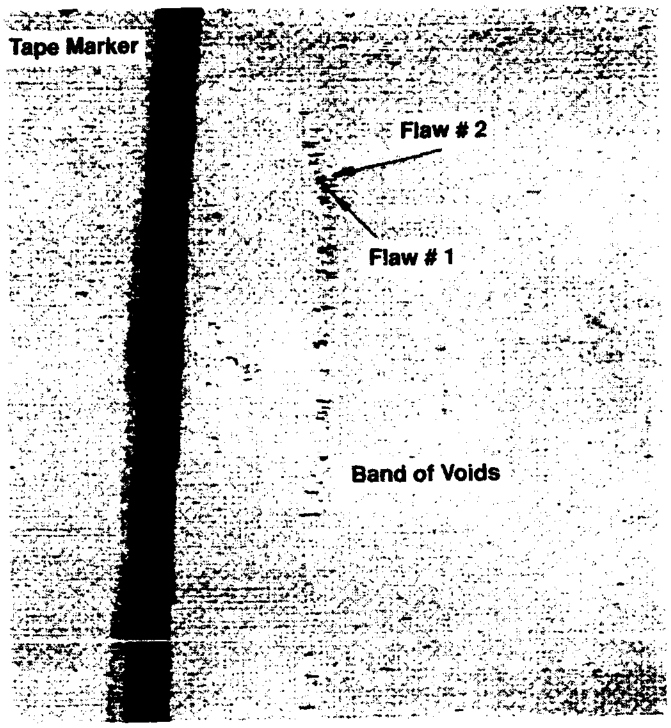

Figure E-7. Ultrasonic C-scan of cylinder #1. Note the narrow band of indications detected with 10 MHz through-transmission.

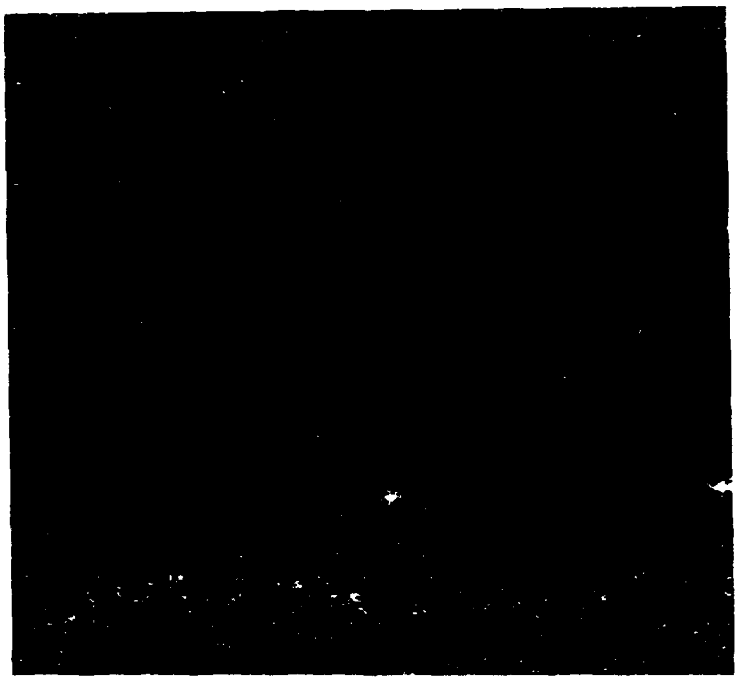

Figure E-8. Images of flaw #1 and #2 indications in cylinder #1 generated by SAM with resolution 0.0015 inch/pixel.

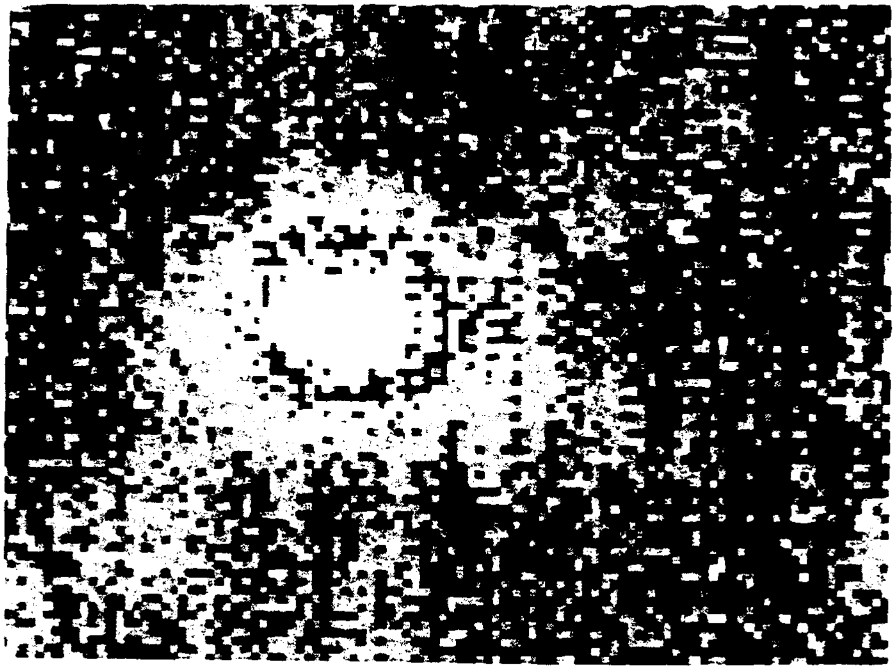

Figure E-9. Enlarged image of flaw #1 indication in cylinder #1 generated by SAM with resolution 0.005 inch/pixel. Estimated size of indication is 0.01–0.015 inch.

Figure E-10. Enlarged image of flaw #2 indication in cylinder #1 generated by SAM with resolution 0.005 inch/pixel. Estimated size of indication is 0.015–0.02 inch.

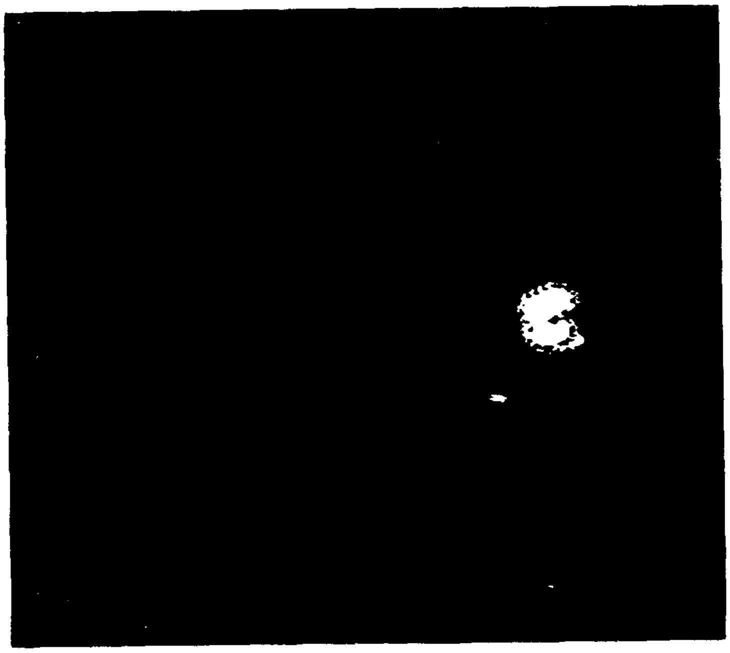

Figure E-11. Image of largest flaw indication in cylinder #3 generated by SAM with resolution of 0.0015 inch/pixel.

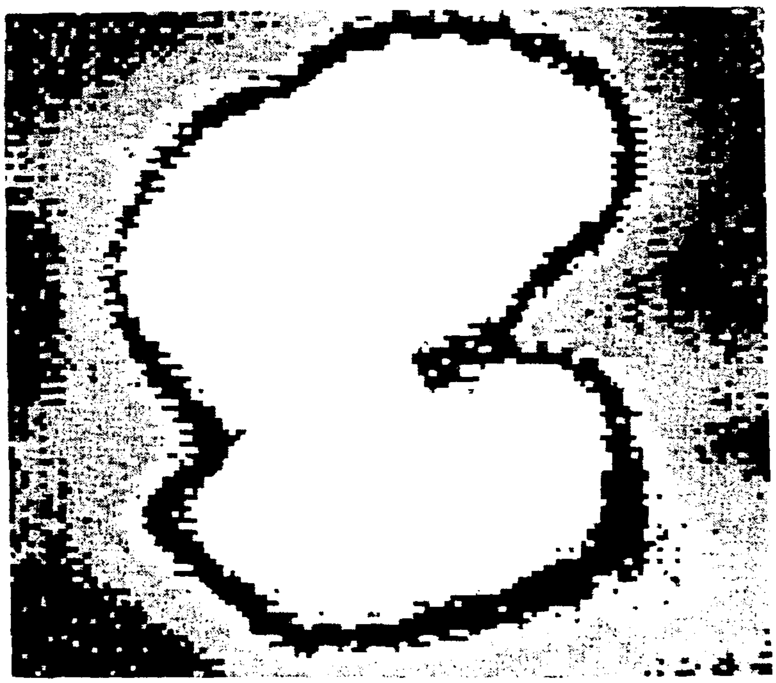

Figure E-12. Enlarged image of largest flaw indication in cylinder #3 generated by SAM with resolution of 0.0005 inch/pixel. Estimated size of indication is 0.057–0.065 inch.

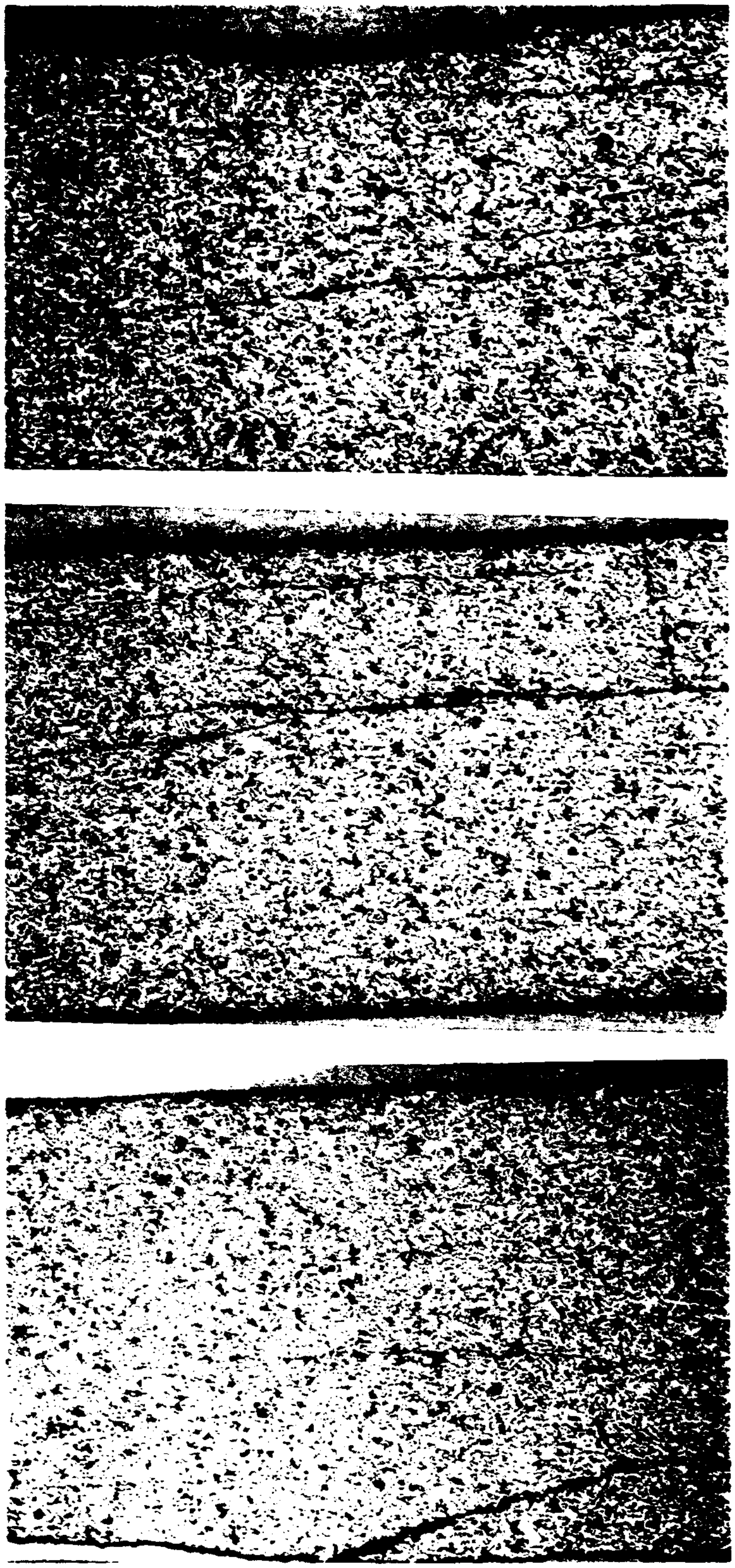

Figure E-13. Photomicrographs of plane bearing surfaces on ceramic spalls from cylinder #4. Note that the predominant orientation of cracks is circumferential.

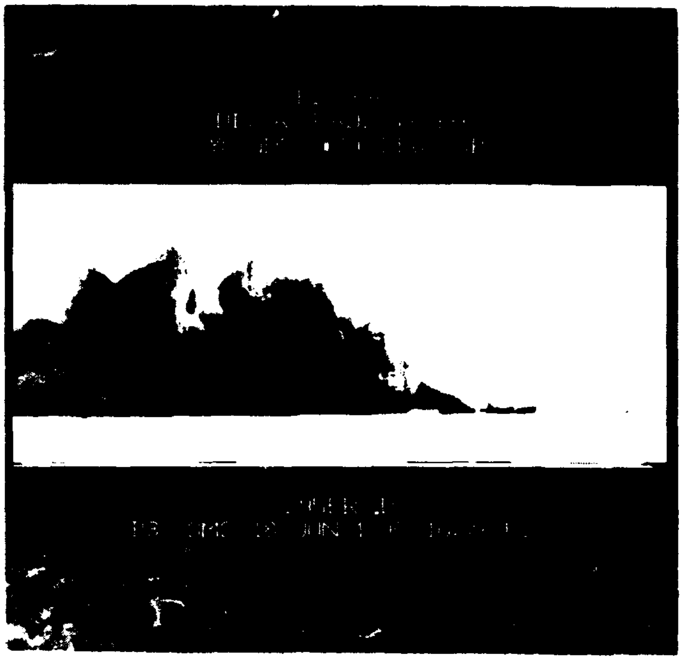

X-Ray Computed Tomography

Digital Radiograph External Spalls

Specimen:
12.00 in OD x 11.176 ir
94% Alumina Ceramic
Cylinder #2

Figure E-14. DR of external spalls visible above metallic end cap on cylinder #2.

X-Ray Computed Tomography

Tomograph Through Cylinder Above End Cap

Specimen:
12.00 in OD x 11.176 in ID
94% Alumina Ceramic
Cylinder #2

Figure E-15. RCT slice through cylinder #2 at one inch evaluation above bottom of cylinder. Note the external spall.

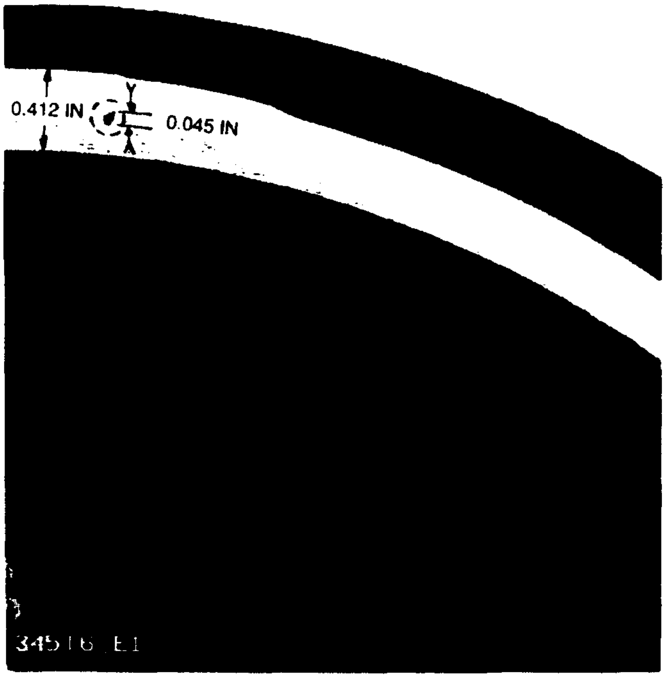

Figure E-16. RCT slice through a large flaw in cylinder #3. The measured size of indication cross section is 0.045 inch. The SAM indication of this flaw is shown in figures E-11 and E-12.

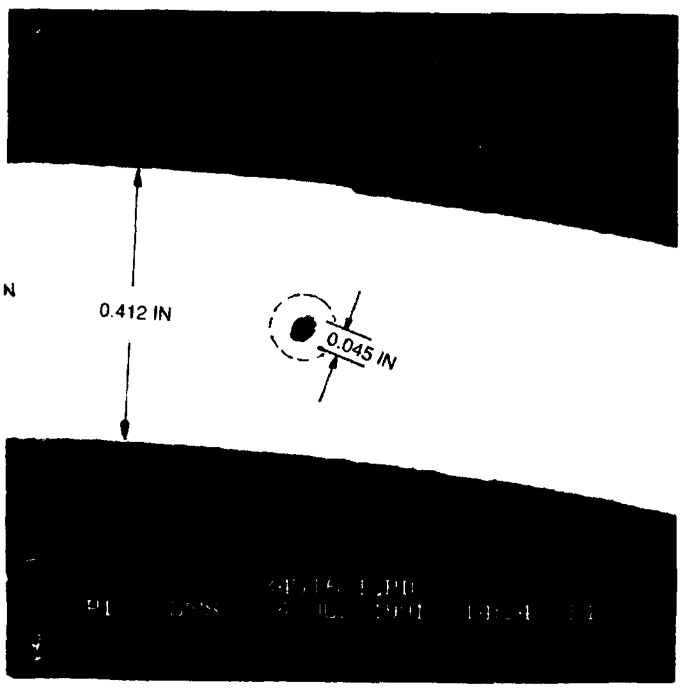

Figure E-17. Enlarged image of RCT slice shown on figure E-16.

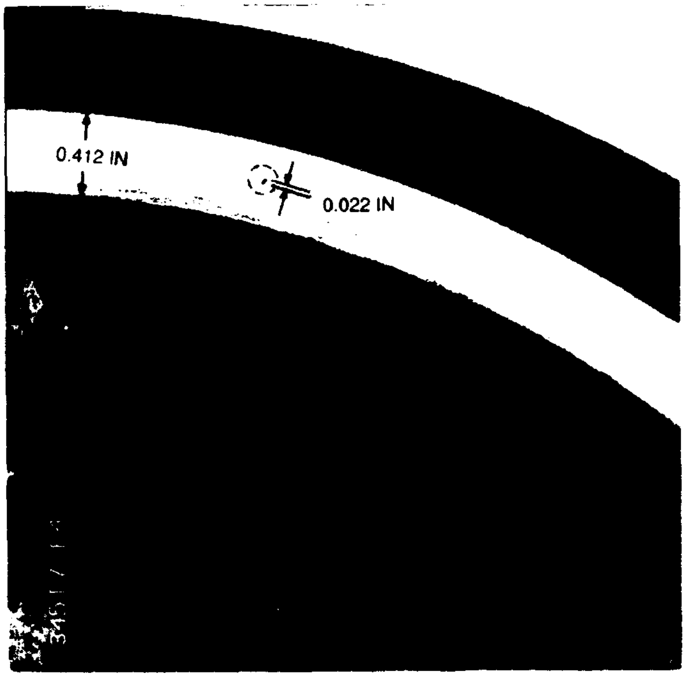

X-Ray Computed Tomography

Tomograph #7
Section E4

Specimen:
12.00 in OD x 11.176 in ID
94% Alumina Ceramic
Cylinder #3

Figure E-18. RCT slice through the smallest flaw in cylinder #3 detected previously by DR.

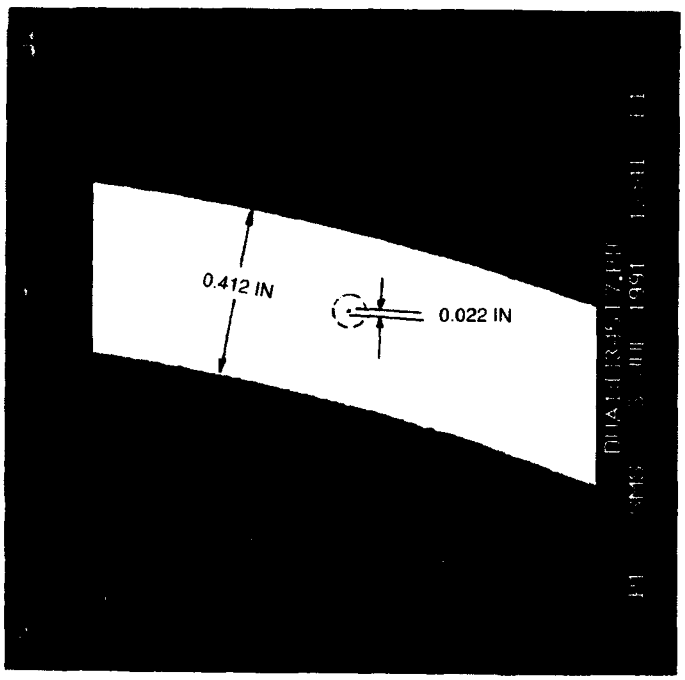

X-Ray Computed Tomography

Tomograph #7
Section E4
Inclusion Detail

Specimen:
12.00 in OD x 11.176 in ID
94% Alumina Ceramic
Cylinder #3

Figure E-19. Enlarged image of RCT slice shown on figure E-18.

Figure E-20. The 13-inch-long cylinder #3 after hydrostatic pressurization to 20,000 psi.

Figure E-21. Cylinder #3 after removal of spalled ends shown on figure D-20.

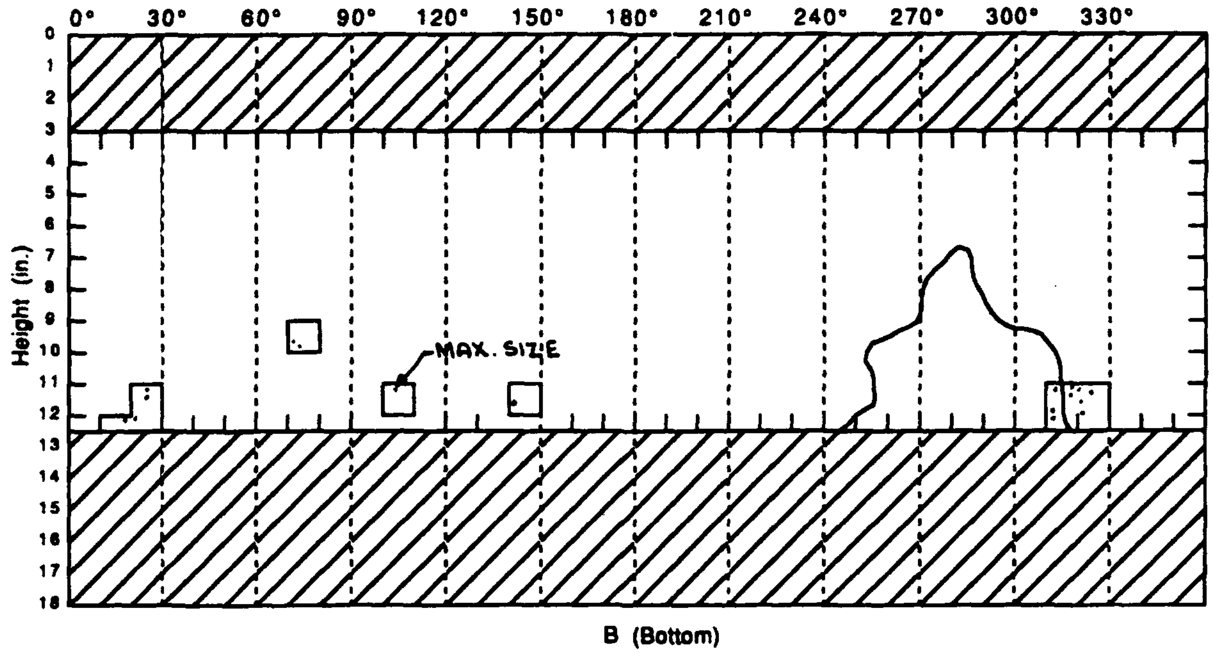

Figure E-22. Indications of flaws detected by film radiography of cylinder #3.

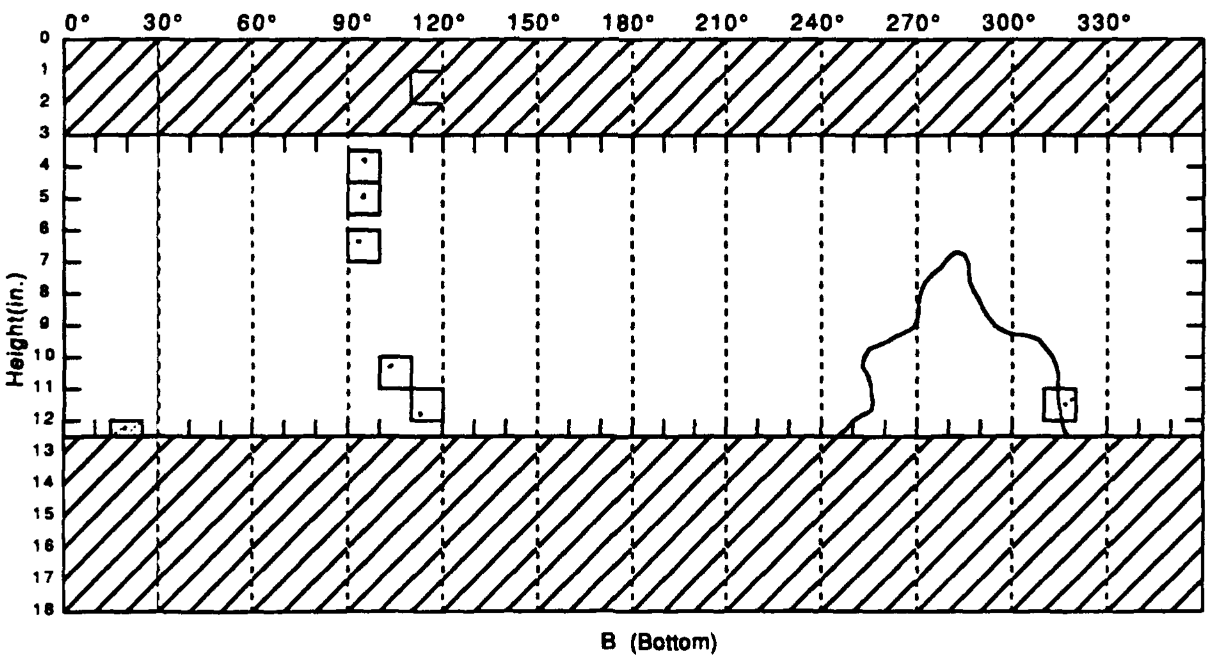

Figure E-23. Indications of flaws detected by SAM of shortened cylinder #3.

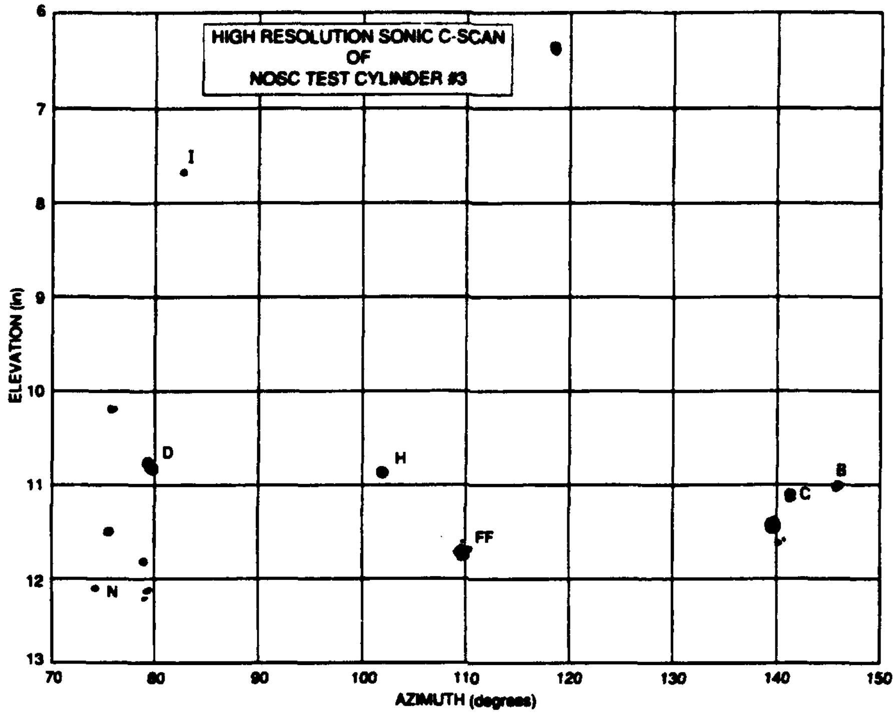

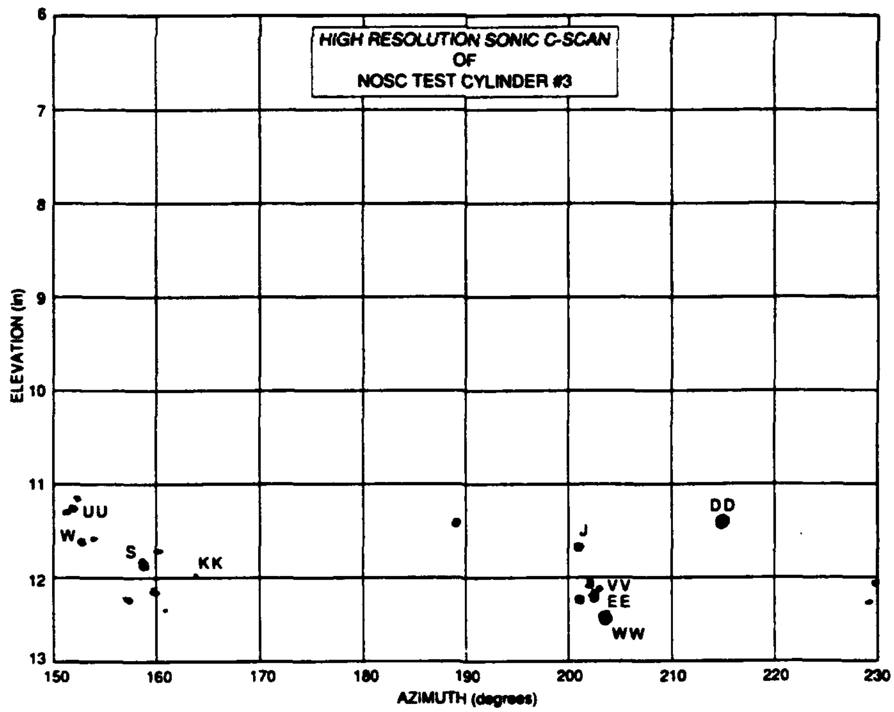

Figure E-24. Industrial-grade ultrasonic C-scan of shortened cylinder #3 using 10 MHz pulse-echo inspection technique, sheet 1.

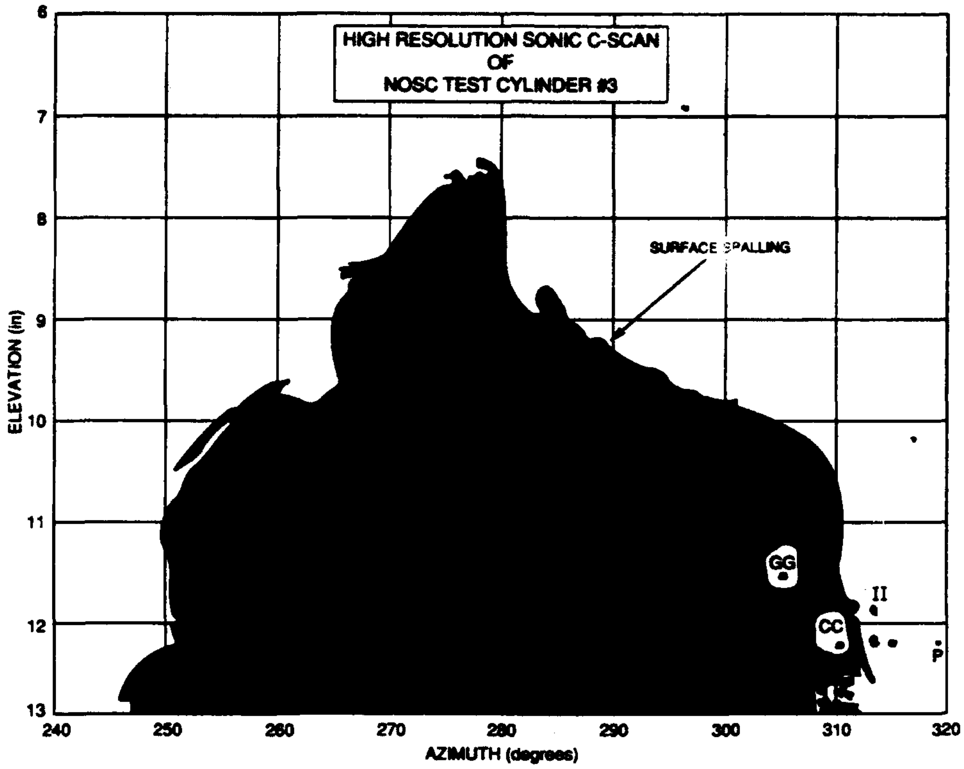

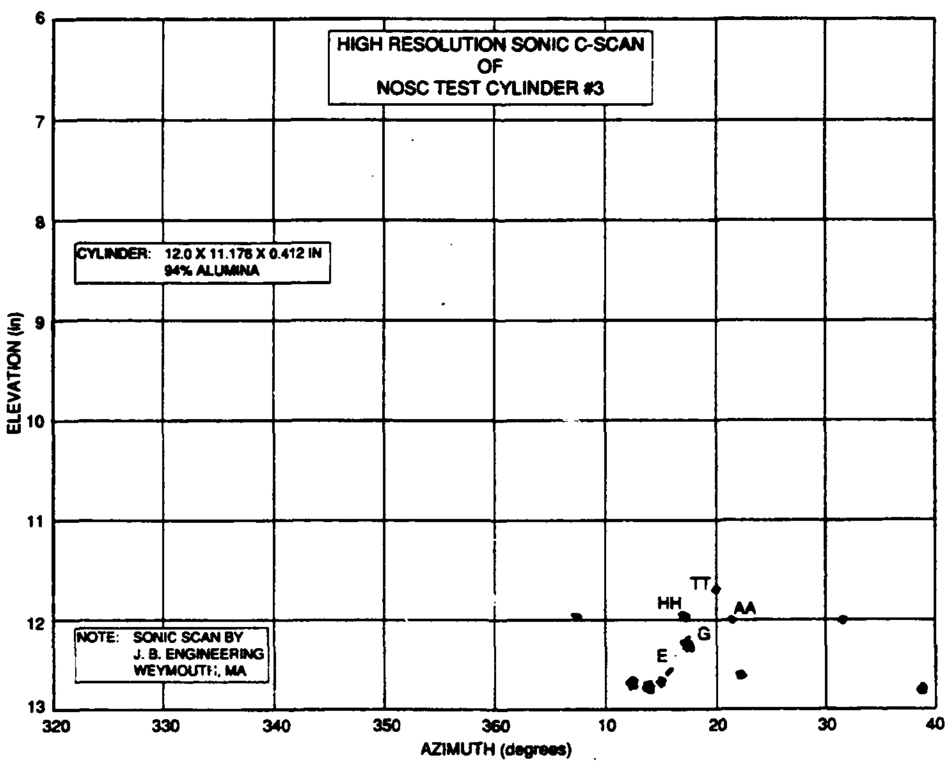

Figure E-24. Industrial-grade ultrasonic C-scan of shortened cylinder #3 using 10 MHz pulse-echo inspection technique, sheet 2.

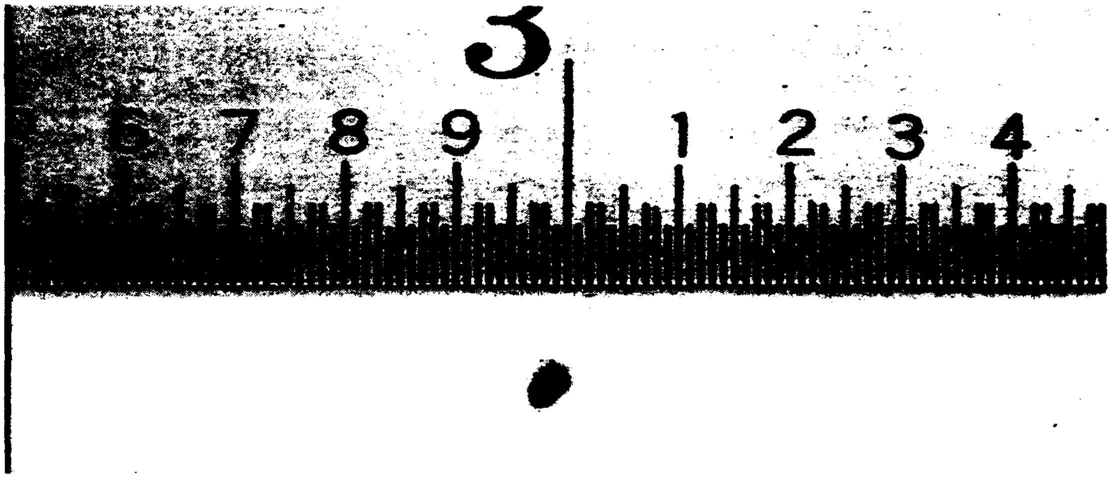

C.
11", 140°, 0.046"

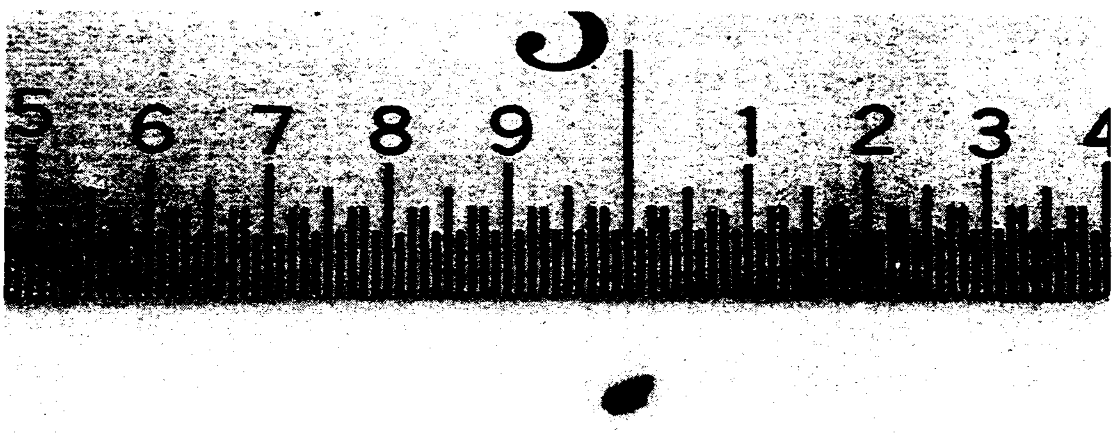

D.
10.5", 80°, 0.062"

Figure E-25. Subsurface flaws C and D uncovered by grinding away external surface of cylinder #3.

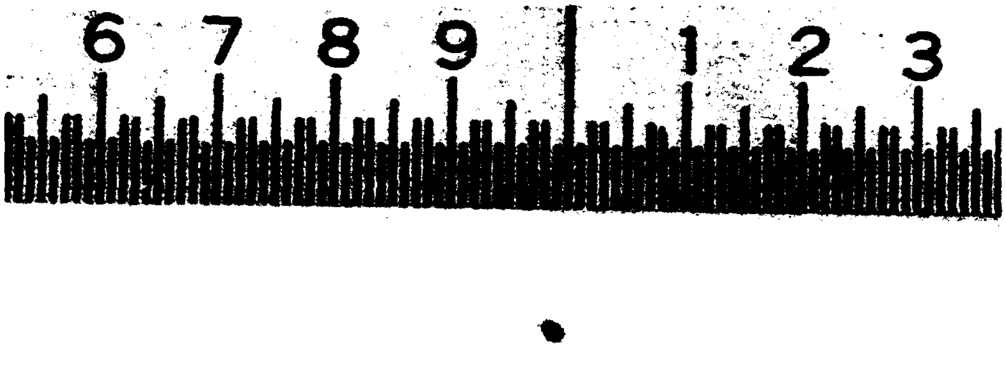

G.
12.25", 20°, 0.140"

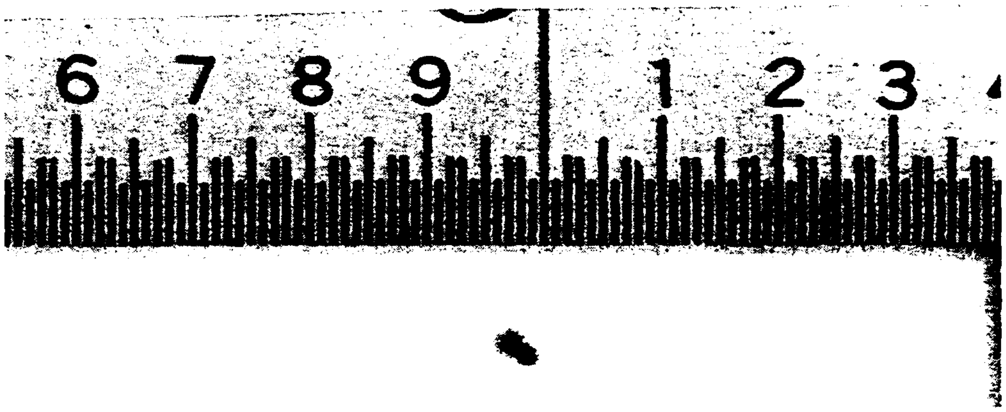

G.
12.25", 20°, 0.148"

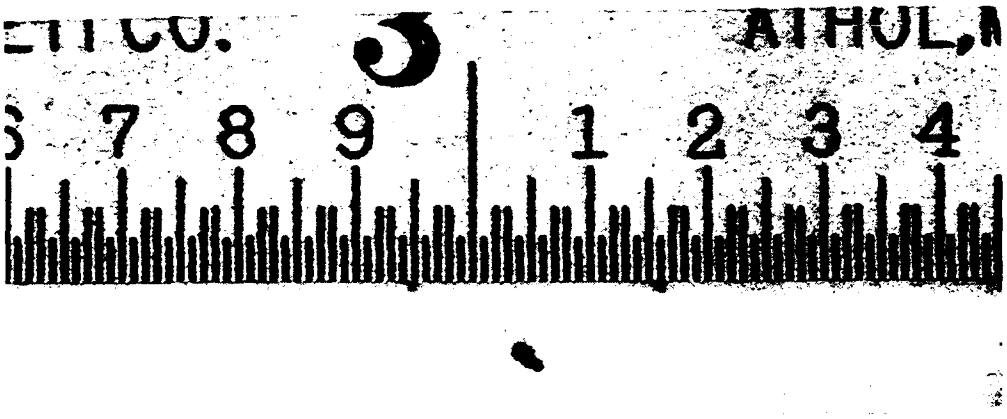

G.
12.25", 20°, 0.150"

Figure E-26. Flaw G cross section uncovered during incremental removal of material from exterior surface of cylinder #3. Note the irregularity of the flaw shape.

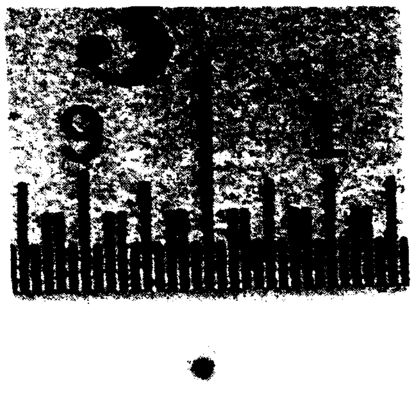

FF.
11.14", 110°, 0.200"

FF.
11.4", 110°, 0.206"

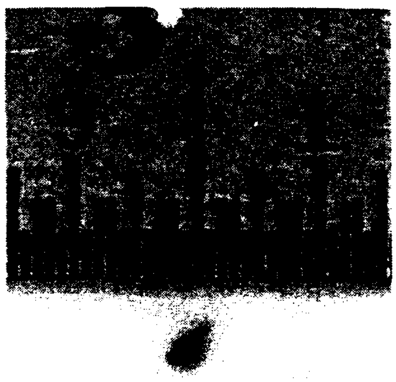

FF.
11.4", 110°, 0.210"

Figure E-27. Flaw FF cross section uncovered during incremental removal of material from exterior surface of cylinder #3.

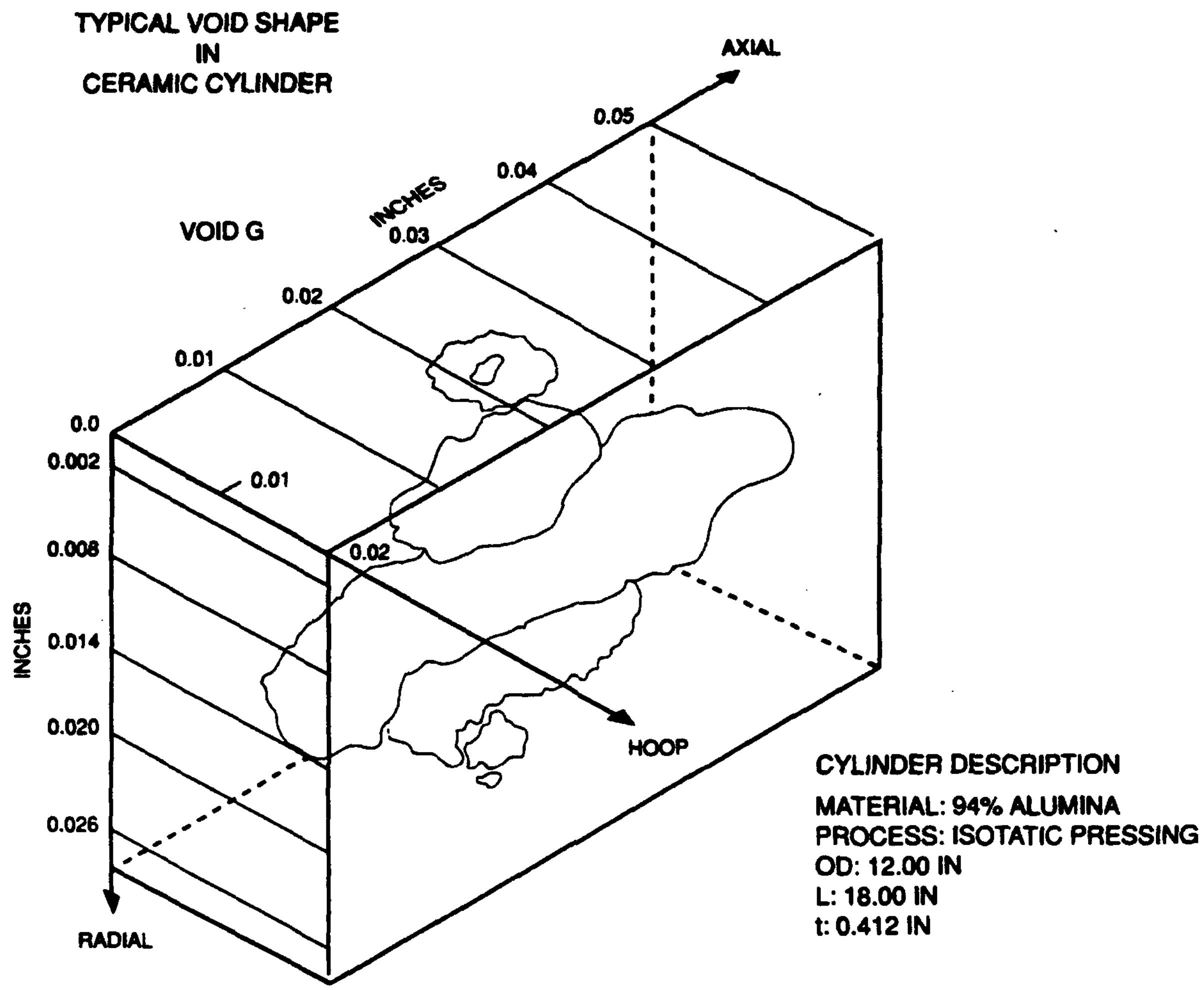

Figure E-28. Three-dimensional reconstruction of a typical flaw on the basis of cross section images uncovered during successive passes of the grinding wheel. Note that the irregularity of the flaw shape makes it impossible to analyze its crack initiation potential by analytical approaches of fracture mechanics.

Table E-1. Critical pressures pressures of 12-inch-diameter ceramic cylinders after testing to proof and design pressures.

	Cylinder 1	Cylinder 2	Cylinder 3	Cylinder 4	
Proof Pressure Tests to 10,000 psi	1	2	3	2	1
Design Pressure Tests to 9000 psi	500 Cycles	90 Cycles	120 Cycles	130 Cycles	80 Cycles
End Cap Design	Mod 1	Mod 0	Mod 0	Mod 0	Mod 0
Surface Spalling –Initiation	None	30 Cycles	40 Cycles	34 Cycles	40 Cycles
–Outside Surface Top	No spalling	6W x 3.5L x 0.125 in T 6W x 1.5L x 0.060 in T	5W x 1.5L x 0.060 in T	6W x 2.5L x 0.125 in T	Minor spalling 0.03 in thick
Bottom	No spalling	5W x 2L x 0.06 in T 5W x 2.5L x 0.03 in T	No spalling	No spalling	Minor Spalling 0.03 thick
–Inside Surface	No spalling	No spalling	No spalling	No spalling	No spalling
Interior Delaminations	None	2W x 4.0 in L 1W x 2.0 in L 2.5W x 2.5 in L	2W x 1 in L Many 1W x 1.0 in L on both bearing surfaces	2W x 4 in L Many 1W x 0.5 in L on both bearing surfaces	Not inspected
Internal Inclusions	None over 0.017 in	Maximum size 0.06 in 0.015 in	None over 0.045 located 0.15 in from exterior surface at midbay	None over 0.015 in	Not inspected
Implosion Pressure	16,5000 psi	13,250 psi	20,000 psi*+	12,100 psi	14,700 psi

Notes: Cylinders are 12.0 in OD x 11.176 in ID x 18.0 in L of 94% alumina ceramic.
Bulkheads are flat steel discs providing radial support.
*Test terminated without implosions,m only circumferential cracks at ends.
+Cylinder was shortened to 13 inches before testing to 20,000 psi

Table E-2. Summary of SAM data for 12-inch OD x 18-inch L x 0.412-inch t alumina cylinders #1, #2, #3, and #4.

CYLINDER	NO. OF SCANS	NO. OF FLAWS DETECTED	GRID LOCATION	DIAMETER OF FLAW (inches)
#1	4	2	100-110° 5th sq. Down	0.017, 0.0105
		1	100-110° 14th Sq. Down	0.0165
#2	15	0	---------	---------
#3	11	1	100-110° 11th Sq. Down	0.057 (0.13 in. from O.D.)
		1	90-100° 7th Sq. Down	0.0105
		2	90-100° 4th & 5th Sq. Down	0.0105, 0.0105
		2	90-100° 5th & 6th Sq. Down	0.012, 0.009
		3	100-110° 11th Sq. Down	0.030, 0.015, 0.0075
		1	110-120° 2nd Sq. Down	0.0135
		2	110-120° 12th Sq. Down	0.018, 0.0135
#4	14	1	90-100° 6th Sq. Down	0.0145
		2	90-100° 9th & 10th Sq. Down	0.0125, 0.007
		1	90-100° 15th & 16th Sq. Down	0.015
		1	70-80° 12th Sq. Down	0.0095
		2	200° 8th Sq. Down	0.011, 0.0075
TOTAL	44	22		Largest - 0.057 (0.13 in. from O.D.)

Table E-3. Summary of indications generated by film radiography of cylinder #3 shortened to 9.5 inches after pressure testing to 20,000 psi.

# of Flaws	Grid Location	Size (in.)
4	10°-30°, 11"-12.5"	largest 0.03 x 0.03
3	70°-80°, 9"-10"	largest 0.03 x 0.02
1	100°-110°, 11"-12"	0.03 x 0.03
1	135°-145°, 11"-12"	0.03 x 0.03
9	310°-330°, 11"-12.5"	largest 0.03 x 0.03

Table E-4. Summary of indications generated by SAM of cylinder #3 shortened to 9.5 inches after pressure testing to 20,000 psi.

# of Flaws	Grid Location	Diameter (in.)
7	18°-21°, 12"-12.5"	0.048, 0.0165, 0.0135, 0.0195, 0.015, 0.015, 0.0405
2	90°-100°, 3.5"-4.5"	0.0105, 0.0105
2	90°-100°, 4.5"-5.5"	0.012, 0.009
1	90°-100°, 6"-7"	0.0105
4	100°-110°, 10"-11"	0.057, 0.030, 0.015, 0.0075
1	110°-120°, 1"-2"	0.0135
2	110°-120°, 11"-12"	0.018, 0.0135
2	313°-316°, 11"-11.5"	0.0225, 0.015

Table E-5. Indications detected by both film radiography (table E-3) and SAM (table E-4) in cylinder #3. The correlation between the two ND inspection techniques is not very high.

# of Flaws	Grid Location	Diameter (in.)
2	18°-21°, 12"-12.5"	0.048, 0.0405
1	100°-110°, 10"-11"	0.057
1	313°-316°, 11"-11.5"	0.0225

Table E-6. Voids detected during progressive removal of material from external surface of 9.5-inch-long cylinder #3, sheet 1.

ID	ELEVATION[1]	AZIMUTH	DEPTH[2]	SIZE
A	10.1	80°	0.015	0.018
B	11.0	145°	0.019	0.018 X 0.025
C	11.0	140°	0.053	0.030 X 0.040
D	10.5	80°	0.057	0.020 X 0.050
E	12.4	15°	0.062	0.010 X 0.024
F	12.5	250°	0.138	0.020
G	12.3	17°	0.148	0.018 X 0.040
H	10.5	103°	0.148	0.020 X 0.030
I	7.3	85°	0.150	0.008 X 0.014
J	11.8	205°	0.157	0.030
BB	11.5	62°	0.160	0.10 Grain
CC	11.2	310°	0.171	0.025 X 0.035
DD	11.1	215°	0.184	0.018 X 0.025
EE	11.9	205°	0.185	0.010 X 0.017
FF	11.4	110°	0.210	0.025 X 0.045
GG	11.5	305°	0.226	0.050
HH	12.0	10°	0.235	0.030

1. Elevation measured from top of cylinder, as per original grid. Bottom of cylinder was spalled end.

2. Depth measured from original outside surface of cylinder to center of void.

3. All dimensions are in inches.

Table E-6. Voids detected during progressive removal of material from external surface of 9.5-inch-long cylinder #3, sheet 2.

ID	Elevation[1]	Azimuth	Depth[2]	Diameter
L	5.0	240°	0.012	0.002
M	4.0	280°	0.040	0.002
N	11.0	75°	0.044	0.005
O	10.8	215°	0.046	0.005
P	12.0	320°	0.047	0.005
Q	11.8	225°	0.064	0.006
R	3.3	225°	0.064	0.006
S	11.5	160°	0.064	0.006
T	9.5	60°	0.134	0.005
U	3.8	335°	0.134	0.002
V	9.7	5°	0.134	0.002
W	11.4	150°	0.136	0.010
X	12.5	265°	0.144	0.006
Y	12.5	275°	0.144	0.006
Z	12.5	45°	0.150	0.006
AA	12.0	21°	0.150	0.008
K	6.8	320°	0.158	0.012
II	11.9	315°	0.163	0.010
JJ	10.2	155°	0.162	0.003
KK	11.9	165°	0.170	0.005
LL	11.6	170°	0.170	0.003
MM	11.6	171°	0.170	0.007
NN	12.5	210°	0.182	0.005
OO	10.8	143°	0.194	0.008
PP	6.8	308°	0.206	0.005
QQ	12.1	277°	0.220	0.010
RR	1.0	157°	0.223	0.003
SS	11.9	310°	0.240	0.007
TT	11.6	20°	0.238	0.012
UU	10.9	155°	0.239	0.003
VV	12.0	205°	0.250	0.005
WW	12.1	205°	0.250	0.001

1. Elevation measured from top of cylinder, as per original grid. Bottom of cylinder was spalled end.

2. Depth measured from original outside surface of cylinder to center of void.

3. All dimensions are in inches.

REPORT DOCUMENTATION PAGE

Form Approved
OMB No. 0704-0188

1. AGENCY USE ONLY *(Leave blank)*

2. REPORT DATE
September 1989
Revised June 1993

3. REPORT TYPE AND DATES COVERED
Final

4. TITLE AND SUBTITLE
EXPLORATORY EVALUATION OF ALUMINA-CERAMIC HOUSINGS FOR DEEP SUBMERGENCE SERVICE
Third Generation Housings; Volume 2: Appendices

5. FUNDING NUMBERS
PE: 0603713N
PROJ: S0397
ACC: DN302232

6. AUTHOR(S)
J. D. Stachiw

7. PERFORMING ORGANIZATION NAME(S) AND ADDRESS(ES)
Naval Command, Control and Ocean Surveillance Center (NCCOSC)
RDT&E Division
San Diego, CA 92152–5000

8. PERFORMING ORGANIZATION REPORT NUMBER
TR 1314

9. SPONSORING/MONITORING AGENCY NAME(S) AND ADDRESS(ES)
Naval Sea Systems Command
Washington, DC 20362

10. SPONSORING/MONITORING AGENCY REPORT NUMBER

11. SUPPLEMENTARY NOTES

12a. DISTRIBUTION/AVAILABILITY STATEMENT
Approved for public release; distribution is unlimited.

12b. DISTRIBUTION CODE

13. ABSTRACT *(Maximum 200 words)*

A test program has been conducted to develop design concepts for assembling large external pressure housings from ceramic cylinders and hemispheres by joining them with removable titanium joint rings and split wedge bands. The proposed design concepts have been validated with 6- and 12-inch-diameter housings assembled from many interchangeable housings components.

The test results show that there appears to be no reduction in structural performance under external pressure associated with (1) linear scaling up of ceramic housing components, and (2) the presence of inclusions or voids <0.05 inch in diameter. Weight-to-displacement of 0.6 has been achieved by housings assembled from 94-percent alumina monocoque cylinders and hemispheres designed not to exceed −150,000 psi compressive stress. The cyclic fatigue life of the ceramic components is determined by the rate of crack growth on the ceramic bearing surfaces under axial bearing loading. The rate of crack growth is minimized by encapsulating the ends of ceramic components in titanium end rings filled with epoxy adhesive. The height of the flanges on the circular, U-shaped end caps is critical for the cyclic fatigue life of the plane bearing surfaces on the ceramic cylinders and hemispheres. The fatigue life of cylinders is >500 pressure cycles to design pressure when their ends are protected by NOSC Mod 1 end caps with flanges whose height h ≈ 3.22x cylinder thickness.

14. SUBJECT TERMS
ceramics
external pressure housing
ocean engineering

15. NUMBER OF PAGES
300

16. PRICE CODE

17. SECURITY CLASSIFICATION OF REPORT	18. SECURITY CLASSIFICATION OF THIS PAGE	19. SECURITY CLASSIFICATION OF ABSTRACT	20. LIMITATION OF ABSTRACT
UNCLASSIFIED	UNCLASSIFIED	UNCLASSIFIED	SAME AS REPORT

21a. NAME OF RESPONSIBLE INDIVIDUAL	21b. TELEPHONE (Include Area Code)	21c. OFFICE SYMBOL
J. D. Stachiw	(619) 553-1875	Code 5602

THE AUTHOR

DR. JERRY STACHIW is Staff Scientist for Marine Materials in the Ocean Engineering Division. He received his undergraduate engineering degree from Oklahoma State University in 1955 and graduate degree from Pennsylvania State University in 1961.

Since that time he has devoted his efforts at various U.S. Navy Laboratories to the solution of challenges posed by exploration, exploitation, and surveillance of hydrospace. The primary focus of his work has been the design and fabrication of pressure resistant structural components of diving systems for the whole range of ocean depths. Because of his numerous achievements in the field of ocean engineering, he is considered to be the leading expert in the structural application of plastics and brittle materials to external pressure housings.

Dr. Stachiw is the author of over 100 technical reports, articles, and papers on design and fabrication of pressure resistant viewports of acrylic plastic, glass, germanium, and zinc sulphide, as well as pressure housings made of wood, concrete, glass, acrylic plastic, and ceramics. His book on "Acrylic Plastic Viewports" is the standard reference on that subject.

For the contributions to the Navy's ocean engineering programs, the Navy honored him with the Military Oceanographer Award and the NCCOSC's RDT&E Division honored him with the Lauritsen-Bennett Award. The American Society of Mechanical Engineers recognized his contributions to the engineering profession by election to the grade of Life-Fellow, as well as the presentation of Centennial Medal, Dedicated Service Award and Pressure Technology Codes Outstanding Performance Certificate.

Dr. Stachiw is past-chairman of ASME Ocean Engineering Division and ASME Committee on Safety Standards for Pressure Vessels for Human Occupancy. He is a member of the Marine Technology Society, New York Academy of Science, Sigma Xi and Phi Kappa Honorary Society.